Investigations on superradiant phases in Landau-quantized graphene

DISSERTATION

ZUR ERLANGUNG DES DOKTORGRADES
DER NATURWISSENSCHAFTEN (DR. RER. NAT.)
DER FAKULTÄT FÜR PHYSIK

DER UNIVERSITÄT REGENSBURG

vorgelegt von

Lisa Heße

aus

Landshut

im Jahr 2017

Das Promotionsgesuch wurde am 02.05.2017 eingereicht.
Das Promotionskolloquium fand am 27.07.2017 statt.

Die Arbeit wurde von Prof. Dr. Klaus Richter angeleitet.

Prüfungsausschuss: Vorsitzender: Prof. Dr. John Lupton
                    1. Gutachter: Prof. Dr. Klaus Richter
                    2. Gutachter: PD Dr. Gernot Schaller
                    weiterer Prüfer: Prof. Dr. Andreas Schäfer

Contents

List of Figures

viii

List of Tables

Chapter 1

Introduction

If the title "king of the elements" [1] was awarded, Carbon would certainly edge out the competition in many ways. No other element is known to combine such a variety of striking chemical and physical properties. Due to its abundance on earth and its unique ability to form a vast variety of chemical compounds Carbon is regarded as one of few elements to be essential for the existence of life. Ever since antiquity, where Carbon compounds were already known[1], this element is playing a seminal role for humankind. From the definition of the Avogadro constant in the 18th century, Carbon as well as its compounds and allotropes constantly gained importance also for various branches of scientific research. However, it is the nature of scientific discourse to yield controversies at certain stages. The same is true for Carbon related research.

The probably most recent and relevant one concerns the thermodynamic stability and thus the existence of an isolated layer of graphite, known as graphene [2, 3]. Theoretical investigations on the remarkable properties of this two-dimensional hexagonal arrangement of Carbon atoms reach back into the year of 1947, where Wallace investigated the band structure of graphite [4] within a tight-binding model. In this seminal work Wallace already pointed out the linear energy dispersion of the band structure close to the corners of the hexagonal Brillouin zone, which was revived a few years later by McClure within the discussion of the nonlinear, strong diamagnetism of graphite [5]. In 1984 DiVincenzo and Mele [6] as well as Semenoff [7] ultimately revealed the mapping of the charge carrier dynamics in the region of linear dispersion onto a two-dimensional Dirac equation with zero rest mass and a constant group velocity $v_{\text{F}} \approx c/300$.
In this early stage however the consideration of a two-dimensional honeycomb lattice mainly served as a mathematical device in order to gain insight into the physical properties of graphite and, later on, fullerenes [8] and carbon nanotubes [9]. Even though, few layers of graphene [10] or even a monolayer of graphene attached to a metal surface [11] have been observed experimentally already at this time, the existence of unsupported graphene remained highly doubted for decades. As pointed out by Peierls [12] and Landau [13, 14] during the 1930s and ultimately summarized by the Mermin-Wagner theorem [15–17], any two-dimensional crystal was regarded to be thermodynamically unstable.
However, this common believe, which was in accordance with several experimental observations [18], faltered with the experimental realization of free-standing graphene by Novoselov, Geim and coworkers in 2004 [19, 20]. These pioneering experiments were

---

[1]in form of charcoal, in Latin: *carbo*

followed by groundbreaking measurements of generic observables proving the pseudo-relativistic dynamics of the charge carriers such as the fractional quantum Hall effect [21, 22], which persists even at room temperature. The experimental evidence of the existence of graphene lead Novoselov and Geim to be awarded with the Nobel Price in 2010 and subsequently opened an entire new subbranch of Carbon based research in the field of condensed-matter physics.

The fascinating nature of graphene results not only from the curiosity of its existence itself but also from the unique charge carrier dynamics close to the corners of the Brillouin zone. The pseudo-relativistic behavior of the fermionic quasiparticles is regarded as the bridge between solid-state and high-energy physics. Moreover, as the valence and conduction band of graphene touch precisely at the corners of the Brillouin zone graphene links the physics of semiconductors and metals with its controllable charge carrier density [19]. Thus investigations of the transport properties of massless Dirac fermions in graphene has naturally become a large area of research [23–25]. Even further, due to its large charge carrier mobility along with their controllable density graphene has the potential to downsize common transistor technology by one order of magnitude accompanied by a significant performance increase compared to ordinary silicon-based devices [26, 27].

The possibilities to study novel or yet unfeasible quantum effects arising from the unique properties of graphene are however not limited to the field of quantum transport. Especially investigations including external gauge potentials hold interesting possibilities for the observation of groundbreaking quantum effects.
Concerning this subfield of graphene related research, the effects emerging from the application of magnetic fields attracted huge interest [24]. The exposure to an uniform perpendicular magnetic field gives rise to a quantization of the energies into discrete degenerate Landau levels similar as it is observable in any other solid-state system. However, the emerging Landau level spectrum in graphene reflects the unique pseudo-relativistic properties in the regime of linear dispersion. This results in a measurable [28–30] energetically non-equidistant spacing of the degenerate Landau levels. Furthermore, according to the electron-hole symmetry of the Dirac cones, a zeroth Landau level is found precisely at the touching point of valence and conduction band. These features give rise to a number of interesting effects reaching from the half-integer quantum Hall effect [21, 22], a giant Faraday effect [31] to the magnetic quantum ratchet effect [32] and also the measurement of the Hofstadter butterfly [33] has been reported. Due to the tunable non-equidistant level spacing and, thus, along with the ability to optically induce frequency-selective cyclotron transitions [28, 34–36] Landau-quantized graphene has also been utilized as a wide-band, tunable THz and IR detector [37] and proposed for Landau-level lasing in this frequency range [38, 39]. Concerning the latter the requirement of population inversion [40, 41] has already been observed experimentally [42–45] in the absence of magnetic fields and it is proposed to persist in Landau-quantized graphene [46] yielding a possibility to realize a wide-range tunable THz Landau-level laser.

Moreover, due to the experimental improvements of the past decades in the field of cavity

quantum electrodynamics, the ultrastrong light-matter coupling regime became experimentally feasible as demonstrated for various condensed-matter systems [47–55]. This coupling range is characterized by the emergence of non-linearities proposing novel effects such as multiphoton Rabi oscillations [56]. Similar investigations for graphene in the absence [57] and presence of magnetic fields [58–60] propose additional signatures arising from the unique pseudo-spin relativistic properties of the material.

Another special quantum effect proposed in the context of cavity quantum electrodynamics in the ultrastrong coupling regime concerns the possible existence of a superradiant phase [61, 62] which can be allocated to the process of collective spontaneous decay. The latter was originally studied by Dicke [63] in 1954 considering the radiative decay of a dense ensemble of distinguishable two-level atoms which is initially prepared in an excited state. Provided that the state of atomic system is symmetric under permutations of individual atoms, which however is identical to their indistinguishability within the setup, they collectively decay under the emission of a coherent radiation flash. The collective interaction of the atomic cloud with electromagnetic radiation enhances the intensity of the emitted light compared to the situation of individually decaying atoms. This cooperative decay is often referred to as Dicke superradiance, which has been observed experimentally in a great variety of different systems ranging from atomic gases [64–70] to circuit quantum electrodynamical setups [71] including investigations of decaying intersubband plasmons [72] and cyclotron resonances [73] in semiconductors.

However, the underlying Dicke model generated a long-term controversy as it is proposed to undergo a second order classical [61] and quantum [62] phase transition from a normal to a superradiant phase in the thermodynamic limit as the ultrastrong critical coupling is exceeded. Thereby, the normal phase is characterized by the ground-state properties of the cavity and the atomic subsystem. By contrast, the superradiant phase where the system has the potential to superradiate [62] is defined by spontaneous macroscopic excitation of both, the atoms and the cavity. Though in driven dissipative systems superradiant critical behavior [74–79] has been observed experimentally in Bose-Einstein condensates [80–83] and atomic gases [84], neither the superradiant classical nor the quantum phase transition has been measured so far in equilibrium, meaning without external driving. This can be explained by means of a no-go theorem [85–91] addressing the originally neglected diamagnetic term which naturally arises from minimal coupling of a parabolic Hamiltonian and prohibits the equilibrium phase transition.

Though the critical behavior proposed for the original Dicke model is regarded as an artifact of approximation, investigations on this peculiar phenomena are still controversial discussed and a matter of current research [92] and especially interesting in the context of graphene [93–95]. Due to the absence of naturally emerging diamagnetic terms in the region of linear dispersion, Landau-quantized graphene offers ideal conditions for the observation of the superradiant phase transition in actual equilibrium [93]. As the degenerate Landau levels are non-equidistant, the transition frequency of the last occupied and first unoccupied level is tunable by the magnetic field and the Fermi level. Thus, the value of the critical coupling is tunable such that a superradiant quantum phase transition is predicted for a large enough Fermi level [93]. However, this proposal completely omits all contributions from filled Landau levels of the valence band as they are regarded to be far off-resonant with the cavity mode. This triggered a controversial discussion [94, 95]

concerning dynamically generated diamagnetic terms which are meant to arise from the occupied Landau states beneath the Fermi level and in turn prohibit superradiant critical behavior. In particular, Refs. [94, 95] perturbatively derive an effective generalized Dicke Hamiltonian for the resonant Landau-level doublet which includes additional, dynamically generated quadratic contributions. The resulting expression however strongly depends on the choice of regularization, which is required as the effective Dirac model artificially assumes unbounded linear energy bands. In general, the proper regularization of the effective Dirac model is still under debate [96, 97]. Nevertheless, neglecting the valence band contribution as well as a second-order perturbative approach applied for the calculation of the diamagnetic terms probably lacks justification when striving a robust prediction for the ultrastrong and, thus, highly non-linear coupling regime.

The aim of this thesis is to constructively contribute to the clarification of the controversial discussion on the existence of superradiant critical behavior in Landau-quantized graphene. Both methods applied for this purpose are chosen with focus on reducing the amount of approximation preferably capturing the entire non-linearity: The first approach concerns a path integral formalism for the calculation of the many-body partition sum on the basis of the effective Dirac model. Within this method it is possible to exactly integrate the fermionic contribution of the entire many-body Hamiltonian and derive an effective action for the cavity mode. However, as the effective Dirac model assumes unbounded linear bands, the effective action requires regularization. This is achieved by two different methods: a rigid ultraviolet cutoff as commonly applied on Landau-quantized graphene [24, 98–102] and a rotating-wave-like approximation yielding a cutoff-independent result similar as applied in Ref. [93]. The predictions obtained within this method are then compared with a numerical tight-binding simulation of the complete band structure of Landau-quantized graphene interacting with a cavity mode. Thereby no further approximations are applied such that the result can be regarded as an independent proof of the analytic prediction.

Additionally, the perturbative approach considered in Ref. [95] is extended to fourth order and evaluated first by using an identical cutoff-independent regularization as applied in the original work. The result for the critical coupling obtained from the effective Dicke model is then compared with the cutoff independent result of the path integral approach. Within the cutoff-independent regularization neither the path integral approach nor the perturbation expansion in second and fourth order yield results that are commensurable with the validity range of the approach. In other words, within this particular choice of regularization, the perturbative approach is a priori not capturing the relevant coupling ranges due to its validity range. However, by allowing for a cutoff-dependent regularization convincing agreement with the path integral approach is obtained for prediction of the phase boundary within the validity range even in second-order approximation.

Outline of this thesis

Part I introduces the theoretical concepts for the investigation on the superradiant critical behavior in Landau-quantized graphene.
To this end, **Chap. 2** briefly outlines the main aspects of the canonical quantization of the electromagnetic field and cavity quantum electrodynamics.

Chap. 3 provides a detailed discussion of the Dicke model starting with the discussion of the Dicke Hamiltonian and the phenomena of Dicke superradiance. Subsequently follows the discussion of the superradiant phase transition with focus on the quantum critical behavior. Thereby a catalog of generic observables indicating and proving the quantum critical behavior is provided. This catalog serves as the basis for the examination of superradiant critical behavior in Landau-quantized graphene as investigated during Part II.

Chap. 4 gives insight into the no-go theorem and provides an outline of proposed exceptions to it according literature. In this chapter also the controversy regarding the superradiant critical behavior in Landau-quantized graphene is picked up.

Chap. 5 provides an introduction into the properties of graphene. Starting at the original single-particle tight-binding Hamiltonian the derivation of the effective Dirac model is outlined and followed by the discussion of Landau quantization and single-particle light-matter interaction within this model. Subsequently follows the construction and discussion of the many-body Hamiltonian of Landau-quantized graphene in the context of cavity quantum electrodynamics.

Part II is regarded as the main part of this thesis where the superradiant quantum phase transition in Landau-quantized graphene is examined.

Chap. 6 discusses the numerical setup of the tight-binding simulation and introduces the parameters of the considered systems. Furthermore, a discussion of the Peierls substitution and an estimation of its range of validity is provided, also in view numerically implementing an electromagnetic vector potential for the cavity mode. The results obtained within the tight-binding simulation are discussed simultaneously with the prediction of the analytic results in the subsequent chapter.

Chap. 7 provides the calculation of the grand-canonical partition sum of the full Landau-quantized many-body Hamiltonian, derived in Chap. 5, within a path integral approach in the thermodynamic limit. A selection of the catalog of typical observables indicating the superradiant quantum phase transition is picked up step by step for two distinct regularization techniques. The mean-field results are then compared with the independent tight-binding simulation proving also the plausibility of the respective regularization method. Thereby the rigid cutoff regularization shows strong agreement with the numerical simulation. On this basis Chap. 7 eventually defines the parameter ranges required for the actual experimental observation of the superradiant quantum phase transition. Furthermore, an analysis of the critical exponents associated with the closure of the excitation gap in the vicinity of the critical point is provided on the basis of the path integral approach.

In **Chap. 8** the perturbative approach applied in Ref. [95] is extended to fourth order. The focus of this investigation mainly lies upon the calculation of the critical point. The effective Dicke-like Hamiltonian derived within this approach is examined using a rigid momentum cutoff and cutoff-independent regularization similar as applied in Ref. [95]. The former predicts the phase boundary in convincing agreement with the path integral approach of the full many-body Hamiltonian. A selection of typical features indicating the superradiant quantum phase transition is then evaluated for the effective Dicke-like Hamiltonian and compared with the path integral results obtained in Chap. 7.

Chap. 9 summarizes the results and provides perspectives for proceeding considerations

on the superradiant phase transition in Landau-quantized graphene.

The **Appendix** complements the Parts I and II by providing technical details and additional information. Thus, in **App. A** a discussion of the Lagrangian and Hamiltonian formulation of classical electrodynamics as the basis for the canonical quantization of electromagnetic radiation is found. **App. B** reviews some basic concepts of single-particle quantum mechanics with special focus on the different dynamical representations and the rotating-frame transformation commonly used in the field of quantum optics. The main aspects of many-body quantum mechanics are summarized in **App. C** recapping the properties of completely symmetrized and anti-symmetrized states which is necessary to understand the concept of indistinguishability in the context of bosonic and fermionic particles. Furthermore a short introduction into the formalism of second quantization and coherent states of both particle species is provided which is necessary to derive the path integral approach for the many-body partition sum examined in **App. D** starting from the familiar single-particle Feynman propagator. **App. E** discusses some useful mathematical tools such as Fourier transformation, Grassmann numbers, Matsubara summation as well as some helpful commutation relations. Finally, **App. F** provides some technical details for the calculation of the fourth-order contribution to the effective Dicke Hamiltonian discussed in Chap. 8.

Part I

Preliminary concepts

Chapter 2

Quantum electrodynamics in Coulomb gauge

In order to understand the physical principles underlying the quantum optical effect of superradiance it is essential to introduce the concepts of electromagnetic radiation and its interaction with charged matter on a basic level beforehand.

In the whole field of quantum optics, the concept of quantizing the electromagnetic field plays a key role by providing the necessary mathematical framework to understand the origin of *vacuum fluctuations* around the zero-point energy. These fluctuations have no classical equivalent and thus in turn are not captured by the classical treatment of radiation based on *Maxwell equations*.

Theoretical investigations on the interaction between a classical electromagnetic field and a quantum state of matter require sufficient insights in the understanding of many optical effects, such as stimulated absorption and emission of radiation [103]. However these, often denoted as *semiclassical*, theories of light-matter interaction are inadequate in the description of several quantum optical effects, such as the Lamb shift [104, 105], the Casimir effect [106–108], the spectral line width of a laser [109, 110] or spontaneous emission [111] and related effects including Dicke superradiance [63]. The common feature of these effects is their explicability based on the introduction of vacuum fluctuations. For instance, the effect of spontaneous emission is accessible through the concept of vacuum fluctuations "stimulating" an excited atom to emit radiation. Furthermore, within a quantized theory of electromagnetic radiation, the introduction of the term *photon* naming the emerging electromagnetic quanta is justified.

Beyond this physical motivation for the necessity of introducing a quantized theory of radiation, in some cases the formalism itself provides technical advantages. According to the different dynamical representations of quantum mechanics as briefly discussed in App. B, the dynamics of the photonic quantities entering the theory are adjustable between either the dependence on time being completely carried by the state vectors or the operators. Therefore also mixed representations according to the interaction picture are possible, see Sec. 3 in App. B. Nevertheless, the Schrödinger picture with constant operators and time-dependent state vectors is exclusively applied throughout this thesis.

2.1 Canonical quantization of the electromagnetic field

In this subsection the derivation of a quantized theory for the free electromagnetic field is outlined. The main aspects of the discussion are leaned on the comprehensive considerations of Ref. [103]. The starting point for the canonical quantization of the electromagnetic field is provided by the postulation of the classical Lagrangian of electrodynamics in accordance with the Maxwell equations.

Similar to classical mechanics the Lagrangian formulation of the respective classical field theory is based on the identification of appropriate generalized coordinates and velocities [112] reflecting the characteristic dynamical properties of the system. The aim is then to derive the momenta conjugate to the independent generalized coordinates of the classical field. Thereby, the field theory of classical electrodynamics can be transformed from the Lagrangian into the Hamiltonian formulation [112] in a similar manner as known from classical mechanics of point particles. Accordingly, the identified generalized coordinates and conjugate momenta for fields satisfy the respective fundamental Poisson brackets [103, 112] wherefore they are also referred to as *canonical* coordinates. The significance of the Poisson bracket (A.50) for theoretical physics is twofold: On the one hand, the validity of the Poisson brackets for a certain set of generalized coordinates and conjugate momenta corresponds to the invariance of the phase-space volume by regarding them as transformations from a different set of canonical coordinates. On the other hand, the Poisson brackets are regarded as the classical equivalent to the canonical commutator relations (C.40) of quantum mechanics [113]. They determine the dynamics of a classical observable (A.51) in a formally similar way as the quantum mechanical commutator in the Heisenberg equation of motion (B.9). This formal coincidence is reasonable in view of *Bohr's correspondence principle* [114], stating that the predictions of quantum mechanics coincide with those of classical physics in the limit of large quantum numbers (or "$\hbar \to 0$"). Therefore the Poisson brackets in classical mechanics and classical field theory can be regarded as the basis for canonical quantization of the respective theory. For more details on the scheme of canonical quantization of the electromagnetic field any standard textbook on quantum optics or quantum electrodynamics is sufficient. e.g. Ref. [103].

It is convenient to start at Maxwell equations (A.1 – A.4), since they offer the most fundamental insight into the properties of the magnetic field $\boldsymbol{B}$ and the electric field $\boldsymbol{E}$ as well as their relation to each other. As outlined of Sec. 1 of App. A, the fields $\boldsymbol{B}$ and $\boldsymbol{E}$ are partially determined from a common vector potential $\boldsymbol{A}$,

$$\boldsymbol{B}(\boldsymbol{q},t) = \nabla \times \boldsymbol{A}(\boldsymbol{q},t), \tag{2.1}$$

$$\boldsymbol{E}(\boldsymbol{q},t) = -\nabla \varphi(\boldsymbol{q},t) - \partial_t \boldsymbol{A}(\boldsymbol{q},t), \tag{2.2}$$

where φ denotes the scalar potential of the electric field. Accordingly, the potentials φ and $\boldsymbol{A}$ can be referred to as generalized coordinates for the fields $\boldsymbol{B}$ and $\boldsymbol{E}$. Thereby the fields $\boldsymbol{B}$ and $\boldsymbol{E}$ are real-valued and invariant under gauge transformations, as outlined of Sec. 1 of App. A. The relations (2.1, 2.2) directly follow from the homogeneous Maxwell equations (A.2, A.4).

For the following discussion it is convenient to represent the fields and the potentials in momentum space. Therefore one applies the Fourier transform, as discussed in Sec. 1 of

App. E, on Eqs. (2.1, 2.2), yielding

$$\tilde{\boldsymbol{B}}(\boldsymbol{k}, t) = i\boldsymbol{k} \times \tilde{\boldsymbol{A}}(\boldsymbol{k}, t), \tag{2.3}$$

$$\tilde{\boldsymbol{E}}(\boldsymbol{k}, t) = -i\boldsymbol{k}\tilde{\varphi}(\boldsymbol{k}, t) - \partial_t \tilde{\boldsymbol{A}}(\boldsymbol{k}, t), \tag{2.4}$$

where $\boldsymbol{k}$ will be associated with the *propagation direction* of the electromagnetic radiation in Coulomb gauge.

2.1.1 Hamiltonian formulation of classical electromagnetism

The dynamics of N point charges q_i interacting with classical radiation is fully determined by the classical Hamiltonian function

$$\mathcal{H}[\{\boldsymbol{q}_i\}, \{\boldsymbol{p}_i\}; \boldsymbol{A}, \boldsymbol{\Pi}] = \mathcal{H}_{\mathrm{matter}}[\{\boldsymbol{q}_i\}, \{\boldsymbol{p}_i\}; \boldsymbol{A}] + \mathcal{H}_{\mathrm{em}}[\boldsymbol{A}, \boldsymbol{\Pi}], \tag{2.5}$$

of the generalized coordinates and momenta of the particles, $\{\boldsymbol{q}_i\}$ and $\{\boldsymbol{p}_i\}$, and the fields, $\boldsymbol{A}$ and $\boldsymbol{\Pi} = \epsilon_0 \partial_t \boldsymbol{A}$ (cf. Sec. 3 of App. A). The contribution

$$\mathcal{H}_{\mathrm{matter}}[\{\boldsymbol{q}_i\}, \{\boldsymbol{p}_i\}; \boldsymbol{A}] = \sum_{i=1}^{N} \frac{[\boldsymbol{p}_i - q_i \boldsymbol{A}(\boldsymbol{q}_i, t)]^2}{2m_i} + V_{\mathrm{C}} \tag{2.6}$$

describes the kinetic properties of the N point charges and the Coulomb interaction among them, denoted by V_{C}. Furthermore, $\{\boldsymbol{q}_i\}$ and $\{\boldsymbol{p}_i\}$ denotes the set of coordinates and momenta of the N point particles. The remaining part of the Hamiltonian function $\mathcal{H}$ describes the kinetics of the free, noninteracting electromagnetic field, reading

$$\mathcal{H}_{\mathrm{em}}[\boldsymbol{A}, \boldsymbol{\Pi}] = \frac{\epsilon_0}{2} \int_{\mathbb{R}^3} \frac{\mathrm{d}^3 k}{(2\pi)^3} \left[\frac{1}{\epsilon_0^2} |\boldsymbol{\Pi}(\boldsymbol{k}, t)|^2 + c^2 k^2 |\tilde{\boldsymbol{A}}(\boldsymbol{k}, t)|^2 \right]. \tag{2.7}$$

Within the derivation of $\mathcal{H}$ from the postulated classical Lagrangian, which is discussed in App. A, one finds for the canonical momenta of the electromagnetic field $\boldsymbol{\Pi} = \epsilon_0 \partial_t \tilde{\boldsymbol{A}}$, see in particular Sec. 3 of App. A. Thus, $\boldsymbol{\Pi}$ is closely related to the electric field $\tilde{\boldsymbol{E}}$ in Fourier space, Eq. (2.4). Moreover, as no time derivative of the scalar potential φ enters the classical Lagrangian, the classical field theory can be transformed into a φ-independent form (cf. Sec. 2 of App. A). With this, the conjugate momenta satisfies $\boldsymbol{\Pi} = -\epsilon_0 \tilde{\boldsymbol{E}}$.

As the classical Hamiltonian function $\mathcal{H}$ is independent on a specific choice of gauge, one may choose a specific constraint for the vector potential $\tilde{\boldsymbol{A}}$ in order to diminish the degrees of freedom entering the theory. Thus, when investigating electromagnetic radiation, it is convenient to choose Coulomb gauge, i.e.

$$\boldsymbol{k} \cdot \tilde{\boldsymbol{A}}(\boldsymbol{k}, t) = 0 \quad \Leftrightarrow \quad \nabla \cdot \boldsymbol{A}(\boldsymbol{q}, t) = 0, \tag{2.8}$$

where the contribution of $\tilde{\boldsymbol{A}}$ parallel to the propagation direction $\boldsymbol{k}$ of the electromagnetic field is set zero. Hence, only the perpendicular or transverse parts of $\tilde{\boldsymbol{A}}$ contribute. As Fig. 2.1 illustrates, this directly yields two perpendicular polarization directions, $\boldsymbol{\eta}_{1,\boldsymbol{k}} \perp \boldsymbol{k}$ and $\boldsymbol{\eta}_{2,\boldsymbol{k}} \perp \boldsymbol{k}$. This is also discussed in more detail in Sec. 2 of App. A. Furthermore, Sec. 4
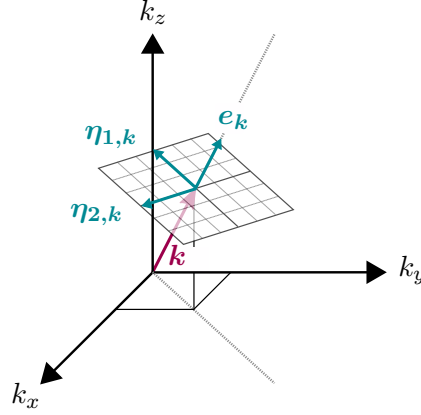
FIGURE 2.1: Illustration of the two independent directions of polarization, $\boldsymbol{\eta}_{1,\boldsymbol{k}}, \boldsymbol{\eta}_{2,\boldsymbol{k}}$, normal to the propagation direction $\boldsymbol{e}_{\boldsymbol{k}} \parallel \boldsymbol{k}$ of the transverse field according to Coulomb gauge, following Ref. [103]. The basis provided by $\boldsymbol{\eta}_{1,\boldsymbol{k}} \perp \boldsymbol{\eta}_{2,\boldsymbol{k}}$ is invariant under rotation with respect to $\boldsymbol{e}_{\boldsymbol{k}}$ axis.

of App. A demonstrates, that the gauge constraint (2.8) directly leads to

$$\tilde{\boldsymbol{A}}_n(\boldsymbol{k}, t) = \boldsymbol{\eta}_{n,\boldsymbol{k}} \tilde{\mathcal{A}}_k \left[\alpha_n(\boldsymbol{k}, t) + \alpha_n^*(-\boldsymbol{k}, t) \right], \tag{2.9}$$

where the normalization factor $\tilde{\mathcal{A}}_k$ is defined by

$$\tilde{\mathcal{A}}_k = \sqrt{\frac{\hbar}{2\epsilon_0 \omega_k}}, \tag{2.10}$$

anticipating the quantum properties of the radiation field as presented subsequently. Thereby $\omega_k = ck$ denotes the radiation frequency and c refers to the speed of light. Furthermore, the Fourier coefficients $\alpha_n(\boldsymbol{k}, t)$ and $\alpha_n^*(-\boldsymbol{k}, t)$, referred to as normal coordinates [103], have the following explicit time dependence

$$\alpha_n(\boldsymbol{k}, t) = \alpha_n(\boldsymbol{k}) e^{-i\omega_k t}, \tag{2.11}$$

$$\alpha_n^*(-\boldsymbol{k}, t) = \alpha_n^*(-\boldsymbol{k}) e^{i\omega_k t}, \tag{2.12}$$

which already reflects the generic properties of electromagnetic radiation with respect to time propagation. The position space representation of $\tilde{\boldsymbol{A}}$, Eq. (2.10), according to Eq. (A.36) further underpins the wave-like properties of the vector potential and thus in turn the fields $\boldsymbol{B}$ and $\boldsymbol{E}$.

The classical Hamiltonian of the free electromagnetic field, $\mathcal{H}_{\text{em}}$, can also be expressed in terms of normal coordinates, yielding

$$\mathcal{H}_{\text{em}}[\boldsymbol{A}, \boldsymbol{\Pi}] = \int_{\mathbb{R}^3} \frac{\mathrm{d}^3 k}{(2\pi)^3} \frac{\hbar \omega_k}{2} \sum_{n=1}^{2} \left[\alpha_n(\boldsymbol{k}, t) \alpha_n^*(\boldsymbol{k}, t) + \alpha_n^*(\boldsymbol{k}, t) \alpha_n(\boldsymbol{k}, t) \right], \tag{2.13}$$

which is already reminiscent of the Hamiltonian of a quantum mechanical oscillator. Along with the Hamiltonian formulation of classical electrodynamics comes the formalism of Poisson brackets determining the dynamics of the corresponding observables. As discussed in Sec. 6 of App. A, the generalized coordinates and conjugate momenta of the particles and the field obey the fundamental Poisson brackets (A.52 A.53, A.54) which provide the basis for the formulation of a quantum mechanical theory of electromagnetic radiation. The main aspects of the canonical quantization of the radiation field is subsequently discussed.

2.1.2 Canonical quantization of the transverse electromagnetic field

According to Dirac [113] quantization of a classical theory is achieved by replacing the Poisson bracket with the commutator (C.40) according to

$$\{f, g\} \mapsto \frac{1}{i\hbar}[\hat{f}, \hat{g}], \tag{2.14}$$

where the classical functions of phase-space coordinates, f and g, are replaced by their operator equivalent, each marked with a caret, i.e.

$$f \mapsto \hat{f}, \quad g \mapsto \hat{g}. \tag{2.15}$$

The r.h.s. of (2.14) is sometimes also referred to as quantum-mechanical Poisson bracket [115]. Applying Dirac's rule onto the generalized coordinates and conjugate momenta, Eqs. (A.29, A.30), along with the respective Poisson brackets (A.52 A.53, A.54) leads from classical field theory to quantum field theory of electrodynamics:

$$\boldsymbol{q}_i \quad \mapsto \hat{\boldsymbol{q}}_i, \qquad \boldsymbol{p}_i \quad \mapsto \hat{\boldsymbol{p}}_i, \tag{2.16}$$

$$\tilde{A}_n(\boldsymbol{k}, t) \mapsto \hat{A}_n(\boldsymbol{k}, t), \quad \tilde{\Pi}_n(\boldsymbol{k}, t) \mapsto \hat{\Pi}_n(\boldsymbol{k}, t), \tag{2.17}$$

where the grapheme $\sim$ marking the Fourier transform of the canonical field coordinates is omitted for convenience. The association of the normal coordinates with operators results in

$$\alpha_n(\boldsymbol{k}, t) \mapsto \hat{a}_{n,\boldsymbol{k}}(t) = \hat{a}_{n,\boldsymbol{k}}e^{-i\omega_k t}, \tag{2.18}$$

$$\alpha_n^*(\boldsymbol{k}, t) \mapsto \hat{a}_{n,\boldsymbol{k}}^\dagger(t) = \hat{a}_{n,\boldsymbol{k}}^\dagger e^{i\omega_k t}, \tag{2.19}$$

where $\hat{a}_{n,\boldsymbol{k}}^\dagger(t)$ and $\hat{a}_{n,\boldsymbol{k}}(t)$ are denoted as creation and annihilation operators of light quanta or *photons* associated with the polarization direction $\boldsymbol{\eta}_{n,\boldsymbol{k}}$. According to the different dynamical representations of quantum mechanics, as discussed in App. B, one can refer to $\hat{a}_n^\dagger(t)$ and $\hat{a}_n(t)$ as represented in Heisenberg or interaction picture. The properties of the creation and annihilation operators in time-independent Schrödinger picture are comprehensively discussed in Sec. 2 of the App. C. Furthermore, according to the operator definitions (2.16, 2.17) the canonical commutation relations are obtained in view of

Dirac's rule:

$$[\hat{\boldsymbol{q}}_{i_\alpha}, \hat{\boldsymbol{p}}_{j_\beta}] = i\hbar\,\delta_{i,j}\delta_{\alpha,\beta}, \tag{2.20}$$

$$[\hat{A}_n(\boldsymbol{k}, t), \hat{\Pi}_{\bar{n}}^\dagger(\boldsymbol{k}', t)] = i\hbar\,\delta_{n,\bar{n}}\delta(\boldsymbol{k} - \boldsymbol{k}'), \tag{2.21}$$

$$[\hat{a}_{n,\boldsymbol{k}}, \hat{a}_{\bar{n},\boldsymbol{k}'}^\dagger] = \delta_{n,\bar{n}}\delta(\boldsymbol{k} - \boldsymbol{k}'), \tag{2.22}$$

where $\alpha, \beta = x, y, z$ in (2.20) denote the operator component of the ith and j^{th} quantum particle along the corresponding space direction. Similar to the Poisson brackets of the corresponding classical observables all other commutators are zero. From the definition of the photonic creation and annihilation operators $\hat{a}_{n,\boldsymbol{k}}^\dagger$ and $\hat{a}_{n,\boldsymbol{k}}$ the corresponding operator component of the electromagnetic vector potential along polarization direction $\eta_{n,\boldsymbol{k}}$ follows directly from (A.37):

$$\hat{\boldsymbol{A}}_n(\hat{\boldsymbol{q}}, t) = \boldsymbol{\eta}_{n,\boldsymbol{k}} \int_{\mathbb{R}^3} \frac{\mathrm{d}^3 k}{(2\pi)^2} \tilde{\mathcal{A}}_k \left[\hat{a}_{n,\boldsymbol{k}}(t)e^{i\boldsymbol{k}\cdot\hat{\boldsymbol{q}}} + \hat{a}_{n,\boldsymbol{k}}^\dagger(t)e^{-i\boldsymbol{k}\cdot\hat{\boldsymbol{q}}} \right]. \tag{2.23}$$

Furthermore, one can define the quantum mechanical Hamiltonian of electrodynamics from its classical counterpart Eqs. (2.5, 2.6, 2.7, A.49):

$$\hat{\mathcal{H}} = \hat{\mathcal{H}}_{\text{matter}} + \hat{\mathcal{H}}_{\text{em}}, \tag{2.24}$$

where each of the contributions reads

$$\hat{\mathcal{H}}_{\text{matter}} = \sum_{i=1}^{N}\sum_{n=1}^{2} \frac{\left[\hat{\boldsymbol{p}}_i - q_i\hat{\boldsymbol{A}}_n(\hat{\boldsymbol{q}}_i, t)\right]^2}{2m_i} + \hat{V}_{\text{C}}, \tag{2.25}$$

$$\hat{\mathcal{H}}_{\text{em}} = \sum_{n=1}^{2} \int_{\mathbb{R}^3} \frac{\mathrm{d}^3 k}{(2\pi)^3} \hbar\omega_k \left(\hat{a}_{n,\boldsymbol{k}}^\dagger \hat{a}_{n,\boldsymbol{k}} + \frac{1}{2} \right). \tag{2.26}$$

The contribution $\propto 1/2$ to the Hamiltonian of the quantum mechanical radiation field in free space (2.26) is associated with the infinite vacuum energy [103]. Since it yields a constant background, it is formally omitted in many quantum optical theories such as the Dicke model discussed in Chap. 3. Note that the integration over wave numbers in the definition of $\hat{\mathcal{H}}_{\text{em}}$ can be regarded as summarizing over the continuum of radiation modes. In most cases, the cumbersome derivation of the Hamiltonian $\hat{\mathcal{H}}$ and its contributions (2.25, 2.26) is shortened by the substitution of

$$\hat{\boldsymbol{p}}_i \mapsto \hat{\boldsymbol{p}}_i - q_i\hat{\boldsymbol{A}}_n(\hat{\boldsymbol{q}}_i, t), \tag{2.27}$$

referred to as the *principle of minimal coupling*.

2.2 Cavity quantum electrodynamics in Coulomb gauge

The main part of this thesis investigates the interaction between Landau-quantized charge carriers in graphene and an electromagnetic cavity mode. By confining the electromagnetic field of free space to a finite volume the properties of the radiation field are influenced by the geometry of the cavity and the boundary conditions of its walls. This holds for classical but also quantum electrodynamics. In case of the latter, the distribution of photons with energy $\hbar\omega_k$ is a continuum in free space. By contrast, only photons with a distinct energy $\hbar\omega_{k_i}$ are able to occupy a cavity. The selection of wave numbers $\boldsymbol{k}_i$ strictly depends on the properties of the cavity walls, as they give rise to characteristic boundary conditions. A prominent example of the altered properties of confined photons compared with those in free space is the Casimir effect [106–108]. Furthermore, the changes in the rate of spontaneous emission of atoms brought into a cavity is another signature of the confinement. Thereby, the emission rate is diminished [116] if the photon frequencies ω_{k_i} are off-resonant with the transition frequency of the atoms. Vice versa, spontaneous emission is enhanced in case of resonance [116]. Thus, also the rate of spontaneous emission of atoms reflects the properties of the cavity boundary conditions. As it might be obvious from the discussion in Sec. 2, the results of the quantization procedure in free space are not generally applicable to confined radiation fields. Generally, before quantizing one has to consistently implement the boundary conditions starting at the solutions to the Helmholtz equation, see Sec. 4 of App. A. The quantization procedure then strongly depends on the geometry and properties of the cavity [117]. Nevertheless the issue of cavity-dependent quantization can be circumvented in case of the validity of dipole approximation. In this case, the relevant spacial dimensions of the atomic or electronic system are much smaller than the wavelength $\lambda = 2\pi/k$ of the cavity mode and the photonic field can be regarded as locally invariant. Accordingly, each component of the vector potential can be approximated as

$$\hat{\boldsymbol{A}}_n(\hat{\boldsymbol{q}}, t) \approx \hat{\boldsymbol{A}}_n = \boldsymbol{\eta}_{n,\boldsymbol{k}} \int_{\mathbb{R}^3} \frac{\mathrm{d}^3 k}{(2\pi)^2} \tilde{\mathcal{A}}_k \left[\hat{a}_{n,\boldsymbol{k}}(t) + \hat{a}^{\dagger}_{n,\boldsymbol{k}}(t)\right], \qquad (2.28)$$

as applied in the standard Dicke model [61–63]. As discussed Subsec. 5.2.3, Eq. (2.28) holds also true when investigating the interaction of Landau-quantized Dirac fermions with a cavity mode.

However, even in the case of Eq. (2.28) being a reasonable approximation there are still signatures of the confinement regarding the wave number $\boldsymbol{k}$ and thus the energy of the photons. For convenience, a rectangular cavity with side lengths L_x, L_y and L_z is chosen during the following. Furthermore, it is assumed, that the spacial extension in x and y direction are much larger than in z direction, i.e. $L_x, L_y \gg L_z$, which is in accordance with other publications investigating the possibility of a superradiant quantum phase transition in Landau-quantized graphene [93–95].

Due to the periodic nature of the electromagnetic field periodic boundary conditions in x and y direction are sufficient. Thereby, the effect of the boundaries in these directions is eliminated in accordance with the spacial dimension. By contrast, the confinement in z direction is assumed to be perfectly conducting. Accordingly, the tangential component of the electric field $\boldsymbol{E}$ and the normal component of the magnetic field $\boldsymbol{B}$ vanish at

$z = 0, L_z$ [117], i.e. $E_x = E_y = B_z = 0$.

Thereby, the wave vector $\boldsymbol{k}$ becomes discretized, $\boldsymbol{k} \mapsto \boldsymbol{k_l} = (k_{l_x}, k_{l_y}, k_{l_z})$, where each component $i = x, y$ is given by [117]

$$k_{l_i} = \frac{2\pi l_i}{L_i}, \tag{2.29}$$

with $l_x, l_y \in \mathbb{Z}$. By contrast, the component in z direction reads [117]

$$k_{l_z} = \frac{\pi l_z}{L_z}, \tag{2.30}$$

with $l_z \in \mathbb{N}_0$, due to the different boundary conditions in this direction. It is also possible to choose the boundary conditions for the walls in x and y direction similar to the one in z direction. In this case k_{l_x} and k_{l_y} would be obtained from conditions similar to Eq. (2.30). Each set of $\boldsymbol{k_l}$ is referred to as a *cavity mode* with energy $\hbar\omega_{k_l}$. According to the discretization of wave vectors the integration entering the definition Hamiltonian $\hat{\mathcal{H}}_{\mathrm{em}}$ (2.26) of the electromagnetic fields needs to be replaced by a sum, i.e.

$$\int_{\mathbb{R}^3} \frac{\mathrm{d}^3 k}{(2\pi)^3} \mapsto \frac{1}{V} \sum_{\boldsymbol{k_l}}. \tag{2.31}$$

Furthermore, the spacial dimension of the cavity is chosen in a way that the mode with lowest, non-zero energy

$$\omega_0 = \min(\{\omega_{|\boldsymbol{k_l}|} > 0, l_x, l_y \in \mathbb{Z}, l_z \in \mathbb{N}_0\}) \tag{2.32}$$

is resonant with some regarded transition. This restriction refers to a *single cavity mode* description. The generalization to a *multimode* case is easily achieved by keeping the summation as the substitute to the integration over the mode continuum according to Eqs. (2.28, 2.31). The corresponding wave vector of a single mode is denoted by $\boldsymbol{k_0}$. For reasons of simplicity and without loss of generality, the polarization of the electromagnetic mode shall be fixed in x direction during this thesis in accordance with Ref. [94]. Then the vector potential is of the form

$$\hat{\boldsymbol{A}}_{\mathrm{em}} = \boldsymbol{e}_x \mathcal{A}_0 [\hat{a}^\dagger(t) + \hat{a}(t)], \tag{2.33}$$

where the operators $\hat{a}^\dagger$ and $\hat{a}$ are defined as

$$\hat{a}^\dagger_{x, \boldsymbol{k_0}}(t) = \sqrt{V} \hat{a}^\dagger(t), \quad \hat{a}_{x, \boldsymbol{k_0}}(t) = \sqrt{V} \hat{a}(t). \tag{2.34}$$

Furthermore the normalization factor $\mathcal{A}_0$ of the cavity mode is obtained as

$$\mathcal{A}_0 = \frac{\tilde{\mathcal{A}}_{|\boldsymbol{k_0}|}}{\sqrt{V}} = \sqrt{\frac{\hbar}{2\epsilon_0 \omega_0 V}}, \tag{2.35}$$

where $\tilde{\mathcal{A}}_{|\boldsymbol{k_0}|}$ as defined in Eq. (A.33).

To summarize, one finds the single-mode Hamiltonian of cavity quantum electrodynamics in dipole approximation by adapting the Hamiltonian of the N-particle system interacting with electromagnetic radiation in free space (2.24, 2.25 2.26) accordingly:

$$\hat{\mathcal{H}}_{\text{matter}} = \sum_{i=1}^{N} \frac{\left[\hat{\boldsymbol{p}}_i - q_i \hat{\boldsymbol{A}}_{\text{em}}\right]^2}{2m_i} + \hat{V}_{\text{C}}, \tag{2.36}$$

$$\hat{\mathcal{H}}_{\text{cav}} = \hbar \omega_0 \left(\hat{a}^\dagger \hat{a} + \frac{1}{2}\right). \tag{2.37}$$

For convenience, the quantum particles are assumed to be identical for the proceeding discussion of the Hamiltonian $\hat{\mathcal{H}} = \hat{\mathcal{H}}_{\text{matter}} + \hat{\mathcal{H}}_{\text{cav}}$. Hence, all particles share the same mass and charge, i.e. $m_i = m$ and $q_i = q \; \forall i = 1, \ldots, N$. By expanding the square in Eq. (2.36) $\hat{\mathcal{H}}_{\text{matter}}$ can be decomposed according to

$$\hat{\mathcal{H}}_{\text{matter}} = \hat{\mathcal{H}}_0 + \hat{\mathcal{H}}_{\text{int}} + \hat{\mathcal{H}}_{\text{dia}}, \tag{2.38}$$

where

$$\hat{\mathcal{H}}_0 = \sum_{i=1}^{N} \frac{\hat{\boldsymbol{p}}_i^2}{2m} + \hat{\mathcal{V}}_{\text{C}}[\hat{\boldsymbol{q}}_1, \ldots, \hat{\boldsymbol{q}}_N] \tag{2.39}$$

denotes the many-body Hamiltonian of N quantum particles in the field-free case. Let $\{|n_i\rangle\}$ denote the complete set of eigenstates of each single-particle contribution to $\hat{\mathcal{H}}_0$, then Eq. (2.39) can be alternatively written as

$$\hat{\mathcal{H}}_0 = \sum_{i=1}^{N} \left(\sum_{n_i} \epsilon_{n_i} |n_i\rangle \langle n_i|\right), \tag{2.40}$$

where ϵ_{n_i} denotes the energy of quantum particle i corresponding to the eigenstate $|n_i\rangle$. Since all quantum particles are regarded to be identical, the particle index i on the energies ϵ_i can be omitted. The second contribution to the Hamiltonian (2.38), $\hat{\mathcal{H}}_{\text{int}}$, describes the interaction between the particles and the cavity mode:

$$\hat{\mathcal{H}}_{\text{int}} = -\frac{q}{m} \sum_{i=1}^{N} \hat{\boldsymbol{p}}_i \cdot \hat{\boldsymbol{A}}_{\text{em}}. \tag{2.41}$$

By deducing the identity

$$\hat{\boldsymbol{p}}_i = i\frac{m}{\hbar}[\hat{\mathcal{H}}_0, \hat{\boldsymbol{q}}_i] \tag{2.42}$$

from the canonical commutation relations for the particle operators $\hat{\boldsymbol{p}}_i$ and $\hat{\boldsymbol{q}}_i$ (2.20), it is possible to expand each single-particle contribution of $\hat{\mathcal{H}}_{\text{int}}$ in the single-particle eigenbasis $\{|n_i\rangle\}$ of $\hat{\mathcal{H}}_0$. Thereby, one inserts resolutions of identity,

$$\sum_{n_i} |n_i\rangle \langle n_i| = 1, \tag{2.43}$$

on each side of the commutator [118] to obtain

$$\hat{\boldsymbol{p}}_i = -i\frac{m}{\hbar q}\sum_{n_i,\bar{n}_i}(\epsilon_{\bar{n}}-\epsilon_n)\hat{\boldsymbol{d}}_{\bar{n}_i,n_i}\,|\bar{n}_i\rangle\,\langle n_i|\,, \tag{2.44}$$

where

$$\hat{\boldsymbol{d}}_{\bar{n}_i,n_i} = e\,\langle\bar{n}_i|\hat{\boldsymbol{q}}_i|n_i\rangle \tag{2.45}$$

denotes the matrix element of the dipole operator [119, 120]. Similar to the single-particle energies, the dipole operator is the same for all quantum particles, since they are regarded as being identical in their internal degrees of freedom. Therefore the indices on the matrix elements can be omitted, i.e. $\hat{\boldsymbol{d}}_{\bar{n}_i,n_i} = \hat{\boldsymbol{d}}_{\bar{n},n}$.

Along with this, the expansion of $\hat{\mathcal{H}}_{\mathrm{int}}$ into eigenstates of the interaction-free Hamiltonian $\hat{\mathcal{H}}_0$ is given by

$$\hat{\mathcal{H}}_{\mathrm{int}} = \sum_{i=1}^{N}\sum_{\bar{n}_i,n_i}\frac{g_{\bar{n}_i,n_i}}{\sqrt{N}}\,|\bar{n}_i\rangle\,\langle n_i|\,[\hat{a}^\dagger(t)+\hat{a}(t)], \tag{2.46}$$

where

$$g_{\bar{n}_i,n_i} = i\sqrt{N}\mathcal{A}_0\frac{\epsilon_{\bar{n}_i}-\epsilon_{n_i}}{\hbar}\,\hat{\boldsymbol{d}}_{\bar{n}_i,n_i}\cdot\boldsymbol{e}_x \tag{2.47}$$

describes the coupling strength between the electrons and the photonic cavity mode. Note that the SI-units of $g_{\bar{n}_i,n_i}$ are Joule. The prefactor $\sqrt{N}$, compensated by its inverse in Eq. (2.46), together with the $\sqrt{V}^{-1}$ proportionality of $\mathcal{A}_0$ ensures the coupling strength to be constant in the thermodynamic limit defined as [62]

$$N\to\infty,\quad V\to\infty,\quad \rho = \frac{N}{V} = \mathrm{const.} \tag{2.48}$$

The coupling constant $g_{\bar{n}_i,n_i}$ is a fixed quantity determined from the properties of the quantum particles and the cavity mode. Keeping this in mind, most of the results for the relevant observables are considered as a function of the coupling strength.

The remaining term in $\hat{\mathcal{H}}_{\mathrm{matter}}$ is given by

$$\hat{\mathcal{H}}_{\mathrm{dia}} = \frac{q^2}{2m}N\hat{\boldsymbol{A}}_{\mathrm{em}}^2 = \kappa[\hat{a}^\dagger(t)+\hat{a}(t)]^2, \tag{2.49}$$

where the factor κ reads

$$\kappa = \frac{q^2\hbar N}{4m\epsilon_0\omega_0 V},\quad [\kappa]_{\mathrm{SI}} = \mathrm{J.} \tag{2.50}$$

This contribution to $\hat{\mathcal{H}}_{\mathrm{matter}}$ is often referred to as *diamagnetic term* since it increases the energy of the system. In various theories on light-matter interaction in cavity QED this diamagnetic term is neglected due to the assumption of κ being small. This is also the case in the Dicke model [63]. The necessity of including the diamagnetic term into the theory [85], especially in the ultrastrong coupling regime, leads to severe changes regarding the existence of the superradiant phase transition as predicted by the Dicke model [61, 62]. This issue is discussed in more detail in Chap. 3.

For the definition of the different coupling regimes according to the relevant energy scales of the considered system see Tab. 3.1.

To summarize this section, the most general Hamiltonian describing the interaction of N quantum particles, each carrying the charge q, with a single cavity mode is given by

$$\hat{\mathcal{H}} = \hbar\omega_0 \left(\hat{a}^\dagger \hat{a} + \frac{1}{2} \right) + \sum_{i=1}^{N} \sum_{n_i} \left[\epsilon_n \left| n_i \right\rangle \left\langle n_i \right| + \sum_{\bar{n}_i} \frac{g_{\bar{n}_i, n_i}}{\sqrt{N}} \left| \bar{n}_i \right\rangle \left\langle n_i \right| [\hat{a}^\dagger(t) + \hat{a}(t)] \right]$$
$$+ \kappa[\hat{a}^\dagger(t) + \hat{a}(t)]^2 \quad (2.51)$$

and provides the basis for a large variety of systems studied in the field of cavity quantum electrodynamics.

The time-dependence of the interaction contributions to $\hat{\mathcal{H}}$ can be transformed in a time-independent representation according to the dynamical representations of quantum mechanics as discussed of App. B. In particular, one can refer to $\hat{\mathcal{H}}$ as represented in the interaction picture. By applying a unitary transformation (B.23) onto $\hat{\mathcal{H}}$ one obtains the time-independent Schrödinger representation of the Hamiltonian (2.51)

$$\hat{\mathcal{H}}_{\mathrm{S}} = \hbar\omega_0 \left(\hat{a}^\dagger \hat{a} + \frac{1}{2} \right) + \sum_{i=1}^{N} \sum_{n_i} \left[\epsilon_n \left| n_i \right\rangle \left\langle n_i \right| + \sum_{\bar{n}_i} \frac{g_{\bar{n}_i, n_i}}{\sqrt{N}} \left| \bar{n}_i \right\rangle \left\langle n_i \right| (\hat{a}^\dagger + \hat{a}) \right] + \kappa(\hat{a}^\dagger + \hat{a})^2.$$
$$(2.52)$$

The transformation of $\hat{\mathcal{H}}$ into $\hat{\mathcal{H}}_{\mathrm{S}}$ is denoted as *rotating frame* transformation in the field of quantum optics. All light-matter interaction Hamiltonians considered in this thesis are regarded in the rotating frame, i.e. the Schrödinger picture. Therefore, the index $_{\mathrm{S}}$ denoting the Schrödinger representation is omitted from now on.

As the Hamiltonian $\hat{\mathcal{H}}$, Eq. (2.52), is a many-body Hamiltonian in general, it captures also effects emerging from the collective interaction of the N quantum particles with the cavity mode. The subsequent discussion investigates these collective radiation effects in more detail, starting from the derivation of of the Dicke Hamiltonian with $\hat{\mathcal{H}}$, Eq. (2.52).

Chapter 3

The Dicke model and the phenomenon of superradiance

The variety of model systems describing the interaction of one cavity mode with $N \geq 1$ approximate two-level atoms provides the well-studied basis for investigating generic quantum optical effects. The microscopic derivation of the corresponding Hamiltonians is generally provided within the scheme discussed in Chap. 2. In particular, the Hamiltonian (2.52) is the microscopic starting point from which the well studied class of two-level models is derived.

The simplest model belonging to this class is the Jaynes-Cummings model [121], which is regarded as a small-coupling approximation of the quantum Rabi model [122–124]. In particular, the Jaynes-Cummings model is obtained from the Rabi Hamiltonian by omitting the so-called counter-rotating terms within rotating-wave approximation. This approximation is justified in the small-coupling regime [125–127]. In both cases, the setup contains a single cavity mode interacting with a single two-level atom. These single-particle models allow detailed investigations of the basic properties of light-matter interaction on a quantum mechanical level and are briefly introduced in Sec. 4 of App. B.

The generalization of the Jaynes-Cummings and the Rabi model to systems with $N > 1$ two-level atoms embedded in a cavity leads to the Tavis-Cummings model [128, 129], valid in the small coupling regime, and the Dicke model [61–63]. Within these many-body models one is able to investigate effects of many-particle light-matter interaction ranging from independent emission of radiation to the collective behavior of the atoms in the radiation field. The latter case was first studied by Dicke [63]. In his seminal work, Dicke demonstrated the enhancement of spontaneously emitted radiation of a dense cloud of $N \gg 1$ excited two-level atoms due to their collective interaction with quantum vacuum fluctuations. Further investigations on the Dicke model in the thermodynamic limit, $N, V \to \infty$ but constant N/V, proposed that the system exhibits classical [61] and quantum [62] critical behavior tied to a spontaneously broken symmetry inherent in the Hamiltonian of the system. In particular, the Dicke model undergoes a second-order phase transition from a normal to a superradiant phase in the ultrastrong coupling regime. Thereby the superradiant phase is characterized by the cavity being spontaneously occupied by a large number $\propto N$ of photons accompanied by a spontaneous polarization of the atoms. Thus, in this new state of matter, the atomic ensemble has the potential to superradiate [62]. At first glance, this collective phenomenon seems peculiar. However, even before discovering the corresponding superradiant thermal [61] and quantum [62] phase transition, Mallory demonstrated [130] that states with

a large number of atoms occupying an excited state are energetically preferable in strong-coupling regimes.

One needs to emphasize, that each of these four models omits the diamagnetic term stemming from the substitution of the kinetic with the canonical momenta in Hamiltonians with parabolic dispersion. Though this approximation is reasonable when investigating small-coupling effects, it lacks justification in an ultrastrong coupling regime. However, ultrastrong coupling is necessary to theoretically obtain the superradiant phase transition [85]. The extension of the Dicke model, including the diamagnetic term as microscopically derived from minimal coupling, Eq. (2.27), in case of a parabolic energy dispersion, see Chap. 2, is referred to as the Hopfield model [131]. The corresponding Hamiltonian provides the correct description of the atomic gas in the ultrastrong coupling regime. Nevertheless, the inclusion of the diamagnetic contribution leads to a no-go theorem [85, 132] for the superradiant phase transition preventing the occurrence of this phenomenon in systems with parabolic energy-momentum dispersion on a fundamental level. This no-go theorem does not necessarily apply onto systems with different energy-momentum dispersion [93] or onto artificial systems where the diamagnetic contribution is not linked to the coupling strength at a similar microscopic level as in an atomic gas. For instance, the existence of a superradiant phase transition is proposed [132] for superconducting Cooper-pair boxes [133–136] coupled to a transmission line resonator [137] even in the presence of a diamagnetic term (cf. Subsec. 4.2).

The afore-mentioned possible exception of the no-go theorem regarding a system with non-quadratic energy-momentum dispersion is discussed in Part II on the example of Landau-quantized graphene. Graphene is known to have a region of linear dispersion close to the corners of the Brillouin zone. Hence, the dynamics of the charge carriers follows a massless Dirac-Weyl equation. Thus, in this regime there are no diamagnetic terms stemming from the band-structure when minimal coupling is applied onto the model. However, there is also the proposal [94, 95] of a dynamical generation of diamagnetic contributions arising from screening effects. Thus, before reviewing the controversy of the potentially existing superradiant phase in graphene, the general properties of this quantum effect are discussed with regard to the original Dicke model.

To this end, the original Dicke Hamiltonian is derived from the general single-mode Hamiltonian, Eq. (2.52), by application of a few additional assumptions. Then, the original discovery of Dicke [63] concerning the collective spontaneous decay of the atomic cloud is outlined. However, the superradiant decay is unaffected by the no-go theorem and has been experimentally verified. By contrast, the thermal and quantum phase transition in equilibrium, i.e. without application of further modulating laser fields, has not been observed experimentally. The properties of the superradiant quantum phase transition are, however, of prior interest for this thesis. Therefore, the characteristic observables indicating the quantum collective and critical behavior are presented and discussed following mainly Refs. [62, 118]. The provided catalog of typical features is then partially picked up in Part II.

3.1 Derivation of the Dicke Hamiltonian

In general, the Dicke model describes the collective interaction of $N \gg 1$ atoms with a single cavity mode as schematically illustrated by Fig. 3.1. The starting point for the derivation of the Dicke Hamiltonian is therefore provided by the result (2.52) of Chap. 2 under the following assumptions:

1. All atoms are identical, but distinguishable [62, 63].

2. There is no overlap of wave functions of different atoms, so that dipole-dipole interactions among them can be neglected [63, 138].

3. The positions of the atoms are fixed, hence there are no interaction effects due to collision and no Doppler effect [63, 138].

4. Dipole approximation is valid. Thus, the atoms occupy a volume smaller than the wavelength λ of the photonic mode [63, 138].

5. There is only one interacting electron per atom [63].

6. Each atom is an approximate two-level system [63].

7. Diamagnetic contributions can be omitted [63].

Thus, the Dicke Hamiltonian is obtained as a specification of the general expression (2.52) describing N quantum particles interacting with a single cavity mode ω_0. Since the microscopically derived Hamiltonian, Eq. (2.52), already satisfies assumptions $1 - 5$ only the restriction of the eigenbasis $\{|n_i\rangle\}$ to two basis states $\{|0_i\rangle, |1_i\rangle\}$ per atom has to be carried out explicitly. Then, by dropping the diamagnetic term, the Dicke Hamiltonian is obtained.

The restricted basis, $\{|0_i\rangle, |1_i\rangle\}$, corresponds to a representation of the special unitary group, $\mathrm{SU}(2)$, which is generated from the identity and *Pauli matrices*:

$$\hat{\sigma}_0^i = \begin{pmatrix} 1 & 0 \\ 0 & 1 \end{pmatrix} = |0_i\rangle \langle 0_i| + |1_i\rangle \langle 1_i|, \quad \hat{\sigma}_y^i = \begin{pmatrix} 0 & -i \\ i & 0 \end{pmatrix} = -i|1_i\rangle \langle 0_i| + i|1_i\rangle \langle 0_i|,$$
$$\hat{\sigma}_x^i = \begin{pmatrix} 0 & 1 \\ 1 & 0 \end{pmatrix} = |0_i\rangle \langle 1_i| + |0_i\rangle \langle 1_i|, \quad \hat{\sigma}_z^i = \begin{pmatrix} 1 & 0 \\ 0 & -1 \end{pmatrix} = \quad |0_i\rangle \langle 0_i| - |1_i\rangle \langle 1_i|. \tag{3.1}$$

It is useful for the following to define [119]

$$\hat{\sigma}_+^i = \frac{\hat{\sigma}_x^i + i\hat{\sigma}_y^i}{2} = \begin{pmatrix} 0 & 1 \\ 0 & 0 \end{pmatrix}, \quad \hat{\sigma}_-^i = \frac{\hat{\sigma}_x^i - i\hat{\sigma}_y^i}{2} = \begin{pmatrix} 0 & 0 \\ 1 & 0 \end{pmatrix}, \tag{3.2}$$

which act onto the ith two-level basis as *raising* $(+)$ and *lowering* $(-)$ operators similar to the creation and annihilation operators for Fock states, discussed in Sec. 2 of App. C. Furthermore, the following commutation relations hold for the Pauli matrices $\hat{\sigma}_z^i$ and $\hat{\sigma}_\pm^j$:

$$[\hat{\sigma}_z^i, \hat{\sigma}_\pm^j] = \pm \delta_{i,j} \hat{\sigma}_\pm^i, \quad [\hat{\sigma}_+^i, \hat{\sigma}_-^j] = 2\delta_{i,j} \hat{\sigma}_z^i, \tag{3.3}$$

where the Kronecker delta $\delta_{i,j}$ indicates that operators from different Hilbert subspaces commute. Due to the isomorphism between SU(2) and the special orthogonal group SO(3) one refers to the two-level atoms as spin-1/2-like system and introduces the corresponding spin operators

$$\hat{s}_k^i = \frac{\hat{\sigma}_k^i}{2}, \quad k = x, y, z. \tag{3.4}$$

The raising and lowering operators in the spin basis are identical to the matrix representation (3.2) yielding

$$\hat{s}_\pm^i = \hat{s}_x^i \pm i\hat{s}_y^i. \tag{3.5}$$

For consistency, the basis is mapped to the spin notation, so that the excited state $|1^i\rangle$ of the ith atom is assigned to the spin-up state $|\uparrow^i\rangle$. The ground state $|0^i\rangle$ is mapped likewise to the spin-down state $|\downarrow^i\rangle$ in this notation. During the following the terms spin and two-level atoms are synonymously used.

Since the spin is an angular momentum [119] the notation of the basis $\{|\downarrow^i\rangle, |\uparrow^i\rangle\}$ can be represented in a mathematical more general way using the common notation $|s^i; m^i\rangle$ for quantum mechanical angular momenta. In this notation each state of the ith spin is described by two quantum numbers, s^i and m^i. Here, s^i refers to the eigenvalue of the total angular momentum operator

$$(\hat{s}^i)^2 = (\hat{s}_x^i)^2 + (\hat{s}_y^i)^2 + (\hat{s}_z^i)^2, \quad (\hat{s}^i)^2 |s^i; m^i\rangle = s^i(s^i + 1) |s^i; m^i\rangle. \tag{3.6}$$

In general, the quantum number s^i is given by either an integer or a half-integer. The latter is the case here, i.e. $s^i = 1/2$. The quantum number m^i refers to the eigenvalue of the $\hat{s}_z^i$ operator

$$\hat{s}_z^i |s^i; m^i\rangle = m^i |s^i; m^i\rangle. \tag{3.7}$$

In general, the quantum number m^i takes the values [119]

$$m^i = -s^i, -(s^i - 1), \dots, (s^i - 1), s^i. \tag{3.8}$$

By regarding a spin-1/2-system m^i assumes the values $\pm 1/2$, where $+$ refers to the spin-up state $|\uparrow^i\rangle$ and $-$ refers to the spin-down state $|\downarrow^i\rangle$. Adjusting the Hamiltonian (2.52) accordingly leads to the following expression

$$\hat{\mathcal{H}} = \hbar\omega_0 \left(\hat{a}^\dagger \hat{a} + \frac{1}{2} \right) + \sum_{i=1}^N \left[\mathcal{E} \hat{s}_0^i + \hbar\Omega\, \hat{s}_z^i + \frac{g}{\sqrt{N}} (\hat{s}_+^i + \hat{s}_-^i)(\hat{a}^\dagger + \hat{a}) \right] + \kappa(\hat{a}^\dagger + \hat{a})^2, \tag{3.9}$$

which is already reminiscent of the Dicke Hamiltonian containing a diamagnetic term. Thereby, $\mathcal{E} = \epsilon_1 + \epsilon_0$ denotes the mean energy and $\hbar\Omega = \epsilon_1 - \epsilon_0$ is the transition frequency of each atom. Furthermore, as the Hamiltonian is Hermitian, it is usual [62, 118] to chose the coupling strength real-valued, reading

$$g = \sqrt{N}\mathcal{A}_0 \frac{\Omega}{\hbar} \hat{\boldsymbol{d}}_{1,0} \cdot \boldsymbol{e}_x, \tag{3.10}$$
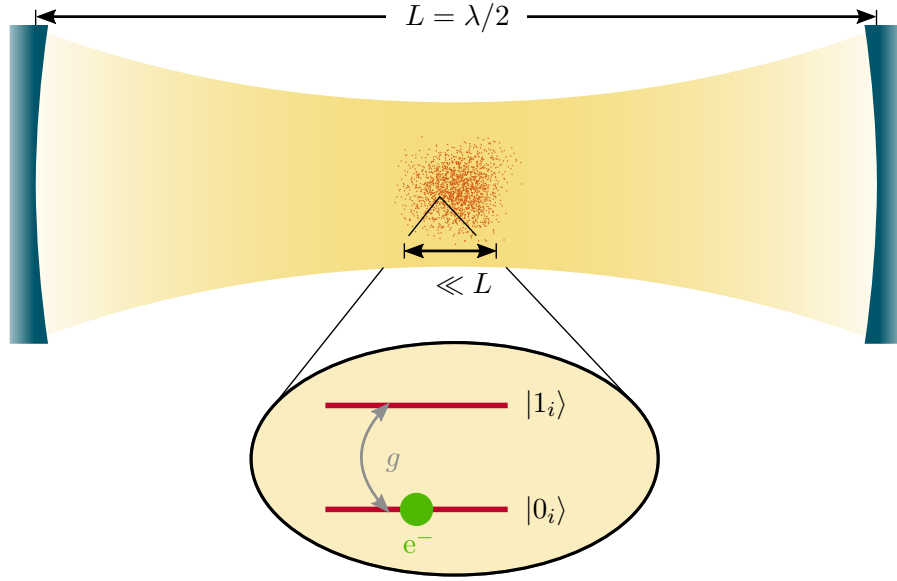
FIGURE 3.1: Inspired by Refs. [118, 139]. Schematic sketch of the configuration in the Dicke model. The blue elements depict the mirrors of the cavity and the yellow shaded region illustrates the area potentially occupied by the photons. The side length of the cavity, L, determines the wave-lengths λ of the optical modes. Since the original Dicke model is a single-mode model, one may assume the corresponding photons to occupy the first fundamental oscillation of the cavity, i.e. $\lambda = 2L$ and $\omega_0 = 2\pi c/\lambda$. The side length L is assumed to be much larger than the size occupied by the atoms (small red dots in the middle of the cavity), justifying dipole approximation. The inset shows the energetic properties of the ith two-level atom. In the depicted example the single-particle system i occupies its ground state $|0_i\rangle$. The coupling strength g is a measure for the probability of the transition between ground state and excited state linked to photon creation and annihilation as encoded in Dicke Hamiltonian (3.11).

This is permitted without loss of generality. Keeping a complex coupling value or assigning the interaction part with an additional imaginary unit yields identical results compared with the convention applied here [132]. Finally, the original Dicke Hamiltonian is obtained by dropping the diamagnetic term $\propto \kappa$. Additionally, the photonic vacuum contribution and the mean-energy term are conveniently omitted since they induce only a constant shift of the energies.

With this, the Dicke Hamiltonian

$$\hat{\mathcal{H}}_{\mathrm{D}} = \hbar\omega_0 \hat{a}^\dagger \hat{a} + \sum_{i=1}^{N} \left[\hbar\Omega \hat{s}_z^i + \frac{g}{\sqrt{N}}(\hat{s}_+^i + \hat{s}_-^i)(\hat{a}^\dagger + \hat{a}) \right] \tag{3.11}$$

is obtained as the many-body generalization of the Rabi Hamiltonian [122–124] (cf. Sec. 4 of App. B).

By expressing the bosonic contribution in the interaction part $\propto g$ in $\hat{\mathcal{H}}_{\mathrm{D}}$ in terms of the

position operator [140], $\hat{x} = 2(\hat{a}^\dagger + \hat{a})$, one may alternatively write

$$\hat{\mathcal{H}}_{\mathrm{D,int}} = \sum_{i=1}^{N} \frac{g}{\sqrt{N}}(\hat{s}_+^i + \hat{s}_-^i)(\hat{a}^\dagger + \hat{a}) \overset{(3.5)}{=} \sum_{i=1}^{N} \frac{g}{\sqrt{N}}\hat{s}_x^i\hat{x}. \tag{3.12}$$

This expression is helpful to gain insights into the properties of the two quantum phases exhibited by the Dicke model as discussed in Sec. 3.3.

Furthermore it is helpful to introduce common terms characterizing the system according to the strength of the coupling parameter g in relation to other relevant energy scales of the model. As enumerated by Tab. 3.1 one distinguishes [124, 141] between a weak, strong, ultrastrong and deep strong coupling regime.

The Dicke Hamiltonian, Eq. (3.11), shows that the underlying model is invariant under permutations of atoms. Therefore, the symmetry properties regarding particle permutation of an initially prepared state are preserved in the dynamical evolution of the system [138]. For example, assume the system to be initially prepared in an excited state which is completely symmetric with respect to particle permutations. As time evolves the system might decay into a state with lower energy after some time t. According to the properties of the Hamiltonian, this final state is then also completely symmetric with respect to permutations of atoms. This is also valid for cascades of decays, such as studied by Dicke [63] yielding the phenomena of *Dicke superradiance* as discussed during the following.

3.2   Collective spontaneous emission

Similar as discussed in Sec. 1 of App. C, the Hilbert space of the particles in the Dicke Hamiltonian and its generalization, Eq. (2.52), is constructed from the tensor products of N single-particle Hilbert spaces. If $\mathbb{H}_s$ denotes the part of the Hilbert space spanned by the ith single-particle two-level basis $\{|m^i\rangle\,;m = \downarrow, \uparrow\}$ one will obtain the complete Hilbert space relevant for the Dicke model by

$$\mathbb{H}_{\mathrm{D}} = \mathbb{H}^+ \left(\bigotimes_{i=1}^{N} \mathbb{H}_s \right), \tag{3.13}$$

where $\mathbb{H}^+$ denotes the Hilbert space of the photonic mode. Accordingly, the basis states of the Dicke Hamiltonian are obtained as product states according to

$$\left\{ |n\rangle \left(\bigotimes_{i=1}^{N} |1/2; m^i\rangle \right) ; m = \pm 1/2; n \in \mathbb{N}_0 \right\}, \tag{3.14}$$

where $|n\rangle$ denotes the Fock state basis of the photonic mode (cf. Sec. 2 of App. C).

Properties	Coupling regime	Comments
$g \ll I_0, \Gamma, \omega_0, \Omega$	weak	• Rotating-wave approximation is valid. • Jaynes-Cummings / Tavis-Cummings model is a good approximation for the quantum Rabi / Dicke model.
$I_0, \Gamma \ll g \ll \omega_0, \Omega$	strong	• Rotating-wave approximation is still valid. • Photon absorption and emission occurs much faster than the cavity decay: coherent quantum Rabi oscillations. • Experimentally observed in various systems: atoms [142], semiconducting quantum dots [143, 144], Cooper-pair boxes [137].
$g \lesssim \omega_0, \Omega$	ultrastrong	• Breakdown of the rotating-wave approximation [125–127]. • Jaynes-Cummings / Tavis-Cummings model becomes insufficient. • Break-down of the standard master equation [145]. • Emergence of non-linearities: multiphoton quantum Rabi oscillations in driven systems [56]. • Ultra-efficient light emission [146, 147]. • New quantum phenomena are proposed such as superradiant phase transition [61, 62]. • Experimentally feasible: superconductor systems [48, 49], semiconductors [47, 51–53, 55], molecules [50] and ferromagnets [54], **strongest coupling recorded so far** [55]: $g = 0.87\hbar\omega_c$
$g \gtrsim \omega_0, \Omega$	deep strong	• Has not been reached experimentally so far. • Proposed [148] breakdown of the Purcell effect [149]: decoupling of light and matter.

TABLE 3.1: Different coupling regimes regarding the relevant energy scales in the Dicke and the quantum Rabi model, according to Refs. [124, 141]. Thereby ω_0 denotes the frequency of the cavity mode, Ω refers to the transition frequency of the two-level atoms and g is the coupling parameter. Furthermore, I_0 and Γ denote the decay rate of each two-level atom and the cavity, respectively. The list of effects emerging for the different coupling regimes is not exhaustive.

3.2.1   Collective spin operators

The introduction of the collective atomic operators [62]

$$J_k = \sum_{i=1}^{N} s_k^i, \quad k = \pm, x, y, z \tag{3.15}$$

not only simplifies the notation of the Dicke Hamiltonian,

$$\hat{\mathcal{H}}_{\mathrm{D}} = \hbar \omega_0 \, \hat{a}^\dagger \hat{a} + \hbar \Omega \, \hat{\mathcal{J}}_z + \frac{g}{\sqrt{N}} (\hat{\mathcal{J}}_+ + \hat{\mathcal{J}}_-)(\hat{a}^\dagger + \hat{a}), \tag{3.16}$$

but also allows a change of basis similar to the standard textbook example concerning the addition of two spins. In view of Eq. (3.5) one finds for the collective raising and lowering operator

$$\hat{\mathcal{J}}_\pm = \hat{\mathcal{J}}_x \pm i \hat{\mathcal{J}}_y. \tag{3.17}$$

With this, in similarity to Eq. (3.12), the alternative representation of interaction part of $\hat{\mathcal{H}}_{\mathrm{D}}$ in terms of the collective angular momentum operator in x-direction is then given by

$$\hat{\mathcal{H}}_{\mathrm{D,int}} = \frac{g}{\sqrt{N}} \hat{\mathcal{J}}_x \hat{x}. \tag{3.18}$$

From Eqs. (3.6, 3.7) follows, that the product basis (3.14) is an eigenbasis for each $(\hat{s}^i)^2$ and $\hat{s}_z^i$ and thus also for any sum of these operators for different atoms. Nevertheless, the basis is not an eigenbasis of the total collective angular momentum operator

$$\hat{\mathcal{J}}^2 = \hat{\mathcal{J}}_x^2 + \hat{\mathcal{J}}_y^2 + \hat{\mathcal{J}}_z^2, \tag{3.19}$$

as it is easily seen from expansion of each operator square in view of Eq. (3.15). One finds for instance:

$$\hat{\mathcal{J}}_x^2 = \sum_{i,j=1}^{N} \hat{s}_x^i \hat{s}_x^j \neq \sum_i (\hat{s}_x^i)^2. \tag{3.20}$$

However, the simultaneous eigenbasis of the collective operators $\hat{\mathcal{J}}^2$ and $\hat{\mathcal{J}}_z$ can be characterized by the two quantum numbers J and M in a similar manner as in the case of a single spin. Thereby, each basis state $|J; M\rangle$ satisfies [119]

$$\begin{aligned} \hat{\mathcal{J}}^2 |J; M\rangle &= J(J+1) |J; M\rangle, \\ \hat{\mathcal{J}}_z |J; M\rangle &= M |J; M\rangle, \end{aligned} \tag{3.21}$$

where J and M assume the values

$$\begin{aligned} J &= \begin{cases} 0, 1, \dots, \frac{N}{2} & \text{for even } N, \\ \frac{1}{2}, \frac{3}{2}, \dots, \frac{N}{2} & \text{for odd } N, \end{cases} \\ M &= -J, -(J-1), \dots, J-1, J. \end{aligned} \tag{3.22}$$

Since both sets of states, $\{|J;M\rangle\}$ and $\{\otimes_{i=1}^{N} |1/2;m^i\rangle\}$, provide a complete orthonormalized basis [119], there exists a unitary transformation

$$|J;M\rangle = \sum_{m^1+\cdots+m^N=M} \mathcal{C}_{m^1,\ldots,m^N;M}^{1/2,\ldots,1/2;J} \left(\otimes_{i=1}^{N} |1/2;m^i\rangle\right), \tag{3.23}$$

promoting the change of basis. The coefficients $\mathcal{C}_{m^1,\ldots,m^N;M}^{1/2,\ldots,1/2;J}$ are referred to as *Clebsch-Gordan coefficients* [119]. The construction of the Clebsch-Gordan coefficients for an arbitrary but fixed number $N > 2$ of spins is, however, not trivial in general [150].

Furthermore, the basis $\{|J;M\rangle\}$ contains states with different symmetry properties regarding the permutation of spins. In a similar manner as discussed in Sec. 1 of App. C for the construction of general many-body states, the relevant part of Hilbert space $\mathbb{H}_D$ spanned by the spin-eigenstates of the Dicke Hamiltonian can be decomposed into three subspaces:

$$\mathbb{H}_D = \mathbb{H}^+ \otimes \left[\tilde{\mathbb{H}}^{\mathrm{sym}} \oplus \tilde{\mathbb{H}}^{\mathrm{anti-sym}} \oplus \tilde{\mathbb{H}}^{\mathrm{mix}}\right], \tag{3.24}$$

where each $\tilde{\mathbb{H}}^{\mathrm{x}}$ is spanned by all basis states with the respective permutation symmetry. Note that the symmetry properties of the subspace $\tilde{\mathbb{H}}^{\mathrm{sym}}$ and $\tilde{\mathbb{H}}^{\mathrm{anti-sym}}$ are similar to $\mathbb{H}^+$ and $\mathbb{H}^-$ discussed in Sec. 1 of App. C. The labels sym and $\mathrm{anti-sym}$ are, however, introduced to avoid confusion. For a fixed value of J the set of symmetrized or anti-symmetrized states with different M are referred to as *multiplets*. The construction of those multiplets from the product basis (3.14) of an arbitrary number N of spins yields entangled and non-separable states [151]. This can even be seen from the example of $N = 2$:

The symmetrized states for $J = 1$ form the *triplet* [92, 119]

$$|J = 1; M = -1\rangle = |\downarrow^1\downarrow^2\rangle, \tag{3.25}$$

$$|J = 1; M = 0\rangle \quad = \frac{|\uparrow^1\downarrow^2\rangle + |\downarrow^1\uparrow^2\rangle}{\sqrt{2}}, \tag{3.26}$$

$$|J = 1; M = +1\rangle = |\uparrow^1\uparrow^2\rangle. \tag{3.27}$$

Accordingly, the anti-symmetrized state

$$|J = 0; M = 0\rangle = \frac{|\uparrow^1\downarrow^2\rangle - |\downarrow^1\uparrow^2\rangle}{\sqrt{2}}, \tag{3.28}$$

is referred to as a singlet. In this example each state of the singlet and triplet with $M = 0$ is an entangled state.

3.2.2 Dicke states

The multiplet of completely symmetric states assigned to the maximal value of the quantum number J, $J_{\mathrm{m}} = N/2$, is referred to as the set of *Dicke states*. In particular, the triplet states (3.25 – 3.27) are Dicke states in a $N = 2$ spin system where J assumes the maximal value of $J_{\mathrm{m}} = 1$ [92]. Dicke coined the name *cooperation number* for the quantum number J_{m} [63].

According to (3.22) there are $N + 1$ Dicke states which can be constructed from the product basis of N single-spin states:

$$|J_{\mathrm{m}}; M = -J_{\mathrm{m}}\rangle \qquad = |\downarrow^1 \downarrow^2 \ldots \downarrow^N\rangle, \tag{3.29}$$

$$|J_{\mathrm{m}}; M = -J_{\mathrm{m}} + 1\rangle = \hat{\mathcal{P}}^{\mathrm{sym}}_{2J_{\mathrm{m}},-J_{\mathrm{m}}+1} \quad |\uparrow^1 \downarrow^2 \ldots \downarrow^N\rangle, \tag{3.30}$$

$$|J_{\mathrm{m}}; M = -J_{\mathrm{m}} + 2\rangle = \hat{\mathcal{P}}^{\mathrm{sym}}_{2J_{\mathrm{m}},-J_{\mathrm{m}}+2} \quad |\uparrow^1 \uparrow^2 \ldots \downarrow^N\rangle, \tag{3.31}$$

$$\vdots$$

$$|J_{\mathrm{m}}; M = +J_{\mathrm{m}}\rangle \qquad = |\uparrow^1 \uparrow^2 \ldots \uparrow^N\rangle. \tag{3.32}$$

The symmetrization operator

$$\hat{\mathcal{P}}^{\mathrm{sym}}_{2J_{\mathrm{m}},M} = \frac{1}{\sqrt{(2J_{\mathrm{m}})!(J_{\mathrm{m}} - M)!(J_{\mathrm{m}} + M)!}} \sum_{\substack{\sigma_{J_{\mathrm{m}}+M} \\ \in S^{2J_{\mathrm{m}}}}} \hat{\mathcal{P}}_{\sigma_{J_{\mathrm{m}}+M}}, \tag{3.33}$$

is similarly defined as the corresponding operator for the construction of completely symmetrized bosonic states, Eq. (C.18). The permutation operator $\hat{\mathcal{P}}_{\sigma_{J_{\mathrm{m}}+M}}$ denotes a linear map associated to each element $\sigma_{J_{\mathrm{m}}+M} \in S^{J_{\mathrm{m}}+M}$ of the permutation group $S^{J_{\mathrm{m}}+M}$. The action of $\hat{\mathcal{P}}_{\sigma_{J_{\mathrm{m}}+M}}$ is in particular given by Eq. (C.12). Each element $\sigma_{J_{\mathrm{m}}+M} \in S^{J_{\mathrm{m}}+M}$ of the group $S^{J_{\mathrm{m}}+M}$ denotes a permutation of $J_{\mathrm{m}} + M$ spin-up states in a set of $N = 2J_{\mathrm{m}}$ spins. Note that the sum over permutations, $\sigma \in S^N$, in the definition of the completely symmetrized bosonic many-body states, Eq. (C.18), includes all possible permutations of a set of N indices. In the case of Eq. (3.33), the normalization factor entering the definition of the symmetrization operator corresponds to the two-particle simplification of the normalization factor obtained for bosonic states according to Eq. (C.18).

The construction of the Dicke states for a given cooperation number $J_{\mathrm{m}} = \max(J)$ from symmetrized single-particle product states is in principle similar to the construction of N-particle Fock states (cf. Sec. 2 of App. C). Moreover, the Dicke states span a Hilbert subspace in which the system is characterized by the indistinguishability of the single-particle subsystems. This is identical to the indistinguishability inherent in the Fock-state description of bosonic or fermionic many-body systems.

3.2.3 Selection rules of the Dicke Hamiltonian

According to the angular momentum algebra, the operators $\hat{\mathcal{J}}_{\pm}$ apparent in $\hat{\mathcal{H}}_{\mathrm{D}}$, Eq. (3.16), act as raising (+) and lowering (−) operators [119] similar to the creation and annihilation operators for Fock states (cf. Sec. 2 of App. C). In particular, their action onto a Dicke state $|J_{\mathrm{m}}, M\rangle$ is given by [62]

$$\hat{\mathcal{J}}_{\pm} |J_{\mathrm{m}}; M\rangle = \sqrt{J_{\mathrm{m}}(J_{\mathrm{m}} + 1) - M(M \pm 1)} |J_{\mathrm{m}}; M \pm 1\rangle, \tag{3.34}$$

yielding the dipole selection rules

$$\Delta J = 0, \quad \Delta M = 1. \tag{3.35}$$

Thus, the cooperation number J_{m} is a good quantum number, as it can also be seen from $[\hat{\mathcal{H}}_{\mathrm{D}}, \hat{\mathcal{J}}^2] = 0$. By contrast the eigenvalue of the $\hat{\mathcal{J}}_z$ operator, M, is not conserved as

Eq. (3.35) or $[\hat{\mathcal{H}}_\mathrm{D}, \hat{\mathcal{J}}_z] \neq 0$ implies.

3.2.4 Dicke superradiance

Suppose the cloud of N two-level atoms described by $\hat{\mathcal{H}}_\mathrm{D}$, Eq. (3.16), to be prepared in the Dicke state $|J_\mathrm{m}; M\rangle$. The cavity is assumed to be in its vacuum state, i.e. there are no photons present. In the course of time, fluctuations of the quantum vacuum trigger the atomic cloud to spontaneously decay from the initial state $|J_\mathrm{m}; M\rangle$ to the final state $|J_\mathrm{m}; M-1\rangle$ in accordance with the selection rules (3.35). As encoded in the interaction term $\propto g$ of $\hat{\mathcal{H}}_\mathrm{D}$ this decay is eventually accompanied by the emission of a photon.
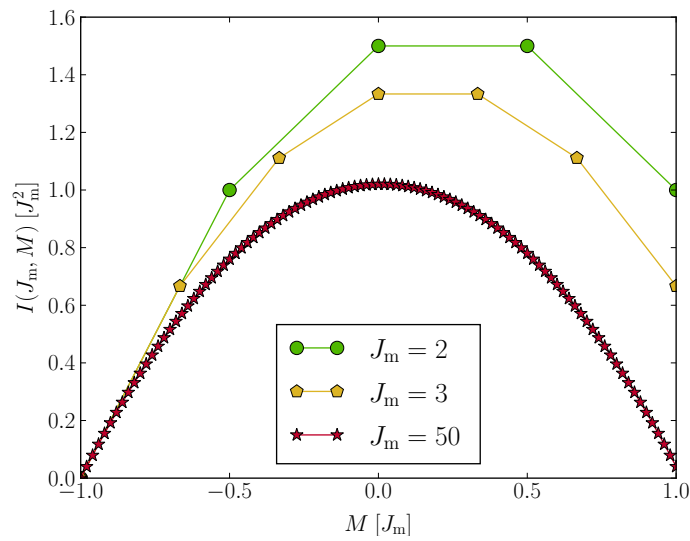
FIGURE 3.2: Rates of spontaneous emission of Dicke states $I(J_\mathrm{m}, M)$, as defined in Eq. (3.36), for different cooperation numbers J_m. As the cooperation number increases the maximum of $I(J_\mathrm{m}, M)$ approaches the vicinity of $M = 0$.

The probability of this event to occur is given by [152]

$$
\begin{aligned}
I(J_\mathrm{m}, M) &= |\langle J_\mathrm{m}; M-1|\, \mathcal{J}_-\, |J_\mathrm{m}; M\rangle|^2 I_0 \\
&= [J_\mathrm{m}(J_\mathrm{m}+1) - M(M-1)]\, I_0,
\end{aligned}
\tag{3.36}
$$

where $I_0 = I(1/2, 1/2)$ denotes the rate of spontaneous emission of a single spin prepared in its excited state $|\uparrow\rangle$.

As time evolves, an initially strongly excited Dicke state, such as $|J_\mathrm{m}, J_\mathrm{m}\rangle$, eventually cascades down the *ladder* of Dicke states [63]

$$
|J_\mathrm{m}, J_\mathrm{m}\rangle \to |J_\mathrm{m}, J_\mathrm{m}-1\rangle \mapsto \cdots \mapsto |J_\mathrm{m}, -J_\mathrm{m}\rangle,
\tag{3.37}
$$

where the rates of the corresponding decays alter according to Eq. (3.36). Figure 3.2 illustrates this for various cooperation numbers.

Furthermore, it can be seen from Fig. 3.2 and Eq. (3.36) that the emission rates for systems with a large number N of spins assume a maximum in the vicinity of $M = 0$:

$$I(J_{\mathrm{m}}, M \approx 0) \approx J_{\mathrm{m}}^2 I_0 = \frac{N^2}{4} I_0. \tag{3.38}$$

The situation $M \approx 0$ corresponds to approximate equality in the population of the single-particle states $|\uparrow\rangle$ and $|\downarrow\rangle$. The scaling of the emission rates with the squared number of two-level atoms for $M \approx 0$ is a feature of the collective behavior of the atomic ensemble [63]. For comparison, if the two-level atoms were spread over the volume of the cavity, such that assumption 4 is not valid anymore, they would radiate incoherently with rates $\propto N$ rather than N^2. This coherent spontaneous emission of radiation was coined by Dicke [63] with the term *superradiance* and Dicke states with $|J_{\mathrm{m}}; M \approx 0\rangle$ are referred to as *superradiant states*.

The existence of superradiant decays have been observed experimentally in various setups ranging from atomic gases [64–70] to circuit quantum electrodynamics [71] and measurements of superradiant decays of intersubband plasmons [72] and cyclotron resonances [73] in semiconductors.

3.3 Superradiant quantum phase transition

The spontaneous collective decay of an ensemble of two-level atoms is in general observable for any coupling parameter $g > 0$ and a large but finite number of atoms. However, in the thermodynamic limit, where the number of atoms approaches an infinite value at constant density, the Dicke model additionally exhibits classical [61, 153] and quantum [62] critical behavior. The transition point is thereby found in the ultrastrong coupling regime, where the coupling strength between the atoms and the cavity mode becomes comparable with their characteristic energy scales. The proposed phase transition of the Dicke model and related systems has given rise to a long-ranged and still ongoing controversy regarding its actual existence in realistic systems. Before entering the main aspects of this discussion around the no-go theorem, the characteristics of the proposed phase transition of the Dicke model are introduced during this section. The following considerations are based on Ref. [62, 118].

Superradiant classical phase transition
By investigating the thermodynamic properties of the exactly solvable Tavis-Cummings model in the thermodynamic limit ($N, V \to \infty$ where $N/V = $ const.), Hepp and Lieb [154] discovered a second-order classical phase transition. The Tavis-Cummings model is similar to the Dicke model where only the energy-conserving contributions $\propto \hat{\mathcal{J}}_- \hat{a}^\dagger + \hat{\mathcal{J}}_+ \hat{a}$ of the interaction term are kept in $\hat{\mathcal{H}}_{\mathrm{D}}$. This approximation is referred to as *rotating-wave approximation* [120] and briefly discussed in Subsec. 4.2 of App. B.
In their work [154] Hepp and Lieb demonstrated that the system described by the corresponding Hamiltonian changes at ultrastrong coupling from the *normal* phase to a *superradiant phase* for $T < T_c$. The normal phase is characterized by the groundstate properties of the noninteracting photonic and atomic subsystem. By contrast, the superradiant
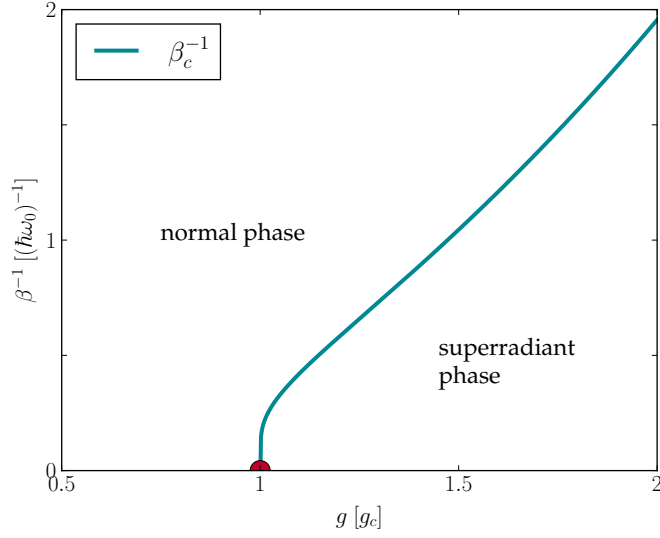
FIGURE 3.3: Phase diagram of the second-order superradiant transition in the Dicke model. The blue line refers to the classical phase boundary $1/\beta_c$ as a function of the coupling parameter g, according to Eq. (3.39). For $\beta^{-1} > \beta_c^{-1}$ the system is in the normal phase, characterized by zero photon occupation and the respective atomic ground states. If the coupling strength g is greater than g_c a decrease of temperature will yield the system to cross the phase boundary resulting in the transition form the normal to the superradiant phase. As T approaches zero, the phase boundary of the thermal phase transition terminates at the quantum critical coupling g_c marked by the red dot. Note that the phase diagram of the second-order quantum phase in this depiction refers only to the one-dimensional g axis at $T = 0$.

phase is characterized by a macroscopic photonic population of the cavity along with excitations of the two-level atoms. Both observables, the photonic cavity occupation and the atomic polarization, are proportional to the number N of atoms in the cavity [154] As the number of atoms is macroscopic ($N \to \infty$), also the photon occupation and the polarization assume macroscopic values. The results concerning the second-order superradiant phase transition of the Tavis-Cummings mode were confirmed by Wang and Hioe [155]. Unfortunately the rotating-wave approximation applied to obtain the Tavis-Cummings model from the Dicke model forfeits validity in the ultrastrong coupling limit, which is required to obtain the superradiant phase transition [125–127].

Nevertheless, Hepp and Lieb proved the existence of the superradiant phase transition in the actual Dicke model [61] as well. This result was confirmed by Ref. [153] using a different approach. The critical temperature for the superradiant phase transition was thereby obtained as [61]

$$\frac{1}{k_{\mathrm{B}}T_c} = \beta_c = \frac{2}{\hbar\Omega}\mathrm{arctanh}\left(\frac{\hbar\omega_0\hbar\Omega}{4g^2}\right), \tag{3.39}$$

differing from the result for the Tavis-Cummings model by the factor of $1/4$ in the argument of the inverse hyperbolic tangent. Within their investigations, Hepp and Lieb observed that the thermal superradiant phase transition in the Dicke model occurs only for couplings g larger than the *critical coupling*

$$g_c = \frac{\hbar}{2}\sqrt{\omega_0 \Omega}. \tag{3.40}$$

Besides the superradiant phase transition driven by thermal fluctuations, the Dicke model exhibits also a *quantum phase transition* from a normal to a superradiant phase as investigated by Emary and Brandes [62]. In contrast to thermal phase transitions occurring for a set of critical parameters as the temperature approaches T_c, quantum phase transitions take place at $T = 0$. They are driven by quantum fluctuations only and thus they have no classical counterpart. As Part II of this thesis focuses mainly on the superradiant quantum critical behavior of Landau-quantized graphene, the main aspects of the quantum phase transition proposed for the Dicke model are discussed subsequently.

Superradiant quantum phase transistion
In equilibrium any system strives to archive a state with minimal energy, quantified by the respective thermodynamic potentials such as the free energy

$$F(T, V, N) = E(T, V, N) - TS \xrightarrow{T \to 0} E(0, V, N). \tag{3.41}$$

When investigating quantum phase transitions one has to consider the limit $T \to 0$ where the free energy F and the internal energy E are identical [156]. Thus, the minimum of the free energy coincides with the quantum mechanical many-body ground-state energy E_0 of the system. The Dicke Hamiltonian and as well as the Hamiltonian considered during the Part II are both of the general form

$$\hat{\mathcal{H}}(g) = \hat{\mathcal{H}}_0 + g\hat{\mathcal{H}}_{\mathrm{int}}. \tag{3.42}$$

$\hat{\mathcal{H}}_0$ describes the dynamics of the quantum particles and the cavity mode without interaction. Hence, the interaction between the photons and the charge carriers of the system is captured in the term $\hat{\mathcal{H}}_{\mathrm{int}}$. Since the Hamiltonian $\hat{\mathcal{H}}$ is a function of the coupling parameter g also the ground-state energy E_0 varies with the coupling strength.
In a weak coupling regime (cf. Tab. 3.1), the energy spectrum of $\hat{\mathcal{H}}$ and thus in turn the properties of the ground-state energy E_0 are dominated by the contribution $\hat{\mathcal{H}}_0$. By contrast, if g exceeds all other relevant energy scales in the model, corresponding to the deep strong coupling regime, the properties of the energy spectrum are governed by the interaction part $\hat{\mathcal{H}}_{\mathrm{int}}$. Depending on the specific details of the contributions $\hat{\mathcal{H}}_0$ and $\hat{\mathcal{H}}_{\mathrm{int}}$ this potentially yield completely different properties of the ground state in either coupling limit.

More precisely, when considering the Dicke Hamiltonian

$$\hat{\mathcal{H}}_{\mathrm{D}} = \hbar\omega_0\,\hat{a}^\dagger\hat{a} + \hbar\Omega\,\hat{\mathcal{J}}_z + \frac{g}{\sqrt{N}}(\hat{\mathcal{J}}_+ + \hat{\mathcal{J}}_-)(\hat{a}^\dagger + \hat{a}), \tag{3.43}$$

the properties of the energy spectrum in the weak coupling regime, $g \ll \hbar\omega_0, \hbar\Omega$, are dominated by the first two contributions on the r.h.s. Hence, the eigenstates are approximately given by the product basis $\{|n\rangle \otimes |J_\mathrm{m}; M\rangle\}$ of Fock states $|n\rangle$ and Dicke states $|J_\mathrm{m}; M\rangle$ (cf. Sec. 2 of App. C and Subsec. 3.2.2 for details). The state of lowest energy corresponds to the product state resulting from the unoccupied cavity and the collective ground state of the ensemble of two-level atoms: $|G_\mathrm{ns}\rangle = |0\rangle \otimes |J_\mathrm{m}; -J_\mathrm{m}\rangle$. The ground-state expectation value of the photon occupation as well as the collective atomic operators in this coupling limit are then given by

$$\langle \hat{a}^\dagger \hat{a} \rangle_{G_\mathrm{ns}} = 0 \tag{3.44}$$

$$\langle \hat{\mathcal{J}}_z \rangle_{G_\mathrm{ns}} = -J_\mathrm{m}, \quad \langle \hat{\mathcal{J}}_x \rangle_{G_\mathrm{ns}} = 0. \tag{3.45}$$

This situation precisely reflects the properties of the normal phase.

In the opposite coupling limit, i.e. $g \gg \hbar\omega_0, \hbar\Omega$, the energetic properties of the hybrid system are dominated by the interaction term $\propto g(\hat{\mathcal{J}}_+ + \hat{\mathcal{J}}_-)(\hat{a}^\dagger + \hat{a})$ of Eq. (3.43), or $\propto g\hat{\mathcal{J}}_x \hat{x}$ according to Eq. (3.18), respectively. The eigenbasis in the deep strong coupling regime is then given by the product basis of the eigenstates of the operators $\hat{\mathcal{J}}_x$ and $\hat{x} \propto (\hat{a}^\dagger + \hat{a})$. As discussed in Subsec. 3.1 of App. C, bosonic coherent states $|\Phi\rangle^+$ are eigenstates of the bosonic annihilation operator $\hat{a}$, where the eigenvalue, denoted by $\sqrt{\alpha}$ for convenience, is in general a complex number. Hence, the eigenvalue equation is given by $\hat{a} |\Phi\rangle^+ = \sqrt{\alpha} |\Phi\rangle^+$. It is intuitive that the bosonic contribution to the ground-state wave function $|G_\mathrm{sp}\rangle$ in this coupling limit is given by some coherent state $|\Phi\rangle^+$. From this it follows that the ground-state expectation values for the photonic occupation and the collective angular momentum operators are of the general form

$$\langle \hat{a}^\dagger \hat{a} \rangle_{G_\mathrm{sp}} = \alpha \tag{3.46}$$

$$\langle \hat{\mathcal{J}}_z \rangle_{G_\mathrm{sp}} = 0, \quad \langle \hat{\mathcal{J}}_x \rangle_{G_\mathrm{sp}} = \pm J_\mathrm{m}, \tag{3.47}$$

where the relations in Eq. (3.47) follow from general angular momentum algebra calculus [119]. A comprehensive discussion on these relations particularly concerning the Dicke model is also provided in Ref. [118]. The properties of the ground-state expectation values (3.46, 3.47) precisely reflect the characteristics of the superradiant phase [61, 62]: A spontaneous, macroscopic polarization of the atoms along with spontaneous photon occupation in the cavity. As it is seen during the following, the photon occupation is also scaling with the number N of atoms embedded in the cavity and therefore it is also referred to as a macroscopic observable.

This intuitive picture provided by both extreme coupling limits, $g \ll \hbar\omega_0, \hbar\Omega$ and $g \gg \hbar\omega_0, \hbar\Omega$, already indicates the existence and main properties of both quantum phases. The aim of the following is to explore these properties on a mathematically sound level also for intermediate coupling strengths close to the critical point. The derived properties yield the basis for investigating the possibility of critical behavior of Landau-quantized graphene which is discussed in Part II. The subsequent discussion is based on considerations of Refs. [62, 118].

It is convenient [62, 157, 158] to introduce the Holstein-Primakoff representation [159–161] of the collective angular momentum operators

$$\hat{\mathcal{J}}_z = (\hat{b}^\dagger \hat{b} - J_{\mathrm{m}}) \tag{3.48}$$

$$\hat{\mathcal{J}}_+ = \hat{b}^\dagger \sqrt{2J_{\mathrm{m}} - \hat{b}^\dagger \hat{b}}, \quad \hat{\mathcal{J}}_- = \sqrt{2J_{\mathrm{m}} - \hat{b}^\dagger \hat{b}} \, \hat{b}, \tag{3.49}$$

where $\hat{b}^\dagger$ and $\hat{b}$ are bosonic operators satisfying the commutation relation $[\hat{b}, \hat{b}^\dagger] = 1$ and $2J_{\mathrm{m}} = N$. This representation corresponds to an exact map. Furthermore, one introduces a displacement [140] of each pair of bosonic operators, $\hat{a}^\dagger$, $\hat{a}$ and $\hat{b}^\dagger$, $\hat{b}$, according to

$$\hat{a}^\dagger = \hat{A}^\dagger + \sqrt{N}\alpha, \quad \hat{b}^\dagger = \hat{B}^\dagger - \sqrt{N}\beta, \tag{3.50}$$

where $\alpha, \beta \in \mathbb{R}$ [62]. The sign in front of each square root can be altered [62]. Note that in the original work of Emary and Brandes the displaced operators (3.50) are introduced without scaling $\propto \sqrt{N}$. The applied notation (3.50) is adopted from Ref. [118] and might provide a more transparent insight into the scaling behavior of the considered quantities. In the end, both approaches yield identical results concerning the atomic polarization and the photon occupation in the ground state. The bosonic operators $\hat{A}^\dagger$ and $\hat{B}^\dagger$ and their Hermitian conjugates, introduced in Eq. (3.50), are regarded as fluctuation operators [62, 118] with vanishing expectation values, i.e. $\langle \hat{A}^\dagger \rangle = \langle \hat{B}^\dagger \rangle = 0$. Along with this, the displacements $\sqrt{N}\alpha$ and $\sqrt{N}\beta$ are interpreted as macroscopic mean fields associated with the photonic cavity occupation and the atomic inversion [62]. This interpretation becomes more obvious during the following. Furthermore, the expectation values of the displaced atomic operators, $\hat{B}^\dagger$ and $\hat{B}$, satisfy [118]

$$\langle \hat{b}^\dagger \rangle \leq \sqrt{N}, \quad \langle \hat{b} \rangle \leq \sqrt{N}, \tag{3.51}$$

for any element of the Hilbert space $\mathbb{H}_{\mathrm{D}}$, Eq. (3.13). Thus, from Eq. (3.50) follows $\sqrt{\beta} \leq 1$ for the atomic mean field [118].

By substitution of the Holstein-Primakoff representation for the collective angular momentum operators (3.48, 3.49) along with application of the displacement (3.50) in the Dicke Hamiltonian (3.43), one obtains

$$\hat{\mathcal{H}}_{\mathrm{D}} = \hbar\omega_0 \left[\hat{A}^\dagger \hat{A} + 2\sqrt{N}\alpha(\hat{A}^\dagger + \hat{A}) + N\alpha \right] + \hbar\Omega \left[\hat{B}^\dagger \hat{B} - 2\sqrt{N}\beta(\hat{B}^\dagger + \hat{B}) + N\beta - J_{\mathrm{m}} \right]$$

$$+ \frac{g}{\sqrt{N}} \left[(\hat{B}^\dagger - \sqrt{N}\beta)\hat{\mathcal{X}} + \hat{\mathcal{X}}(\hat{B} - \sqrt{N}\beta) \right] \left[(\hat{A}^\dagger + \hat{A}) + 2\sqrt{N}\alpha \right], \tag{3.52}$$

where $\hat{\mathcal{X}}$ denotes the square root assigned to the raising and lowering operators in Holstein-Primakoff representation (3.49). It is useful to rewrite $\hat{\mathcal{X}}$ in the following manner

$$\hat{\mathcal{X}} = \sqrt{N}\gamma\sqrt{1 - \frac{\hat{B}^\dagger \hat{B} - (\hat{B}^\dagger + \hat{B})\sqrt{N}\beta}{N\gamma}}, \tag{3.53}$$

where $\gamma = 1 - \beta$. In the thermodynamic limit, only terms up to $\mathcal{O}(1/\sqrt{N})$ contribute to the Hamiltonian. By expanding $\hat{\mathcal{X}}$ into orders of N,

$$\hat{\mathcal{X}} = \sqrt{N\gamma}\left[1 + \sqrt{\beta}\frac{\hat{B}^\dagger + \hat{B}}{2\sqrt{N}\gamma} - \beta\frac{\hat{B}^\dagger\hat{B}}{2N\gamma} - \beta\frac{(\hat{B}^\dagger + \hat{B})^2}{8N\gamma^2} + \mathcal{O}\left(\frac{1}{\sqrt{N}^3}\right)\right], \tag{3.54}$$

one obtains for $\hat{\mathcal{H}}_\mathrm{D}$, in the notation of Ref. [118], the power series

$$\hat{\mathcal{H}}_\mathrm{D} = N\hat{\mathcal{H}}_{\mathrm{D},0} + \sqrt{N}\hat{\mathcal{H}}_{\mathrm{D},1} + \hat{\mathcal{H}}_{\mathrm{D},2} + \mathcal{O}(1/\sqrt{N}). \tag{3.55}$$

The contributions remaining in the limit $N \to \infty$ are then given by

$$\hat{\mathcal{H}}_{\mathrm{D},0} = \hbar\omega_0\,\alpha + \hbar\Omega\left(\beta - \frac{1}{2}\right) - 4g\sqrt{\alpha\beta\gamma}, \tag{3.56}$$

$$\hat{\mathcal{H}}_{\mathrm{D},1} = (\hat{B}^\dagger + \hat{B})\left(2g\sqrt{\alpha\gamma} - 2g\sqrt{\frac{\alpha}{\gamma}}\beta - \hbar\Omega\,\sqrt{\beta}\right) + (\hat{A}^\dagger + \hat{A})\left(\hbar\omega_0\,\sqrt{\alpha} - 2g\sqrt{\beta\gamma}\right), \tag{3.57}$$

$$\hat{\mathcal{H}}_{\mathrm{D},2} = \hbar\omega_0\,\hat{A}^\dagger\hat{A} + \left(\hbar\Omega + 2g\sqrt{\frac{\alpha\beta}{\gamma}}\right)\hat{B}^\dagger\hat{B}$$
$$+ g\sqrt{\frac{\alpha\beta}{\gamma}}\left(1 + \frac{1}{2}\frac{\beta}{\gamma}\right)(\hat{B}^\dagger + \hat{B})^2 + g\left(\sqrt{\gamma} - \frac{\beta}{\sqrt{\gamma}}\right)(\hat{B}^\dagger + \hat{B})(\hat{A}^\dagger + \hat{A}). \tag{3.58}$$

This intermediate result is in accordance with Ref. [118] and also Ref. [62] when accounting for the deviations in the definition of the displaced operators (3.50). The decomposition of $\hat{\mathcal{H}}_\mathrm{D}$ into powers of N also sorts the Hamiltonian with respect to its dependence on powers of fluctuation operators. Thus, the contribution $\hat{\mathcal{H}}_{\mathrm{D},0}$ depends only on real numbers. Due to $\hat{\mathcal{H}}_{\mathrm{D},0}$ entering the Dicke Hamiltonian with a prefactor of N, it provides the dominant contribution in the thermodynamic limit. In consequence, the ground-state properties are dominated by this term [62, 118]. By contrast, the contribution $\hat{\mathcal{H}}_{\mathrm{D},1}$ is linear and $\hat{\mathcal{H}}_{\mathrm{D},2}$ is bi-linear in the fluctuation operators. The latter describes the dynamics of quantum fluctuations above the ground state. The interpretation of $\hat{\mathcal{H}}_{\mathrm{D},1}$ lapses as this contribution vanishes during the procedure of minimization of $\hat{\mathcal{H}}_{\mathrm{D},0}$ [62] as subsequently demonstrated.

By noting that the prefactors of $\hat{\mathcal{H}}_{\mathrm{D},1}$, assigned to the photonic and the atomic degrees of freedom, can be obtained from $\hat{\mathcal{H}}_{\mathrm{D},0}$ by differentiation with respect to $\sqrt{\alpha}$ and $\sqrt{\beta}$ [118] one is able to rewrite $\hat{\mathcal{H}}_{\mathrm{D},1}$ in the following manner:

$$\hat{\mathcal{H}}_{\mathrm{D},1} = (\hat{B}^\dagger + \hat{B})\frac{\partial\hat{\mathcal{H}}_{\mathrm{D},0}}{\partial\sqrt{\beta}} + (\hat{A}^\dagger + \hat{A})\frac{\partial\hat{\mathcal{H}}_{\mathrm{D},0}}{\partial\sqrt{\alpha}}. \tag{3.59}$$

Without the restriction of $\sqrt{\alpha}$ and $\sqrt{\beta}$ being real-valued as initially imposed for the sake of simplicity, the prefactors of the contribution $\hat{\mathcal{H}}_{\mathrm{D},2}$ can also be obtained from $\hat{\mathcal{H}}_{\mathrm{D},0}$ in a similar manner [118].

In order to investigate the properties of the superradiant quantum phase transition, one

needs to find the ground-state energy of the Dicke Hamiltonian (3.41). Since the dominant contribution in the thermodynamic limit is provided by $\hat{\mathcal{H}}_{D,0}$, which solely is a function of the real-valued displacements $\sqrt{\alpha}$ and $\sqrt{\beta}$, the ground-state is found by minimization of $\hat{\mathcal{H}}_{D,0}$ with respect to the displacements [62, 118]. According to mathematical analysis the extrema of $\hat{\mathcal{H}}_{D,0}$ fulfill the condition

$$\frac{\partial \hat{\mathcal{H}}_{D,0}}{\partial \sqrt{\beta}} = 0, \quad \frac{\partial \hat{\mathcal{H}}_{D,0}}{\partial \sqrt{\alpha}} = 0, \tag{3.60}$$

which simultaneously imposes that $\hat{\mathcal{H}}_{D,1} = 0$ [62, 118].
The mean field configurations satisfying Eq. (3.60) are equivalent to an energetic minimum, if the corresponding Hessian

$$H_{\hat{\mathcal{H}}_{D,0}}(\sqrt{\alpha}, \sqrt{\beta}) = \begin{pmatrix} \frac{\partial^2 \hat{\mathcal{H}}_{D,0}}{\partial \sqrt{\alpha} \partial \sqrt{\alpha}} & \frac{\partial^2 \hat{\mathcal{H}}_{D,0}}{\partial \sqrt{\alpha} \partial \sqrt{\beta}} \\ \frac{\partial^2 \hat{\mathcal{H}}_{D,0}}{\partial \sqrt{\beta} \partial \sqrt{\alpha}} & \frac{\partial^2 \hat{\mathcal{H}}_{D,0}}{\partial \sqrt{\beta} \partial \sqrt{\beta}} \end{pmatrix} = \begin{pmatrix} 2\hbar\omega_0 & 4g\frac{2\beta-1}{\sqrt{1-\beta}} \\ 4g\frac{2\beta-1}{\sqrt{1-\beta}} & 2\hbar\Omega + 4g\sqrt{\alpha\beta}\frac{3-2\beta}{\sqrt{1-\beta^3}} \end{pmatrix} \tag{3.61}$$

is positive definite at these points. A necessary condition for a matrix to be positive definite is its determinant being positive.

By explicit consideration of the functional dependence of $\hat{\mathcal{H}}_{D,0}$ on the mean fields, $\sqrt{\alpha}$ and $\sqrt{\beta}$, one is able to rewrite the minimization conditions (3.60) in the following manner:

$$\begin{aligned} \sqrt{\beta}\left(1 - 2\beta - \zeta^2\right) &= 0, \\ \sqrt{\alpha} - \frac{2g}{\hbar\omega_0}\sqrt{\beta(1-\beta)} &= 0, \end{aligned} \tag{3.62}$$

where

$$\zeta = \frac{g_c}{g}, \quad g_c = \frac{\hbar\sqrt{\omega_0\Omega}}{2}. \tag{3.63}$$

There are two sets of solutions satisfying the condition (3.62):

1. A trivial solution

$$\sqrt{\alpha_{\mathrm{np}}} = 0, \quad \sqrt{\beta_{\mathrm{np}}} = 0, \tag{3.64}$$

   where the determinant of the corresponding Hessian is given by

$$\det\left[H_{\hat{\mathcal{H}}_{D,0}}(\sqrt{\alpha_{\mathrm{np}}}, \sqrt{\beta_{\mathrm{np}}})\right] = 16g^2(\zeta^2 - 1) = 16(g_c^2 - g^2). \tag{3.65}$$

   Hence, the mean-field configuration $\sqrt{\alpha_{\mathrm{np}}}$ and $\sqrt{\beta_{\mathrm{np}}}$ corresponds to the state of minimal energy in the coupling regime $g < g_c$ which is associated with the normal phase of the system [62]. The corresponding Hamiltonian in this parameter range consists only of the contribution arising from quantum fluctuations above the constant ground-state energy

$$E_0^{\mathrm{np}} = -N\frac{\hbar\Omega}{2}, \tag{3.66}$$

as it can be seen from Eqs. (3.55 – 3.58). Hence, the Dicke Hamiltonian in this phase reads

$$\hat{\mathcal{H}}_{\mathrm{D}}^{\mathrm{np}} = \hbar\omega_0\, \hat{A}^\dagger\hat{A} + \hbar\Omega\, \hat{B}^\dagger\hat{B} + g(\hat{B}^\dagger + \hat{B})(\hat{A}^\dagger + \hat{A}) + E_0^{\mathrm{np}}. \tag{3.67}$$

2. The minimization condition (3.62) posses also the non-trivial solution

$$\sqrt{\alpha_{\mathrm{sp}}} = \pm\frac{g}{\hbar\omega_0}\sqrt{1-\zeta^4}, \quad \sqrt{\beta_{\mathrm{sp}}} = \pm\sqrt{\frac{1-\zeta^2}{2}}, \tag{3.68}$$

where $\zeta = g_c/g$ and the determinant of the Hessian

$$\det\left[H_{\hat{\mathcal{H}}_{\mathrm{D},0}}(\sqrt{\alpha_{\mathrm{sp}}}, \sqrt{\beta_{\mathrm{sp}}})\right] = 32g^2(1-\zeta^2) = 32(g^2 - g_c^2) \tag{3.69}$$

is positive for $g > g_c$. Hence, the mean-field configuration (3.68), illustrated in Fig. 3.6, yields the ground state in this coupling range. In accordance with Ref. [62], one finds the Hamiltonian in this parameter range to read

$$\hat{\mathcal{H}}_{\mathrm{D}}^{\mathrm{sp}} = \hbar\omega_0\, \hat{A}^\dagger\hat{A} + \hbar\Omega\left(1+\frac{1}{\zeta^2}\right)\hat{B}^\dagger\hat{B} + \hbar\Omega\frac{(1-\zeta^2)(3+\zeta^2)}{8\zeta^2(1+\zeta^2)}(\hat{B}^\dagger + \hat{B})^2$$

$$+ g\sqrt{\frac{2\zeta^4}{1+\zeta^2}}(\hat{B}^\dagger + \hat{B})(\hat{A}^\dagger + \hat{A}) + E_0^{\mathrm{sp}}(g). \tag{3.70}$$

The ground-state energy E_0^{sp} is a monotonically decreasing function for $g > g_c$,

$$E_0^{\mathrm{sp}}(g) = -N\frac{\hbar\Omega}{4}\left(\zeta^2 + \frac{1}{\zeta^2}\right) = -N\frac{\hbar\Omega}{4}\left[\left(\frac{g_c}{g}\right)^2 + \left(\frac{g}{g_c}\right)^2\right], \tag{3.71}$$

as Figs. 3.4, 3.5 a) illustrate. Hence, the mean-field configuration (3.68) precisely yields the ground state in the coupling regime, where the trivial solution for the mean fields (3.64) does not satisfy the minimization condition (3.65) anymore. The properties arising from minimizing the mean-field configuration (3.68) for $g > g_c$ correspond to the superradiant phase [62] as subsequently demonstrated by investigating a variety of characteristic physical observables.

The solutions of the minimization condition (3.62) in both coupling ranges, $g \gtrless g_c$, provide the basis for the following discussion of a selection of characteristic observables featuring the emergence of the quantum phase transition. Moreover, the general properties of these observables are not tied to the Dicke model only and thus they can rather be regarded as the typical characteristics of a second-order superradiant quantum phase transition. Thus, the selection of observables discussed in Subsecs. 3.1 – 3.4 of this section serves as the foundation for the discussion of collective radiation effects in more complex systems, such as Landau-quantized graphene.
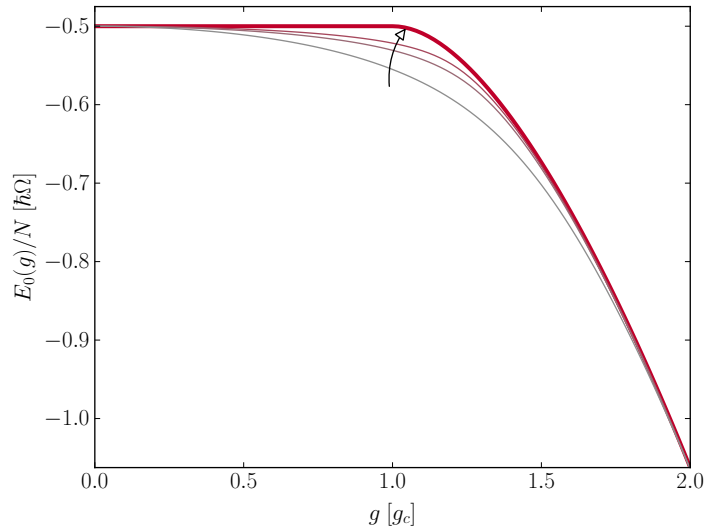
FIGURE 3.4:   Ground-state energy $E_0(g)$ (thick red) of the Dicke Hamiltonian (3.43) as a function of the coupling g at resonance, $\omega_0 = \Omega$, in the thermodynamic limit [62]. The thin curves represent the corresponding observable for the finite values of $N = 3, 6, 9$ obtained from numerical diagonalization [162, 163] of $\hat{\mathcal{H}}_{\mathrm{D}}$ according to Eq. (3.43). As N increases the finite-size result approaches $E_0(g)$ (3.72).

3.3.1   Ground-state energy and the order of the phase transition

Figure 3.4 shows the functional behavior of the ground-state energy,

$$E_0(g) = \begin{cases} -N\frac{\hbar\Omega}{2}, & \text{for } g < g_c, \\ -N\frac{\hbar\Omega}{4}\left[\left(\frac{g_c}{g}\right)^2 + \left(\frac{g}{g_c}\right)^2\right], & \text{for } g > g_c, \end{cases} \tag{3.72}$$

of the Dicke model in the thermodynamic limit at resonance, $\omega_0 = \Omega$. Even though also the ground-state energy for finite-N Dicke systems is depicted in Fig. 3.4 one is referred to Subsec. 3.3.2 for a brief discussion of the effect of finite N on the superradiant quantum phase transition. Furthermore, Subsec. 3.3.2 addresses the issue of resonance and off-resonance, respectively, in the context of the superradiant phase transition.

To continue with the discussion of the ground-state energy in the thermodynamic limit, one distinguishes different orders of quantum and classical phase transitions according to the mathematical properties of the free energy as a function of g. As the free energy coincides with the ground-state energy $E_0(g)$ in the former case, a quantum phase transition will be referred to as being of nth order if only the first $n-1$ partial derivatives $\partial_g^i E_0(g)$, $i = 0, 1, \ldots, n-1$, are continuous functions of g. In different words, the nth partial derivative, $\partial_g^n E_0(g)$, is the first one showing a discontinuity as the coupling parameter approaches a *critical* value g_c of a quantum phase transition of order n. Note that this classification of phase transition also applies for thermal phase transitions. Thereby the order of the transition is determined by the discontinuity of the nth partial derivative

of the respective thermodynamic potential, for instance the free energy (3.41).

In particular, the superradiant thermal and quantum phase transitions in the Dicke model are both of second order [61, 62]. Concerning the latter, the ground-state energy is an analytic function of the coupling strength, where its second partial derivative is discontinuous at g_c (3.40) [62]. From the theory of classical critical behavior stems the term *continuous* phase transition denoting transitions of second order and higher. This due to the *latent heat*, defined as the first derivative of the respective thermodynamic potential with respect to T, being continuous in this case. These characteristics of second-order phase transitions are depicted in Fig. 3.5 on the particular ground-state energy of the Dicke model [62] in the thermodynamic limit as well as for finite numbers of N.
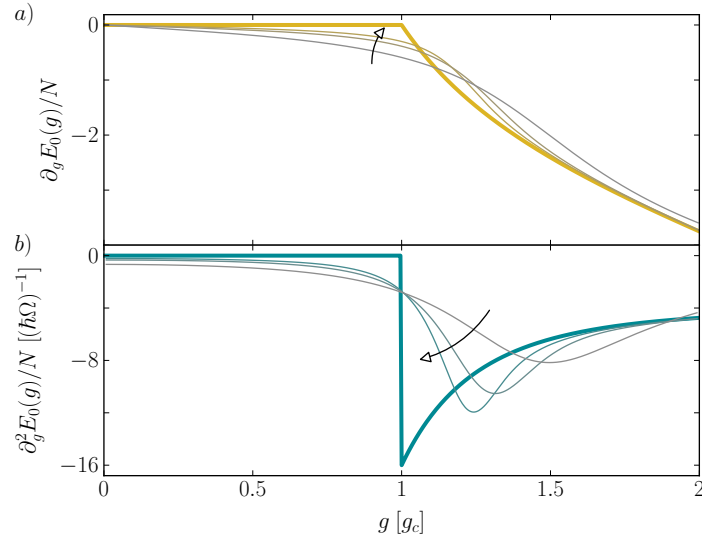
FIGURE 3.5: Panel a) shows the first derivative of ground-state energy $E_0(g)$, Eq. (3.72), of the Dicke Hamiltonian (3.43) as a function of the coupling g at resonance, $\omega_0 = \Omega$ in the thermodynamic limit (thick, orange) among results for finite $N = 3, 6, 9$ (thin). The result for $N \to \infty$ is continuous though non-analytic at the critical point, $g = g_c$. This is a characteristic feature of second-order quantum phase transitions. The finite-N results illustrate the meaning of the thermodynamic limit for the superradiant quantum phase transition, as the lack of the non-analyticity at the critical point. This becomes even more obvious in view of Panel b), where the second partial derivatives of the ground-state energies are depicted. In the thermodynamic limit (thick blue), the system shows a discontinuity at $g = g_c$. By contrast, the finite-N results (thin) obtained from numerical diagonalization [162, 163] of the Dicke Hamiltonian (3.43) lack this discontinuity even though approaching it as N increases.

By contrast, first-order transitions are denoted as *discontinuous* since the latent heat is discontinuous in a respective thermal phase transition of this order. Similarly, the first partial derivative of $E_0(g)$ is discontinuous in case of a first-order quantum phase transition. If $\partial_g E_0(g)$ referred to the ground-state energy $E_0'(g)$ of some hypothetic system undergoing a first-order quantum phase transition, Panel a) and b) of Fig. 3.5 would

depict the respective characteristic behavior of $E_0'(g)$ and $\partial_g E_0'(g)$. An example for a first-order phase transition is also found in the context of superradiance by investigating a three-level-Λ generalization of Dicke Hamiltonian [164].

3.3.2 Mean-field solutions, the thermodynamic limit and resonance
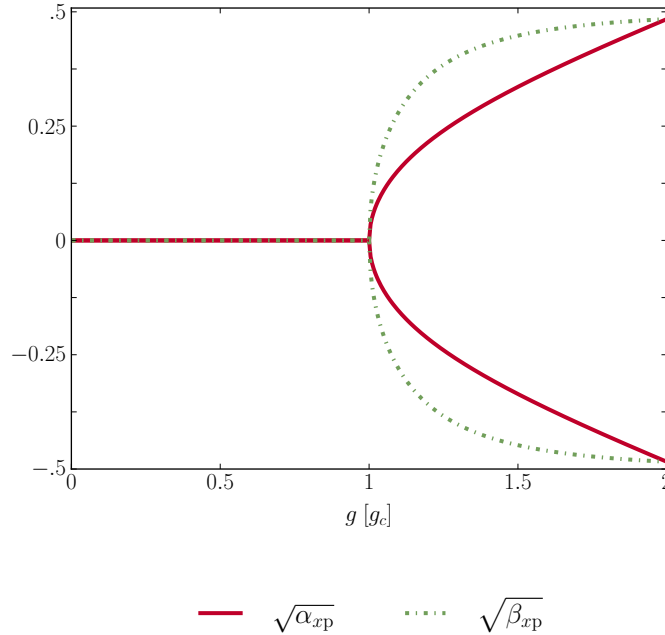
FIGURE 3.6: Illustration of the mean-field solutions, $\sqrt{\alpha_{x\mathrm{p}}}$, $\sqrt{\beta_{x\mathrm{p}}}$, of the minimization condition (3.62) in the thermodynamic limit at resonance. For $g < g_c$ the ground-state properties of the Dicke model are determined by the trivial solution of the mean-field configuration (3.64), $\sqrt{\alpha_{\mathrm{np}}} = \sqrt{\beta_{\mathrm{np}}} = 0$. This corresponds to the normal phase. In the superradiant phase, $g > g_c$, the non-trivial solution (3.68), $\sqrt{\alpha_{\mathrm{sp}}} \neq 0$, $\sqrt{\beta_{\mathrm{sp}}} \neq 0$, yields the ground state of the Dicke Hamiltonian (3.55).

Figure 3.6 illustrates the minimizing mean-field solutions (3.64, 3.68) for the displaced Dicke Hamiltonian (3.55) in both phases at resonance, $\omega_0 = \Omega$.

Thermodynamic limit and finite systems

The mean-field approach (3.50) will be appropriate only if quantum fluctuations are small [156]. This is certainly true in the thermodynamic limit since the ratios of the excitation energies $\epsilon_\pm$ of the quantum fluctuations (cf. Subsec. 3.3.4) and the ground-state energy E_0 (cf. Subsec. 3.3.1) vanish as $N \to \infty$. Hence, the mean-field configurations (3.64, 3.68) and any observable related to them are precisely valid only in the thermodynamic limit where the Dicke Hamiltonian is integrable.

By contrast, for a finite number N of atoms the Dicke Hamiltonian is not integrable [62, 165–170]. In this case, the system shows signatures of quantum chaos [62, 165, 167–171] indicated by typical features for instance emerging in the nearest-neighbor level spacing [62, 165].

Furthermore, for finite N the system exhibits what is called one or multiple smooth *superradiant quantum phase crossovers* [172–174] which converge to the superradiant quantum phase transition indicated by non-analyticities in the respective observables at $g = g_c$, as the thermodynamic limit is restored. This convergence from a smooth phase boundary, for $N < \infty$, to a sharp one in the thermodynamic limit is of rather general nature but, however, it does not necessarily hold for all kinds of second-order quantum phase crossovers and transitions [175, 176].

The properties of finite-N Dicke systems, depicted in Figs. 3.4, 3.5, 3.7 and 3.8, are obtained from numerical diagonalization of $\hat{\mathcal{H}}_D$ according to Eq. (3.43) under usage of the numerical Python package QuTiP [162, 163]. Thereby, the Fock space of the unbounded bosonic operators of the radiation mode, reading in matrix representation

$$\hat{a}^\dagger = \sum_{n=0}^{\infty} \sqrt{n+1} \, |n+1\rangle \, \langle n| \,, \quad \hat{a} = \sum_{n=0}^{\infty} \sqrt{n+1} \, |n\rangle \, \langle n+1| \,, \tag{3.73}$$

need to be handled with care to achieve convergence of the considered observables. For small N as it is the case in Figs. 3.4, 3.5, 3.7 and 3.8 this can be accomplished by truncating the Fock basis in Eq. (3.73) at a sufficiently large N_{tr}. For $N \gg 1$ the assurance of convergence within this method becomes numerically challenging. In this situation, usage of coherent-state representation of the bosonic creation and annihilation operators provides an elegant method to circumvent this issue in case of the Dicke Hamiltonian as demonstrated in Ref. [177].

A comprehensive discussion of finite-N effects would go beyond the scope of this thesis. Therefore one is referred to the literature for further details on, for instance, the finite-N scaling properties [79, 178, 179] of the observables discussed during the following or the emergence of entanglement between the field and the atoms [166, 180, 181] as a signature of $N < \infty$.

Resonance, off-resonance and the classical oscillator limit

In general, resonance is not mandatory for the emergence of neither the superradiant quantum nor the superradiant classical phase transition [182–186]. The same holds for superradiant quantum phase crossovers emerging for finite-N Dicke systems in a detuned cavity [173, 174, 187–189]. Though resonance is subsequently chosen for convenience when illustrating the functional behavior of the physical observables in accordance with Ref. [62], even far off-resonant atoms interact collectively in the ultrastrong coupling regime [182–184, 186]. Thus, by assuming the transition frequency Ω to be fixed, the value of the critical coupling (3.40) varies with the frequency ω_0 of the cavity mode and might be tunable in this sense in accordance with the validity of the dipole approximation.

Note that these arguments apply also for the spontaneous collective decay [63] discussed in Sec. 3.2 even though in this case resonance between atoms and the field enhances the

probability of the spontaneous decay.

Returning to the discussion of superradiant quantum phase crossovers in finite N-systems, one can mime a situation similar to the thermodynamic limit by consideration of

$$\frac{\Omega}{\omega_0} \to \infty, \quad \frac{g}{\hbar\omega_0} \to \infty, \quad \frac{1}{g_c} = \frac{2}{\hbar\sqrt{\omega_0\Omega}} = \text{const.}, \tag{3.74}$$

which refers to an extreme example of cavity-atom detuning. One can interpret this "alternative thermodynamic limit", also referred to as the *classical oscillator limit* [174, 190], as follows:

Either the atomic transition frequency Ω is kept constant while the cavity frequency ω_0 tends to zero or, vice versa, ω_0 is kept constant while Ω becomes arbitrary large. The former case is probably experimentally more interesting when dealing with a certain species of atoms where the transition frequencies are rather determined by elementary properties. Even in the case of tunable transition frequencies, as it is the case in Landau-quantized graphene, the limit $\Omega \to \infty$ would correspond to infinitely large and therefore experimentally infeasible magnetic fields. Thus, the assumption $\omega_0 \to 0$ corresponds to an infinitely large wave-length $\lambda = c/\omega_0$ perfectly serving the condition of valid dipole approximation. Even though neither the thermodynamic limit (2.48) nor the condition (3.74) reflect a realistic situation concerning an experimental setup, the classical oscillator limit might yield some advantages in this context. This condition resembles the superradiant quantum phase transition for $N < \infty$ [174, 190] even in the case of $N = 1$ [188, 189, 191] where the Dicke Hamiltonian coincides with the Rabi Hamiltonian. Without going into the details, the derivation scheme can be adopted from the one applied for the thermodynamic limit, discussed in the beginning of the section, yielding again mean-field solutions which minimize the ground-state energy in each phase.

Thus, to summarize, taking off-resonance between the field and the atoms into account yields an alternative approach for the discovery of a superradiant quantum phase transition even in the case of finite N.

Even though one can strictly speak of a superradiant quantum phase transition only in the thermodynamic or classical oscillator limit, the terms transition and crossover for $N < \infty$ are not distinguished by most authors. This convention will be adopted during the following.

Furthermore, the interaction of a cavity mode with an additional far-detuned two-level atom is proposed [192] to provide a possibility for an adiabatic measurement of the superradiant phase.

With this, the classical oscillator limit is set aside and the discussion of the selection of characteristic observables indicating the superradiant quantum phase transition in the thermodynamic limit, $N, V \to \infty$, $N/V = \text{const.}$, is continued during the following.

3.3.3 Spontaneous photon occupation, atomic inversion and polarization

The most insistent signature of the superradiant phase transition concerns the spontaneous macroscopic photonic occupation of the cavity along with the spontaneous polarization of the atomic cloud [61, 62]. The main properties of these observables were already indicated by Eqs. (3.44 – 3.47) in the discussion of both extreme coupling limits, the weak and the deep strong coupling regime. Nevertheless, from the definition of the displaced operators $\hat{a}^\dagger$ and $\hat{b}^\dagger$, Eq. (3.50), follows for the expectation value of the photon number operator

$$\langle \hat{a}^\dagger \hat{a} \rangle = N\alpha. \tag{3.75}$$

Likewise, one finds for the expectation value of the atomic inversion in view of Eqs. (3.48, 3.50) the expression

$$\langle \hat{\mathcal{J}}_z \rangle = \langle \hat{b}^\dagger \hat{b} \rangle - J_\mathrm{m} = N \left(\beta - \frac{1}{2} \right) \leq \frac{N}{2}. \tag{3.76}$$

Furthermore, the expectation value of $\hat{\mathcal{J}}_x$ also reflects the collective polarization of the atomic cloud and is obtained from Eqs. (3.49, 3.50):

$$\langle \hat{\mathcal{J}}_x \rangle = \frac{\langle \hat{\mathcal{J}}_+ + \hat{\mathcal{J}}_- \rangle}{2} = -N\sqrt{\beta}\sqrt{1-\beta}. \tag{3.77}$$

Since quantum phase transition are phenomena regarding the ground-state properties of the system, the physical observables (3.75 – 3.77) need to be evaluated with respect to the ground state in order to show their characteristic behavior in both quantum phases. From minimizing the mean-field contribution $\hat{\mathcal{H}}_{\mathrm{D},0}$ to the Dicke Hamiltonian the ground-state values for $\sqrt{\alpha}$ and $\sqrt{\beta}$ are already obtained in Eqs. (3.64, 3.68). Therefore, it follows straightforward for the photonic occupation in the ground state

$$\frac{\langle \hat{a}^\dagger \hat{a} \rangle_0}{N} = \begin{cases} 0, & \text{for } g < g_c, \\ \frac{g_c^2}{\hbar\omega_0} \left[\left(\frac{g}{g_c} \right)^2 - \left(\frac{g_c}{g} \right)^2 \right], & \text{for } g > g_c, \end{cases} \tag{3.78}$$

in accordance with Refs. [62, 118]. Panel a) of Fig. 3.7 illustrates this characteristic behavior as a function of the coupling parameter g where the spontaneous photon occupation is seen for couplings $g > g_c$. The atomic observables in the ground state are obtained as

$$\frac{\langle \hat{\mathcal{J}}_z \rangle_0}{N} = \begin{cases} -\frac{1}{2}, & \text{for } g < g_c, \\ -\frac{1}{2} \left(\frac{g_c}{g} \right)^2, & \text{for } g > g_c, \end{cases} \tag{3.79}$$

$$\frac{\langle \hat{\mathcal{J}}_x \rangle_0}{N} = \begin{cases} 0, & \text{for } g < g_c, \\ \mp \frac{1}{2}\sqrt{1 - \left(\frac{g_c}{g} \right)^4}, & \text{for } g > g_c, \end{cases} \tag{3.80}$$

in accordance with Refs. [62, 118]. For couplings $g < g_c$ the atomic cloud is in the collective ground-state arising from each atom occupying its single-particle ground state in the normal phase as indicated by the expectation value of $\hat{\mathcal{J}}_z$. Likewise, $\langle \hat{\mathcal{J}}_x \rangle_0$ is zero in this coupling regime. For couplings $g > g_c$ the ground-state properties are dominated by the interaction part of the Dicke Hamiltonian as the non-zero value of $\langle \hat{\mathcal{J}}_x \rangle_0$ indicates. As

the coupling g increases, the system approaches an equal occupation of single-particle ground states and excited states. Thus, the ground-state expectation value of $\hat{\mathcal{J}}_z$ approaches zero in the deep strong coupling regime, where $\langle\hat{\mathcal{J}}_x\rangle_0 \to \mp N/2$, as Panel b) of Fig. 3.7 illustrates.
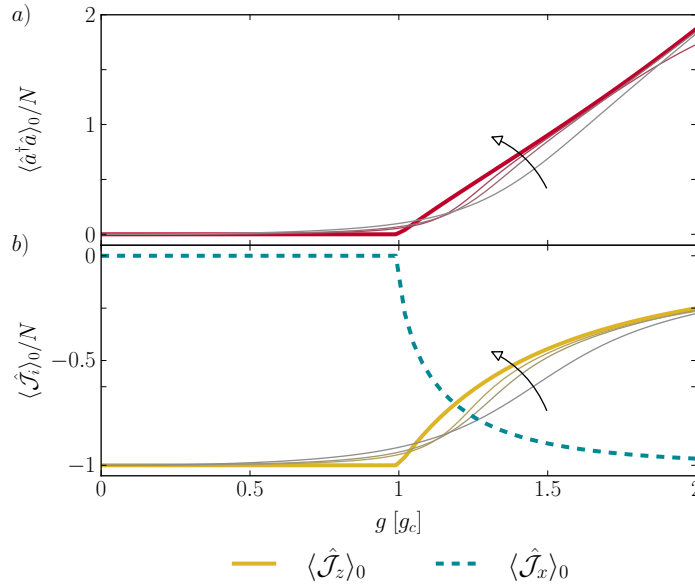
FIGURE 3.7: Ground-state expectation values of a) the cavity occupation (thick) and b) the atomic inversion $\hat{\mathcal{J}}_z$ (thick, solid, orange) and the atomic polarization $\hat{\mathcal{J}}_x$ (thick, dashed, blue) for the Dicke model in the thermodynamic limit. For convenience, only the negative value of $\langle\hat{\mathcal{J}}_x\rangle_0$ is depicted. All values refer to the resonant case at $T = 0$, hence depicting the quantum critical behavior. At the critical coupling g_c, each of the observables changes its properties in a continuous but non-analytic way. This characteristic feature of second-order quantum phase transitions [156] lacks in the corresponding results for finite $N = 3, 6, 9$ (thin), where the change between both phases occurs rather smooth.

To summarize, all three observables change their properties as $g \to g_c$ in a characteristic way. As typical for quantum phase transitions of second order [156], this change yields a non-analyticity at the critical value g_c. This can also be seen from both panels of Fig. 3.7.

3.3.4   Vanishing excitation gap

By investigating the ground-state energy and the expectation values of the photonic cavity occupation and the atomic observables $\hat{\mathcal{J}}_x$, $\hat{\mathcal{J}}_z$ (cf. Subsecs. 3.3.1, 3.3.3) only the scalar part of the Dicke Hamiltonian, $\hat{\mathcal{H}}_{D,0}$, is considered. Nevertheless, keeping in mind that $\hat{\mathcal{H}}_{D,1}$ vanishes within the procedure of minimization, also the fluctuation operator $\hat{\mathcal{H}}_{D,2}$ is affected by the quantum critical behavior in a characteristic way. Thus, to derive the excitation spectrum [62, 156] the operator $\hat{\mathcal{H}}_{D,2}$ is diagonalized in both phases. To this

end, one first applies a canonical transformation onto each pair of bosonic operators [62],

$$\hat{x} = \sqrt{\frac{\hbar}{2\omega_0}}(\hat{A}^\dagger + \hat{A}), \quad \hat{p}_x = i\sqrt{\frac{\hbar\omega_0}{2}}(\hat{A}^\dagger - \hat{A}),$$

$$\hat{y} = \sqrt{\frac{\hbar}{2\Omega}}(\hat{B}^\dagger + \hat{B}), \quad \hat{p}_y = i\sqrt{\frac{\hbar\Omega}{2}}(\hat{B}^\dagger - \hat{B}), \tag{3.81}$$

similar as for investigating two ordinary quantum harmonic oscillators of particles with mass $m = 1$. After substitution of (3.81) into $\hat{\mathcal{H}}_{D,2}$ its diagonalization is performed separately in both phases, each by means of a Bogoliubov transformation [193, 194]. Thereby one applies a rotation of the coordinate system according to

$$\hat{x}^{x\mathrm{p}} = \hat{q}_1^{x\mathrm{p}}\cos\gamma^{x\mathrm{p}} + \hat{q}_2^{x\mathrm{p}}\sin\gamma^{x\mathrm{p}},$$
$$\hat{y}^{x\mathrm{p}} = -\hat{q}_1^{x\mathrm{p}}\sin\gamma^{x\mathrm{p}} + \hat{q}_2^{x\mathrm{p}}\cos\gamma^{x\mathrm{p}}, \tag{3.82}$$

where the angle $\gamma^{x\mathrm{p}}$ can be chosen in a way that both harmonic oscillators are precisely decoupled. Following Ref. [62] the choice

$$\gamma^{x\mathrm{p}} = \begin{cases} \frac{1}{2}\arctan\left[\left(\frac{2}{\hbar}\right)^2 \frac{2gg_c}{\Omega^2 - \omega_0^2}\right], & \text{for } x = \mathrm{n} \Leftrightarrow g < g_c, \\ \frac{1}{2}\arctan\left[\left(\frac{2}{\hbar}\right)^2 \frac{2g_c^2}{\Omega^2\left(\frac{g}{g_c}\right)^4 - \omega_0^2}\right], & \text{for } x = \mathrm{s} \Leftrightarrow g > g_c \end{cases} \tag{3.83}$$

satisfies this aim. By applying another canonical transformation,

$$\hat{q}_1^{x\mathrm{p}} = \frac{\hbar}{\sqrt{2\epsilon_-^{x\mathrm{p}}}}(\hat{C}_{x\mathrm{p}}^\dagger + \hat{C}_{x\mathrm{p}}), \quad \hat{p}_1^{x\mathrm{p}} = i\sqrt{\frac{\epsilon_-^{x\mathrm{p}}}{2}}(\hat{C}_{x\mathrm{p}}^\dagger - \hat{C}_{x\mathrm{p}}),$$

$$\hat{q}_2^{x\mathrm{p}} = \frac{\hbar}{\sqrt{2\epsilon_+^{x\mathrm{p}}}}(\hat{D}_{x\mathrm{p}}^\dagger + \hat{D}_{x\mathrm{p}}), \quad \hat{p}_2^{x\mathrm{p}} = i\sqrt{\frac{\epsilon_+^{x\mathrm{p}}}{2}}(\hat{D}_{x\mathrm{p}}^\dagger - \hat{D}_{x\mathrm{p}}), \tag{3.84}$$

one is then able to obtain the eigenbasis representation of the fluctuation operator $\hat{\mathcal{H}}_{D,2}$,

$$\hat{\mathcal{H}}_{D,2}^{x\mathrm{p}} = \epsilon_-^{x\mathrm{p}}(g)\,\hat{C}_{x\mathrm{p}}^\dagger\hat{C}_{x\mathrm{p}} + \epsilon_+^{x\mathrm{p}}(g)\,\hat{D}_{x\mathrm{p}}^\dagger\hat{D}_{x\mathrm{p}}, + \frac{\epsilon_-^{x\mathrm{p}}(g) + \epsilon_+^{x\mathrm{p}}(g)}{2} \tag{3.85}$$

in terms of the bosonic fluctuation operators $\hat{C}_{x\mathrm{p}}^\dagger$, $\hat{C}_{x\mathrm{p}}$ and $\hat{D}_{x\mathrm{p}}^\dagger$, $\hat{D}_{x\mathrm{p}}$ in the normal, $x = \mathrm{n}$, and the superradiant phase, $x = \mathrm{s}$. Thereby each pair of the bosonic fluctuation operators, $\hat{C}_{x\mathrm{p}}^\dagger$, $\hat{C}_{x\mathrm{p}}$ and $\hat{D}_{x\mathrm{p}}^\dagger$, $\hat{D}_{x\mathrm{p}}$, addresses a different Hilbert subspace. Hence, $\hat{C}_{x\mathrm{p}}^\dagger$, $\hat{C}_{x\mathrm{p}}$ and $\hat{D}_{x\mathrm{p}}^\dagger$, $\hat{D}_{x\mathrm{p}}$ satisfy the commutation relations:

$$[\hat{C}_{x\mathrm{p}}, \hat{C}_{x\mathrm{p}}^\dagger] = 1, \quad [\hat{D}_{x\mathrm{p}}, \hat{D}_{x\mathrm{p}}^\dagger] = 1, \tag{3.86}$$

where all other commutators are zero. At zero coupling, the collective mode associated with $\hat{C}_{x\mathrm{p}}^\dagger$, $\hat{C}_{x\mathrm{p}}$ arise from the photonic degrees of freedom [62]. Hence, ϵ_- is referred to as the photonic branch. Likewise, ϵ_+ denotes the atomic branch since $\hat{D}_{x\mathrm{p}}^\dagger$, $\hat{D}_{x\mathrm{p}}$ are associated with the collective atomic degrees of freedom at zero coupling. The energies

of these fundamental excitations are given by [62]

$$
\frac{\sqrt{2}}{\hbar}\epsilon_{\pm}(g) = \begin{cases} \left[\omega_0^2 + \Omega^2 \pm \sqrt{[\omega_0^2 - \Omega^2]^2 + 16g^2\omega_0\Omega}\right]^{\frac{1}{2}}, & \text{for } g < g_c, \\[2ex] \left[\omega_0^2 + \Omega^2\left(\frac{g}{g_c}\right)^2 \pm \sqrt{[\omega_0^2 - \Omega^2\left(\frac{g}{g_c}\right)^2]^2 + 4\omega_0\Omega}\right]^{\frac{1}{2}}, & \text{for } g > g_c, \end{cases}
\tag{3.87}
$$

and are thus independent on the number N of atoms. This is in accordance with the nature of the mean-field approach (3.50) which is only valid if quantum fluctuations are small compared to the mean-field ground-state energy. Since $E_0 \propto N$ this condition is satisfied in the thermodynamic limit.

In both phases, the excitation energies $\epsilon_{\pm}$ are real-valued only in the coupling range declared on the r.h.s. of Eq. (3.87). Figure 3.8 illustrates the functional behavior of the collective eigenmodes $\epsilon_{\pm}$ as the coupling strength g varies. According to Ref. [62] the atomic branch ϵ_+ continuously increases for increasing g and approaches $4g^2/(\hbar\omega_0)$ in the limit $g \to \infty$. By contrast, as $g \to g_c$, the energy gap between the ground-state energy and the photonic branch ϵ_- closes from either direction according the power law [62]

$$
\epsilon_-(g \approx g_c) \approx \sqrt{\frac{32g_c^3(\hbar\omega_0)^2}{16g_c^4 + (\hbar\omega_0)^2}} \, |g_c - g|^{z\bar{\nu}}.
\tag{3.88}
$$

The closure of the excitation gap related to the photonic branch is characteristic feature for second-order quantum phase transitions [62, 156]. The critical exponent of the power law is given by [62]

$$
z\bar{\nu} = 1/2.
\tag{3.89}
$$

According to Ref. [62] $z = 2$ denotes the dynamical critical exponent and $\bar{\nu} = 1/4$ is related to the power law of the characteristic length scale of the system, $l_-^{x\mathrm{p}} \propto 1/\sqrt{\epsilon_-^{x\mathrm{p}}}$, in the vicinity of the critical point g_c. Thus, as g approaches this point, l_- diverges as $|g - g_c|^{-\bar{\nu}}$ from either direction revealing the scale invariance of fluctuations at the transition point [156].

The scale invariance can also be seen from investigating the wave functions of the fluctuation operator in the $q_1^{x\mathrm{p}}$-$q_2^{x\mathrm{p}}$ plane. For instance, the ground-state wave function of $\hat{\mathcal{H}}_{\mathrm{D},2}^{x\mathrm{p}}$ is given by the product of two normalized Gaussian functions [62],

$$
\Psi_0^{x\mathrm{p}}(q_1, q_2) = G_-^{x\mathrm{p}}(q_1)G_+^{x\mathrm{p}}(q_2), \quad G_{\pm}^{x\mathrm{p}}(q) = \left(\frac{\epsilon_{\pm}^{x\mathrm{p}}}{\pi\hbar^2}\right)^{\frac{1}{4}} \exp\left[-\frac{\epsilon_{\pm}^{x\mathrm{p}}}{2\hbar^2}q^2\right],
\tag{3.90}
$$

where the superscript $^{x\mathrm{p}}$ on the coordinates q_1 and q_2, marking the respective phase, is omitted for brevity. The variance of each Gaussian wave packet, $(\sigma_{\pm}^{x\mathrm{p}})^2 = \hbar^2/\epsilon_{\pm}^{x\mathrm{p}}$, is a measure for its spacial extent. Hence, in agreement with the previous considerations, the variance is determined by the characteristic length in each phase: $(\sigma_{\pm}^{x\mathrm{p}})^2 \propto (l_{\pm}^{x\mathrm{p}})^2$. At zero coupling, the wave function is rotationally symmetric and centered around the origin. As g approaches the critical coupling, Ψ_0^{np} squeezes in the direction of q_2 and stretches along the q_1-axis, as Fig. 3.9 illustrates. Thereby Ψ_0^{np} is depicted in the x-y plane for convenience [62]. The transformation from the coordinate system q_1^{np}-q_2^{np} to the x-y representation is promoted by the inverse of the Bogoljubov transformation (3.82).
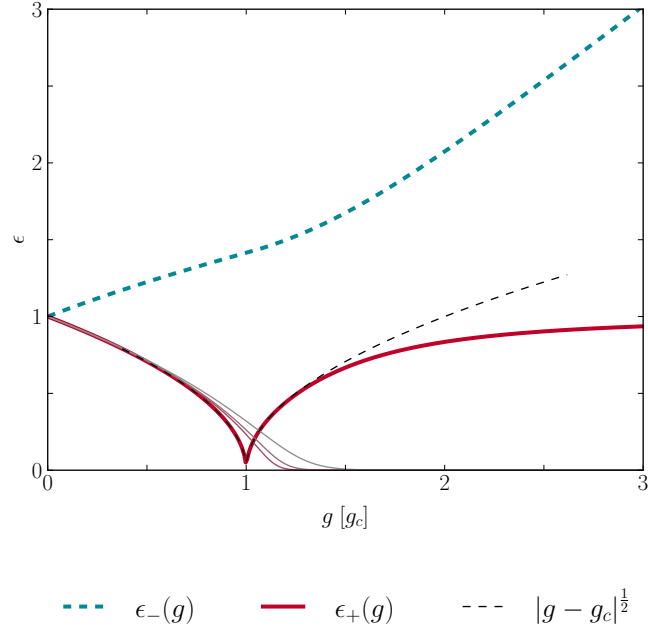
FIGURE 3.8: Fundamental excitations $\epsilon_\pm$ of quantum fluctuations of the Dicke Hamiltonian above the ground state as a function of g. The system is assumed to be in the thermodynamic limit and at resonance, $\omega_0 = \Omega$. As g approaches the critical value g_c, the energy gap of the photonic branch ϵ_- (thick, solid, red) narrows and closes precisely at g_c according to the power law $\propto |g_c - g|^{\frac{1}{2}}$ (thin, dashed, black). The energy gap of atomic branch ϵ_+ (thick, dotted, blue) continuously increases with increasing g. The closing of the energy gap at the critical value g_c is a characteristic signature for second-order quantum phase transitions in most cases [62, 156]. The photonic branch in case of a finite number of atoms (thin, solid), where $N = 3, 6, 9$, approaches the mean-field values for $g < g_c$ as N increases. Above the critical coupling, the finite-N excitation energies approach zero featuring the symmetry properties of the corresponding finite-N Dicke Hamiltonian.

Furthermore, Fig. 3.9 illustrates the symmetry properties of the system in the normal phase, which are indicated by the invariance of Ψ_0^{np} with respect to rotations of π around the origin [62]. As subsequently discussed, this parity symmetry breaks down as the system crosses the phase boundary at g_c.

3.3.5 Breakdown of the parity symmetry

Another characteristic signature of second-order quantum phase transitions concerns the breakdown of parity symmetry [62] as the system undergoes the second-order superradiant quantum phase transition.
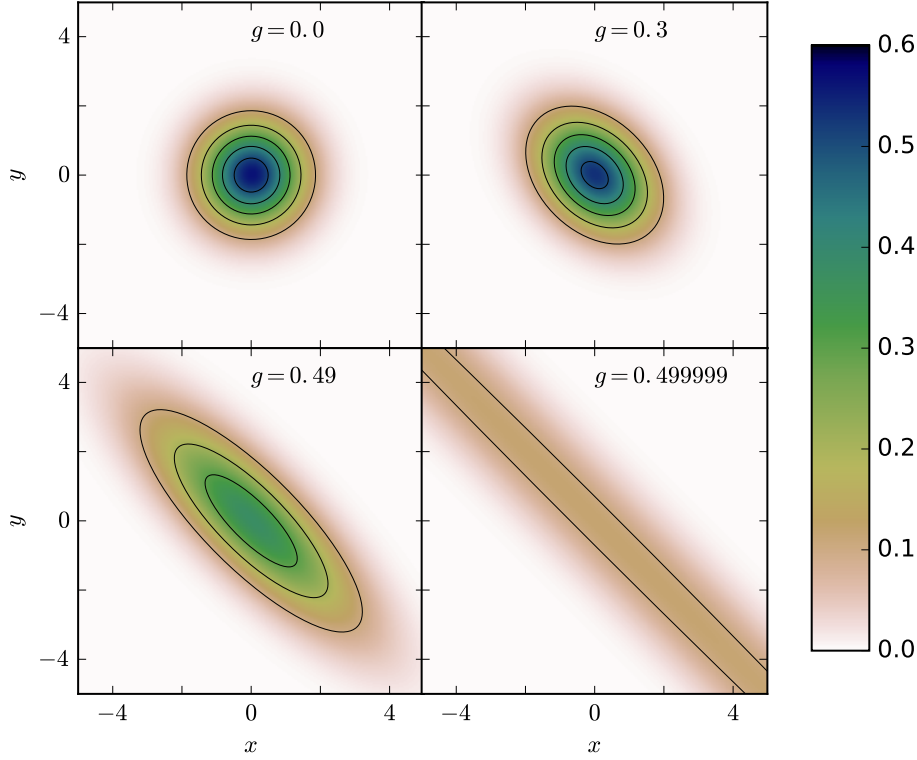
FIGURE 3.9: Illustration of the ground-state wave function of the fluctuation operator in the normal phase of the finite-N Dicke model following Ref. [62]. The system is at resonance and $N = 50$ in each panel. Furthermore, the black lines mark isolines spaced by the value 0.1. For all coupling values $< g_c$ the wave function is also an eigenfunction of the parity operator $\hat{\Pi}^{\mathrm{np}}$ indicated by its invariance under rotation of π around the origin. As the coupling increases, the wave function gets stretched in the direction of $q_1 = x \cos \gamma^{\mathrm{np}} - y \sin \gamma^{\mathrm{np}}$ and squeezed along the orthogonal axis $q_2 = x \sin \gamma^{\mathrm{np}} + y \cos \gamma^{\mathrm{np}}$. In each of the directions the spacial extent is associated with a characteristic length, l_- and l_+, respectively. The latter diverges with $|g - g_c|^{1/2}$ in the vicinity of the transition point.

Normal phase

In the normal phase, the parity operator [62, 118],

$$\hat{\Pi} = e^{i\pi\left(\hat{a}^\dagger \hat{a} + \hat{\mathcal{J}}_z + J_{\mathrm{m}}\right)} = e^{i\pi\left(\hat{a}^\dagger \hat{a} + \hat{b}^\dagger \hat{b}\right)}, \tag{3.91}$$

commutes with the fluctuation operator $\hat{\mathcal{H}}^{\mathrm{np}}_{\mathrm{D},2}$ and thus in turn with the corresponding Dicke Hamiltonian $\hat{\mathcal{H}}^{\mathrm{np}}_{\mathrm{D}}$ (3.67). Due to the vanishing mean-field solutions (3.64), $\sqrt{\alpha_{\mathrm{np}}}$ and $\sqrt{\beta_{\mathrm{np}}}$, in the respective coupling range, $g < g_c$, the displaced operators (3.50), $\hat{a}^\dagger$ and $\hat{b}^\dagger$, coincide with the fluctuation operators, $\hat{A}^\dagger$ and $\hat{B}^\dagger$. Hence, the parity operator in the

normal phase can be specified according to

$$\hat{\Pi}^{\mathrm{np}} = e^{i\pi\left(\hat{A}^\dagger\hat{A} + \hat{B}^\dagger\hat{B}\right)}, \tag{3.92}$$

where the commutation of $\hat{\mathcal{H}}^{\mathrm{np}}_{\mathrm{D},2}$ and $\hat{\Pi}^{\mathrm{np}}$ is then easily deduced from the discussion in Sec. 4 of App. E. Note that the parity operator (3.91, 3.92) is formally similar to the parity operator of a two-dimensional harmonic oscillator [195].

The commutation of $\hat{\mathcal{H}}^{\mathrm{np}}_{\mathrm{D},2}$ with $\hat{\Pi}$ indicates that both operators share a common eigenbasis [62, 119]. For instance, Fig. 3.9 shows the ground-state wave function Ψ^{np}_0 of the fluctuation operator for various coupling strengths in the normal phase. Incidentally focusing on the symmetry properties of Ψ^{np}_0 only, one is referred to Subsec. 3.3.4 for the discussion of the deformation of Ψ^{np}_0 as g increases. It is obvious from each panel of Fig. 3.9 that the corresponding ground-state wave function is invariant under rotations of π around the origin. This precisely corresponds to action of the parity operator onto the wave function and thus to the parity symmetry of the corresponding fluctuation operator in the normal phase. The parity symmetry of excited states can also be proven [62].

The argument of the exponential in the parity operator (3.91, 3.92) counts the total number of excitation quanta in the system [62]. Likewise, the operator $\hat{a}^\dagger\hat{a} + \hat{\mathcal{J}}_z + J_{\mathrm{m}}$ or $\hat{a}^\dagger\hat{a} + \hat{b}^\dagger\hat{b}$ is referred to as the excitation number operator [62]. Its eigenvalues are easily found in terms of the product basis of Dicke states $|J_{\mathrm{m}}; M\rangle$, see Subsec. 3.2.2, and Fock states $|n\rangle$, $\{|n\rangle \otimes |J_{\mathrm{m}}; M\rangle\}$, reading

$$\left(\hat{a}^\dagger\hat{a} + \hat{\mathcal{J}}_z + J_{\mathrm{m}}\right)|n\rangle \otimes |J_{\mathrm{m}}; M\rangle = (n + M + J_{\mathrm{m}})|n\rangle \otimes |J_{\mathrm{m}}; M\rangle. \tag{3.93}$$

As discussed in Subsec. 3.2.1 the quantum number M is bounded by J_{m}. By contrast, the quantum number n associated with the number of photons in the cavity is unbounded. Hence, the eigenvalues of the excitation number operator (3.93) are either even or odd resulting in eigenvalues $+1$ or -1 of the parity operator $\hat{\Pi}$ (3.91). The states associated with the positive eigenvalue of $\hat{\Pi}$ are referred to as having positive parity and vice versa. Therefore, each state $|n\rangle \otimes |J_{\mathrm{m}}; M\rangle$ of the basis can be associated with a distinct parity. For instance, the ground-state $|0\rangle \otimes |J_{\mathrm{m}}; -J_{\mathrm{m}}\rangle$ in the normal phase has positive parity as it follows from Eq. (3.93).

Superradiant phase

By contrast, the parity is not a good quantum number in the superradiant phase [62, 118], where $g > g_c$ and the Dicke Hamiltonian is given by Eq. (3.70). This can also be seen from the considerations in Sec. 4 of App. E, keeping in mind that the displaced operators (3.50), $\hat{a}^\dagger$ and $\hat{b}^\dagger$, do not coincide with the fluctuation operators, $\hat{A}^\dagger$ and $\hat{B}^\dagger$. This follows form the finite values of the mean fields (3.68) within this coupling regime so that $\hat{\Pi}$ for $g > g_c$ is given by

$$\hat{\Pi}^{\mathrm{sp}} \propto e^{i\pi\left[\hat{A}^\dagger\hat{A} + 2\sqrt{N\alpha_{\mathrm{sp}}}(\hat{A}^\dagger + \hat{A}) + \hat{B}^\dagger\hat{B} - 2\sqrt{N\beta_{\mathrm{sp}}}(\hat{B}^\dagger + \hat{B})\right]}. \tag{3.94}$$

Figure 3.10 shows the behavior of the ground-state wave function Ψ^{sp}_0 of the fluctuation operator in the superradiant phase for a finite system of $N = 50$ atoms. Even though
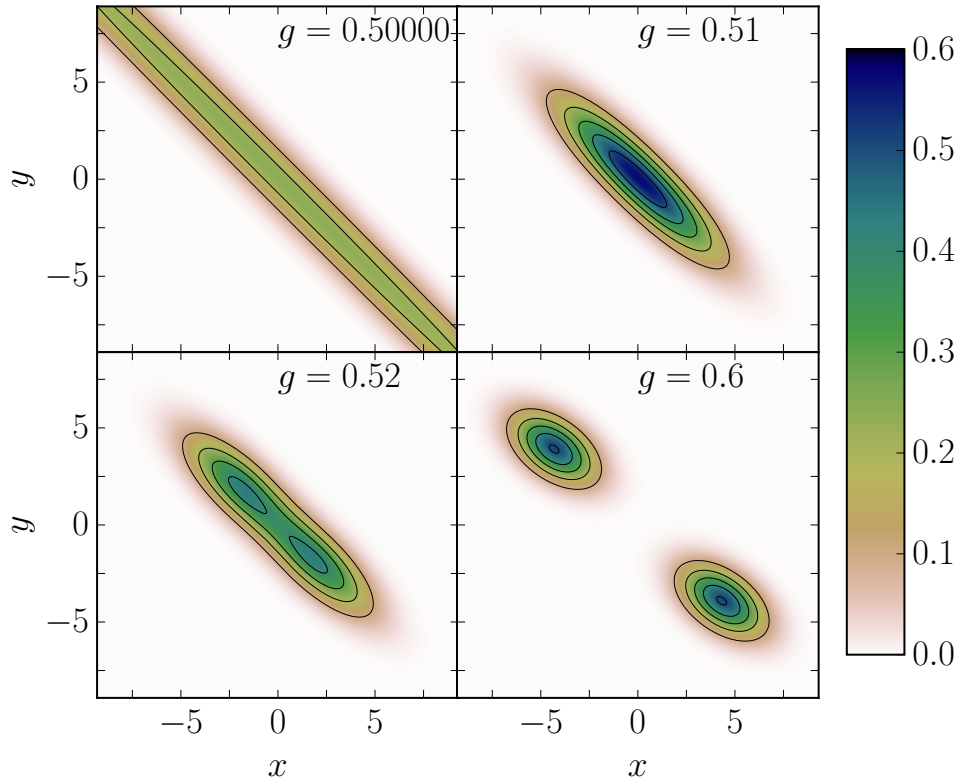
FIGURE 3.10: Illustration of the ground-state wave function of the fluctuation operator in the superradiant phase of the finite-N Dicke model according to Ref. [62]. The system is at resonance and $N = 50$ in each panel. Furthermore, the black lines mark isolines, spaced by the value 0.1. As the coupling increases the wave function separates into two lobes with a displacement proportional to $\propto \sqrt{gN}$. For finite N, there remains a non-zero overlap of both lobes in the superradiant phase for finite $g \gtrsim g_c$. The system retains its parity symmetries also in the superradiant case. This can be seen from the invariance of the respective wave functions under rotation of π around the origin as each of the four panels shows. By contrast, in the thermodynamic limit, both lobes are spread infinitely far away from each other for any value $g > g_c$. Thereby, each lobe corresponding to one realization of the mean-field configuration (3.68). Thus, in the thermodynamic limit, the system loses its invariance under π-rotation around the origin as the phase boundary is crossed. This corresponds to a breakdown of the parity symmetry. Nevertheless, each lobe retains locally invariant under rotation of π around the local maximum. The bottom right panel can be regarded to indicate these local symmetry properties even though it depicts the case of finite N.

in finite-N systems the parity retains a good quantum number also in the superradiant phase, the depicted example helps to understand the breakdown of the parity symmetry in the thermodynamic limit. Hence, as the system crosses the phase boundary at $g = g_c$ the wave function spreads into two lobes with a separation proportional to $\propto \sqrt{gN}$ [62].

If $N < \infty$, as it is the case in Fig. 3.10, there remains a non-zero overlap of both lobes close to the critical point. By contrast, in the thermodynamic limit, the lobs are instantaneously separated infinitely far away from each other as the system crosses the critical point. This results from the displacement initially applied to the photonic and atomic operators (3.50) and the procedure of diagonalization of $\hat{\mathcal{H}}_{D,2}$ discussed in Subsec. 3.3.4. In the thermodynamic limit, each of the two lobes corresponds to one realization of the two mean-field configurations (3.68) denoted by either the $+$ or the $-$ sign. Thereby the wave function obviously loses its invariance under π-rotation around the origin which corresponds to the breakdown of the parity symmetry. For an explicit discussion of the derivation of Ψ_0^{sp} one is referred to Refs. [62, 165]. There, one also finds a detailed consideration of the properties of Ψ_0^{sp} for $N < \infty$ considering aspects of quantum chaos in the superradiant phase.

To summarize this subsection, the superradiant quantum phase transition of the Dicke model in the thermodynamic limit is accompanied with a breakdown of the discrete parity symmetry of the states promoted by the operator $\hat{\Pi}$. In general, the breakdown of a characteristic symmetry inherent in the system is also a typical feature of a second-order quantum phase transition [156].

3.3.6 Summary and remarks

Subsections 3.3.1 – 3.3.5 catalog a selection of generic features of the superradiant quantum phase transition of the Dicke model in the thermodynamic limit. The derivation of the characteristic observables is based on a mean-field ansatz yielding distinct ground-state properties in both quantum phases. In the normal phase, $g < g_c$, the ground-state of the hybrid system is determined by the ground-state properties of both subsystems. Hence, in average, the photon occupation vanishes along with each atom occupying its single-particle ground-state. As the phase boundary is crossed, the ground-state properties of the system drastically change. Thus, in the superradiant phase for $g > g_c$, the state of minimal energy is accompanied by a spontaneous photonic occupation of the cavity and the collective excitation of the atoms. Both observables scale with the number of atoms and hence they are macroscopic quantities in the thermodynamic limit. By investigating the low-energy excitations above the collective ground state, one finds the excitation gap of the photonic branch closing at the transition point following a power law with universal exponents. Similarly, the corresponding characteristic length diverges as the system approaches the critical point. This scale invariance of quantum fluctuations in the vicinity of g_c can also be seen from the wave function. Furthermore, the wave function gives insight into the breakdown of the parity symmetry of the Dicke Hamiltonian in the superradiant phase. Among others, these quantities and properties are generic features of quantum phase transitions and provide the basis for the discussion of the collective behavior of Landau-quantized graphene embedded in an optical cavity (cf. Part II).

Furthermore, all considerations made in this thesis refer to the superradiant quantum phase transition in the so-called equilibrium, meaning no further driving fields are applied to the system. The opposite situation is referred to as an nonequilibrium setup.

Theoretical investigations on nonequilibrium superradiant quantum phase transitions can be found in the literature [74–79]. Some of the proposals suggest multi-level atoms driven by an external laser field such that the effective Hamiltonian is given by a Dicke Hamiltonian [74, 75]. Based on this approach, superradiant phase transitions in driven systems have been experimentally observed for atoms [84] and Bose-Einstein condensates [80–83].

An experimental observation of the equilibrium superradiant phase transition has not been reported so far even though the required ultrastrong coupling regime has been reached experimentally for cyclotron transitions of two-dimensional electron gases [52, 55]. The highest coupling strength ever recorded [55] lies with $g = 0.87\hbar\omega_c$ at $T = 10\,\mathrm{K}$ clearly above the critical value offered by the Dicke model, presupposing the validity of g_c in this situation. Additional interaction effects [196] or the issue that dipole approximation is not strictly valid in the setup of Refs. [52, 55] could potentially explain the critical point to be shifted to higher values.

Nevertheless, it is more reasonable to explain the absence of the equilibrium superradiant phase transition in the corresponding experiments by means of a no-go theorem applicable to systems with parabolic energy-momentum dispersion in Coulomb gauge. The no-go theorem addresses the diamagnetic term emerging from minimal coupling applied to a parabolic dispersion which is omitted in the Dicke model. As recognized by K. Rzażewski *et al.* [85] the diamagnetic contributions to the Dicke Hamiltonian cannot be neglected in the ultrastrong coupling regime. Moreover, as the diamagnetic term in the Dicke model is microscopically linked to the interaction term (cf. Chap. 2) it cannot be tuned arbitrarily. The explicit consideration of this contribution to $\hat{\mathcal{H}}_\mathrm{D}$ yields a no-go theorem that prohibits the superradiant quantum and classical phase transition [85]. The formulation of the no-go theorem has given rise to a still ongoing controversial discussion [88, 89, 185, 197, 198] concerning its validity. Especially the approaches of Refs. [88, 89, 198] are interesting as they address this issue on a more fundamental level than the derivation of the effective one-mode Dicke Hamiltonian and the no-go theorem itself. The foundation of these considerations is outlined in Subsec. 4.2. However, the prohibition of the superradiant phase transition in the original Dicke model due to the diamagnetic contribution and thus the validity of the no-go theorem is widely regarded as being proven [85–91]. Even further, the presence of the diamagnetic term manifests as a blue-shift in the quasiparticle energies and has also been observed experimentally in ultrastrongly coupled cyclotron transitions of two-dimensional electron gases [55].

In order to provide some insights into this issue, the derivation of the no-go theorem is outlined and proposed exceptions of it are discussed in the next chapter.

Chapter 4

No-go theorem for the superradiant phase transition of the Dicke model

The derivation of the no-go theorem for the superradiant phase transition of the Dicke model requires two steps. The first one concerns the ground-state properties of the generalized Dicke model consisting of the original Dicke Hamiltonian (3.43) and the diamagnetic contribution (2.49),

$$\hat{\mathcal{H}}_{\text{gD}} = \hat{\mathcal{H}}_{\text{D}} + \kappa(\hat{a}^\dagger + \hat{a})^2. \tag{4.1}$$

In particular, one aims for the derivation of a condition which connects the prefactor κ and the coupling strength g and ensures the determinant of the Hessian (3.61) to vanish. The second step concerns the proof of the validity of this condition based on the microscopic properties of κ and g (cf. Chap. 2) under application of the Thomas-Reiche-Kuhn (TRK) sum rule [199–202].

4.1 Estimation of a critical condition in the presence of diamagnetic terms

Application of the Holstein-Primakoff transformation (3.48, 3.49) onto the atomic collective spin-operators in $\hat{\mathcal{H}}_{\text{D}}$ and definition of the displaced operators, similar to Eq. (3.50), yields $\hat{\mathcal{H}}_{\text{D}}$ to be given by the expression (3.52) and the diamagnetic term to read

$$\hat{\mathcal{H}}_{\text{dia}} = \kappa \left[(\hat{A}^\dagger + \hat{A}) + 2\sqrt{N}\alpha \right]^2 = \kappa \left[(\hat{A}^\dagger + \hat{A})^2 + 4\sqrt{N}\alpha(\hat{A}^\dagger + \hat{A}) + 4N\alpha \right]. \tag{4.2}$$

With this one can decompose $\hat{\mathcal{H}}_{\text{gD}}$ into a power series of different orders of N similar to Eq. (3.55). Likewise, the contribution to this power series relevant for the ground-state properties is the one $\propto N$ reading

$$\hat{\mathcal{H}}_{\text{gD},0} = \hat{\mathcal{H}}_{\text{D},0} + 4\kappa\alpha \overset{(3.56)}{=} (\hbar\omega_0 + 4\kappa) \, \alpha + \hbar\Omega \left(\beta - \frac{1}{2} \right) - 4g\sqrt{\alpha\beta(1-\beta)}. \tag{4.3}$$

Again the ground state of this contribution is obtained by evaluating the equivalent to Eqs. (3.60, 3.62) yielding

$$
\sqrt{\beta} \left[1 - 2\beta - (4\kappa + \hbar\omega_0) \frac{\hbar\Omega}{4g^2} \right] = 0,
$$
$$
\sqrt{\alpha} - \frac{2g}{4\kappa + \hbar\omega_0} \sqrt{\beta(1 - \beta)} = 0.
$$

(4.4)

By sending $\kappa \to 0$, the minimization criterion coincides with the one obtained for the original Dicke model (3.62). Evaluation of the determinant of the corresponding Hessian provides the information whether the trivial mean-field configuration

$$
\sqrt{\alpha_{\mathrm{np}}} = 0, \quad \sqrt{\beta_{\mathrm{np}}} = 0,
$$

(4.5)

corresponds to a minimum of $\hat{\mathcal{H}}_{\mathrm{gD},0}$, i.e.

$$
\det \left[H_{\hat{\mathcal{H}}_{\mathrm{gD},0}}(\sqrt{\alpha_{\mathrm{np}}}, \sqrt{\beta_{\mathrm{np}}}) \right] = 16 \left[(g_c^2 + \kappa\hbar\Omega) - g^2 \right] \overset{!}{>} 0.
$$

(4.6)

Obviously this will be satisfied if $(g_c^2 + \hbar\Omega\kappa) > g^2$. As long as this condition is fulfilled the system is in the normal phase. The criterion for a quantum phase transition to occur is the determinant of the Hessian evaluated at $\sqrt{\alpha_{\mathrm{np}}}$, $\sqrt{\beta_{\mathrm{np}}}$ to change its sign as g crosses a critical value $\tilde{g}_c$. This ultimately requires κ to satisfy

$$
\kappa < \frac{g^2}{\hbar\Omega},
$$

(4.7)

in accordance with the literature [85–91]. Whether the condition (4.7) is eventually fulfilled strictly depends on the microscopic properties of κ and g. For any Hamiltonian with parabolic momentum dependence κ and g are linked to each other by the principle of minimal coupling (2.27) and thus both quantities cannot be tuned independently. This can be seen from the TRK sum rule as discussed during the following.

4.2   TRK sum rule and the no-go theorem

From the derivation of the general Hamiltonian for quantum electrodynamics in Chap. 2, one finds the following microscopic properties for the prefactor κ, Eq. (2.50):

$$
\kappa = N \frac{e^2 \hbar^2}{2m} \frac{1}{2\hbar\epsilon_0\omega_0 V}.
$$

(4.8)

Note that this result already contains the constraint of identical particles indicated by the factor of N. Likewise, the coupling strength for the Dicke model is defined in Eq. (3.10) and reads

$$
g^2 = N \mathcal{A}_0^2 \frac{\Omega^2}{\hbar^2} |\boldsymbol{d}_{1,0} \cdot \boldsymbol{e}_x|^2 \leq N \mathcal{A}_0^2 \frac{\Omega^2}{\hbar^2} |\boldsymbol{d}_{1,0}|^2, \quad \mathcal{A}_0 = \sqrt{\frac{\hbar}{2\epsilon_0\omega_0 V}}.
$$

(4.9)

Thereby $\boldsymbol{d}_{1,0} = \langle 1^i | \hat{\boldsymbol{d}} | 0^i \rangle$ denotes the matrix element of the dipole operator $\hat{\boldsymbol{d}} = -e\hat{\boldsymbol{q}}_i$ for the transition between the two states $|0^i\rangle \leftrightarrow |1^i\rangle$ of the ith two-level approximated atom. The inequality in Eq. (4.9) results from the Cauchy-Schwartz inequality [203] where $|e_x|^2 = 1$ was used.

As neatly presented in Ref. [118] the condition

$$\sum_n (\epsilon_n - \epsilon_m) \langle m | \hat{F} | n \rangle \langle n | \hat{F} | m \rangle = \frac{1}{2} \langle m | [\hat{F}, [\hat{H}, \hat{F}]] | m \rangle \tag{4.10}$$

refers to a generalized formulation of the TRK sum rule [199–202] and holds for any operator $\hat{F}$ and the eigenspectrum $\{\epsilon_n, |n\rangle\}$ of an arbitrary Hamiltonian $\hat{H}$. For convenience, the quantities in Eq. (4.10) are assumed to denote single-particle operators, states and energies.

Now, by supposing the Hamiltonian to be quadratic in the momentum of the ith particle with charge q_i, i.e. $\hat{H} = \hat{\boldsymbol{p}}_i^2/(2m)$, one easily obtains the following relations:

$$-\frac{i\hbar}{m_i} \hat{\boldsymbol{p}}_i = [\hat{\mathcal{H}}, \hat{\boldsymbol{q}}_i], \qquad \frac{\hbar^2}{m_i} = [\hat{\boldsymbol{q}}_i, [\hat{\mathcal{H}}, \hat{\boldsymbol{q}}_i]] \quad \Rightarrow \quad \frac{q_i^2 \hbar^2}{m_i} = [\hat{\boldsymbol{d}}_i, [\hat{\mathcal{H}}, \hat{\boldsymbol{d}}_i]]. \tag{4.11}$$

Hence, by associating $\hat{F} = \hat{\boldsymbol{d}}_i$, Eq. (4.10) specifies to

$$\sum_{n_i} (\epsilon_{n_i} - \epsilon_{m_i}) \langle m^i | \hat{\boldsymbol{d}}_i | n^i \rangle \langle n^i | \hat{\boldsymbol{d}}_i | m^i \rangle = \sum_{n_i} (\epsilon_{n_i} - \epsilon_{m_i}) \left| \langle n^i | \hat{\boldsymbol{d}}_i | m^i \rangle \right|^2 = \frac{q_i^2 \hbar^2}{2m_i}. \tag{4.12}$$

By summation over all quantum particles, $i = 1, \ldots, N$, one finds the TRK sum rule in its original form [199–202]:

$$\sum_{i=1}^{N} \left[\sum_{n_i} (\epsilon_{n_i} - \epsilon_{m_i}) \left| \langle n^i | \hat{\boldsymbol{d}}_i | m^i \rangle \right|^2 \right] = \sum_{i=1}^{N} \frac{q_i^2 \hbar^2}{2m_i}. \tag{4.13}$$

The application to the generalized Dicke Hamiltonian (4.2) is then achieved by claiming that all quantum particles are identical atoms, i.e. $m_i = m$, $q_i = -e$ $\forall i = 1, \ldots, N$, and restricting each single-particle basis $\{|n^i\rangle\}$ to the two-level approximation. Thus, the TRK sum rule for $\hat{\mathcal{H}}_{\text{gD}}$ is given by

$$N\hbar\Omega \left| \hat{\boldsymbol{d}}_{1,0} \right|^2 = N \frac{e^2 \hbar^2}{2m} \overset{(4.8)}{=} \kappa \, 2\hbar\epsilon_0 \omega_0 V. \tag{4.14}$$

The l.h.s. can be associated with the squared coupling strength (4.9) yielding

$$\frac{g^2}{\hbar\Omega} 2\hbar\epsilon_0 \omega_0 V \leq N\hbar\Omega \left| \hat{\boldsymbol{d}}_{1,0} \right|^2. \tag{4.15}$$

Finally, by combines Eqs. (4.14, 4.15) one obtains

$$\frac{g^2}{\hbar\Omega} \leq \kappa, \tag{4.16}$$

which clearly contradicts relation (4.7). However, relation (4.7) needs to be satisfied for the persistence of the superradiant phase transition in the presence of the diamagnetic term. As the TRK sum rule applied onto the generalized Dicke model, Eq. (4.16), originates from generic quantum mechanical and mathematical considerations it is regarded as being irrevocably valid under the applied assumptions. Consequently, it prohibits the occurrence of superradiant critical behavior of the generalized Dicke model in equilibrium. This statement is referred to as the no-go theorem [85–91].

According to Ref. [190] the no-go theorem also prohibits the superradiant quantum phase transition of the finite-N Dicke model in the classical oscillator limit (cf. Subsec. 3.3.2).

In atomic or solid state physics, the TRK sum rule is often also referred to as f-sum rule. As in the discussed example of the no-go theorem, f-sum rules provide a powerful basis when estimating the validity of certain approximations or effective models [99, 204, 205].

4.3   Remarks on the no-go theorem

Even though Dicke superradiance (cf. Sec. 3.2) is not the focus of this thesis, one has to emphasize that the no-go theorem is not restricting the spontaneous superradiant decay. The same holds for critical behavior of driven systems depending on the specific details of the respective setup. Hence, the nonequilibrium superradiant phase transitions [74–79] have been observed experimentally in Bose-Einstein condensates [80–83] and atomic gases [84].

In the following three proposed exceptions of the no-go theorem are introduced. Each of these proposals has risen a controversial discussion addressing mostly quite fundamental aspects of the respective theory. In order to provide some insights into the complexity entailed in the corresponding investigations on superradiance, the corresponding scientific discourses are also briefly touched during the following.

4.3.1   Removal of diamagnetic terms by gauge transformations

There are proposals [88, 89, 198] addressing the validity of the diamagnetic term and hence the no-go theorem on a profound level based on gauge arguments. The main aspect of Refs. [88, 89] concerns an unitary transformation of the classical [88, 89] Hamiltonian of electrodynamics (2.5, 2.6, 2.7) from Coulomb to dipole gauge. The transformation is analogous to the Power-Zienau-Woolley transformation [206] in free space [88, 89] and crucially needs to be applied before the two-level approximation and the restriction to one preferred cavity mode [88, 89]. The striking features of the transformed Hamiltonian can be summarized as follows:

1. After careful examination, the Hamiltonian appears in advantageous manner, as the canonical momenta of the particles is replaced by their kinetic ones yielding gauge invariance to persist the two-level approximation.

2. The diamagnetic contribution to the Hamiltonian is fully compensated by atomic polarization terms appearing in the procedure of transformation.

3. The Coulomb term, appearing in the transformed Hamiltonian, contains also contributions originating from the interaction of the particles with the boundary of the cavity.

If starting from the classical Hamiltonian function [88, 89], the canonical quantization is then similarly achieved as discussed in Subsec. 2.1.2. Finally, the restriction of the quantized Hamiltonian to a two-level description ultimately yields the precise Dicke Hamiltonian $\hat{\mathcal{H}}_{\mathrm{D}}$ which naturally omits a diamagnetic term and thus dissolves the no-go theorem [88, 89]. Hence, within dipole gauge [88, 89] the existence of the superradiant phase transition seems to be naturally possible.

However, the discussion concerning the no-go theorem preventing the superradiant phase transition in the Dicke model is still ongoing as Ref. [207] doubts the validity of this noticeable result regarding the cancellation of the diamagnetic contributions and atomic polarization.

4.3.2 Circuit quantum electrodynamics in Coulomb gauge

Regarding the equilibrium situation without any external driving, there is the proposal of the no-go theorem to be not strictly valid in certain cases of circuit quantum electrodynamics. In particular, Nataf and Ciuti suggest a setup where N Cooper-pair boxes are capacitively coupled to a transmission line resonator [132]. Their considerations are based on an effective model [137] commonly used in the description of systems in the field of circuit quantum electrodynamics. Due to the capacitative coupling, the Cooper-pair occupation of each box can be controlled by a back-gate voltage corresponding to the chemical potential in condensed matter physics. By assuming each box to be occupied by n Cooper-pairs, the authors of Ref. [132] restrict their considerations on the transition between the last occupied and first unoccupied state of each box. Hence, by dropping the information about all other occupied states, the problem is reduced to an effective two-level description of each box. However, as a potential superradiant quantum phase transition does not require resonance and is meant to occur in the ultrastrong coupling regime it is not obvious that a two-level restriction, achieved by dropping all other states of the system, provides a sufficient description of the situation. Though within this approach, a quantum critical point is found in dependence of the Cooper-pair box occupation number n in the thermodynamic limit even in the presence of a diamagnetic contribution [132]. Hence, the equivalent to the condition (4.7) is satisfied. The invalidity of the no-go theorem is drawn back onto the specific properties of the wave functions [132] such that a condition similar to Eq. (4.16) does not hold for the considered system.
This promising result of Nataf and Ciuti [132] has risen a controversial discussion [208–211] regarding the validity of the standard effective model [137] in the required thermodynamic limit. Moreover, the authors of Ref. [208] derive a no-go theorem for the regarded system from first principles similar to the considerations valid for the original Dicke model. Nevertheless, the approach discussed in Ref. [208] ignores the finite occupation of each Cooper-pair box [209] which plays a crucial role in the results of Ref. [132].

4.3.3   Systems with linear dispersion in Coulomb gauge

There is another potential exception to the no-go theorem of the equilibrium superradiant phase transition regarding systems with linear energy-momentum dispersion. From first inspection, these systems naturally go without a diamagnetic term and thus without a no-go theorem even within the principle of minimal coupling. For instance, graphene has a region of pseudo-relativistic dispersion close to the corners of its hexagonal Brillouin zone. By applying an additional magnetic field perpendicular to the graphene flake the energies become discretized into degenerate, non-equidistant Landau levels allowing investigations of optically induced cyclotron transitions [93].

Starting from the full tight-binding Hamiltonian of the system, Hagenmüller and Ciuti demonstrate [93] the existence of quantum critical behavior of Landau-quantized graphene in dependence of the chemical potential. To this end, they expand the full tight-binding Hamiltonian in the region of linear dispersion up to third order. Hence, their approach also includes diamagnetic terms originating from the distortion of the band structure as moving away from the corners of the Brillouin zone.

However, the validity of this promising result was criticized by Ref. [94] where the authors focus on the effective Dirac model for graphene under aspects of linear response theory applied to the limit of vanishing photon energy. Thus, within second-order perturbation theory the authors of Ref. [94] calculate the energy shift induced by interaction between photons and Landau-quantized charge carriers in graphene supposing a finite Fermi level. According to the order of approximation the energy correction is paramagnetic and quadratic in the vector potential hence formally similar to a diamagnetic term but opposite in sign. As the effective Dirac model assumes unbounded linear energy bands, the contribution from the conduction band yields divergence and thus needs to regularized by an ultraviolet cutoff. The paramagnetic energy shift is then dependent on the cutoff. However, a rigid ultraviolet cutoff is known to break gauge invariance in minimal coupling models such that the authors of Ref. [94] "restore" the gauge invariance of their theory by adding the cutoff-dependent energy shift of an undoped valence band to the Hamiltonian *by hand*. According to the electron-hole symmetry of both bands the energy shift is precisely compensated which the authors of Ref. [94] interpret as a proof for the absence of a superradiant quantum phase transition.

The approach of Ref. [94] is considered in Ref. [95] in a mathematically more rigorous manner based on perturbative Schrieffer-Wolff transformations [204, 212–214] up to second order. Thereby an effective generalized Dicke-Hamiltonian is derived which includes dynamically generated diamagnetic contributions. Within the order and the range of validity of this approximation, these terms are found to prohibit a superradiant quantum phase transition [95]. This ansatz is discussed in more detail in Chap. 8 where also an extension of the perturbative Schrieffer-Wolff expansion up to fourth order is provided.

However, as discussed in Part II in more detail, the cutoff-independent value for the critical point obtained within the path integral approach lies beyond the validity of the perturbative ansatz of Ref. [95] even in fourth-order approximation. By contrast, the path integral and the perturbative approach show convincing agreement when regularized with a rigid ultraviolet cutoff.

As already briefly addressed in Subsec. 4.3.1, the restriction of the basis by means of a ultraviolet momentum cutoff violates gauge invariance in Coulomb gauge. In the context of the Dicke model, this issue generates rarely as much confusion as in the context of graphene. However, the technique of cutoff regularization is commonly used when investigating the response of graphene to electromagnetic vector potentials within the effective Dirac model [24, 100–102] even in the derivation of proper f-sum rules for graphene [98, 99]. Moreover, it is also often considered as justified even in the presence of electromagnetic potentials since the band edges of graphene are naturally bounded and hence also the region of linear dispersion is finite. Though it is convenient to apply a rigid ultraviolet cutoff up to order of the band width [24, 98–102], the proper regularization of the Dirac description under these aspects is still a subject of debate [96, 97] and also an issue discussed in this thesis.

In order to contribute to this controversy one needs to be familiar with the graphene specific properties arising from the hexagonal lattice within a tight-binding approach. To this end, the main aspects of the electronic properties of graphene are introduced in the following chapter.

Chapter 5

Graphene

This chapter briefly outlines the most important properties of graphene which are necessary to understand the exceptional properties of this two-dimensional Carbon material. As Carbon is the sixth element of the periodic table, each atom consists of six electrons, where the $1s^2$ shell is completely filled with two electrons. The second shell is partially filled and characterized by the electronic configuration $2s^2 2p^2$ in atomic Carbon. These electrons are available to form covalent bonds to neighboring atoms.

The lattice structure of the two known natural allotropes of Carbon, diamond and graphite or graphene, respectively, can be explained within the concept of hybridization [215] where linear combinations of the atomic orbitals form new hybrid orbitals. These hybrid orbitals differ from the atomic ones in energy, binding angles and binding distances. For instance, by combining the wave functions of three of the four electrons in the second shell one obtains three planar $2sp^2$ hybrid orbitals where the axes along maximal probability are separated by $120°$ from each other. When these hybrid orbitals covalently bind to neighboring $2sp^2$-hybridized Carbon atoms, a hexagonal lattice structure naturally arises. Each remaining electron per atom occupies the $2p_z$ orbital perpendicular to the plane spanned by the $2sp^2$ orbitals and characterizes the electronic properties of the system.

The band structure arising from the $2sp^2$ is obtained within a single-particle tight-binding description based on the properties of the hexagonal lattice as discussed subsequently. The linear dispersion close to the corners of the Brillouin zone follows directly from the band structure and results in the effective single-particle Dirac model for graphene. The discussion of these characteristic properties is provided during this chapter and based on Refs. [23, 216].

Subsequent to the derivation of the effective Dirac model follows the investigation of Landau quantization in the region of linear dispersion based on Ref. [24]. The discussion of the single-particle properties is completed by the consideration of an additional vector potential determining an electromagnetic cavity mode. As dipole approximation is required over the whole range of this thesis a discussion of its validity range is provided. In the end, the complete single-particle Hamiltonian of Landau-quantized graphene interacting with one cavity mode is transformed into a many-body Hamiltonian within second quantization. The resulting Hamiltonian provides then the basis for the discussion of superradiant critical behavior in Part II.

5.1   Lattice properties

Graphene consists of $2sp^2$-hybridized Carbon atoms arranged in a triangular Bravais lattice with a two-atomic basis. As Fig. 5.1 a) illustrates, the Bravais lattice is generated from iterative shifts of the primitive unit cell spanned by the primitive unit vectors

$$\boldsymbol{a}_1 = \begin{pmatrix} a \\ 0 \end{pmatrix}, \quad \boldsymbol{a}_2 = \begin{pmatrix} \frac{a}{2} \\ \frac{\sqrt{3}a}{2} \end{pmatrix}, \tag{5.1}$$

where $a = \sqrt{3}a_{CC}$ denotes the lattice constant of the triangular Bravais lattice and $a_{CC} \approx 1.42\,\text{Å}$ is the Carbon-Carbon binding distance in $2sp^2$ hybridization. The position of each unit cell is then uniquely defined by a Bravais lattice vector,

$$\boldsymbol{R}_i = n_1\boldsymbol{a}_1 + n_2\boldsymbol{a}_2, \quad n_1, n_2 \in \mathbb{Z}. \tag{5.2}$$

Even though both atoms in each unit cell are identical Carbon atoms, one may label them with A and B. The ensemble of all A atoms in the lattice compound form the triangular sublattice A. Similarly, all B atoms form the triangular sublattice B. The position of the A and B Carbon atom with respect to their corresponding unit cell, positioned at $\boldsymbol{R}_i$, is given by [216]

$$\boldsymbol{d}_A = \begin{pmatrix} 0 \\ 0 \end{pmatrix}, \quad \boldsymbol{d}_B = \begin{pmatrix} 0 \\ \frac{a}{\sqrt{3}} \end{pmatrix}. \tag{5.3}$$

Thus the position of each atom in the hexagonal lattice is uniquely defined by the vector $\boldsymbol{R}_i + \boldsymbol{d}_\alpha$, where $\alpha = A, B$. According to the lattice properties of graphene shown in Fig. 5.1 a), each Carbon atom has three nearest neighbors within the Carbon-Carbon binding distance. For instance, the three nearest neighbors of an atom in sublattice A are found at the positions [216]

$$\boldsymbol{\delta}_1 = \begin{pmatrix} 0 \\ \frac{a}{\sqrt{3}} \end{pmatrix}, \quad \boldsymbol{\delta}_2 = \begin{pmatrix} \frac{a}{2} \\ -\frac{a}{2\sqrt{3}} \end{pmatrix}, \quad \boldsymbol{\delta}_3 = \begin{pmatrix} -\frac{a}{2} \\ -\frac{a}{2\sqrt{3}}, \end{pmatrix} \tag{5.4}$$

and belong to sublattice B. Likewise, the three nearest neighbors of one atom in the sublattice B belong to sublattice A and can be found at $-\boldsymbol{\delta}_i$, $i = 1, 2, 3$.

The reciprocal lattice of the triangular Bravais lattice is again triangular and spanned by the reciprocal lattice vectors [216]

$$\boldsymbol{b}_1 = \begin{pmatrix} \frac{2\pi}{a} \\ \frac{2\pi}{\sqrt{3}a} \end{pmatrix}, \quad \boldsymbol{b}_2 = \begin{pmatrix} 0 \\ \frac{4\pi}{\sqrt{3}a} \end{pmatrix}. \tag{5.5}$$

By constructing the Wigner-Seitz cell of the reciprocal lattice one finds the first Brillouin zone of graphene which is illustrated in Fig. 5.1 b). The hexagonal shape of the first Brillouin zone solely originates from the lattice structure of the underlying Bravais lattice and is independent of the number of atoms per unit cell [216]. Furthermore, any vector in reciprocal space is defined as a sum of multiples of $\boldsymbol{b}_1$ and $\boldsymbol{b}_2$. Hence, four of the six corners of the first Brillouin can be mapped onto only two inequivalent corners which
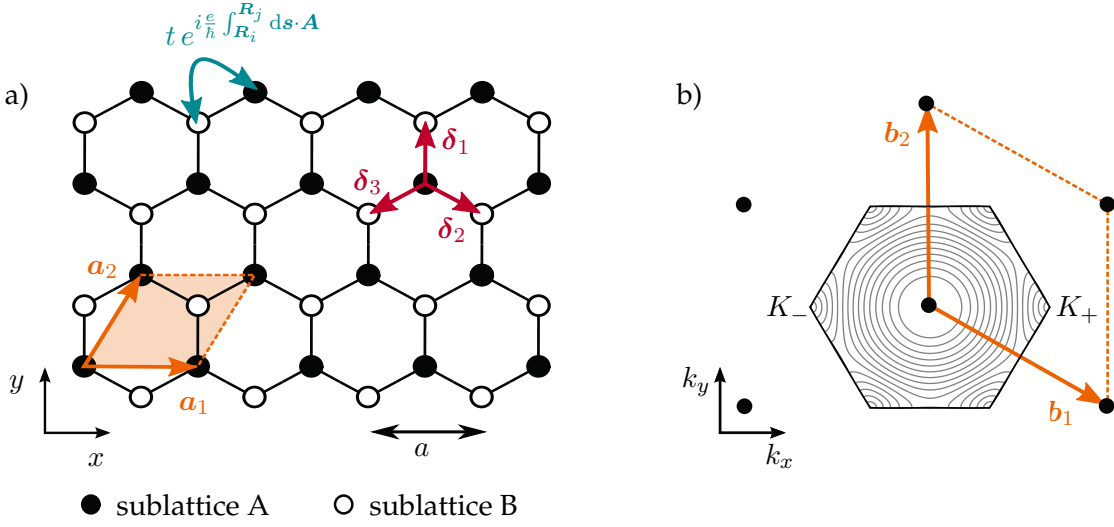
FIGURE 5.1: Inspired by Refs. [23, 216]. Panel a) sketches a small flake of graphene in the x-y plane. The hexagonal lattice structure is composed from a triangular unit cell (orange shaded region) spanned by the lattice vectors $\boldsymbol{a}_1$ and $\boldsymbol{a}_2$ and the two-atomic basis A and B. Each carbon atom has three nearest neighbors found in the direction of each $\boldsymbol{\delta}_i$ with respect to the sublattice A. The lattice constant $a = \sqrt{3}a_{\mathrm{CC}}$, where $a_{\mathrm{CC}} \approx 1.42\,\text{Å}$ is carbon-carbon binding length in $2sp^2$ hybridization. The presence of electromagnetic vector potentials modifies the hopping parameter by means of the Peierls substitution. Panel b) illustrates the reciprocal lattice spanned by the lattice vectors $\boldsymbol{b}_1$ and $\boldsymbol{b}_2$ along with the first hexagonal Brillouin zone where equipotential lines of the band structure are marked.

are often denoted as the K- and K'-point. By introducing the valley index $\tau = \pm 1$, the location of these points can be chosen, for instance, at [216]

$$\boldsymbol{K}_\tau = \begin{pmatrix} \tau\frac{4\pi}{3a} \\ 0 \end{pmatrix}, \tag{5.6}$$

as shown in Fig. 5.2 b). For convenience, the K-point shall be associated with $\tau = +1$ whereas the $\tau = -1$ denotes the K' point. Furthermore, the term valley index stems from the valley-like shape of the band structure in the vicinity of the K- and K'-point as it can be seen from Fig. 5.2.

5.2 Single-particle tight-binding Hamiltonian and the effective Dirac model

According to the electronic configuration of Carbon in $2sp^2$ hybridization there are three of the four electrons of the second atomic shell participating in the covalent bonds with neighboring atoms. The remaining electron occupies the $2p_z$ and dominates the electronic properties of the material. The tight-binding model for graphene is therefore a theory of the dynamics of the $2p_z$ electrons and thus derived as a mean-field description [217] of

the most general single-particle Hamiltonian

$$\hat{H} = \frac{\hat{\boldsymbol{p}}^2}{2m} + V_{\text{eff}}(\hat{\boldsymbol{x}}) + V_{\text{ext}}(\hat{\boldsymbol{x}}). \tag{5.7}$$

The effective potential V_{eff} stems from the underlying lattice including the atomic cores and bounded electrons as well as interactions among them [216]. All external potentials applied to the system are summarized in V_{ext}.

The main aspect of the development of a single-particle tight-binding model is due to the assumption of the electrons being rather tightly bound to the atomic core. Therefore, the orbital of the electrons roughly coincide with the atomic orbitals where a finite overlap of corresponding neighboring sites is taken into account. Thus, the expansion of $\hat{H}$ into a local basis of each $2p_z$ electron according to the properties of the underlying lattice is a suitable ansatz in this case. The wave functions of neighboring $2p_z$ electrons are assumed to overlap and the amount of energy needed to change from one site to another one is quantified by the corresponding matrix element which is referred to as a hopping parameter.

According to the lattice properties of graphene, each electron in a $2p_z$ orbital is characterized by the two position labels, i and α, and the spin quantum number s. This is summarized by the state vector $|i, \alpha, s\rangle$. As spin interactions are not particularly considered during this thesis, one may abbreviate the state vector with $|i, \alpha\rangle$ and account for the spin degree by means of a two-fold degeneracy of each state. Thus, the expansion of the single-particle Hamiltonian into the states $|i, \alpha\rangle$ yields [216]

$$\hat{H}_{\text{TB}} = \sum_{i,\alpha;j,\beta} t_{i,\alpha;j,\beta} \, |i, \alpha\rangle \, \langle j, \beta| \, , \tag{5.8}$$

where the matrix element $t_{i,\alpha;j,\beta} = \langle j, \beta|\hat{H}_{\text{TB}}|i, \alpha\rangle$ is defined as [4, 216]

$$t_{i,\alpha;j,\beta} = \begin{cases} V_i + M_i, & \text{if } i = j, \alpha = \beta = \text{A}, \\ V_i - M_i, & \text{if } i = j, \alpha = \beta = \text{B}, \\ -t, & \text{if } i, \alpha \text{ and } j, \beta \text{ are nearest neighbors}. \end{cases} \tag{5.9}$$

in nearest-neighbor approximation. Note that this result corresponds to the spin-less case in accordance with Ref. [216]. The on-site potentials V_i and M_i in Eq. (5.9) arise from the external potential V_{ext}. Thereby V_i denotes a potential which is constant or slowly varying on the inter-atomic scale. By contrast, M_i is referred to as a staggered potential and takes rapidly varying contributions of V_{ext} into account. A staggered potential is typically expected when the graphene flake is placed onto a substrate which breaks the symmetry between both sublattices [218]. Furthermore, in the absence of external potentials V_i and M_i are zero.

The matrix element of nearest-neighbor states is referred to as the hopping parameter and assumes the value $t = 2.7\,e\text{V}$ [219, 220].

The aim of the following is to calculate the band structure arising from the tight-binding

Hamiltonian $\hat{H}_{\text{TB}}$. This is most conveniently achieved by introducing the set of orthonormal tight-binding sums [4, 221]

$$|\Phi_\alpha(\boldsymbol{k})\rangle = \frac{1}{\sqrt{N_{\text{C}}}} \sum_{\boldsymbol{R}_i} e^{i\boldsymbol{k}\cdot(\boldsymbol{R}_i+\boldsymbol{d}_\alpha)} |i,\alpha\rangle, \quad \langle\Phi_\alpha(\boldsymbol{k})|\Phi_\beta(\boldsymbol{k}')\rangle = \delta_{\alpha,\beta}\delta_{\boldsymbol{k},\boldsymbol{k}'}, \tag{5.10}$$

where $\alpha = \text{A}, \text{B}$ and N_{C} denotes the number of unit cells assembling the graphene flake. As $|\Phi_\alpha(\boldsymbol{k})\rangle$ is a periodic function of the lattice points it satisfies the Bloch theorem [216]. Hence, $\boldsymbol{k}$ is associated with the Bloch vector. Along with this and the ansatz

$$|\varphi(\boldsymbol{k})\rangle = \varphi_{\text{A}}(\boldsymbol{k})\,|\Phi_{\text{A}}(\boldsymbol{k})\rangle + \varphi_{\text{B}}(\boldsymbol{k})\,|\Phi_{\text{B}}(\boldsymbol{k})\rangle, \tag{5.11}$$

the diagonalization of $\hat{H}_{\text{TB}}$ is reduced to an eigenproblem of the coefficient or envelope functions $\varphi_\alpha(\boldsymbol{k})$, $\alpha = \text{A}, \text{B}$. The eigenvalue equation for envelope function can then be written as [216]

$$H(\boldsymbol{k})\begin{pmatrix}\varphi_{\text{A}}(\boldsymbol{k})\\\varphi_{\text{B}}(\boldsymbol{k})\end{pmatrix} = \begin{pmatrix}H_{\text{AA}}(\boldsymbol{k}) & H_{\text{AB}}(\boldsymbol{k})\\H_{\text{BA}}(\boldsymbol{k}) & H_{\text{BB}}(\boldsymbol{k})\end{pmatrix}\begin{pmatrix}\varphi_{\text{A}}(\boldsymbol{k})\\\varphi_{\text{B}}(\boldsymbol{k})\end{pmatrix} = E(\boldsymbol{k})\begin{pmatrix}\varphi_{\text{A}}(\boldsymbol{k})\\\varphi_{\text{B}}(\boldsymbol{k})\end{pmatrix}, \tag{5.12}$$

where the matrix elements $H_{\alpha\beta}(\boldsymbol{k}) = \langle\Phi_\alpha(\boldsymbol{k})|\hat{H}_{\text{TB}}|\Phi_\beta(\boldsymbol{k})\rangle$ are obtained from Eq. (5.9). The 2×2-matrix representation of the effective eigenvalue problem, Eq. (5.12), naturally arises from the two-atomic basis A and B of the triangular Bravais lattice. The evalua-
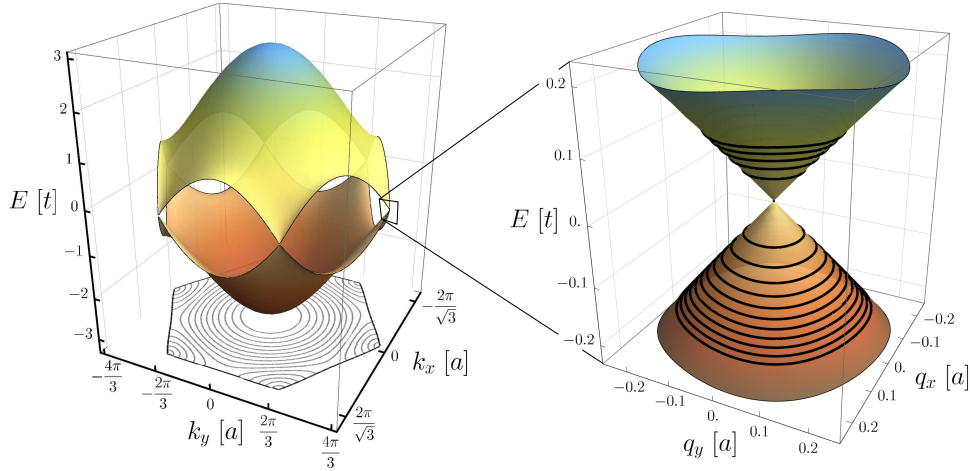
FIGURE 5.2: Inspired by Ref. [23, 216]: Band structure of the $2p_z$-orbital envelope functions φ_α of bulk graphene in the first Brillouin zone in nearest-neighbor hopping approximation according to Eq. (5.15). No external potentials were considered, i.e. $M = V_0 = 0$. Without external potentials or doping the valence band is completely filled whereas the conduction band is empty. At the corners of the hexagonal Brillouin zone valence and conduction band touch each other. The band structure is linear in the vicinity of these points as the inset on the r.h.s. shows. In this region of the band structure the dynamics of charge carriers is determined by an effective Dirac Hamiltonian. The black lines mark non-equidistant Landau levels matched to the Dirac cone.

tion of $H(\boldsymbol{k})$ is proceeded under the assumption of uniform external potentials, $V_i = V_0$

and $M_i = M \; \forall i = 1, \cdots, N_C$. Then one finds for the matrix elements $H_{\alpha\beta}(\boldsymbol{k})$ in particular [216]

$$\langle \Phi_A(\boldsymbol{k}) | \hat{H}_{TB} | \Phi_A(\boldsymbol{k}) \rangle = V_0 + M, \qquad \langle \Phi_A(\boldsymbol{k}) | \hat{H}_{TB} | \Phi_B(\boldsymbol{k}) \rangle = -t \sum_{i=1}^{3} e^{i\boldsymbol{k}\cdot\boldsymbol{\delta}_i},$$

$$\langle \Phi_B(\boldsymbol{k}) | \hat{H}_{TB} | \Phi_A(\boldsymbol{k}) \rangle = -t \sum_{i=1}^{3} e^{-i\boldsymbol{k}\cdot\boldsymbol{\delta}_i}, \quad \langle \Phi_B(\boldsymbol{k}) | \hat{H}_{TB} | \Phi_B(\boldsymbol{k}) \rangle = V_0 - M, \tag{5.13}$$

so that the 2×2 Hermitian matrix $H(\boldsymbol{k})$ in Eq. (5.12) takes the following form [216]

$$H(\boldsymbol{k}) = V_0 \, \sigma_0 + M \, \sigma_z - t \left[\left(\sum_{i=1}^{3} \cos(\boldsymbol{k} \cdot \boldsymbol{\delta}_i) \right) \sigma_x - \left(\sum_{i=1}^{3} \sin(\boldsymbol{k} \cdot \boldsymbol{\delta}_i) \right) \sigma_y \right]. \tag{5.14}$$

Thereby σ_i, $i = x, y, z$ denote Pauli matrices as defined in Eq. (3.1). As the Pauli matrices are often associated with the description of a spin-1/2 system, σ_i, $i = x, y, z$ in $H(\boldsymbol{k})$ is referred to as the pseudo-spin degree of freedom which emerges from the two-atomic basis A and B. In the terminology of pseudos-spins $(\varphi_A, \varphi_B)^T$ is referred to as a two-component pseudo-spinor.

By solving the eigenproblem (5.12), the energy dispersion $E(\boldsymbol{k})$ is straightforwardly found from diagonalization of Eq. (5.14):

$$E_{\pm}(\boldsymbol{k}) = V_0 \pm \sqrt{M^2 + t^2 \left[3 + 2\cos(k_x a) + 4\cos\left(\frac{k_x a}{2}\right) \cos\left(\frac{\sqrt{3}k_y a}{2}\right) \right]}. \tag{5.15}$$

The negative and positive sign refers to the valence and conduction band, respectively. The band structure determined by Eq. (5.15) is illustrated in Fig. 5.2 for $V_{ext} = 0$. This result is in convincing agreement with experimental measurements [222].

As staggered potentials are not relevant for the scope of this thesis, M is set zero during the following. By contrast, V_0 is associated with back-gate voltage tuning the Fermi level and thus it is kept non-zero. For $V_0 = 0$, as shown in Fig. 5.2, the valence band is completely filled whereas the conduction band is empty. If a non-zero potential V_0 is considered, the band structure will be accordingly shifted in energy.

5.2.1 Effective Dirac model for low-energy excitations

Close to the corners of the Brillouin zone, both bands form valleys from either direction and touch precisely at the K- and K'-point. This can also be seen from Fig 5.2. The dispersion is approximately linear in the vicinity of the touching points Thus, from the expansion of $E_{\pm}(\boldsymbol{k})$ around $\boldsymbol{K}_{\pm}$ one finds [4]:

$$E_{\pm}(\boldsymbol{K}_\tau + \boldsymbol{q}) \approx V_0 \pm \hbar v_F |\boldsymbol{q}|, \tag{5.16}$$

which is valid up to $|E_\pm| \lesssim 0.7\,t$ [223]. For larger energies the shape of the valleys trigonally warp such that higher orders of the expansion around $\boldsymbol{K}_\tau$ should be considered [23, 24]. The trigonal warping of the valleys can also be seen in the density plots in Figs. 5.1 b), 5.2 and the tight-binding simulation discussed in Part II.

As $E_\pm(\boldsymbol{K}_\tau + \boldsymbol{q})$ is reminiscent of the dispersion of a relativistic particle with zero rest mass and constant velocity $v_{\mathrm{F}} = \sqrt{3}at/(2\hbar) \approx 10^6\,\mathrm{m/s}$, one refers to low-energy excitations around the K- and K'-point as massless pseudo-relativistically Dirac fermions. Therefore, the valleys close to the K- and K'-point are also often called Dirac cones. The dynamics of the low-energy excitations is determined from a massless Dirac equation in either valley which is obtained from the expansion of Eq. (5.14) around $\boldsymbol{K}_\pm$ [216]:

$$H_\tau(\boldsymbol{q}) = H(\boldsymbol{K}_\tau + \boldsymbol{q}) \approx V_0\sigma_0 + \hbar v_{\mathrm{F}} \left(\tau\sigma_x q_x + \sigma_y q_y\right). \tag{5.17}$$

This mapping was first recognized by DiVincenzo and Mele [6] as well as Semenoff [7] in 1984. In the notation applied to Eq. (5.17) the valley degree of freedom, τ, additionally spans a two-dimensional subspace and thus can be associated with a set of Pauli matrices τ_i, $i = x, y, z$, and the unit matrix τ_0. Accordingly, the 2×2 Dirac equation (5.17) in either valley can be gathered into a 4×4 Dirac equation which simultaneously accounts for the contributions from both valleys:

$$\hat{H}' = v_{\mathrm{F}} \left(\tau_z \otimes \sigma_x \hat{p}_x + \tau_0 \otimes \sigma_y \hat{p}_y\right), \tag{5.18}$$

where $\hat{p}_i = \hbar\hat{q}_i$, for $i = x, y$. Accordingly, the wave function can be written in terms of a four-component pseudo-spinor

$$\Phi' = \begin{pmatrix} \varphi_{\mathrm{A}} & \varphi_{\mathrm{B}} & \varphi'_{\mathrm{A}} & \varphi'_{\mathrm{B}} \end{pmatrix}^T, \tag{5.19}$$

where φ_α and φ'_α, $\alpha = \mathrm{A, B}$, refers to the K- and K'-point, respectively. This valley-anisotropic form of the effective Dirac description can be transformed into a valley-isotropic representation [224],

$$\hat{H} = \hat{U}\hat{H}'\hat{U}^\dagger = v_{\mathrm{F}}\,\tau_0 \otimes \boldsymbol{\sigma} \cdot \hat{\boldsymbol{p}}, \tag{5.20}$$

under application of the unitary transformation

$$\hat{U} = \frac{\tau_0 + \tau_z}{2} \otimes \sigma_0 - i\frac{\tau_0 - \tau_z}{2} \otimes \sigma_y. \tag{5.21}$$

Thereby, the vector notation $\boldsymbol{\sigma} = (\sigma_x, \sigma_y)^T$ and $\hat{\boldsymbol{p}} = (\hat{p}_x, \hat{p}_y)^T$ was used. The valley-isotropic equivalent of wave function Φ' is given by

$$\Phi = \hat{U}\Phi' = \begin{pmatrix} \varphi_{\mathrm{A}} & \varphi_{\mathrm{B}} & -\varphi'_{\mathrm{B}} & \varphi'_{\mathrm{A}} \end{pmatrix}^T. \tag{5.22}$$

The valley-isotropic representation will be the preferred one during this thesis.

5.2.2   Landau-level quantization in the effective Dirac model

In this section the effect of an uniform magnetic field which is applied perpendicular to the graphene plane is investigated within the effective Dirac model. For convenience, the graphene flake is assumed to lie in the x-y-plane. Throughout this thesis, the vector potential determining the magnetic field is chosen in Landau gauge,

$$\boldsymbol{A}_0(\boldsymbol{r}) = -By\boldsymbol{e}_x \quad \Leftrightarrow \quad \boldsymbol{B} = \nabla \times \boldsymbol{A}_0(\boldsymbol{r}) = B\boldsymbol{e}_z, \tag{5.23}$$

where $\boldsymbol{e}_i$ denotes the unit vector in i-direction.

In the effective Dirac model the coupling between the uniform perpendicular magnetic field (5.23) and the electronic degree of freedom is accomplished by means of minimal coupling, Eq (2.27). Thereby the kinetic momentum $\hat{\boldsymbol{p}}$ is substituted by the canonical momentum [119]:

$$\hat{\boldsymbol{p}} \mapsto \hat{\boldsymbol{\Pi}}_0 = \hat{\boldsymbol{p}} + e\hat{\boldsymbol{A}}_0. \tag{5.24}$$

The Hamiltonian (5.20) transforms then according to

$$\hat{H} \mapsto \hat{H}_0 = v_{\mathrm{F}}\, \tau_0 \otimes \boldsymbol{\sigma} \cdot \hat{\boldsymbol{\Pi}}_0. \tag{5.25}$$

The diagonalization of $\hat{H}_0$ yields the characteristic Landau levels of graphene [24, 225]:

$$\epsilon_{\lambda,n} = \lambda\, \hbar\omega_c\, \sqrt{n} \propto \sqrt{B}\sqrt{n}, \tag{5.26}$$

where $n \in \mathbb{N}_0$ denotes the Landau level index. The cyclotron frequency is defined as

$$\omega_c = \sqrt{2}\frac{v_{\mathrm{F}}}{l_B}, \quad l_B = \sqrt{\frac{\hbar}{eB}}, \tag{5.27}$$

where l_B denotes the magnetic length. The $\sqrt{B}$-proportionality of ω_c as well as the $\sqrt{n}$-scaling behavior of the eigenenergies reflect the pseudo-relativistic character of the quasi-particle dynamics close to the K- and K'-point and is depicted in Fig. 6.1.

For convenience, the collective index $N = (\lambda, n)$ is introduced along with the following convention:

$$\begin{aligned} N = (+1, n) &\quad \text{denotes a conduction band state and} \\ -N = (-1, n) &\quad \text{refers to a valence band state.} \end{aligned} \tag{5.28}$$

Within this notation, one obtains the eigenstate of $\hat{H}_0$, Eq. (5.25), in form of a four-component spinor,

$$\Phi_{N,k}(\boldsymbol{r}) = \begin{pmatrix} \Psi^{+1}_{N,k}(\boldsymbol{r}) \\ \Psi^{-1}_{N,k}(\boldsymbol{r}) \end{pmatrix}, \quad \Psi^{\tau}_{N,k}(\boldsymbol{r}) = \langle \boldsymbol{r}|N,k\rangle_{\tau}, \tag{5.29}$$

where the two-component spinor in either valley is given by [24, 225]

$$|N, k\rangle_\tau = \frac{1}{\sqrt{2}} \begin{pmatrix} w_{-,n} |n - 1, k\rangle \\ \lambda\, w_{+,n} |n, k\rangle \end{pmatrix}. \tag{5.30}$$

Note that each component of $|N, k\rangle_\tau$ denotes a wave function in the respective sublattice A and B according to the generic definition (5.22) in valley-isotropic representation. The position-space representation of each sublattice contribution $|m, k\rangle$, where $m = n - 1, n$, is identical to an eigenfunction of the quantum harmonic oscillator [119] in y-direction and a free wave in x-direction:

$$\langle \boldsymbol{r} | m, k\rangle = \frac{e^{ikx}}{\sqrt{L}} \frac{e^{-\zeta^2/2}}{\sqrt{2^m m!}} \mathrm{H}_m(\zeta), \quad \zeta = y - l_B^2 k. \tag{5.31}$$

Thereby, $\mathrm{H}_m(\zeta)$ denotes the mth Hermite polynomial [203] and L refers to the spacial extension of the graphene flake in x- and y-direction. Accordingly, the two-component spinors form a complete set of orthonormalized eigenstates, $\{|N, k\rangle_\tau\, | \lambda = \pm 1, n \in \mathbb{N}_0, k = 1, ..., \mathcal{N}, \tau = \pm 1\}$, in the corresponding valley subspace τ of $\hat{H}_0$, Eq. (5.25). Furthermore, the prefactors entering each sublattice contribution in Eq. (5.30),

$$w_{\pm,n} = \sqrt{1 \pm \delta_{n,0}}, \tag{5.32}$$

ensure the correct normalization of the zeroth Landau level wave function [24, 225].

Different from the eigenenergies ϵ_N (5.26) the two- and four-component spinors, Eqs. (5.29, 5.30), depend on the quantum number k. According to the chosen gauge, the quantum number $k = 1, \dots, \mathcal{N}$, describes the eigenvalues of the magnetic translation operator $\hat{T}_x$ in x-direction and is a conserved quantity [226]. From the k-independence of the energy spectrum (5.26) follows the $\mathcal{N}$-fold degeneracy of each Landau level. The degeneracy $\mathcal{N}$ is thereby proportional to the flux trough the system and thus tunable. In particular, from generic phase space arguments [227, 228] and Bohr-Sommerfeld quantization [229] follows:

$$\mathcal{N} = g_\mathrm{s} g_\mathrm{v} \frac{S}{(2\pi l_B^2)} = g_\mathrm{s} g_\mathrm{v} \frac{S}{a^2} \varphi_0^2, \tag{5.33}$$

where $S = L^2$ represents the area of the flake and

$$\varphi_0 = \frac{a}{\sqrt{2\pi} l_B} \quad \Leftrightarrow \quad \varphi = \frac{S}{a^2} \varphi_0 \tag{5.34}$$

denotes the flux through one unit cell. Similarly, φ as defined on the r.h.s. of Eq. (5.34) denotes the total flux through the system.

Besides the each two-fold spin- and valley-degeneracy, $g_\mathrm{s} = g_\mathrm{v} = 2$, the degeneracy of each Landau level is similar in the case of an ordinary two-dimensional electron gas. Note that the valley degeneracy, g_v, only needs to be explicitly taken into account in the absence of inter-valley scattering processes.

In the following, the effect of an additional electromagnetic vector potential is investigated within the effective Dirac model.

5.2.3   Single-particle light-matter interaction Hamiltonian

In this subsection, the coupling of Landau-quantized charge carriers with a single cavity mode is discussed. To this end, the vector potential $\hat{\boldsymbol{A}}_{\mathrm{em}}$ of the electromagnetic mode is introduced. Similar to the quantizing vector potential in Landau gauge, $\hat{\boldsymbol{A}}_0$, the interaction enters the effective Dirac Hamiltonian by means of minimal coupling [119]. Therefore, the canonical momentum $\hat{\boldsymbol{\Pi}}_0$, Eq. (5.24), is modified in the following way:

$$\hat{\boldsymbol{\Pi}}_0 \mapsto \hat{\boldsymbol{\Pi}}' = \hat{\boldsymbol{\Pi}}_0 + e\hat{\boldsymbol{A}}_{\mathrm{em}}(\hat{\boldsymbol{r}}). \tag{5.35}$$

Likewise, the effective Dirac Hamiltonian $\hat{H}$, defined in Eq. (5.20), decomposes according to

$$\hat{H} \mapsto \hat{H}_0 + \hat{H}_{\mathrm{i}}, \qquad \hat{H}_{\mathrm{i}} = v_{\mathrm{F}} e\, \tau_0 \otimes \boldsymbol{\sigma} \cdot \hat{\boldsymbol{A}}_{\mathrm{em}}(\hat{\boldsymbol{r}}), \tag{5.36}$$

where $\hat{H}_0$ is given by Eq. (5.25) The contribution $\hat{H}_{\mathrm{i}}$ encodes then the interaction of a single Dirac fermion with the radiation field and is discussed during the following.

Similar as for the Dicke model and in accordance with Refs. [93–95], the electromagnetic vector potential is considered within dipole approximation. Hence any spacial variance of the cavity mode is neglected, i.e.

$$\hat{\boldsymbol{A}}_{\mathrm{cav}}(\hat{\boldsymbol{r}}) \approx \hat{\boldsymbol{A}}_{\mathrm{em}} = \sqrt{\frac{\hbar}{2\omega_0 \epsilon V}}\, \boldsymbol{e}_{\mathrm{em}}(\hat{a} + \hat{a}^\dagger), \tag{5.37}$$

where $\epsilon = \epsilon_0 \epsilon_{\mathrm{r}}$. Thereby ϵ_0 denotes the vacuum permittivity and ϵ_{r} is the dimensionless relative permittivity of a dielectric medium inside the cavity. If not stated different, $\epsilon_{\mathrm{r}} = 1$ will be assumed during this thesis.

The application of dipole approximation is in accordance with the literature [93–95] and also fairly justified as it is seen from the following:
Suppose the frequency of the cavity mode to be given by $\omega_0 = s\omega_c$, where $s > 0$ is a dimensionless scaling factor and ω_c denotes the cyclotron frequency of graphene (5.27). Without a dielectric medium the wavelength of the lowest cavity excitation is then given by $\lambda = 2\pi c/\omega_0$, where c refers to the speed of light. Furthermore, the typical length scales of the charge carriers in Landau-quantized graphene are determined by the lattice constant a and the magnetic length l_B, Eq. (5.27). Hence, the condition

$$1 \ll \frac{\sqrt{\pi}c}{s v_{\mathrm{F}}} \approx \frac{600}{s} \tag{5.38}$$

accounts for the validity of the dipole approximation. As $s \leq 1$ for any inter-band transition frequency, the inequality (5.38) is certainly fulfilled in this case. In accordance with Refs. [94, 95], the polarization direction of the electromagnetic mode shall be chosen along x-direction, $\boldsymbol{e}_{\mathrm{em}} = \boldsymbol{e}_x$, and the spacial extension of the cavity in x- and y-direction are assumed to coincide with those of the graphene sample. The volume of the cavity is then given by $V = S \cdot L_z$, where it is assumed that $L_z \ll L$.

Furthermore, the time-independent appearance of $\hat{\boldsymbol{A}}_{\mathrm{em}}$ in Eq. (5.37) refers to the Schrödinger picture which is exclusively preferred during this thesis. Nevertheless, one can easily transform this time-independent representation into a time-dependent one by means of an unitary transformation as discussed in App. B.

The bosonic ladder operators $\hat{a}$ and $\hat{a}^\dagger$ annihilate and create photonic quanta with frequency $\omega_0 = \pi c/(\sqrt{\epsilon_{\mathrm{r}}} L_z)$ in the cavity. Further details on the canonical quantization of the electromagnetic field can be found in Chap. 2. Furthermore, one finds a discussion about the properties of the bosonic creation and annihilation operators, $\hat{a}^\dagger$ and $\hat{a}$, in App. C.

Adopting the previously discussed steps, the interaction Hamiltonian $\hat{H}_{\mathrm{i}}$ particularizes accordingly,

$$\hat{H}_{\mathrm{i}} = 2\frac{g}{\sqrt{\mathcal{N}}}(\hat{a} + \hat{a}^\dagger)\,\tau_0 \otimes \sigma_x, \tag{5.39}$$

with the coupling parameter g defined as

$$g = \frac{\sqrt{\mathcal{N}}}{2}v_{\mathrm{F}}e\mathcal{A}_0 = \hbar\omega_c\sqrt{\frac{\alpha}{2\pi\sqrt{\epsilon_{\mathrm{r}}}}} \approx 0.0341\,\epsilon_{\mathrm{r}}^{-\frac{1}{4}}\,\hbar\omega_c \tag{5.40}$$

and in accordance with the literature [93–95].. Thereby, $\alpha = e^2/(4\pi\epsilon_0\hbar c) \approx 1/137$ denotes the fine-structure constant. Note that the Landau-level degeneracy $\mathcal{N}$ now takes the role of the number of two-level atoms, N, in the original Dicke model (cf. Chap. 3). Within this particular definition of g, Eq. (5.40), the factor of 2 in Eq. (5.39) is precisely compensated by the normalization factor in the definition of the two-component Landau-quantized spinor when $\hat{H}_{\mathrm{i}}$ is transformed into its many-body equivalent. This corresponds to g quantifying the coupling strength of the interaction of precisely one Dirac fermion with the cavity mode. Similar as for an ordinary system with parabolic dispersion (cf. Chap. 2) the coupling strength is determined by the properties of the electronic and photonic subsystem and thus it is not tunable arbitrarily. Nevertheless, the coupling strength will be varied for the analysis of the critical behavior during this thesis. To this end, g_{r} shall denote the actual coupling strength as obtained from Eq. (5.40) and g refers to a tunable parameter. Hence, any critical coupling strength g_c extracted for the variable g from the considerations in Part II will be compared to the actual coupling strength g_{r} in order to estimate the actual feasibility of the critical behavior in equilibrium.

Summarizing, the total Hamiltonian describing a Landau-quantized particle interacting with a single cavity mode is given by

$$\hat{H} = \hat{H}_{\mathrm{cav}} + \hat{H}_0 + \hat{H}_{\mathrm{i}}, \qquad \hat{H}_{\mathrm{cav}} = \hbar\omega\,\hat{a}^\dagger\hat{a}, \tag{5.41}$$

where $\hat{H}_0$ and $\hat{H}_{\mathrm{i}}$ are defined in Eq. (5.25) and Eq. (5.39), respectively. The operator $\hat{H}_{\mathrm{cav}}$ describes the energetic properties of the radiation field similar to a quantum harmonic oscillator (cf. Chap. 2). For $g \neq 0$, the eigenbasis of the total Hamiltonian $\hat{H}$ is given by dressed states [230] which differs from the common eigenbasis of $\hat{H}_{\mathrm{cav}}$ and $\hat{H}_0$. The latter is given by the product basis $\{|a\rangle \otimes |N, k\rangle_\tau\}$ in either valley.

Both single-particle Dirac operators, $\hat{H}_0$ and $\hat{H}_i$, are isotropic in the valley degree of freedom and no further valley-scattering processes are considered during this thesis. Therefore, the tensor products between valley and pseudo-spin space in Eqs. (5.25, 5.39) are dropped such that $\hat{H}_0$ and $\hat{H}_i$ reduce from an each 4×4 to an each 2×2 Dirac operator. Likewise, the eigenbasis of the reduced operator $\hat{H}_0$ is given by the set of two-component spinors $\{|N, k\rangle\}$ according to Eq. (5.30). The Landau level degeneracy $\mathcal{N}$ accounts then for the valley degree of freedom as already anticipated in Eq. (5.33).

5.3 Many-body Hamiltonian for the effective Dirac model

In order to study collective effects due to the correlated interaction of Landau-quantized fermionic charge carriers with a radiation mode, it is convenient to translate the first-quantized Hamiltonian $\hat{H}$ into a many-body operator $\hat{\mathcal{H}}$. Preferably, the formalism of *second quantization* accomplishes this scope in the most comprehensive way. Thereby the resulting Hamiltonian naturally accounts for the indistinguishability and symmetry of the considered fermionic and bosonic particles species according to anti-commutation and commutation relations of the respective particle creating and annihilating operators.

As discussed in Subsec. 2.5 of App. C, the fermionic many-body equivalent of the single-particle Hamiltonian $\hat{H}$, Eq. (5.41), is obtained from the following expression

$$\hat{\mathcal{H}} = \sum_{N,k} \sum_{N',k'} \hat{c}^\dagger_{N,k} \langle N, k|\hat{H}|N', k'\rangle \hat{c}_{N',k'}, \tag{5.42}$$

where the matrix elements $\langle N, k|\hat{H}|N', k'\rangle$ are defined in the basis of the two-component spinors, Eq. (5.30). The summation over the valley-degeneracy is encoded in k, k' which assume the values $k, k' = 1, \ldots, \mathcal{N}$, with $\mathcal{N}$ denoting the Landau-level degeneracy according to Eq. (5.33). The summation over collective indices N, N', as defined in Eq. (5.28), is carried out over infinitely extended linear bands. This artifact of the effective Dirac model yields divergence of contributions which arise from the valence band. Thus, a proper regularization is required when investigating the partition sum as discussed in Part II in more detail.

The fermionic creation and annihilation operators introduced in Eq. (5.42), $\hat{c}^\dagger_{N,k}$ and $\hat{c}_{N',k'}$, obey the anti-commutation relations

$$\left\{\hat{c}_{N,k}, \hat{c}^\dagger_{N',k'}\right\} = \delta_{\lambda,\lambda'}\delta_{n,n'}\delta_{k,k'}, \quad \left\{\hat{c}_{N,k}, \hat{c}_{N',k'}\right\} = \left\{\hat{c}'_{N,k}, \hat{c}^\dagger_{N',k'}\right\} = 0, \tag{5.43}$$

as discussed in App. C in more detail. With this it is straightforward to obtain the many-body equivalent of the total single-particle Hamiltonian, Eq. (5.41):

$$\hat{\mathcal{H}} = \hat{\mathcal{H}}_{\text{cav}} + \hat{\mathcal{H}}_0 + \hat{\mathcal{H}}_i, \tag{5.44}$$

where $\hat{\mathcal{H}}_{\text{cav}}$ is identical to $\hat{H}_{\text{cav}}$, i.e.

$$\hat{\mathcal{H}}_{\text{cav}} = \hbar\omega\,\hat{a}^\dagger\hat{a}. \tag{5.45}$$

The second term in Eq. (5.44) describes the kinetic part of the Landau-quantized many-
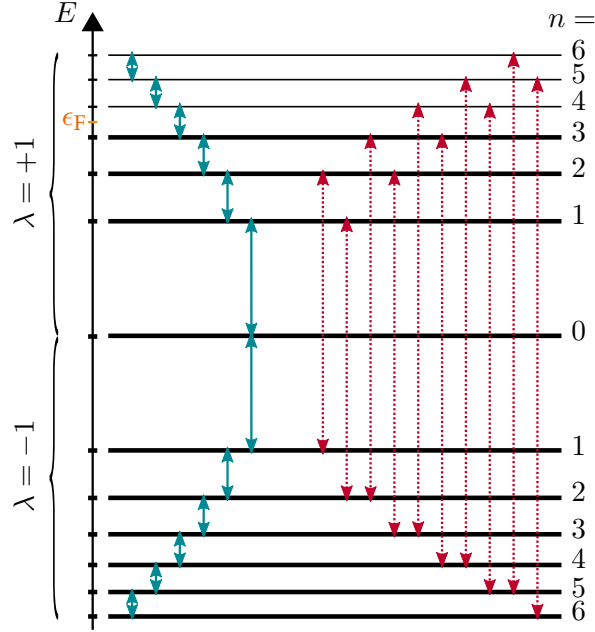
FIGURE 5.3: Illustration of optical transitions captured by the interaction Hamiltonian $\hat{\mathcal{H}}_i$ according to Eqs. (5.47, 5.48). Each arrow represents a dipole allowed optical transition between two Landau levels, i.e. $\Delta n = \pm 1$ independent on the band indices λ and λ' of initial and final state. One distinguishes between intra-band (solid, blue) and inter-band (dotted, red) transitions. In case of intra-band or cyclotron excitations initial and final state are both found within either the valence band ($\lambda = -1$) or the conduction band ($\lambda = +1$). An inter-band transition optically couples a state within the valence band with one lying in the conduction band. Each energy level below the Fermi level ϵ_F is occupied by $\mathcal{N}$ electrons.

body system:

$$\hat{\mathcal{H}}_0 = \sum_{N,k} \epsilon_N \hat{c}^\dagger_{N,k} \hat{c}_{N,k}. \tag{5.46}$$

Finally, the third part in Eq. (5.44) defines the many-body interaction of charge carriers with the cavity mode and is of the following form:

$$\hat{\mathcal{H}}_i = \frac{g}{\sqrt{\mathcal{N}}} (\hat{a} + \hat{a}^\dagger) \sum_{N,N',k} \hat{c}^\dagger_{N,k} \mathcal{M}_{N,N'} \hat{c}_{N',k}. \tag{5.47}$$

Thereby, the matrix elements $\mathcal{M}_{N,N'}$ are associated with a symmetric matrix $\mathcal{M}$ and encode the graphene specific dipole-selection rules,

$$\mathcal{M}_{N,N'} = \lambda \, w_{+,n} w_{-,n'} \, \delta_{n+1,n'} + \lambda' \, w_{+,n'} w_{-,n} \, \delta_{n,n'+1}, \tag{5.48}$$

where the weighting functions $w_{\pm,n}$ are defined in Eq. (5.32). The expressions obtained for each of the three contributions to the many-body Hamiltonian $\hat{\mathcal{H}}$ are in accordance with Ref. [95].

For the discussion in Chap. 8 it is useful to introduce the decomposition of each matrix element into $\mathcal{M}_{N,N'} = m_{N,N'} + m_{N',N}$ where the component $m_{N,N'}$ is defined as

$$m_{N,N'} = \lambda \, w_{+,n} w_{-,n'} \, \delta_{n+1,n'} = m_{N,N'}^{\dagger}. \tag{5.49}$$

Along with this, the interaction Hamiltonian can be decomposed accordingly into $\hat{\mathcal{H}}_{\mathrm{i}} = \hat{h}_{\mathrm{i}} + \hat{h}_{\mathrm{i}}^{\dagger}$, where

$$\hat{h}_{\mathrm{i}} = \frac{g}{\sqrt{\mathcal{N}}} (\hat{a} + \hat{a}^{\dagger}) \sum_{N,N',k} \hat{c}_{N,k}^{\dagger} \, m_{N,N'} \, \hat{c}_{N',k} \neq \hat{h}_{\mathrm{i}}^{\dagger}. \tag{5.50}$$

It follows from Eq. (5.48) that the interaction Hamiltonian does not account for transitions between different values of k according to the dipole approximation. Consequently, only Landau levels with subsequent Landau index, $\Delta n = \pm 1$, are optically coupled. This selection rule is independent on the band indices of initial and final state, λ and λ'. Figure 5.3 illustrates the characteristic dipole selection rules.

At some stages during the following the k-dependence of the fermionic operators will be absorbed into the collective index for the sake of brevity:

$$\hat{c}_{N,k}^{\dagger} \leftrightarrow \hat{c}_{N}^{\dagger}, \quad \hat{c}_{N,k} \leftrightarrow \hat{c}_{N}. \tag{5.51}$$

The anti-commutation relations (5.43) remain of course unaffected by this short-hand notation. Furthermore, the term *intra-band* transition is introduced for transitions inside one band, i.e. $\lambda = \lambda'$. Note that inter-band transitions are also often referred to as *cyclotron transitions*. Consequently, the term *inter-band* transition refers to the optical coupling of two Landau states each in one of the two band, i.e. $\lambda \neq \lambda'$.

In the noninteracting case, $g = 0$, each Landau-levels with $\epsilon_N < \epsilon_{\mathrm{F}}$ is occupied by $\mathcal{N}$ electrons, whereas all Landau-levels with $\epsilon_N > \epsilon_{\mathrm{F}}$ are completely empty at $T = 0$. This precisely refers to the scenario considered during Part II of this thesis. In accordance with the literature [93–95] it is assumed that the Fermi level lies between the two Landau levels M and $M + 1$ in the valence band. In particular, ϵ_{F} satisfies

$$\epsilon_{\mathrm{F}} = \frac{\epsilon_{M+1} + \epsilon_M}{2}. \tag{5.52}$$

The transition frequency of the corresponding cyclotron transition is then given by

$$\hbar \Omega_M = \epsilon_{M+1} - \epsilon_M = \frac{(\hbar \omega_c)^2}{2\epsilon_{\mathrm{F}}}. \tag{5.53}$$

The relation between the transition frequency and the Fermi level follows from the definition of the Landau levels, Eq. (5.26), and basic calculus.

During the following discussion of the superradiant critical behavior, resonance of the transition frequency Ω_M and the cavity mode ω_0 may be assumed for convenience at certain stages. However, as discussed in Subsec. 3.3.2 this is no requirement for the emergence of a superradiant phase transition. Furthermore, in similarity to the Dicke model

the critical point is found in the ultrastrong coupling regime (cf. Chap. 7), which is characterized by the emergence of non-linearities and hence a breakdown of the validity of ordinary perturbation theory.

Thus, in the ultrastrong coupling regime, also excitations from energetically lower or already partially populated Landau levels above the Fermi level might occur in accordance with the dipole selection rules and Pauli blocking. However, in order to account for these processes, a brute restriction of the former to a two-level description including only the resonant level doublet will certainly be not beneficial. The path integral approach for the partition sum, which is discussed in Chap. 7, provides a considerably better approach as one is able to exactly integrate over the fermionic contribution and thus account for all conceivable transitions encoded in $\hat{\mathcal{H}}$. Thereby Pauli blocking is automatically considered within the accompanied formalism of Matsubara summation.

Within a different approach an effective two-level Hamiltonian for the resonant Landau-level doublet M and $M+1$ can be derived as discussed in Chap. 8. The ansatz is based on Ref. [95] and is provided by a perturbative Schrieffer-Wolff transformation. However, the investigations of Ref. [95] are extended from second to fourth order and discussed within two different regularization approaches similar as for the path integral method. The resulting Hamiltonian simplifies then to a generalized Dicke Hamiltonian with additional contributions $\propto (\hat{a}^\dagger + \hat{a})^2$ stemming from the screening of the occupied Landau levels beneath the Fermi level. Different from Ref. [95], also a rigid ultraviolet cutoff is applied for regularization.

Part II

Superradiant critical behavior of Landau-quantized graphene

Chapter 6

Numerical tight-binding simulation

The analytic results obtained in Chap. 7 are supported by a numerical tight-binding simulation of the entire energy spectrum of rectangular graphene flakes embedded in an optical cavity. The numerical approach includes also an uniform perpendicular magnetic field similar to the analytic approach. Thus, the tight-binding Hamiltonian $\hat{H}_{\mathrm{TB}}$, Eq. (5.8), needs to be extended in order to investigate the effect of both vector potentials. This is discussed during the following. Furthermore, the calculation of the relevant observables, the photon occupation and the ground-state energy, based on the tight-binding spectrum is outlined subsequently. The chapter is completed with a brief discussion of the details of the numerical implementation.

6.1 Tight-binding model in the presence of vector potentials

The implementation of a vector potential $\boldsymbol{A}$ into a tight-biding model is commonly achieved by means of the Peierl's phase [231]

$$t_{i,\alpha;j,\beta} \mapsto t_{i,\alpha;j,\beta} \exp\left[i\frac{e}{\hbar}\int_{\boldsymbol{R}_j+\boldsymbol{d}_\beta}^{\boldsymbol{R}_i+\boldsymbol{d}_\alpha} \mathrm{d}\boldsymbol{s} \cdot \boldsymbol{A}(\boldsymbol{x})\right], \tag{6.1}$$

where the integration contour has to be taken along the straight line [221, 232] connecting the lattice points $\boldsymbol{R}_j + \boldsymbol{d}_\beta$ and $\boldsymbol{R}_i + \boldsymbol{d}_\alpha$. This might be justified in a nearest-neighbor model, but raises the question of the proper implementation when considering tight-binding models with higher-order neighbor hoppings or three-dimensional lattices [232]. However, as the Peierl's phase lacks a rigorous derivation from first principles its validity in any case is not guaranteed [233, 234]. Moreover, according to W. Kohn, the substitution (6.1) provides a rather "uncontrolled approximation" [235] leaving doubts on the validity of the results obtained therefrom in general.

Nevertheless, as the Peierl's phase is a widely used technique when accounting for the effects of magnetic fields in tight-binding models there are investigations [236] for a derivation based on the properties of the tight-binding sums (5.10) and a minimal coupling Hamiltonian obtained from Eq. (5.7). It is found [236] that within a nearest-neighbor tight-binding model the Peierl's phase (6.1) will provide a suitable ansatz for the implementation of a magnetic field

1. if the corresponding vector potential is slowly varying with respect to the lattice constant a and

2. if the magnetic flux through one unit cell is small:

$$\varphi_0 = \frac{e}{h} B a^2 = \left(\frac{a}{\sqrt{2\pi} l_B} \right)^2 \ll 1. \tag{6.2}$$

Roughly spoken, $\varphi_0 \ll 1$ will be fairly satisfied for any magnetic field up to $B \approx 1000\,\mathrm{T}$.

In the course of these constraints, the Peierl's substitution is commonly used in tight-binding simulations of graphene under the influence of a magnetic field and yields consistency with the effective Landau-quantized Dirac model in the region of linear dispersion [237]. Furthermore, the Dirac model is in accordance with experimental results [21, 22, 28, 28–33, 37] also in the presence of magnetic fields and thus the Peierl's phase is regarded as a suitable approach for the implementation of magnetic fields into a tight-binding simulation of graphene. The agreement between analytic model and numerical simulation in the presence of a uniform perpendicular magnetic field can also be seen from Fig. 6.1. Thereby, the energy spectra of quadratic graphene flakes of various sizes are shown as a function of the flux (5.34) through the system. The quantizing vector potential $\boldsymbol{A}_0$ was chosen in Landau gauge, as defined in Eq. (5.23), and was numerically implemented by means of a Peierl's phase. The vertical lines in Fig. 6.1 mark the flux values, $\varphi = 12.5$ and $\varphi = 18$, for which the calculation of the partition sum is performed later on. It is easily seen that the condition $\varphi_0 \ll 1$ is satisfied in any case.

The energy spectra in Fig. 6.1 clearly depict the condensation or clustering of single-particle energy levels in the vicinity of analytically predicted Landau levels. However, as the simulated systems are of rather small spacial extension one may account for trigonal warping as an extension to the effective Dirac model in the region $E \gtrsim 0.7\,t$. Thereby the next order in the expansion of $H(\boldsymbol{k})$, Eq. (5.14), around the Dirac cones into powers of $|\boldsymbol{q}|a$ is taken into account yielding [24]

$$\tilde{\epsilon}_N = \epsilon_N \left(1 - \kappa |N| \right), \quad \kappa = \frac{w^2}{8} \left(\frac{a}{l_B} \right)^2 \tag{6.3}$$

where ϵ_N denotes a Landau level within Dirac approximation, Eq. (5.26), and $w = 0.1025$ is a fitting parameter. Figure 6.1 shows, that this correction however loses importance as the system size increases. This is easily understood by noting that κ scales with $1/L^2$ when regarded as function of the flux φ.
As $E \lesssim t$ roughly coincides with the validity range of the continuum model obtained for first- and second-order expansion of $H(\boldsymbol{k})$, one can understand this energy threshold as an ultraviolet cutoff of the effective Dirac model [223] or its equivalent when accounting for trigonal warping. Thus, one finds a magnetic-field dependent Landau-level cutoff ν satisfying $E \lesssim t$,

$$\epsilon_\nu = \hbar \frac{\sqrt{2} v_{\mathrm{F}}}{l_B} \sqrt{\nu} \approx t \quad \Leftrightarrow \quad \nu \approx \frac{10^4}{B\,[\mathrm{T}]} \tag{6.4}$$

in accordance with the literature [24, 223]. In general, when evaluating the analytical approaches in Chap. 7 and 8 within cutoff regularization one refers to this as Landau-level cutoff.

The validity range of the effective model, $E \approx t$, is also revealed by the tight-binding spectra shown in Fig. 6.1: The Landau clustering breaks down above a certain energy where the spectra are then superimposed by higher order contributions to the tight-binding model and finite-size effects. As the graphene flakes considered during this thesis are rather small, the cutoff energy $E \lesssim t$ applies only for roughly $\varphi \gtrsim 15$. This is due to finite-size effects competing with the Landau-level clustering for fluxes $\varphi \lesssim 15$. In turn this yields a smaller number of Landau levels to be actually resolved in the region of linear dispersion as predicted by the continuum model, Eq. (6.4). Thus, when directly comparing a numerical result obtained for $\varphi < 15$ one needs to adjust the value of ν entering the analytic approach accordingly. The particular values for ν extracted from the tight-binding spectra are listed in Tab. 6.1.

Except for a true spin degeneracy the numerically obtained Landau-level clusters actually are not degenerate. However, one can introduce an approximate degeneracy $\mathcal{N}_{\mathrm{TB}}$ counting the number of levels which cluster in the vicinity of an analytic Landau level. During this thesis, any level which deviates by less than 0.2% from the position of an analytic Landau level is regarded as contributing to $\mathcal{N}_{\mathrm{TB}}$. Table 6.1 provides an overview of $\mathcal{N}_{\mathrm{TB}}$ obtained for the systems depicted in Fig. 6.1. As a consequence of finite-size effects and as apparent from the levels between subsequent Landau clusters in the tight-binding spectra, Fig. 6.1, the approximate degeneracy $\mathcal{N}_{\mathrm{TB}}$ is smaller than the analytically predicted one. However, since sizes of the graphene flakes are rather small, the number of Landau level clusters resolved in the region of approximate linear dispersion is small but increases with increasing system size. From a computational point of view larger systems including magnetic fields are feasible within an acceptable amount of calculation time. However, as discussed in Sub. 6.3 in more detail, this becomes challenging when considering the effect of a cavity mode determined by the vector potential $\boldsymbol{A}_{\mathrm{em}}$, as defined in Eq. (5.37). As the system is not in the thermodynamic limit, a mean-field approach for the bosonic degree of freedom is not applicable. Thus, the photonic degree of freedom enters the simulation microscopically by implementing a truncated matrix representation of the creation and annihilation operators as already briefly touched in Subsub. 3.3.2:

$$\hat{a}^{\dagger}_{N_{\mathrm{tr}}} = \sum_{n=0}^{N_{\mathrm{tr}}} \sqrt{n+1} \, |n+1\rangle \langle n|, \quad \hat{a}_{N_{\mathrm{tr}}} = \sum_{n=0}^{N_{\mathrm{tr}}} \sqrt{n+1} \, |n\rangle \langle n+1|. \tag{6.5}$$

The dimension of the corresponding Fock space, $\dim(\mathbb{H}^{+}) = N_{\mathrm{tr}} + 1$, has to be chosen large enough in order to provide convergence of the eigensprectrum. For the calculations presented during this thesis $N_{\mathrm{tr}} = 3$ provided remarkably good convergence for the relevant parameter ranges. Thus, in analogy to the criterion (6.2), one can estimate the validity range of the Peierl's phase when implementing the truncated electromagnetic vector potential, $\hat{\boldsymbol{A}}^{N_{\mathrm{tr}}}_{\mathrm{em}} = \mathcal{A}_{0} \boldsymbol{e}_{\mathrm{em}} (\hat{a}^{\dagger}_{N_{\mathrm{tr}}} + \hat{a}_{N_{\mathrm{tr}}})$, in dipole approximation:

$$\frac{e}{\hbar} a \mathcal{A}_{0} ||\hat{a}^{\dagger}_{N_{\mathrm{tr}}} + \hat{a}_{N_{\mathrm{tr}}}||_{2} \stackrel{(5.40)}{=} \frac{2a}{\hbar v_{\mathrm{F}}} \sqrt{N_{\mathrm{tr}}(1+N_{\mathrm{tr}})} \frac{g}{\sqrt{\mathcal{N}_{\mathrm{TB}}}} \ll 1. \tag{6.6}$$

Thereby it was used, that the norm of the truncated bosonic operator sum is given by

$$||\hat{a}^\dagger_{N_{\mathrm{tr}}} + \hat{a}_{N_{\mathrm{tr}}}||_2 = \left(\sum_{i,j=1}^{N_{\mathrm{tr}}} a_{i,j}^2\right)^{\frac{1}{2}} = \sqrt{N_{\mathrm{tr}}(1 + N_{\mathrm{tr}})}. \tag{6.7}$$

By defining the modified coupling strength,

$$g_{\mathrm{TB}} = \frac{g}{e\sqrt{\mathcal{N}_{\mathrm{TB}}}}, \quad [g_{\mathrm{TB}}] = e\mathrm{V}, \tag{6.8}$$

which will be varied within the numerical simulation, the estimation of the validity range (6.6) can be further specified for the relevant case, $N_{\mathrm{tr}} = 3$:

$$g_{\mathrm{TB}} \ll \frac{\hbar v_{\mathrm{F}}}{2ea}\frac{1}{\sqrt{N_{\mathrm{tr}}(1 + N_{\mathrm{tr}})}} \approx \frac{1}{3}\,e\mathrm{V}. \tag{6.9}$$

As long as g_{TB} satisfies this relation, the Peierl's phase is regarded to yield solid results. In Chap. 7 the critical behavior indicated by the numerical simulation is compared with the analytic prediction obtained for varying g within the path integral approach. In particular, when obtaining some critical value $g_{\mathrm{TB},c}$ one explicitly has to account for the Landau-level degeneracy $\mathcal{N}_{\mathrm{TB}}$ obtained from the tight-binding spectra when comparing with an analytically g_c. This can be regarded as a consistency check of both approaches.

Despite this, one should ensure that the actual coupling strength g_{r}, as given by the r.h.s. of Eq. (5.40), is compatible with the criterion (6.9). This is crucial, as it determines the quality of the predictions obtained within the numerical approach. Thus, by setting $g = g_{\mathrm{r}}$ in the definition of g_{TB} one finds from Eq. (6.9):

$$\varphi_0 \ll 9\,\sqrt{\epsilon_{\mathrm{r}}}\mathcal{N}_{\mathrm{TB}}, \tag{6.10}$$

which is certainly satisfied for the relevant parameters and in agreement with the criterion $\varphi_0 \ll 1$. If this relation was not fulfilled, investigations on the equilibrium superradiant phase transition within the tight-binding approach would forfeit their significance as the essential criterion for the theoretical chance to numerically reach the relevant parameter range, $g_{\mathrm{TB},c} < g_{\mathrm{r}}/(e\sqrt{\mathcal{N}_{\mathrm{TB}}})$, would be invalid in the first place. This criterion could not been satisfied within the simulations carried out during this thesis which is due to the small size of the considered systems. However, the signatures of superradiance obtained from the tight-binding approach $g_{\mathrm{TB},c} > g_{\mathrm{r}}/(e\sqrt{\mathcal{N}_{\mathrm{TB}}})$ are in convincing agreement with analytic predictions as discussed in Chap. 7. When extrapolating this agreement to the simulation of larger systems one will probably find the criterion $g_{\mathrm{TB},c} < g_{\mathrm{r}}/(e\sqrt{\mathcal{N}_{\mathrm{TB}}})$ to be satisfied.

6.2 Thermodynamic properties

As the validity ranges for the implementation of both vector potentials, $\boldsymbol{A}_0$ and $\hat{\boldsymbol{A}}_{\mathrm{em}}$, by means of Peierl's phases are pinned, one can proceed with the discussion of the generalized tight-binding Hamiltonian on the basis of Eq. (5.8). The bosonic creation and

annihilation operators are implemented as truncated matrices of dimension $N_{tr} + 1$, according to Eq. (6.5), such that the hopping elements of the original tight-binding model are generalized to matrices with identical dimension. Thus, the generalized tight-binding Hamiltonian studied throughout this thesis is of the following form

$$\hat{H}_{TB} = \sum_{i,\alpha;j,\beta} t_{i,\alpha;j,\beta}(B) |i,\alpha\rangle \langle j,\beta| \otimes \hat{T}_{i,\alpha;j,\beta}, \tag{6.11}$$

where the hopping element

$$t_{i,\alpha;j,\beta} = \begin{cases} -\mu, & \text{if } i = j, \alpha = \beta, \\ -t \exp\left[i\frac{e}{\hbar} \int_{\boldsymbol{R}_j+\boldsymbol{d}_\beta}^{\boldsymbol{R}_i+\boldsymbol{d}_\alpha} \mathrm{d}\boldsymbol{s} \cdot \boldsymbol{A}_0(\boldsymbol{x})\right], & \text{if } i, \alpha \text{ and } j, \beta \text{ are nearest neighbors}, \end{cases} \tag{6.12}$$

accounts for the quantizing vector potential $\boldsymbol{A}_0$ in Landau gauge as defined in Eq. (5.23). The tight-binding Hamiltonian is complemented with the hopping matrix $\hat{T}_{i,\alpha;j,\beta}$ of dimension $N_{tr} + 1$ which accounts for truncated bosonic Fock space in the model. The equivalent to the on-site hopping element, $i = j, \alpha = \beta$, is then given by

$$\hat{T}_{i,\alpha;i,\alpha} = \hbar\omega_0 \hat{a}^\dagger_{N_{tr}} \hat{a}_{N_{tr}}, \tag{6.13}$$

where $\hat{a}^\dagger_{N_{tr}}$ and $\hat{a}_{N_{tr}}$ are defined in Eq. (6.5). Similar to the quantizing vector potential, $\boldsymbol{A}_0$, also the electromagnetic vector potential, $\hat{\boldsymbol{A}}_{em}^{N_{tr}}$, is included by means of the Peierl's phase, Eq. (6.1), which additionally modulates the hopping parameter according to

$$\hat{T}_{i,\alpha;j,\beta} = \exp\left[i\, g_{TB}\left(\frac{2ae}{\hbar v_F}(\hat{a}^\dagger_{N_{tr}} + \hat{a}_{N_{tr}}) \int_{\boldsymbol{R}_j+\boldsymbol{d}_\beta}^{\boldsymbol{R}_i+\boldsymbol{d}_\alpha} \mathrm{d}\boldsymbol{s} \cdot \boldsymbol{e}_{em}\right)\right]. \tag{6.14}$$

The variable coupling strength is chosen as $g_{TB} = g/(e\sqrt{\mathcal{N}_{TB}})$ such that the approximate Landau-level degeneracy $\mathcal{N}_{TB}$, Tab. 6.1, has to be explicitly taken into account for comparison with an analytic prediction. Likewise, the numerically obtained observables stemming from the partition sum have to be explicitly normalized by the approximate degeneracy. This provides an additional check of the consistency of the tight-binding simulation and the analytic prediction, discussed in Chap. 7.

The numerical implementation of the rectangular graphene flakes of various sizes, Tab. 6.1, is carried out using the Python package Kwant [238]. After setting up the system, one calculates the many-body partition sum from the single-particle energies similar as discussed in Sec. 3 in App. D. As the Hamiltonian consists of a fermionic and a bosonic contribution, one has to account for the different quantum statistics when tracing. This is most easily achieved by partial tracing over either the bosonic or fermionic part and then eventually take the trace over the remaining subsystem. Therefore, consider the partition sum of the Hamiltonian (6.11) in the following form

$$\mathcal{Z}_{TB} = \mathrm{Tr}\left[e^{-\beta\hat{H}_{TB}}\right] = \sum_{n=0}^{N_{tr}} \sum_{k,\gamma} \langle n| \langle k,\gamma| e^{-\beta\hat{H}_{TB}} |k,\gamma\rangle |n\rangle = \sum_{n=0}^{N_{tr}} \langle n| e^{-\beta\hat{H}_{eff}} |n\rangle, \tag{6.15}$$

where $\{|n\rangle\,;\,n=0,\ldots,N_{\mathrm{tr}}\}$ and $\{|k,\gamma\rangle\,;\,k=1,\ldots,N_{\mathrm{C}},\gamma=\mathrm{A},\mathrm{B}\}$ shall denote the eigen-basis in the bosonic and fermionic space. Thereby, N_{C} denotes the number of unit cells composing the graphene flake. If $\{|n\rangle\}$ and $\{|k,\gamma\rangle\}$ denote a basis different from the eigenbasis, the former will easily be transformed into the latter by an appropriate unitary transformation.

For the evaluation of the tight-binding simulation during this thesis, the fermionic degree of freedom is chosen to be traced out first, as the r.h.s. of Eq. (6.15) indicates.

To ensure that the evaluated observables are well-defined, it is necessary to normalize the partition sum $\mathcal{Z}_{\mathrm{TB}}$ with the one of the noninteracting system, $\mathcal{Z}_{0,\mathrm{TB}}$, obtained for $g=0$ [239, 240]. Thus, one defines $\bar{\mathcal{Z}}_{\mathrm{TB}} = \mathcal{Z}_{\mathrm{TB}}/\mathcal{Z}_{0,\mathrm{TB}}$. From the partition sum $\bar{\mathcal{Z}}_{\mathrm{TB}}$ one then finds the photonic occupation of the cavity and the mean-energy as the thermal or ensemble average

$$\langle \hat{a}^\dagger_{N_{\mathrm{tr}}} \hat{a}_{N_{\mathrm{tr}}} \rangle = -\frac{1}{\beta}\partial_{\hbar\omega_0}\log(\bar{\mathcal{Z}}_{\mathrm{TB}}), \quad E_{\mathrm{TB}} = \langle \hat{H}_{\mathrm{eff}} \rangle = -\partial_\beta \log(\bar{\mathcal{Z}}_{\mathrm{TB}}). \qquad (6.16)$$

In the limit $\beta \to \infty$, these thermal averages coincide with the ground-state values of the corresponding observables. As this is numerically not feasible, one chooses β as large as possible whereas convergence may be assured. For the evaluation presented during Chap. 7, $\beta = 1000/(\hbar\omega_c)$ was chosen. This value corresponds to a temperature $T \lesssim 10\,\mathrm{K}$ where the particular value depends on the size of the system. Thus, the obtained results may be referred to as the ground-state properties of the tight-binding system.

6.3   Remarks on the tight-binding simulation

During this thesis, the analytic results obtained within the effective Dirac model are un-derpinned by numerical tight-binding simulations of a rectangular graphene flake with various side lengths, as itemized in Tab. 6.1. To this end, the Python package Kwant [238] is used to setup the hexagonal lattice structure based on the Hamiltonian $\hat{\mathbb{H}}_{\mathrm{TB}}$ defined in Eq. (6.11). According to the choice of the spacial extension, the graphene flake is as-sembled from $N_{\mathrm{C}} = 2689, 1368$ or 625 atoms which equals the number of single-particle states in the system. Thus the dimension of the Hilbert space corresponding to $\hat{H}_{\mathrm{TB}}$ is given by $\dim(\mathbb{H}_{\mathrm{TB}}) = N_{\mathrm{C}}$ where the valley degree of freedom is automatically taken into account. By contrast, one explicitly has to account for the two-fold spin degeneracy of the tight-binding states when comparing the numerical results with analytic predictions.

By implementation of a cavity vector potential, according to Eq. (6.14), the total Hilbert space of the system is extended by the dimension of the bosonic Fock space, $\dim(\mathbb{H}^+) = N_{\mathrm{tr}} + 1$, yielding $\dim(\mathbb{H}^+ \otimes \mathbb{H}_{\mathrm{TB}}) = (N_{\mathrm{tr}} + 1)N_{\mathrm{C}}$ in total.

For the computation of the effective energy spectrum of the bosonic mode, the total Hamiltonian is implemented as a dense matrix requiring the allocation of $16[(N_{\mathrm{tr}}+1)N_{\mathrm{C}}]^2$ B of memory when working with double precision complex floats. Thereby, for instance, the calculation of the effective Hamiltonian $\hat{H}_{\mathrm{eff}}$ for one g value and $L = 8.5\,\mathrm{nm}$, $N_{\mathrm{tr}} = 3$ consumes approximately $21\,\mathrm{h}$ of computation time on a $3.5\,\mathrm{GHz}$ core and requires $2\,\mathrm{GB}$ of memory. By working with sparse matrices the amount of required memory would

System	N	$\varphi = 12.5$		$\varphi = 18$	
		$\mathcal{N}_{\mathrm{TB}}$	ν	$\mathcal{N}_{\mathrm{TB}}$	ν
8.5 nm	0	40		42	
	1	12	3	14	4
	2	4		4	
6 nm	0	32		32	
	1	12	3	12	3
	2	4		2	
4 nm	0	20	2	22	2
	1	12		10	

TABLE 6.1: Approximate degeneracy $\mathcal{N}_{\mathrm{TB}}$ of different Landau levels N obtained from the tight-binding simulation for various system sizes and fluxes. For each Landau level index N any single-particle energy that deviates by $< 0.2\%$ from the analytical prediction (accounting for trigonal warping, red lines in Fig. 6.1) is counted as a Landau level. Furthermore, the spin degeneracy was taken explicitly into account by an additional factor of 2. The deviations from the analytically obtained degeneracy $\mathcal{N} = 4\varphi$, according to Eq. (5.33), result from finite-size effects. However, the numerical values for $\mathcal{N}_{\mathrm{TB}}$ for each Landau level $N > 0$ and flux value deviate only slightly among the differently scaled systems. The given values for ν are extracted from the tight-binding spectra, Fig. 6.1, as well and correspond to the actual number of resolved Landau-level clusters for either flux value.

clearly be decreased and hence larger flake sizes would be feasible. However, the aim of the tight-binding simulation is to provide an independent approach which is able to capture signatures of the light-matter interaction also arising from the band structure beyond the Dirac model and thus including also higher order terms of the electromagnetic vector potential. Especially concerning the proposed dynamically generated quadratic terms prohibiting the superradiant quantum phase transition [94, 95], a tight-binding computation of the complete band structure yields the probably most reliable and robust reference in this context. Unfortunately, the performance of diagonalization routines rapidly drops when computing the entire eigenspectrum of a matrix within a sparse matrix approach. In particular, the calculation time has been found to double compared with the diagonalization of an identical dense matrix. In view of the available resources, the choice of a dense matrix approach to the disadvantage of the flake size appeared to be more efficient in the course of this thesis.

During the next chapter a path integral approach for the many-body Hamiltonian in Dirac approximation is considered and and partially compared with the tight-binding simulation.
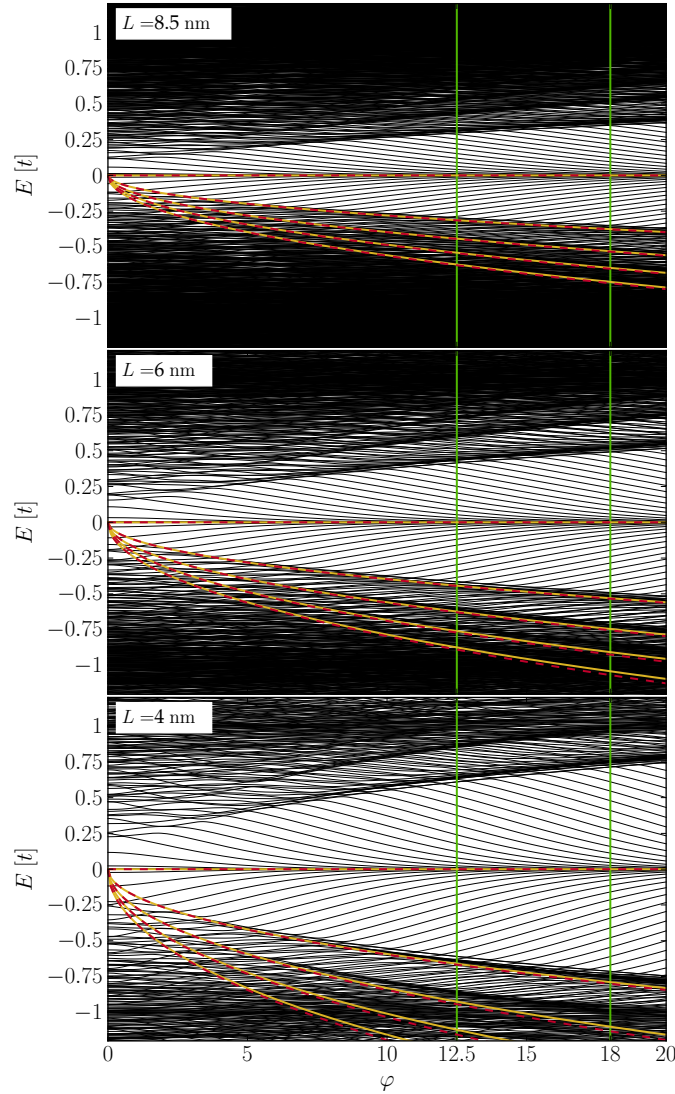
FIGURE 6.1: Energy spectra of quadratic graphene flakes with various side lengths as a function of the normalized flux φ through each system. For $\varphi \gtrsim 5$ the condensation of single-particle energies into Landau levels is clearly visible. According to the rather small spacial extension of the flakes, only a small number of Landau levels is formed within the region of approximate linear dispersion $E \lesssim t$. As the size of the flake increases also the number of Landau levels formed within this region increases. For energies $\gtrsim 0.7\,t$ the warping of the valleys can be seen from the deviation of the bare Landau levels, Eq. (5.26), in Dirac approximation (thick red dashed lines in the valence band) and the numerical simulation. Accounting for this effect in an extended effective description [24] (thick yellow solid lines in the valence band) yields convincing agreement of the analytic theory and the numerical simulation. The vertical green line marks the flux value applied for the numerical simulations of radiation effects throughout this thesis.

Chapter 7

Path integral approach for the many-body partition sum

In this chapter the thermodynamic properties of the many-body Hamiltonian for Landau-quantized graphene interacting with a single cavity mode are derived. The focus lies thereby on the effective Dirac model and is based on the many-body Hamiltonian considered in Sec. 5.3. The results obtained within this chapter are compared with the results of the numerical tight-binding simulation introduced Chap. 6. The analytic considerations are based on a path integral approach in the thermodynamic limit which allows an exact integration of the fermionic degree of freedom.

As a first step, the partition sum of the many-body system is evaluated in the normal phase which is determined from the individual ground-state properties of the cavity and the solid-state subsystem. By integration over the fermionic degree of freedom one obtains an effective action for the bosonic subsystem.
However, as already pointed out during Subsec. 4.3.3, the analytic approach requires regularization as the Dirac model for graphene artificially assumes unbounded bands. The issue of reasonable regularization though is still a subject of research [24, 96–102], especially in context of gauge fields where a rigid ultraviolet momentum cutoff breaks gauge invariance. Despite this crucial argument however the validity range of the effective Dirac model for graphene is limited to a region close to the corners of the Brillouin zone. This validity range is also revealed by the tight-binding simulation, discussed in Chap. 6, as the Landau-level clustering of the tight-binding eigenenergies breaks down rather suddenly for energies above a certain value. This value can be associated with the validity range of the effective Dirac description or its extension accounting for trigonal warping of the Dirac cones. Thus, one of two regularization approaches discussed during the following corresponds to a rigid ultraviolet momentum cutoff in accordance with the literature [24, 98–102]. Thereby, the sums over the Landau-level indices in the many-body Hamiltonian, Eq. (5.42), are truncated at a Landau-level cutoff ν which is in general obtained from Eq. (6.4) in accordance with the literature [24, 223]. However, for the comparison with the particular tight-binding setups, discussed in Chap. 6, the cutoff ν is chosen from the actual number of resolved Landau-level clusters in the tight-binding spectra, Fig. 6.1. The corresponding values are summarized in Tab. 6.1. The results obtained from the cutoff-regularized analytic approach are then compared with the tight-binding simulation.
Furthermore, a regularization approach based on the suggestion of Ref. [93] is applied for

comparison. Thereby, far off-resonant contributions to the interaction Hamiltonian are omitted. In particular, one neglects all dipole-allowed transitions stemming from the valence band into the conduction band when imposing the Fermi level to lie in the conduction band between the Landau-level doublet M and $M + 1$. Within this approach cutoff-independent results for the corresponding observables are obtained and then again compared with the tight-binding simulation.

Having defined both regularization methods, one proceeds with the evaluation of the effective action in the normal phase. From the second derivative of the effective action one finds that the normal phase will correspond to the actual ground-state only if the coupling is smaller than a critical value. This critical point however depends on the choice of regularization. This is the first important intermediate result of this chapter as the derived criterion indicates quantum criticality in a similar manner as the Hessian discussed for the Dicke model in Chap. 3.

Before the evaluation of the path integral is performed for couplings larger than the critical one, a comparison with the critical points extracted from the numerical simulation is performed. Finally, the parameter ranges actually required to reach the critical points are determined for either regularization method . This is crucial as this thesis solely investigates the critical behavior of Landau-quantized graphene in equilibrium and thus without external driving. In equilibrium, however, the actual coupling strength of the Dirac fermions with the cavity mode are certainly determined from microscopic properties of both subsystems and thus it is rather not tunable (cf. Sec. 5.2.3). Hence, the system will only be able to cross the critical point in equilibrium if the actual coupling strength exceeds the predicted phase boundary. As the critical points for either regularization depend on at least the Fermi level one is finally able to determine the parameter ranges required for the actual coupling strength to naturally cross the phase boundary.

Subsequent to this follows the discussion of the path integral approach beyond the critical point where the trivial solution no longer corresponds to the ground state of the hybrid system. In addition to the thermodynamic limit also the properties of quantum fluctuations are discussed during the following. The analytic results are then again compared with the numerical simulation.

7.1 Derivation of the critical point

The evaluation of the many-body partition sum,

$$\mathcal{Z} = \text{Tr}\left[\mathrm{e}^{-\beta\left(\hat{\mathcal{H}} - \mu\hat{\mathcal{N}}\right)}\right], \tag{7.1}$$

is achieved by means of a path integral approach similar to the one discussed in Refs. [239, 241, 242] in the context of the original Dicke model. The derivation of the path integral representation for a many-body partition sum is discussed in Sec. 3 of App. D and based on the evaluation of the trace within the basis of bosonic and fermionic coherent states (cf. Subsec. 3.1 of App. C). In this basis the bosonic operators of the cavity mode, $\hat{a}^{\dagger}$ and $\hat{a}$, are replaced by complex-valued fields, $\alpha^*(\tau)$ and $\alpha(\tau)$, where τ denotes the Euclidean time. These fields correspond to the eigenvalues of the bosonic annihilation operator in

the basis of bosonic coherent states. Likewise, one finds the eigenvalues of the fermionic annihilation operator in the basis of fermionic coherent states to be given by Grassmann numbers (cf. Sec. 2 in App. E). It is convenient to introduce a short-hand vector notation for the fermionic degree of freedeom according to

$$\boldsymbol{\rho}_k^\dagger(\tau) = \begin{pmatrix} c_{-\nu,k}^\dagger(\tau) & c_{-(\nu-1),k}^\dagger(\tau) & \cdots & c_{0,k}^\dagger(\tau) & \cdots & c_{\nu-1,k}^\dagger(\tau) & c_{\nu,k}^\dagger(\tau) \end{pmatrix},$$

$$\boldsymbol{\rho}_k(\tau) = \begin{pmatrix} c_{-\nu,k}(\tau) & c_{-(\nu-1),k}(\tau) & \cdots & c_{0,k}(\tau) & \cdots & c_{\nu-1,k}(\tau) & c_{\nu,k}(\tau) \end{pmatrix}^T,$$

(7.2)

where each component of $\boldsymbol{\rho}_k^\dagger$ and $\boldsymbol{\rho}_k$ is a Grassmann field associated with the corresponding set of quantum numbers. Note that the applied notation, $(\lambda_\nu\nu, k) = (\lambda_\nu, \nu, k)$, refers to the collective index notation introduced in Eq. (5.28). From Eq. (D.71) one finds then the path integral representation of the partition sum (7.1) to be given by

$$\bar{\mathcal{Z}} = \frac{\mathcal{Z}}{\mathcal{Z}_0} = \frac{\oint \mathcal{D}[\alpha] \oint \mathcal{D}[\{\boldsymbol{\rho}_k\}] e^{-\mathcal{S}_E[\alpha^*,\alpha;\{\boldsymbol{\rho}_k^\dagger,\boldsymbol{\rho}_k\}]}}{\oint \mathcal{D}[\alpha] \oint \mathcal{D}[\{\boldsymbol{\rho}_k\}] e^{-\mathcal{S}_E^0[\alpha^*,\alpha;\{\boldsymbol{\rho}_k^\dagger,\boldsymbol{\rho}_k\}]}}.$$

(7.3)

The definition of the integration measure is found in Eq. (D.65). The normalization with $\mathcal{Z}_0$ of the noninteracting system, $g = 0$, ensures $\bar{\mathcal{Z}}$ to be well-defined [239, 240]. The Euclidean action $\mathcal{S}_E$ in the exponential of $\mathcal{Z}$ is defined by

$$\mathcal{S}[\alpha^*, \alpha; \{\boldsymbol{\rho}_k^\dagger, \boldsymbol{\rho}_k\}] = \int_0^\beta d\tau \left[\alpha^*(\tau)\partial_\tau\alpha(\tau) + \sum_{k=1}^{\mathcal{N}} \boldsymbol{\rho}_k^\dagger(\tau)\partial_\tau\boldsymbol{\rho}_k(\tau) \right.$$

$$\left. + \mathcal{H}[\alpha^*(\tau), \alpha(\tau); \{\boldsymbol{\rho}_k^\dagger(\tau), \boldsymbol{\rho}_k(\tau)\}] - \mu\tilde{\mathcal{N}}[\{\boldsymbol{\rho}_k^\dagger(\tau), \boldsymbol{\rho}_k(\tau)\}] \right]$$

$$= \mathcal{S}_+[\alpha^*, \alpha] + \mathcal{S}_{\text{mix}}[\alpha^*, \alpha; \{\boldsymbol{\rho}_k^\dagger, \boldsymbol{\rho}_k\}],$$

(7.4)

where the index E denoting the underlying Euclidean metric is omitted from now on. Likewise, one obtains $\mathcal{S}_E^0$ by setting $g = 0$ in Eq. (7.4). According to the symmetry properties of bosonic and fermionic particles, the complex and Grassmann fields satisfy periodic and anti-periodic boundary conditions, respectively:

$$\alpha^*(0) = \alpha^*(\beta), \quad \alpha^*(0) = \alpha^*(\beta),$$

$$\boldsymbol{\rho}_k^\dagger(0) = -\boldsymbol{\rho}_k^\dagger(\beta), \quad \boldsymbol{\rho}_k(0) = -\boldsymbol{\rho}_k(\beta).$$

(7.5)

To proceed the evaluation of the effective action for the bosonic mode it is beneficial to Fourier transform the Euclidean-time representation into a Matsubara-sum representation. To this end, one applies the following identities

$$\alpha^*(\tau) = \frac{1}{\sqrt{\beta}} \sum_{\omega_n^+} \tilde{\alpha}_N^* e^{i\omega_n^+\tau}, \quad \alpha(\tau) = \frac{1}{\sqrt{\beta}} \sum_{\omega_n^+} \tilde{\alpha}_N e^{-i\omega_n^+\tau},$$

$$\boldsymbol{\rho}^\dagger(\tau) = \frac{1}{\sqrt{\beta}} \sum_{\omega_n^-} \tilde{\boldsymbol{\rho}}_n^\dagger e^{i\omega_n^-\tau}, \quad \boldsymbol{\rho}(\tau) = \frac{1}{\sqrt{\beta}} \sum_{\omega_n^-} \tilde{\boldsymbol{\rho}}_n e^{-i\omega_n^-\tau},$$

(7.6)

which leave the measures of the field integral unchanged. Thereby, $\omega_n^+ = 2n\pi/\beta$ and $\omega_n^- = (2n+1)\pi/\beta$, $n \in \mathbb{Z}$, denote bosonic and fermionic Matsubara frequencies, respectively. The formalism associated with Matsubara frequencies provides an elegant method to ensure the correct implementation of the symmetric and anti-symmetric boundary conditions (7.5).

The pure bosonic part of the action is then found as

$$\mathcal{S}_+[\tilde{\alpha}^*, \tilde{\alpha}] = \sum_{\omega_N^+} \tilde{\alpha}_N^* \left(-i\omega_N^+ + \hbar\omega_0\right) \tilde{\alpha}_N. \tag{7.7}$$

The remaining contribution, $\mathcal{S}_{\mathrm{mix}}$, in Eq. (7.4) composites from fermionic and bosonic contributions due to the interaction part of the many-body Hamiltonian. It is convenient to write the mixed contribution in the following form

$$\mathcal{S}_{\mathrm{mix}}[\tilde{\alpha}^*, \tilde{\alpha}; \{\tilde{\boldsymbol{\rho}}_k^\dagger, \tilde{\boldsymbol{\rho}}_k\}] = \sum_k \sum_{\omega_p^-, \omega_q^-} \tilde{\rho}_{n,k}^\dagger \left[-\mathbb{G}_0^{-1}\delta_{p,q} + \mathbb{M}[\tilde{\alpha}^*, \tilde{\alpha}]\right] \tilde{\rho}_{q,k}, \tag{7.8}$$

where $\mathbb{G}_0^{-1}$ denotes the inverse of the free Green's function of the fermionic subsystem. Consequently, $\mathbb{M}$ accounts for the light-matter interaction. Both quantities are each defined by matrices of $\dim = 2\nu + 1$ in the basis of Grassmann-field vectors defined in Eq. (7.2). In this basis, the matrix elements of $\mathbb{G}_0^{-1}$ and $\mathbb{M}$ read

$$-\left(\mathbb{G}_0^{-1}\right)_{K,L} = \left[-i\omega_p^- + (\epsilon_K - \mu)\right]\delta_{K,L} \tag{7.9}$$

$$\left(\mathbb{M}[\tilde{\alpha}^*, \tilde{\alpha}]\right)_{K,L} = \frac{g}{\sqrt{\mathcal{N}}}\left[\tilde{\alpha}_{K-L}^* + \tilde{\alpha}_{L-K}\right]\mathcal{M}_{K,L}, \tag{7.10}$$

where $\mathcal{M}_{K,L}$ encodes the dipole-selection rules according to Eq. (5.48). Both matrices are independent on the quantum number k which accounts for the Landau-level degeneracy.

As a first step, the field integral over the fermionic degrees of freedom is carried out yielding an effective action for the bosonic mode (cf. Sec. 3 of App. D):

$$\bar{\mathcal{Z}} = (\mathcal{Z}_0^+)^{-1} \oint \mathcal{D}[\tilde{\alpha}]e^{-\mathcal{S}_+[\tilde{\alpha}^*, \tilde{\alpha}]}\left[\prod_{\omega_n^-} \det\left[\mathbb{1} - \mathbb{G}_0\mathbb{M}[\tilde{\alpha}^*, \tilde{\alpha}]\right]\right]^{\mathcal{N}}$$

$$= (\mathcal{Z}_0^+)^{-1} \oint \mathcal{D}[\tilde{\alpha}]e^{-\mathcal{S}_+[\tilde{\alpha}^*, \tilde{\alpha}] + \mathcal{N}\log[\det[\mathbb{1} - \mathbb{G}_0\mathbb{M}[\tilde{\alpha}^*, \tilde{\alpha}]]]}. \tag{7.11}$$

Thereby, $\mathcal{Z}_0^+$ denotes the partition sum of the free cavity mode [240]:

$$\mathcal{Z}_0^+ = \frac{1}{2\sinh\left(\frac{\beta}{2}\hbar\omega_0\right)}. \tag{7.12}$$

The power of $\mathcal{N}$ results from the degeneracy of each Landau level. Furthermore, the product over fermionic Matsubara frequencies was absorbed into the determinant in the second line of Eq. (7.11).

This intermediate result refers to an exact integration over the fermionic degree of freedom. However, due to the complexity of the underlying model, the examination of the sum or product, respectively, over the fermionic Matsubara frequencies is analytically challenging for arbitrary large ν in a general case. Thus, a numerical approach is advantageous in most cases. However, the exact value of the critical point can be analytically derived from Eq. (7.11) as it is shown during the following.

To proceed the evaluation of the effective action for the bosonic mode, one substitutes $\tilde{\alpha}^* \mapsto \sqrt{\mathcal{N}}\tilde{\alpha}^*, \tilde{\alpha} \mapsto \sqrt{\mathcal{N}}\tilde{\alpha}$ such that the partition sum can be written as

$$\bar{\mathcal{Z}}\mathcal{Z}_0^+ = \mathcal{N} \oint \mathcal{D}[\tilde{\alpha}]e^{-\mathcal{N}\Phi[\tilde{\alpha}^*,\tilde{\alpha}]}, \quad \Phi[\tilde{\alpha}^*,\tilde{\alpha}] = \mathcal{S}_+[\tilde{\alpha}^*,\tilde{\alpha}] - \log\left[\det\left[\mathbb{1} - \mathbb{G}_0\mathbb{M}[\tilde{\alpha}^*,\tilde{\alpha}]\right]\right]. \quad (7.13)$$

In the thermodynamic limit, where $\mathcal{N} \to \infty$ is assumed, the dominant contribution to the partition sum arises from field configurations which correspond to a minimum of the phase functional $\Phi[\tilde{\alpha}^*, \tilde{\alpha}]$. Thus, analogous to Hamilton's princple minimizing the phase of the single-particle quantum propagator, one finds the minima of $\Phi[\tilde{\alpha}^*, \tilde{\alpha}]$ by evaluation of

$$\frac{\delta}{\delta\tilde{\alpha}_N}\Phi[\tilde{\alpha}^*,\tilde{\alpha}]\bigg|_{\alpha_0^*,\alpha_0} = 0, \quad \frac{\delta}{\delta\tilde{\alpha}_N^*}\Phi[\tilde{\alpha}^*,\tilde{\alpha}]\bigg|_{\alpha_0^*,\alpha_0} = 0. \quad (7.14)$$

One can show [239] that the corresponding field configuration α_0^*, α_0 is static, i.e. independent on Matsubara frequencies. Furthermore, this field configuration is real-valued, i.e. $\alpha_0^* = \alpha_0$. This is due to $\log\left[\det\left[\mathbb{1} - \mathbb{G}_0\mathbb{M}\right]\right]$ being symmetric in $\tilde{\alpha}^*$ and $\tilde{\alpha}$. Thus, the functional derivative of this expression with respect to $\tilde{\alpha}^*$ is identical with the one carried out with respect to $\tilde{\alpha}$ when evaluated at a static configuration. This becomes more clear during the following, where it is also proven that the trivial solution α_0 always satisfies Eq. (7.14).

Thus, before proceeding the evaluation of the path integral in the thermodynamic limit, consider the functional derivative of $\log\left[\det\left[\mathbb{1} - \mathbb{G}_0\mathbb{M}\right]\right]$:

$$F[\alpha_N^*, \alpha_{-N}] = \frac{\delta}{\delta\tilde{\alpha}_N}\log\left[\det\left[\mathbb{1} - \mathbb{G}_0\mathbb{M}\right]\right] = \frac{\delta}{\delta\tilde{\alpha}_{-N}^*}\log\left[\det\left[\mathbb{1} - \mathbb{G}_0\mathbb{M}\right]\right]$$
$$= \mathrm{Tr}\left[(\mathbb{1} - \mathbb{G}_0\mathbb{M})^{-1}\frac{\delta(-\mathbb{G}_0\mathbb{M})}{\delta\tilde{\alpha}_N}\right], \quad (7.15)$$

where the trace is carried out in the basis [241]

$$\mathrm{Tr}\left[\mathrm{O}\right] = \frac{1}{\beta}\sum_{\omega_n^-}\int_0^\beta \mathrm{d}\tau e^{i\omega_n^-\tau}\left[\sum_I O_{I,I}\right]e^{-i\omega_n^-\tau}. \quad (7.16)$$

Thereby, the innermost sum refers to the trace in the basis of the Grassmann vectors, Eq. (7.2). or a fixed value of k.
By defining the abbreviation $\mathbb{A}[-i\omega_n^-; \tilde{\alpha}^*, \tilde{\alpha}] = \mathbb{1} - \mathbb{G}_0\mathbb{M}[\tilde{\alpha}^*, \tilde{\alpha}]$ and using $\delta\tilde{\alpha}_M/(\delta\tilde{\alpha}_N) =$

$\delta_{M,N}$ one obtains for Eq. (7.15) in particular

$$F[\tilde{\alpha}_N^*, \tilde{\alpha}_{-N}] = \frac{1}{\beta} \sum_{\omega_n^-} \sum_I \left(\mathbb{A}^{-1}[-i\omega_n^- - \mu, \tilde{\alpha}_N^*, \tilde{\alpha}_{-N}](-\mathbb{G}_0\mathbb{M}[0,1]) \right)_{I,I}$$

$$= \frac{1}{\beta} \sum_{\omega_n^-} \frac{\partial_A G_\nu[-i\omega_n^- - \mu, A]}{G_\nu[-i\omega_n^- - \mu, A]} \Bigg|_{A = \tilde{\alpha}_N^* + \tilde{\alpha}_{-N}}. \quad (7.17)$$

where G_ν is understood as an ordinary polynomial function of even powers of A, i.e. $G_\nu[p, A] = \sum_{i=0}^{\nu} c_{2i}(p) A^{2i}$. Due to the specific properties of the interaction term, captured in the matrix $\mathbb{M}$, one is able to iterate G_ν for a given cutoff $\nu \geq 2$ from

$$G_L[p, A] = \begin{cases} p + \epsilon_L, & \text{for } L = 0, \\ B_L[p, A]G_{L-1}[p, A], & \text{for } L = 1, \\ B_L[p, A]G_{L-1}[p, A] + C_{L-1}[p, A]G_{L-2}[p, A], & \text{for } L \geq 2, \end{cases} \quad (7.18)$$

where ϵ_L denotes the Landau level energy assigned with the collective index $L = (\lambda_l, l)$ and

$$B_L[p, A] = p^2 - (\epsilon_L^2 + 2w_{+,L-1}^2 A^2), \quad (7.19)$$

$$C_L[p, A] = -2w_{+,L}^2 \epsilon_L^2 A^2. \quad (7.20)$$

The normalization $w_{+,L}$ is defined in Eq. (5.32). Furthermore, $G_\nu(p)$ can also be understood as a polynomial in p of order $2\nu + 1$ as it is seen from Eqs. (7.18, 7.19, 7.20). By carrying out the partial derivative of $G_\nu[p, A]$ with respect to the parameter A, one finds for $F[\tilde{\alpha}_N^*, \tilde{\alpha}_{-N}]$

$$F[\tilde{\alpha}_N^*, \tilde{\alpha}_{-N}] = A \times \frac{1}{\beta} \sum_{\omega_n^-} \frac{\sum_{i=0}^{\nu-1}(2i+1)c_{2i+2}(-i\omega_n^- - \mu)A^{2i}}{\sum_{i=0}^{\nu} c_{2i}(-i\omega_n^- - \mu)A^{2i}} \Bigg|_{A = \tilde{\alpha}_N^* + \tilde{\alpha}_{-N}}, \quad (7.21)$$

which is an odd function of A. The poles of the denominator as a function of $-i\omega_n^-$ correspond to the eigenvalues of the Hamiltonian associated with the mixed action $\mathcal{S}_{\text{mix}}$. Thus, an analytic evaluation of the sum over Matsubara frequencies requires these eigenvalues to be also known analytically. However, as there exists no generic procedure for finding the roots of a polynomial of order $n > 4$, this task is preferably performed numerically when choosing a reasonable cutoff $\nu \geq 2$ and $A \neq 0$.
Thus, proceeding the discussion of Eq. (7.14) at the static configuration α_0^*, α_0 one obtains

$$\frac{\delta}{\delta\tilde{\alpha}_N} \Phi[\tilde{\alpha}^*, \tilde{\alpha}] \Bigg|_{\alpha_0^*, \alpha_0} = \hbar\omega_0 \, \alpha_0^* - F(\alpha_0^*, \alpha_0) = 0, \quad (7.22)$$

$$\frac{\delta}{\delta\tilde{\alpha}_N^*} \Phi[\tilde{\alpha}^*, \tilde{\alpha}] \Bigg|_{\alpha_0^*, \alpha_0} = \hbar\omega_0 \, \alpha_0 - F(\alpha_0^*, \alpha_0) = 0, \quad (7.23)$$

which are simultaneously satisfied only if $\alpha_0^* = \alpha_0$. Furthermore, from Eq. (7.21) directly follows that the trivial solution, $\alpha_0 = 0$, always satisfies Eqs. (7.22, 7.23). Similar as in the

discussion of the original Dicke model this solution is associated with the normal phase of the system if it is minimizing the phase function. However, whether $\alpha_0 = 0$ actually corresponds to a minimum of the phase function $\Phi(\alpha_0, \alpha_0)$ for any choice of parameters depends on the properties of $F(\alpha_0^*, \alpha_0)$ and requires

$$\frac{\partial^2}{\partial \alpha^2} \Phi(\alpha, \alpha) \bigg|_{\alpha_0} > 0. \tag{7.24}$$

This condition is identical with the claim of a positive definite Hessian discussed during the introduction of the Dicke model (cf. Chap. 3). If the condition (7.24) is violated for a certain parameter g at $\alpha_0 = 0$, the trivial solution will not correspond to the minimum of the phase function anymore. In this case, a different, non-trivial solution of Eqs. (7.22, 7.23) will alternatively satisfy Eq. (7.24) and hence determine a different ground state of the system.

The evaluation of Eq. (7.24) for the trivial solution yields the value of the critical coupling in case that a second-order phase transition exists. During the following, this condition is examined within two different techniques of regularization. The first one is provided by a rotating-wave like approximation yielding a cutoff-independent result for the critical point. Within this approach inter-band transitions are omitted in analogy to Ref. [93]. However, during this thesis a slight variation of the regularization approach suggested in Ref. [93] will be applied: The transition between the valence-band Landau level $N = -1$ and the zeroth Landau level will be included as the corresponding transition frequency is identical with the transition between the zeroth Landau level and $N = +1$ in the conduction band. Thus, excitations from $N = -1$ into the zeroth and also into the first Landau level in the conduction band are likely in an ultrastrong coupling regime especially when the system is filled up to $M = 0$.

Despite this exception, the rotating-wave like approximation is achieved by claiming $\lambda = \lambda'$ in the matrix elements $\mathcal{M}_{N,N'}$, Eq. (5.48). This differs from the ordinary rotating-wave approximation discussed in Subsec. 4.2 of App. B which omits all counter-rotating terms. The Hamiltonian within the rotating-wave like approximation however still contains counter-rotating terms stemming from inter-band transitions. Without providing a rigorous justification of this approach one may point out that especially for a Fermi level above $M \gg 1$ inter-band transitions are far-off resonant. Thus, excitations from a valence-band Landau-level into an empty one in the conduction band requires multi-photon processes involving a large number of photons. In particular, for a cavity which lowest eigenmode is resonant with the transition $\epsilon_{M+1} - \epsilon_M$, a dipole allowed transition from the valence band state $-M$ into $M + 1$ requires the absorption of $\approx 4M$ photons of frequency Ω_M to compensate the energy difference. However, as multphotonic events are likely to occur in ultrastrong coupling regimes a rigorous justification should be provided especially when convincing agreement of the results with other methods is obtained.

The second regularization method applied during the following is given by the ultraviolet Landau-level cutoff ν being kept when evaluating Eq. (7.24) for $\alpha_0 = 0$.

By introducing a new parameter γ controlling the intra-band transitions in the interaction Hamiltonian, one is able to evaluate Eq. (7.24) for both approaches at once. Thus, define

$$\tilde{\mathcal{M}}_{N,N'}^{\gamma} = \lambda(w_{+,n}w_{-,n'}\,\delta_{n+1,n'} + w_{+,n'}w_{-,n}\,\delta_{n,n'+1}) - \lambda\gamma w_{+,n'}w_{-,n}\,\delta_{n,n'+1}, \tag{7.25}$$

which coincides with $\mathcal{M}_{N,N'}$ if $\gamma = 1$ and omits inter-band transitions for $\gamma = 0$. The definition of $\mathbb{M}$, given in Eq. (7.10), is then adapted likewise through the following. Note that for $\gamma = 0$ this definition of $\tilde{\mathcal{M}}_{N,N'}^{\gamma}$ yields an identical regularization as suggested in Ref. [93] where all inter-band transitions are omitted. During this thesis, the transition between the Landau level $N = -1$ and the zeroth Landau level is however explicitly considered. As the corresponding definition of $\tilde{\mathcal{M}}_{N,N'}^{\gamma}$ is easily adapted but yields a cumbersome expression, one stays with Eq. (7.25) for the sake of brevity and keeps in mind the exception for $N = -1$. Any result discussed during the following precisely refers to this modification.

From the derivation of the function $F(\alpha, \alpha)$ one obtains the second derivative of the fermionic contribution to the action with respect to the static, real-valued field α as

$$
\begin{aligned}
\partial_\alpha F^\gamma(\alpha, \alpha)|_{\alpha_0 = 0} &= -\operatorname{Tr}\left[(\mathbb{1} - \mathbb{G}_0 \mathbb{M}^\gamma)^{-1} \frac{\partial(-\mathbb{G}_0 \mathbb{M}^\gamma)}{\partial \alpha} (\mathbb{1} - \mathbb{G}_0 \mathbb{M}^\gamma)^{-1} \frac{\partial(-\mathbb{G}_0 \mathbb{M}^\gamma)}{\partial \alpha} \right]\Bigg|_{\alpha_0 = 0} \\
&= -\operatorname{Tr}\left[(-\mathbb{G}_0) \frac{\partial \mathbb{M}^\gamma}{\partial \alpha} (-\mathbb{G}_0) \frac{\partial \mathbb{M}^\gamma}{\partial \alpha} \right] \\
&= \frac{1}{\beta} \sum_{\omega_n^-} \frac{\partial_A^2 G_\nu[-i\omega_n^- - \mu, A]}{G_\nu[-i\omega_n^- - \mu, A]}\Bigg|_{A=0},
\end{aligned}
$$
(7.26)

where it was used that $\partial_A^2 G_\nu|_0 = 0$. Unfortunately, for $\gamma \neq 1$ the polynomial $G_\nu(p)$ cannot be casted in a convenient form similar to Eq. (7.18). However, the product of matrices in second line of Eq. (7.26) is easily evaluated for $\alpha_0 = 0$ yielding

$$
\partial_\alpha F^\gamma(\alpha, \alpha)|_{\alpha_0 = 0} = -\frac{8g^2}{\beta} \sum_{\omega_n^-} \sum_{L=0}^{\nu-1} U_L^\gamma(-i\omega_n^- - \mu),
$$
(7.27)

where the summands $U_L^\gamma(p)$ are given by

$$
U_L^\gamma(p) = \begin{cases} \frac{4p}{(p+\epsilon_0)[p^2 - \epsilon_1^2]}, & \text{for } L = 0, \\ \frac{p^2 + (1-\gamma^2)\epsilon_L \epsilon_{L+1}}{[p^2 - \epsilon_L^2][p^2 - \epsilon_{L+1}^2]}, & \text{else.} \end{cases}
$$
(7.28)

In a next step one evaluates the sum over fermionic Matsubara frequencies. This is most easily achieved by means of residue calculus as discussed in Sec. 3 in App. E. Thus, one obtains for Eq (7.27)

$$
\partial_\alpha F^\gamma(\alpha, \alpha)|_{\alpha_0 = 0} = -8g^2 \sum_{L=1}^{\nu} \bar{U}_L^\gamma f(\epsilon_L, \mu)
$$
(7.29)

where $\bar{U}_L^\gamma$ is defined as

$$\bar{U}_L^\gamma = \begin{cases} \frac{2}{\Delta_{L,L-1}} + \frac{-\Delta_{L+1,-L}+\gamma^2\Delta_{L+1,L}}{\Delta_{L+1,L}\Delta_{L+1,-L}}, & \text{for } L = 1, \\ \frac{\Delta_{L,-(L-1)}+\gamma^2\Delta_{L,L-1}}{\Delta_{L,L-1}\Delta_{L,-(L-1)}} + \frac{-\Delta_{L+1,-L}+\gamma^2\Delta_{L+1,L}}{\Delta_{L+1,L}\Delta_{L+1,-L}}, & \text{for } 1 < L < \nu, \\ \frac{\Delta_{L,-(L-1)}+\gamma^2\Delta_{L,L-1}}{\Delta_{L,L-1}\Delta_{L,-(L-1)}}, & \text{for } L = \nu, \end{cases} \tag{7.30}$$

using $\Delta_{K,L} = \epsilon_K - \epsilon_L$. Thereby, the index notation refers to the collective index notation introduced in Eq. (5.28). The function

$$f(\epsilon_L, \mu) = -\frac{1}{2}\left[\tanh\left(\frac{\beta}{2}(\epsilon_L - \mu)\right) + \tanh\left(\frac{\beta}{2}(\epsilon_L + \mu)\right)\right] \overset{\beta \to \infty}{=} -\Theta(\epsilon_L - \mu) \tag{7.31}$$

results from the Fermi-Dirac distribution entering the evaluation of the Matsubara sum. Thus, by setting $T = 0$ and $2\mu = \epsilon_{M+1} + \epsilon_M$, Eq. (7.29) can be simplified according to

$$\partial_\alpha F^\gamma(\alpha, \alpha)\big|_{\alpha_0=0} = 8g^2 \sum_{L=M+1}^\nu \bar{U}_L^\gamma. \tag{7.32}$$

Despite the claim of electron-hole symmetric single-particle energies ϵ_L no further information about the particular definition of ϵ_L entered the intermediate result for $\bar{U}_L^\gamma$ and thus in turn Eq. (7.32). During the following, the single-particle energies ϵ_L are associated with the Landau levels of graphene within Dirac approximation as given in Eq. (5.26). The results derived from the corresponding expression of $\partial_\alpha F^\gamma(\alpha, \alpha)\big|_0$ then reveal the properties of the Landau-quantized Dirac fermions interacting with a cavity mode. However, when comparing the results obtained from this analytic approach with those of the numerical tight-binding simulation it is beneficial to account for trigonal warping in the evaluation of Eqs. (7.30, 7.32). This is reasonable, as the spacial extension of the simulated graphene flakes is rather small and in turn the number of resolved Landau levels in the region of linear dispersion is limited to at most four Landau levels in each band for the considered fluxes (cf. Fig. 6.1 and Tab. 6.1). Thus, to provide the comparability of both approaches also for larger fillings one needs to take trigonal warping of the Dirac cones into account. This is achieved by evaluation of Eq. (7.30) for the modified energy levels $\tilde{\epsilon}_L$ as defined in Eq. (6.3).

Proceeding the discussion for ϵ_L denoting a Landau level in Dirac approximation, the sum over $\bar{U}_L^\gamma$ is easily evaluated. Thereby, one finds for $\Delta_{L+1,L}\Delta_{L+1,-L} = \hbar\omega_c$ in the denominator of the summands $\bar{U}_L^\gamma$ which are then further simplified according to

$$\hbar\omega_c \bar{U}_L^\gamma = \begin{cases} (2\delta_{L,1} + \sqrt{L-1} - \sqrt{L+1})(1-\gamma^2), & \text{for } 1 \le L < \nu, \\ \sqrt{\nu}(1+\gamma^2) + \sqrt{\nu-1}(1-\gamma^2), & \text{for } L = \nu, \end{cases} \tag{7.33}$$

Thus, the result for rigid cutoff regularization is straight forwardly obtained by putting $\gamma = 1$:

$$\partial_\alpha F^1(\alpha, \alpha)\big|_{\alpha_0=0} = 16g^2 \frac{\sqrt{\nu}}{\hbar\omega_c}. \tag{7.34}$$

The cutoff-independent result for $\partial_\alpha F(\alpha, \alpha)|_0$ is, however, also easily obtained from re-ordering the sum over $\bar{U}_L^\gamma$ with $\gamma = 0$, yielding

$$\partial_\alpha F^0(\alpha, \alpha)\big|_{\alpha_0=0} = 8g^2 \left[\frac{2\delta_{M,0}}{\hbar\omega_c} + \frac{1}{\hbar\Omega_M} \right]. \tag{7.35}$$

By inserting these results into the second derivative of the phase function with respect to α, one finds

$$
\begin{aligned}
\partial_\alpha^2 \Phi^\gamma(\alpha, \alpha)\big|_{\alpha_0=0} &= 2\hbar\omega_0 - \partial_\alpha F^\gamma(\alpha, \alpha)\big|_{\alpha_0=0} \\
&= \begin{cases}
16 \frac{\sqrt{\nu}}{\hbar\omega_c} \left[\left(\frac{\hbar\sqrt{\omega_0\omega_c}}{2\sqrt{2\nu}} \right)^2 - g^2 \right], & \text{for } \gamma = 1, \\[3mm]
8 \left(\frac{2\delta_{M,0}}{\hbar\omega_c} + \frac{1}{\hbar\Omega_M} \right) \left[\left(\frac{\hbar\sqrt{\omega_0\left(\omega_c/(2\delta_{M,0})+\Omega_M\right)}}{2} \right)^2 - g^2 \right], & \text{for } \gamma = 0.
\end{cases}
\end{aligned}
\tag{7.36}
$$

These equations precisely define the critical points for either regularization. In particular, the trivial solution will correspond to a minimum of the phase function only if the coupling g is smaller than either

$$g_{c,\nu} = \frac{\hbar\sqrt{\omega_0\omega_c}}{2\sqrt{2\nu}}, \tag{7.37}$$

in case of a rigid ultraviolet cutoff, or

$$g_{c,M} = \frac{\hbar\sqrt{\omega_0\left(\omega_c/(2\delta_{M,0}) + \Omega_M\right)}}{2}. \tag{7.38}$$

when inter-band excitations are dropped. The latter is similar to the result derived in Ref. [93] where all inter-band transitions are omitted. In reality though at most one of these approaches matches the actual situation in the system. Thus, either $g_{c,\nu}$ or $g_{c,M}$ determines the phase boundary of the true system. From the Dirac model itself however one will not be able to conclude which of these proposed critical points corresponds to the actual phase boundary of Landau-quantized graphene. This issue is related to the discussion of proper regularization of the unbounded valence band when applying the low-energy approximation onto the tight-binding description of graphene [94–97]. Especially in the presence of gauge fields a rigid ultraviolet momentum cutoff is known to violate gauge invariance which is a serious aspect from a theoretical perspective. However, in reality, the band structure of graphene is naturally bounded and thus also the region where the effective Dirac model provides a reasonable approximation is finite. This is, for instance, illustrated in Fig. 6.1, where the energy spectra of differently sized graphene flakes in the presence of a magnetic field are numerically calculated within a tight-binding approach. The Landau-level clustering appearing in these spectra occurs only in a region $|E| \lesssim t$ which roughly matches the validity range of the effective Dirac model. As leaving this energy range, the Landau-level clustering suddenly breaks down in the numerical spectra. Though this breakdown rather results from warping of the Dirac cones when moving away from the K- and K'-point than from a rigid cutoff

the latter seems to provide a reasonable regularization for an analytic approach in this context. Thus, regarding $|E| \lesssim t$ as a reasonable choice in accordance with the literature [24, 223] one finds the Landau-level cutoff ν as defined in Eq. (6.4). Note that this definition yields a magnetic field-dependent cutoff ν.

However, as gauge violation is a crucial issue, one strives for a cutoff-independent formulation of the respective theory also in the context of superradiance in graphene [93–95]. Thus, picking up the discussion about the importance of far off-resonant contributions stemming from inter-band transitions, one arrives at the proposed phase boundary $g_{c,M}$. At first glance, the underlying regularization method might seem justified as the probability for multiphotonic events involving a large number of photons can be estimated to be rather small. However, these arguments are likely based on a perturbative ansatz of which it is known that its validity fades for ultrastrong couplings (cf. Tab. 3.1) as required to reach $g_{c,M}$, Eq. (7.38).

To clarify which of both regularization techniques rather resembles the actual properties of graphene the results obtained for either approach are compared with a numerical tight-binding simulation of graphene (cf. Chap. 6 for details on the numerical setup). Within the numerical calculation the full band structure of graphene is considered and thus the results naturally account also for higher order terms as those captured by the effective Dirac model. Thus, also quadratic contributions stemming from the warping of the bands are certainly included. Furthermore, the numerical simulation accounts for any light-matter interaction contribution which naturally arises from the Hamiltonian in dipole approximation. Consequently, the numerical tight-binding results include intra- as well as inter-band processes corresponding to their actual weighting. Finally, the comparison of the numerical results with the analytic predictions identifies one of the two regularization methods to yield convincing agreement. However, to provide the suitable analytical bases for this comparison one has to account for trigonal warping as apparent from the tight-binding spectra, Fig. 6.1. Substitution of ϵ_L with $\tilde{\epsilon}_L = \epsilon_L(1 - \kappa|L|)$ rises the value of $\bar{U}_L^\gamma$, Eq. (7.30), and thus in turn the critical points, $g_{c,M}$ and $g_{c,\nu}$, are shifted to lower values. Thereby, $\kappa > 0$ corresponds to a small correction parameter and is given in Eq. (6.3). By identical evaluation of the previous steps, one finds the cutoff-independent value of the critical coupling to be precisely given by

$$\tilde{g}_{c,M} = \frac{\hbar \sqrt{\omega_0 \left(\omega_c/(2\delta_{M,0}) + \tilde{\Omega}_M \right)}}{2} < g_{c,M}, \tag{7.39}$$

where $\hbar\tilde{\Omega}_M = \tilde{\epsilon}_{M+1} - \tilde{\epsilon}_M$. Thus, the result retains the cutoff independence when trigonal warping is considered.

The evaluation of the equivalent of Eq. (7.36) for $\gamma = 1$ yields

$$\tilde{g}_{c,\nu} = \frac{\hbar \sqrt{\omega_0 \omega_c}}{2 \sqrt{2 v(\kappa)}} < g_{c,\nu}, \tag{7.40}$$

where $v(\kappa)$ corresponds to rather cumbersome expression when exactly carrying out the sum over $\bar{U}_L^1$ according to Eq. (7.32). By a Taylor series expansion of $\bar{U}_L^1$ around $\kappa = 0$ one

finds in first-order approximation:

$$v(\kappa) \approx \sqrt{\nu} + \kappa \left[\sqrt{\nu}(3\nu - 2) + 4\zeta_{-\frac{1}{2}}(\nu - 1) - 4\delta_{M,0} - 4\zeta_{-\frac{1}{2}}(M + 1) \right], \qquad (7.41)$$

where $\zeta_x(z)$ denotes the Hurwitz zeta function [203]. For the comparison with the simulation however the exact value of $v(\kappa)$ will be applied.

Table 7.1 enumerates the values of the critical points extracted from the tight-binding simulations and provides a comparison of these values with the analytic prediction for either regularization. The numerical results are obtained from the evaluation of the photon occupation (cf. Subsec. 7.2.2) as a function of the coupling g_{TB} as defined in Eq. (6.8). According to the definition of g_{TB}, the approximate Landau-level degeneracy $\mathcal{N}_{\mathrm{TB}}$ of the Landau-level clusters in the tight-binding spectra, Fig. 6.1, has to be explicitly taken into account for the comparison with the analytic result. In particular, Tab. 7.1 compares $\tilde{g}_{c,\mathrm{TB}} = e\sqrt{\mathcal{N}_{\mathrm{TB}}}\, g_{c,\mathrm{TB}}$ with the analytically predicted phase boundary. The values of $\mathcal{N}_{\mathrm{TB}}$ are thereby found in Tab. 6.1. Furthermore, the Landau-level cutoff ν entering the analytic expressions $g_{c,\nu}$, Eq. (7.37), and $\tilde{g}_{c,\nu}$, Eq. (7.40), were chosen in accordance with the actual number of resolved Landau-level clusters in the tight-binding spectra. The corresponding values are also enumerated in Tab. 6.1. The tight-binding systems cover a variety of different values for ν, ranging from $\nu = 2$ to $\nu = 4$, such that Tab. 7.1 provides a comprehensive comparison of the critical points. This is complemented by the evaluation of the simulation and the analytic approach for different Fermi levels. Despite slight deviations the numerical results for the critical point coincide remarkably well with $\tilde{g}_{c,\nu}$ where trigonal warping is considered. For the larger systems, $L \approx 8.5\,\mathrm{nm}$ and $L \approx 6\,\mathrm{nm}$, also the comparison with the cutoff-dependent critical point obtained within Dirac approximation, $g_{c,\nu}$, yields satisfying agreement with the numerical values. This does not hold for the cutoff-independently regularized equivalents where almost all sets of parameters show significant deviations from the numerical result.

Before proceeding with the further evaluation of the path integral and the comparison of the analytic predictions obtained therefrom with the numerical simulation, it is important to emphasize that the comparison of the critical points extracted from the tight-binding simulation with the results $\tilde{g}_{c,x}$, $x = M, \nu$, represents an extension to the Dirac model. This extension is solely required as the simulated systems are small. If considering systems with side lengths in a few hundred nano- or even micrometer range, the necessity for a trigonal-warping extension will fade as the number of Landau levels in the linear energy regime increases for constant flux values. Simultaneously, the significance of the correction diminishes for a fixed flux through the system since $\kappa \propto \varphi/L^2$. This can also be seen from Tab. 7.1, as the deviations of the tight-binding result for the critical point and $g_{c,\nu}$ narrow when the system size increases. Likewise, the deviations of the tight-binding result $\tilde{g}_{c,\mathrm{TB}}$ from $\tilde{g}_{c,\nu}$ and $g_{c,\nu}$ for the smallest system, $L \approx 4\,\mathrm{nm}$, are largest compared with the results of $L \approx 6\,\mathrm{nm}$ and $8.5\,\mathrm{nm}$. This indicates signatures of finite-size effects which are however not further investigated during this thesis. Summarizing, the convincing agreement of $\tilde{g}_{c,\mathrm{TB}}$ and $\tilde{g}_{c,\nu}$ is interpreted as cutoff regularization provides a well-suited approach for the prediction of the critical point. By contrast, the cutoff-independent regularization method suggested by Ref. [93] fails in the attempt of proper description of the

System	M	$\varphi = 12.5$				
		$\tilde{g}_{c,\mathrm{TB}}\,[\hbar\omega_c]$	$\tilde{g}_{c,\mathrm{TB}}/\tilde{g}_{c,\nu}$	$\tilde{g}_{c,\mathrm{TB}}/g_{c,\nu}$	$\tilde{g}_{c,\mathrm{TB}}/\tilde{g}_{c,M}$	$\tilde{g}_{c,\mathrm{TB}}/g_{c,M}$
8.5 nm	0	0.195	1.002	0.990	0.785	0.779
	1	0.150	1.021	0.985	0.752	0.723
	2	0.139	1.046	0.983	0.931	0.872
6 nm	0	0.2	1.000	0.978	0.813	0.799
	1	0.153	1.021	0.949	0.799	0.738
	2	0.126	1.018	0.894	0.911	0.793
4 nm	0	0.205	1.003	0.958	0.853	0.820
	1	0.151	1.036	0.871	0.878	0.727
System	M	$\varphi = 18$				
		$\tilde{g}_{c,\mathrm{TB}}\,[\hbar\omega_c]$	$\tilde{g}_{c,\mathrm{TB}}/\tilde{g}_{c,\nu}$	$\tilde{g}_{c,\mathrm{TB}}/g_{c,\nu}$	$\tilde{g}_{c,\mathrm{TB}}/\tilde{g}_{c,M}$	$\tilde{g}_{c,\mathrm{TB}}/g_{c,M}$
8.5 nm	0	0.208	1.075	1.057	0.842	0.831
	1	0.158	1.097	1.041	0.809	0.765
	2	0.122	1.003	0.917	0.847	0.769
6 nm	0	0.200	1.010	0.978	0.819	0.799
	1	0.147	1.020	0.916	0.800	0.712
	2	0.105	0.904	0.745	0.811	0.661
4 nm	0	0.205	1.022	0.957	0.867	0.819
	1	0.134	1.005	0.773	0.858	0.645

TABLE 7.1: Critical couplings $\tilde{g}_{c,\mathrm{TB}}$, third column, extracted from the analysis of the photon occupation within the tight-binding simulation. Thereby, M refers to the filling of the system. For the evaluation of the numerical simulation and the analytic approach resonance was imposed. The values of the approximate Landau-level degeneracy, $\mathcal{N}_{\mathrm{TB}}$, where explicitly taken into account according to Tab. 6.1. Thus, g_{TB} as defined in Eq. (6.8) entered the simulation such that $\tilde{g}_{c,\mathrm{TB}} = e\sqrt{\mathcal{N}_{\mathrm{TB}}}\, g_{c,\mathrm{TB}}$ is the quantity which is compared with the analytically obtained values for the critical point. Hence, $\tilde{g}_{c,\mathrm{TB}}$ is compared with the analytical result obtained within cutoff regularization for trigonal-warping correction (fourth column) and for the Dirac model (fifth column). Likewise, the sixth and seventh column compare $\tilde{g}_{c,\mathrm{TB}}$ with the cutoff-independent equivalents. The cutoffs for the analytic evaluation of $\tilde{g}_{c,\nu}$, Eq. (7.37), and $g_{c,\nu}$, Eq. (7.40), respectively, were chosen from the numerical tight-binding spectra, depicted in Fig. 6.1 and enumerated in Tab. 6.1. The deviation of the tight-binding result $\tilde{g}_{c,\mathrm{TB}}$ are smallest when compared with the trigonal-warping corrected cutoff-dependent analytic prediction. Further details on the tight-binding simulations are found in Chap. 6.

critical points obtained from the simulation.

In Subsec. 7.2.1 and 7.2.2 the comparison of the numerical simulation and the path integral approach within both regularization methods is continued and extended to the

discussion of the ground-state energy and the photon occupation. With this the discussion of the analytic approach is continued and focused on the Dirac approximation.

Having derived the phase boundary for either regularization, one is able to estimate the parameters of the system required to actually reach these critical points. In equilibrium, the coupling strength of the charge carriers with the cavity mode is determined by the microscopic properties of both subsystems (cf. Subsec. 5.2.3) and thus rather rarely tunable. In particular, the coupling is given by $g_r = \hbar\omega_c/\sqrt{2\pi 137\sqrt{\epsilon_r}}$, Eq. (5.40), where $\epsilon_r = 1$ shall be assumed from now on. Thus, a possible phase transition will only occur if $g_r > g_{c,x}$, $x = M, \nu$. From this inequality one is eventually able to define the required filling and, in case of $g_{c,\nu}$, the magnetic field for which the system is expected to leave the normal phase.

In the case of cutoff-independent regularization, this inequality is easily evaluated at resonance,

$$g_r > g_{c,M} \quad \Leftrightarrow \quad M > 53, \tag{7.42}$$

in accordance with Ref. [93]. As M denotes the last occupied Landau level, the system is expected to naturally exhibit an equilibrium phase transition for a sufficient large Fermi level.

By contrast, the critical point $g_{c,\nu}$ is determined by the Fermi level and the value of the cutoff or the magnetic field, respectively, as well. Thus, one expects the system to leave the normal phase when

$$
\begin{aligned}
g_r > g_{c,\nu} \quad \Leftrightarrow \quad B\,[\mathrm{T}] &< \frac{32 \times 10^4}{18769\pi^2}(1 + 2M + 2\sqrt{M(M+1)}) \\
&\approx 1.72746 \times (1 + 2M + 2\sqrt{M(M+1)}).
\end{aligned}
\tag{7.43}
$$

For different values of M this results in a phase diagram as depicted in Fig. 7.1. From Fig. 7.1 it becomes clear that one is able to cross the phase boundary by either tuning the Fermi level or the magnetic field or both at once. Within this approach, the superradiant quantum phase transition is predicted to occur at rather small fillings and magnetic fields. This contrasts the result obtained for cutoff-independent regularization, where the phase boundary is found at large fillings. If cutoff-regularization resembles the true properties of the system as indicated by the comparison of the critical points obtained from the independent tight-binding simulation, this result will be remarkable as the critical point is predicted for an experimentally feasible parameter range concerning both variables, M and B. For instance, the spectroscopic experiments reported in Refs. [28–30] show convincing resolution of Landau levels up to $M = 5$ for a magnetic field range of a few Tesla. Furthermore, recent experiments [55] have shown that the required ultrastrong coupling regime is also feasible.

7.2   The partition sum in the thermodynamic limit

The previous discussion demonstrated the existence of a critical point $g_{c,x}$, $x = M, \nu$, for Landau-quantized graphene in Dirac approximation. The critical point is thereby determined from $\partial_\alpha^2 \Phi^\gamma(\alpha, \alpha)\big|_0 = 0$ which means that the trivial solution, $\alpha_0 = 0$, of $\partial_\alpha \Phi^\gamma(\alpha, \alpha) = 0$ no longer corresponds to the minimum of the phase function when the
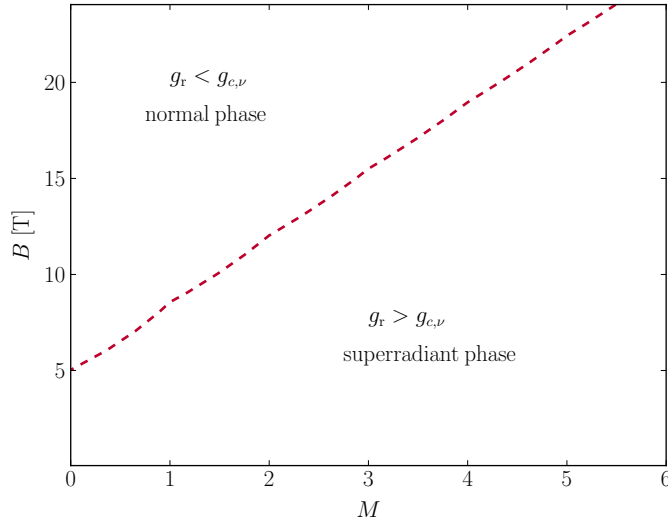
FIGURE 7.1: Phase diagram of the superradiant critical behavior within cutoff regularization. The cutoff is thereby determined by Eq. (6.4). The dashed curve corresponds to the phase boundary of the system. For any choice of the parameter set (M, B) referring to point below the phase boundary the system is expected to be in the superradiant phase. By contrast, a point above the phase boundary refers to the normal phase of the system.

coupling g exceeds the critical point. Thus, in the regime $g > g_{c,x}$, $x = M, \nu$, a yet unknown non-trivial $\alpha_0 \neq 0$ solution of $\partial_\alpha^2 \Phi^\gamma(\alpha, \alpha)$ minimizes the phase function $\Phi^\gamma(\alpha, \alpha)$. Note that the non-trivial solutions α_0 also carry a label γ denoting the chosen regularization approach according to the definition of the modified matrix elements $\mathcal{M}_{N,N''}^\gamma$, Eq. (7.25). However, for the sake of brevity, this subscript is omitted.

As the square of the minimizing solution α_0 is associated with the cavity occupation, the trivial solution corresponds to the normal phase of the system where the ground-state properties of the system are governed by the ground states of the photonic and electronic subsystem. Then for $\beta \to \infty$, the non-trivial solution $\alpha_0 \neq 0$ for $g > g_{c,x}$, $x = M, \nu$, describes the ground-state properties of the system in the superradiant phase which are precisely characterized by a spontaneous photonic occupation of the cavity. This is identical with the discussion of the mean-field solution for the ordinary Dicke model (cf. Chap. 3).

However, as already pointed out, the task of finding the non-trivial solutions of Eq. (7.14) is analytically challenging but in the thermodynamic limit easily accomplished within a numerical approach.

Thus, consider again the phase functional in the thermodynamic limit evaluated at a real-valued static field α,

$$\Phi^\gamma(\alpha, \alpha) = \mathcal{S}_+(\alpha, \alpha) - \log\left[\det\left[\mathbb{1} - \mathbb{G}_0 \mathbb{M}^\gamma(\alpha, \alpha)\right]\right]. \tag{7.44}$$

The expression in the argument of the functional determinant represents a matrix in the basis of the Grassmann vectors $\tilde{\rho}^{\dagger}$ and $\tilde{\rho}$ similar as defined in Eq. (7.2). From the discussion in Sec. 3 in App. D one finds for the fermionic contribution to $\Phi(\alpha, \alpha)$:

$$\log\left[\det\left[\mathbb{1} - \mathbb{G}_0\mathbb{M}^{\gamma}(\alpha, \alpha)\right]\right] \overset{(E.41)}{=} \sum_j \log\left[1 \mp e^{-\beta[\bar{\epsilon}_j^{\gamma}(\alpha) - \mu]}\right] = -\beta\Omega_-^{\gamma}(\alpha, \alpha), \qquad (7.45)$$

where, $\bar{\epsilon}_j^{\gamma}(\alpha)$ denotes the energy of the single-particle state j obtained from diagonalization of $\mathbb{1} - \mathbb{G}_0\mathbb{M}^{\gamma}(\alpha, \alpha)$ at $\omega_n^- = 0$. The fermionic grand-canonical potential is denoted by $\Omega_-^{\gamma}(\alpha, \alpha)$. Thus, the evaluation of the Matsubara sum encoded in this expression corresponds to a weighted summation over eigenvalues $\bar{\epsilon}_j^{\gamma}(\alpha)$. These eigenvalues are then obtained numerically. Finally, by minimization of

$$\Phi^{\gamma}(\alpha, \alpha) = \beta\left[\hbar\omega_0\alpha^2 + \Omega_-^{\gamma}(\alpha, \alpha)\right] \qquad (7.46)$$

one finds the real-valued static solutions α_0 according to Eqs. (7.22, 7.23).

One approximates then the field integral defining the partition sum by a static Gaussian expansion around the minimizing field configuration:

$$\Phi^{\gamma}(\alpha, \alpha) \approx \Phi^{\gamma}(\alpha_0, \alpha_0) + \frac{1}{2}\left.\partial_{\alpha}^2\Phi^{\gamma}(\alpha, \alpha)\right|_{\alpha_0}(\alpha - \alpha_0)^2, \qquad (7.47)$$

where $\alpha(\tau) = \alpha$ refers to a static configuration in the vicinity of α_0 and $\left.\partial_{\alpha}^2\Phi^{\gamma}(\alpha, \alpha)\right|_{\alpha_0} > 0$. This method is known as the method of steepest descent or stationary phase approximation in case of a complex exponential (cf. Sec. 1 in App. D). Note that this order of approximation completely suppresses quantum fluctuations and the resulting expression for the phase function captures only the dominant mean-field contribution identical to the term $\hat{\mathcal{H}}_{D,0}$ in the discussion of the Dicke model (cf. Chap. 3). A discussion of quantum fluctuations is however found in Sec. 7.3.

By carrying out the integration over $\mathrm{Im}[\alpha]$ and $\mathrm{Re}[\alpha]$ one eventually finds for the normalized partition sum

$$\bar{\mathcal{Z}}_{\mathrm{SPA}} = (\mathcal{Z}_0^+)^{-1}\sqrt{\frac{2}{\hbar\omega_0\beta|\left.\partial_{\alpha}^2\Phi^{\gamma}(\alpha, \alpha)\right|_{\alpha_0}|}}e^{-\mathcal{N}\Phi^{\gamma}(\alpha_0, \alpha_0)}, \qquad (7.48)$$

where the notation of Ref. [95] was adopted. During the following, the ground-state energy and the photon occupation are evaluated in the thermodynamic limit. These observables are then also compared with the tight-binding equivalent during the following.

7.2.1 Ground-state energy

One obtains the ground-state energy of the system in the thermodynamic limit from

$$\frac{E_0}{\mathcal{N}} = -\lim_{\beta\to\infty}\partial_{\beta}\log\bar{\mathcal{Z}}_{\mathrm{SPA}}. \qquad (7.49)$$

Thereby, the meaning of this observable is identical to the one of the corresponding mean-field quantity arising from $\hat{\mathcal{H}}_{D,0}$ in the discussion of the Dicke model (cf. Chap. 3). Similarly, the derivatives of the ground-state energy with respect to the coupling parameter provide insight into the order of the underlying phase transition. Figure 7.2 a) shows
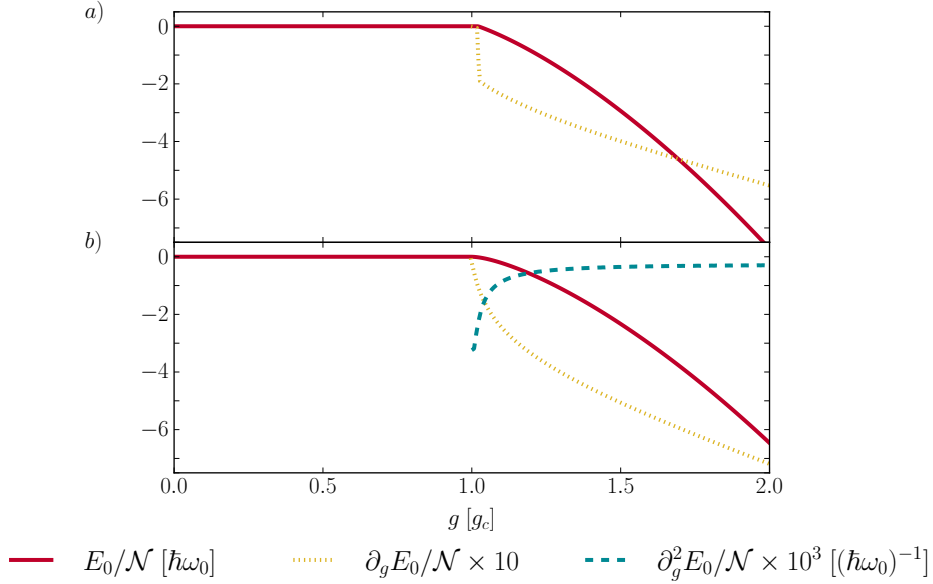
FIGURE 7.2: Ground-state energy and its derivatives with respect to the coupling g for a) cutoff-independent regularization and b) cutoff regularization at resonance. The Fermi level was chosen between $M = 1$ and $M + 1$ and the cutoff was set at $\nu = 4$ in panel b). Panel a) shows typical signatures of a first-order quantum phase transition as the first-order derivative is discontinuous. By contrast, panel b) depicts the features of a second-order quantum phase transition (cf. Subsec. 3.3.1).

the ground-state energy and its first derivative as a function of the coupling parameter g for the cutoff-independently regularized partition sum. Likewise, Fig. 7.2 b) illustrates the ground-state energy as well as its first and second derivative when a rigid ultraviolet cutoff is applied at $\nu = 4$. The cavity mode is assumed to be resonant with the transition frequency of the last occupied and first unoccupied Landau level, $M = 1$ and $M + 1$, respectively. The cutoff-independent result seen in panel a) shows signatures of a first-order quantum phase transition for this particular choice of the Fermi level. As this investigation goes beyond the discussion found in Ref. [93] no comparison of this result with the literature can be carried out. Panel b) of Fig. 7.2 shows typical features of a second-order quantum phase transition similar to the one exhibited by the original Dicke model (cf. Sec. 3.3).

A comparison with the tight-binding results for the ground-state energy, Fig. 7.3, shows qualitative agreement with E_0 depicted in Fig. 7.2 b) where cutoff-regularization has been applied. In particular, the behavior of the first- and second-order derivative of the tight-binding result for E_0 also show signatures of a second-order quantum phase transition even though finite-size effects are apparent. This general behavior is also revealed by the
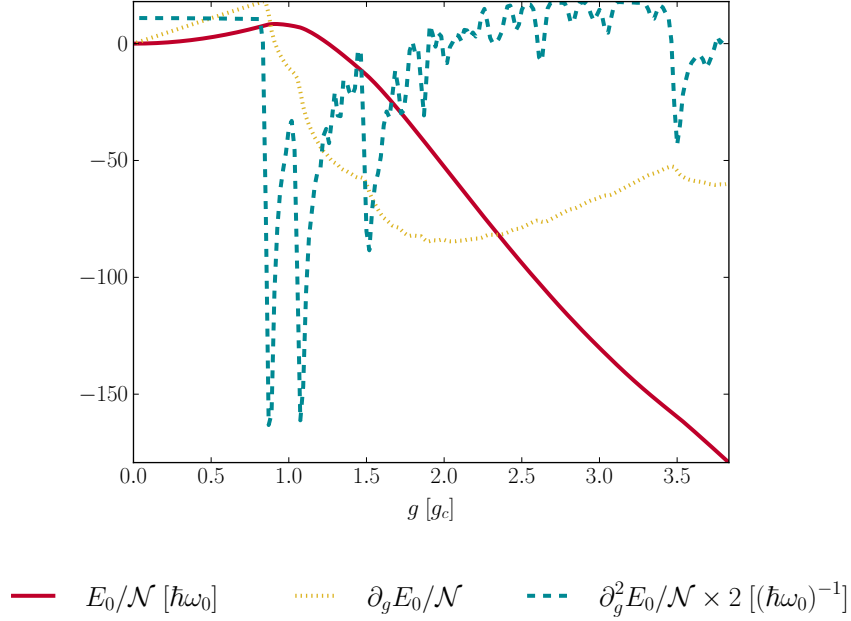
FIGURE 7.3: Ground-state energy and its derivatives with respect to the coupling g obtained from the tight-binding simulations for identical parameters as shown in Fig. 7.2. The slight increase of the ground-state energy (solid) for $g < \tilde{g}_{c,\mathrm{TB}}$ is probably due to finite-size effects. The first-order derivative is continuous at any depicted point. This does not hold for the second-order derivative which discontinuously changes its value as the critical point is crossed. This behavior is a generic feature of a second-order quantum phase transition.

photon occupation as it discussed during the following.

7.2.2   Photon occupation

The photon occupation of the cavity is derived from the partition sum in the thermo-dynamic limit. The ground-state properties of this observable are in particular obtained from

$$\frac{\langle \hat{a}^\dagger \hat{a} \rangle_0}{\mathcal{N}} = \frac{\alpha_0^2}{\mathcal{N}} = - \lim_{\beta \to \infty} \frac{1}{\beta} \partial_{\hbar\omega_0} \log \bar{\mathcal{Z}}_{\mathrm{SPA}}, \tag{7.50}$$

which is easily verified in view of Eq. (7.48). Thus, in the thermodynamic limit the ground-state occupation of the cavity is identical with the squared value of the mini-mizing field configuration α_0. Again, α_0 corresponds to the equivalent of the mean field α introduced in the discussion of the Dicke Hamiltonian in Sec. 3.3.

In the superradiant phase, α_0 is obtained numerically from minimizing the phase function $\Phi(\alpha, \alpha)$. Fig. 7.4 exemplarily illustrates the behavior of the cutoff-regularized phase $\Phi^1(\alpha, \alpha)$ as a function of the real-valued static field configuration α for various values of the coupling. It can be seen that the trivial solution, $\alpha_0 = 0$, corresponds to a minimum of the phase for $g < g_{c,\nu}$. As the coupling approaches the critical point, the phase function flattens and exhibits a new global minimum at $\alpha_0 \neq 0$ when the phase boundary is

crossed. Then, the trivial solution no longer corresponds to the global minimum of the system and the second derivative of the phase function evaluated at this point changes its sign. This particular behavior is regarded a generic feature of a second-order quantum phase transition. This is contrasted by Fig. 7.5 which shows the equivalent situation
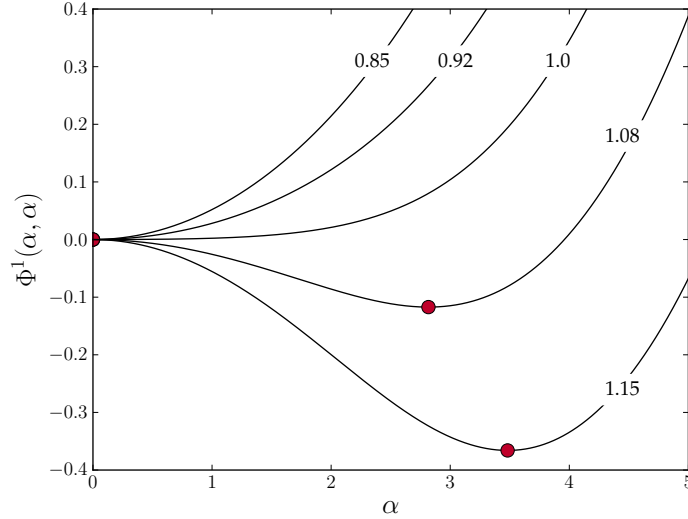
FIGURE 7.4: Phase function of the cutoff-regularized system at resonance. The cutoff was chosen at $\nu = 4$ and the system is filled up to the Landau level $M = 1$. The numbers associated with each line refer to the value of the coupling normalized by the critical coupling according to Eq. (7.37). The minimum of the phase function, α_0, is marked with the red dot for each coupling value. In the normal phase, $g < g_{c,\nu}$, the trivial solution corresponds to the minimum of the phase function. As the system approaches the critical point, the phase function flattens and a new minimum appears for $\alpha_0 \neq 0$. This is accompanied by a sign change of the second derivative of the phase function at $\alpha_0 = 0$.

when the rotating wave-like approximation is applied for regularization. The behavior seen in Fig. 7.5 is typical for a first-order quantum phase transition: The trivial solution corresponds to a global minimum for small couplings $g < g_{c,M}$. As the coupling rises, the trivial solution corresponds to a local minimum as another local minimum appears at $\alpha_0 \neq 0$. In this intermediate coupling regime both local minima compete for minimizing the phase function. For large enough couplings however the non-trivial solution, $\alpha_0 \neq 0$, corresponds again to a global minimum. The critical point obtained in Sec. 7.1 however refers to a second-order quantum phase transition and is unsuitable for the prediction of a the critical point in case of a first-order quantum phase transition. This can be seen from Fig. 7.5. The extraction of α_0 from the phase function then yields a discontinuity in the value of the photon occupation as a certain coupling is exceeded. This particular behavior can also be seen from expansion of the phase function around $\alpha_0 = 0$. Thus, consider

$$\Phi^\gamma(\alpha, \alpha) \approx \frac{A^\gamma}{2}\alpha^2 + \frac{B^\gamma}{4}\alpha^4, \tag{7.51}$$
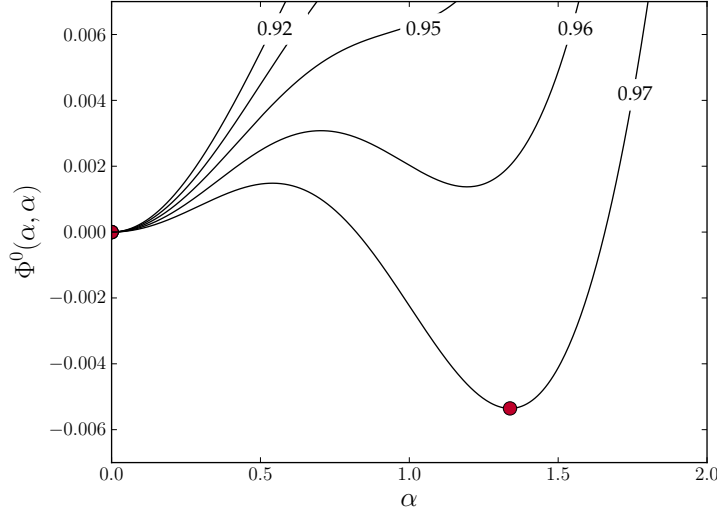
FIGURE 7.5: Phase function of the rotating-wave like regularized system at resonance. The system is filled up to the Landau level $M = 1$. Each line refers to a different coupling strength and the red dots mark the position of the minima of the phase function. The depicted behavior is typical for a first-order quantum phase transition: As the coupling increases, the initial global minimum of the phase function in the normal phase, $\alpha_0 = 0$, transforms into a local minimum along with the appearance of another local minimum at $\alpha_0 \neq 0$. For large enough couplings, however, the non-trivial solution α_0 corresponds to a global minimum. The critical coupling predicted from the considerations in Sec. 7.1 refers to a second-order quantum phase transition and thus is not compatible with the transition point of this actual first-order phase transition.

where

$$A^\gamma = \partial_\alpha^2 \Phi^\gamma(\alpha, \alpha)\big|_{\alpha_0=0} \overset{(7.36)}{\propto} g_{c,\gamma}^2 - g^2, \tag{7.52}$$

$$B^\gamma = \partial_\alpha^4 \Phi^\gamma(\alpha, \alpha)\big|_{\alpha_0=0} = \mathrm{Tr}\left[\mathbb{G}_0 \frac{\partial \mathbb{M}^\gamma}{\partial \alpha} \mathbb{G}_0 \frac{\partial \mathbb{M}^\gamma}{\partial \alpha} \mathbb{G}_0 \frac{\partial \mathbb{M}^\gamma}{\partial \alpha} \mathbb{G}_0 \frac{\partial \mathbb{M}^\gamma}{\partial \alpha}\right]_{\alpha=0}, \tag{7.53}$$

in analogy to the Landau theory of phase transitions [14]. Note that any odd product of $\mathbb{G}_0 \partial_\alpha \mathbb{M}^\gamma$ yields a vanishing trace according to the properties of the matrices. A second-order quantum phase transition requires $B^\gamma > 0$ [14]. The photon occupation is then approximately given by $\alpha^2 \approx -A^\gamma/B^\gamma$ [14]. If $B^\gamma < 0$, the phase transition will certainly be of a different order. The fourth-order derivative of the phase function is obtained within an analogous procedure as discussed in Sec. 7.1 for the second-order derivative.

Within the rotating wave-like approximation this yields

$$\partial_\alpha^4 \Phi^0(\alpha, \alpha)\big|_{\alpha_0=0} = \begin{cases} 128 \frac{g^4}{(\hbar\omega_c)^3} \frac{1}{M+1} \left(\frac{1}{\sqrt{M+1}} - \frac{1}{\sqrt{M+2}} \right) > 0, & \text{for } M = 0, \\ 32 \frac{g^4}{(\hbar\omega_c)^3} (\sqrt{M+1} + \sqrt{M})^2 \left(\sqrt{M} - \sqrt{M+2} \right) < 0, & \text{for } M = 1, \\ 32 \frac{g^4}{(\hbar\omega_c)^3} \left[(\sqrt{M} - \sqrt{M-1}) - (\sqrt{M+2} - \sqrt{M+1}) \right] > 0, & \text{for } M > 1. \end{cases}$$

(7.54)

Thus, it can be seen that the coefficient B^0 for $M = 1$ is negative whereas it is positive for all other values of the filling.

For the sake of completion one finds one finds for the cutoff-dependent regularized coefficient B^1:

$$\partial_\alpha^4 \Phi^1(\alpha, \alpha)\big|_{\alpha_0=0} = 128 \frac{g^4}{(\hbar\omega_c)^3} \sqrt{\nu} \left[2\sqrt{\nu}(\sqrt{\nu} - \sqrt{\nu-1}) - 1) \right] > 0 \quad \Leftrightarrow \quad \nu > 1, \quad (7.55)$$

which is positive for all values of $\nu > 1$ and thus corresponds to a second-order transition.

However, no signatures of a first-order transition could be found from the evaluation of tight-binding results as Fig. 7.6 b) shows for an identical filling of $M = 1$. The depicted data clearly indicates a second-order transition as the behavior of the photon occupation is continuous close to the critical point. A similar behavior can be seen for the photon occupation obtained from the cutoff-regularized phase function, Fig. 7.6 a).

Thus, before proceeding the discussion of the details of Fig. 7.6 the intermediate result for the cutoff-independent approach is summarized:

The deviations of the critical coupling predicted for the path integral approach and the tight-binding simulation, Tab. 7.1, are largest when regularized by means of the rotating-wave like approximation which is similarly applied in Ref. [93]. The variant of this approach applied during this thesis predicts a first-order quantum phase transition for a filling up to $M = 1$ which seems not to be replicated by the tight-binding simulation. Thus, due to these significant deviations from the simulation one concludes that this particular choice of regularization provides an insufficient ansatz for the description of the processes occurring in the system. For this reason, the focus of the remaining chapter solely lies upon the cutoff-regularized approach. With this, the discussion of Fig. 7.6 is proceeded.

Both panels of Fig. 7.6 show an increasing photon occupation for increasing ν. The tight-binding results correspond thereby to the systems and parameters as found in the right column of Tab. 6.1, i.e. $\varphi = 18$. The approximate Landau-level degeneracy has been explicitly taken into account for normalization of the photon occupation and the extraction of the critical points found in Tab. 7.1. Besides the convincing agreement in the qualitative scaling behavior of the photon occupation for different values of the Landau-level cutoff ν, deviations in the behavior appear close to the critical point. The path integral approach predicts a rather steep increase for any depicted set of parameters whereas the tight-binding result shows an approximate linear dependence. Furthermore, the path integral result overestimates the photon occupation obtained from the tight-binding simulation by a factor of ≈ 4. These deviations might result from finite-effects even though the path integral result showed identical behavior close to $\tilde{g}_{c,\nu}$ when trigonal warping of
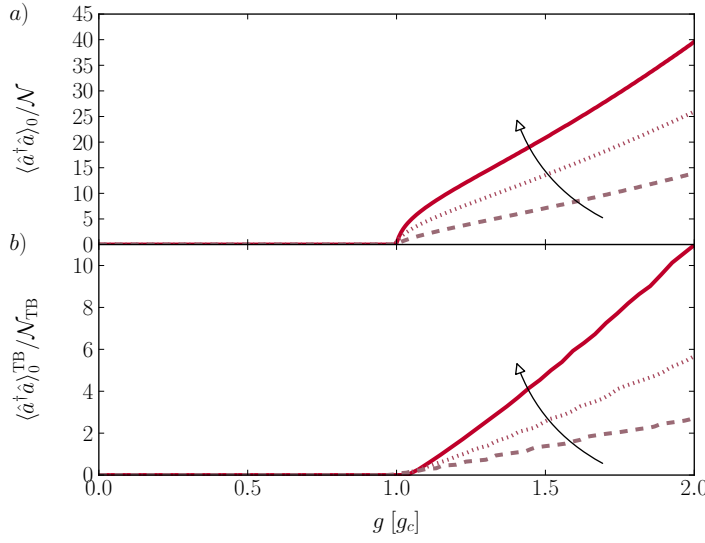
FIGURE 7.6: Photon occupation obtained from a) the path integral approach within cutoff regularization and b) the tight-binding simulation at resonance for various cutoffs: $\nu = 4, 3, 2$ (solid, dotted, dashed). The arrows indicate the direction of raising values of nu. The tight-binding results are obtained for the systems and parameters according to the right column of Tab. 6.1, i.e. $\varphi = 18$. The depicted systems are filled up to Landau level $M = 1$ and show typical behavior of a second-order quantum phase transition. From comparison of both panels follows that the qualitative behavior of the photon occupation for rising Landau-level cutoffs is identical. However, the path integral approach predicts a steep increase of the photon occupation close to $g_{c,\nu}$ whereas the tight-binding simulations shows a linear behavior in this region.

the Landau levels was considered. However, this extension of the model accounts only for the correction of the energy levels but omits higher order contributions of the electromagnetic vector potential to the interaction Hamiltonian of the analytic approach.

Even though deviations are apparent, the qualitative agreement of both approaches is convincing when keeping in mind that the tight-binding simulation refers to a purely microscopic approach solely based on lattice properties of graphene. As the simulated systems are finite and compared to a continuum model in the thermodynamic limit it is even more remarkable that the results of the former show a sharp phase boundary. When considering the original Dicke model, the phase boundary is smoothened for finite N such that one refers to the corresponding transition rather as a phase crossover than a phase transition (cf. Subsec. 3.3.2). However, the sharp phase boundary emerging for the finite-$\mathcal{N}$ tight-binding simulation even retains for very small $\mathcal{N}$ as Fig. 7.7 b) shows. Thereby, the photon occupation of the system $L \approx 8.5\,\mathrm{nm}$ is shown for various fillings and accordingly varying $\mathcal{N}_{\mathrm{TB}}$ as it can be seen from Tab. 6.1. The smallest approximate Landau-level degeneracy shown in Fig. 7.7 b) corresponds to $\mathcal{N}_{\mathrm{TB}} = 4$ for the system being filled up to $M = 2$. Besides the sharp phase boundary retaining also for this small value of $\mathcal{N}_{\mathrm{TB}}$ and the previously mentioned deviations at $g \gtrsim g_c$, the tight-binding simulation qualitatively agrees again with the cutoff-regularized path integral equivalent

shown in Fig. 7.7 a). Thereby, identical parameters were chosen. Thus, for a rising Fermi level also the values of the photon occupation rise. This holds even for the photon occupation obtained from the simulation at $M = 2$ as shown in Fig. 7.7 b) even though the results only slightly exceeds the equivalent obtained for $M = 1$.
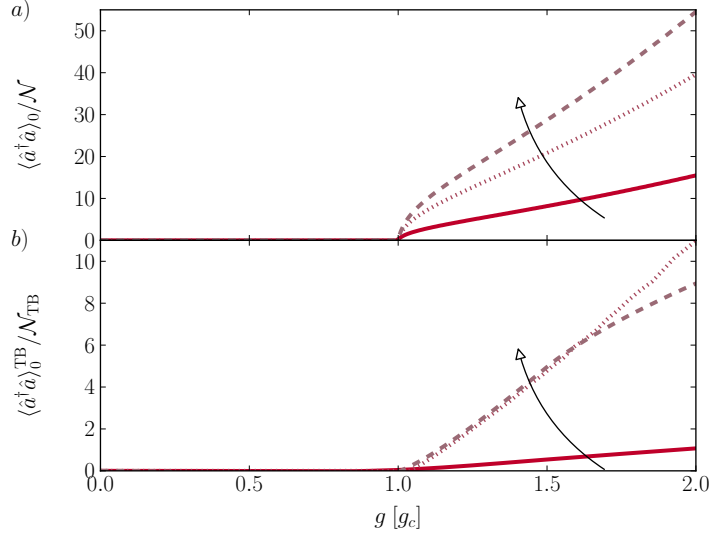
FIGURE 7.7: Photon occupation obtained from the path integral approach within cutoff regularization, a), and the tight-binding simulation, b), at resonance for various fillings: $M = 0, 1, 2$ (solid, dotted, dashed). The cutoff was chosen at $\nu = 4$ in both cases. Again, the qualitative behavior of both approaches differs close to critical point. However, both approaches show an increase of the photon occupation for increasing filling. This holds also for the tight-binding result even though the photon occupation for $M = 2$ only slightly exceeds the equivalent obtained for $M = 1$. All data sets depicted in panel b) are obtained for the system with $L \approx 8.5\,\text{nm}$.

With this, the discussion of quantum fluctuations and the derivation of the excitation spectrum is provided during the following. Thereby, cutoff regularization will be solely applied.

7.3 Quantum fluctuations above the ground-state

When aiming for the description of quantum fluctuations above the ground state one expands the phase functional $\Phi[\tilde{\alpha}^*, \tilde{\alpha}]$, Eq. (7.13), in second-order approximation around the real-valued static field configuration α_0 [239, 241, 242].
Let $\tilde{\beta}_N^*$ and $\tilde{\beta}_N$ denote the fluctuation fields in the vicinity of the static solution α_0. By defining [241, 242]

$$\tilde{\alpha}_N^* = \frac{1}{\sqrt{\mathcal{N}}}\left(\tilde{\beta}_N^* - \alpha_0\right), \quad \tilde{\alpha}_N = \frac{1}{\sqrt{\mathcal{N}}}\left(\tilde{\beta}_N - \alpha_0\right), \tag{7.56}$$

similar to the displacements (3.50) applied onto the Dicke model, one finds for the Gaussian expansion of the phase functional

$$\Phi^\gamma[\tilde{\alpha}^*, \tilde{\alpha}] \approx \Phi^\gamma(\alpha_0, \alpha_0) + \frac{1}{2\mathcal{N}} \sum_{\omega_M^+, \omega_N^+} \begin{pmatrix} \tilde{\alpha}_M^* & \tilde{\alpha}_M \end{pmatrix} \delta^2 \Phi_{M,N}^\gamma \begin{pmatrix} \tilde{\alpha}_N^* \\ \tilde{\alpha}_N \end{pmatrix}, \qquad (7.57)$$

where the variation $\delta^2 \Phi_{N,M}^\gamma$ is given by [241, 242]:

$$\delta^2 \Phi_{M,N}^\gamma = \begin{pmatrix} \delta^2 \Phi_{M,N}^{\gamma,1,1} & \delta^2 \Phi_{M,N}^{\gamma,1,2} \\ \delta^2 \Phi_{M,N}^{\gamma,2,1} & \delta^2 \Phi_{M,N}^{\gamma,2,2} \end{pmatrix}. \qquad (7.58)$$

The last term on the r.h.s. of Eq. (7.57) is analogous to the contribution $\hat{\mathcal{H}}_{D,2}$ capturing the quantum fluctuations in the Dicke model. As shown in Ref. [118], one is also able to obtain the coefficients defining $\hat{\mathcal{H}}_{D,2}$ from the second-order derivate of the mean-field configuration $\hat{\mathcal{H}}_{D,0}$ with respect to the mean fields. The matrix elements $\delta^2 \Phi_{N,M}^{\gamma,i,j}$ are particularly defined by

$$\begin{aligned}
\delta^2 \Phi_{M,N}^{\gamma,1,1} &= \left. \frac{\delta^2 \Phi^\gamma[\tilde{\alpha}^*, \tilde{\alpha}]}{\delta \tilde{\alpha}_M^* \delta \tilde{\alpha}_N^*} \right|_{\tilde{\alpha}^*=\tilde{\alpha}=\alpha_0} = \delta_{M,-N} R^\gamma(i\omega_M^+), \\
\delta^2 \Phi_{M,N}^{\gamma,1,2} &= \left. \frac{\delta^2 \Phi^\gamma[\tilde{\alpha}^*, \tilde{\alpha}]}{\delta \tilde{\alpha}_M^* \delta \tilde{\alpha}_N} \right|_{\tilde{\alpha}^*=\tilde{\alpha}=\alpha_0} = \delta_{M,N} \ S^\gamma(i\omega_M^+), \\
\delta^2 \Phi_{M,N}^{\gamma,2,1} &= \left. \frac{\delta^2 \Phi^\gamma[\tilde{\alpha}^*, \tilde{\alpha}]}{\delta \tilde{\alpha}_M \delta \tilde{\alpha}_N^*} \right|_{\tilde{\alpha}^*=\tilde{\alpha}=\alpha_0} = \delta_{M,N} \ S^\gamma(i\omega_M^+), \\
\delta^2 \Phi_{M,N}^{\gamma,2,2} &= \left. \frac{\delta^2 \Phi^\gamma[\tilde{\alpha}^*, \tilde{\alpha}]}{\delta \tilde{\alpha}_M \delta \tilde{\alpha}_N} \right|_{\tilde{\alpha}^*=\tilde{\alpha}=\alpha_0} = \delta_{M,-N} R^\gamma(i\omega_M^+),
\end{aligned} \qquad (7.59)$$

where the notation introduced in Ref. [242] was adopted. From Eqs. (7.15, 7.17) one finds further

$$\begin{aligned}
\delta^2 \Phi_{M,N}^{\gamma,1,1} &= - \left. \frac{\delta}{\delta \tilde{\alpha}_M^*} F[\alpha_{-N}^*, \alpha_N] \right|_{\alpha_0} \\
&= \frac{1}{\beta} \sum_{\substack{\omega_n^-, \omega_m^- \\ n-m=M}} \sum_I \left(\mathbb{A}^{-1}[-i\omega_n^- - \mu, \alpha_0, \alpha_0](-\mathbb{G}_0(i\omega_n^-)\mathbb{M}[1,0]) \right. \\
&\qquad \times \left. \mathbb{A}^{-1}[-i\omega_n^- - \mu, \alpha_0, \alpha_0](-\mathbb{G}_0(i\omega_m^-)\mathbb{M}[1,0]) \right)_{I,I} \delta_{M,-N}, \\
\delta^2 \Phi_{M,N}^{\gamma,2,1} &= \left. \frac{\delta}{\delta \tilde{\alpha}_M} \left((-i\omega_N^+ + \hbar\omega_0)\tilde{\alpha}_N - F[\alpha_{-N}^*, \alpha_N] \right] \right|_{\alpha_0} \\
&= \left[\hbar\omega_0 + \frac{1}{\beta} \sum_{\substack{\omega_n^-, \omega_m^- \\ n-m=M}} \sum_I \left(\mathbb{A}^{-1}[-i\omega_n^- - \mu, \alpha_0, \alpha_0](-\mathbb{G}_0(i\omega_n^-)\mathbb{M}[1,0]) \right. \right. \\
&\qquad \times \left. \left. \mathbb{A}^{-1}[-i\omega_n^- - \mu, \alpha_0, \alpha_0](-\mathbb{G}_0(i\omega_m^-)\mathbb{M}[0,1]) \right)_{I,I} \right] \delta_{M,N}.
\end{aligned} \qquad (7.60)$$

Based on the numerically obtained α_0 these expressions are then also numerically evaluated. The fermionic Matsubara sums are thereby transformed into a sum over residue (cf. Sec. 3 in App. E) which is then evaluated by numerical integration in the complex plane under usage of the residue theorem. The resulting expressions for $R(i\omega_M^+)$ and $S(i\omega_M^+)$ then yield the excitation spectrum of the quantum fluctuations which is seen from the following [239, 242]:
Supposing to know $R(i\omega_M^+)$ and $S(i\omega_M^+)$ for a given bosonic Matsubara frequency ω_M^+, one finds for the partition sum [239, 242]:

$$\bar{\mathcal{Z}} \approx \bar{\mathcal{Z}}_{\text{SPA}} \oint \mathcal{D}[\tilde{\boldsymbol{\alpha}}] e^{-\mathcal{S}_{\text{G}}[\{\tilde{\boldsymbol{\alpha}}^*, \tilde{\boldsymbol{\alpha}}\}]} \tag{7.61}$$

where the action of the quantum fluctuations in Gaussian approximation is given by

$$\mathcal{S}_{\text{G}}[\{\tilde{\boldsymbol{\alpha}}^*, \tilde{\boldsymbol{\alpha}}\}] = \sum_{\omega_M^+ \geq 0} \tilde{\boldsymbol{\alpha}}_M^\dagger \, \mathbb{S}(i\omega_M^+) \, \tilde{\boldsymbol{\alpha}}_M, \quad \mathbb{S}(\omega_N^+) = \begin{pmatrix} S^\gamma(i\omega_M^+) & R^\gamma(i\omega_M^+) \\ R^\gamma(i\omega_M^+) & S^\gamma(-i\omega_M^+). \end{pmatrix} \tag{7.62}$$

Thereby, the vector notation $\tilde{\boldsymbol{\alpha}}_M^\dagger = (\tilde{\alpha}_M^* \; \tilde{\alpha}_{-M}^*)$, $\tilde{\boldsymbol{\alpha}}_N = (\tilde{\alpha}_M \; \tilde{\alpha}_{-M})^T$ for the fluctuation fields was introduced. The path integral over the fluctuation fields is then easily evaluated yielding $\bar{\mathcal{Z}} \approx \bar{\mathcal{Z}}_{\text{SPA}}[\det \mathbb{S}(i\omega_M^+)]^{-1}$. By application of a suitable unitary transformation $\mathbb{U}^\dagger \mathbb{S}(ip) \mathbb{U} = \tilde{\mathbb{S}}(ip)$, where $\tilde{\mathbb{S}}(ip)$ is supposed to be diagonal, one finds for the functional determinant

$$\left[\det \mathbb{S}(i\omega_M^+)\right]^{-1} \overset{(D.75)}{=} \prod_{\omega_M^+ > 0} \left[\left(\omega_M^{+\,2} + \epsilon_+^{\gamma\,2}\right)\left(\omega_M^{+\,2} + \epsilon_-^{\gamma\,2}\right)\right]^{-1}, \tag{7.63}$$

which is reminiscent of the partition sum of two uncoupled harmonic oscillators, Eq. (7.12), when carrying out the Matsubara product. The eigenenergies of $\mathbb{S}(0)$, $\epsilon_\pm^\gamma$, are then associated with the eigenmodes of the quantum fluctuations above the ground state analogous as discussed in Subsec. 3.3.4 on the example of the original Dicke model. Thus, ϵ_+^γ is associated with the atomic or fermionic branch. Likewise, ϵ_-^γ denotes the photonic branch which is of particular interest. This is due to ϵ_-^γ vanishes as the system approaches the critical point. The closure of the excitation gap between the ground-state energy E_0 and the photonic branch is a feature of second-order quantum phase transitions and typically tied to a diverging characteristic length at the phase boundary (cf. Subsec. 3.3.4). This means that fluctuations which drive the quantum phase transition occur at any scale of the characteristic length. The divergence of the characteristic length and thus in turn the closure of the excitation gap is often governed by a power law with universal critical exponents (cf. Subsec. 3.3.4). With this the results obtained within the path integral approach for cutoff regularization are evaluated during the following.

Figure 7.8 shows the excitation spectrum of the path integral approach. Different from the symmetric power law valid for the original Dicke model, the photonic branch shown in Fig. 7.8 is governed by an asymmetry concerning the critical exponents when approaching g_c either from the normal or the superradiant phase. For the particular case shown in
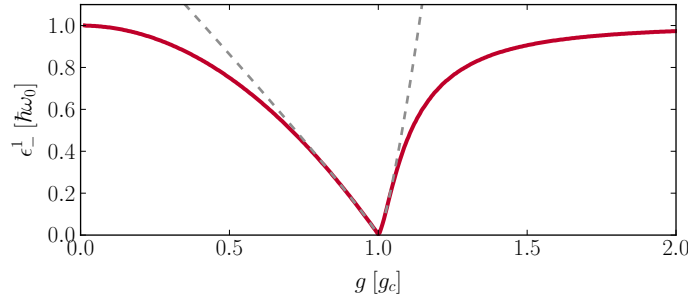
FIGURE 7.8: Excitation spectrum of the photonic branch obtained within the path integral approach for $\gamma = 1$ (cutoff regularization). The red solid line refers to a Fermi level between $M = 0$ and $M + 1$ and $\nu = 5$ at resonance. The power law is governed by different critical exponents when approaching g_c from either the normal or the superradiant phase.

Fig. 7.8, $M = 0$ and $\nu = 5$, the power law is given by

$$
\epsilon_-^1 \propto \begin{cases} [g_{c,\nu} - g]^{z^{\mathrm{np}}\bar{\nu}}, & \text{for } g < g_c, \ z^{\mathrm{np}} \approx 3.75, \\ [g - g_{c,\nu}]^{z^{\mathrm{sp}}\bar{\nu}}, & \text{for } g > g_c, \ z^{\mathrm{sp}} \approx 5.00, \end{cases} \tag{7.64}
$$

where $z^{x\mathrm{p}}$, $x = \mathrm{n}, \mathrm{s}$, denotes the dynamical critical exponent in the normal and the superradiant phase, respectively. Furthermore, $\bar{\nu} = 1/4$ is related to the power law of the characteristic length scale of the system (cf. Subsec. 3.3.4). Figure 7.9 a) shows the excitation spectrum for various Fermi levels and Fig. 7.9 b) for different Landau-level cutoffs. Despite slight deviations seen in Fig. 7.9 a) in the superradiante phase, the critical exponents are approximately identical for the depicted parameters.

With this, the main results of this chapter are summarized during the following.

7.4   Summary

The investigation of key features indicating a superradiant phase transition within the path integral approach showed distinct signatures of this collective radiation effect. This holds also for the numerical tight-binding simulation which is solely based on microscopic information about the underlying lattice and the photons. The comparison of the simulation and the analytic approach shows convincing agreement with the path integral predictions obtained for cutoff regularization. This holds for the prediction of the critical points extracted from the simulation for various sets of parameters especially when a trigonal-warping correction of the analytic Landau levels is taken into account. This is necessary, as the simulated systems are rather small. Furthermore, the ground-state energy shows typical signatures of a second-order transition in both cases. This is also seen from the evaluation of the photon occupation. Thereby, qualitative agreement in the scaling behavior of this observable for different Landau-level cutoffs and Fermi levels has been found. However, the path integral result predicts a rather steep increase of the photon occupation close to the critical point. This differs from the approximate linear
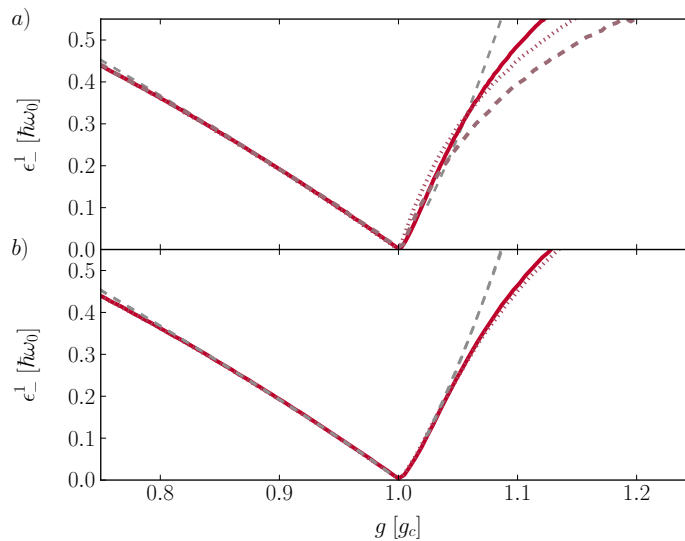
FIGURE 7.9: Excitation spectrum of the photonic branch obtained within the path integral approach for $\gamma = 1$ (cutoff regularization). Panel a) depicts the photonic branch for $\nu = 4$ and different values of the filling: $M = 0$ (solid), $M = 1$ (dotted) and $M = 2$ (dashed). The power law in the normal phase is identical for all parameters. In the superradiant phase slight deviations appear. Panel b) shows the photonic branch for constant fillings, $M = 0$, but different cutoffs, $\nu = 5$ (solid) and $\nu = 4$. Both parameters yield convincing agreement close to the critical point.

behavior of the equivalent obtained from the simulation.

The cutoff-independent regularization approach, based on a rotating-wave like approximation as suggested by Ref. [93], failed in the proper description of the tight-binding results. In particular, the critical point is overestimated in both orders of approximation. However, the deviations obtained for the ground-state energy and the photon occupation are even more crucial as the cutoff-independently regularized path integral approach predicts a first-order quantum phase transition for a system filled up to Landau level $M = 1$. This behavior could not be observed from the tight-binding simulation. As this regularization approach omits inter-band transitions one concludes that these contributions play a crucial role in the properties of the superradiant phase. The failure of this approach might probably be due to similar arguments as applied onto the original rotating-wave approximation in the ultrastrong coupling regime [125–127].

Thus, when regarding the cutoff-regularized results as providing a suitable ansatz for the description of the actual processes in the system one finds the phase transition occurring for rather low magnetic fields and fillings. This parameter range is already experimentally feasible [28–30].

However, as the path integral approach provides rather rare insight into the details of the processes, one aims for a more transparent approach. As suggested by Ref. [95] this

can be achieved by means of a perturbative Schrieffer-Wolff transformation which yields an effective Dicke-like Hamiltonian with a two-level description of the last occupied and first unoccupied Landau level. This approach will be discussed and extended to the next order of approximation during the next chapter.

Chapter 8

Derivation of a generalized Dicke Hamiltonian

In this section the derivation of an effective two-level Hamiltonian for Landau-quantized graphene interacting with a cavity mode is presented. The approach is based on the technique of Ref. [95]. Similar to the investigations discussed in Chap. 7, the Fermi level is assumed to lie between the Landau levels M and $M + 1$. The aim of the following discussion is to decouple this pair from the full system, meaning from all other dipole allowed transitions involving either Landau level M or $M + 1$. The resulting effective two-level Hamiltonian might then offer a more transparent view on the collective behavior of graphene in the superradiant phase than the path integral approach provides.

The task of decoupling is accomplished by the *Schrieffer-Wolff* (SW) method [204, 212–214]. Thereby a unitary transformation is applied onto the many-body Hamiltonian which yields the operator to decompose into two distinct components each acting onto disjoint parts of the full Hilbert space.
The SW method is in general applicable to any Hamiltonian of the family $\hat{\mathcal{H}} = \hat{\mathcal{H}}_0 + g\,\hat{\mathcal{V}}$ as long as $\hat{\mathcal{H}}_0$ provides a *spectral gap* $\Delta \ll 2||\hat{\mathcal{V}}||$ separating the two respective subspaces. In most cases [204, 212–214] this operation yields a perturbative power series expansion for the generator of the unitary transformation into powers of the expansion parameter $\propto g$. The effective Hamiltonian is then also obtained as a perturbative power series up to a certain order of the expansion parameter. Whereas absolute convergence is ensured in a single-particle case when $g < \Delta/(2||\hat{\mathcal{V}}||)$, it is not mandatory for a comparable many-body Hamiltonian [214]. This results from $||\hat{\mathcal{V}}||$ being proportional to the number of electrons inside the system which yields the SW transformation to be inconclusively well-defined [214]. Consequently the power series expansion for the SW generator and thus in turn for the effective Hamiltonian might be valid only up to a certain order and the reliability of the results must be handled with great care.

When aiming for the derivation of the effective two-level Hamiltonian, one follows Ref. [95] in a first step by evaluating the lowest order of approximation within identical regularization. In this order of approximation the expansion of the transformed Hamiltonian decomposes into two parts:
The first one, a Dicke-type Hamiltonian with a two-level structure, describes the resonant Landau level pair M and $M + 1$ with additional terms quadratic in the bosonic operators $\hat{a}^\dagger + \hat{a}$ and the coupling parameter. These terms are related to the diamagnetic

current-current response of the system and they cancel with the paramagnetic current-current response, originating from linear light-matter coupling contributions, in the static limit [95]. This preserves gauge invariance.

The second contribution to the transformed Hamiltonian contains the information about all remaining Landau levels including the complete valence band and the conduction band, except of the Landau-level doublet M and $M + 1$. However, the remaining terms corresponding to the second part of the transformed Hamiltonian are still coupled among themselves by dipole allowed transitions encoded in the remaining interaction Hamiltonian. The diagonalization of the second part is then achieved by means of another SW transformation. The fermionic degrees of freedom are then treated as a mean field for the photons at $T = 0$ where the resulting expression is related to the density-density response of the system [95]. This gives rise to a global contribution which is quadratic in the coupling parameter and the bosonic mode. In accordance with the preserved gauge invariance, this global quadratic contribution vanishes in the static limit.

The contributions obtained within this second SW transformations require reasonable regularization as they stem from the entire unbounded valence band. According to Ref. [95] one regularizes in two steps. First, one applies an ultraviolet cutoff and extracts the cutoff-dependent terms of the corresponding results. Second, one subtracts these cutoff-dependent, gauge violating terms obtaining a cutoff-independet result.

Beside small deviations in the details of these terms, one obtains the same overall conclusion as drawn by the authors of Ref. [95] concerning the potential existence of a superradiant phase:

The value of the critical coupling g_c, extracted from the effective Hamiltonian, lies at least one order of magnitude beyond the validity of the SW approach when regularized similar as in Ref. [95]. Therefore no prediction about the existence of a superradiant phase can be made within this order of approximation.

In a second step one extends the effective Hamiltonian up to fourth order which is the next non-vanishing order with respect to the quadratic contributions. The effective Hamiltonian then contains not only terms $\propto (\hat{a}^\dagger + \hat{a})^2$ with quadratic but also quartic coupling. The resulting terms are then also treated as a mean field and regularized similarly as the second-order approximation in Ref. [95].

In summary one arrives at the fourth-order equivalent of the *generalized Dicke Hamiltonian* obtained in Ref. [95]. However, within identical regularization as provided in Ref. [95], there is no signature of a superradiant phase in graphene in fourth-order approximation.

This result is contrasted by similar considerations where the rigid ultraviolet cutoff is kept. Though not gauge invariant, this regularization is also identically applied onto the effective action within the path integral approach (cf. Chap. 7) and yields convincing agreement between the latter and the numerical tight-binding simulation. Moreover, the SW approach within cutoff regularization yields good agreement with the aforementioned approaches and indicates also a superradiant quantum phase transition.

However, the value of the critical coupling predicted by the path integral approach and the criterion $g < \Delta/(2||\hat{\mathcal{V}}||)$, limiting the validity of the perturbative SW method, are incommensurate when strictly applied such that agreement of both approaches is not

mandatory. The authors of Ref. [95] refer to a softened criterion solely based on the spectral gap between the Landau-level doublet M and $M + 1$ and neighboring levels when estimating the validity range of the SW approach. The cutoff-dependent result obtained within the path integral approach is compatible with this softened criterion for a proper choice of ν which however does not hold for the cutoff-independent regularization.

8.1 Decomposition of the Hilbert space

According to Ref. [95] the Fermi level is assumed to lie in the conduction band, $\lambda = +1$, between Landau level M and $M + 1$. During this Chapter the collective index notation introduced in Eq. (5.28) will be applied. The frequency of the corresponding cyclotron transition is given by

$$\hbar\Omega_M = \epsilon_{M+1} - \epsilon_M. \tag{8.1}$$

Following Ref. [95], the cavity mode ω_0 is assumed to be resonant with Ω_M when evaluating the results.

In order to decouple the resonant Landau level pair, M and $M + 1$, from the complete Hamiltonian, Eq. (5.44), detailed considerations on the corresponding Hilbert space appear to be crucial.

Even though the single-particle Hamiltonian $\hat{H}$, Eq. (5.41), cannot be diagonalized by means of the eigenbasis of $\hat{H}_{\text{cav}}$ and $\hat{H}_0$, $\{|a\rangle \otimes |N, k\rangle\}$, one is able to represent the Hilbert space spanned by the eigenstates of $\hat{H}$ as the tensor product

$$\mathbb{H} = \mathbb{H}^+ \otimes \mathbb{H}^- \tag{8.2}$$

of the Hilbert spaces $\mathbb{H}^+$ and $\mathbb{H}^-$ as discussed in App. C. Here, $\mathbb{H}^+$ refers to the Hilbert space spanned by the bosonic states $\{|a\rangle\}$, which refer to the radiation mode inside the cavity. The complete fermionic Hilbert space $\mathbb{H}^-$ is spanned by all Landau levels and therefore a tensor product itself, reading

$$\mathbb{H}^- = \bigotimes_{n,\lambda} \mathbb{L}^n_\lambda, \qquad \mathbb{L}^n_\lambda = \{(\lambda, n, k) | \, \forall \, k = 1, ..., \mathcal{N}\}. \tag{8.3}$$

Here, $\mathbb{L}^n_\lambda$ represents the subspace of the $\mathcal{N}$-fold degenerate n^{th} Landau level in the energy band λ. For the sake of clearness, the collective index notation, as introduced in Eq. (5.28) is skipped in the notation of the Landau-level Hilbert subspaces. Note that $\mathbb{L}^n_\lambda$ is also a tensor product, namely of $\mathcal{N}$ different k states. Furthermore, one constructs the $2^\mathcal{N}$-fold subspace $\mathbb{H}^-_{\text{M}} \subseteq \mathbb{H}^-$ spanned by the resonant level pair, M and $M + 1$, and defines the complement $\mathbb{H}^-_{\text{N}} \subseteq \mathbb{H}^-$ as

$$\mathbb{H}^-_{\text{M}} = \mathbb{L}^m_+ \otimes \mathbb{L}^{m+1}_+, \qquad \mathbb{H}^-_{\text{N}} = \mathbb{H}^- \, / \, \mathbb{H}^-_{\text{M}}. \tag{8.4}$$

This decomposition is naturally applicable to the complete Hilbert space $\mathbb{H}$ as defined in Eq. (8.2),

$$\mathbb{H}_M = \mathbb{H}^+ \otimes \mathbb{H}_M^-, \qquad \mathbb{H}_N = \mathbb{H}^+ \otimes \mathbb{H}_N^-. \tag{8.5}$$

Since the kinetic Hamiltonian $\hat{\mathcal{H}}_0$, Eq. (5.46), contains only particle conserving fermionic number operators, the decomposition of the fermionic Hilbert space $\mathbb{H}^+$ is also applicable to $\hat{\mathcal{H}}_0$. Thus, the operator decomposes into

$$\hat{\mathcal{H}}_{0,M} + \hat{\mathcal{H}}_{0,N} = \hat{\mathcal{H}}_0 : \mathcal{F}_-(\mathbb{H}^-) \mapsto \mathcal{F}_-(\mathbb{H}^-). \tag{8.6}$$

whereas each term on the l.h.s. is an automorphism and therefore particle conserving on the level of the corresponding Fock subspace:

$$\hat{\mathcal{H}}_{0,X} : \mathcal{F}_-(\mathbb{H}_X^-) \mapsto \mathcal{F}_-(\mathbb{H}_X^-), \qquad X = M, N. \tag{8.7}$$

Regarding the definition of $\hat{\mathcal{H}}_0$ (5.46) one particularizes

$$\hat{\mathcal{H}}_{0,M} = \sum_k \left[\epsilon_M \hat{c}_{M,k}^\dagger \hat{c}_{M,k} + \epsilon_{M+1} \hat{c}_{M+1,k}^\dagger \hat{c}_{M+1,k} \right], \tag{8.8}$$

$$\hat{\mathcal{H}}_{0,N} = \sum_{N \in \mathbb{H}_N^-} \epsilon_N \hat{c}_{N,k}^\dagger \hat{c}_{N,k}, \tag{8.9}$$

where $\hat{\mathcal{H}}_{0,M}$ is already reminiscent of a two-level Hamiltonian for the Landau-level doublet M and $M+1$. This is discussed in more detail in Subsec. 8.2.4.

However, a similar direct decomposition of the interaction Hamiltonian $\hat{\mathcal{H}}_i$ (5.47) into two linear operators, each describing an automorphism on one of the Fock subspaces $\mathcal{F}(\mathbb{H}_M)$ and $\mathcal{F}(\mathbb{H}_N)$, is not possible. This can be seen immediately from Fig. 8.1: Each Landau state with $n > 1$ is coupled to four other Landau states by dipole allowed optical transitions, whereas the first / zeroth Landau level is involved in three / two transitions. This complex ladder-like coupling of Landau states arises from the dipole selection rules, Eq. (5.48). Even though the interaction Hamiltonian $\hat{\mathcal{H}}_i$ (5.47) conserves the total number of particles, there are contributions changing the subspace occupation by one particle, i.e.

$$\hat{c}_{N_M,k}^\dagger \hat{c}_{M,k} : \hat{S}_-(\mathbb{H}^{\otimes n_{N_M}} \otimes \mathbb{H}^{\otimes n_M}) \mapsto \hat{S}_-(\mathbb{H}^{\otimes n_{N_M}+1} \otimes \mathbb{H}^{\otimes n_M-1}), \tag{8.10}$$

$$\hat{c}_{M,k}^\dagger \hat{c}_{N_M,k} : \hat{S}_-(\mathbb{H}^{\otimes n_{N_M}} \otimes \mathbb{H}^{\otimes n_M}) \mapsto \hat{S}_-(\mathbb{H}^{\otimes n_{N_M}-1} \otimes \mathbb{H}^{\otimes n_M+1}). \tag{8.11}$$

As denoted by red arrows in Fig. 8.1, one identifies the single-particle Hilbert subspace $\mathbb{H}_{N_M}^- \subseteq \mathbb{H}_N^-$ spanned by six Landau levels,

$$\mathbb{H}_{N_M}^- = \mathbb{L}_+^{m+2} \otimes \mathbb{L}_+^{m-1} \otimes \mathbb{L}_-^{m-1} \otimes \mathbb{L}_-^m \otimes \mathbb{L}_-^{m+1} \otimes \mathbb{L}_-^{m+2}, \tag{8.12}$$

which are optically coupled to the resonant level pair spanning $\mathbb{H}_M^-$. The action of the corresponding fermionic ladder operators yields then a coupling between the Fock subspaces according to Eqs. (8.10, 8.11). The associated terms of the interaction Hamiltonian therefore prohibit the direct decomposition of $\hat{\mathcal{H}}_i$ into parts similar to Eq. (8.6).
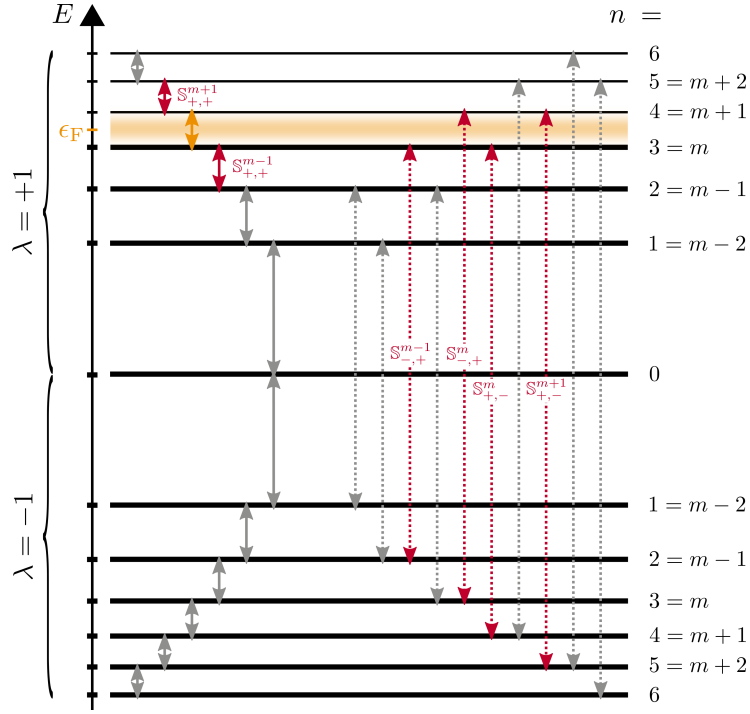
FIGURE 8.1: Each arrow represents a dipole allowed, optical transition between two Landau levels. Thereby one can distinguish intra-band (solid) and inter-band (dotted) excitations. The decomposition of the complete Hilbert space $\mathbb{H}^-$ into two-component subspaces $\mathbb{S}^n_{\lambda,\lambda'} = \mathbb{L}^n_\lambda \otimes \mathbb{L}^{n+1}_{\lambda'}$ spanned by two Landau levels which are connected via optical transitions $\lambda n \leftrightarrow \lambda'(n+1)$ is obvious. The energy levels below the Fermi level ϵ_F are each occupied by $\mathcal{N}$ electrons symbolized by bold lines. The resonant two-level subsystem (orange arrow, orange shaded) is coupled to six other allowed transitions (red arrows) each spanning up a two-component subspace (f.l.t.r.: $\mathbb{S}^{m+1}_{+,+}$, $\mathbb{S}^{m-1}_{+,+}$, $\mathbb{S}^{m-1}_{-,+}$, $\mathbb{S}^m_{-,+}$, $\mathbb{S}^m_{+,-}$, $\mathbb{S}^{m+1}_{+,-}$). All remaining transitions are depicted by gray arrows.

8.1.1 Block-diagonal and block-off-diagonal operators

However, as discussed in Sec. 8.2, the interaction Hamiltonian can be decoupled into two linear operators, each acting solely onto one of the subspaces $\mathcal{F}(\mathbb{H}_M)$, $\mathcal{F}(\mathbb{H}_N)$ by means of the SW method [204, 212–214]. Within this complex procedure it is necessary to handle the decomposition of the Hilbert space as well as the corresponding parts of the interaction Hamiltonian with care.

For this purpose and in order to construct the unitary operator accomplishing the decoupling of $\hat{\mathcal{H}}_i$, it is reasonable to introduce a few definitions according to Ref. [214].

Let $\hat{P}_X$ denote the single-particle projector onto the subspace $\mathbb{H}_X$, i.e.

$$\hat{P}_X = \sum_{X \in \mathbb{H}_X^-} \mathbb{1}^+ \otimes \hat{p}_X. \tag{8.13}$$

Thereby $\mathbb{1}^+$ corresponds to the identity operating in the bosonic Hilbert subspace and

$\hat{p}_X = \sum_k |X,k\rangle \langle X,k|$ denotes the projector onto the single Landau subspace $\mathbb{L}_\lambda^x$. Then, $\hat{P}_M$ and $\hat{P}_N$ represent the projectors onto the subspace $\mathbb{H}_M$ and $\mathbb{H}_N$, respectively. According to the definition of both subspaces, Eqs. (8.4, 8.5), one finds that $\hat{P}_N$ is the orthogonal complement to $\hat{P}_M$ and vice versa. Therefore, $\hat{P}_N \hat{P}_M = 0$ and the sum of both projectors reflects the completeness of basis states by definition such that $\hat{P}_M + \hat{P}_N = \mathbb{1}^+ \otimes 1^-$ holds true.

Further, one refers to the space of linear operators acting onto the Hilbert space $\mathbb{H}$ as $\mathbb{S}(\mathbb{H})$ and denotes any linear map $\mathcal{S} : \mathbb{S}(\mathbb{H}) \mapsto \mathbb{S}(\mathbb{H})$ acting on $\mathbb{S}(\mathbb{H})$ with the term *superoperator*. In accordance with Ref. [214] the term *block-off-diagonal* is introduced if a linear operator $\hat{\mathcal{X}}$ obeys

$$\mathcal{O}(\hat{\mathcal{X}}) = \hat{\mathcal{X}} = \begin{pmatrix} 0 & \hat{\mathcal{X}}_{M,N} \\ \hat{\mathcal{X}}_{N,M} & 0 \end{pmatrix}, \tag{8.14}$$

where the simplest definition of the superoperator $\mathcal{O}(\hat{\mathcal{X}})$ reads

$$\mathcal{O}(\hat{\mathcal{X}}) = \hat{P}_M \hat{X} \hat{P}_N + \hat{P}_N \hat{X} \hat{P}_M. \tag{8.15}$$

Thus, block-off-diagonal operators impart the coupling between the Fock subspaces corresponding to $\mathbb{H}_M^-$ and $\mathbb{H}_{N_M}^- \subseteq \mathbb{H}_N^-$ by means of particle exchange as described in Eqs. (8.10, 8.11). The term *block-diagonal* accounts then for a linear operator $\hat{\mathcal{X}}$ which conserves the occupation number of the decomposed Fock subspaces corresponding to $\mathbb{H}_M$ and $\mathbb{H}_N$. Accordingly, a block-diagonal operator $\hat{\mathcal{X}}$ obeys

$$\mathcal{D}(\hat{\mathcal{X}}) = \hat{\mathcal{X}} = \begin{pmatrix} \hat{\mathcal{X}}_{M,M} & 0 \\ 0 & \hat{\mathcal{X}}_{N,N} \end{pmatrix}, \tag{8.16}$$

where the action of the superoperator $\mathcal{D}(\hat{\mathcal{X}})$ on a many-body operator $\hat{\mathcal{X}}$ is described by

$$\mathcal{D}(\hat{\mathcal{X}}) = \hat{P}_M \hat{X} \hat{P}_M + \hat{P}_N \hat{X} \hat{P}_N. \tag{8.17}$$

By contrast to the block-off-diagonal operators, block-diagonal operators are automorphisms with respect to the respective subspaces. With these definitions one is able to decompose the full many-body Hamiltonian of Landau-quantized graphene, as discussed in Sec. 5.3, into its block-diagonal and block-off diagonal contributions with respect to the Landau-level doublet M and $M+1$.

8.1.2 Decomposition of the many-body Hamiltonian

For the following it is useful to introduce the notation $\hat{\mathcal{H}}_{i,X,Y}$ for the projection

$$\hat{\mathcal{H}}_{i,X,Y} = \hat{P}_X \hat{\mathcal{H}}_i \hat{P}_Y = \frac{g}{\sqrt{\mathcal{N}}} (\hat{a}^\dagger + \hat{a}) \sum_{\substack{X \in \mathbb{H}_X^- \\ Y \in \mathbb{H}_Y^-}} \delta_{k,k'} \hat{c}_{X,k}^\dagger \mathcal{M}_{X,Y} \hat{c}_{Y,k'}, \tag{8.18}$$

where the summation is carried out over all three quantum numbers according to the definition of the corresponding Hilbert subspaces $\mathbb{H}_X^-$ and $\mathbb{H}_Y^-$, where X, Y = M, N. Note that the projection yields an Hermitian operator only if X = Y. In this case the index

notation $\hat{\mathcal{H}}_{i,X,X} = \hat{\mathcal{H}}_{i,X}$ is abbreviated for convenience. When $X \neq Y$, the Hermitian conjugate of $\hat{\mathcal{H}}_{i,X,Y}$ needs to be explicitly taken into account. Along with the definition of block-diagonal and block-off-diagonal operators the interaction $\hat{\mathcal{H}}_i = g(\hat{\mathcal{V}}_d + \hat{\mathcal{V}}_o)$, where

$$g\hat{\mathcal{V}}_d = \mathcal{D}(\hat{\mathcal{H}}_i) = \hat{\mathcal{H}}_{i,M} + \hat{\mathcal{H}}_{i,N}, \tag{8.19}$$

denotes the block-diagonal part of the interaction Hamiltonian. For the following discussion it is beneficial to introduce the decomposition $\hat{\mathcal{V}}_d = \hat{v} \otimes \hat{V}_d$, where the bosonic part is defined as

$$\hat{v} = \frac{\hat{a}^\dagger + \hat{a}}{\sqrt{\mathcal{N}}}. \tag{8.20}$$

Thus, the fermionic part of the block-diagonal perturbation is defined by the Hermitian operator

$$\hat{V}_d = \sum_{M,M' \in \mathbb{H}_M^-} \delta_{k,k'} \, \hat{c}_{M,k}^\dagger \, \mathcal{M}_{X,Y} \, \hat{c}_{M',k'} + \sum_{N,N' \in \mathbb{H}_N^-} \delta_{k,k'} \, \hat{c}_{N,k}^\dagger \, \mathcal{M}_{X,Y} \, \hat{c}_{N',k'}. \tag{8.21}$$

Thereby, the contribution operating on the resonant subspace $\mathbb{H}_M$ is explicitly given by

$$\hat{\mathcal{H}}_{i,M} = \frac{g}{\sqrt{\mathcal{N}}} (\hat{a}^\dagger + \hat{a}) \sum_k w_{+,M} \left[\hat{c}_{M+1,k}^\dagger \hat{c}_{M,k} + \hat{c}_{M,k}^\dagger \hat{c}_{M+1,k} \right] \tag{8.22}$$

and is already reminiscent of an two-level Hamiltonian. This becomes even more apparent after application of the Schwinger-Wigner map between fermionic operators and Pauli matrices as discussed in Subsec. 8.2.4.

The block-off-diagonal part of the interaction Hamiltonian is given by

$$g\hat{\mathcal{V}}_o = \mathcal{O}(\hat{\mathcal{H}}_i) = \hat{\mathcal{H}}_{i,M,N_M} + \hat{\mathcal{H}}_{i,N_M,M}. \tag{8.23}$$

where the dipole selection rules (5.48) were applied. Therefore, not the complete Hilbert subspace $\mathbb{H}_N$ is relevant for the block-off-diagonal operator $\hat{\mathcal{V}}_o$, but only states coupled directly via dipole allowed transitions to the resonant Landau level pair, as depicted in Fig. 8.1. These states span the subspace $\mathbb{H}_{N_M} \subseteq \mathbb{H}_N$ as defined in Eq. (8.12).

Note that the kinetic part of the Hamiltonian, $\hat{\mathcal{H}}_0$, is block-diagonal by definition and can thus be decomposed into both blocks according to Eqs. (8.6, 8.7). Similar to the decomposition of $\hat{\mathcal{V}}_d$ into bosonic and fermionic part, one can write $\hat{\mathcal{V}}_o = \hat{v} \otimes (\hat{V}_o + \hat{V}_o^\dagger)$, where the bosonic component is given by Eq. (8.20) and the fermionic degrees of freedom are stored in

$$\hat{V}_o = \sum_{\substack{M \in \mathbb{H}_M^- \\ N \in \mathbb{H}_{N_M}^-}} \hat{c}_{M,k}^\dagger \, \mathcal{M}_{M,N} \, \hat{c}_{N,k} \neq \hat{V}_o^\dagger. \tag{8.24}$$

The SW method discussed in Subsec. 8.2 targets these block-off-diagonal contributions of the total Hamiltonian with the aim of conveying them into block-diagonal terms by means of a suitable unitary transformation.

This notation, i.e. small letters denoting a bosonic contribution and capital ones referring to a fermionic part, deviates from the notation introduced in App. C and preferably used throughout this thesis. However, this notation yields cumbersome expressions when evaluating nested commutators during the following, such that it is replaced by the previously introduced one during this chapter.

Thus summarizing, the total many-body Hamiltonian (5.44) can be rewritten in the following way,

$$\hat{\mathcal{H}} = \hat{\mathcal{H}}_{\text{cav}} + \hat{\mathcal{H}}_0 + g\hat{\mathcal{V}}_d + g\hat{\mathcal{V}}_o, \tag{8.25}$$

where the first three terms on the r.h.s. are indeed block-diagonal operators and only the last term appears to be block-off-diagonal. Note that the photonic part $\hat{\mathcal{H}}_{\text{cav}}$ is regarded as a block-diagonal operator similar as $\hat{\mathcal{H}}_0$ since it is particle conserving in the same sense.

8.2 Decoupling of the two-level subsystem

In this section the SW method [204, 212–214] is applied onto the total many-body Hamiltonian $\hat{\mathcal{H}}$, Eq. (8.25), with the aim of decoupling the resonant Landau level pair, spanning $\mathbb{H}_{\text{M}}^-$, from all other dipole allowed transitions up to fourth-order approximation.

Therefore, the main characteristics of the SW method are briefly introduced and the scheme of constructing the transformation operator $\hat{\mathcal{U}} = e^{\hat{\mathcal{S}}}$ is sketched according to Ref. [214]. Thereby, $\hat{\mathcal{S}} = \mathcal{O}(\hat{\mathcal{S}})$ denotes the anti-Hermitian, block-off-diagonal generator of the transformation. The main aspect of this technique is to treat the interaction part $\propto g$ in the total Hamiltonian, as defined in Eq. (8.25), as a perturbation of the unperturbed Hamiltonian $\hat{\mathcal{H}}_{\text{cav}} + \hat{\mathcal{H}}_0$. The generator $\hat{\mathcal{S}}$ is then constructed for the unperturbed Hamiltonian which is supposed to be diagonalizable exactly, whereas the eigenbasis of the total Hamiltonian, Eq. (8.25), is unknown. For that reason, the construction of the transformation operator $\hat{\mathcal{S}}$ and therefore the derivation of a block-diagonal transformed Hamiltonian $\hat{\mathcal{H}}^{\text{eff}}$ is accomplished by means of a perturbative power series expansion of $\hat{\mathcal{S}}$

$$\hat{\mathcal{S}} = \sum_{n=1}^{\infty} \hat{\mathcal{S}}_n g^n, \qquad \hat{\mathcal{S}}_n^{\dagger} = -\hat{\mathcal{S}}_n \tag{8.26}$$

The series expansion of $\hat{\mathcal{S}}$ yields in turn a perturbative power series for the approximately block-diagonal Hamiltonian

$$\hat{\mathcal{H}}^{\text{eff}} = e^{\hat{\mathcal{S}}}\,\hat{\mathcal{H}}\,e^{-\hat{\mathcal{S}}} \approx \mathcal{D}(\hat{\mathcal{H}}^{\text{eff}}) = \begin{pmatrix} \hat{\mathcal{H}}_{\text{M}}^{\text{eff}} & 0 \\ 0 & \hat{\mathcal{H}}_{\text{N}}^{\text{eff}} \end{pmatrix}, \tag{8.27}$$

where a spectral gap Δ between both subspaces, $M \in \mathbb{H}_{\text{M}}^-$ and $N \in \mathbb{H}_{\text{N}_{\text{M}}}^-$, is required. For Landau-quantized graphene with a Fermi level between the levels M and $M+1$ the spectral gap is particularly given by [95, 214]

$$\Delta = \min(|\hbar\omega_0 - |\epsilon_M - \epsilon_N||)_{M \in \mathbb{H}_{\text{M}}, N \in \mathbb{H}_{\text{M}_{\text{N}}}} = |\hbar\omega_0 - \hbar\Omega_{M+1}|, \tag{8.28}$$

where $\hbar\Omega_{M+1}$ is analogously defined as in Eq. (8.1). The perturbative series expansion is convergent for couplings

$$g < \rho_0 = \frac{\Delta}{||\hat{\mathcal{V}}_d + \hat{\mathcal{V}}_o||} \frac{1}{16(1 + \frac{4\hbar}{\pi\Delta})} \tag{8.29}$$

as the rigorous derivation in Ref. [214] proofs. For single particle concerns, this require-ment ensures even absolute convergence of the perturbative series [214]. However, con-vergence of this approach is highly questionable in many-body systems as addressed in Ref. [214] for a general case. This is due to the norm of the perturbation scaling with the number of particles in the system which is, in the case of Landau-quantized graphene, $||\hat{\mathcal{V}}_d + \hat{\mathcal{V}}_o|| \leq (2\nu + 1)\mathcal{N}$. Thereby, ν denotes the ultraviolet Landau-level cutoff and $\mathcal{N}$ is the level degeneracy. Contrarily, the spectral gap is constant regardless of the number of particles described by the many-body model. Thus, the disc of convergence, Eq. (8.29), narrows with increasing particle number. The thermodynamic limit, $\mathcal{N} \to \infty$, or the claim $\nu \to \infty$, as proposed in Ref. [95], ultimately destroys the validity of this approach. Furthermore, according to Ref. [214], convergence will be partially restored if truncating the perturbative power series expansion for the generator $\hat{S}$ at some order. This is also adopted here, truncating after third order which yields an approximately block-diagonal Hamiltonian in fourth order of g. This is in contrast to Ref. [95], where only the first order of $\hat{S}$ is considered. Furthermore, in Ref. [95] condition (8.29) is softened such that

$$g < \tilde{\rho}_0 = \Delta. \tag{8.30}$$

is regarded as proving convergence. This completely omits the ν-dependent norm of the perturbation $\hat{\mathcal{V}}_d + \hat{\mathcal{V}}_o$.

Condition (8.29) is not compatible at all with the critical couplings $g_{c,\nu}$ and $g_{c,M}$ obtained from the path integral approach within both regularizations given in Eqs. (7.37, 7.38). By contrast, the softened condition (8.30) is compatible with the value of the critical point ob-tained within the cutoff-regularized path integral approach, $g_{c,\nu}$, Eq. (7.37), for sufficient values of ν:

$$\nu > \frac{(\omega_0\omega_c)^2}{64(\omega_0 - \Omega_{M+1})^4} \overset{\omega_0=\Omega_M}{\approx} M^3(M+1)^2. \tag{8.31}$$

Thus, during the following, relation (8.30) will provide the reference for the estimation of the validity range.

8.2.1 Construction of the unitary Schrieffer-Wolff transformation

In order to proceed the subspace decoupling, one needs to find the SW generator $\hat{S}$ accomplishing the transformation (8.27) from the block-off diagonal Hamiltonian $\hat{\mathcal{H}}$ to the approximate block-diagonal Hamiltonian $\hat{\mathcal{H}}^{\text{eff}}$. By application of the *Baker-Campbell-Hausdorff formula* [243–245], Eq. (B.26), the transformation (8.27) takes the form

$$\hat{\mathcal{H}}^{\text{eff}} = \sum_{n=0}^{\infty} \frac{[\hat{S}, \hat{\mathcal{H}}]_n}{n!}, \tag{8.32}$$

where the nested commutators are given by $[\hat{\mathcal{S}}, \hat{\mathcal{H}}]_n = [\hat{\mathcal{S}}, [\hat{\mathcal{S}}, \hat{\mathcal{H}}]]_{n-1}$ and $[\hat{\mathcal{S}}, \hat{\mathcal{H}}]_0 = \hat{\mathcal{H}}$. By inserting the perturbative series for the SW generator $\hat{\mathcal{S}}$, Eq. (8.26), and the definition of $\hat{\mathcal{H}}$, Eq. (8.25), one is able to expand each nested commutator into powers of g. This yields for instance

$$
\begin{aligned}
[\hat{\mathcal{S}}, \hat{\mathcal{H}}]_1 \approx {} & g[\hat{\mathcal{S}}_1, \hat{\mathcal{H}}_{\text{cav}} + \hat{\mathcal{H}}_0] + g^2([\hat{\mathcal{S}}_2, \hat{\mathcal{H}}_{\text{cav}} + \hat{\mathcal{H}}_0] + [\hat{\mathcal{S}}_1, \hat{\mathcal{V}}_d + \hat{\mathcal{V}}_o]) \\
& + g^3([\hat{\mathcal{S}}_3, \hat{\mathcal{H}}_{\text{cav}} + \hat{\mathcal{H}}_0] + [\hat{\mathcal{S}}_2, \hat{\mathcal{V}}_d + \hat{\mathcal{V}}_o]) + g^4([\hat{\mathcal{S}}_4, \hat{\mathcal{H}}_{\text{cav}} + \hat{\mathcal{H}}_0] + [\hat{\mathcal{S}}_3, \hat{\mathcal{V}}_d + \hat{\mathcal{V}}_o]).
\end{aligned}
\tag{8.33}
$$

Nested commutators for larger n are obtained likewise and can be found in Ref. [214]. One choses then $\hat{\mathcal{S}}_n$ such that the block-off diagonal contributions for the nth power of g in the expansion (8.32) are compensated by the commutator $[\hat{\mathcal{S}}_n, \hat{\mathcal{H}}_{\text{cav}} + \hat{\mathcal{H}}_0]$. This yields the following relations for the lowest order of g:

$$
[\hat{\mathcal{S}}_1, \hat{\mathcal{H}}_{\text{cav}} + \hat{\mathcal{H}}_0] = -\hat{\mathcal{V}}_o,
\tag{8.34}
$$

from which it can be concluded that $\hat{\mathcal{S}}_1$ is a block-off diagonal, anti-Hermitian operator [214]. This holds also for the higher orders of g [214],

$$
[\hat{\mathcal{S}}_2, \hat{\mathcal{H}}_{\text{cav}} + \hat{\mathcal{H}}_0] = -[\hat{\mathcal{S}}_1, \hat{\mathcal{V}}_d],
\tag{8.35}
$$

$$
[\hat{\mathcal{S}}_3, \hat{\mathcal{H}}_{\text{cav}} + \hat{\mathcal{H}}_0] = -[\hat{\mathcal{S}}_2, \hat{\mathcal{V}}_d] - \frac{1}{3}[\hat{\mathcal{S}}_1, [\hat{\mathcal{S}}_1, \hat{\mathcal{V}}_o]],
\tag{8.36}
$$

$$
[\hat{\mathcal{S}}_4, \hat{\mathcal{H}}_{\text{cav}} + \hat{\mathcal{H}}_0] = -[\hat{\mathcal{S}}_3, \hat{\mathcal{V}}_d] - \frac{1}{3}[\hat{\mathcal{S}}_2, [\hat{\mathcal{S}}_1, \hat{\mathcal{V}}_o]] - \frac{1}{3}[\hat{\mathcal{S}}_1, [\hat{\mathcal{S}}_2, \hat{\mathcal{V}}_o]].
\tag{8.37}
$$

Moreover, these equations precisely define the contributions $\hat{\mathcal{S}}_n$ of the power series expansion of the generator $\hat{\mathcal{S}}$.
Following Ref. [214], each $\hat{\mathcal{S}}_n$ is then systematically obtained from

$$
\hat{\mathcal{S}}_1 = \mathcal{L}(\hat{\mathcal{V}}_o),
\tag{8.38}
$$

$$
\hat{\mathcal{S}}_2 = \mathcal{L}([\hat{\mathcal{S}}_1, \hat{\mathcal{V}}_d]),
\tag{8.39}
$$

$$
\hat{\mathcal{S}}_3 = \mathcal{L}([\hat{\mathcal{S}}_2, \hat{\mathcal{V}}_d]) + \frac{1}{3}\mathcal{L}([\hat{\mathcal{S}}_1, [\hat{\mathcal{S}}_1, \hat{\mathcal{V}}_o]]),
\tag{8.40}
$$

$$
\hat{\mathcal{S}}_4 = \mathcal{L}([\hat{\mathcal{S}}_3, \hat{\mathcal{V}}_d]) + \frac{1}{3}\mathcal{L}([\hat{\mathcal{S}}_2, [\hat{\mathcal{S}}_1, \hat{\mathcal{V}}_o]]) + \frac{1}{3}\mathcal{L}([\hat{\mathcal{S}}_1, [\hat{\mathcal{S}}_2, \hat{\mathcal{V}}_o]]),
\tag{8.41}
$$

where $\mathcal{L}$ defines the superoperator transforming a Hermitian block-off-diagonal operator $\hat{\mathcal{X}}$ into its anti-Hermitian counterpart [214]:

$$
\mathcal{L}(\hat{\mathcal{X}}) = \int_0^\infty dt\, e^{-t(\hat{\mathcal{H}}_{\text{cav}} + \hat{\mathcal{H}}_0)} \hat{P}_{\text{M}} \hat{\mathcal{X}} \hat{P}_{\text{N}} - \int_0^\infty dt\, \hat{P}_{\text{N}} \hat{\mathcal{X}} \hat{P}_{\text{M}} e^{-t(\hat{\mathcal{H}}_{\text{cav}} + \hat{\mathcal{H}}_0)} \leq \frac{||\hat{\mathcal{X}}||}{\Delta},
\tag{8.42}
$$

The inductive rule for constructing the series coefficients $\hat{\mathcal{S}}_n$ for an arbitrary order n can be found in Ref. [214] where each contribution $\hat{\mathcal{S}}_n$ can be expressed in terms of the lowest order term, $\hat{\mathcal{S}}_1$. This recipe allows to systematically derive the generator $\hat{\mathcal{S}}$ of the SW transformation term by term.

8.2.2 Derivation of the effective block-diagonal Hamiltonian

From the remaining terms of the series expansion (8.32) one constructs the effective Hamiltonian, which is in fourth-order approximation of the form:

$$\hat{\mathcal{H}}^{\text{eff}} \approx \hat{\mathcal{H}}_{\text{cav}} + \hat{\mathcal{H}}_0 + g\hat{\mathcal{V}}_d + \sum_{n=2}^{4} g^n \hat{\mathcal{H}}^{(n)} \approx \begin{pmatrix} \hat{\mathcal{H}}_{\text{M}}^{\text{eff}} & 0 \\ 0 & \hat{\mathcal{H}}_{\text{N}}^{\text{eff}} \end{pmatrix}. \tag{8.43}$$

Thereby, the second to fourth-order contributions are given by [214]

$$\hat{\mathcal{H}}^{(2)} = \frac{1}{2}[\hat{\mathcal{S}}_1, \hat{\mathcal{V}}_o], \tag{8.44}$$

$$\hat{\mathcal{H}}^{(3)} = \frac{1}{2}[\hat{\mathcal{S}}_2, \hat{\mathcal{V}}_o], \tag{8.45}$$

$$\hat{\mathcal{H}}^{(4)} = \frac{1}{2}[\hat{\mathcal{S}}_3, \hat{\mathcal{V}}_o] - \frac{1}{24}[\hat{\mathcal{S}}_1, [\hat{\mathcal{S}}_1, [\hat{\mathcal{S}}_1, \hat{\mathcal{V}}_o]]], \tag{8.46}$$

where the generalization to higher orders of the expansion is discussed in Ref. [214] in great detail.

As the construction of the SW generators $\hat{\mathcal{S}}_n$ is inductive and all terms of the series expansion can be expressed by the lowest order generator, $\hat{\mathcal{S}}_1$, it is convenient to write the third and fourth-order contribution to $\hat{\mathcal{H}}^{\text{eff}}$ in terms of $\hat{\mathcal{S}}_1$:

$$\hat{\mathcal{H}}^{(3)} = \frac{1}{2}[\hat{\mathcal{V}}_o, \mathcal{L}([\hat{\mathcal{V}}_d, \hat{\mathcal{S}}_1])], \tag{8.47}$$

$$\hat{\mathcal{H}}^{(4)} = -\frac{1}{2}[\hat{\mathcal{V}}_o, \mathcal{L}([\hat{\mathcal{V}}_d, \mathcal{L}([\hat{\mathcal{V}}_d, \hat{\mathcal{S}}_1])])] - \frac{1}{6}[\hat{\mathcal{V}}_o, \mathcal{L}([\hat{\mathcal{S}}_1, [\hat{\mathcal{S}}_1, \hat{\mathcal{V}}_o]])] - \frac{1}{24}[\hat{\mathcal{S}}_1, [\hat{\mathcal{S}}_1, [\hat{\mathcal{S}}_1, \hat{\mathcal{V}}_o]]]. \tag{8.48}$$

After calculation of each contribution $\hat{\mathcal{H}}^{(n)}$, one obtains an expression which is approximately block-diagonal. The terms operating on the Hilbert subspace of the Landau-level doublet M and $M+1$, $\mathbb{H}_{\text{M}}$, is transformed into a Dicke-like Hamiltonian by associating the fermionic creation and annihilation operators with Pauli matrices. Following Ref. [95], the remaining part, which operates onto the Hilbert subspace $\mathbb{H}_{\text{N}}$, is then approximately diagonalized by means of another SW transformation. These terms are then treated as a mean field for the Landau level doublet M and $M+1$ and thus are evaluated within the ground-state expectation value. However, as the aim of this chapter focuses onto the derivation of a value for the critical coupling within this approach, only contributions of $\hat{\mathcal{H}}^{(n)}$ that are $\propto (\hat{a}^\dagger + \hat{a})^2$ will be important. This is crucial to the derivation of the third and fourth-order contribution as the calculation dramatically simplifies under this restriction (cf. Subsecs. 8.2.6 and 8.2.7). With this, the derivation of the second to fourth-order contribution is discussed during the following.

8.2.3 Second-order correction to the effective Hamiltonian

Before evaluating the second-order contribution of the effective Hamiltonian, $\hat{\mathcal{H}}^{\text{eff}}$, one needs to construct the SW generator $\hat{\mathcal{S}}_1$. This is achieved by combination of Eqs. (8.42, 8.38) with Eq. (8.23) such that one finds in analogy to Ref. [95] the block-off-diagonal,

anti-Hermitian generator

$$\hat{\mathcal{S}}_1 = \sum_{\substack{M \in \mathbb{H}_M^- \\ N \in \mathbb{H}_{N_M}^-}} \left(\hat{s}_{M,N} \otimes \hat{S}_{M,N} - \hat{s}_{M,N}^\dagger \otimes \hat{S}_{M,N}^\dagger \right), \tag{8.49}$$

where the fermionic part is defined as

$$\hat{S}_{M,N} = \hat{c}_M^\dagger \, \mathcal{M}_{M,N} \, \hat{c}_N \tag{8.50}$$

The bosonic operator $\hat{s}_{M,N}$ is then given by

$$\hat{s}_{M,N} = \frac{\hat{a} A_{M,N}^{-1} + \hat{a}^\dagger A_{M,N}^{+1}}{\sqrt{\mathcal{N}}}, \tag{8.51}$$

where the scalar function

$$A_{M,N}^{\pm x} = \frac{1}{\Delta_{M,N} \pm x\hbar\omega} = -A_{N,M}^{\mp}, \qquad \text{and } \Delta_{M,N} = \epsilon_M - \epsilon_N \tag{8.52}$$

results from the integration over t in the definition of the superoperator $\mathcal{L}$, Eq. (8.42). In Eq. (8.52), x defines any integer number. For convenience, the explicit notation of $\pm x$ in the case of $x = 1$ will be abbreviated by $\pm$. Since $\Delta_{M,N} = -\Delta_{N,M}$ and thus in turn $\hat{s}_{N,M} = -\hat{s}_{M,N}^\dagger$, the generator $\hat{\mathcal{S}}_1$ is anti-Hermitian since the bosonic operator $\hat{s}_{N,M}$ is anti-Hermitian.

Only states of the subspaces $\mathbb{H}_M$ and $\mathbb{H}_{N_M} \subseteq \mathbb{H}_N$ are contributing to $\hat{\mathcal{S}}_1$, Eq. (8.49), which results from the dipole selection rules encoded in $\mathcal{M}_{M,N}$, Eq. (5.48), and is in accordance with the definition of the block-off-diagonal parts of the interaction Hamiltonian, $\hat{\mathcal{V}}_o$ (8.23).

For the sake of simplification one introduces the short-hand notation

$$\hat{\mathcal{S}}_1 = \hat{s} \otimes \hat{S} - \hat{s}^\dagger \otimes \hat{S}^\dagger \tag{8.53}$$

for the SW generator keeping the summation over the quantum numbers according to Eq. (8.49).

With this, one is ready to consider the second-order contribution to the effective Hamiltonian from Eq. (8.44). Thus, it is beneficial to expand the commutator according to

$$2\hat{\mathcal{H}}^{(2)} = [\hat{s}, \hat{v}] \otimes (\hat{V}_o + \hat{V}_o^\dagger)\hat{S} - [\hat{s}^\dagger, \hat{v}] \otimes (\hat{V}_o + \hat{V}_o^\dagger)\hat{S}^\dagger + \hat{s}\hat{v} \otimes [\hat{S}, \hat{V}_o^\dagger] - \hat{s}^\dagger\hat{v} \otimes [\hat{S}^\dagger, \hat{V}_o], \tag{8.54}$$

which follows from basic commutator algebra. Furthermore, it was used that the commutators

$$[\hat{S}, \hat{V}_o] = [\hat{S}^\dagger, \hat{V}_o^\dagger] = 0, \tag{8.55}$$

which follows from the dipole selection rules and the definitions of the Hilbert subspaces.

However, Eq. (8.54) can be simplified in view of the definition of each entering component. Thus, one finds for the commutators

$$[\hat{s}, \hat{v}]_{M,N} = -\frac{[\hat{a}, \hat{a}^\dagger]}{\mathcal{N}} \mathcal{C}_{M,N}, \tag{8.56}$$

$$[\hat{s}^\dagger, \hat{v}]_{M,N} = \frac{[\hat{a}, \hat{a}^\dagger]}{\mathcal{N}} \mathcal{C}_{M,N}, \tag{8.57}$$

$$[\hat{S}, \hat{V}_o^\dagger]_{M,N,\bar{M},\bar{N}} = \mathcal{M}_{M,N} \mathcal{M}_{\bar{M},\bar{N}} (\hat{c}_M^\dagger \hat{c}_{\bar{M}} \delta_{N,\bar{N}} - \hat{c}_{\bar{N}}^\dagger \hat{c}_N \delta_{M,\bar{M}}), \tag{8.58}$$

$$[\hat{S}^\dagger, \hat{V}_o]_{M,N,\bar{M},\bar{N}} = -\mathcal{M}_{M,N} \mathcal{M}_{\bar{M},\bar{N}} (\hat{c}_{\bar{M}}^\dagger \hat{c}_M \delta_{N,\bar{N}} - \hat{c}_N^\dagger \hat{c}_{\bar{N}} \delta_{M,\bar{M}}), \tag{8.59}$$

where the indices labeling the commutators indicate the, for instance, M^{th} and N^{th} summand in the definition of $\hat{\mathcal{S}}_1$, Eq. (8.49). In Eqs. (8.56, 8.57) the following definition was used:

$$\mathcal{C}_{M,N} = A_{M,N}^+ - A_{M,N}^- = -\frac{2\,\hbar\omega_0}{\Delta_{M,N}^2 - (\hbar\omega_0)^2}. \tag{8.60}$$

As the commutator of the bosonic creation and annihilation operators in Eqs. (8.56, 8.57) yields the identity, the terms in Eq. (8.54) associated with these commutators are constant with respect to the bosonic contribution and thus they are irrelevant for the calculation of the critical coupling. Furthermore, these terms are of an order $\leq \mathcal{O}(1)$ and thus yield no dominant contribution in the thermodynamic limit, $\mathcal{N} \to \infty$. Thus, keeping only the last two already block-diagonal contributions in Eq. (8.54), one finds for the second-order correction to the effective Hamiltonian in view of the dipole selection rules and the definition of the relevant subspaces $\mathbb{H}_{\text{M}}^-$, $\mathbb{H}_{\text{N}_{\text{M}}}^-$:

$$\hat{\mathcal{H}}^{(2)} = \frac{(\hat{a}^\dagger + \hat{a})^2}{2\mathcal{N}} \sum_{\substack{M \in \mathbb{H}_{\text{M}}^- \\ N \in \mathbb{H}_{\text{N}_{\text{M}}}^-}} \mathcal{D}_{M,N} \mathcal{M}_{M,N}^2 \, (\hat{c}_M^\dagger \hat{c}_M - \hat{c}_N^\dagger \hat{c}_N) = \hat{\mathcal{H}}_{\text{M}}^{(2)} + \hat{\mathcal{H}}_{\text{N}_{\text{M}}}^{(2)}. \tag{8.61}$$

This expression is indeed block-diagonal as well as diagonal. Thereby the following relation was used:

$$(\hat{a}^\dagger + \hat{a})\mathcal{D}_{M,N} = \hat{s}_{M,N} + \hat{s}_{M,N}^\dagger, \quad \text{where } \mathcal{D}_{M,N} = A_{M,N}^+ + A_{M,N}^- = \frac{2\,\hbar\omega_0}{\Delta_{M,N}^2 - (\hbar\omega_0)^2}. \tag{8.62}$$

The application of the dipole selection rules $\mathcal{M}_{M,N}$, Eq. (5.49), explicitly yields for $\hat{\mathcal{H}}_{\text{M}}^{(2)}$:

$$\begin{aligned}
\hat{\mathcal{H}}_{\text{M}}^{(2)} = \frac{(\hat{a}^\dagger + \hat{a})^2}{2\mathcal{N}} &\left[\left[w_{+,M-1}^2 \left(\mathcal{D}_{M,M-1} + \mathcal{D}_{M,-(M-1)} \right) + w_{+,M}^2 \mathcal{D}_{M,-(M+1)} \right] \hat{c}_M^\dagger \hat{c}_M \right. \\
&\left. + \left[w_{+,M+1}^2 \left(\mathcal{D}_{M+1,M+2} + \mathcal{D}_{M+1,-(M+2)} \right) + w_{+,M}^2 \mathcal{D}_{M+1,-M} \right] \hat{c}_{M+1}^\dagger \hat{c}_{M+1} \right].
\end{aligned} \tag{8.63}$$

The details of this contributions are discussed in Subsec. 8.2.4. The remaining contribution $\hat{\mathcal{H}}_{\mathrm{N_M}}^{(2)}$ is given by

$$
\begin{aligned}
\hat{\mathcal{H}}_{\mathrm{N_M}}^{(2)} = -\frac{(\hat{a}^\dagger + \hat{a})^2}{2\mathcal{N}} \Big[&w_{+,M+1}^2 \mathcal{D}_{M+1,-(M+2)} \hat{c}_{-(M+2)}^\dagger \hat{c}_{-(M+2)} \\
&+ w_{+,M}^2 \mathcal{D}_{M,-(M+1)} \hat{c}_{-(M+1)}^\dagger \hat{c}_{-(M+1)} \\
&+ w_{+,M+1}^2 \mathcal{D}_{M+1,-M} \hat{c}_{-M}^\dagger \hat{c}_{-M} + w_{+,M-1}^2 \mathcal{D}_{M,-(M-1)} \hat{c}_{-(M-1)}^\dagger \hat{c}_{-(M-1)} \\
&+ w_{+,M-1}^2 \mathcal{D}_{M,M-1} \hat{c}_{M-1}^\dagger \hat{c}_{M-1} + w_{+,M+1}^2 \mathcal{D}_{M+1,M+2} \hat{c}_{M+2}^\dagger \hat{c}_{M+2} \Big].
\end{aligned}
\tag{8.64}
$$

The discussion of this contribution is postponed until Sec. 8.3.

So far, the effective Hamiltonian is of the form

$$
\hat{\mathcal{H}}^{\mathrm{eff}} = \hat{\mathcal{H}}_{\mathrm{cav}} + \left(\hat{\mathcal{H}}_{0,\mathrm{M}} + g\hat{\mathcal{V}}_{d,\mathrm{M}} + g^2 \hat{\mathcal{H}}_{\mathrm{M}}^{(2)} \right) + \left(\hat{\mathcal{H}}_{0,\mathrm{N}} + g\hat{\mathcal{V}}_{d,\mathrm{N}} + g^2 \hat{\mathcal{H}}_{\mathrm{N_M}}^{(2)} \right) + \sum_{n=3}^{4} g^n \hat{\mathcal{H}}^{(n)}, \tag{8.65}
$$

where $\hat{\mathcal{H}}^{(3)}$ and $\hat{\mathcal{H}}^{(4)}$ are still unknown. Despite the block-diagonal perturbations, $\hat{\mathcal{V}}_{d,\mathrm{M}}$ and $\hat{\mathcal{V}}_{d,\mathrm{N}}$, the expressions in the brackets are diagonal operators. For the construction of the Dicke-like Hamiltonian, all operators assigned to the Hilbert subspace $\mathbb{H}_{\mathrm{M}}$ will be associated with an effective two-level system. All remaining terms in the Hilbert subspace $\mathbb{H}_{\mathrm{N}}$ are then treated as a mean field for the effective two-level system. Thus, one needs to diagonalize the perturbation $\hat{\mathcal{V}}_{d,\mathrm{N}}$ which is approximately achieved by means of another SW transformation. However, unlike the operator contribution $\hat{\mathcal{H}}_{\mathrm{M}}^{\mathrm{eff}}$ projected onto the resonant Fock subspace $\mathcal{F}(\mathbb{H}_{\mathrm{M}})$, the complement $\hat{\mathcal{H}}_{\mathrm{N}}^{\mathrm{eff}}$ operates on a Fock subspace corresponding to the single-particle Hilbert space $\mathbb{H}_{\mathrm{N}}$, Eqs. (8.4, 8.5), which contains infinitely many Landau levels. This is an artifact of the effective Dirac model on which the considerations are based. Especially terms contained in the corresponding part of the interaction Hamiltonian, $\hat{\mathcal{H}}_{\mathrm{i,N}}$, will yield a divergence in the limit $\nu \to \infty$ if not regularized properly. This issue is addressed in Sec. 8.3, where the diagonalization of $\hat{\mathcal{V}}_{d,\mathrm{N}}$ is demonstrated along with the discussion of $\hat{\mathcal{H}}_{\mathrm{N_M}}^{(2)}$. Before proceeding with the derivation of the third- and fourth-order contribution to $\hat{\mathcal{H}}^{\mathrm{eff}}$, the Dicke-like two-level Hamiltonian of the Landau-level doublet M and $M+1$ is discussed.

8.2.4   Effective Dicke-type Hamiltonian of the resonant subsystem

This subsection investigates the Hamiltonian of the Landau-level doublet M and $M+1$. The contributions arising from

$$
\hat{\mathcal{H}}_{\mathrm{M}}^{\mathrm{eff}} = \hat{\mathcal{H}}_{0,\mathrm{M}} + \hat{\mathcal{H}}_{\mathrm{i,M}} + g^2 \hat{\mathcal{H}}_{\mathrm{M}}^{(2)} \tag{8.66}
$$

give rise to an effective two-level description reminiscent of a generalized Dicke Hamiltonian. Thereby $\hat{\mathcal{H}}_{0,\mathrm{M}}$ is defined in Eq. (8.8) and $\hat{\mathcal{H}}_{\mathrm{i,M}}$ corresponds to Eq. (8.22). Likewise, $\hat{\mathcal{H}}_{\mathrm{M}}^{(2)}$ is found in Eq. (8.63) and gives rise to terms $\propto (\hat{a}^\dagger + \hat{a})^2$ on a microscopic level [95].

For the further discussion it is convenient to write $\hat{\mathcal{H}}_{\mathrm{M}}^{(2)}$ as

$$\hat{\mathcal{H}}_{\mathrm{M}}^{(2)} = \frac{(\hat{a}^\dagger + \hat{a})^2}{\mathcal{N}} \sum_k \left[G_M^{\omega_0} \hat{c}_M^\dagger \hat{c}_M + G_{M+1}^{\omega_0} \hat{c}_{M+1}^\dagger \hat{c}_{M+1} \right], \tag{8.67}$$

where the functions $G_M^{\omega_0}$ and $G_{M+1}^{\omega_0}$ are given by

$$2\,G_M^{\omega_0} = w_{+,M-1}^2[\mathcal{D}_{M,M-1} + \mathcal{D}_{M,-(M-1)}] + w_{+,M}^2 \mathcal{D}_{M,-(M+1)}, \tag{8.68}$$

$$2\,G_{M+1}^{\omega_0} = w_{+,M+1}^2[\mathcal{D}_{M+1,M+2} + \mathcal{D}_{M+1,-(M+2)}] + w_{+,M}^2 \mathcal{D}_{M+1,-M}. \tag{8.69}$$

The definition of $\mathcal{D}_{N,N'}$ is found in Eq. (8.62). The details of Eqs. (8.68, 8.69) are revealed by applying the definition of $\mathcal{D}_{N,N'} \propto \Delta_{N,N'}$, Eq. (8.62), and $\Delta_{N,N'} = \epsilon_N - \epsilon_{N'}$ according to Eq. (8.51). By exploiting the sign convention of the collective index notation, Eq. (5.28), one finds $-N$ to refer to a state in the valence band. Thus, $\epsilon_{-N} = -\epsilon_N$ and $\mathcal{D}_{M,-(M+1)} = \mathcal{D}_{M+1,-M}$. Consequently, the last terms on the r.h.s. of Eqs. (8.68, 8.69) are identical. Furthermore, each of the square brackets of Eqs. (8.68, 8.69) is of the general form

$$\begin{aligned}
\mathcal{D}_{N,N'} + \mathcal{D}_{N,-N'} &= \frac{(\Delta_{N,N'} + \Delta_{N,-N'})[\Delta_{N,N'}\Delta_{N,-N'} - (\hbar\omega)^2]}{[\Delta_{N,N'}^2 - (\hbar\omega)^2][\Delta_{N,-N'}^2 - (\hbar\omega)^2]} \\
&= \frac{2\epsilon_N[(\epsilon_N^2 - \epsilon_{N'}^2) - (\hbar\omega)^2]}{(\epsilon_N^2 - \epsilon_{N'}^2)^2 - 2(\hbar\omega)^2(\epsilon_N^2 + \epsilon_{N'}^2) + (\hbar\omega)^4},
\end{aligned} \tag{8.70}$$

where $N, N' = M, M-1$ in case of Eq. (8.68) and $N, N' = M+1, M+2$ if regarding Eq. (8.69). In view of the definition of the Landau level spectrum (5.26) the expression can then be rewritten as

$$\mathcal{D}_{N,N'} + \mathcal{D}_{N,-N'} = \frac{\omega_c}{\hbar} \frac{2\sqrt{n}[(n-n')\omega_c^2 - \omega_0^2]}{(n-n')^2\omega_c^4 - 2(n+n')\omega_c^2\omega_0^2 + \omega_0^4}, \tag{8.71}$$

yielding in particular

$$2\,G_M^{\omega_0} = \frac{\omega_c}{\hbar} \left[\frac{w_{+,M-1}^2 \cdot [2\sqrt{M}(\omega_c^2 - \omega_0^2)]}{\omega_0^4 - 2(2M-1)\omega_c^2\omega_0^2 + \omega_c^4} + \frac{w_{+,M}^2 \cdot (\sqrt{M+1} + \sqrt{M})}{(\sqrt{M+1} + \sqrt{M})^2\omega_c^2 - \omega_0^2} \right], \tag{8.72}$$

$$2\,G_{M+1}^{\omega_0} = \frac{\omega_c}{\hbar} \left[-\frac{w_{+,M+1}^2 \cdot [2\sqrt{M+1}(\omega_c^2 + \omega_0^2)]}{\omega_0^4 - 2(2M+3)\omega_c^2\omega_0^2 + \omega_c^4} + \frac{w_{+,M}^2 \cdot (\sqrt{M+1} + \sqrt{M})}{(\sqrt{M+1} + \sqrt{M})^2\omega_c^2 - \omega_0^2} \right]. \tag{8.73}$$

At resonance, $\omega_0 = \Omega_M$, both expressions simply further and read

$$G_M^{\Omega_M} = \frac{\epsilon_{\mathrm{F}}}{(\hbar\omega_c)^2} \left[w_{+,M-1}^2\, M + \frac{w_{+,M}^2}{4\sqrt{M+1}\sqrt{M}} \right], \tag{8.74}$$

$$G_{M+1}^{\Omega_M} = \frac{\epsilon_{\mathrm{F}}}{(\hbar\omega_c)^2} \left[\frac{w_{+,M}^2}{4\sqrt{M+1}\sqrt{M}} + w_{+,M+1}^2\,(M+1) \right], \tag{8.75}$$

where the Fermi energy

$$\epsilon_{\mathrm{F}} = \frac{\epsilon_{M+1} + \epsilon_M}{2} = \frac{\hbar\omega_c^2}{2\Omega_M} \tag{8.76}$$

is related to the mean energy of the resonant-two level subsystem and to the inverse of the transition frequency Ω_M, Eq. (8.1). From Eqs. (8.74, 8.75) one finds that $G_{M+1}^{\Omega_M} > G_M^{\Omega_M} > 0$.

By substituting the *Schwinger-Wigner representation* of the fermionic operators acting onto the subspace of the Landau-level doublet M and $M + 1$,

$$\tau_k^+ = \hat{c}_{M+1,k}^\dagger \hat{c}_{M,k}, \qquad \tau_k^z = \hat{c}_{M+1,k}^\dagger \hat{c}_{M+1,k} - \hat{c}_{M,k}^\dagger \hat{c}_{M,k},$$
$$\tau_k^- = \hat{c}_{M,k}^\dagger \hat{c}_{M+1,k}, \qquad \tau_k^0 = \hat{c}_{M+1,k}^\dagger \hat{c}_{M+1,k} + \hat{c}_{M,k}^\dagger \hat{c}_{M,k}, \tag{8.77}$$

in Eq. (8.66), one finds $\hat{\mathcal{H}}_{\mathrm{M}}^{\mathrm{eff}}$ revealing a two-level structure reminiscent of the Dicke Hamiltonian, Eq. (3.11), including additional terms $\propto (\hat{a}^\dagger + \hat{a})^2$ on a microscopic level. The operators τ_k^i, $i = +, -, z$ represent two-dimensional Pauli matrices of the kth particle and τ_k^0 corresponds to the two-dimensional unit matrix. Within this mapping of fermionic operators to Pauli matrices and vice versa, Eq. (8.77), all commutation as well as anti-commutation relations retain. Thus, the fermionic character of the operators remains valid in the Schwinger-Wigner representation such that $\hat{\mathcal{H}}_{\mathrm{M}}^{\mathrm{eff}}$ can be rewritten as

$$\hat{\mathcal{H}}_{\mathrm{M}}^{\mathrm{eff}} = \sum_{k=1}^{\mathcal{N}} \left[\epsilon_{\mathrm{F}} \tau_k^0 + \frac{\hbar\Omega_M}{2} \tau_k^z + g \frac{(\hat{a}^\dagger + \hat{a})}{\sqrt{\mathcal{N}}} w_{+,M} (\tau_k^- + \tau_k^+) \right.$$
$$\left. + g^2 \frac{(\hat{a}^\dagger + \hat{a})^2}{\mathcal{N}} \kappa_M^z \tau_k^z + g^2 \frac{(\hat{a}^\dagger + \hat{a})^2}{\mathcal{N}} \kappa_M \tau_k^0 \right]. \tag{8.78}$$

Thereby ϵ_{F} and Ω_M are defined in Eq. (8.76) and Eq. (8.1), respectively, and

$$\kappa_M^z = \frac{1}{2} \left(G_{M+1}^{\omega_0} - G_M^{\omega_0} \right), \qquad \kappa_M = \frac{1}{2} \left(G_{M+1}^{\omega_0} + G_M^{\omega_0} \right), \tag{8.79}$$

where $G_M^{\omega_0}$ and $G_{M+1}^{\omega_0}$ are defined in Eq. (8.68) and Eq. (8.69), respectively.

8.2.5 Comparison to the literature

The exterior appearance of the effective two-level Hamiltonian $\hat{\mathcal{H}}_{\mathrm{M}}^{\mathrm{eff}}$ (8.78) matches with Eq. (34) of Ref. [95]. However, in this thesis two deviating formal conventions were applied:
First, different from the convention defined in Ref. [214], the coupling parameter g appears as a prefactor in the derivations related to the second-order correction of the effective Hamiltonian. Thus, κ_M^z and κ_M appear to be independent on g in this thesis. By contrast, the authors of Ref. [95] absorb the prefactor g^2 into their definition of κ^z and κ, Eqs. (35-38) in Ref. [95].

Second, in this thesis a different sign convention of the term $\propto \kappa_M^z$ is used. The convention applied within this thesis arises naturally from the application of the Schwinger-Wigner representation of the fermionic operators. However, the authors of Ref. [95] introduce an extra minus sign in their definition of $\propto \kappa_M^z$ yielding also an negative sign in their analogue of $\hat{\mathcal{H}}_{\mathrm{M}}^{\mathrm{eff}}$.

Keeping the two deviations in mind and adjusting the results of Ref. [95] according to the conventions used during this thesis, one refers to κ^z and κ, Eqs. (35-38) in Ref. [95], as $\bar{\kappa}_M^z$ and $\bar{\kappa}_M$ during the following. By application of these formal deviations one would fairly expect both results for the effective two-level Hamiltonian to coincide, i.e. $\bar{\kappa}_M^z = \kappa_M^z$ and $\bar{\kappa}_M = \kappa_M$.

Even though the previously discussed conventions were carefully adapted, the results for κ_M^z and κ_M obtained within this thesis differ from those stated in Eqs. (35-38) of Ref. [95]. This becomes most obvious under the consideration of resonance, i.e. $\omega_0 = \Omega_M$, and assumption of $M \geq 2$ where all prefactors $w_{+,n} = 1$. In this case, one obtains for κ_M and κ_M^z from Eq. (8.79):

$$\kappa_M^z\big|_{\omega_0=\Omega_M} = \frac{\epsilon_{\mathrm{F}}}{(\hbar\omega_c)^2} < \frac{1}{\hbar\Omega_M}, \tag{8.80}$$

$$\kappa_M\big|_{\omega_0=\Omega_M} = \frac{\epsilon_{\mathrm{F}}}{(\hbar\omega_c)^2}\left[(2M+1) + \frac{1}{2\sqrt{M+1}\sqrt{M}}\right] < \frac{M+1}{\hbar\Omega_M}, \tag{8.81}$$

whereas the authors of Ref. [95] state in Eqs. (54, 55) of their work

$$\bar{\kappa}_M^z\big|_{\omega_0=\Omega_M} = \frac{\sqrt{M}}{2\hbar\omega_c}, \tag{8.82}$$

$$\bar{\kappa}_M\big|_{\omega_0=\Omega_M} = \frac{1}{\hbar\omega_c}\left[2(M+1)\frac{\epsilon_{\mathrm{F}}}{\hbar\omega_c} - \frac{3}{2}\sqrt{M} + \frac{1}{\sqrt{M}\sqrt{M+1}}\left(\frac{\hbar\omega_c}{\epsilon_{\mathrm{F}}}\right)^3\right]. \tag{8.83}$$

Figure 8.2 a) depicts the differences between the κ_M^z and κ_M at resonance, Eqs. (8.80, 8.81), from the results stated in Ref. [95] according to Eqs. (8.82, 8.83). The deviation in each case is given by $\sqrt{M+1}/(2\hbar\omega_c)$ indicating the difference to origin from the calculation of $G_{M+1}^{\omega_0}$ as Fig. 8.2 b) supports. Thereby $\bar{G}_M^{\omega_0}$ as well as $\bar{G}_{M+1}^{\omega_0}$ are extracted from $\bar{\kappa}_M^z$ and $\bar{\kappa}_M$, respectively, according to Eq. (8.79). With this, one finds $G_M^{\Omega_M}$ to coincide with $\bar{G}_M^{\Omega_M}$, whereas the result obtained within this thesis for $G_{M+1}^{\Omega_M}$ differs from $\bar{G}_{M+1}^{\Omega_M}$ by the $\sqrt{M+1}/(\hbar\omega_c)$.

8.2.6 Third-order correction to the effective Hamiltonian

As the focus of this chapter lies mainly on the derivation of the critical coupling within the effective Dicke-type Hamiltonian, only contributions up to second order of the bosonic operators are relevant. This follows from calculation of the second derivative of the action with respect to the bosonic mean field at $\alpha = 0$ in the thermodynamic analogous as discussed in Chap. 7. Thus, one easily finds that the third-order correction yields no contribution to the critical coupling. To this end, recall the definition of the third-order
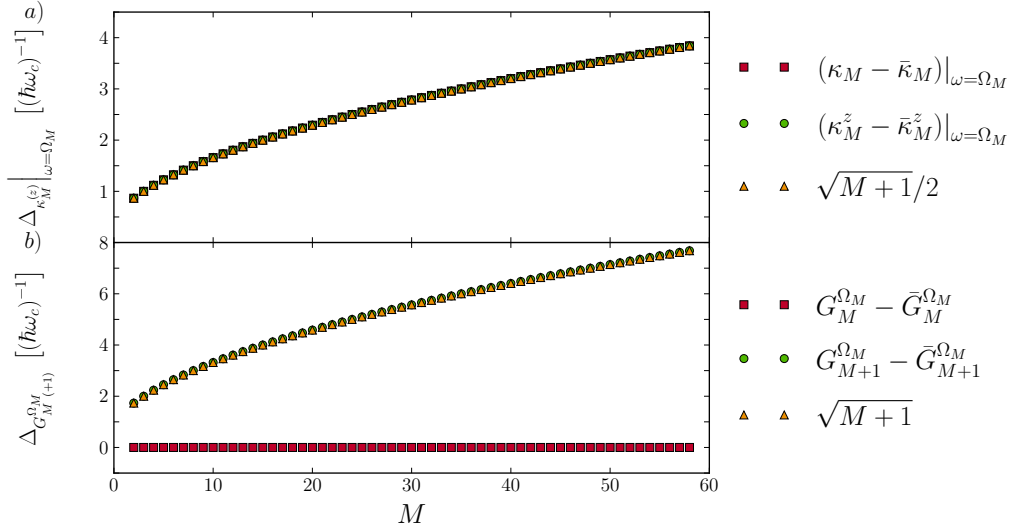
FIGURE 8.2: Comparison of results obtained within this thesis with those stated in Ref. [95], marked by an overline in each case, at resonance. In each panel the corresponding observables are shown as a function of the lower Landau level index M of the resonant two-level subsystem. Panel a) shows the difference of the results for κ_M (8.81) with $\bar{\kappa}_M$ (8.83) (red squares) and the deviation of $\bar{\kappa}_M^z$ (8.81) from κ_M^z (8.82) (green circles), both at resonance. Both of the results obtained within this thesis deviate with an amount of $\sqrt{M+1}/(2\hbar\omega_c)$ (orange triangles) from the results shown in Ref. [95], such that all three coincide perfectly. Panel b) depicts the differences $G_M^{\Omega_M} - \bar{G}_M^{\Omega_M}$ (red squares) and $G_{M+1}^{\Omega_M} - \bar{G}_{M+1}^{\Omega_M}$ (green circles), where the former yields zero. Therefore $G_M^{\Omega_M}$ and $\bar{G}_M^{\Omega_M}$, extracted from $\bar{\kappa}_M^z$ and $\bar{\kappa}_M$ according to Eq. (8.79), coincide. Contrarily, $\bar{G}_{M+1}^{\Omega_M}$ deviates from the result $G_{M+1}^{\Omega_M}$ obtained within this thesis by the amount of $\sqrt{M+1}/(\hbar\omega_c)$ (orange triangles), as the coincidence of both curves demonstrates.

correction, Eq. (8.47):

$$\hat{\mathcal{H}}^{(3)} \propto [\hat{\mathcal{V}}_o, \mathcal{L}([\hat{\mathcal{V}}_d, \hat{\mathcal{S}}_1])]. \tag{8.84}$$

Despite of the action of the superoperator $\mathcal{L}$, which adds, loosely spoken, scalar weighting functions to the bosonic operator contributions, $\hat{\mathcal{H}}^{(3)}$ is of the general form

$$[\hat{d} \otimes \hat{D}, [\hat{c} \otimes \hat{C}, \hat{b}, \otimes \hat{B}]]. \tag{8.85}$$

Applying the decomposition of each operator contribution into bosonic and fermionic part and expanding the commutators, one finds two classes of contributions. The first one is given by the nested commutator of fermionic operators, similar to

$$\hat{d}\hat{c}\hat{a} \otimes [\hat{D}, [\hat{C}, \hat{B}]] \propto \frac{(\hat{a}^\dagger + \hat{a})^3}{\sqrt{\mathcal{N}}^3}. \tag{8.86}$$

As the power of the bosonic operators is larger than 2 these contributions will not contribute to the value of the critical coupling. The second class of commutator contributions

is of the form

$$\hat{b}[\hat{d}, \hat{c}] \otimes [\hat{C}, \hat{B}]\hat{D} \propto \frac{\hat{a}^\dagger + \hat{a}}{\sqrt{\mathcal{N}}^3}. \tag{8.87}$$

However, also this class yields no contribution to the critical coupling as the second derivative in the thermodynamic limit simply vanishes when evaluated in the ensemble average. Thus, as there is no contribution to g_c stemming from the third-order correction of the effective Hamiltonian, one can proceed with the discussion of the fourth-order contribution.

8.2.7 Fourth-order correction to the effective Hamiltonian

To begin the examination of the contribution to g_c originating from the fourth-order correction it is helpful to review $\hat{\mathcal{H}}^{(4)}$ according to Eq. (8.48):

$$\hat{\mathcal{H}}^{(4)} = -\frac{1}{2}[\hat{\mathcal{V}}_o, \mathcal{L}([\hat{\mathcal{V}}_d, \mathcal{L}([\hat{\mathcal{V}}_d, \hat{\mathcal{S}}_1])])] - \frac{1}{6}[\hat{\mathcal{V}}_o, \mathcal{L}([\hat{\mathcal{S}}_1, [\hat{\mathcal{S}}_1, \hat{\mathcal{V}}_o]])] - \frac{1}{24}[\hat{\mathcal{S}}_1, [\hat{\mathcal{S}}_1, [\hat{\mathcal{S}}_1, \hat{\mathcal{V}}_o]]]. \tag{8.88}$$

The following discussion is based on similar arguments as the one applied onto the third-order correction. However, as it subsequently becomes clear, the fourth order yields a dominant contribution to the value of critical coupling in the thermodynamic limit. The term dominant refers to contributions of the order $\geq \mathcal{O}(\mathcal{N})$. Thereby, especially terms in the order of $\geq \mathcal{O}[(\hat{a}^\dagger + \hat{a})^2]$ are taken into account since they will contribute as $\geq \mathcal{O}(\mathcal{N})$ if the system exhibits a superradiant phase in the thermodynamic limit. Then, a mean-field description similar to Eq. (3.50) will be applicable to the bosonic operators such that $\hat{a}^\dagger, \hat{a} \propto \sqrt{N\alpha}$ (cf. Subsec. 3.3.2.)

The definition of $\hat{\mathcal{H}}^{(4)}$ results in a rather elongated expression and the evaluation of each single contribution yields quite complex equations of which the most yield no contribution to g_c according to similar arguments as applied onto the third-order correction. Thus, it is essential to extract the main characteristics of the contributing parts beforehand. Again, one can sketch each part of $\hat{\mathcal{H}}^{(4)}$ in the following way

$$[\hat{e} \otimes \hat{E}, [\hat{d} \otimes \hat{D}, [\hat{c} \otimes \hat{C}, \hat{b}, \otimes \hat{B}]]], \tag{8.89}$$

where small and capital letters refer to bosonic and fermionic contributions, respectively. Again, only terms $\propto (\hat{a}^\dagger + \hat{a})^2$ hold the potential to be relevant for the calculation of g_c. The corresponding class of commutators obtained from the generic expression (8.89) can be characterized by

$$\hat{e}\hat{b}[\hat{d}, \hat{c}] \otimes [\hat{E}, [\hat{C}, \hat{B}]\hat{D}] = \hat{e}\hat{b}[\hat{d}, \hat{c}] \otimes [\hat{E}, [\hat{C}, \hat{B}]]\hat{D} + \hat{e}\hat{b}[\hat{d}, \hat{c}] \otimes [\hat{C}, \hat{B}][\hat{E}, \hat{D}] \propto \frac{(\hat{a}^\dagger + \hat{a})^2}{\mathcal{N}^2}, \tag{8.90}$$

resulting in expressions each involving four fermionic operators. These four-operator terms will be evaluated by means of the Wick theorem [204] during the following. Thereby non-physical terms are automatically excluded from the theory [204] and the operator is decomposable into one and two-body interaction terms. Thus, any product of four fermionic operators can be expanded into a sum of normal ordered terms relative to the

ground state of the system [204]:

$$
\begin{aligned}
\hat{c}_W^\dagger \hat{c}_V^\dagger \hat{c}_Y \hat{c}_Z = \quad & n_W^- \delta_{W,Z}\, n_V^- \delta_{V,Y} \; - \; n_W^- \delta_{W,Y}\, n_V^- \delta_{V,Z} \\
& + n_W^- \delta_{W,Z} \,:\! \hat{c}_V^\dagger \hat{c}_Y \!:\, + \; n_V^- \delta_{V,Y} \,:\! \hat{c}_W^\dagger \hat{c}_Z \!: \\
& - n_W^- \delta_{W,Y} \,:\! \hat{c}_V^\dagger \hat{c}_Z \!:\, - \; n_V^- \delta_{V,Z} \,:\! \hat{c}_W^\dagger \hat{c}_Y \!: \\
& + \,:\! \hat{c}_W^\dagger \hat{c}_V^\dagger \hat{c}_Y \hat{c}_Z \!:,
\end{aligned}
\tag{8.91}
$$

where n_W^- denotes the occupation of the Landau level W. For non-zero temperatures, n_W^- is given by the Fermi-Dirac distribution. Each Kronecker delta in Eq. (8.91) is explicitly given by, for instance, $\delta_{W,Z} = \delta_{\lambda_w,\lambda_z} \delta_{w,z} \delta_{k_w,k_z}$. Furthermore, the operator components $:\! \hat{c}_V^\dagger \hat{c}_Y \!:$ are regarded as fluctuations above the ground-state occupation with zero manybody ground-state expectation value [204], denoted by $\langle \ldots \rangle_0$. Thus, the ground-state average of the four-electron interaction is given by expression (8.91):

$$
\langle \hat{c}_W^\dagger \hat{c}_V^\dagger \hat{c}_Y \hat{c}_Z \rangle_0 = n_W^- \delta_{W,Z}\, n_V^- \delta_{V,Y} - n_W^- \delta_{W,Y}\, n_V^- \delta_{V,Z}.
\tag{8.92}
$$

According to Ref. [204], the second and third line in Eq. (8.91) describes the interaction of a fermion with other fermions and hence, is regarded as a contribution to the self-energy or self-interaction of fermionic particles. The remaining term in the last line of Eq. (8.91) describes the actual two-body interaction free of self-energy contributions [204].

Likewise, one can express any product of one fermionic creation and annihilation operator in terms of its average ground-state value and quantum fluctuations [204],

$$
\hat{c}_V^\dagger \hat{c}_Y = n_V^- \delta_{V,Y} + \,:\! \hat{c}_V^\dagger \hat{c}_Y \!:, \quad \Leftrightarrow \quad \langle \hat{c}_V^\dagger \hat{c}_Y \rangle_0 = n_V^- \delta_{V,Y}.
\tag{8.93}
$$

The relations (8.91, 8.93) are exact expressions. As the focus of this consideration mainly addresses the ground-state properties the results obtained from the four-operator contributions will be evaluated with respect to the ground-state expectation value (8.92). Thus, for the sake of abbreviation, the following discussion will only include the first line of Eq. (8.91) even when the ground-state expectation value has not been explicitly applied yet.

In the thermodynamic limit, a non-vanishing, dominant contribution arises from Eq. (8.89) only if the fermionic contributions $\propto \mathcal{N}^2$. This is due to similar arguments as applied onto the second-order correction. Thus, relevant terms require two distinct summations over the quantum number k which accounts for the Landau-level degeneracy, $\mathcal{N}$. As the fermionic operators are linked to each other by the commutators and the matrix elements encoding the dipole allowed transitions, Eq. (5.48), only the second part in the middle of Eq. (8.89) is relevant as it can be seen from the following considerations:

Starting with the discussion of the nested commutator in the middle of Eq. (8.89). The fermionic contributions of this expression are generally given by the relation

$$
[\hat{E}, [\hat{C}, \hat{B}]] \hat{D} \propto \left(\mathcal{M}_{W,X} \mathcal{M}_{X,U} \mathcal{M}_{U,Y}\, \hat{c}_{W,k}^\dagger \hat{c}_{Y,k} \right) \left(\mathcal{M}_{V,Z}\, \hat{c}_{V,k'}^\dagger \hat{c}_{Z,k'} \right),
\tag{8.94}
$$

where short-hand notation for the fermionic operators, introduced in Eq. (5.51), was substituted by the explicit one accounting for the quantum numbers k and k'. So far, this contribution seems to involve summations over two distinct quantum numbers counting

the level degeneracy, k and k'. However, this is due to Eq. (8.94) containing unphysical contributions which vanish when brought into normal ordered form:

$$[\hat{E}, [\hat{C}, \hat{B}]]\hat{D} \propto -\mathcal{M}_{W,X}\mathcal{M}_{X,U}\mathcal{M}_{U,Y}\mathcal{M}_{V,Z} \left(\hat{c}^\dagger_{W,k}\hat{c}^\dagger_{V,k'}\hat{c}_{Y,k}\hat{c}_{Z,k'} - \hat{c}^\dagger_{W,k}\hat{c}_{Z,k'}\delta_{V,Y}\delta_{k',k} \right).$$
(8.95)

Thereby, the fermionic anti-commutation relations (C.43, C.44) were used (cf. App. C). The one-body contribution already connects both distinct sums over k and k' and thus this term is at most $\propto \mathcal{N}$ or, together with the factor of $1/\mathcal{N}^2$ in the original expression (8.90), of $\leq \mathcal{O}[(\hat{a}^\dagger + \hat{a})^2/\mathcal{N}] \leq \mathcal{O}(1)$ in total. Regarding the remaining two-body term in Eq. (8.95), the only contribution from Eq. (8.91) which survives the ground-state average and yields no connection between k and k' is

$$- n^-_{W,k}\delta_{W,Y}\, n^-_{V,k'}\delta_{V,Z}.$$
(8.96)

However, by substitution into Eq. (8.95) one finds that contributions arising therefrom are forbidden by the dipole selection rules, Eq. (5.48). Thus, the contribution arising from the nested fermionic commutator is of $\leq \mathcal{O}[(\hat{a}^\dagger + \hat{a})^2/\mathcal{N}] \leq \mathcal{O}(1)$ in total and thus not relevant for the following.

With this, the remaining contribution of this class of commutators, Eq. (8.89), is considered. The fermionic part of the second term the middle of Eq. (8.89) is generally represented by

$$[\hat{C}, \hat{B}][\hat{E}, \hat{D}] \propto \left(\mathcal{M}^2_{W,Y}\, \hat{c}^\dagger_{W,k}\hat{c}_{W,k} \right) \left(\mathcal{M}^2_{V,Z}\, \hat{c}^\dagger_{V,k'}\hat{c}_{V,k'} \right)$$
(8.97)

and involves also two sums over the level degeneracy. In particular, each commutator in Eq. (8.97) is similar to the commutators obtained for the second-order contribution, Eqs. (8.58, 8.59). However, from Eq. (8.97) one still cannot tell whether these two distinct sums remain when canceling non-physical terms. Thus, the operator components are brought into normal ordering yielding

$$[\hat{C}, \hat{B}][\hat{E}, \hat{D}] \propto -\mathcal{M}^2_{W,Y}\mathcal{M}^2_{V,Z} \left(\hat{c}^\dagger_{W,k}\hat{c}^\dagger_{V,k'}\hat{c}_{W,k}\hat{c}_{V,k'} - \hat{c}^\dagger_{W,k}\hat{c}_{V,k'}\delta_{V,W}\delta_{k',k} \right),$$
(8.98)

where, again, the fermionic one-body contribution yields at most $\propto \mathcal{N}$. The relevant terms for the two-body part arising from the equivalent to Eq. (8.91) reduce to

$$- n^-_{W,k}\, n^-_{V,k'}$$
(8.99)

in similarity to Eq. (8.96) where $W = Y$ and $V = Z$. Note that the indices Y and Z in the dipole matrix element remain unchanged as Eq. (8.91) addresses only the indices of the operators. Hence, in Eq. (8.98) the sum over the Landau-level degeneracy remains for each fermionic commutator. Thus, each fermionic commutator contributes a factor of $\mathcal{N}$ which gives a factor of $\mathcal{N}^2$ in total. Along with the factor of $1/\mathcal{N}^2$ in the original expression (8.90) the contributions arising from these commutators are of $\mathcal{O}[(\hat{a}^\dagger + \hat{a})^2]$. Consequently, the terms stemming from this part hold the potential for a relevant contribution to g_c in the thermodynamic limit.

However, the details of these contributions strongly depend on the definition of $\hat{\mathcal{H}}^{(4)}$

and have to evaluated carefully by means of the previously discussed arguments. The derivation of these terms is found in App. F, such that only the results are stated here. The ensemble average of the fourth-order contribution to the decoupled Hamiltonian $\hat{\mathcal{H}}^{\text{eff}}$ can be written as

$$\langle \hat{\mathcal{H}}^{(4)} \rangle_0 = (\hat{a}^\dagger + \hat{a})^2 \, \chi_{M,\nu}^{(4)}(\hbar\omega_0), \tag{8.100}$$

where the function $\chi_{M,\nu}^{(4)}$ can be decomposed into its ν-independent and -dependent parts, $\chi_{M,\nu}^{(4)} = \chi_M^{(4)} + \chi_\nu^{(4)}$, where

$$\chi_M^{(4)}(\hbar\omega_0) = \frac{1}{4}\left[\mathcal{W}_{M+1,-M}(M) + \mathcal{W}_{M+1,-(M+2)}(M) + \mathcal{Y}(M)\right], \tag{8.101}$$

$$\chi_\nu^{(4)}(\hbar\omega_0) = -\frac{1}{4}\left[\mathcal{W}'_{M+1,-M}(\nu) + \mathcal{W}'_{M+1,-(M+2)}(\nu)\right]. \tag{8.102}$$

By defining

$$\mathcal{CD}_{M,N} = \mathcal{C}_{M,N}\mathcal{D}_{M,N} = -\frac{4\Delta_{M,N}\hbar\omega_0}{[\Delta_{M,N}^2 - (\hbar\omega_0)^2]^2} \xrightarrow{\omega_0 \to 0} 0, \tag{8.103}$$

$$\mathcal{E}_{K,L}^{M,N} = -\frac{2\Delta_{K,L}}{\Delta_{M,N}^2 - \Delta_{K,L}^2}. \tag{8.104}$$

one finds for the components of the ν-independent contribution, $\chi_M^{(4)}$:

$$\begin{aligned}
\mathcal{W}_{K,L}(M) &= \mathcal{CD}_{K,L} \times \left[J_{M+3}(\Delta_{K,L}) + 2\mathcal{D}_{K,L} - \mathcal{E}_{M+1,M}^{K,L} - \mathcal{E}_{M+3,M+2}^{K,L} - \mathcal{E}_{M+3,-(M+2)}^{K,L}\right] \\
&= \mathcal{CD}_{K,L} \times \left[J_{M+3}(\Delta_{K,L}) + \frac{4\Delta_{K,L}}{\Delta_{K,L}^2 - (\hbar\omega_0)^2} + \frac{2\hbar\Omega_M}{\Delta_{K,L}^2 - (\hbar\Omega_M)^2}\right. \\
&\quad \left. + \frac{4\,\hbar\omega_c\left[\Delta_{K,L}^2 - (\hbar\omega_c)^2\right]\sqrt{M+3}}{\Delta_{K,L}^4 + (\hbar\omega_c)^4 - 2\Delta_{K,L}^2(\hbar\omega_c)^2\left[1 + 2(M+2)\right]}, \right]
\end{aligned} \tag{8.105}$$

with $\mathcal{D}_{K,L}$ defined in Eq. (8.62), and

$$\begin{aligned}
\mathcal{Y}(M) &= \mathcal{CD}_{M+1,-M}\mathcal{D}_{M+1,-(M+2)} + \mathcal{CD}_{M+1,-(M+2)}\mathcal{D}_{M+1,-M} \\
&= \frac{8\,\hbar\omega_0\Delta_{M+1,-M}\Delta_{M+1,-(M+2)}\left[2(\hbar\omega_0)^2 - \Delta_{M+1,-M}^2 - \Delta_{M+1,-(M+2)}^2\right]}{\left[(\hbar\omega_0)^2 - \Delta_{M+1,-M}^2\right]^2\left[(\hbar\omega_0)^2 - \Delta_{M+1,-(M+2)}^2\right]^2}.
\end{aligned} \tag{8.106}$$

Likewise, the function $\mathcal{W}'_{K,L}(\nu)$ entering $\chi_M^{(4)}$ is given by

$$\begin{aligned}
\mathcal{W}'_{K,L}(\nu) &= \mathcal{CD}_{K,L} \times \left[J^{\nu-2}(\Delta_{K,L}) - \mathcal{E}_{\nu,\nu-1}^{K,L} + \mathcal{E}_{\nu,-(\nu-1)}^{K,L}\right] \\
&= \mathcal{CD}_{K,L} \times \left[J^{\nu-2}(\Delta_{K,L}) - \frac{4\hbar\omega_c\left[(\hbar\omega_c)^2 + \Delta_{K,L}^2\right]\sqrt{\nu-1}}{\Delta_{K,L}^4 + (\hbar\omega_c)^4 - 2\Delta_{K,L}^2(\hbar\omega_c)^2\left[1 + 2(\nu-1)\right]}\right].
\end{aligned} \tag{8.107}$$

In Eqs. (8.105, 8.107) J_{M+3} and $J^{\nu-2}$ correspond to the evaluation of the integral approximation of the sum over $2\mathcal{E}^{K,L}_{N+1,-N}$ (cf. Eq. (F.35)) at the lower and upper integration boundary, respectively. In particular, one finds

$$J^{\nu-2}_{M+3}(\Delta_{M,N}) = J^{\nu-2}(\Delta_{M,N}) - J_{M+3}(\Delta_{M,N})$$
$$= \left[\frac{4\sqrt{o}}{\hbar\omega_c} + \frac{\Delta_{M,N}}{(\hbar\omega_c)^2} \log\left(\frac{2\,\hbar\omega_c\sqrt{o} - \Delta_{M,N}}{2\,\hbar\omega_c\sqrt{o} + \Delta_{M,N}} \right) \right]^{o=\nu-2}_{o=M+3}, \quad (8.108)$$

which yields the dominant contribution to $\mathcal{W}_{K,L}(M)$ and $\mathcal{W}'_{M,N}(\nu)$. The functional behavior of both components, $\chi^{(4)}_M(\hbar\omega_0)$ and $\chi^{(4)}_\nu(\hbar\omega_0)$, is illustrated in Fig. 8.3 with respect to M at resonance, where both parts give a positive contribution for $M \geq 4$.
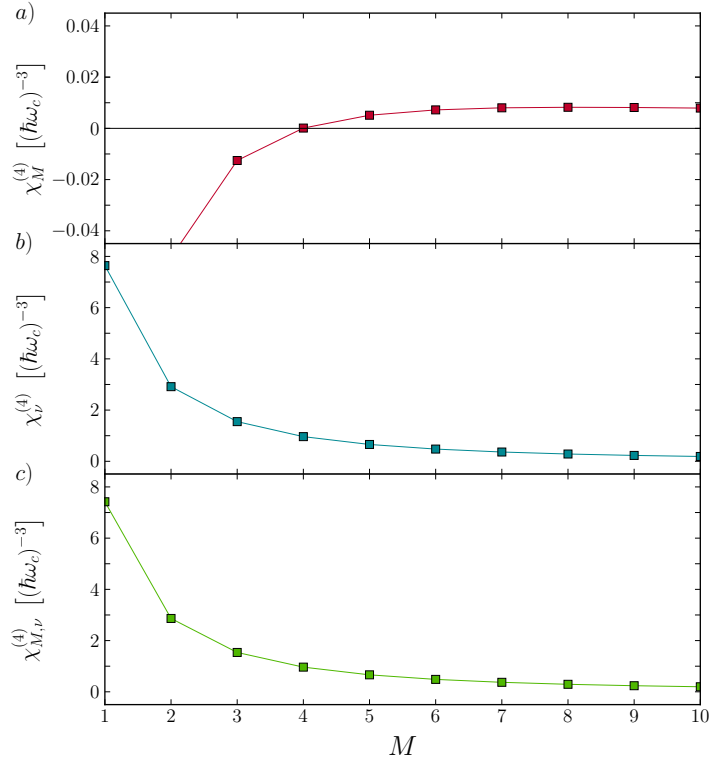
FIGURE 8.3: Functional dependence of the fourth-order contribution to the decoupled Hamiltonian $\hat{\mathcal{H}}^{\text{eff}}$ at resonance. Panel a) shows the ν-independent part of $\chi^{(4)}_{M,\nu}$ according to Eq. (8.101). This term yields a positive contribution for $M \geq 4$. Panel b) depicts the ν-dependent contribution to $\chi^{(4)}_{M,\nu}$, as given in Eq. (8.102). The value of ν is chosen from Eq (6.4) at $B = 5$ T. This contribution is positive for all $M \geq 0$. Panel c) shows the sum of both contributions.

The effective block-diagonal Hamiltonian in fourth-order approximation is now of the form

$$\hat{\tilde{\mathcal{H}}}^{\text{eff}} = \hat{\mathcal{H}}_{\text{cav}} + \hat{\mathcal{H}}^{\text{eff}}_M + \left(\hat{\mathcal{H}}_{0,\text{N}} + g\hat{\mathcal{V}}_{d,\text{N}} + g^2\hat{\mathcal{H}}^{(2)}_{\text{N}_M} \right) + g^4 \langle \hat{\mathcal{H}}^{(4)} \rangle_0, \quad (8.109)$$

where $\hat{\mathcal{H}}_{\mathrm{M}}^{\mathrm{eff}}$, Eq. (8.78), is of the form of a generalized Dicke Hamiltonian with quadratic contributions on a microscopic level. The fourth-order correction $\hat{\mathcal{H}}^{(4)}$ is evaluated within the ensemble average at $T = 0$ and defined in Eq. (8.100). The following section discusses the approximate diagonalization of the perturbation $\hat{\mathcal{V}}_{d,\mathrm{N}}$ up to fourth order of g.

8.3   Diagonalization of the remaining operator contributions

In this section the perturbative diagonalization [95] of the remaining contribution of Eq. (8.65),

$$\hat{\mathcal{H}}_{\mathrm{N}}^{\mathrm{eff}} = \hat{\mathcal{H}}_{\mathrm{cav}} + \hat{\mathcal{H}}_{0,\mathrm{N}} + \hat{\mathcal{H}}_{\mathrm{i},\mathrm{N}}, \tag{8.110}$$

is discussed. Thereby, the interaction Hamiltonian $\hat{\mathcal{H}}_{\mathrm{i},\mathrm{N}}$ is treated as a block-off diagonal contribution. The definition of block-off and block-diagonal operators differs in its details from the previously discussed case. Any operator, that is diagonal, i.e. consists of terms $\propto \hat{c}_N^\dagger \hat{c}_N$, is referred to as block-diagonal. Likewise, the terms $\propto \hat{c}_N^\dagger \hat{c}_{N''}$, where $N \neq N'$, are denoted as block-off diagonal. The approximate diagonalization of block-off diagonal contributions is accomplished by means of another fourth-order SW transformation as applied in Sec. 8.2 where it is aimed for the decoupling of the block-off-diagonal operator contribution $\hat{\mathcal{V}}_o$. Within the scope of diagonalizing $\hat{\mathcal{H}}_{\mathrm{N}}^{\mathrm{eff}}$, one needs to adjust the definition of block-diagonal and block-off-diagonal operators and construct an appropriate unitary transformation $\hat{\mathcal{T}} = e^{\hat{\mathcal{R}}}$ such that the transformed Hamiltonian provides

$$\hat{\mathcal{H}}_{\mathrm{D}} = e^{\hat{\mathcal{R}}} \, \hat{\mathcal{H}}_{\mathrm{N}}^{\mathrm{eff}} \, e^{-\hat{\mathcal{R}}} = \hat{\mathcal{H}}_{\mathrm{cav}} + \hat{\mathcal{H}}_{0,\mathrm{N}} + \sum_{n=2}^{4} g^n \hat{\mathcal{H}}_{\mathrm{N}}^{(n)} = \sum_{N \in \mathbb{H}_{\mathrm{N}}} \hat{\mathcal{W}}_N \, \hat{c}_N^\dagger \hat{c}_N. \tag{8.111}$$

Thereby $\hat{\mathcal{W}}_N$ represents a bosonic operator related to the eigenenergies of the transformed Hamiltonian. In the end of this Section, the effective Hamiltonian, Eq. (8.109), will be of the form

$$\hat{\tilde{\mathcal{H}}}^{\mathrm{eff}} = \hat{\mathcal{H}}_{\mathrm{cav}} + \hat{\mathcal{H}}_{\mathrm{M}}^{\mathrm{eff}} + \hat{\mathcal{H}}_{0,\mathrm{N}} + g^2 (\langle \hat{\mathcal{H}}_{\mathrm{N}_{\mathrm{M}}}^{(2)} \rangle_0 + \langle \hat{\mathcal{H}}_{\mathrm{N}}^{(2)} \rangle_0) + g^4 (\langle \hat{\mathcal{H}}^{(4)} \rangle_0 + \langle \hat{\mathcal{H}}_{\mathrm{N}}^{(4)} \rangle_0), \tag{8.112}$$

where $\hat{\mathcal{H}}_{\mathrm{N}}^{(2)}$ and $\hat{\mathcal{H}}_{\mathrm{N}}^{(4)}$ correspond to the second- and fourth-order contribution of the approximate diagonalization according to Eq. (8.111).

The construction of the generator $\hat{\mathcal{R}}$ is achieved by the technique provided in Subsec. 8.2.1 for the example of $\hat{\mathcal{S}}$. Since the construction scheme is only depending on the definition of block-diagonal and block-off-diagonal operator contributions, it is adjustable to the scope of diagonalizing $\hat{\mathcal{H}}_{\mathrm{N}}^{\mathrm{eff}}$. According to Eqs. (8.14, 8.15), one redefines the term block-diagonal-off, if a linear operator $\hat{\mathcal{X}}$ obeys $\mathcal{D}'(\hat{\mathcal{X}}) = \hat{\mathcal{X}}$, where

$$\mathcal{D}'(\hat{\mathcal{X}}) = \hat{P}_N \, \hat{X} \, \hat{P}_{N'} + \hat{P}_{N'} \, \hat{X} \, \hat{P}_N \tag{8.113}$$

exploiting the projector definition according to the r.h.s. of Eq. (8.13). The definition of block-diagonal operators according to Eqs. (8.16, 8.17) remains valid. Therefore, the operators $\hat{\mathcal{H}}_{0,\mathrm{N}}$, Eq. (8.9), and $\hat{\mathcal{H}}_{\mathrm{N}_{\mathrm{M}}}^{(2)}$, Eq. (8.64), are already block-diagonal such that one refers

to $\hat{\mathcal{H}}_{\text{i,N}}$ as a block-off-diagonal operator:

$$g\hat{\mathcal{V}}'_o = \mathcal{D}'(\hat{\mathcal{H}}_{\text{i,N}}) = \hat{v} \otimes (\hat{V_o}' + \hat{V}'^{\dagger}_o), \tag{8.114}$$

where the bosonic contribution is defined in Eq. (8.20). However, the fermionic contribution is given by

$$\hat{V_o}' = \sum_{N,N'} m_{N,N'} \, \hat{c}^{\dagger}_N \hat{c}_{N'}, \tag{8.115}$$

where $m_{N,N'}$ is defined in Eq. (5.49). The explicit decomposition of the Hermitian operator $\hat{\mathcal{H}}_{\text{i,N}}$ into its non-Hermitian components, as Eq. (8.114) shows, is beneficial, as the results obtained in Sec. 8.2 can mainly be adopted.

Thus, the derivation of the generator $\hat{\mathcal{R}}$ is similarly accomplished as demonstrated in Subsec. 8.2.1 for $\hat{\mathcal{S}}$. As the perturbation is purely block-off diagonal, the equivalents of Eqs. (8.34 – 8.36) are given by

$$[\hat{\mathcal{R}}_1, \hat{\mathcal{H}}_{\text{cav}} + \hat{\mathcal{H}}_{0,\text{N}}] = -\hat{\mathcal{V}}'_o, \tag{8.116}$$

$$[\hat{\mathcal{R}}_2, \hat{\mathcal{H}}_{\text{cav}} + \hat{\mathcal{H}}_{0,\text{N}}] = 0, \tag{8.117}$$

$$[\hat{\mathcal{R}}_3, \hat{\mathcal{H}}_{\text{cav}} + \hat{\mathcal{H}}_{0,\text{N}}] = -\frac{1}{3}[\hat{\mathcal{R}}_1, [\hat{\mathcal{R}}_1, \hat{\mathcal{V}}'_o]]. \tag{8.118}$$

Thus, in analogy to the superoperator $\mathcal{L}$, Eq. (8.42) one defines

$$\mathcal{L}'(\hat{\mathcal{X}}) = \int_0^{\infty} \mathrm{d}t \, e^{-t\,(\hat{\mathcal{H}}_{\text{cav}} + \hat{\mathcal{H}}_{0,\text{N}})} \hat{P}_{\text{N}} \, \hat{\mathcal{X}} \, \hat{P}_{\text{N}'} - \int_0^{\infty} \mathrm{d}t \, \hat{P}_{\text{N}'} \, \hat{\mathcal{X}} \, \hat{P}_{\text{N}} e^{-t\,(\hat{\mathcal{H}}_{\text{cav}} + \hat{\mathcal{H}}_{0,\text{N}})} \leq \frac{||\hat{\mathcal{X}}||}{\Delta} \tag{8.119}$$

to obtain

$$\hat{\mathcal{R}}_1 = \mathcal{L}'(\hat{\mathcal{V}}_o), \tag{8.120}$$

$$\hat{\mathcal{R}}_2 = 0, \tag{8.121}$$

$$\hat{\mathcal{R}}_3 = \frac{1}{3}\mathcal{L}'([\hat{\mathcal{R}}_1, [\hat{\mathcal{R}}_1, \hat{\mathcal{V}}'_o]]). \tag{8.122}$$

Note that in this case the second-order generator is already zero. Thereby, the second to fourth-order contributions of the approximate diagonal Hamiltonian, $\hat{\mathcal{H}}_{\text{D}}$ are then given by [214]

$$\hat{\mathcal{H}}^{(2)}_{\text{N}} = \frac{1}{2}[\hat{\mathcal{R}}_1, \hat{\mathcal{V}}'_o], \tag{8.123}$$

$$\hat{\mathcal{H}}^{(3)}_{\text{N}} = 0, \tag{8.124}$$

$$\hat{\mathcal{H}}^{(4)}_{\text{N}} = -\frac{1}{6}[\hat{\mathcal{V}}'_o, \mathcal{L}'([\hat{\mathcal{R}}_1, [\hat{\mathcal{R}}_1, \hat{\mathcal{V}}'_o]])] - \frac{1}{24}[\hat{\mathcal{R}}_1, [\hat{\mathcal{R}}_1, [\hat{\mathcal{R}}_1, \hat{\mathcal{V}}'_o]]], \tag{8.125}$$

where $\hat{\mathcal{H}}_{\mathrm{N}}^{(3)}$ is also zero right away. Again, each $\hat{\mathcal{H}}_{\mathrm{N}}^{(n)}$ can be obtained from the lowest SW generator $\hat{\mathcal{R}}_1$, which is given by

$$\hat{\mathcal{R}}_1 = \sum_{N,N' \in \mathbb{H}_{\mathrm{N_M}}^-} \left(\hat{r}_{N,N'} \otimes \hat{R}_{N,N'} - \hat{r}_{N,N'}^\dagger \otimes \hat{R}_{N,N'}^\dagger \right), \tag{8.126}$$

where the fermionic part reads

$$\hat{R}_{N,N'} = \hat{c}_N^\dagger \, m_{N,N'} \, \hat{c}_{N'}. \tag{8.127}$$

The bosonic contribution is defined as

$$\hat{r}_{N,N'} = \frac{\hat{a} A_{N,N'}^{-1} + \hat{a}^\dagger A_{N,N'}^{+1}}{\sqrt{\mathcal{N}}}, \tag{8.128}$$

where $A_{N,N'}^{\pm x}$ is identical to Eq. (8.52).

8.3.1   Second-order contribution

With this the second-order contribution to $\hat{\mathcal{H}}_{\mathrm{D}}$ is found by evaluation of

$$2\hat{\mathcal{H}}_{\mathrm{N}}^{(2)} = [\hat{r}, \hat{v}] \otimes (\hat{V}_o' + \hat{V}_o'^\dagger)\hat{R} - [\hat{r}^\dagger, \hat{v}] \otimes (\hat{V}_o' + \hat{V}_o'^\dagger)\hat{R}^\dagger$$
$$+ \hat{r}\hat{v} \otimes [\hat{R}, \hat{V}_o'] - \hat{r}^\dagger \hat{v} \otimes [\hat{R}^\dagger, \hat{V}_o'^\dagger] - \hat{r}^\dagger \hat{v} \otimes [\hat{R}^\dagger, \hat{V}_o'] + \hat{r}\hat{v} \otimes [\hat{R}, \hat{V}_o'^\dagger], \quad (8.129)$$

in analogy to Eq. (8.54). Note that in Eq. (8.129) the short-hand notation

$$\hat{\mathcal{R}}_1 = \hat{r} \otimes \hat{R} - \hat{r}^\dagger \otimes \hat{R}^\dagger \tag{8.130}$$

was used. Thereby, one has to keep in mind the summation over the quantum numbers as precisely defined by Eq. (8.126).

During this evaluation, the relevant contribution arise from the last two commutators in the second line of Eq. (8.129), in analogy to the discussion in Sec. 8.2. However, this results from the dipole selection rules and the microscopic definition of $\hat{\mathcal{R}}$ and $\hat{\mathcal{V}}_o'$ and can be seen as follows: Similar to Eqs. (8.56 – 8.57), the first two commutators of Eq. (8.129),

$$[\hat{r}, \hat{v}]_{N,N'} = -\frac{[\hat{a}, \hat{a}^\dagger]}{\mathcal{N}} \mathcal{C}_{N,N'}, \tag{8.131}$$

$$[\hat{r}^\dagger, \hat{v}]_{N,N'} = \frac{[\hat{a}, \hat{a}^\dagger]}{\mathcal{N}} \mathcal{C}_{N,N'}, \tag{8.132}$$

where $\mathcal{C}_{N,N'}$ is defined in Eq. (8.60), give only a constant contribution with respect to the bosonic part. Thus these terms are omitted. The first two commutators in the second line of Eq. (8.129),

$$[\hat{R}, \hat{V}_o']_{N,N',\bar{N},N''} = m_{N,N'} m_{\bar{N},N''}(\hat{c}_N^\dagger \hat{c}_{N''} \delta_{N',\bar{N}} - \hat{c}_{\bar{N}}^\dagger \hat{c}_{N'} \delta_{N,N''}), \tag{8.133}$$

$$[\hat{R}^\dagger, \hat{V}_o'^\dagger]_{N,N',\bar{N},N''} = -m_{N,N'} m_{\bar{N},N''}(\hat{c}_{N''}^\dagger \hat{c}_{\bar{N}} \delta_{N',\bar{N}} - \hat{c}_{N'}^\dagger \hat{c}_{\bar{N}} \delta_{N,N''}), \tag{8.134}$$

yield terms which vanish in the ground-state average. Thus, the only relevant contribution arises from the last two commutators in the second line of Eq. (8.129):

$$[\hat{R}, \hat{V}_o'^{\dagger}]_{N,N',\bar{N},N''} = m_{N,N'} m_{\bar{N},N''} (\hat{c}_N^{\dagger} \hat{c}_{\bar{N}} \delta_{N',N''} - \hat{c}_{N''}^{\dagger} \hat{c}_{N'} \delta_{N,\bar{N}}), \tag{8.135}$$

$$[\hat{R}^{\dagger}, \hat{V}_o']_{N,N',\bar{N},N''} = -m_{N,N'} m_{\bar{N},N''} (\hat{c}_{\bar{N}}^{\dagger} \hat{c}_N \delta_{N',N''} - \hat{c}_{N'}^{\dagger} \hat{c}_{N''} \delta_{N,\bar{N}}). \tag{8.136}$$

From the definition of the matrix elements $m_{N,N'}$, Eq. (5.49), it follows that the operator contributions in Eqs. (8.135, 8.136) are already diagonal. Thus, one finds for $\hat{\mathcal{H}}_N^{(2)}$ after relabeling the indices

$$\begin{aligned}
\hat{\mathcal{H}}_N^{(2)} &= \frac{(\hat{a}^{\dagger} + \hat{a})^2}{2\mathcal{N}} \sum_{N,N'} m_{N,N'}^2 \mathcal{D}_{N,N'} (\hat{c}_N^{\dagger} \hat{c}_N - \hat{c}_{N'}^{\dagger} \hat{c}_{N'}) \\
&= \frac{(\hat{a}^{\dagger} + \hat{a})^2}{2\mathcal{N}} \sum_{N,N'} \left(m_{N,N'}^2 \mathcal{D}_{N,N'} - m_{N',N}^2 \mathcal{D}_{N',N} \right) \hat{c}_N^{\dagger} \hat{c}_N,
\end{aligned} \tag{8.137}$$

where the definition of $\mathcal{D}_{N,N'}$ is found in Eq. (8.62). At this point it is beneficial to include $\hat{\mathcal{H}}_{N_M}^{(2)}$ into the evaluation. By expansion of $\hat{\mathcal{M}}_{M,N}^2 = m_{M,N}^2 + m_{N,M}^2$ one finds under application of the symmetry properties of $\hat{\mathcal{D}}_{M,N}$ for Eq. (8.64)

$$\begin{aligned}
\hat{\mathcal{H}}_{N_M}^{(2)} &= -\frac{(\hat{a}^{\dagger} + \hat{a})^2}{2\mathcal{N}} \sum_{\substack{M \in \mathbb{H}_M \\ N \in \mathbb{H}_N}} (m_{M,N}^2 \mathcal{D}_{M,N} + m_{N,M}^2 \mathcal{D}_{M,N}) \hat{c}_N^{\dagger} \hat{c}_N \\
&= -\frac{(\hat{a}^{\dagger} + \hat{a})^2}{2\mathcal{N}} \sum_{\substack{M \in \mathbb{H}_M \\ N \in \mathbb{H}_N}} (m_{M,N}^2 \mathcal{D}_{M,N} - m_{N,M}^2 \mathcal{D}_{N,M}) \hat{c}_N^{\dagger} \hat{c}_N,
\end{aligned} \tag{8.138}$$

which yields in combination with Eq. (8.137) the quantum number N' to be defined within the complete fermionic Hilbert space. Thus for the proceeding, one defines $\hat{\bar{\mathcal{H}}}^{(2)} = \hat{\mathcal{H}}_N^{(2)} + \hat{\mathcal{H}}_{N_M}^{(2)}$. By evaluation of the summation over k, which is encoded in the short-hand notation, and subsequent evaluation of the sum over N' one finds for $\hat{\bar{\mathcal{H}}}^{(2)}$:

$$\begin{aligned}
\hat{\bar{\mathcal{H}}}^{(2)} &= \frac{(\hat{a}^{\dagger} + \hat{a})^2}{2} \sum_N \left[w_{+,N}^2 \left(\mathcal{D}_{N,N+1} + \mathcal{D}_{N,-(N+1)} \right) - w_{+,N-1}^2 \left(\mathcal{D}_{N-1,N} + \mathcal{D}_{-(N-1),N} \right) \right] \hat{c}_N^{\dagger} \hat{c}_N \\
&= \frac{(\hat{a}^{\dagger} + \hat{a})^2}{2} \sum_N \left[w_{+,N}^2 \left(-\mathcal{D}_{N+1,N} + \mathcal{D}_{N+1,-N} \right) + w_{+,N-1}^2 \left(\mathcal{D}_{N,N-1} + \mathcal{D}_{N,-(N-1)} \right) \right] \hat{c}_N^{\dagger} \hat{c}_N
\end{aligned} \tag{8.139}$$

where the symmetry properties of $\mathcal{D}_{N,N'}$ were applied in the second line. By taking the ground-state expectation value of $\hat{\bar{\mathcal{H}}}^{(2)}$ the fermionic operators can be substituted by the Fermi-Dirac distribution

$$\langle \hat{c}_N^{\dagger} \hat{c}_N \rangle_0 = n_T^-(\epsilon_N) = \frac{1}{\exp\left[\beta(\epsilon_N - \epsilon_F)\right] + 1}. \tag{8.140}$$

Thus, one finds for $T = 0$, where the Fermi-Dirac distribution is a Heaviside step function, $n_T^-(\epsilon_N) \overset{T\to\infty}{\longrightarrow} n^-(\epsilon_N) = \Theta(\epsilon_F - \epsilon_N)$:

$$
\begin{aligned}
\langle \hat{\bar{\mathcal{H}}}^{(2)} \rangle_0 = \frac{(\hat{a}^\dagger + \hat{a})^2}{2} & \Bigg[\sum_{|N|=0}^{M-1} \Big[w_{+,N}^2 \left(-\mathcal{D}_{N+1,N} + \mathcal{D}_{N+1,-N} \right) \\
& \qquad\qquad + w_{+,N-1}^2 \left(\mathcal{D}_{N,N-1} + \mathcal{D}_{N,-(N-1)} \right) \Big] \\
& + \sum_{|N|=0}^{M-1} \Big[w_{+,N}^2 \left(-\mathcal{D}_{-(N+1),-N} + \mathcal{D}_{-(N+1),N} \right) \\
& \qquad\qquad + w_{+,N-1}^2 \left(\mathcal{D}_{-N,-(N-1)} + \mathcal{D}_{-N,N-1} \right) \Big] \\
& + \sum_{|N|=M}^{\nu-1} \Big[w_{+,N}^2 \left(-\mathcal{D}_{-(N+1),-N} + \mathcal{D}_{-(N+1),N} \right) \\
& \qquad\qquad + w_{+,N-1}^2 \left(\mathcal{D}_{-N,-(N-1)} + \mathcal{D}_{-N,N-1} \right) \Big] \Bigg],
\end{aligned}
\tag{8.141}
$$

where it was explicitly accounted for both bands encoded in the short-hand notation $N = (\lambda, n) = (\lambda, |N|)$. The terms in the first two lines correspond to the contribution from the conduction band levels beneath the last occupied Landau level M according to the definition of the Hilbert subspace $\mathbb{H}_N$. The remaining two sums refer to the contribution arising from the filled levels in the valence band. As the effective Dirac model artificially assumes unbounded bands, one has to introduce an ultraviolet cutoff ν similar as in the evaluation of the effective action of the bosonic field discussed in Chap. 7. Rigid cutoff regularization avoids the divergence arising from the boundless valence band. From a theoretical point of view however this is always an issue in the presence of electromagnetic potentials in Coulomb gauge as gauge symmetry is broken. Despite this crucial argument, cutoff regularization seems, however, to be justified when remembering that the Dirac description is an effective model approximating the band-structure only for small energy excitations. Thus, the numerical tight-binding simulation, which serves as an independent reference, shows cutoff-like bounds for the Landau-clustered region (cf. Fig. 6.1) and the comparison of the cutoff-regularized path integral results with the numerical simulation are in striking agreement. Therefore, the results obtained in this Chapter are also evaluated for a rigid cutoff and compared with the corresponding predictions of the path integral approach and the numerical simulation. Furthermore, the regularization approach of Ref. [95] yields a cutoff-independent result and is adopted in addition. Likewise, this approach is then compared with the cutoff-independent regularization of the path integral approach. The discussion of this regularization method is found after the further discussion of $\langle \hat{\bar{\mathcal{H}}}^{(2)} \rangle_0$ in the next paragraph.

The contributions in the first and second line of Eq. (8.141) precisely cancel according to the symmetry properties of $\mathcal{D}_{N,N'}$. Thus, the remaining terms can then be written as

$$
\langle \hat{\bar{\mathcal{H}}}^{(2)} \rangle_0 = (\hat{a}^\dagger + \hat{a})^2 \, \chi_{M,\nu}^{(2)}(\hbar\omega_0),
\tag{8.142}
$$

where

$$
\chi_{M,\nu}^{(2)}(\hbar\omega_0) = -\frac{1}{2}\left[\mathcal{J}_M^{\nu-2}(\hbar\omega_0) + w_{+,M-1}^2\left(\mathcal{D}_{M,M-1} + \mathcal{D}_{M,-(M-1)}\right)\right.
$$
$$
\left. + w_{+,\nu-1}^2\left(-\mathcal{D}_{\nu,\nu-1} + \mathcal{D}_{\nu,-(\nu-1)}\right)\right], \quad (8.143)
$$

with $\mathcal{J}_M^{\nu-2}(\hbar\omega_0)$ defined in Eq. (F.35). Following Ref. [95], the contribution $\langle\hat{\bar{\mathcal{H}}}^{(2)}\rangle_0$ has to vanish in the limit $\hbar\omega_0 \to 0$ as static, homogeneous vector potentials have no effect on the dynamics of charges and can always be removed by a gauge transformation. However, $\chi_{M,\nu}^{(2)}(\hbar\omega_0)$ assumes the value

$$
\chi_{M,\nu}^{(2)}(0) = -\frac{1}{2}\left[2\sum_{|N|=M}^{\nu-2} w_{+,N}^2\frac{1}{\Delta_{N+1,-N}} + w_{+,M-1}^2\left(\frac{1}{\Delta_{M,M-1}} + \frac{1}{\Delta_{M,-(M-1)}}\right)\right]
$$
$$
+ w_{+,\nu-1}^2\left(-\frac{1}{\Delta_{\nu,u-1}} + \frac{1}{\Delta_{\nu,-(\nu-1)}}\right) \quad (8.144)
$$

at $\hbar\omega_0 = 0$ and is certainly not zero. According to Ref. [95], this contribution has to be subtracted from $\chi_{M,\nu}^{(2)}(\hbar\omega_0)$ in order to restore gauge symmetry in the static limit. Note that this context of gauge symmetry is essentially different from the discussion of broken gauge symmetry in cutoff-regularized systems. Thus, by defining

$$
\tilde{\mathcal{D}}_{M,N} = \mathcal{D}_{M,N} - \mathcal{D}_{M,N}|_{\hbar\omega_0=0} = \frac{2(\hbar\omega_0)^2}{\Delta_{M,N}\left[\Delta_{M,N}^2 - (\hbar\omega_0)^2\right]}, \quad (8.145)
$$

$$
\mathcal{I}_M^{\nu-2}(\hbar\omega_0) = \mathcal{J}_M^{\nu-2}(\hbar\omega_0) - \mathcal{J}_M^{\nu-2}(0) = 2\sum_{|N|=M}^{\nu-2} w_{+,N}\tilde{\mathcal{D}}_{N+1,-N}, \quad (8.146)
$$

one finds the function

$$
\tilde{\chi}_{M,\nu}^{(2)}(\hbar\omega_0) = \chi_{M,\nu}^{(2)}(\hbar\omega_0) - \chi_{M,\nu}^{(2)}(0)
$$
$$
= -\frac{1}{2}\left[\mathcal{I}_M^{\nu-2}(\hbar\omega_0) + w_{+,M-1}^2\left(\tilde{\mathcal{D}}_{M,M-1} + \tilde{\mathcal{D}}_{M,-(M-1)}\right)\right. \quad (8.147)
$$
$$
\left. + w_{+,\nu-1}^2\left(-\tilde{\mathcal{D}}_{\nu,\nu-1} + \tilde{\mathcal{D}}_{\nu,-(\nu-1)}\right)\right],
$$

which vanishes properly in the static limit and therefore will be referred to in the evaluation of $\langle\hat{\bar{\mathcal{H}}}^{(2)}\rangle_0$. Similar to $\mathcal{J}_M^{\nu-2}$ being bound by the integrals $J_{M+1}^{\nu-2}$ and $J_M^{\nu-2}$, Eq. (8.108), one finds the lower and upper bound for $\mathcal{I}_M^{\nu-2}$ as

$$
I_{M+1}^{\nu-2}(\hbar\omega_0) \leq \mathcal{I}_M^{\nu-2}(\hbar\omega_0) \leq I_M^{\nu-2}(\hbar\omega_0), \quad (8.148)
$$

where

$$I_M^{\nu-2}(\hbar\omega_0) = I^{\nu-2}(\hbar\omega_0) - I_M(\hbar\omega_0) = \left[\frac{\hbar\omega_0}{(\hbar\omega_c)^2}\log\left(\frac{2\,\omega_c\sqrt{O}-\omega_0}{2\,\omega_c\sqrt{O}+\omega_0}\right)\right]_M^{\nu-2}. \tag{8.149}$$

The short-hand notation introduced in the middle of this expression reads as follows: I carrying a super- or subscript corresponds to the evaluation of the expression on the r.h.s. of Eq. (8.149) with respect to the upper or lower boundary. The integral approximation for the sum $\mathcal{I}_M^{\nu-2}$ converges in the limit $\nu \to \infty$ according to

$$I_M^\infty(\hbar\omega_0) = \lim_{\nu\to\infty} I_M^{\nu-2}(\hbar\omega_0) = -I_M(\hbar\omega_0). \tag{8.150}$$

Thus, also the sum $\mathcal{I}_M^\infty = \lim_{\nu\to\infty}\mathcal{I}_M^{\nu-2}$ converges as it is bounded by I_{M+1}^∞ and I_M^∞. Further, the remaining terms in Eq. (8.147) are given by

$$\tilde{\mathcal{D}}_{M,M-1} + \tilde{\mathcal{D}}_{M,-(M-1)} = \frac{4\sqrt{M}\left(\frac{\omega_0}{\omega_c}\right)^2\left[4M-3-(\frac{\omega_0}{\omega_c})^2\right]}{\hbar\omega_c\left[1+(2-4M)\left(\frac{\omega_0}{\omega_c}\right)^2+\left(\frac{\omega_0}{\omega_c}\right)^4\right]}, \tag{8.151}$$

$$-\tilde{\mathcal{D}}_{\nu,\nu-1} + \tilde{\mathcal{D}}_{\nu,-(\nu-1)} = -\frac{4\sqrt{\nu-1}\left(\frac{\omega_0}{\omega_c}\right)^2\left[4\nu-1-(\frac{\omega_0}{\omega_c})^2\right]}{\hbar\omega_c\left[1+(2-4\nu)\left(\frac{\omega_0}{\omega_c}\right)^2+\left(\frac{\omega_0}{\omega_c}\right)^4\right]}. \tag{8.152}$$

It is beneficial for the following discussion to introduce the decomposition $\tilde{\chi}_{M,\nu}^{(2)}$ into its ν-independent and -dependent parts according to

$$\tilde{\chi}_{M,\nu}^{(2)}(\hbar\omega_0) = \tilde{\chi}_M^{(2)}(\hbar\omega_0) + \tilde{\chi}_\nu^{(2)}(\hbar\omega_0), \tag{8.153}$$

where

$$\tilde{\chi}_M^{(2)}(\hbar\omega_0) = -\frac{1}{2}\left[-I_M(\hbar\omega_0) + w_{+,M-1}^2\left(\tilde{\mathcal{D}}_{M,M-1}+\tilde{\mathcal{D}}_{M,-(M-1)}\right)\right], \tag{8.154}$$

$$\tilde{\chi}_\nu^{(2)}(\hbar\omega_0) = -\frac{1}{2}\left[I_{\nu-2}(\hbar\omega_0) + w_{+,\nu-1}^2\left(-\tilde{\mathcal{D}}_{\nu,\nu-1}+\tilde{\mathcal{D}}_{\nu,-(\nu-1)}\right)\right]. \tag{8.155}$$

Both components are negative at resonance, as illustrated by Fig. (8.4) as a function of M. When investigating the effective Hamiltonian within rigorous ultraviolet cutoff regularization, one refers to the contribution

$$\langle\hat{\tilde{\mathcal{H}}}^{(2)}\rangle_0^{M,\nu} = (\hat{a}^\dagger+\hat{a})^2\,\tilde{\chi}_{M,\nu}^{(2)}(\hbar\omega_0). \tag{8.156}$$

For the discussion in Sec. 8.4 it is beneficial to rewrite the cutoff-independent contribution in the following way

$$
\begin{aligned}
\tilde{\chi}_M^{(2)}(\hbar\omega_0) &= \frac{1}{2}I_M(\hbar\omega_0) + \frac{w_{+,M}^2}{2}\mathcal{D}_{M+1,-M} + w_{+,M-1}^2\frac{2\sqrt{M}}{\hbar\omega_c} - (\kappa - \kappa_z) \\
&= \frac{1}{2}I_M(\hbar\omega_0) + \frac{(\hbar\omega_0)^2}{2\epsilon_{\mathrm{F}}[(2\epsilon_{\mathrm{F}})^2 - (\hbar\omega_0)^2]} + \frac{2w_{+,M-1}^2 - 1}{\hbar\Omega_M} - (\kappa - \kappa_z)
\end{aligned}
\tag{8.157}
$$

This intermediate result coincides so far with the results of Ref. [95].
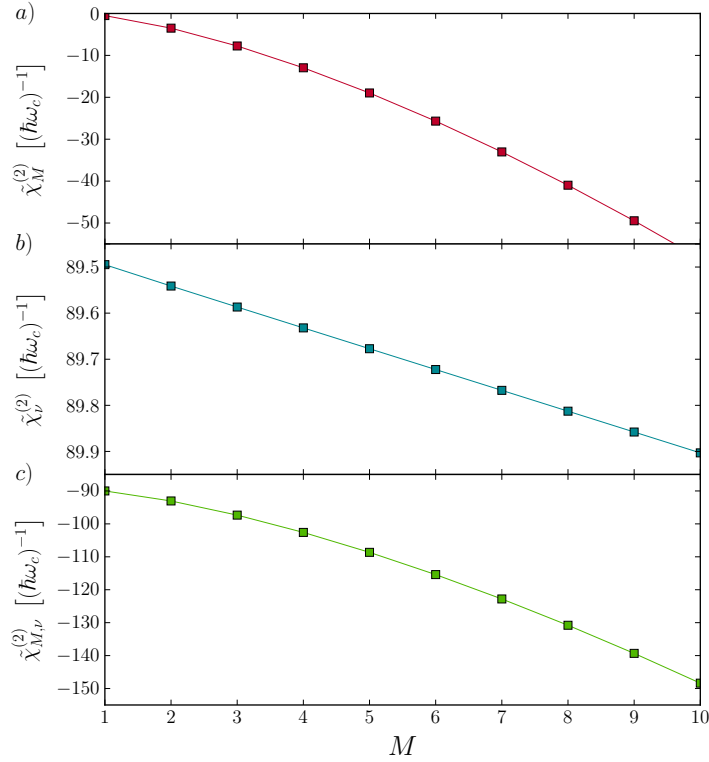
FIGURE 8.4: Dependence of the second-order contribution to the approximately diagonalized Hamiltonian $\hat{\mathcal{H}}_{\mathrm{D}}$ as a function of the Landau-level index M. The functions $\tilde{\chi}_M^{(2)}$, panel a), and $\tilde{\chi}_\nu^{(2)}$, panel b), are both evaluated at resonance and yield a negative contribution. The ultraviolet cutoff is chosen from Eq. (6.4) for $B = 5$ T. Panel c) illustrates the sum of both contributions.

However, the authors of Ref. [95] subtract all cutoff-depended terms of $\tilde{\chi}_{M,\nu}^{(2)}$ in a second step to achieve a ν-independent result. Then, the limit $\nu \to \infty$, as artificially required by the effective Dirac model, is trivially taken as a last step. Thus, one defines the regularized function

$$
\langle \hat{\tilde{\mathcal{H}}}^{(2)} \rangle_0^{M,\mathrm{reg}} = (\hat{a}^\dagger + \hat{a})\,\tilde{\chi}_M^{(2)}(\hbar\omega_0),
\tag{8.158}
$$

where only the ν-independent part of $\tilde{\chi}^{(2)}_{M,\nu}$, defined in Eq. (8.154), enters. This term is identical with the final result of Ref. [95] in the second-order approximation.

8.3.2 Fourth-order contribution

As the third order vanishes straight from the beginning, the discussion of the fourth order, Eq. (8.125), is continued. For the identification of the relevant contributions, identical arguments as discussed in Subsec. 8.2.7 are applied. Thus, the only relevant contributions for the value of g_c are quadratic in the bosonic operators and arise from the nested commutators which decompose into two distinct commutators of each two fermionic operators, Eq. (8.97). By careful examination, as shown in Sec. 2 of App. F, one finds

$$\langle \hat{\mathcal{H}}^{(4)}_{\mathrm{N}} \rangle_0 = (\hat{a}^\dagger + \hat{a})^2 \, \chi^{(4)}_{\mathrm{N},M,\nu}(\hbar\omega_0), \tag{8.159}$$

where $\chi^{(4)}_{\mathrm{N},M,\nu} = \chi^{(4)}_{\mathrm{N},M} + \chi^{(4)}_{\mathrm{N},\nu}$ decomposes into a ν-independent and -dependent part, $\chi^{(4)}_{\mathrm{N},M}$ and $\chi^{(4)}_{\mathrm{N},\nu}$, respectively. The latter is given by

$$\chi^{(4)}_{\mathrm{N},M}(\hbar\omega_0) = \frac{1}{2} \left[-K_{M+3}(\hbar\omega_0) + w^2_{+,M+2} \left(\mathcal{CD}_{M+3,M+2} + \mathcal{CD}_{M+3,-(M+2)} \right) \right]$$
$$\times \left[-J_{M+3}(\hbar\omega_0) + w^2_{+,M+2} \left(\mathcal{D}_{M+3,M+2} + \mathcal{D}_{M+3,-(M+2)} \right) \right], \tag{8.160}$$

where $\mathcal{CD}_{M,N}$ is defined in Eq. (8.103) and

$$K^{\nu-2}_{M+3}(\hbar\omega_0) = K^{\nu-2}(\hbar\omega_0) - K_{M+3}(\hbar\omega_0)$$
$$= \left[\frac{2 \times 2\,\hbar\omega_c\sqrt{o}\,\hbar\omega_0}{\hbar\omega_c\left[(2\,\hbar\omega_c\sqrt{o})^2 - (\hbar\omega_0)^2\right]} - \frac{1}{(\hbar\omega_c)^2} \log\left(\frac{2\,\omega_c\sqrt{o} - \omega_0}{2\,\omega_c\sqrt{o} + \omega_0} \right) \right]^{o=\nu-2}_{o=M+3} \tag{8.161}$$

corresponds to the integral approximation of the sum over $2\mathcal{CD}_{N+1,-N}$ according to Eq. (F.67). Likewise, $J^{\nu-2}_{M+3}$ denotes an integral representation of the sum over $2\mathcal{D}_{N+1,-N}$, which is identical to Eq. (8.108). The details of $\chi^{(4)}_{\mathrm{N},M}$ are found in Eq. (F.71). This function is positive for all values of M at resonance, as Fig. 8.5 a) shows. Further, the cutoff-dependent contribution reads

$$\chi^{(4)}_{\mathrm{N},\nu}(\hbar\omega_0) = \frac{1}{2} \left[K^{\nu-2}(\hbar\omega_0) + w^2_{+,\nu-1} \left(-\mathcal{CD}_{\nu,\nu-1} + \mathcal{CD}_{\nu,-(\nu-1)} \right) \right]$$
$$\times \left[J_{\nu-2}(\hbar\omega_0) + w^2_{+,\nu-1} \left(-\mathcal{D}_{\nu,\nu-1} + \mathcal{D}_{\nu,-(\nu-1)} \right) \right]$$
$$+ \frac{1}{2} \left[K^{\nu-2}(\hbar\omega_0) + w^2_{+,\nu-1} \left(-\mathcal{CD}_{\nu,\nu-1} + \mathcal{CD}_{\nu,-(\nu-1)} \right) \right]$$
$$\times \left[-J_{M+3}(\hbar\omega_0) + w^2_{+,M+2} \left(\mathcal{D}_{M+3,M+2} + \mathcal{D}_{M+3,-(M+2)} \right) \right]$$
$$+ \frac{1}{2} \left[-K_{M+3}(\hbar\omega_0) + w^2_{+,M+2} \left(\mathcal{CD}_{M+3,M+2} + \mathcal{CD}_{M+3,-(M+2)} \right) \right]$$
$$\times \left[J_{\nu-2}(\hbar\omega_0) + w^2_{+,\nu-1} \left(-\mathcal{D}_{\nu,\nu-1} + \mathcal{D}_{\nu,-(\nu-1)} \right) \right] \tag{8.162}$$

and its explicit form is given in Eq. (F.72). At resonance, $\chi^{(4)}_{\mathrm{N},\nu}$ yields a negative contribution for all values of M and ν which are compatible with the validity of this perturbative

approach in the sense of Eq. (8.31). Figure 8.5 b) illustrates $\chi_{N,\nu}^{(4)}$ as a function of M.

As $\mathcal{CD} \to 0$ in the static limit, also $\chi_{N,M}^{(4)}$ and $\chi_{N,M}^{(4)}$ vanish. Thus, there is no require-ment for a similar regularization as applied onto the second-order contribution (cf. Sub-sec. 8.3.1). However, also this contribution is examined within the cutoff-independent regularization approach used in Ref. [95]. To this end, one subtracts all ν-dependent terms, i.e. $\chi_{N,\nu}^{(4)}$, from $\chi_{N,M,\nu}^{(4)}$ when referring to this regularization method.

The comparison of $\chi_{M,\nu}^{(4)}$, illustrated in Fig. 8.3, with $\chi_{N,M,\nu}^{(4)}$, illustrated in Fig. 8.5, shows that the latter provides the dominant contribution to the fourth-order correction. Further-more, the cutoff-independent parts of the functions $\chi_{M,\nu}^{(4)}$ and $\chi_{N,M,\nu}^{(4)}$ yield both a positive contribution whereas the cutoff-independent second-order term $\tilde{\chi}_{M}^{(2)}$, shown in Fig. 8.4, is negative at resonance.
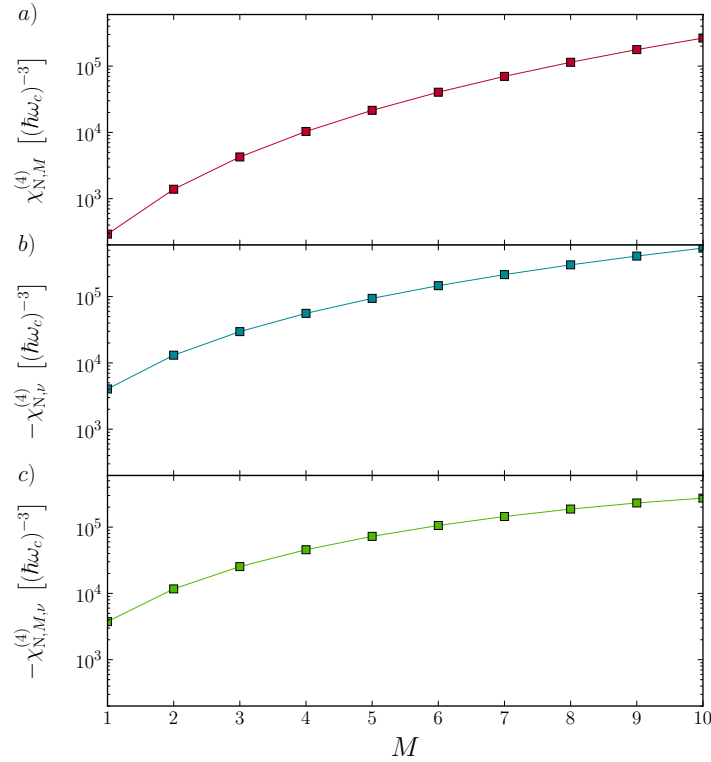
FIGURE 8.5: Dependence of the functions $\chi_{N,M}^{(4)}$, panel a), and $-\chi_{N,\nu}^{(4)}$, panel b), on the Landau-level index M at resonance. In panel b) the ultraviolet cutoff is chosen from Eq. (6.4) at $B = 5$ T. The ν-independent contribution, $\chi_{N,M}^{(4)}$, is positive for all values of M. By contrast, $\chi_{N,\nu}^{(4)}$ is negative on the depicted interval of M. The comparison with Figs. 8.3, 8.4 for identical parameters shows that $\chi_{N,M}^{(4)}$ and $\chi_{N,\nu}^{(4)}$ yields the dominant contribution to the fourth-order correction of the diagonalized Hamiltonian $\hat{\mathcal{H}}_{D}$. Panel c) shows the negative of the sum of both contributions, i.e. $-\chi_{N,M,\nu}^{(4)}$.

8.3.3 The generalized Dicke Hamiltonian

Before the derivation of the critical coupling is performed the final result for the effective Hamiltonian, Eq. (8.112), is summarized.

According to the previous discussion, one finds for Eq. (8.112) the expression

$$\hat{\tilde{\mathcal{H}}}^{\text{eff}} = \hat{\mathcal{H}}_{\text{cav}} + \hat{\mathcal{H}}_{\text{M}}^{\text{eff}} + \hat{\mathcal{H}}_{0,\text{N}} + g^2(\hat{a}^\dagger + \hat{a})^2 \tilde{\chi}_{M,\nu}^{(2)} + g^4(\hat{a}^\dagger + \hat{a})^2 \left[\chi_{M,\nu}^{(4)} + \chi_{\text{N},M,\nu}^{(4)} \right], \quad (8.163)$$

which provides an extension of the ansatz discussed in Ref. [95] from second to fourth order. The dynamically generated quadratic contributions in second-order approximation, $\tilde{\chi}_{M,\nu}^{(2)}(\hbar\omega_0)$, as well as the fourth-order contributions, $\chi_{M,\nu}^{(4)}(\hbar\omega_0)$ and $\chi_{\text{N},M,\nu}^{(4)}(\hbar\omega_0)$, vanish in the static limit, $\omega_0 \to 0$. Moreover, the cutoff-independent parts of the second- and fourth-order corrections are opposite in sign when resonance is imposed. By contrast, the dominant cutoff-dependent parts, $\tilde{\chi}_\nu^{(2)}$ and $\chi_{\text{N},\nu}^{(4)}$, are negative in both orders of approximation. This is illustrated by Fig. 8.6.

For the subsequent discussion of the critical behavior it is convenient to drop all terms which yield only a constant shift of the energies with respect to the bosonic mode. Thus, the term $\propto \epsilon_F$ in $\hat{\mathcal{H}}_{\text{M}}^{\text{eff}}$, Eq. (8.78), can be omitted during the following. Hence, in analogy to Ref. [95], one defines

$$\hat{\mathcal{H}}_{\text{M}} = \sum_{k=1}^{\mathcal{N}} \left[\frac{\hbar\Omega_M}{2}\tau_k^z + g\frac{(\hat{a}^\dagger + \hat{a})}{\sqrt{\mathcal{N}}} w_{+,M}(\tau_k^- + \tau_k^+) + g^2\frac{(\hat{a}^\dagger + \hat{a})^2}{\mathcal{N}} \left(\kappa_M^z \tau_k^z + \kappa_M \tau_k^0 \right) \right]. \quad (8.164)$$

Furthermore, the constant contribution $\hat{\mathcal{H}}_{0,\text{N}}$ can be omitted. Thus, one defines the generalized Dicke Hamiltonian for Landau-quantized graphene within rigid cutoff regularization as

$$\hat{\mathcal{H}}_{\text{GDH}} = \hat{\mathcal{H}}_{\text{cav}} + \hat{\mathcal{H}}_{\text{M}} + g^2(\hat{a}^\dagger + \hat{a})^2 \tilde{\chi}_{M,\nu}^{(2)} + g^4(\hat{a}^\dagger + \hat{a})^2 \tilde{\chi}_{M,\nu}^{(4)}, \quad (8.165)$$

where $\tilde{\chi}_{M,\nu}^{(4)} = \chi_{M,\nu}^{(4)} + \chi_{\text{N},M,\nu}^{(4)}$.

The cutoff-independent equivalent of the generalized Dicke Hamiltonian is then obtained in analogy to the second-order approximation of Ref. [95] by subtracting all ν-dependent terms from $\hat{\mathcal{H}}_{\text{GDH}}$. Thus, one finds

$$\hat{\mathcal{H}}_{\text{GDH}}^{\text{reg}} = \hat{\mathcal{H}}_{\text{cav}} + \hat{\mathcal{H}}_{\text{M}} + g^2(\hat{a}^\dagger + \hat{a})^2 \tilde{\chi}_M^{(2)} + g^4(\hat{a}^\dagger + \hat{a})^2 \tilde{\chi}_M^{(4)}. \quad (8.166)$$

Note that the symmetry properties of both Hamiltonians, $\hat{\mathcal{H}}_{\text{GDH}}$ and $\hat{\mathcal{H}}_{\text{GDH}}^{\text{reg}}$, are analogous to those of the original Dicke model (cf. Sec. 3.3.5). Though not explicitly proven during the following, one will expect the parity symmetry assigned with the commutation of the Hamiltonian with the parity operator, Eq. (3.91), to be broken if a superradiant phase transition is exhibited by the model. This can be deduced from the considerations in Sec. 4 of App. E.

During the following, the critical behavior of $\hat{\mathcal{H}}_{\text{GDH}}$ and $\hat{\mathcal{H}}_{\text{GDH}}^{\text{reg}}$ is analyzed and compared with the results from the path integral approach.
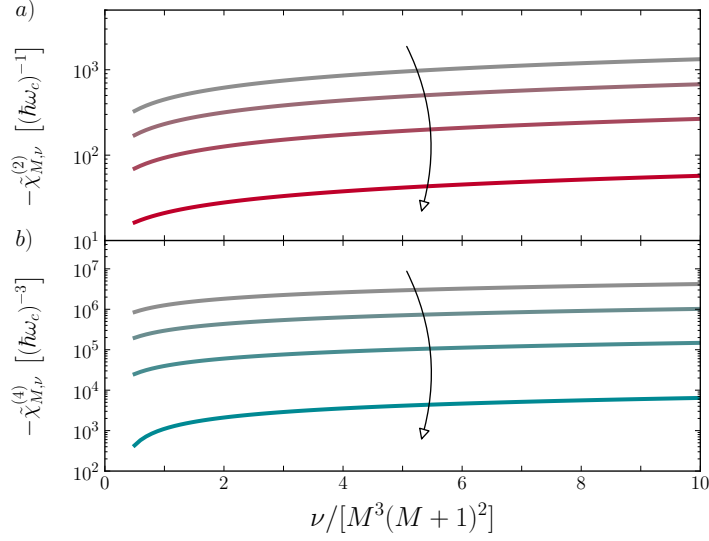
FIGURE 8.6: Dependence of the second- and fourth-order contribution to the generalized Dicke Hamiltonian as a function of the normalized cut-off $\nu/[M^3(M+1)^2]$. All data points shown for $\nu/[M^3(M+1)^2] > 1$ are in accordance with the validity range of this perturbative approach, Eq.(8.31). Panel a) shows the negative of the second-order contribution $\tilde{\chi}^{(2)}_{M,\nu}$, Eq. (8.153) for $M = 2, 4, 6, 8$. The arrows point along increasing M. Panel b) shows the negative of the fourth-order contribution $\tilde{\chi}^{(4)}_{M,\nu}$ composited from $\chi^{(4)}_{M,\nu}$, Eqs. (8.101, 8.102) and $\chi^{(4)}_{N,M,\nu}$, Eqs. (8.162, 8.162), for identical values of M.

8.4 Critical behavior of the generalized Dicke Hamiltonian

The analysis of the generalized Dicke Hamiltonian is performed within a path integral approach similar to the investigations of Wang and Hioe [155] on the original Dicke model. This approach was also used in Ref. [95] for the analysis of the corresponding cutoff-independent generalized Dicke Hamiltonian in second-order approximation. However, also the approach based on the Holstein-Primakoff transformation (cf. Sec. 3.3) of the collective spin operators would be suitable. Both approaches are expected to yield identical results.

Thus, one starts with the partition sum in the grand-canonical ensemble,

$$\mathcal{Z} = \text{Tr}\left[e^{-\beta(\hat{\tilde{\mathcal{H}}}^{\text{eff}} - \mu\hat{\mathcal{N}})}\right], \tag{8.167}$$

where $\hat{\mathcal{N}} = \sum_{N,k} \hat{c}^\dagger_{N,k}\hat{c}_{N,k}$ denotes the many-body number operator. By further inspection of the exponent, one finds for $\mu = \epsilon_{\text{F}}$

$$\hat{\tilde{\mathcal{H}}}^{\text{eff}} - \mu\hat{\mathcal{N}} = \hat{\mathcal{H}}_{\text{GDH}} + (\hat{\mathcal{H}}_{0,\text{N}} - \mu\hat{\mathcal{N}}'), \tag{8.168}$$

where $\hat{\mathcal{N}}' = \hat{\mathcal{N}} - \sum_k (n^-_{M,k} + n^-_{M+1,k})$. As the last term on the r.h.s. only shifts the energy of the system by a constant amount it can be omitted during the following. For the sake of brevity, the following discussion is formally referred to the cutoff-regularized generalized Dicke model. Thus, by omitting all cutoff-dependent terms in the respective equations and definition one easily obtains their cutoff-independent equivalent, Eq. (8.166), as considered in Ref. [95].

The partition sum is then evaluated either by the approach discussed in Ref. [155], keeping the spin-representation, or by a more generalized approach based on the fermionic representation of the Pauli matrices, Eq. (8.77), as shown in Refs. [95, 239, 242]. To keep the discussion as general as possible, the latter is chosen during the following.

Thus consider the normalized many-body partition sum of the grand-canonical ensemble according to Eq. (8.167) in path integral representation

$$\tilde{\mathcal{Z}} = \frac{\mathcal{Z}}{\mathcal{Z}_0} = \frac{\oint \mathcal{D}[\alpha] \oint \mathcal{D}[\{\boldsymbol{\rho}_k\}] e^{-\mathcal{S}_{\mathrm{E}}[\alpha^*,\alpha;\{\boldsymbol{\rho}_k^\dagger,\boldsymbol{\rho}_k\}]}}{\oint \mathcal{D}[\alpha] \oint \mathcal{D}[\{\boldsymbol{\rho}_k\}] e^{-\mathcal{S}_{\mathrm{E}}^0[\alpha^*,\alpha;\{\boldsymbol{\rho}_k^\dagger,\boldsymbol{\rho}_k\}]}}, \tag{8.169}$$

where $\mathcal{S}_E$ and $\mathcal{S}_E^0$ denote the Euclidean action of the interacting and noninteracting system, respectively. Furthermore, $\alpha^*, \alpha \in \mathbb{C}$ denotes the complex field of the bosonic mode. Likewise, $\boldsymbol{\rho}_k^\dagger$ and $\boldsymbol{\rho}_k$ describes the vector representation of the fermionic subsystem in terms of Grassmann numbers or fields (cf. Sec. 2 in App. E). As any contribution yielding only a constant energy shift is omitted, $\boldsymbol{\rho}_k^\dagger$ and $\boldsymbol{\rho}_k$ refer only to the Landau-level doublet M and $M+1$ and thus is given by

$$\boldsymbol{\rho}_k^\dagger = \begin{pmatrix} c^\dagger_{M+1,k} & c^\dagger_{M,k} \end{pmatrix}, \quad \boldsymbol{\rho}_k = \begin{pmatrix} c_{M+1,k} & c_{M,k} \end{pmatrix}^T, \tag{8.170}$$

where each component is a Grassmann number. This is analogous to the definition (7.2). The integration measures in Eq. (8.169) are given by Eq. (D.65) in Sec. 3 of App. D, where also further details on the evaluation of many-body partitions sums are found. The Euclidean action in Eq. (8.169) can be decomposed according to

$$\begin{aligned} \mathcal{S}[\alpha^*,\alpha;\{\boldsymbol{\rho}_k^\dagger,\boldsymbol{\rho}_k\}] = \int_0^\beta \mathrm{d}\tau \, \Bigg[& \alpha^*(\tau)\partial_\tau\alpha(\tau) + \sum_{k=1}^{\mathcal{N}} \boldsymbol{\rho}_k^\dagger(\tau)\partial_\tau\boldsymbol{\rho}_k(\tau) \\ & + \mathcal{H}_{\mathrm{GDH}}[\alpha^*(\tau),\alpha(\tau);\{\boldsymbol{\rho}_k^\dagger(\tau),\boldsymbol{\rho}_k(\tau)\}] \Bigg] \\ = & \, \mathcal{S}_+[\alpha^*,\alpha] + \mathcal{S}_{\mathrm{mix}}[\alpha^*,\alpha;\{\boldsymbol{\rho}_k^\dagger,\boldsymbol{\rho}_k\}], \end{aligned} \tag{8.171}$$

where the index E is omitted for brevity. The first contribution, $\mathcal{S}_+$ only contains bosonic degrees of freedom and is given by

$$\mathcal{S}_+[\alpha^*,\alpha] = \int_0^\beta \mathrm{d}\tau \, \Big[\alpha^*(\tau) \, (\partial_\tau + \hbar\omega_0) \, \alpha(\tau) + [\alpha^*(\tau) + \alpha^*(\tau)]^2 \, \mathcal{X}(g) \Big], \tag{8.172}$$

where $\mathcal{X}(g) = g^2 \tilde{\chi}^{(2)}_{M,\nu} + g^4 \tilde{\chi}^{(2)}_{M,\nu}$ when evaluating the fourth order of approximation. For

the evaluation of the second order, one puts $\mathcal{X}(g) = g^2 \tilde{\chi}_{M,\nu}^{(2)}$. The mixed contribution to the Euclidean action contains fermionic and bosonic contributions due to the light-matter interaction term and reads

$$\mathcal{S}_{\text{mix}}[\alpha^*, \alpha; \{\boldsymbol{\rho}_k{}^\dagger, \boldsymbol{\rho}_k\}] = \sum_k \int_0^\beta \mathrm{d}\tau\, \boldsymbol{\rho}_k^\dagger(\tau)\, [\mathbb{1} - \mathbb{G}_0 \mathbb{M}[\alpha^*, \alpha]]\, \boldsymbol{\rho}_k(\tau), \qquad (8.173)$$

where $-\mathbb{G}_0^{-1} = \partial_\tau \sigma^0 + \frac{\Omega_0}{2}\sigma^z$ denotes the inverse of the Green's function of the noninteracting two-level subsystem. The k-independent matrix is then given by

$$\mathbb{M}[\alpha^*, \alpha] = \left[\frac{g}{\sqrt{\mathcal{N}}} w_{+,M}\, [\alpha^*(\tau) + \alpha(\tau)]\, \sigma^x + \frac{g^2}{\mathcal{N}}\, [\alpha^*(\tau) + \alpha(\tau)]^2 \left(\kappa_M \sigma^0 + \kappa_M^z \sigma^z \right) \right]. \qquad (8.174)$$

By rescaling the complex fields $\alpha^*(\tau) \mapsto \sqrt{\mathcal{N}}\alpha^*(\tau)$, $\alpha(\tau) \mapsto \sqrt{\mathcal{N}}\alpha(\tau)$ and integrating over the fermionic degree of freedom one finds for the partition sum

$$\tilde{\mathcal{Z}} = (\mathcal{Z}_0^+)^{-1} \mathcal{N} \oint \mathcal{D}[\alpha] e^{-\mathcal{N}\Phi[\alpha^*, \alpha]}, \quad \Phi[\alpha^*, \alpha] = \mathcal{S}_+[\alpha^*, \alpha] - \log\left[\det\left[\mathbb{1} - \mathbb{G}_0\mathbb{M}[\alpha^*, \alpha]\right]\right], \qquad (8.175)$$

where the phase Φ can be regarded as an effective action for the bosonic mode. The partition sum $\mathcal{Z}_0^+$ of the free cavity mode is introduced in Chap. 7 and explicitly defined in Eq. (7.12). Similar as discussed in Chap. 7, one evaluates the remaining integral in Eq. (8.175) in the thermodynamic limit by means of the method of steepest descent. This is justified as the dominant contribution to the partition sum in this limit arise from the extrema of the phase functional. One can prove [239] that the corresponding field configurations $\alpha_0^*(\tau) = \alpha_0$, $\alpha_0^*(\tau) = \alpha_0$ are static, i.e. independent on the Euclidean time, and defined by

$$\frac{\delta}{\delta\alpha(\tau')} \Phi[\alpha^*(\tau), \alpha(\tau)]\bigg|_{\alpha_0^*, \alpha_0} = 0, \quad \frac{\delta}{\delta\alpha^*(\tau')} \Phi[\alpha^*(\tau), \alpha(\tau)]\bigg|_{\alpha_0^*, \alpha_0} = 0. \qquad (8.176)$$

From inspection of the phase Φ further follows $\alpha_0^* = \alpha_0$ such that the integration over the imaginary part in Eq. (8.175) can also been carried out exactly in stationary phase approximation. Thus one finds in analogy to the discussion in Chap. 7 and the considerations in Ref. [95]

$$\bar{\mathcal{Z}}_{\text{SPA}} = (\mathcal{Z}_0^+)^{-1} \sqrt{\frac{2}{\beta\hbar\omega_0 |\partial_\alpha^2 \Phi(\alpha, \alpha)|_{\alpha_0}|}} e^{-\mathcal{N}\Phi(\alpha_0, \alpha_0)}, \qquad (8.177)$$

where $\partial_\alpha^2 \Phi(\alpha, \alpha)|_{\alpha_0} > 0$. When accounting only for the relevant real-valued static fields $\alpha = \alpha^*$ the phase function is easily evaluated:
To this end, evaluate the fermionic grand-canonical potential encoded in $\log\det(\mathbb{1} - \mathbb{G}_0\mathbb{M})$ as discussed in Sec. 3 of App. D. Thus, by diagonalizing the matrix given in the argument of the determinant for $\omega_n^- = 0$ one finds,

$$\epsilon_\pm(\alpha) = 4g^2\alpha^2\kappa_M \pm \sqrt{4g^2\alpha^2 + (\hbar\Omega_M/4 + 2g^2\alpha^2\kappa_M^z)} \qquad (8.178)$$

which then yields for $\log \det(\mathbb{1} - \mathbb{G}_0 \mathbb{M})$ according to Eqs. (D.73, D.76)

$$-\beta \Omega_-(\alpha) = \log\left[\det\left[\mathbb{1} - \mathbb{G}_0 \mathbb{M}\left[\alpha^*, \alpha\right]\right]\right] = \sum_{i=\pm} \log\left[1 + e^{-\beta \epsilon_i(\alpha)}\right]. \tag{8.179}$$

Under usage of the relation

$$\log\left[1 + e^a e^b\right] + \log\left[1 + e^a e^{-b}\right] = a + \log 2 + \log\left[\cosh a + \cosh b\right] \tag{8.180}$$

the fermionic grand-canonical potential is further simplified yielding

$$\begin{aligned}
-\beta \Omega_-(\alpha) = -\beta 4 g^2 \alpha^2 \kappa_M + \log 2 + \log\bigg[&\cosh\left(\beta 4 g^2 \alpha^2\right) \\
&+ \cosh\left(\beta\sqrt{4 g^2 \alpha^2 + (\hbar \Omega_M/4 + 2 g^2 \alpha^2 \kappa_M^z)}\right)\bigg]
\end{aligned} \tag{8.181}$$

in agreement with Ref. [95]. Dropping the constant term one finally finds for the phase function

$$\begin{aligned}
\Phi(\alpha, \alpha) = \beta\left[\hbar \omega_0 + 4 \mathcal{X}(g) + 4 g^2 \kappa_M\right]\alpha^2 - \log\bigg[&\cosh\left(\beta 4 g^2 \alpha^2\right) \\
&+ \cosh\left(\beta\sqrt{4 g^2 \alpha^2 + (\hbar \Omega_M/4 + 2 g^2 \alpha^2 \kappa_M^z)}\right)\bigg]
\end{aligned} \tag{8.182}$$

in accordance with Ref. [95]. When evaluating $\partial_\alpha \Phi(\alpha, \alpha)|_{\alpha_0} = 0$ one finds always the trivial-solution $\alpha_0 = 0$ similar as discussed for the original Dicke model (cf. Sec. 3.3). This solution corresponds to the normal phase of the system. The ground-state properties are then determined by $\alpha_0 = 0$ which corresponds to the ground-state of the noninteracting cavity as α_0^2 is associated with the photonic cavity occupation. However, if there exists an additional solution $\alpha_0 \neq 0$ which yields a global minimum of the effective action Φ the superradiant phase will be indicated and α_0^2 corresponds then to the photonic occupation of the cavity. In addition, the trivial solution does not correspond to a minimum of the effective action anymore which yields a change of the sign in second derivative of the phase function at $\alpha_0 = 0$ (cf. Fig. (8.11). Thus, by consideration of

$$\frac{\partial^2}{\partial^2 \alpha}\Phi(\alpha, \alpha)\bigg|_{\alpha_0=0} = 0 \qquad \Leftrightarrow \qquad g = g_c \tag{8.183}$$

one eventually finds a critical point g_c. In second-order approximation, i.e. $\mathcal{X}(g) = g^2 \tilde{\chi}_{M,\nu}^{(2)}$ one obtains

$$g_{c,M,\nu}^{(2)} = \frac{\hbar \Omega_M}{2}\sqrt{-\frac{1}{\rho_{M,\nu}}}. \tag{8.184}$$

in analogy to Ref. [95]. The function $\rho_{M,\nu}$ also appears in fourth-order approximation, i.e. $\mathcal{X}(g) = g^2 \tilde{\chi}_{M,\nu}^{(2)} + g^4 \tilde{\chi}_{M,\nu}^{(4)}$,

$$g_{c,M,\nu}^{(4)} = \sqrt{-\frac{\rho_{M,\nu} + \sqrt{-\tilde{\chi}_{M,\nu}^{(4)} \cdot (\hbar\Omega_M)^3 + \rho_{M,\nu}^2}}{2\tilde{\chi}_{M,\nu}^{(4)}\hbar\Omega_M}}. \tag{8.185}$$

and is given by

$$\rho_{M,\nu} = -1 + \left(\tilde{\chi}_{M,\nu}^{(2)} + \kappa_M - \kappa_M^z\right)\hbar\Omega_M. \tag{8.186}$$

In order to actually describe an actual critical point, $g_{c,M,\nu}^{(n)}$ needs to be real-valued. Relating this requirement of $g_c \in \mathbb{R}$ to the Holstein-Primakoff approach discussed in Sec. 3.3 on the example of the original Dicke model precisely corresponds to a Hessian $\propto (g_c^2 - g^2)$. A complex-valued critical coupling would transform Eq. (3.65) into an expression $\propto (g_c^2 + g^2)$ which could never be satisfied. Thus, $g_{c,M,\nu}^{(n)} \in \mathbb{R}$ is the first necessary condition for the model to describe criticality. Whether real-valued critical point in either order of approximation can be obtained for suitable values of M and ν ultimately depends on the details of the entering contributions.

Thus, assuming $g_{c,M,\nu}^{(n)} \in \mathbb{R}$ for the moment, the second necessary condition for the model holding an appropriate and robust prediction of the critical behavior is the satisfaction of the validity range of the SW approach according to Eq. (8.30). These two requirements address rather theoretical aspects providing an estimation of the critical behavior of the respective model approximated by the SW approach up to n^{th} order. However, when asking weather the described system is indeed able to approach criticality in equilibrium and under realistic conditions one also has to account for the actual coupling g_{r} determined by the microscopic properties of the hybrid system. In particular, one expects a superradiant phase transition to occur, when the intrinsic coupling exceeds the predicted value of the critical coupling for certain parameters. As this is in turn only provided when also g_{r} lies within the validity range of the SW ansatz, one can summarize

$$g_{c,M,\nu}^{(n)} < g_{\text{r}} < \Delta \stackrel{(8.30)}{=} |\hbar\omega_0 - \hbar\Omega_{M+1}|, \tag{8.187}$$

which has to be satisfied in order to describe realistic critical behavior within the SW method.

Thus, the following investigates the validity of these conditions for cutoff-independent and -dependent regularization. During the proceeding resonance and $M > 0$ are imposed. Furthermore, one assumes $\epsilon_{\text{r}} = 1$, such that

$$g_{\text{r}} \stackrel{(8.28)}{=} \hbar\omega_c\sqrt{\frac{\alpha}{2\pi}} \approx 0.0341\,\hbar\omega_c. \tag{8.188}$$

The generalization to $\epsilon_{\text{r}} \neq 1$ is found in Ref. [95] and, anyways, easily obtained $\epsilon_{\text{r}} \neq 1$ shifts only the value of the actual coupling g_{r} but leaves the results of the SW approach unaffected.

8.4.1 Cutoff-independent regularization

Even though the reference for the critical coupling obtained within cutoff-independent regularization of the path integral approach exceeds the validity range of the perturbative Schrieffer-Wolff transformation one may, nevertheless, evaluate the latter. As the second-order of the cutoff-independent regularized generalized Dicke model is examined in Ref. [95] in great detail, the discussion shall be abbreviated and restricted to a graphical analysis. Thus, Fig. 8.7 shows the equivalent of the in Ref. [95] considered second-order approximation of the generalized Dicke model for Landau-quantized graphene. In this order of approximation, the requirement of $g_{c,M,\nu}^{(2)} \in \mathbb{R}$ is satisfied. However, the critical point predicted by Eq. (8.184) lies at least one order of magnitude beyond the validity range of the underlying approximation. Thus, no robust prediction can be drawn from this result which is in agreement with the conclusion of Ref. [95].

Similarly, also the cutoff-independent result $g_{c,M}$ obtained from the path integral approach, Eq. (7.38), exceeds the validity range of the SW approach as Fig. 8.7 demonstrates. Furthermore, g_r/Δ is also shown in Fig. 8.7 for $\epsilon_r = 1$. Any value of the relative permittivity different from 1 would only shift this reference but leaves the result of the SW approach unaffected.

It is important to emphasize that from $g_{c,M}^{(2)}/\Delta > 1$ one can only conclude that the predicted critical point lies beyond the validity of the perturbative approach on which the evaluation is based on. In this case, the results cannot be regarded as robust. Therefore, from this result one is not able to estimate the critical behavior of the original model as a possible critical point might actually be found in a parameter range beyond the validity of the SW ansatz.

To proceed the discussion, the fourth order of approximation is evaluated.

However, it is easy to see that not even the first necessary condition of a real-valued $g_{c,M}^{(4)}$ is satisfied. This is seen from inspection of the argument of the innermost square root in the definition (8.185). As $\tilde{\chi}_M^{(4)} > 0$ and at least three orders of magnitude larger than $\rho_M^2 > 0$ (cf. Figs. 8.3 a), 8.4 a) and 8.5 a)), the argument of the innermost square root in (8.185) yields a negative value as illustrated by Fig. 8.8. Thus, no real-valued $g_{c,M}^{(4)}$ is found within a valid parameter range. Again, this result disallows the conclusion of the absence of criticality in the underlying model. The SW method is a perturbative approach which, even when the validity range is handled with great care, is not necessarily yielding a convergent result in many-body considerations.

Anyways, as the cutoff-dependent regularization showed convincing agreement of the path integral result with the tight-binding simulation, one evaluates the SW approach within cutoff regularization during the following.

8.4.2 Rigid cutoff regularization

Now the results for the critical coupling in second- and fourth-order approximation are evaluated on the basis of the cutoff-regularized functions $\tilde{\chi}_{M,\nu}^{(n)}$. As these functions are dominated by the negative contribution arising from the cutoff a real-valued second-order result $g_{c,M,\nu}^{(2)}$ (cf. Fig. 8.4 c)) is ensured. This holds also for the fourth order and it is roughly seen from the following:

FIGURE 8.7: Comparison of the cutoff-independent results for the critical coupling with the actual coupling g_r and the validity range of the SW, approach according to Eq. (8.30), at resonance. The shown data points are normalized by the spectral gap Δ, Eq. (8.28), which estimates the validity of the SW ansatz according to Ref. [95]. The actual coupling g_r, (grey diamonds), obtained from the microscopic properties of the system is compatible with the validity range of the SW ansatz for $M \leq 2$. Note that $\epsilon_r \neq 1$ would only shift the data points to lower values. However, both cutoff-independent values for the critical coupling exceed the validity range of the SW approach and g_r. Thereby, the second-order approximation $g_{c,M}^{(2)}$, (blue squares), is at least one order of magnitude larger than g_r and far beyond the validity range. The path integral result $g_{c,M}/\Delta > 1$, (red triangles), is also not compatible with the latter.
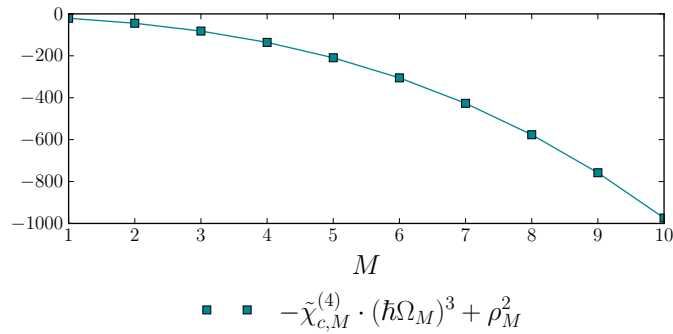
FIGURE 8.8: Argument of the innermost square root of the fourth-order result for the critical coupling, Eq. (8.185), in cutoff-independent regularization. The data points are shown for the resonant case.

Inspection of the functions $\tilde{\chi}_{M,\nu}^{(4)}$ shows, that the dominant contribution arises from the cutoff-dependent terms (cf. Figs. 8.3 c), 8.5 c)). As the result for $\tilde{\chi}_{M,\nu}^{(4)}$ is negative, the argument of the innermost square root in $g_{c,M,\nu}^{(4)}$, Eq. (8.185), is positive and thus in turn the innermost square root is real-valued and $\geq |\rho_{M,\nu}|$. This yields a positive numerator in Eq. (8.185) such that the argument of the outermost square root is positive and thus

a real-valued prediction of the critical coupling is expected also in fourth-order approximation.

The precise value of the second- and fourth-order results however depend on the choice of parameters. As $\tilde{\chi}_{M,\nu}^{(n)}$, $n = 2, 4$, are rather complicated functions of M and ν a graphical analysis of the results for the critcal coupling at resonance should be sufficient for a first insight.
Thus, Fig. 8.9 b) shows the second- and fourth-order result for the critical coupling obtained within the SW approach as a function of M. The cutoff is obtained from Eq. (6.4) for $B = 5$ T. For both orders of approximation the depicted data points are compatible with the validity range of the SW approach when $M \leq 3$ for this particular choice of the magnetic field. The comparison with the path integral result $g_{c,\nu}$, Eq. (7.37), demonstrates good agreement with $g_{c,M,\nu}^{(2)}$ even though the latter is slightly underestimating the former. This is shown in Fig. 8.9 a). In fourth order the deviations of the SW result with the path integral reference $g_{c,\nu}$ increase. In particular, the critical point is clearly underestimated in this order of approximation as Fig. 8.9 b) shows. This picks up the discussion about the convergence of the SW perturbation series outlined in Sec. 8.2. However, as the second-order yields convincing agreement, truncation of the perturbative series expansion of the effective Hamiltonian after second order should be sufficient for the following.

Figure 8.10 complements the evaluation of the second- and fourth-order results by showing the dependence of the corresponding critical couplings on the cutoff as a function of the magnetic field. The Fermi level is therefore chosen above $M = 1$. One finds again good agreement of the second-order SW result and the path integral approach. Similarly, the fourth order underestimates the critical coupling obtained within the path integral approach. For this specific choice of M critical behavior is predicted within both analytic approaches when $B \lesssim 7$ T in accordance with the phase diagram obtained for the path integral result, Fig. 7.1. The choice of ϵ_F close to the Dirac point is reasonable, as $g_r > g_{c,\bar{M},\nu}^{(2)}$ will be satisfied for $\bar{M} > M$ at fixed ν if $g_r > g_{c,M,\nu}^{(2)}$. This follows from $g_{c,M,\nu}^{(2)}$ being, similar as $g_{c,\nu}$, Eq. (7.37), a monotonous decreasing function of M at fixed ν. However, for $\bar{M} + 1 \gtrsim \nu^{1/5}$ one leaves the validity range of the SW ansatz.
Thus, restricting the following discussion onto the second-order of approximation, one finds the solutions to Eq. (8.176) in the thermodynamic limit as

$$\frac{\alpha_0^2}{\mathcal{N}} = \begin{cases} 0 & \text{for } g < g_{c,M,\nu}^{(2)}, \\ -\frac{1+\hbar\Omega_M\kappa_M^z}{8g^2(\kappa_M^z)^2} + \tilde{\delta}_{M,\nu}\frac{4g^2(\tilde{\chi}_{M,\nu}^{(2)}+\kappa_M)+\hbar\omega_0}{8g^2(\kappa_M^z)^2}\sqrt{1+2\kappa_M^z\hbar\Omega_M}, & \text{for } g > g_{c,M,\nu}^{(2)}, \end{cases} \tag{8.189}$$

where

$$\tilde{\delta}_{M,\nu} = \left[16g^4\left[(\tilde{\chi}_{M,\nu}^{(2)} + \kappa)^2 - (\kappa_M^z)^2\right] + 8g^2(\tilde{\chi}_{M,\nu}^{(2)} + \kappa)\hbar\omega_0 + (\hbar\omega_0)^2\right]^{-\frac{1}{2}}. \tag{8.190}$$

These results precisely coincide with the location of the minima of $\Phi(\alpha, \alpha)$ as Fig. 8.11 shows for $M = 1$ and ν chosen according to Eq. (6.4) at $B = 5$ T. The cavity occupation as function of the coupling is depicted in Fig. 8.12 at resonance. Thereby, panel a) shows the cavity occupation for $M = 1$ and various cutoffs according to Eq. (6.4) and $B = 1$, 2
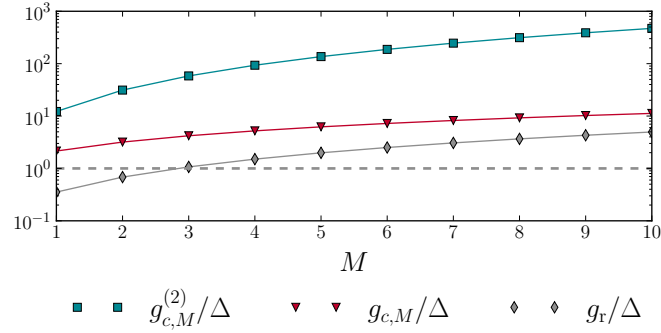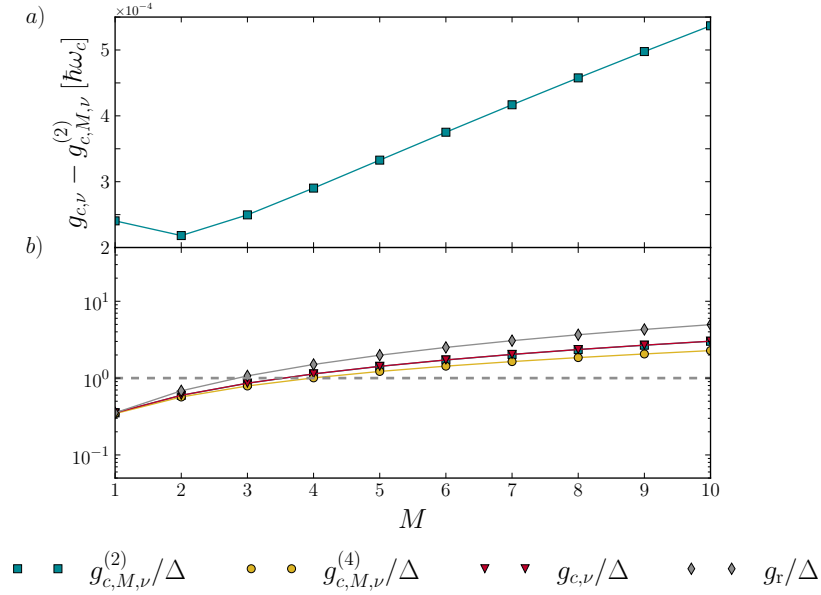
FIGURE 8.9: Comparison of the cutoff-dependent results for the critical coupling with g_r and the validity range of the SW approach, Eq. (8.30), at resonance and as a function M. The cutoff ν was chosen from Eq. (6.4) at $B = 5$ T. Panel a) shows that the second-order result $g_{c,M,\nu}^{(2)}$ slightly underestimates the path integral prediction $g_{c,\nu}$. Panel b) depicts the nth-order result $g_{c,M,\nu}^{(n)}$, ($n = 2$: blue squares, $n = 4$: yellow dots), in comparison with $g_{c,\nu}$, (red triangles), and the actual coupling g_r, (grey diamonds), normalized by the spectral gap Δ, Eq. (8.28). The fourth-order result, $g_{c,M,\nu}^{(4)}$, clearly underestimates the path integral prediction $g_{c,\nu}$. The actual coupling of the system, g_r, exceeds both predictions for critical couplings in the depicted range of M. Further, $g_{c,M,\nu}^{(2)}$ and $g_{c,\nu}$ are compatible with the validity range of the former for $M \leq 3$.

and 3 T. The qualitative scaling behavior with varying ν is thereby identical to one obtained for the cutoff-regularized path integral result (cf. 7.6). However, the comparison shows deviations close to the critical point and in the dependence on g. According to Eq. (8.189), the photon occupation scales with the squared coupling as it is also seen from Fig. 8.12 a). However, the path integral approach shows a rather linear scaling after a steep increase close to the critical point.

The deviations in the scaling of the photon occupation with rising Fermi level are however crucial. As Fig. 8.12 b) illustrates, the value of the photon occupation obtained from the generalized Dicke Hamiltonian decreases for a rising Fermi level. This contradicts the behavior found from the identically regularized path integral approach, shown in Fig. 7.7.

Regardless of these deviations one may though consider quantum fluctuations. As a final proof of the critical behavior one considers the excitation gap of quantum fluctuations above the ground state (cf. Subsec. 3.3.4). To hold the discussion simple, the quantum
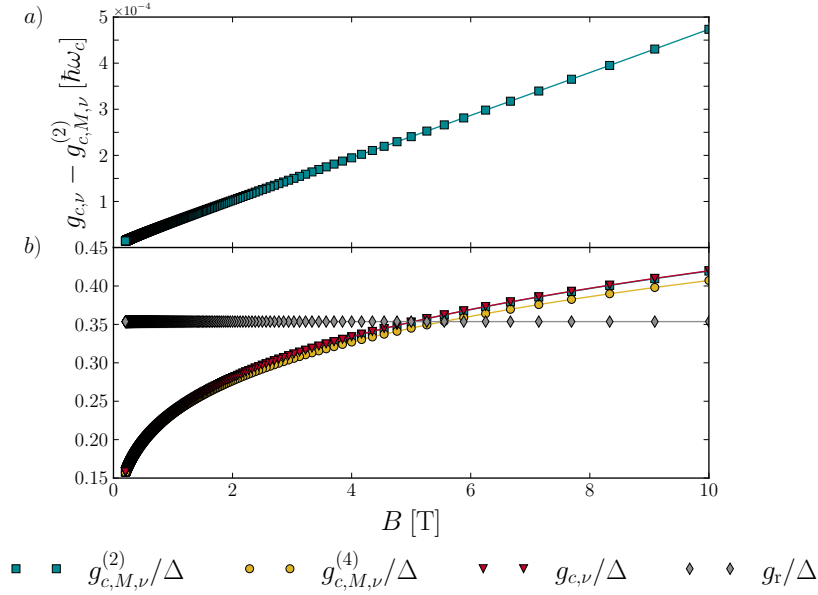
FIGURE 8.10: Comparison of the cutoff-dependent results for the critical coupling with g_r and the validity range of the SW approach, Eq. (8.30), at resonance. The data points are shown as a function ν or B according to Eq. (6.4), respectively. The Fermi level lies between $M = 1$ and $M + 1 = 2$. Panel a) again shows the deviation of the second-order result from the path integral reference $g_{c,\nu}$ as a function of the field. In particular, $g_{c,M,\nu}^{(2)}$ slightly underestimates $g_{c,\nu}$. Panel b) depicts the nth-order result $g_{c,M,\nu}^{(n)}$, ($n = 2$: blue squares, $n = 4$: yellow dots), in comparison with $g_{c,\nu}$, (red triangles), and the actual coupling g_r, (grey diamonds), normalized by the spectral gap Δ, Eq. (8.28). For the chosen Fermi level, both approaches yield a critical coupling $< g_r$ for fields up to ≈ 5 T. The fourth-order result, $g_{c,M,\nu}^{(4)}$ which clearly underestimates $g_{c,\nu}$ similar as seen in Fig. 8.9 b).

fluctuations are considered in the normal phase, $\alpha_0 = 0$, only. Thus, one expands the phase functional $\Phi[\alpha^*, \alpha]$ in second order around the real-valued static extreme point $\alpha_0 = 0$ in accordance with Refs. [95, 242]. It is convenient to apply the following identity

$$\log\left[\det\left[\mathbb{1} - \mathbb{G}_0\mathbb{M}[\alpha^*, \alpha]\right]\right] = \log\left[\det\left[-\mathbb{G}_0^{-1}\right]\right] + \text{Tr}\left[\log\left[\mathbb{1} - \mathbb{G}_0\mathbb{M}[\alpha^*, \alpha]\right]\right]$$

$$= \log\left[\det\left[-\mathbb{G}_0^{-1}\right]\right] - \sum_{n=1}^{\infty} \frac{\text{Tr}\left[(\mathbb{G}_0\mathbb{M}[\alpha^*, \alpha])^n\right]}{n}, \quad (8.191)$$

where only terms which are quadratic in the bosonic fields contribute to the Gaussian expansion of the phase functional around its extreme point $\alpha_0 = 0$. Thus, one finds the quadratic approximation of the Euclidean action, Eq. (8.171), as

$$\mathcal{S}_G[\alpha^*, \alpha; \{\boldsymbol{\rho}_k^\dagger, \boldsymbol{\rho}_k\}] = \mathcal{S}_+[\alpha^*, \alpha] - \log\left[\det\left[-\mathbb{G}_0^{-1}\right]\right] + \text{Tr}\left[\mathbb{G}_0\mathbb{B}\right] + \frac{1}{2}\text{Tr}\left[\mathbb{G}_0\mathbb{A}\mathbb{G}_0\mathbb{A}\right], \quad (8.192)$$

in analogy to Ref. [95]. The fields, $\alpha^*(\tau)$ and $\alpha(\tau)$, are now associated with small bosonic
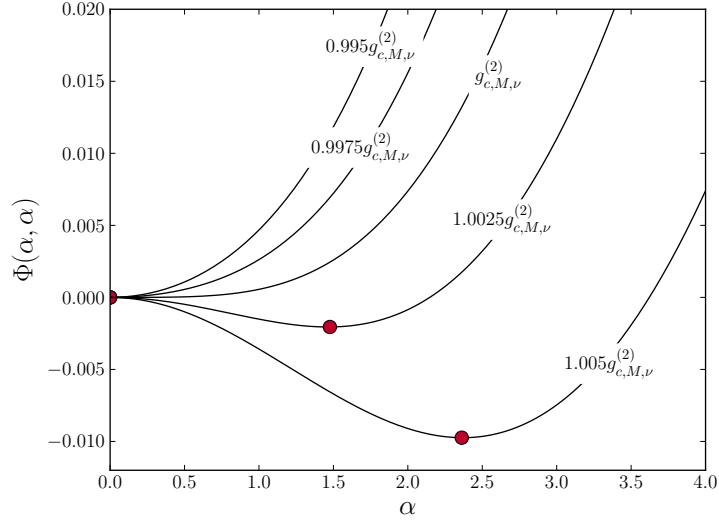
FIGURE 8.11: Illustration of the phase function in second-order approximation within cutoff regularization for various coupling strength in the thermodynamic limit for $B = 5$ T and $M = 1$. The red dots mark the position of the minima in accordance with Eq. (8.189). The behavior of the phase function is typical for second-order phase transitions.

fluctuations above the stationary minimum of the phase function in the normal phase. The bosonic action $\mathcal{S}_+$ is found in Eq. (8.172) and

$$\mathbb{A}[\alpha^*, \alpha] = \frac{g}{\sqrt{\mathcal{N}}} w_{+,M} \left[\alpha^*(\tau) + \alpha(\tau) \right] \sigma^x, \tag{8.193}$$

$$\mathbb{B}[\alpha^*, \alpha] = \frac{g^2}{\mathcal{N}} \left[\alpha^*(\tau) + \alpha(\tau) \right]^2 (\kappa_M \sigma^0 + \kappa_M^z \sigma^z), \tag{8.194}$$

in agreement with Ref. [95]. The trace appearing in the Gaussian approximation of the action, $\mathcal{S}_{\mathrm{G}}$, is carried out in the basis [241]

$$\mathrm{Tr}\left[O(\tau) \right] = \frac{1}{\beta} \sum_{\omega_n^-} \int_0^\beta \mathrm{d}\tau e^{i\omega_n^- \tau} \left[\sum_i O_{i,i}(\tau) \right] e^{-i\omega_n^- \tau}, \tag{8.195}$$

where the innermost sum refers to the trace over the products of Pauli matrices as resulting from the corresponding expressions. The outermost sum over fermionic Matsubara frequencies, $\omega_n^- = (2n+1)\pi/\beta$ for $n \in \mathbb{Z}$, is evaluated in a last step using residue calculus as discussed in Sec. 3 of App. E.

By defining the Fourier transformation of the bosonic fluctuations

$$\alpha^*(\tau) = \frac{1}{\sqrt{\beta}} \sum_{\omega_n^+} \tilde{\alpha}_n^* e^{i\omega_n^+ \tau}, \quad \alpha(\tau) = \frac{1}{\sqrt{\beta}} \sum_{\omega_n^+} \tilde{\alpha}_n e^{-i\omega_n^+ \tau}, \tag{8.196}$$
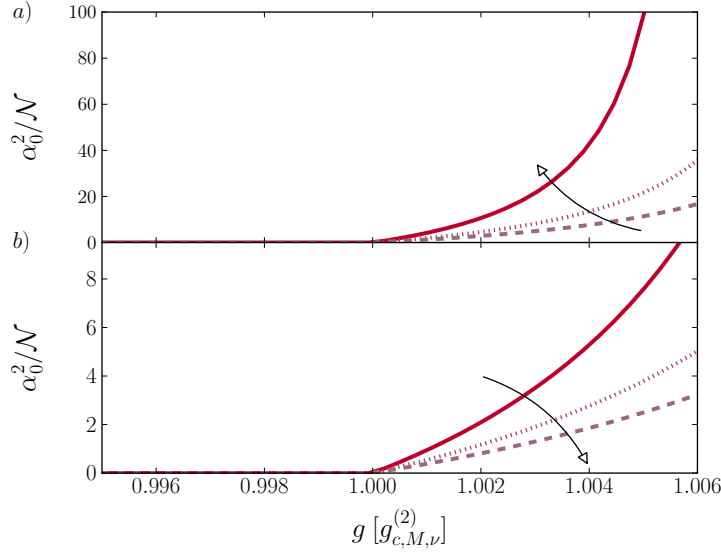
FIGURE 8.12: Photon occupation in the thermodynamic limit for various cutoffs, a), and fillings, b). In panel a) the cutoffs were chosen from Eq. (6.4) for $B = 1$ T (solid), 2 T (dotted) and 3 T (dashed) at resonance. In each case, the system is filled up to Landau level $M = 1$. Panel b) shows the photon occupation for $B = 5$ T and $M = 2$ (solid), $M = 3$ (dotted) and $M = 4$ (dashed). The arrows mark the direction of rising cutoff, a), and filling, b), respectively. Any choice of parameters is in accordance with the validity range of the approach.

where $\omega_n^+ = 2n\pi/\beta$, $n \in \mathbb{Z}$, denotes bosonic Matsubara frequencies, one finds for the first trace in Eq. (8.192)

$$
\begin{aligned}
\text{Tr}\,[\mathbb{G}_0\mathbb{B}] &= \frac{g^2}{\beta} \sum_{\omega_N^+, \omega_n^-} \left[\tilde{\alpha}_N^* \tilde{\alpha}_{-N}^* + \tilde{\alpha}_N \tilde{\alpha}_{-N} + 2\tilde{\alpha}_N^* \tilde{\alpha}_N \right] \frac{-(-i\omega_n^-)\kappa_M + \frac{\hbar\Omega_M}{2}\kappa_M^z}{(-i\omega_n^-)^2 - (\frac{\hbar\Omega_M}{2})^2} \\
&\overset{(E.38)}{=} g^2 \sum_{\omega_N^+} \left[\tilde{\alpha}_N^* \tilde{\alpha}_{-N}^* + \tilde{\alpha}_N \tilde{\alpha}_{-N} + 2\tilde{\alpha}_N^* \tilde{\alpha}_N \right] \left[\kappa_M - \kappa_M^z \tanh\left(\beta\frac{\hbar\Omega_M}{4}\right) \right],
\end{aligned}
\tag{8.197}
$$

Likewise, the second trace in Eq. (8.192) is obtained as

$$
\begin{aligned}
\text{Tr}\,[\mathbb{G}_0\mathbb{A}\mathbb{G}_0\mathbb{A}] &= \frac{2g^2}{\beta} \sum_{\substack{\omega_n^- \omega_m^- \\ n-m=N}} \frac{(\tilde{\alpha}_{n-m}^* + \tilde{\alpha}_{m-n})(\tilde{\alpha}_{m-n}^* + \tilde{\alpha}_{n-m})\left[-\omega_n^- \omega_m^+ - \left(\frac{\hbar\Omega_M}{2}\right)^2 \right]}{\left[(-i\omega_n^-)^2 - \left(\frac{\hbar\Omega_M}{2}\right)^2 \right]\left[(-i\omega_m^-)^2 - \left(\frac{\hbar\Omega_M}{2}\right)^2 \right]} \\
&\overset{(E.38)}{=} 2g^2 \sum_{\omega_N^+} \left[\tilde{\alpha}_N^* \tilde{\alpha}_{-N}^* + \tilde{\alpha}_N \tilde{\alpha}_{-N} + 2\tilde{\alpha}_N^* \tilde{\alpha}_N \right] \frac{\hbar\Omega_M \tanh\left(\beta\frac{\hbar\Omega_M}{4}\right)}{(-i\omega_N^+)^2 - (\hbar\Omega_M)^2}.
\end{aligned}
$$

$$
\tag{8.198}
$$

To proceed, it is convenient to transform use the Fourier representation of $\mathcal{S}_+$ accordingly,

$$\mathcal{S}_+[\tilde{\alpha}^*, \tilde{\alpha}] = \sum_{\omega_N^+} \left[\tilde{\alpha}_N^* \left(-i\omega_N^+ + \hbar\omega_0 \right) \tilde{\alpha}_N + \mathcal{X}(g) \left(\tilde{\alpha}_N^* \tilde{\alpha}_{-N}^* + \tilde{\alpha}_N \tilde{\alpha}_{-N} + 2\tilde{\alpha}_N^* \tilde{\alpha}_N \right) \right], \quad (8.199)$$

such that the Gaussian action of the fluctuation fields can be written as [242]

$$\mathcal{S}_G[\{\tilde{\alpha}^*, \tilde{\alpha}\}] = \sum_{\omega_N^+ \geq 0} \tilde{\boldsymbol{\alpha}}_N^\dagger \, \mathbb{S}(i\omega_N^+) \, \tilde{\boldsymbol{\alpha}}_N, \quad \mathbb{S}(\omega_N^+) = \begin{pmatrix} S(i\omega_N^+) & R(i\omega_N^+) \\ R(i\omega_N^+) & S(-i\omega_N^+), \end{pmatrix} \quad (8.200)$$

where $\tilde{\boldsymbol{\alpha}}_N^\dagger = (\tilde{\alpha}_N^* \; \tilde{\alpha}_{-N}^*)$, $\tilde{\boldsymbol{\alpha}}_N = (\tilde{\alpha}_N \; \tilde{\alpha}_{-N})^T$ and

$$S(i\omega_N^+) = -i\omega_N^+ + \hbar\omega_0 + 2\mathcal{X}(g) + 2g^2 \left[\kappa_M - \left(\kappa_M^z + \frac{\hbar\Omega_M}{(\omega_N^+)^2 + (\hbar\Omega_M)^2} \right) \tanh\left(\beta \frac{\hbar\Omega_M}{4} \right) \right],$$

$$R(i\omega_N^+) = 2\mathcal{X}(g) + 2g^2 \left[\kappa_M - \left(\kappa_M^z + \frac{\hbar\Omega_M}{(\omega_N^+)^2 + (\hbar\Omega_M)^2} \right) \tanh\left(\beta \frac{\hbar\Omega_M}{4} \right) \right]. \quad (8.201)$$

The corresponding path integral over the fluctuating fields can now be evaluated exactly and the eigenvalues of the fluctuating fields correspond to the poles of $(\det \mathbb{S})^{-1}$ (cf. Sec. 3 of App. D). The determinant of $\mathbb{S}$ is easily obtained and given by

$$\det \mathbb{S}(i\omega_N^+) = \prod_{N \geq 0} \left[(\omega_N^+)^2 + (\hbar\omega_0)^2 + 4g^2 \hbar\omega_0 \left[\tilde{\chi}_{M,\nu}^{(2)} + \kappa_M \right. \right.$$

$$\left. \left. - \left(\kappa_M^z + \frac{\hbar\Omega_M}{(\omega_N^+)^2 + (\hbar\Omega_M)^2} \right) \tanh\left(\beta \frac{\hbar\Omega_M}{4} \right) \right] \right], \quad (8.202)$$

where the explicit definition of $\mathcal{X}$ in second-order approximation was used. This result is in accordance with Ref. [95]. From analytic continuation $\omega_N^+ \mapsto -iE$ [239, 241, 242] one finds then the eigenenergies of the fluctuations above the ground-state at $T = 0$

$$2\epsilon_\pm^2 = (\hbar\omega_0)^2 + (\hbar\Omega_M)^2 + 4g^2(\rho_{M,\nu} + 1) \pm \left[\left[(\hbar\Omega_M)^2 - (\hbar\omega_0)^2 \right]^2 + 16g^2 \hbar\omega_0 \hbar\Omega_M \right.$$

$$\left. + 8g^2(\rho_{M,\nu} + 1) \left(2g^2(\rho_{M,\nu} + 1) \right) + (\hbar\omega_0)^2 - (\hbar\Omega_M)^2 \right]^{\frac{1}{2}}, \quad (8.203)$$

which coincide in the absence of the dynamically generated terms, i.e. $\rho_{M,\nu} = -1$, with the fluctuation energies in the original Dicke model (cf. Subsec. 3.3.4). Figure 8.13 shows the photonic branch in the normal phase as a function of g at $M = 1$ and $B = 5$ T. The excitation gap narrows as g approaches the critical point and vanishes precisely at $g = g_{c,M,\nu}^{(2)}$. The closure of the excitation gap is associated with the divergence of the characteristic length scales of the system and thus a typical feature for continuous quantum phase transitions [156]. The power law determining the behavior close to the critical point is thereby similar to the one valid in the original Dicke model, Eq. (3.88), but deviates from the path integral approach of the full-many body Hamiltonian. This is shown in Fig. 8.13.
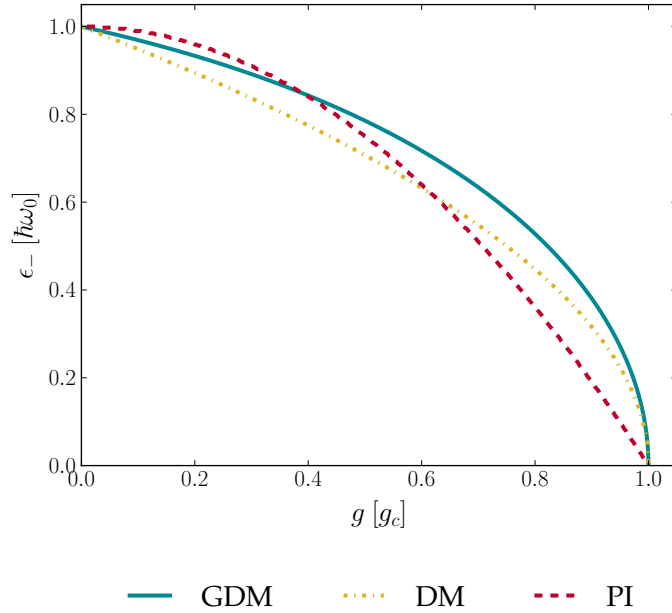
FIGURE 8.13: Excitation spectra of the photonic branch for $B = 5$ T and $M = 1$ as a function of the coupling for the generalized Dicke Hamiltonian (solid, blue), the path integral reference (red, dotted) and the original Dicke model (dashed, yellow). The closure of the gap between the photonic branch ϵ_- and the ground-state energy at the critical point is clearly seen in all three cases. The photonic branches of the generalized Dicke Hamiltonian and the original Dicke model follow an identical power law, Eq. (3.88), close to the critical point. The path integral approach of the full many-body Hamiltonian differs from this behavior.

8.5 Summary

Despite some deviations in the details of the second-order contributions to the effective Dicke Hamiltonian, the main result of Ref. [95] remains valid when choosing an identical, cutoff-independent regularization approach. However, the interpretation of these results might be altered. The authors of Ref. [95] conclude from the critical point being predicted for a parameter regime that exceeds the validity range of the underlying perturbative SW approach that superradiance is prohibited in Landau-quantized graphene. However, the only statement which can safely be concluded is that within the validity range of the approach under usage of the proposed cutoff-independent regularization no superradiant phase transition is predicted. The broad statement of a phase transition to be generally prohibited is certainly ambitious when applying an approach with a narrow validity range in the first place. Anyway, the limitation of the allowed parameter ranges within this particular regularization can be regarded as the bottleneck of the considerations of Ref. [95], as even the actual coupling of the system is rarely compatible with it.

However, when allowing for rigid ultraviolet cutoff regularization the predicted critical point is found within the validity range of the SW approach. Especially the second-order

approximation predicts the critical point almost identical to the result obtained within the path integral approach of the full-many body Hamiltonian. However, the deviations of the results for the investigated selection of key features indicating superradiance, the photon occupation and the excitation spectrum, intimate that the effective Dicke model is not providing a sufficient substitute of the full many-body Hamiltonian. The most crucial deviation concerns the scaling behavior of the photon occupation for rising Fermi level. In particular, the result obtained from the generalized Dicke Hamiltonian contradicts the behavior obtained for the path integral approach as well as the tight-binding simulation. Furthermore, the limited validity range of this approach is an issue which is circumvented when applying the path integral approach of the full many-body Hamiltonian.

Chapter 9

Conclusion and outlook

During this thesis the equilibrium superradiant phase transition of Landau-quantized graphene has been considered. The focus of the investigation has mainly addressed the quantum critical behavior of the system within Dirac approximation. The aim of this thesis was to provide a constructive contribution to the controversial discussion [93–95] about the existence of this collective radiation phenomenon in Landau-quantized graphene. The theoretical investigations have been partially supported with an independent tight-binding simulation of graphene which was solely based on microscopic information. A similar numerical approach has not been applied in previous publications on this particular subject [93–95].

9.1   Summary of the thesis and conclusion

For the purpose of this thesis, the main aspects of the underlying theoretical concepts were introduced in Part I.

As the phenomenon of superradiance is a purely quantum effect and requires the concept of quantum vacuum fluctuations, the foundations of the canonical quantization of the electromagnetic field and its interaction with charged matter were introduced in Chap. 2. This was complemented by a brief introduction into the quantum optical subfield of cavity quantum electrodynamics.

Based on these concepts, the original Dicke model was derived in Chap. 3. Then, the phenomenon of Dicke superradiance, denoting the collective spontaneous decay of a dense cloud of two-level atoms prepared in an excited state, was introduced. This discussion was complemented by investigating the second-order superradiant phase transition exhibited by the underlying model in the thermodynamic limit. Thereby, a catalog of generic features indicating the corresponding quantum phase transition was derived and discussed step by step. It was seen that the typical ground-state observables, cavity occupation, atomic polarization and the ground-state energy, are extensive quantities in the superradiant phase and thus scale with the number of atoms. Furthermore, the excitation spectrum of quantum fluctuations was discussed with the focus on the photonic branch. The gap between the photonic branch and the ground-state energy closes as the system approaches the critical point from either direction according to a power law with universal exponents. In contrast to Dicke superradiance, the superradiant phase transition is an artifact of inappropriate approximation applied onto the derivation of the Dicke Hamiltonian. The correction of this insufficiency gives rise to a no-go theorem prohibiting superradiant phase transitions in systems with parabolic dispersion.

The derivation of the no-go theorem was provided by Chap. 4 and supplemented by the discussion of three recently proposed exceptions to it. One of these proposals [93] precisely concerns the emergence of a superradiant quantum phase transition in Landau-quantized graphene as the original no-go theorem does not apply onto systems with linear dispersion. After a brief summary of the controversial discussion [94, 95] which was triggered by this proposal, the main properties of graphene were introduced in Chap. 5 on the basis of the lattice properties of the material.

Thus, the effective Dirac model was derived as a low-energy approximation in the vicinity of the K- and K'-point and discussed in the presence of a quantizing uniform magnetic field which gives rise to Landau quantization. Then, after the discussion of the single-particle light-matter interaction Hamiltonian in Dirac approximation, the many-body Hamiltonian of the Landau-quantized graphene embedded in an optical cavity was derived in second quantization. The resulting expression provided the basis for the investigations on the superradiant quantum critical behavior discussed in Part II.

Some of the analytic results obtained in Part II have been underpinned by a numerical tight-binding simulation based on a microscopic implementation of both, the hexagonal lattice and the cavity mode. Therefore, the properties of the numerical setup were discussed in Chap. 6, starting with the evaluation of the validity range of the Peierl's substitution which provides the generic basis for the implementation of vector potentials into tight-binding simulations. The electromagnetic vector potential was thereby implemented within matrix representation of the bosonic operators in a truncated Hilbert space. Thereby convergence with respect to the dimension of the truncated Hilbert space was ensured and obtained for remarkably low dimensions compared with similar investigations concerning the original Dicke mode. Complementing, the formation of Landau-level clusters in the simulated finite-size systems of various spacial extension was discussed and compared with the effective Dirac description and its extension accounting for trigonal warping of the Dirac cones. It has been found that the tight-binding spectra approximately reveal the validity range of the analytic Dirac model. This is indicated by a rather sudden breakdown of the formation of Landau-level clusters above a certain energy threshold due to further warping of the bands when moving away from the Dirac points. Furthermore, a criterion for the evaluation of the approximate degeneracy of the Landau-level clusters has been formulated. The values of the approximate degeneracy have then been extracted from the considered tight-binding spectra. This is crucial, as the approximate degeneracy of the Landau-level clusters takes the role of the number of atoms in the Dicke model and explicitly entered the simulation to provide an additional proof of the consistency for the comparison with the analytic results. Remarkably, it has been found that the tight-binding simulation shows distinct signatures of superradiance as the photonic occupation of the cavity rises from zero to a non-zero value when a critical coupling is exceeded. Thereby, the complete tight-binding spectrum was considered. The evaluation of the simulation results however was performed in Chap. 7 by simultaneous comparison with analytic predictions.

For the analytical examination of the superradiant critical behavior of Landau-quantized graphene within Dirac approximation two approaches have been chosen. The first method was investigated in Chap. 7 and is provided by a path integral approach for the grand-canonical partition sum of the many-body Hamiltonian. This approach allows an exact

integration of the fermionic degree of freedom. The second approach, found in Chap. 8, is identical with the technique applied in Ref. [95] where a generalized Dicke Hamiltonian for the last occupied and first unoccupied Landau level is perturbatively derived by means of a many-body Schrieffer-Wolff transformation. This approach has been extended from second- to fourth-order approximation during this thesis.

As both approaches are based on the effective Dirac model, proper regularization of contributions stemming from the valence band was required. For each analytic approach two regularization techniques have been considered: The first one is similar for both approaches and provided by the introduction of a rigid ultraviolet momentum cutoff. Though violating gauge invariance in the presence of gauge potentials this technique is commonly applied when investigating light-matter interaction effects in graphene [24, 98–102]. The second regularization method differs for both analytic approaches but yields a cutoff-independent result in both cases. In case of the path integral approach this regularization method is provided by a rotating-wave like approximation which omits inter-band transitions as proposed in Ref. [93]. Thereby, a slight modification of the particular approach suggested in Ref. [93] has been considered. The cutoff-independent regularization of the SW ansatz was adopted from Ref. [95] and results from subtraction of all cutoff-dependent contributions from the considered terms in the effective Hamiltonian.

The particular investigations discussed in Chap. 7 are further summarized as follows:
After exactly integrating over the fermionic degree of freedom, the effective action resulting for the bosonic mode has first been studied analytically in the normal phase within both regularization methods. In the thermodynamic limit, an analytic expression for the critical point has been found for either regularization. This point is associated with the normal phase no longer determining the ground-state properties of the system and thus indicating critical behavior in analogy to similar considerations on the Dicke model. The critical points in Dirac approximation were then compared with the actual coupling strength of the system which is determined by the microscopic properties of the Dirac fermions and the cavity mode. Thereby, the parameter ranges required to actually reach the critical point in equilibrium have been pinned for either regularization. It has been found that the cutoff-independent result predicts a phase boundary at large fillings in accordance with Ref. [93] where similar regularization is applied. This has been contrasted by the cutoff-regularized phase boundary which is predicted for rather low and experimentally feasible [28–30] fillings and magnetic fields. The analytical calculation of the critical coupling has been extended by a small trigonal-warping correction of the Landau levels for comparison with the independent tight-binding simulation. It has been found that the corresponding cutoff-regularized result convincingly predicts the critical point emerging from the simulation whereas the cutoff-independent one overestimates the numerical result. This indicates that cutoff regularization provides a proper description of the actual properties of graphene in this context.
The comparison of the ground-state energy and the cavity occupation has confirmed this further: Thereby, the evaluation of the partition sum beyond the critical point was performed numerically. The photonic occupation and the ground-state energy then have been compared with the tight-binding simulation. It has been found that the path integral approach as well as the independent tight-binding approach show distinct signatures of

superradiance as the photon occupation above the critical coupling assumes a non-zero value. Thereby, the tight-binding result indicates a second-order quantum phase transition similar as obtained from the path integral approach for cutoff regularization. This has been contrasted by investigating the cutoff-independent equivalent which exhibits a first-order quantum phase transition when the Fermi level lies between the Landau levels $M = 1$ and $M + 1$. From this crucial deviation along with the insufficiencies regarding the proper prediction of the critical point when comparing with the numerical simulation the following conclusion has been drawn:

This particular choice of regularization provides an inadequate description of the actual processes in the system. In consequence, inter-band transitions seem to play a crucial role in the emergence of superradiance in Landau-quantized graphene.

Thus, the cutoff-regularized result for the photon occupation and the tight-binding simulation show convincing qualitative agreement concerning the scaling of this observable with respect to the cutoff and the filling. In both cases, the value of photon occupation increases as the respective parameter rises. Even though the approximate degeneracy of the Landau-level clusters appearing in the tight-binding spectra are finite and far from resembling a thermodynamic limit, a rather sharp phase boundary has been found in the evaluation of the photon occupation.

However, also differences in the cutoff-regularized result for the photon occupation and the tight-binding simulation have been seen. The former predicts a rather steep increase of the photon occupation close to the critical coupling. This deviates from the rather linear behavior obtained from the simulation. Furthermore, the path integral approach has been found to overestimate the value of the photon occupation compared with the tight-binding simulation. Whether this results from finite-size effects affecting the latter requires further investigations.

Nevertheless, the cutoff-regularized path integral approach resembles a number of key features which emerge from the tight-binding simulation. This includes in particular the proper prediction of the critical point, the order of the phase transition and the qualitative scaling behavior of the photon occupation for different values of the cutoff and the Fermi level. Thus, this approach can be regarded as a suitable ansatz for the investigation of collective radiation effects in Landau-quantized graphene. However, the argument of gauge violence tied to this approach still requires further discussion on a fundamental level.

Further investigations on the spectrum of quantum fluctuations above the ground-state of the path integral approach within cutoff regularization have shown an asymmetric closure of the excitation gap. Thereby, the critical exponents depend on the direction from which the phase boundary is approached. This contrasts the behavior of the corresponding quantity in the original Dicke model where the critical exponents of the power law are identical for either direction.

Chapter 8 provided an extension of the considerations discussed in Ref. [95]. Thereby, an effective Dicke-like Hamiltonian for the last occupied and first unoccupied Landau level has been derived by means of a Schrieffer-Wolff transformation. This perturbative approach has been extended from second order, as considered in Ref. [95], to fourth order. Within this approach additional terms which are quadratic in the bosonic mode appear as

dynamically generated corrections of the Dicke-like Hamiltonian. In addition to the regularization approach applied in Ref. [95] also cutoff regularization has been investigated. By identical evaluation as found in Ref. [95], small deviations in the details of the effective contributions to the Hamiltonian arising from the transformation have been found in comparison with Ref. [95]. However, from the evaluation of the cutoff-independent effective Hamiltonian in second-order approximation no prediction of critical behavior could be made. This is due to the critical point obtained within this approach lying beyond the validity range of the Schrieffer-Wolff approach. This validity range is thereby determined by the transition frequency of the last occupied and the first unoccupied Landau level and narrows as the filling increases. The conclusion drawn in this thesis differs from the one provided in Ref. [95], where the authors interpret an identical result as a modified no-go theorem for the emergence of superradiance in graphene. From the fourth-order result derived within this thesis no critical point could be found at all. As convergence of the perturbation series obtained from Schrieffer-Wolff approach is not mandatory in a many-body case, this result provides no robust justification for similar conclusion as drawn by Ref. [95].

By allowing for cutoff-dependent regularization, the predicted phase boundary is compatible with the validity range of the approach when the cutoff is much larger than the Landau level index of the last occupied level. In this parameter range also convincing agreement with the phase boundary obtained within the path integral approach for an identical regularization has been found especially for the second-order approximation. However, the perturbative result slightly underestimates the path integral prediction. This underestimation is enhanced in fourth-order approximation of the effective Dicke-like Hamiltonian. The photon occupation in second-order approximation shows also typical characteristics of a second-order quantum phase transition with a quadratic dependence on the coupling parameter. The scaling with varying cutoff is thereby similar to the one obtained for the photon occupation of the path integral approach and the simulation. However, a parabolic dependence on the coupling parameter could not be found in the evaluation of the approaches, discussed in Chap. 6 and 7. Note that a direct comparison of the simulation with the perturbation approach has not been possible during this thesis. This is due to the latter requiring values for the cutoff which were not feasible within the simulation. Even more crucial is however the deviation of the scaling behavior of the photon occupation for varying Fermi level. The effective Dicke-like Hamiltonian predicts a decrease of the photon occupation as the Landau level increases. This contradicts the results obtained from the path integral approach and the tight-binding simulation. The excitation spectrum obtained for the normal phase of the second-order effective Dicke-like Hamiltonian within cutoff regularization also shows deviations from the path integral equivalent. The power law associated with the vanishing photonic branch close to the critical point rather reveals the critical exponents obtained for the original Dicke model than the one found for the path integral equivalent for identical parameters.

With this, the main conclusion of the investigations discussed in this thesis can be drawn: The comparison of the critical points and the photon occupation resulting from the tight-binding simulation has indicated that each of the considered approaches fails in the proper description when the regularization is chosen cutoff-independent. In contrast,

any of the three considered approaches shows distinct signatures of a second-order superradiant quantum phase transition in Landau-quantized graphene when a rigid ultraviolet cutoff is applied. Thereby, convincing agreement of all approaches has been found for the phase boundary. According to the path integral approach and the simulation this phase boundary is predicted for an experimentally already feasible parameter range [28–30, 55] The applied analytic methods qualitatively resemble the scaling behavior of the photon occupation obtained for the simulation for different values of the cutoff. However, the scaling behavior predicted from the perturbative approach for different Fermi levels contradicts the results obtained from the path integral approach and the simulation.

Despite all remaining open questions, the results obtained within this thesis might though provide a constructive contribution to the controversial discussion about the existence of a superradiant phase transition. Especially the tight-binding simulation brought in new aspects concerning the issue of regularization tied to the effective Dirac description of the system in this context. The application of an ultraviolet cutoff is commonly used in related subfields of graphene research [24, 98–102] but has not been investigated in the context of superradiance [93–95]. However, this regularization approach is still under recent debate [96, 97]. Thus, also the understanding of superradiant critical behavior in Landau-quantized graphene requires further research in this context. Thereby, new paths for scientific research related to the phenomena of collective radiation might be opened under theoretical but also experimental perspectives.

9.2 Proposals for future investigations

The analysis of the differences emerging from the considered approaches certainly requires further investigation. Thereby, also effects stemming from a finite Landau-level degeneracy could be included as a correction to the thermodynamic limit. This can be achieved for both analytic methods within a perturbative expansion into orders of the degeneracy similar as considered in Refs. [79, 178, 179, 239] for the original Dicke model. Additionally, one should aim for the completion of catalog of generic features presented on the example of the original Dicke model. This concerns in particular the polarization of the solid state system and the identification of the symmetry which broken in the superradiant phase.

Furthermore, it would be interesting to investigate a slightly modified Schrieffer-Wolff transformation within cutoff-regularization. In particular, Ref. [95] proposes a transformation where the complete valence band is "integrated", i.e. compensated by an appropriate transformation. The effective Hamiltonian will not be reminiscent of an extended Dicke model but might offer further insights into the underlying processes from an altered perspective. The evaluation of the resulting Hamiltonian can then be achieved by meas of a path integral approach. The advantage of this modification is due to an extended validity range of the perturbation series as the energy gap of the corresponding block-diagonal subspaces is determined by the transition energy of the zeroth and first Landau level.

An interesting path for further considerations in this subfield of graphene research would be provided by additionally investigating Coulomb interaction. This has already been briefly touched in Ref. [93] finding the critical point to persist within similar cutoff-independent regularization as applied in Chap. 7 of this thesis. However, it would be interesting how this result is altered when differently regularized and compared with a numerical simulation.

Another novel path concerns the effect of the superradiant phase on the transport properties of graphene. This is interesting as transport has been rarely considered in the entire field of research on collective radiation phenomena. However, studies on a single-particle system in a state analogous to Dicke superradiance propose [246] distinct changes in the transport properties such as a maximization of the electronic transmission at the transition point. Thus, investigating the effect of the superradiant phase in the context of Landau-quantized graphene holds the potential to gain further insight into the underlying processes. Thereby one might also obtain further signatures of the superradiant state of the system. This in turn might open new possibilities for experimental measurements of superradiance in Landau-quantized graphene.

Appendix A

Classical electrodynamics in Coulomb gauge

This chapter provides the derivation of the classical Hamiltonian function describing the interaction of N point charges with electromagnetic radiation. To this end, one starts with the postulation of the classical Lagrangian for electrodynamics based on the Maxwell equations and the Lorentz force law. From the Lagrangian formulation based on generalized coordinates and velocities one is then able to identify the canonical momenta and thus transfer the classical field theory into the Hamiltonian formulation. One key quantity of the Hamiltonian formalism is given by the fundamental Poisson brackets which determine the dynamics of the considered system. Moreover, the fundamental Poisson brackets provide the formal basis for the formulation of a quantized theory. In particular, the quantum theory of electrodynamics is derived from the fundamental Poisson brackets of corresponding classical field theory (cf. Chap. 2). The following discussion is mostly leaned on Ref. [103].

A.1 Maxwell equations

Since Maxwell equations provide the connection between the electric and the magnetic field $\boldsymbol{E}$ and the magnetic field $\boldsymbol{B}$ on the most fundamental level of electrodynamics it is convenient to recapitulate them when investigating on classical electromagnetic radiation. The Maxwell equations in general, differential representation read

$$\nabla \times \boldsymbol{B}(\boldsymbol{q}, t) - \mu_0 \epsilon_0 \partial_t \boldsymbol{E}(\boldsymbol{q}, t)) = \mu_0 \boldsymbol{j}(\boldsymbol{q}, t), \tag{A.1}$$

$$\nabla \times \boldsymbol{E}(\boldsymbol{q}, t) + \partial_t \boldsymbol{B}(\boldsymbol{q}, t) = 0, \tag{A.2}$$

$$\nabla \cdot \boldsymbol{E}(\boldsymbol{q}, t) = \frac{\rho}{\epsilon_0}, \tag{A.3}$$

$$\nabla \cdot \boldsymbol{B}(\boldsymbol{q}, t) = 0, \tag{A.4}$$

where ϵ_0 and μ_0 denote the *vacuum permittivity* and *permeability*, respectively. In free space, meaning vanishing charge and current densities, $\rho = 0$ and $\boldsymbol{j} = 0$, the Maxwell equations (A.1 – A.3) are also known as *Ampere law*, *Faraday law* and *Gauss law*, respectively.
Further details concerning Maxwell equations in the presence of a dielectric medium with finite permittivity ϵ_r and permeability μ_r can be found in any textbook on classical quantum electrodynamics, such as Ref. [247]. As a first important insight one can conclude

from Eq. (A.4) that there exist no magnetic monopoles. Consequently, the magnetic field $\boldsymbol{B}$ can be represented as the rotation of a vector potential $\boldsymbol{A}$, i.e. $\boldsymbol{B} = \nabla \times \boldsymbol{A}$. This holds true for any choice of $\boldsymbol{B}$ since the divergence of the curl of any vector field yields the zero and vice versa. Similar to this also the curl of the gradient of any arbitrary scalar field Λ results in the zero vector, as easily proven. Consequently, the vector potential $\boldsymbol{A}$ is not unique but only fixed up to the gradient of a *gauge field* Λ without affecting the magnetic field, i.e.

$$\boldsymbol{B}(\boldsymbol{q}, t) = \nabla \times \left[\boldsymbol{A}(\boldsymbol{q}, t) + \nabla \Lambda(\boldsymbol{q}, t) \right]. \tag{A.5}$$

Inserting this identity for the magnetic field into Eq. (A.2) one finds for the electric field in a similar manner

$$\boldsymbol{E}(\boldsymbol{q}, t) = -\nabla \Phi(\boldsymbol{q}, t) - \partial_t \left[\boldsymbol{A}(\boldsymbol{q}, t) + \nabla \Lambda(\boldsymbol{q}, t) \right]. \tag{A.6}$$

The presence of a time-dependent magnetic field $\boldsymbol{B}$ induces an electric vortex field in addition to the electric field resulting from the scalar potential $\Phi(\boldsymbol{q}, t)$. According to Eq. (A.2) the gauge invariance of the magnetic field (A.5) extends to the electric field according to Eq. (A.6).

For the derivation of the Hamiltonian function of classical electromagnetism, it is convenient, to use the Fourier transform (cf. Sec. E.1) of the magnetic and electric field, yielding

$$\tilde{\boldsymbol{B}}(\boldsymbol{k}, t) = i\boldsymbol{k} \times \tilde{\boldsymbol{A}}(\boldsymbol{k}, t), \tag{A.7}$$

$$\tilde{\boldsymbol{E}}(\boldsymbol{k}, t) = -i\boldsymbol{k}\tilde{\varphi}(\boldsymbol{k}, t) - \partial_t \tilde{\boldsymbol{A}}(\boldsymbol{k}, t), \tag{A.8}$$

without the gauge field Λ. During the following, $\boldsymbol{k}$ will be associated with the *propagation direction* of the electromagnetic field.

A.2   Lagrangian of classical electromagnetism

According to the basic ideas underlying the Lagrangian formulation of classical mechanics one constructs the *Lagrangian of classical electromagnetism* $\mathcal{L}_{\text{em}}$ precisely in the way that the inhomogeneous Maxwell equations (A.1, A.3) are obtained from the Euler-Lagrange equations corresponding to $\mathcal{L}_{\text{em}}$ with respect to the generalized coordinates $\tilde{\varphi}$, $\tilde{\boldsymbol{A}}$ and the generalized velocities $\dot{\tilde{\varphi}}$, $\partial_t \tilde{\boldsymbol{A}}$ [103]. The homogeneous Maxwell equations enter the Lagrangian by means of the relations (A.7, A.8) for the fields $\tilde{\boldsymbol{B}}$, $\tilde{\boldsymbol{E}}$ and the potentials $\tilde{\varphi}$, $\tilde{\boldsymbol{A}}$. Regarding these constrains, the Lagrangian of classical electromagnetism in momentum space is postulated to read [103]

$$\mathcal{L}_{\text{em}}[\tilde{\varphi}, \tilde{\boldsymbol{A}}; \partial_t \tilde{\varphi}, \partial_t \tilde{\boldsymbol{A}}] = \int_{\mathbb{R}^3} \frac{\mathrm{d}^3 k}{(2\pi)^3} L'_{\text{em}}[\tilde{\varphi}, \tilde{\boldsymbol{A}}; \partial_t \tilde{\varphi}, \partial_t \tilde{\boldsymbol{A}}], \tag{A.9}$$

where L'_{em} denotes the *Lagrangian density*, defined as

$$L'_{\text{em}}[\tilde{\varphi}, \tilde{\boldsymbol{A}}; \partial_t \tilde{\varphi}, \partial_t \tilde{\boldsymbol{A}}] = \frac{\epsilon_0}{2} \left[\left| \tilde{\boldsymbol{E}}(\boldsymbol{k}, t) \right|^2 - c^2 \left| \tilde{\boldsymbol{B}}(\boldsymbol{k}, t) \right|^2 \right] - \tilde{\rho}(\boldsymbol{k}, t)\tilde{\varphi}(-\boldsymbol{k}, t) + \tilde{\boldsymbol{j}}(\boldsymbol{k}, t) \cdot \tilde{\boldsymbol{A}}(-\boldsymbol{k}, t). \tag{A.10}$$

The moduli squared of the fields $\tilde{B}$, $\tilde{E}$ enter due to the constraint of a real-valued Lagrangian and fields in position space [103]. More generally, any Fourier transform entering the Lagrangian has to fulfill the relation

$$\tilde{f}(-\boldsymbol{k}) = \tilde{f}^*(\boldsymbol{k}) \tag{A.11}$$

in order to provide a real-valued Lagrangian and thus in turn real-valued fields $\boldsymbol{B}$, $\boldsymbol{E}$. The implementation of this constraint into the definition of $\mathcal{L}_{\text{em}}$ is formally achieved by the restriction [103] of the integration from the complete reciprocal space $\mathbb{R}^3$ to the *reciprocal half space* $\mathbb{H}^3 = \{(k_x, k_y, k_z) | k_x \geq 0\}$ in Eq. (A.9). This is reasonable since by knowing the value of an observable $\tilde{f}$ in the half space $\mathbb{H}^3$ one also knows its value in the complementary half space by complex conjugation according to the constraint (A.11). The corresponding Lagrangian is therefore obtained from

$$\mathcal{L}_{\text{em}}[\tilde{\varphi}, \tilde{\boldsymbol{A}}; \partial_t \tilde{\varphi}, \partial_t \tilde{\boldsymbol{A}}] = \int_{\mathbb{H}^3} \frac{\mathrm{d}^3 k}{(2\pi)^3} L_{\text{em}}[\tilde{\varphi}, \tilde{\boldsymbol{A}}; \partial_t \tilde{\varphi}, \partial_t \tilde{\boldsymbol{A}}], \tag{A.12}$$

with L_{em} defined as

$$L_{\text{em}}[\tilde{\varphi}, \tilde{\boldsymbol{A}}; \partial_t \tilde{\varphi}, \partial_t \tilde{\boldsymbol{A}}] = \epsilon_0 \left[\left| \tilde{\boldsymbol{E}}(\boldsymbol{k}, t) \right|^2 - c^2 \left| \tilde{\boldsymbol{B}}(\boldsymbol{k}, t) \right|^2 \right]$$
$$- \tilde{\rho}^*(\boldsymbol{k}, t)\tilde{\varphi}(\boldsymbol{k}, t) - \tilde{\rho}(\boldsymbol{k}, t)\tilde{\varphi}^*(\boldsymbol{k}, t) + \tilde{\boldsymbol{j}}^*(\boldsymbol{k}, t) \cdot \tilde{\boldsymbol{A}}(\boldsymbol{k}, t) + \tilde{\boldsymbol{j}}(\boldsymbol{k}, t) \cdot \tilde{\boldsymbol{A}}^*(\boldsymbol{k}, t). \tag{A.13}$$

Thereby the first and third contribution in the second line of Eq. (A.13) result from the Fourier transform of the products $\rho\varphi$ and $\boldsymbol{j} \cdot \boldsymbol{A}$, respectively, known as *Plancherel identity* (E.3) in view of (A.11). Contrarily, the second and fourth contribution in the second line of Eq. (A.13) arise from the restriction of $\boldsymbol{k} \in \mathbb{H}^3$ in view of Eq. (A.11).
In Eq. (A.13) ϵ_0 and c denote the universal constants vacuum permittivity and and speed of light. Furthermore,

$$\tilde{\rho}(\boldsymbol{k}, t) = \sum_{j=1}^{N} q_j e^{-i\boldsymbol{k}\cdot\boldsymbol{q}_j} \quad \Leftrightarrow \quad \rho(\boldsymbol{q}, t) = \sum_j q_j \delta(\boldsymbol{q} - \boldsymbol{q}_j) \tag{A.14}$$

denotes the charge density of N point charges q_j, each localized at the position $\boldsymbol{q}_j$ in reciprocal (left) and real space (right). For the sake of clearness, normal letters refer to scalar observables in the chosen notation convention. Hence, q_j denotes the charge of the jth particle. By contrast, bold letters denote vector quantities, such as the position of the jth particle, $\boldsymbol{q}_j$. The charge current associated with the motion of these particles is defined as

$$\tilde{\boldsymbol{j}}(\boldsymbol{k}, t) = \sum_{j=1}^{N} q_j \dot{\boldsymbol{q}}_j e^{-i\boldsymbol{k}\cdot\boldsymbol{q}_j} \quad \Leftrightarrow \quad \boldsymbol{j}(\boldsymbol{q}, t) = \sum_j q_j \dot{\boldsymbol{q}}_j \delta(\boldsymbol{q} - \boldsymbol{q}_j). \tag{A.15}$$

Therefore the last four contributions to the r.h.s. of Eq. (A.13) describe the interaction of the particles with the electromagnetic field. As a consequence of the gauge invariance of the fields $\tilde{\boldsymbol{B}}, \tilde{\boldsymbol{E}}$ also the Lagrangian density (A.13) and thus the Lagrangian (A.12) is invariant under gauge transformations [103].

Choosing a specific gauge function Λ (A.5, A.6) diminishes the degrees of freedom entering the theory. Therefore, the choice of a specific gauge function Λ or *gauge fixing* often yields a formal simplification. Throughout this thesis, the gauge degree of freedom shall be fixed to *Coulomb gauge*,

$$\boldsymbol{k} \cdot \tilde{\boldsymbol{A}}(\boldsymbol{k}, t) = 0 \quad \Leftrightarrow \quad \nabla \cdot \boldsymbol{A}(\boldsymbol{q}, t) = 0, \tag{A.16}$$

which is the most appropriate choice regarding investigations on electromagnetic radiation [103]. Thereby the part of $\tilde{\boldsymbol{A}}$ which is parallel to $\boldsymbol{k}$, also referred to as *longitudinal* part, is set to zero. The vector potential is then fully described by the *transverse* part $\tilde{\boldsymbol{A}}_{\perp}$. For that reason Coulomb gauge is sometimes also referred to as *transverse gauge* or *radiation gauge*, according to the purely transverse properties of electromagnetic radiation.
The longitudinal and transverse part of $\tilde{\boldsymbol{A}}$ are formally obtained from

$$\begin{aligned} \tilde{\boldsymbol{A}}_{\|}(\boldsymbol{k}, t) &= \boldsymbol{e}_{\boldsymbol{k}}\, \tilde{A}_{\|}(\boldsymbol{k}, t), \\ \tilde{\boldsymbol{A}}_{\perp}(\boldsymbol{k}, t) &= \tilde{\boldsymbol{A}}(\boldsymbol{k}, t) - \tilde{\boldsymbol{A}}_{\|}(\boldsymbol{k}, t), \end{aligned} \tag{A.17}$$

where $\tilde{A}_{\|}(\boldsymbol{k}, t) = \boldsymbol{e}_{\boldsymbol{k}} \cdot \tilde{\boldsymbol{A}}(\boldsymbol{k}, t)$ is a complex number and $\boldsymbol{e}_{\boldsymbol{k}} = \boldsymbol{k}/k$, with $k = |\boldsymbol{k}|$, denotes the unit vector parallel to $\boldsymbol{k}$ as Fig. 2.1 depicts. According to the gauge condition (A.16) $\tilde{\boldsymbol{A}}_{\perp}$ is in general described by two independent components

$$\tilde{\boldsymbol{A}}_{\perp}(\boldsymbol{k}, t) = \tilde{\boldsymbol{A}}_{\perp,1}(\boldsymbol{k}, t) + \tilde{\boldsymbol{A}}_{\perp,2}(\boldsymbol{k}, t), \quad \tilde{\boldsymbol{A}}_{\perp,1}(\boldsymbol{k}, t) \perp \tilde{\boldsymbol{A}}_{\perp,2}(\boldsymbol{k}, t). \tag{A.18}$$

These components can be expressed in terms of the basis vectors $\boldsymbol{\eta}_{1,\boldsymbol{k}} \perp \boldsymbol{\eta}_{2,\boldsymbol{k}}$, spanning the plane perpendicular to the *propagation direction* $\boldsymbol{e}_{\boldsymbol{k}}$ as Fig. 2.1 illustrates. Therefore, each of the independent $\tilde{\boldsymbol{A}}_{\perp,n}$ components reads

$$\tilde{\boldsymbol{A}}_{\perp,n}(\boldsymbol{k}, t) = \boldsymbol{\eta}_{n,\boldsymbol{k}}\, \tilde{A}_{\perp,n}(\boldsymbol{k}, t), \quad n = 1, 2, \tag{A.19}$$

where $\tilde{A}_{\perp,n}(\boldsymbol{k}, t) = \boldsymbol{\eta}_{n,\boldsymbol{k}} \cdot \tilde{\boldsymbol{A}}(\boldsymbol{k}, t)$ is a complex number in general. The charge current $\tilde{\boldsymbol{j}}$ can be decomposed into its longitudinal and transverse part similar to Eq. (A.17). Thereby, the scalar product of $\tilde{\boldsymbol{j}}_{\|}$ with $\tilde{\boldsymbol{A}}_{\perp}$ is zero.
Summarizing, the Lagrangian density L_{em} in Coulomb gauge reads

$$\begin{aligned} L_{\text{em}}[\tilde{\varphi}, \tilde{\boldsymbol{A}}_{\perp}; \partial_t \tilde{\varphi}, \partial_t \tilde{\boldsymbol{A}}_{\perp}] = \epsilon_0 &\left[\left| i\boldsymbol{k}\tilde{\varphi} - \partial_t \tilde{\boldsymbol{A}}_{\perp} \right|^2 - c^2 \left| i\boldsymbol{k} \times \tilde{\boldsymbol{A}}_{\perp} \right|^2 \right] \\ &- \tilde{\rho}^* \tilde{\varphi} - \tilde{\rho}\tilde{\varphi}^* + \tilde{\boldsymbol{j}}_{\perp}^* \cdot \tilde{\boldsymbol{A}}_{\perp} + \tilde{\boldsymbol{j}}_{\perp} \cdot \tilde{\boldsymbol{A}}_{\perp}^*, \end{aligned} \tag{A.20}$$

where the definitions of the fields $\tilde{\boldsymbol{B}}, \tilde{\boldsymbol{E}}$ according to Eqs. (A.7, A.8) entered. As the charge current $\tilde{\boldsymbol{j}}$, Eq. (A.15), is explicitly dependent on the generalized velocities $\dot{\boldsymbol{q}}_i$ of the point charges also the Lagrangian density L_{em} carries an explicit dependence on $\dot{\boldsymbol{q}}_i$, $i = 1, \dots, N$.
For the sake of brevity and simplicity the arguments of the functions entering the Lagrangian density L_{em} are mostly omitted during the following.

The result is further simplified by expanding the first modulus squared on the r.h.s. under application of the gauge constraint (A.16):

$$L_{\text{em}}[\tilde{\varphi}, \tilde{\boldsymbol{A}}_\perp; \partial_t \tilde{\varphi}, \partial_t \tilde{\boldsymbol{A}}_\perp] = \epsilon_0 \left[|i\boldsymbol{k}\tilde{\varphi}|^2 + \left|\partial_t \tilde{\boldsymbol{A}}_\perp\right|^2 - c^2 \left|i\boldsymbol{k} \times \tilde{\boldsymbol{A}}_\perp\right|^2 \right]$$
$$- \tilde{\rho}^* \tilde{\varphi} - \tilde{\rho}\tilde{\varphi}^* + \tilde{\boldsymbol{j}}_\perp^* \cdot \tilde{\boldsymbol{A}}_\perp + \tilde{\boldsymbol{j}}_\perp \cdot \tilde{\boldsymbol{A}}_\perp^*. \quad \text{(A.21)}$$

Note that the Lagrangian density L_{em} is independent of the generalized velocity $\dot{\tilde{\varphi}}$. Therefore the scalar potential is regarded to be a static variable which can be eliminated from the Lagrange density L_{em} by solving the corresponding Euler-Lagrange equation for $\tilde{\varphi}^*$

$$0 = \frac{\partial L_{\text{em}}}{\partial \tilde{\varphi}^*} = \epsilon_0 k^2 \tilde{\varphi}(\boldsymbol{k}, t) - \tilde{\rho}(\boldsymbol{k}, t) \quad \Leftrightarrow \quad \tilde{\varphi}(\boldsymbol{k}, t) = \frac{\tilde{\rho}(\boldsymbol{k}, t)}{\epsilon_0 k^2}. \quad \text{(A.22)}$$

Different from the discrete case of point particles, the Euler-Lagrange equations for the classical fields can also be obtained from the Lagrangian density [103]. By defining functional derivatives it is also possible to equivalently derive the Euler-Lagrange equations from the Lagrangian itself [103].
However, substituting the result (A.22) for $\tilde{\varphi}$ into L_{em} (A.21) results, after some rearrangements of the terms related to $\tilde{\varphi}$, in

$$L_{\text{em}}[\tilde{\boldsymbol{A}}_\perp; \partial_t \tilde{\boldsymbol{A}}_\perp] = \tilde{L}_{\text{em}}[\tilde{\boldsymbol{A}}_\perp; \partial_t \tilde{\boldsymbol{A}}_\perp] - \frac{2}{\epsilon_0} \frac{|\tilde{\rho}(\boldsymbol{k}, t)|^2}{k^2}, \quad \text{(A.23)}$$

where $\tilde{L}_{\text{em}}$ is defined by

$$\tilde{L}_{\text{em}}[\tilde{\boldsymbol{A}}_\perp; \partial_t \tilde{\boldsymbol{A}}_\perp] = \epsilon_0 \left[\left|\partial_t \tilde{\boldsymbol{A}}_\perp\right|^2 - c^2 \left|i\boldsymbol{k} \times \tilde{\boldsymbol{A}}_\perp\right|^2 \right] + \tilde{\boldsymbol{j}}_\perp^* \cdot \tilde{\boldsymbol{A}}_\perp + \tilde{\boldsymbol{j}}_\perp \cdot \tilde{\boldsymbol{A}}_\perp^*. \quad \text{(A.24)}$$

The static scalar potential $\tilde{\varphi}$ is successfully eliminated from the Lagrangian density and thus from the Lagrangian $\mathcal{L}_{\text{em}}$, Eq. (A.12), so that both dependent only on the generalized coordinate $\tilde{\boldsymbol{A}}$ and corresponding velocity $\partial_t \tilde{\boldsymbol{A}}$. The last term in the second line of Eq. (A.23) can be identified with the Coulomb potential [103] after insertion of L_{em} (A.23) into the Lagrangian $\mathcal{L}_{\text{em}}$ (A.12):

$$V_{\text{C}} = \frac{2}{\epsilon_0} \int_{\mathbb{H}^3} \frac{\mathrm{d}^3 k}{(2\pi)^3} \frac{|\tilde{\rho}(\boldsymbol{k}, t)|^2}{k^2} = \Sigma_{\text{C}} + \sum_{i>j} \frac{q_i q_j}{4\pi\epsilon_0 |\boldsymbol{q}_i - \boldsymbol{q}_j|}, \quad \text{(A.25)}$$

where Σ_{C} denotes the divergent self energy. The second term in Eq. (A.25) describes the electrostatic interaction of all point charges.
The Lagrangian $\mathcal{L}_{\text{em}}$ (A.12) is therefore of the following form

$$\mathcal{L}_{\text{em}}[\tilde{\boldsymbol{A}}_\perp; \partial_t \tilde{\boldsymbol{A}}_\perp] = \tilde{\mathcal{L}}_{\text{em}}[\tilde{\boldsymbol{A}}_\perp; \partial_t \tilde{\boldsymbol{A}}_\perp] - V_{\text{C}}, \quad \text{(A.26)}$$

where $\tilde{\mathcal{L}}_{\mathrm{em}}$ arises from $\tilde{L}_{\mathrm{em}}$, reading

$$\tilde{\mathcal{L}}_{\mathrm{em}}[\tilde{\boldsymbol{A}}_\perp; \partial_t \tilde{\boldsymbol{A}}_\perp] = \int_{\mathbb{H}^3} \frac{\mathrm{d}^3 k}{(2\pi)^3} \left\{ \epsilon_0 \left[\left| \partial_t \tilde{\boldsymbol{A}}_\perp \right|^2 - c^2 \left| i\boldsymbol{k} \times \tilde{\boldsymbol{A}}_\perp \right|^2 \right] + \tilde{\boldsymbol{j}}_\perp^* \cdot \tilde{\boldsymbol{A}}_\perp + \tilde{\boldsymbol{j}}_\perp \cdot \tilde{\boldsymbol{A}}_\perp^* \right\}. \tag{A.27}$$

By aiming at a comprehensive description of the dynamics of a system of N charged particles interacting with the electromagnetic field one also has to take into account the kinetic energy of the particles. The Lagrangian of this combined system is then given by [103]

$$\mathcal{L}[\{\boldsymbol{q}_i\}, \tilde{\boldsymbol{A}}_\perp; \{\dot{\boldsymbol{q}}_i\}, \partial_t \tilde{\boldsymbol{A}}_\perp] = \sum_{i=1}^{N} \frac{m_i}{2} \dot{\boldsymbol{q}}_i^2 - V_{\mathrm{C}} + \tilde{\mathcal{L}}_{\mathrm{em}}[\tilde{\boldsymbol{A}}_\perp; \{\dot{\boldsymbol{q}}_i\}, \partial_t \tilde{\boldsymbol{A}}_\perp], \tag{A.28}$$

assuming that there are no further external potentials acting on the particles. Furthermore, the argument of the Lagrangian $\tilde{\mathcal{L}}_{\mathrm{em}}$ accounts now explicitly for the dependence of the generalized velocities $\{\dot{\boldsymbol{q}}_i\}$ of the point charges due to the definition of the charge current $\tilde{\boldsymbol{j}}$ according to Eq. (A.15). The mass of the i-th particle is denoted by m_i and $\{\boldsymbol{q}_i\}$ represents a short-hand notation for the generalized coordinates $\boldsymbol{q}_1, \ldots, \boldsymbol{q}_N$ of the particles. Thereby, the generalized coordinate of each of the particles denotes an object in $\mathbb{R}^3$ in general. Similarly, $\{\dot{\boldsymbol{q}}_i\}$ denote the corresponding generalized velocities $\dot{\boldsymbol{q}}_1, \ldots, \dot{\boldsymbol{q}}_N$. Note that the Euler-Lagrange equations of $\mathcal{L}$ based on the generalized coordinates and velocities of the particles yield the Lorentz force law [103].

Since the entire subsequent discussion is exclusively concerned with the transverse part $\tilde{\boldsymbol{A}}_\perp$ of $\tilde{\boldsymbol{A}}$, the index $\perp$ is omitted in order to simplify the notation from now on.

A.3 Conjugate momenta of particle and field coordinates

In order to find the classical Hamilton function corresponding to the *Legendre transform* of the Lagrangian $\mathcal{L}$ (A.28) the momenta conjugate to the dynamical coordinates of the particles, $\boldsymbol{q}_i$, and fields, $\tilde{\boldsymbol{A}}$, need to be identified. According to classical mechanics there are as many conjugate momenta as dynamical coordinates entering the Lagrangian. In view of Eq. (A.28) the conjugate momentum of the ith charged particle is given by

$$\boldsymbol{p}_i = \frac{\partial \mathcal{L}}{\partial \dot{\boldsymbol{q}}_i} = m_i \dot{\boldsymbol{q}}_i + q_i \boldsymbol{A}(\boldsymbol{q}_i, t), \tag{A.29}$$

where the second term on the r.h.s. results from the $\dot{\boldsymbol{q}}_i$-dependence of the charge current (A.15) entering the contribution $\tilde{\mathcal{L}}_{\mathrm{em}}$ and thus full Lagrangian $\mathcal{L}$ according to Eqs. (A.27, A.28).

Similarly, the conjugate momenta for the fields $\boldsymbol{B}$, $\boldsymbol{E}$ are obtained by differentiation of the Lagrangian density $\tilde{L}_{\mathrm{em}}$, Eq. (A.24), with respect to each component of the generalized velocity $\partial_t \tilde{\boldsymbol{A}}_n^*$ [103]:

$$\tilde{\boldsymbol{\Pi}}_n(\boldsymbol{k}, t) = \frac{\partial \tilde{L}_{\mathrm{em}}}{\partial (\partial_t \tilde{\boldsymbol{A}}_n^*)} = \epsilon_0 \partial_t \tilde{\boldsymbol{A}}_n(\boldsymbol{k}, t), \tag{A.30}$$

where $n = 1, 2$ refers to the two directions of polarization, $\boldsymbol{\eta}_{1,\boldsymbol{k}}$ and $\boldsymbol{\eta}_{2,\boldsymbol{k}}$, according to the decomposition of the vector potential (A.18, A.19).

A.4 Helmholtz equation and normal coordinates

Before moving to the classical Hamiltonian of electrodynamics as the basis for the canonical quantization of the electromagnetic field, the calculation of the Euler-Lagrange equations for the classical field coordinates, $\tilde{\boldsymbol{A}}$ and $\partial_t \tilde{\boldsymbol{A}}$, shall clarify the main characteristics of classical radiation. The Euler-Lagrange equation can be obtained from the Lagrangian density in reciprocal space (A.24) by differentiation with respect to the generalized coordinates $\tilde{\boldsymbol{A}}_n^*$ and velocities $\partial_t \tilde{\boldsymbol{A}}_n^*$:

$$0 = \frac{\mathrm{d}}{\mathrm{d}t} \frac{\partial L_{\mathrm{em}}}{\partial(\partial_t \tilde{\boldsymbol{A}}_n^*)} - \frac{\partial L_{\mathrm{em}}}{\partial \tilde{\boldsymbol{A}}_n^*} = \epsilon_0 \left[\partial_t^2 + c^2 k^2 \right] \tilde{\boldsymbol{A}}_n(\boldsymbol{k}, t) - \tilde{\boldsymbol{j}}_n(\boldsymbol{k}, t). \tag{A.31}$$

Where the identity $\boldsymbol{k} \times (\boldsymbol{k} \times \tilde{\boldsymbol{A}}) = \boldsymbol{k}(\boldsymbol{k} \cdot \tilde{\boldsymbol{A}}) - (\boldsymbol{k} \cdot \boldsymbol{k})\tilde{\boldsymbol{A}}$ was applied. Using the gauge condition (A.16) and $\boldsymbol{k} \cdot \boldsymbol{k} = |k|^2$ yields the corresponding expression proportional to c^2 in Eq. (A.31). The application of the gauge condition in the derivation of Eq. (A.31) emphasizes the transverse character of the electromagnetic vector potential and thus according to Eqs. (A.7, A.8), of the fields $\tilde{\boldsymbol{B}}$, $\tilde{\boldsymbol{E}}$.

This inhomogeneous differential equation can also be obtained from Maxwell equations (A.1 – A.4), proving consistency of the Lagrangian formulation. The homogeneous part of (A.31), i.e. $\tilde{\boldsymbol{j}}_n = 0$, refers to the classical *wave equation* of electrodynamics in free space, referred to as the *Helmholtz equation*. The solutions for each polarization direction are of the form [103]

$$\tilde{\boldsymbol{A}}_n(\boldsymbol{k}, t) = \boldsymbol{\eta}_{n,\boldsymbol{k}} \tilde{\mathcal{A}}_k \left[\alpha_n(\boldsymbol{k}, t) + \alpha_n^*(-\boldsymbol{k}, t) \right], \tag{A.32}$$

where the normalization factor $\tilde{\mathcal{A}}_k$ is defined by

$$\tilde{\mathcal{A}}_k = \sqrt{\frac{\hbar}{2\epsilon_0 \omega_k}}, \tag{A.33}$$

anticipating the quantum properties of the radiation field, which are discussed in Chap. 2. In Eq. (A.33) $\omega_k = ck$ denotes the radiation frequency. In classical electrodynamics the normalization factor $\tilde{\mathcal{A}}_k$ is mostly absorbed into the *normal coordinates* [103]

$$\alpha_n(\boldsymbol{k}, t) = \alpha_n(\boldsymbol{k}) e^{-i\omega_k t}, \tag{A.34}$$

$$\alpha_n^*(-\boldsymbol{k}, t) = \alpha_n^*(-\boldsymbol{k}) e^{i\omega_k t}, \tag{A.35}$$

which are regarded as independent Fourier coefficients for each polarization direction n. The constraint (A.11), which connects an observable in the opposite half space $\tilde{\mathbb{H}}^3 = \{(k_x, k_y, k_z) | k_x < 0\}$ with its conjugate in $\mathbb{H}^3$, is not applicable to $\alpha_n(\boldsymbol{k}, t)$ and $\alpha_n^*(-\boldsymbol{k}, t)$ each by its own, i.e. $\alpha_n(-\boldsymbol{k}, t) \neq \alpha_n^*(\boldsymbol{k}, t)$. This is important to realize since $\alpha_n(\boldsymbol{k}, t)$ and $\alpha_n^*(-\boldsymbol{k}, t)$ are associated with the annihilation and creation operator during the procedure of canonical quantization. To obtain the solution to the Helmholtz equation in position

space, one can consider the Fourier transform of each component $\tilde{\boldsymbol{A}}_n(\boldsymbol{k}, t)$ according to

$$
\begin{aligned}
\boldsymbol{A}_n(\boldsymbol{q}, t) &= \frac{1}{2} \int_{\mathbb{H}^3} \frac{\mathrm{d}^3 k}{(2\pi)^2} \left[\tilde{\boldsymbol{A}}_n(\boldsymbol{k}, t) e^{i\boldsymbol{k} \cdot \boldsymbol{q}} + \tilde{\boldsymbol{A}}_n(-\boldsymbol{k}, t) e^{-i\boldsymbol{k} \cdot \boldsymbol{q}} \right] \\
&= \frac{1}{2} \boldsymbol{\eta}_{n,\boldsymbol{k}} \int_{\mathbb{H}^3} \frac{\mathrm{d}^3 k}{(2\pi)^2} \tilde{\mathcal{A}}_k \left\{ \left[\alpha_n(\boldsymbol{k}, t) + \alpha_n^*(-\boldsymbol{k}, t) \right] e^{i\boldsymbol{k} \cdot \boldsymbol{q}} + \left[\boldsymbol{k} \to -\boldsymbol{k} \right] e^{-i\boldsymbol{k} \cdot \boldsymbol{q}} \right\}.
\end{aligned}
\tag{A.36}
$$

By evaluating the integral over the complete reciprocal space, $\boldsymbol{A}_n$ takes the simplified form

$$
\boldsymbol{A}_n(\boldsymbol{q}, t) = \boldsymbol{\eta}_{n,\boldsymbol{k}} \int_{\mathbb{R}^3} \frac{\mathrm{d}^3 k}{(2\pi)^2} \tilde{\mathcal{A}}_k \left[\alpha_n(\boldsymbol{k}, t) e^{i\boldsymbol{k} \cdot \boldsymbol{q}} + \alpha_n^*(\boldsymbol{k}, t) e^{-i\boldsymbol{k} \cdot \boldsymbol{q}} \right].
\tag{A.37}
$$

In the source-free case ($\rho = 0$, $\boldsymbol{j} = 0$), the magnetic field (A.7) reads

$$
\tilde{\boldsymbol{B}}_n(\boldsymbol{k}, t) = i\boldsymbol{k} \times \tilde{\boldsymbol{A}}_n(\boldsymbol{k}, t) = \boldsymbol{e}_{\boldsymbol{k}} \times \boldsymbol{\eta}_{n,\boldsymbol{k}} \tilde{\mathcal{B}}_k \left[\alpha_n(\boldsymbol{k}, t) + \alpha_n^*(-\boldsymbol{k}, t) \right],
\tag{A.38}
$$

with $\tilde{\mathcal{B}}_k = ik\,\tilde{\mathcal{A}}_k$. For the electric field (A.8) one finds

$$
\tilde{\boldsymbol{E}}_n(\boldsymbol{k}, t) = -\partial_t \tilde{\boldsymbol{A}}_n(\boldsymbol{k}, t) = \boldsymbol{\eta}_{n,\boldsymbol{k}} \tilde{\mathcal{E}}_k \left[\alpha_n(\boldsymbol{k}, t) - \alpha_n^*(-\boldsymbol{k}, t) \right],
\tag{A.39}
$$

where $\tilde{\mathcal{E}}_k = i\omega_k\,\tilde{\mathcal{A}}_k$. Due to the outer product between the unit vector $\boldsymbol{e}_{\boldsymbol{k}}$ in propagation direction and the polarization vector $\boldsymbol{\eta}_{n,\boldsymbol{k}}$ the magnetic field at a given time t is perpendicular to the corresponding electric field $\tilde{\boldsymbol{E}}$ and the vector potential $\tilde{\boldsymbol{A}}$. Even though both fields $\tilde{\boldsymbol{B}}$, $\tilde{\boldsymbol{E}}$ lie at any time t in the plane normal to the direction of propagation $\boldsymbol{e}_{\boldsymbol{k}}$ as expected for transverse waves (see Fig. 2.1 for illustration).
According to Eq. (A.32) the generalized velocities and conjugate momenta $\tilde{\boldsymbol{\Pi}}_n$ (A.30) can be expressed in terms of the normal coordinates:

$$
\tilde{\boldsymbol{\Pi}}_n(\boldsymbol{k}, t) = \epsilon_0 \partial_t \tilde{\boldsymbol{A}}_n(\boldsymbol{k}, t) = -\epsilon_0 \boldsymbol{\eta}_{n,\boldsymbol{k}} \tilde{\mathcal{E}}_k \left[\alpha_n(\boldsymbol{k}, t) - \alpha_n^*(-\boldsymbol{k}, t) \right].
\tag{A.40}
$$

From there it directly follows

$$
\alpha_n(\boldsymbol{k}, t) = \frac{\tilde{A}_n(\boldsymbol{k}, t) + \frac{i}{\epsilon_0 \omega_k} \tilde{\Pi}_n(\boldsymbol{k}, t)}{2\tilde{\mathcal{A}}_k},
\tag{A.41}
$$

$$
\alpha_n^*(-\boldsymbol{k}, t) = \frac{\tilde{A}_n(\boldsymbol{k}, t) - \frac{i}{\epsilon_0 \omega_k} \tilde{\Pi}_n(\boldsymbol{k}, t)}{2\tilde{\mathcal{A}}_k},
\tag{A.42}
$$

where $\tilde{A}_n = \boldsymbol{\eta}_{n,\boldsymbol{k}} \cdot \tilde{\boldsymbol{A}}_n$ and $\tilde{\Pi}_n = \boldsymbol{\eta}_{n,\boldsymbol{k}} \cdot \tilde{\boldsymbol{\Pi}}_n$, as defined in Eq. (A.19). This relation between the normal coordinates and the field coordinates and conjugate momenta emphasizes the independence of the former.

A.5 The classical Hamilton function of electrodynamics

Knowing the conjugate momenta p_i and $\mathbf{\Pi}$ of the point charges and the fields $B, \tilde{E}$ yields the classical Hamiltonian of electrodynamics as the Legendre transform of $\mathcal{L}$ (A.28):

$$\mathcal{H} = \sum_{i=1}^{N} p_i \cdot \dot{q}_i + \int_{\mathbb{H}^3} \frac{\mathrm{d}^3 k}{(2\pi)^3} \left[\tilde{\mathbf{\Pi}} \cdot \partial_t \tilde{A}^* + \tilde{\mathbf{\Pi}}^* \cdot \partial_t \tilde{A} \right] - \mathcal{L}[\{q_i\}, \tilde{A}, \{\dot{q}_i\}, \partial_t \tilde{A}]. \qquad (A.43)$$

In view of Eq. (A.28) the classical Hamilton function can be decomposed into one part $\mathcal{H}_{\mathrm{matter}}$ containing all particle degrees of freedom and their interaction with the field, i.e.

$$\mathcal{H}[\{q_i\}, \{p_i\}; A, \mathbf{\Pi}] = \mathcal{H}_{\mathrm{matter}}[\{q_i\}, \{p_i\}; A] + \mathcal{H}_{\mathrm{em}}[A, \mathbf{\Pi}], \qquad (A.44)$$

Hence, the second part, $\mathcal{H}_{\mathrm{em}}$, describes the dynamics of the fields in the source-free space.

$$\begin{aligned}
\mathcal{H}_{\mathrm{matter}}[\{q_i\}, \{p_i\}; A] &= \sum_{i=1}^{N} \left[p_i \cdot \dot{q}_i - \frac{m_i}{2} \dot{q}_i^2 - \int_{\mathbb{H}^3} \frac{\mathrm{d}^3 k}{(2\pi)^3} \left\{ \tilde{j}^* \cdot \tilde{A} + \tilde{j} \cdot \tilde{A}^* \right\} \right] + V_{\mathrm{C}} \\
&= \sum_{i=1}^{N} \left[p_i \cdot \dot{q}_i - \frac{m_i}{2} \dot{q}_i^2 - \int_{\mathbb{R}^3} \mathrm{d}^3 q \, q_i \delta(q - q_i) \dot{q}_i \cdot A(q, t) \right] + V_{\mathrm{C}} \\
&= \sum_{i=1}^{N} \left[p_i \cdot \dot{q}_i - \frac{m_i}{2} \dot{q}_i^2 - q_i \dot{q}_i \cdot A(q_i, t) \right] + V_{\mathrm{C}}
\end{aligned}$$

$$(A.45)$$

where the Plancherel identity (E.3) is used in (A.45) to transform the integral from reciprocal to position space. By substituting the generalized velocities of the particles $\dot{q}_i$ according to (A.29) the Hamilton function of the particles is of the familiar form

$$\mathcal{H}_{\mathrm{matter}}[\{q_i\}, \{p_i\}; A] = \sum_{i=1}^{N} \frac{[p_i - q_i A(q_i, t)]^2}{2m_i} + V_{\mathrm{C}}. \qquad (A.46)$$

The remaining part describes the dynamics of the fields. Similar to the corresponding Lagrangian the Hamilton function

$$\mathcal{H}_{\mathrm{em}}[A, \mathbf{\Pi}] = \int_{\mathbb{R}^3} \frac{\mathrm{d}^3 k}{(2\pi)^3} H_{\mathrm{em}}[A, \mathbf{\Pi}] \qquad (A.47)$$

can be expressed in terms of the *Hamiltonian density* H_{em}. By using $(k \times \tilde{A}) \cdot (k \times \tilde{A}^*) = (k \cdot \tilde{A}^*)(k \cdot \tilde{A}) - (k \cdot k)(\tilde{A} \cdot \tilde{A}^*)$ in view of the gauge condition (A.16) in order to transform the second modulus squared in (A.27), the Hamiltonian density H_{em} reads:

$$H_{\mathrm{em}}[A, \mathbf{\Pi}] = \frac{\epsilon_0}{2} \left[\frac{1}{\epsilon_0^2} |\mathbf{\Pi}(k, t)|^2 + c^2 k^2 |\tilde{A}(k, t)|^2 \right]. \qquad (A.48)$$

Note that H_{em} is evaluated over the complete reciprocal space $\mathbb{R}^3$ for convenience. It is also possible to define the Hamiltonian density H'_{em} on the half space $\mathbb{H}^3$, where the

simple relation $H'_{\text{em}} = 2H_{\text{em}}$ is valid. By using the representation of field coordinates and conjugate momenta in terms of normal coordinates (A.32, A.40), the Hamiltonian density takes the form

$$H_{\text{em}} = \frac{\hbar\omega_k}{2} \sum_{n=1}^{2} \left[\alpha_n(\boldsymbol{k}, t)\alpha_n^*(\boldsymbol{k}, t) + \alpha_n^*(\boldsymbol{k}, t)\alpha_n(\boldsymbol{k}, t) \right], \qquad (A.49)$$

where $-\boldsymbol{k} \mapsto \boldsymbol{k}$ is applied on the last term of the r.h.s. in accordance with $\mathcal{H}_{\text{em}}$ being defined on the complete reciprocal space.

A.6 Poisson brackets of the field coordinates

The Hamiltonian formulation of the respective classical theory described by a set of $3N$ independent generalized coordinates q_i and conjugate momenta p_i comes along with the definition of the *Poisson bracket*:

$$\{f, g\}_{\boldsymbol{q},\boldsymbol{p}} = \sum_{i=1}^{3N} \left(\frac{\partial f}{\partial q_i}\frac{\partial g}{\partial p_i} - \frac{\partial f}{\partial p_i}\frac{\partial g}{\partial q_i} \right), \qquad (A.50)$$

where f, g denote functions of the classical phase-space coordinates. One can prove that the dynamics of a classical observable F is then determined by

$$\frac{\mathrm{d}F}{\mathrm{d}t} = \{F, \mathcal{H}\} + \frac{\partial F}{\partial t}, \qquad (A.51)$$

similar to the description of the dynamics of a quantum mechanical operator within the Heisenberg equation of motion (B.9). Furthermore by knowing the independent generalized coordinates and conjugate momenta of the N particles one can evaluate the Poisson brackets therefore,

$$\begin{aligned}
\{\boldsymbol{q}_{i_\alpha}, \boldsymbol{p}_{j_\beta}\}_{\boldsymbol{q},\boldsymbol{p}} &= \delta_{i,j}\delta_{\alpha,\beta}, \\
\{\boldsymbol{q}_{i_\alpha}, \boldsymbol{q}_{j_\beta}\}_{\boldsymbol{q},\boldsymbol{p}} &= \{\boldsymbol{p}_{i_\alpha}, \boldsymbol{p}_{j_\beta}\}_{\boldsymbol{q},\boldsymbol{p}} = 0,
\end{aligned} \qquad (A.52)$$

where $\alpha, \beta = x, y, z$ denotes the spacial degree of freedom of particle i and j, respectively. Any set of independent generalized coordinates and conjugate momenta satisfying similar relations is referred to as a set of *canonical* coordinates. Some authors [248] denote these relations (A.52) as *fundamental* Poisson brackets. In analogy the fundamental Poisson brackets for the independent components $\tilde{A}_n, \tilde{\Pi}_{\bar{n}}^*$ and normal coordinates $\alpha_n(\boldsymbol{k}, t)$, $\alpha_n^*(\boldsymbol{k}, t)$ of the fields [249] are given by

$$\{\tilde{A}_n(\boldsymbol{k}, t), \tilde{\Pi}_{\bar{n}}^*(\boldsymbol{k}', t)\}_{\boldsymbol{q},\boldsymbol{p}} = \delta_{n,\bar{n}}\delta(\boldsymbol{k} - \boldsymbol{k}'), \qquad (A.53)$$

$$\{\alpha_n(\boldsymbol{k}, t), \alpha_{\bar{n}}^*(\boldsymbol{k}', t)\}_{\boldsymbol{q},\boldsymbol{p}} = \frac{1}{i\hbar}\delta_{n,\bar{n}}\delta(\boldsymbol{k} - \boldsymbol{k}'), \qquad (A.54)$$

where $\boldsymbol{k}, \boldsymbol{k}' \in \mathbb{H}^3$. All other Poisson brackets constructed from $\tilde{A}_n$ and $\boldsymbol{\Pi}_{\bar{n}}^*$ are zero. Note that due to Coulomb gauge fixing (A.16) the representation of the Poisson bracket

in position space yields a slight modification concerning the δ distribution as comprehensively discussed in Ref. [103].

Appendix B

Dynamical representations of quantum mechanics

This section summarizes and defines the main characteristics of the three most commonly used dynamical pictures of quantum mechanics: the *Schrödinger picture*, the *Heisenberg picture* and the *interaction picture*[1]. Within the mathematical framework quantum mechanics is based on, all three representations are equivalent and interchangeable ways to describe the evolution of quantum systems in time. The transformation from one of these pictures into another one resembles a change of basis with respect to the time dependencies of the physical quantities. It is accomplished by means of a unitary transformation, called the *time-evolution operator* $\hat{U}(t', t)$.

Before discussing the formal differences between the three dynamical representations a few technical terms should be defined. Further details on this topic can be found in any textbook on quantum mechanics, e.g. Ref. [119].

According to the *postulates of quantum mechanics* [119] the state i of a quantum system is completely characterized by its *ket* $|\varphi_i\rangle$. This abstract quantity is an element of a linear vector space, known as the *Hilbert space* $\mathbb{H}$. In position-space representation the ket $|\varphi_i\rangle$ is associated with the quadratically integrable wave function $\varphi_i(\boldsymbol{q}) = \langle\boldsymbol{q}|\varphi\rangle_i$ of the quantum system. The measurable probability of finding the considered quantum particle at position q is given by the modulus squared of the wave function. Furthermore it is also postulated that every measurable physical *observable* $a_i \in \mathbb{R}$ is an eigenvalue of a linear self-adjoint or *Hermitian operator* $\hat{A}$ acting on the vector space of states $\mathbb{H}$, so that

$$\hat{A}|\varphi_i\rangle = a_i|\varphi_i\rangle, \tag{B.1}$$

where $\{|\varphi_i\rangle\,; i = 1, 2, \ldots, n\}$ represents the basis of the Hermitian operator $\hat{A}$. Equation (B.1) holds true for any most general quantum mechanical system, such as in the description of a spin-1/2 particle or a quantum harmonic oscillator. However there is one exception where the equivalence to Eq. (B.1) plays a superordinate role in physics:

In analogy to classical mechanics, the operator associated to the energy ϵ_i of a quantum system is referred to as the *Hamiltonian* $\hat{H}$. Thus, the corresponding eigenvalue equation reads

$$\hat{H}|\psi_i\rangle = \epsilon_i|\psi_i\rangle. \tag{B.2}$$

The basis states $\{|\phi_i\rangle\,; i = 1, 2, \ldots, n\}$ are called *stationary states*. This terminology refers

---

[1]The interaction picture is sometimes referred to as Dirac picture.

to the time independence of all related, measurable physical quantities such as the probability $\langle \boldsymbol{q}|\psi_i\rangle = |\psi_i(\boldsymbol{q})|$ of finding the quantum particle with energy ϵ_i at position $\boldsymbol{q}$. By contrast, measurable observables that result from a superposition of single stationary states $|\psi_i\rangle$ of a certain Hamiltonian, i.e.

$$|\varphi\rangle = \sum_i c_i |\psi_i\rangle,\tag{B.3}$$

have a distinct dependence on time. Thereby the Hamiltonian acts as the generator of the time-evolution of state vectors or operators mediated by the operator [119]

$$\hat{U}(t',t) = e^{-\frac{i}{\hbar}\hat{H}(t'-t)}.\tag{B.4}$$

The time-dependent representation of the state vectors $|\varphi_i\rangle$ or operators $\hat{F}$ depend on the choice of dynamic representation which is discussed in the following.

Though not mandatory it is convenient [119] to start at the Schrödinger picture, which is also the representation used throughout this thesis.

B.1 Schrödinger picture

The main characteristics of the Schrödinger picture are [119]

1. the time dependence is completely carried by the state vectors $|\psi(t)\rangle_{\mathrm{S}}$,

2. all operators are time independent $\hat{F}_{\mathrm{S}} = \mathrm{const.}$, when not explicitly time-dependent.

The evolution of the state i from an initial time t to a final time $t' > t$ is provided by the time-evolution operator $\hat{U}(t',t)$ in the following manner

$$|\psi(t')\rangle_{i,\mathrm{S}} = \hat{U}(t',t)\,|\psi_i(t)\rangle_{\mathrm{S}}.\tag{B.5}$$

By combining Eqs. (B.2, B.4, B.5) the dynamics of a stationary state $|\psi(t)\rangle_{i,\mathrm{S}}$ is determined by the time-dependent version of the Schrödinger equation

$$\hat{H}_{\mathrm{S}}\,|\psi_i(t)\rangle_{\mathrm{S}} = i\hbar\partial_t\,|\psi_i(t)\rangle_{\mathrm{S}}.\tag{B.6}$$

Since $\{|\psi_i(t)\rangle_{\mathrm{S}}\,; i = 1, 2, \ldots, n\}$ denotes a complete set of basis states of the Hamiltonian $\hat{H}$ any arbitrary, time-dependent state $|\varphi(t)\rangle$ can be constructed according to Eq. (B.3).

B.2 Heisenberg picture

The main characteristics of the Heisenberg picture can be considered as inverse to the Schrödinger picture with respect to the formal time dependence of the physical quantities [119]:

1. all state vectors are time independent $|\psi\rangle_{\mathrm{H}} = \mathrm{const.}$,

2. the time dependence is completely carried by the operators $\hat{F}_{\mathrm{H}}(t)$.

Therefore stationary states are truly independent of the time. The evolution of an operator $\hat{F}_{\mathrm{H}}(t)$ from an initial time $t_{\mathrm{i}} = 0$ to a final time t_{f} can be derived from Eq. (B.5) by calculating the expectation value of an operator $\hat{F}_{\mathrm{S}}$ in the Schrödinger picture

$$_{\mathrm{S}}\langle\psi(t)|\,\hat{F}_{\mathrm{S}}\,|\psi(t)\rangle_{\mathrm{S}} = {}_{\mathrm{S}}\langle\psi(0)|\,\hat{U}^{\dagger}(t,0)\hat{F}_{\mathrm{S}}\hat{U}(t,0)\,|\psi(0)\rangle_{\mathrm{S}}\,, \tag{B.7}$$

stating that

$$\hat{F}_{\mathrm{H}}(t) = \hat{U}^{\dagger}(t,0)\hat{F}_{\mathrm{S}}\,\hat{U}(t,0). \tag{B.8}$$

Equivalent to the dynamical description of state vectors by the time-dependent Schrödinger equation (B.6) in the Schrödinger picture the dynamics of the time-dependent operator $\hat{F}_{\mathrm{H}}(t)$ in the Heisenberg representation is determined by

$$\frac{d}{dt}\hat{F}_{\mathrm{H}}(t) = \frac{i}{\hbar}\left[\hat{H}_{\mathrm{S}},\hat{F}_{\mathrm{H}}(t)\right] + \partial_{t}\hat{F}_{\mathrm{H}}(t), \tag{B.9}$$

which is known as the *Heisenberg equation of motion*. The canonical commutator $[.,.] = [.,.]_{-}$ is defined in Eq. (C.40). Heisenberg's equation of motion is formally similar to formulation of the equation of motion for a classical observable (A.51).

B.3 Interaction picture

The interaction picture can be regarded as the interface between Schrödinger and Heisenberg picture in a way that both, the operators and the states, formally carry time dependence [119]. Usually it is applied for quantum systems with a decomposable Hamiltonian

$$\hat{H}_{\mathrm{S}}(t) = \hat{H}_{\mathrm{S},0} + \hat{V}_{\mathrm{S}}(t), \tag{B.10}$$

where ideally $\hat{H}_{\mathrm{S},0}$ is exactly solvable. Furthermore, $\hat{H}_{\mathrm{S},0}$ shall not explicitly depend on time. In the most general case $\hat{V}_{\mathrm{S}}(t)$ can be understood as a perturbation or interaction term which might explicitly depend on time and which does not necessarily commute with $\hat{H}_{\mathrm{S},0}$, i.e. $[\hat{H}_{\mathrm{S},0},\hat{V}_{\mathrm{S}}(t)] \neq 0$. The aim is to find a solution to the corresponding time-dependent Schrödinger equation,

$$\hat{H}_{\mathrm{S}}\,|\psi_{i}(t)\rangle_{\mathrm{S}} = \left(\hat{H}_{\mathrm{S},0} + \hat{V}_{\mathrm{S}}(t)\right)|\psi_{i}(t)\rangle_{\mathrm{S}} = i\hbar\partial_{t}\,|\psi_{i}(t)\rangle_{\mathrm{S}}\,. \tag{B.11}$$

By defining a new time-evolution operator generated only from $\hat{H}_{\mathrm{S},0}$,

$$\hat{u}(t) = e^{\frac{i}{\hbar}\hat{H}_{\mathrm{S},0}t}, \tag{B.12}$$

one can define a state vector in the interaction picture as

$$|\psi_{i}(t)\rangle_{\mathrm{I}} = \hat{u}(t)\,|\psi_{i}(t)\rangle_{\mathrm{S}}\,. \tag{B.13}$$

Likewise, the interaction picture representation of a potentially explicit time-dependent operator $\hat{O}(t)$ is defined by

$$\hat{O}_{\mathrm{I}}(t) = \hat{u}^{\dagger}(t)\hat{O}\hat{u}(t). \tag{B.14}$$

Within the interaction picture one as able to describe the time-evolution of a state vector $|\psi_i(t)\rangle_{\mathrm{I}}$ only by regarding the perturbation term $\hat{V}_{\mathrm{I}}(t)$, i.e.

$$i\hbar\frac{\mathrm{d}}{\mathrm{d}t}|\psi_i(t)\rangle_{\mathrm{I}} = \hat{V}_{\mathrm{I}}(t)|\psi_i(t)\rangle_{\mathrm{I}}. \tag{B.15}$$

This directly follows from the total derivative of $|\psi_i(t)\rangle_{\mathrm{I}}$ with respect to t as easily proven in view of Eq. (B.13) and by application of the Schrödinger equation, Eq. (B.11).

Furthermore one is able to derive a differential equation equivalent to Eq. (B.15) for the interaction picture representation of time-evolution operator $\hat{U}(t',t)$ as defined by Eq. (B.4) in consideration of the corresponding Hamiltonian $\hat{H}(t)$, Eq. (B.10). This directly follows from inserting

$$|\psi_i(t')\rangle_{\mathrm{I}} = \hat{u}(t')\hat{U}(t',t)|\psi_i(t)\rangle_{\mathrm{S}} = \hat{U}_{\mathrm{I}}(t',t)|\psi_i(t)\rangle_{\mathrm{I}} \tag{B.16}$$

into Eq. (B.17):

$$i\hbar\frac{\mathrm{d}}{\mathrm{d}t'}\hat{U}_{\mathrm{I}}(t',t) = \hat{V}_{\mathrm{I}}(t')\hat{U}_{\mathrm{I}}(t',t). \tag{B.17}$$

B.4   Rotating frame in quantum optics

Especially in the field of quantum optics the explicitly time-independent Schrödinger picture representation of a Hamiltonian or parts of it are referred to as the *rotating frame*. The relation between the interaction picture and the Schrödinger picture representation might sometimes cause confusion especially in this field. This results from the naturally time-dependent appearance of the photonic operators (2.18) after canonically quantizing the classical radiation field, as discussed in Sec. 2. Furthermore in many quantum optics textbooks the distinction between Schrödinger and interaction picture is rarely found. During this thesis the following convention is applied: If one defines this time-dependent occurrence of the related Hamiltonian as its interaction picture representation one finds the, ideally time independent, Schrödinger picture representation by the inverse of the transformation (B.14). The following, rather explicitly discussed, example shall avoid confusion concerning the time dependence of the considered light-matter interaction Hamiltonian during this thesis.

B.4.1   Quantum Rabi Hamiltonian

Suppose a two-level atom interacting with a cavity mode, known as the *Rabi Hamiltonian* [122–124] as found in various textbooks [120]

$$\hat{H}(t) = \hat{H}_{\mathrm{cav}} + \hat{H}_{\mathrm{atom}} + \hat{H}_{\mathrm{int}}(t), \tag{B.18}$$

where each of the three contributions is defined as

$$\hat{H}_{\mathrm{cav}} \quad = \hbar\omega_0\hat{a}^\dagger\hat{a}, \tag{B.19}$$

$$\hat{H}_{\mathrm{atom}} = \hbar\Omega\,\hat{s}_z, \tag{B.20}$$

$$\hat{H}_{\mathrm{int}}(t) = g(\hat{s}_+ + \hat{s}_-)[\hat{a}^\dagger(t) + \hat{a}(t)]. \tag{B.21}$$

Thereby ω_0 denotes the frequency of the radiation mode. Likewise, Ω denotes the transition frequency of the two-level system, which couples with a strength g to the radiation mode. As introduced in Sec. 3.1, $\hat{s}_i$, $i = zm\pm$ denote spin matrices. The time-dependence of creation and annihilation operator, resulting naturally from canonical quantization, reads

$$\hat{a}^\dagger(t) = \hat{a}^\dagger e^{-i\omega_0 t}, \quad \hat{a}(t) = \hat{a}e^{i\omega_0 t}, \tag{B.22}$$

where $\hat{a}^\dagger, \hat{a}$ are time-independent operators, i.e. $\partial_t \hat{a}^\dagger = \partial_t \hat{a} = 0$. According to the previous discussion $\hat{a}^\dagger, \hat{a}$ correspond to the Schrödinger picture as proven during the following. Details on the properties of bosonic creation and annihilation operator $\hat{a}^\dagger, \hat{a}$ are discussed in Sec. C.2. According to the previous consideration $\hat{H}$ is represented in the interaction picture. This is demonstrated by applying the inverse of the transformation defined in Eq. (B.14) on $\hat{H}$. Since all time dependence in the Hamiltonian is assigned to the photonic degree of freedom, it is sufficient to define

$$\hat{u}(t) = e^{\frac{i}{\hbar}\hat{H}_{\mathrm{cav}}t}. \tag{B.23}$$

According to $[\hat{H}_{\mathrm{cav}}, \hat{H}_{\mathrm{cav}}] = [\hat{H}_{\mathrm{cav}}, \hat{H}_0] = 0$, the operators $\hat{H}_{\mathrm{cav}}$ and $\hat{H}_{\mathrm{atom}}$ remain invariant under transformation with respect to $\hat{u}(t)$. Along with this, the Rabi Hamiltonian in Schrödinger picture is obtained from the transformation of the interaction part only, i.e.

$$\hat{H}_{\mathrm{S}} = \hat{u}(t)\hat{H}(t)\hat{u}^\dagger(t) = \hat{H}_{\mathrm{cav}} + \hat{H}_{\mathrm{atom}} + \hat{H}_{S,\mathrm{int}}, \tag{B.24}$$

whereas the interaction part explicitly reads

$$\hat{H}_{S,\mathrm{int}} = \hat{u}(t)\hat{H}_{\mathrm{int}}(t)\hat{u}^\dagger(t) = g(\hat{s}_+ + \hat{s}_-)\,\hat{u}(t)[\hat{a}^\dagger(t) + \hat{a}(t)]\hat{u}^\dagger(t) \tag{B.25}$$

Allowing for the *Baker-Campbell-Hausdorff formula* [243–245]

$$e^{\hat{A}}\hat{B}e^{-\hat{A}} = \sum_{i=0}^{\infty} \frac{[\hat{A}, \hat{B}]_i}{i!}, \quad \text{where } [\hat{A}, \hat{B}]_i = [\hat{A}, [\hat{A}, \hat{B}]_{i-1}], \text{ and } [\hat{A}, \hat{B}]_0 = \hat{B}, \tag{B.26}$$

one finds in view of the commutation-relation of $\hat{a}^\dagger, \hat{a}$ (C.41) for the creation and annihilation operators in Eq. (B.25) in the Schrödinger picture

$$\hat{a}_{\mathrm{S}}^\dagger = e^{i\omega_0 \hat{a}^\dagger \hat{a} t}\,\hat{a}^\dagger(t)e^{-i\omega_0 \hat{a}^\dagger \hat{a} t} = \sum_{k=0}^{\infty} \frac{(i\omega_0 t)^k}{k!}\ \hat{a}^\dagger(t) = e^{i\omega_0 t}\ \hat{a}^\dagger(t), \tag{B.27}$$

$$\hat{a}_{\mathrm{S}} = e^{i\omega_0 \hat{a}^\dagger \hat{a} t}\,\hat{a}(t)\ e^{-i\omega_0 \hat{a}^\dagger \hat{a} t} = \sum_{k=0}^{\infty} \frac{(-i\omega_0 t)^k}{k!}\ \hat{a}(t) = e^{-i\omega_0 t}\ \hat{a}(t). \tag{B.28}$$

Application of Eq. (B.22) results in time-independent operators $\hat{a}^\dagger, \hat{a}$. Consequently, the time-independent Rabi Hamiltonian in Schrödinger picture explicitly reads

$$\hat{H}_{\mathrm{S}} = \hbar\omega_0 \hat{a}^\dagger \hat{a} + \hbar\Omega\,\hat{s}_z + g(\hat{s}_+ + \hat{s}_-)(\hat{a}_{\mathrm{S}}^\dagger + \hat{a}_{\mathrm{S}}). \tag{B.29}$$

The example can be extended to any Hamiltonian with similar appearance of the photonic operators, so that the transformation from interaction to Schrödinger picture is also

valid in the case of the light-matter interaction term (5.47) considered during this thesis. Furthermore, one can easily prove that also powers of $[\hat{a}^\dagger(t) + \hat{a}(t)]$, as they enter the diamagnetic term (2.49), can be analogously transformed into the time-independent Schrödinger representation. Since the Schrödinger picture is the preferred one in this thesis, the indices $_S$ are dropped.

B.4.2 Rotating-wave approximation and the Jaynes-Cummings model

The Heisenberg picture of the time-independent Rabi Hamiltonian (B.29) gives some further insights into dynamics of the interaction term. By application of the unitary transformation (B.8) generated by the full Rabi Hamiltonian one obtains

$$\hat{H}_H = \hat{H}_{\text{cav}} + \hat{H}_{\text{atom}} + \hat{H}_{H,\text{int}}(t), \tag{B.30}$$

where $\hat{H}_{\text{cav}}$ and $\hat{H}_{\text{atom}}$ remain unaffected by the transformation. Hence they are given by Eqs. (B.19, B.20). The interaction part in Heisenberg representation is obtained by means of similar considerations than made in Eqs. (B.27, B.28), whereas now also the atomic operators have to be transformed, resulting in

$$\hat{H}_{H,\text{int}}(t) \propto [\hat{s}_+(t) + \hat{s}_-(t)][\hat{a}^\dagger(t) + \hat{a}(t)] = [\hat{s}_+ e^{-i\hbar\Omega t} + \hat{s}_- e^{i\hbar\Omega t}][\hat{a}^\dagger e^{-i\hbar\omega_0 t} + \hat{a} e^{i\hbar\omega_0 t}]. \tag{B.31}$$

By expanding the brackets on the r.h.s. it becomes most obvious in the case of resonance, i.e. $\Omega = \omega_0$, that the so-called counter-rotating terms

$$\hat{s}_+ \hat{a}^\dagger e^{-i\hbar(\Omega+\omega_0)t} \overset{\Omega=\omega_0}{=} \hat{s}_+ \hat{a}^\dagger e^{-2i\hbar\omega_0 t}, \quad \hat{s}_- \hat{a} e^{i\hbar(\Omega+\omega_0)t} \overset{\Omega=\omega_0}{=} \hat{s}_- \hat{a} e^{2i\hbar\omega_0 t} \tag{B.32}$$

oscillate significantly faster than the so-called energy-conserving terms

$$\hat{s}_+ \hat{a} e^{-i\hbar(\Omega-\omega_0)t} \overset{\Omega=\omega_0}{=} \hat{s}_+ \hat{a}, \quad \hat{s}_- \hat{a}^\dagger e^{i\hbar(\Omega-\omega_0)t} \overset{\Omega=\omega_0}{=} \hat{s}_- \hat{a}^\dagger. \tag{B.33}$$

As a consequence, under time average and in the small-coupling regime [125–127], the dominant contribution to the dynamics of the system originates from the latter. Neglecting the counter-rotating terms is called *rotating-wave approximation* [120] and leads from the quantum Rabi model to the *Jaynes-Cummings model* [121]:

$$\hat{H}_{\text{JC}} = \hbar\omega_0 \hat{a}^\dagger \hat{a} + \hbar\Omega\, \hat{s}_z + g(\hat{s}_+ \hat{a} + \hat{s}_- \hat{a}^\dagger). \tag{B.34}$$

Appendix C

Many-body quantum systems

Investigations on quantum effects emerging from the interaction of a variety of indistinguishableparticles, such as the collective phenomena of the superradiant phase transition, require an extension of the standard formulation of quantum mechanics as a single-particle theory. Thereby the concept of indistinguishability of identical particles defines one of the essential differences between classical and quantum mechanics (cf. App C). Different from classical mechanics quantum mechanics assumes impossibility of identifying one specific particle in a group of N identical quantum particles without influencing its state [119]. This assumption stays in alignment with experimental observations up to this day.

C.1 From indistinguishability to bosons and fermions

The mathematical framework for a theory of $N > 1$ indistinguishable particles is provided by a Hilbert space $\mathbb{H}_N$ constructed as the tensor product of single-particle Hilbert spaces $\mathbb{H}$

$$\mathbb{H}_N = \bigotimes_{\alpha=1}^{N} \mathbb{H}. \tag{C.1}$$

Thereby the basis of the product space $\mathbb{H}_N$ is given by the tensor product of orthonormal basis states $\{|\psi_i\rangle\}$ assigned to each single-particle Hilbert space $\mathbb{H}$, reading

$$\left\{ |\Psi_A\rangle = |\psi_{i_1}, \psi_{i_2}, \ldots, \psi_{i_N}\rangle = \bigotimes_{\alpha=1}^{N} |\psi_{i_\alpha}\rangle \right\}. \tag{C.2}$$

The numbering superscript indices in Eq. (C.2) are applied for book-keeping reasons rather than ordering at this stage. The dimension of the many-body basis set $\{|\Psi_A\rangle\}$ (C.2) is determined by the dimension $\dim(\{|\psi_i\rangle\})$ of each single-particle basis set and the number of particles N, i.e. $\dim(\{|\Psi_A\rangle\}) = N \cdot \dim(\{|\psi_i\rangle\})$, where $\dim(\{|\psi_i\rangle\})$. At some passages during the following the index i labeling the i-th component of the single-particle basis $\{|\psi_i\rangle\}$ might be dropped for reasons of simplicity. Therefore the short-hand notation

$$|\psi_{i_1}, \psi_{i_2}, \ldots, \psi_{i_N}\rangle = |\psi^1, \psi^2, \ldots, \psi^N\rangle \tag{C.3}$$

is used by keeping in mind that each ψ on the r.h.s. represents a complete set of single-particle basis states.

Furthermore, the construction of a product space $\mathbb{H}_N$ is not limited to a finite number of particles N.

For reasons of simplicity during the following it is assumed that each single-particle basis $\{|\psi_i\rangle\}$ describes a complete set of orthonormalized eigenvectors of a given single-particle Hamiltonian $\hat{H}$, i.e.

$$\hat{H}|\psi_i\rangle = \epsilon_i|\psi_i\rangle, \tag{C.4}$$

$$\langle\psi_i|\psi_j\rangle = \delta_{i,j}, \tag{C.5}$$

$$\sum_i |\psi_i\rangle\langle\psi_i| = 1. \tag{C.6}$$

Consequently, the product basis $\{|\Psi_A\rangle\}$ (C.2) represents a complete set of orthonormalized eigenvectors to the corresponding many-body Hamiltonian of N indistinguishable particles

$$\hat{\mathcal{H}} = \sum_{\alpha=1}^{N} \hat{H}_\alpha, \tag{C.7}$$

so that the many-body equivalent to Eqs. (C.4–C.6) read

$$\hat{\mathcal{H}}|\Psi_A\rangle = E_A\Psi_A, \tag{C.8}$$

$$\langle\Psi_A|\Psi_B\rangle = \delta_{A,B}, \tag{C.9}$$

$$\sum_A |\Psi_A\rangle\langle\Psi_A| = 1. \tag{C.10}$$

It might be useful for the understanding of the following discussion to explicit execute the summation concerning the completeness of the basis $\{|\Psi_A\rangle\}$ yielding Eq. (C.10) to read

$$
\begin{aligned}
1 = \sum_A |\Psi_A\rangle\langle\Psi_A| &= \sum_{i_1,i_2,\ldots,i_N} |\psi_{i_1},\psi_{i_2},\ldots,\psi_{i_N}\rangle\langle\psi_{i_1},\psi_{i_2},\ldots,\psi_{i_N}| \\
&= \sum_{i_1,i_2,\ldots,i_N} \bigotimes_{\alpha=1}^{N} |\psi_{i_\alpha}\rangle \bigotimes_{\alpha=1}^{N} \langle\psi_{i_\alpha}|,
\end{aligned}
\tag{C.11}
$$

where each sum over i_β, $\beta = 1, 2, \ldots, N$, denotes the summation over the corresponding complete set of single-particle basis states $\{|\psi_{i_\beta}\rangle\}$.

C.1.1 The symmetric group S^N on $\mathbb{H}_N$

According to abstract algebra, one can define the symmetric group S^N on the set of, yet disordered, indices $\{1, 2, \ldots, N\}$ [250]. Thereby each element $\sigma \in S^N$ of the symmetric group is a unique permutation operation performed on the set of indices. Accordingly, there is a linear unitary map $\hat{\mathcal{P}}_\sigma : \mathbb{H}_N \to \mathbb{H}_N$ assigned to each $\sigma \in S^N$ which is uniquely defined by its action an a state vector

$$\hat{\mathcal{P}}_\sigma |\psi^1, \psi^2, \ldots, \psi^N\rangle = |\psi^{\sigma(1)}, \psi^{\sigma(2)}, \ldots, \psi^{\sigma(N)}\rangle. \tag{C.12}$$

Thereby, each permutation operation $\sigma \in S^N$ can be obtained from the composition of transpositions [250], defined as the exchange of two elements of the set $\{1, 2, \ldots, N\}$. Depending on the number $M(\sigma)$ of transpositions one can define two classes of permutations $\sigma \in S^N$ according to their parity. Permutations that result from an even number $M(\sigma)$ of transpositions are referred to as even permutations. By contrast, permutations composited from an odd number of transpositions are called odd permutations. Likewise one can define the sign of a permutation by its parity according to

$$\mathrm{sgn}(\sigma) = (-1)^{M(\sigma)} = \begin{cases} +1, & \text{for even } \sigma, \\ -1, & \text{for odd } \sigma. \end{cases} \tag{C.13}$$

C.1.2 Exchange symmetry

As a consequence of the concept of indistinguishability of N identical quantum particles the physical state of the system needs to remain unaffected by the permutation of indices attached to the particles according to Eq. (C.2).

This is known as *exchange symmetry* and it is exactly provided by the completely symmetric and anti-symmetric state vectors as it becomes obvious during the following discussion. Furthermore, any Hermitian single-particle operator $\hat{A}$ and thus in turn any many-body operator composited therefrom similar to Eq. (C.7), is regarded to be invariant under the action of a permutation operator $\hat{\mathcal{P}}_\sigma$, i.e.

$$\hat{A} = \hat{\mathcal{P}}_\sigma^\dagger \hat{A} \hat{\mathcal{P}}_\sigma. \tag{C.14}$$

C.1.3 Totally symmetric and anti-symmetric states: bosons and fermions

There exist two distinct irreducible representations of the symmetric group on $\{1, 2, \ldots, N\}$, corresponding to a completely symmetric and a completely antisymmetric arrangement of the set of indices [115, 250]. Therefore, a basis vector $|\Psi_A\rangle^+ \in \mathbb{H}_N$ that remains invariant under an arbitrary permutation $\sigma \in S^N$,

$$\hat{\mathcal{P}}_\sigma |\Psi_A\rangle^+ = |\Psi_A\rangle^+, \tag{C.15}$$

is referred to as *completely symmetric*. All completely symmetric basis vectors span the symmetric Hilbert subspace $\mathbb{H}_N^+ \subset \mathbb{H}_N$. By contrast a basis vector $|\Psi_A\rangle^- \in \mathbb{H}_N$ fulfilling

$$\hat{\mathcal{P}}_\sigma |\Psi_A\rangle^- = \mathrm{sgn}(\sigma) |\Psi_A\rangle^- \tag{C.16}$$

is called *completely anti-symmetric*. Analogous the anti-symmetric Hilbert subspace $\mathbb{H}_N^- \subset \mathbb{H}_N$ is spanned by all completely anti-symmetric state vectors. The remaining part of the N-particle Hilbert space is spanned by states with mixed permutation symmetry and is denoted with $\mathbb{H}_N^{\mathrm{mix}} \subset \mathbb{H}_N$. The direct sum of all three subspaces reassembles the complete N-particle Hilbert space $\mathbb{H}_N$, i.e.

$$\mathbb{H}_N = \mathbb{H}_N^+ \oplus \mathbb{H}_N^- \oplus \mathbb{H}_N^{\mathrm{mix}}. \tag{C.17}$$

As discussed during the following, the symmetric and anti-symmetric Hilbert subspace are of superordinate interest in physics due to their association with elementary particles.

Defining the symmetrization and anti-symmetrization operator [115, 119], respectively

$$\hat{\mathcal{P}}_N^+ = \frac{1}{\sqrt{N! \prod_i (n_i!)}} \sum_{\sigma \in S^N} \hat{\mathcal{P}}_\sigma, \tag{C.18}$$

$$\hat{\mathcal{P}}_N^- = \frac{1}{N!} \sum_{\sigma \in S^N} \text{sgn}(\sigma) \hat{\mathcal{P}}_\sigma, \tag{C.19}$$

each acting as projectors on $\mathbb{H}_N^+$ and $\mathbb{H}_N^-$, respectively. The normalization factor of the symmetrization operator differs from the normalization of the anti-symmetrized equivalent. This accounts precisely for the properties of symmetrization. The claim for a symmetric wave function with respect to permutation of particle indices is in accordance with one or more particles carrying the same index and thus in turn occupying the same quantum state i. n_i denotes the occupation of the respective single-particle state. Consequently one has to normalize the completely symmetrized wave function in this case as denoted in (C.18). Thereby, the sum over all single-particle occupation numbers n_i has to satisfy $\sum_i n_i = N$. Similar considerations on the anti-symmetrized projector precisely yield the normalization given in Eq. (C.19). This is due to the single-particle occupation being restricted to $n_i \leq 1$ within the claim for anti-symmetric properties of the wave function, known as *Pauli-exlusion principle* which is outlined in Subsec. C.1.4.

Both projectors (C.18, C.19) reflect the orthogonality of the Hilbert-space decomposition (C.17) by their orthogonality with respect to each other, i.e. $\hat{\mathcal{P}}_N^+ \hat{\mathcal{P}}_N^- = 0$ [115, 119]. The application of the symmetrization or anti-symmetrization operator on a basis vector $|\Psi_A\rangle \in \mathbb{H}_N$ yields a completely symmetrized or anti-symmetrized basis vector [1] of $\mathbb{H}^+$ and $\mathbb{H}^-$, respectively,

$$|\Psi_A\rangle^\pm = \hat{\mathcal{P}}_N^\pm |\Psi_A\rangle, \tag{C.20}$$

whereas the formulation of an equivalent to Eqs. (C.8–C.11) for $\{|\Psi_A\rangle^\pm\}$ is obvious. Particles described by a completely symmetrized state vector are called *bosons*, whereas one refers to particles with a anti-symmetric state vector as *fermions*.[2]

C.1.4 Pauli-exclusion principle

As a logical consequence of the completely anti-symmetric properties of the state vector associated with system of N indistinguishable fermions, it follows that two or more fermions cannot occupy the same single-particle state k at once. This becomes obvious by considering a completely the anti-symmetrized state vector

$$|\psi^1, \psi^2, \ldots, \psi_{k_\alpha}, \ldots, \psi_{l_\beta}, \ldots, \psi^N\rangle^- = -|\psi^1, \psi^2, \ldots, \psi_{l_\beta}, \ldots, \psi_{k_\alpha}, \ldots, \psi^N\rangle^-. \tag{C.21}$$

---

[1] The anti-symmetrized basis vector can also be represented in terms of a determinant, called the *Slater determinant* [251].

[2] There is a species of quasiparticles, called anyons [252, 253], which are neither described by a symmetrized nor an anti-symmetrized state vector. Therefore states characterizing an anyon are an element of the subspace of mixed states $\mathbb{H}_N^{\text{mix}}$ (C.17). Referring to literature, a discussion of these kinds of quasiparticles would go far beyond the scope of this thesis.

Assuming equality of the single-particle states k_α and l_β, i.e. $|\psi_{k_\alpha}\rangle = |\psi_{l_\beta}\rangle$ Eq. (C.21) is only fulfilled if

$$\left.|\psi^1, \psi^2, \ldots, \psi_{k_\alpha}, \ldots, \psi_{l_\beta}, \ldots, \psi^N\rangle^-\right|_{k_\alpha = l_\beta} = 0. \tag{C.22}$$

Therefore each fermion in the system has to differ from another one in at least one quantum number.

C.1.5 Spin-statistics theorem

Anticipating the different quantum statistics inherent to bosons and fermions, the spin-statistics theorem provides a theoretical formulation [254] of the following empirical observation [255]:

1. Particles with an **integer spin** follow a quantum statistics associated with the properties of a **symmetric state vector**, referred to as *Bose-Einstein statistics*.

2. Particles with a **half-integer spin** follow a quantum statistics associated with the properties of an **anti-symmetric state vector**, referred to as *Fermi-Dirac statistics*.

In different word, it states that bosons always have an integer spin, whereas fermions are particles with half-integer spin.

C.2 Second quantization

The more reasonable an approach based on state vectors is in single-particle quantum mechanics the more cumbersome it becomes in a many-body formulation of quantum theory, especially in situations where the number of indistinguishable particles is large. The formalism of second quantization provides a more elegant, transparent and efficient way to account for the indistinguishability and symmetry of the bosonic and fermionic many-body systems.

C.2.1 Fock states and Fock space

The basic quantity in this formalism is the occupation number n_i of a single-particle state i. Thereby one can set up an occupation-number representation of basis vectors, referred to as *Fock states*, which fully characterize symmetrized or anti-symmetrized basis vector $|\Psi_A\rangle^\pm$ according to their occupation n_i of a single-particle state i, i.e.

$$|\Psi_A\rangle_N^\pm = |n_1, n_2, \ldots\rangle_N^\pm, \tag{C.23}$$

where N denotes the number of indistinguishable particles. From the orthonormalization of the single-particles basis $\{|\psi_i\rangle\}$ directly follows the orthonormalization of the Fock basis states, i.e.

$$_N^\pm\langle n_1, n_2, \ldots | \bar{n}_1, \bar{n}_2, \ldots\rangle_{\bar{N}}^\pm = \delta_{N,\bar{N}} \prod_i \delta_{n_i, \bar{n}_i}. \tag{C.24}$$
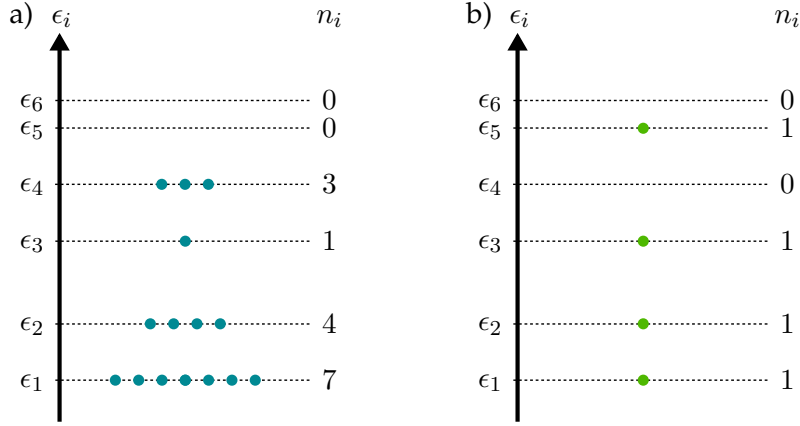
FIGURE C.1: Occupation scheme of a a) bosonic and b) fermionic many-body system. The number n_i of indistinguishable bosonic paticles (blue dots) occupying a single-particle state i with energy ϵ_i is not restricted due to their symmetrized state vector. However, the fermionic occupation n_i (green dots) of a single-particle state i is restricted to one at most.

Accordingly, the resolution of identity in this basis reads

$$\sum_{\substack{n_1, n_2, \dots \\ \sum_i n_i = N}} |n_1, n_2, \dots\rangle_N^{\pm}{}_N^{\pm}\langle n_1, n_2, \dots| = 1. \tag{C.25}$$

As a consequence of their permutation symmetry and depicted by Fig. C.1, the occupation of single-particle states in case of bosons with identical quantum numbers differ quite fundamentally from those of fermions with identical quantum numbers. Whereas the occupation of a single-particle state i is not restricted in the former case, fermions are allowed to occupy a single particle state i only once accounting for the Fermi-exclusion principle, i.e.

$$n_i = \begin{cases} 0, 1, 2, \dots & \text{for bosons,} \\ 0, 1 & \text{for fermions.} \end{cases} \tag{C.26}$$

The state vector characterizing the bosonic many-body state depicted in Fig. C.1 a) therefore reads

$$|\Psi_A\rangle_{15}^+ = |7, 4, 1, 3, 0, 0\rangle_{15}^+. \tag{C.27}$$

Accordingly, the state vector describing the fermionic many-body state illustrated by Fig. C.1 b) is is determined by the Fock state

$$|\Psi_A\rangle_4^- = |1, 1, 1, 0, 1, 0\rangle_4^-. \tag{C.28}$$

Thereby the Hilbert space spanned by Fock states (C.23) containing $N = \sum_i n_i$ indistinguishable particles is given by $\mathbb{H}_N^\pm$, according to Eq. (C.1) Any N-particle state vector in
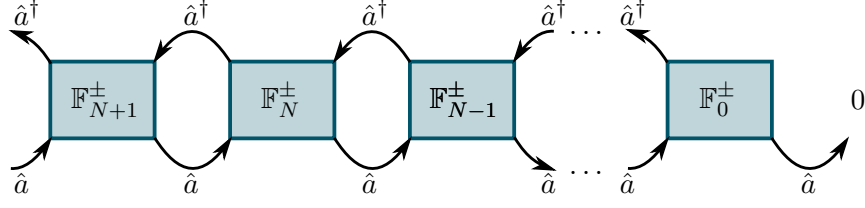
FIGURE C.2: Illustration of the action of creation and annihilation operator $\hat{a}^\dagger$ and $\hat{a}$ as generators of finite-particle Fock subspaces. Thereby the action of each creation operator $\hat{a}^\dagger$ is defined by adding a particle to the system yielding an enlargement of the N-particle Hilbert space $\hat{a}^\dagger : \mathbb{H}_N^\pm \to \mathbb{H}_{N+1}^\pm$. Likewise, the annihilation operator $\hat{a}$ destroys a particle in a N-particle system resulting in the diminishment of the Hilbert space from $\hat{a} : \mathbb{H}_N^\pm \to \mathbb{H}_{N-1}^\pm$. Accordingly a system of N indistinguishable particles can iteratively be created by repeated action of creation operators on the vacuum state.

this space can be represented as a linear superposition of Fock basis states in the follwoing way

$$|\Phi\rangle_N^\pm = \sum_{\substack{n_1, n_2, \dots \\ \sum_i n_i = N}} c_{n_1, n_2, \dots} |n_1, n_2, \dots\rangle_N^\pm, \tag{C.29}$$

where $c_{n_1, n_2, \dots} \in \mathbb{C}$ denotes the expansion coefficient. This coefficient is a measure for the overlap of the state $|\Phi\rangle^\pm$ with the corresponding Fock state $|n_1, n_2, \dots\rangle_N^\pm$ and therefore a measure for the probability of the system to be in the specific occupation configuration represented by the Fock state. The Hilbert space without any restriction on the number of identical particles is referred to as the *Fock space*, which constructed from the direct sum of all N-particle Hilbert spaces $\mathbb{H}_N^\pm$ according to

$$\mathbb{F}^\pm = \bigoplus_{N=0}^\infty \mathbb{H}_N^\pm, \tag{C.30}$$

whereas $\mathbb{H}_0^\pm$ refers to *vacuum space* spanned by a single basis state $|0\rangle$ called the *vacuum state*. In view of Eq. (C.29) any general state $|\Psi\rangle^\pm \in \mathbb{F}^\pm$, unrestricted with respect to the total number of particles N, can be written as

$$|\Phi\rangle^\pm = \sum_{N=0}^\infty |\Phi\rangle_N^\pm = |n_1, n_2, \dots\rangle^\pm, \tag{C.31}$$

where the r.h.s. denots a common short-hand notation.

C.2.2 Creation and annihilation operators

Within the occupation-number representation one can define linear operators $\hat{b}_i^\dagger, \hat{b}_i$: $\mathbb{F}^\pm \to \mathbb{F}^\pm$ connecting many-body Hilbert spaces with different particle numbers as Fig. C.2 demonstrates. Thereby, the operator $\hat{b}_i^\dagger$ adds a particle in the single-particle state i to a

system of N indistinguishable particles,

$$\hat{b}_i^\dagger : \mathbb{H}_N^\pm \to \mathbb{H}_{N+1}^\pm, \quad |n_1, \ldots, n_i, \ldots\rangle_N^\pm \mapsto (\pm 1)^{s_i} \sqrt{n_i + 1} \, |n_1, \ldots, n_i + 1, \ldots\rangle_{N+1}^\pm, \quad \text{(C.32)}$$

and is therefore referred to as *creation operator*. Its adjoint counterpart, the *annihilation operator* $\hat{b} = (\hat{b}^\dagger)^\dagger$ diminishes the number of particles occupying the single-particle state i by one. Therefore $\hat{b}_i$ is defined by the map

$$\hat{b}_i : \mathbb{H}_N^\pm \to \mathbb{H}_{N-1}^\pm, \quad |n_1, \ldots, n_i, \ldots\rangle_N^\pm \mapsto (\pm 1)^{s_i} \sqrt{n_i} \, |n_1, \ldots, n_i - 1, \ldots\rangle_{N-1}^\pm. \quad \text{(C.33)}$$

The factors $(\pm)^{s_i}$, where $s_i = \sum_{j=1}^{i-1} n_i$, on the r.h.s. of Eqs. (C.32, C.33) account for the appropriate sign of the anti-symmetrized state.
In case of a bosonic N-particle state the factors are equal to one.
Also for fermionic particles the general definition of the $\hat{b}^\dagger$ and $\hat{b}$ according to Eqs. (C.32, C.33) can be further simplified. Since the creation of another fermionic particle in an already occupied single-particle state i is not possible due to the Fermi-exclusion principle the action of the creation operator C.32 can be further specified to

$$\hat{b}_i^\dagger \, |n_1, n_2, \ldots, n_i, \ldots\rangle_N^- = (-1)^{s_i} \delta_{n_i,0} \, |n_1, n_2, \ldots, n_i + 1, \ldots\rangle_{N+1}^-. \quad \text{(C.34)}$$

Accordingly, a fermionic particle can only be annihilated in a single-particle state i if this state is occupied, so that Eq. (C.33) reads

$$\hat{b}_i \, |n_1, n_2, \ldots, n_i, \ldots\rangle_N^- = (-1)^{s_i} \delta_{n_i,1} \, |n_1, n_2, \ldots, n_i - 1, \ldots\rangle_{N-1}^\pm. \quad \text{(C.35)}$$

Within the definition of the creation operator (C.32, C.34) any N-particle Fock state can be constructed by repeated application of $\hat{b}_i^\dagger$ on the vacuum state [140, 256, 257]:

$$|n_1, n_2, \ldots\rangle_N^\pm = \prod_{\substack{i \\ \sum_i n_i = N}} \frac{(\hat{b}_i^\dagger)^{n_i}}{\sqrt{n_i!}} \, |0\rangle. \quad \text{(C.36)}$$

To keep the subsequent discussion as general as possible, $\hat{b}_i^\dagger$, $\hat{b}_i$ functions as space holder for either a bosonic or a fermionic pair of creation and annihilation operators. At some stages it will be necessary to specify the consideration to either bosons or fermions. In this case, the following notation is used: Bosonic creation and annihilation operators for a single-particle state i are denoted by

$$\hat{a}_i^\dagger, \hat{a}_i : \mathbb{F}^+ \to \mathbb{F}^+ \quad \Leftrightarrow \quad \hat{a}_i^\dagger : \mathbb{H}_N^+ \to \mathbb{H}_{N+1}^+, \quad \hat{a}_i : \mathbb{H}_N^+ \to \mathbb{H}_{N-1}^+. \quad \text{(C.37)}$$

Likewise,

$$\hat{c}_i^\dagger, \hat{c}_i : \mathbb{F}^- \to \mathbb{F}^- \quad \Leftrightarrow \quad \hat{c}_i^\dagger : \mathbb{H}_N^- \to \mathbb{H}_{N+1}^-, \quad \hat{c}_i : \mathbb{H}_N^- \to \mathbb{H}_{N-1}^- \quad \text{(C.38)}$$

refers to the fermionic equivalent.

C.2.3 Number operators

From Eqs. (C.32, C.33) follows that the Fock state (C.23) is an eigenstate of the operator

$$\hat{b}_i^\dagger \hat{b}_i = \hat{n}_i, \tag{C.39}$$

referred to as the *number operator* of the single-particle state i. The eigenvalues of n_i are the corresponding occupation numbers n_i of the state.

C.2.4 Canonical commutation and anti-commutation relations

According to the formal similarity to the *Poisson bracket* of the canonical phase-space coordinates (q_i, p_j) in classical mechanics the operation

$$[\hat{A}, \hat{B}]_{-x} = \hat{A}\hat{B} - x\hat{B}\hat{A}, \tag{C.40}$$

for some arbitrary operators $\hat{A}$ and $\hat{B}$, is referred to as *canonical commutator* if $x = +1$ and *anti-commutator* if $x = -1$. The term "canonical" refers to the formal coincidence with the Poisson brackets of classical mechanics, as briefly addressed in Sub. A.6. The anti-commutator is often also denoted by curled brackets, i.e. $[.,.]_{+1} = \{.,.\}$. Likewise, plane brackets $[.,.]$ refer to the commutator $[.,.]_{-1}$. During this thesis, this notation is precisely applied.

From action of the bosonic and fermionic creation and annihilation operators on a Fock state, as defined by Eqs. (C.32, C.33), one can deduce the respective canonical commutation and anti-commutation relations reflecting the symmetrization and anti-symmetrization of the corresponding N-particle Hilbert subspace $\mathbb{H}_N^\pm$.

Bosonic operators $\hat{a}_j^\dagger, \hat{a}_i : \mathbb{F}^+ \to \mathbb{F}^+$ fulfill the canonical commutation relation

$$[\hat{a}_i, \hat{a}_j^\dagger]_- = \delta_{i,j}, \tag{C.41}$$

$$[\hat{a}_i, \hat{a}_j]_- = [\hat{a}_i^\dagger, \hat{a}_j^\dagger]_- = 0, \quad \forall i, j. \tag{C.42}$$

Similar, fermionic $\hat{c}_j^\dagger, \hat{c}_i : \mathbb{F}^- \to \mathbb{F}^-$ fulfill the canonical anti-commutation relation

$$[\hat{c}_i, \hat{c}_j^\dagger]_+ = \delta_{i,j}, \tag{C.43}$$

$$[\hat{c}_i, \hat{c}_j]_+ = [\hat{c}_i^\dagger, \hat{c}_j]_+ = 0, \quad \forall i, j. \tag{C.44}$$

From Eqs. (C.41, C.43) relations one can derive more relations between creation and annihilation operators. For this thesis the following ones are especially important:

$$[\hat{a}_i^\dagger \hat{a}_j, \hat{a}_k]_- = -\hat{a}_j \delta_{i,k}, \quad [\hat{a}_i^\dagger \hat{a}_j, \hat{a}_k^\dagger]_- = \hat{a}_i^\dagger \delta_{j,k}. \tag{C.45}$$

Even though fermions follow the anti-commutation relation (C.43), there is a useful expression concerning their behavior within a commutator operation:

$$[\hat{c}_i^\dagger \hat{c}_j, \hat{c}_k^\dagger \hat{c}_l]_- = \hat{c}_i^\dagger \hat{c}_l \delta_{j,k} - \hat{c}_k^\dagger \hat{c}_j \delta_{i,l}. \tag{C.46}$$

C.2.5   Transformation of many-particle operators into Fock-state notation

The formalism of second quantization based on the Fock-state representation of completely symmetrized and anti-symmetrized state vectors unfolds its actual significance by investigating on the transformation of many-particle operators within this formalism. Supposing a general many-body operator $\hat{\mathcal{A}} = \sum_{\gamma=1}^{N} \hat{A}_\gamma$ composed from single-particle operators $\hat{A}_\gamma$. By inserting a resolution of identity in terms of the symmetrized or anti-symmetrized (C.20) version of Eq. (C.11) each on the left and right hand side of the many-body operator $\hat{\mathcal{A}}$ one obtains

$$\hat{\mathcal{A}}^\pm = \sum_{\gamma,A,B} |\Psi_A\rangle^\pm {}^\pm\langle\Psi_A|\hat{A}_\gamma|\Psi_B\rangle^\pm {}^\pm\langle\Psi_B|. \tag{C.47}$$

For the moment, one might focus on the matrix element ${}^\pm\langle\Psi_A|\hat{A}_\gamma|\Psi_B\rangle^\pm$. According to the definition of each set of symmetrized and anti-symmetrized many-body basis vectors (C.20) as the tensor product of single-particle basis vectors (C.2) the matrix element reads

$$^\pm\langle\Psi_A|\hat{A}_\gamma|\Psi_B\rangle^\pm = \bigotimes_{\alpha=1}^{N} \langle\psi_{i_\alpha}|\hat{\mathcal{P}}_N^\pm\hat{A}_\gamma\hat{\mathcal{P}}_N^\pm \bigotimes_{\beta=1}^{N}|\psi_{j_\beta}\rangle. \tag{C.48}$$

According to the permutation invariance (C.14, C.18, C.19) of each single-particle operator one can replace $\hat{\mathcal{P}}_N^\pm\hat{A}_\gamma\hat{\mathcal{P}}_N^\pm$ with $\hat{A}_\gamma$ in Eq. (C.48). Any matrix element between single-particle basis states of different Hilbert subspaces, i.e. $\alpha = \beta$, give zero due to their orthogonality (C.5). Furthermore, only single-particle basis vectors of the Hilbert subspace γ are affected by the single-particle operator $\hat{A}_\gamma$. All remaining contributions with $\alpha \neq \gamma$ result in a scalar product. Accordingly, Eq. (C.48) simplifies to

$$\begin{aligned}
^\pm\langle\Psi_A|\hat{A}_\gamma|\Psi_B\rangle^\pm &= \langle\psi_{i_\gamma}|\hat{A}_\gamma|\psi_{j_\gamma}\rangle \bigotimes_{\substack{\alpha=1\\\alpha\neq\gamma}}^{N} \langle\psi_{i_\alpha}|\psi_{j_\alpha}\rangle\, \delta_{\alpha,\beta} \\
&= \langle\psi_{i_\gamma}|\hat{A}_\gamma|\psi_{j_\gamma}\rangle \prod_{\substack{\alpha=1\\\alpha\neq\gamma}}^{N} \delta_{i_\alpha,j_\alpha}\delta_{\alpha,\beta},
\end{aligned} \tag{C.49}$$

whereas the orthonormality of the single-particle basis vectors (C.5) entered the second step. The matrix element in Eq. (C.49) is just a complex number independent on the label assigned to a Hilbert subspace, so that

$$A_{i,j} = \langle\psi_{i_\gamma}|\hat{A}_\gamma|\psi_{j_\gamma}\rangle. \tag{C.50}$$

The result for the matrix element (C.49) is inserted into Eq. (C.47). Similar to Eq. (C.48) one applies the definition of the symmetrized and anti-symmetrized basis vectors (C.2,

C.20) for the remaining bra and ket in (C.47), so that

$$\hat{\mathcal{A}}^{\pm} = \left[\frac{1}{N} \sum_{\gamma=1}^{N} \sum_{i,j} \hat{\mathcal{P}}_1^{\pm} \left| \psi_i \right\rangle A_{i,j} \left\langle \psi_i \right| \hat{\mathcal{P}}_1^{\pm} \right] \otimes \left[\sum_{i_1,\dots,i_{N-1}} \hat{\mathcal{P}}_{N-1}^{\pm} \bigotimes_{\alpha=1}^{N-1} \left| \psi_{i_\alpha} \right\rangle \bigotimes_{\alpha=1}^{N-1} \left\langle \psi_{i_\alpha} \right| \hat{\mathcal{P}}_{N-1}^{\pm} \right].$$

(C.51)

The factor N^{-1} in the first bracket is compensated by the summation over γ. By applying the Fock state representation (C.30) of the bra and ket in view of Eq. (C.36) in both brackets of (C.51) yields

$$\hat{\mathcal{A}}^{\pm} = \hat{b}_i^{\dagger} A_{i,j} \hat{b}_j \cdot \left[\sum_{\substack{n_1,n_2,\dots \\ \sum_i n_i = N-1}} \prod_{\substack{i \\ \sum_i n_i = N-1}} \frac{(\hat{b}_i^{\dagger})^{n_i}}{\sqrt{n_i!}} \left| 0 \right\rangle \left\langle 0 \right| \frac{(\hat{b}_i)^{n_i}}{\sqrt{n_i!}} \right].$$

(C.52)

The bracket in Eq. (C.52) equals the resolution of identity of a system with $N - 1$ indistinguishable particles according to Eqs. (C.25, C.36).

With this, Eq. (C.52) simplifies by adopting the operator notation of the commutation and anti-commutation relations assigned to bosonic (C.41) and fermionic particles (C.43) to one of the main results of this section, reading

$$\hat{\mathcal{A}}^{+} = \sum_{i,j} \hat{a}_i^{\dagger} A_{i,j} \hat{a}_j, \quad \hat{\mathcal{A}}^{-} = \sum_{i,j} \hat{c}_i^{\dagger} A_{i,j} \hat{c}_j.$$

(C.53)

The main characteristics of the formalism of second quantization, as encoded in Eq. (C.53), can be summarized as follows:

1. The entire information about the permutation symmetry of the considered species of particles is encoded in the creation and annihilation operators according to their corresponding commutation (C.41) or anti-commutation relation (C.43).

2. The construction of a bosonic ($+$) or fermionic ($-$) many-body operator $\hat{\mathcal{A}}^{\pm}$ from a known single-particle operator $\hat{A}$ boils down to the calculation of its matrix elements $A_{i,j}$ multiplied by the corresponding creation and annihilation operators, $\hat{a}_i^{\dagger}, \hat{a}_j$ and $\hat{c}_i^{\dagger}, \hat{c}_j$ respectively, in a chosen single-particle basis $\{|\psi_i\rangle\}$.

Furthermore, supposing $\{|\psi_i\rangle\}$ to denote the eigenbasis of the single-particle operator $\hat{A}$, the diagonalized many-body Hamiltonian takes the following form

$$\hat{\mathcal{A}}^{\pm} = \sum_i a_i \hat{n}_i,$$

(C.54)

where a_i denotes the eigenvalue of $\hat{A}$ to the eigenstate $|\psi_i\rangle$. Thus from Eq. (C.54) that the eigenvalues of a many-body operators are given by the sum over single-particle eigenvalues weighted by the occupation of the corresponding single-particle state.

Within a similar scheme one can derive the second-quantized formulation of many-body operators describing interactions between particles [256].

C.3 Functional field integral – many-body path integrals

The aim of this subsection is the derivation of formalism for the calculation of the many-body partition sum based on a functional field integral. Thereby the basic idea and the construction scheme is very similar as outlined in Chap. D for the construction of a path-integral representation of the single-particle propagator and the partition sum (D.36):

1. Decompose the exponential of the many-body Hamiltonian into N infinitesimal (complex) time slices.

2. Choose a proper basis representation for the insertion of resolution of identity between each pair of time-sliced exponentials.

3. Take the limit of $N \to \infty$ from a discrete set of time-slices to a continuous time.

In the almost trivial case of knowing the eigenbasis of the many-body Hamiltonian this scheme is easily adopted to the many-body case. Nevertheless, in most cases analytic diagonalization is hard to archive especially when considering a more complicated form of the Hamiltonian than in the example of (C.54). This is already the case, when creation and annihilation operator appear in a Hamiltonian not in form of a product of equal ratio, but, for example, as a sum of both $(\hat{a}^\dagger + \hat{a})$. As demonstrated in Eqs. (C.32, C.33), the Fock basis is the eigenbasis of neither $\hat{a}^\dagger$ nor $\hat{a}$, so that accomplishing task 2. of the construction scheme by means of Fock states yields a cumbersome procedure. The introduction of *coherent states* as actual eigenstates of the annihilation operator circumvents this issue as discussed during the following.

According to Eqs. (C.31, C.36) an arbitrary symmetrized or anti-symmetrized many-body state vector is of the form [140, 256, 257]

$$|\Phi\rangle^\pm = \sum_{n_1,\ldots,n_i,\ldots} c_{n_1,\ldots,n_i,\ldots} \prod_j \frac{(\hat{b}_j^\dagger)^{n_j}}{\sqrt{n_j!}} |0\rangle^\pm . \tag{C.55}$$

The absence of the total number of particles N marking the state where restrictions on the total number of particles N are not necessary in general.
The aim of the following is to solve the eigenvalue equation

$$\hat{b}_i |\Phi\rangle^\pm = b_i |\Phi\rangle^\pm \tag{C.56}$$

for a the annihilation operator of a single-particle state i. According to the different symmetry of both species of particles, bosons and fermions, the following derivations are separately carried out for each focusing on the most important aspects regarding this thesis. For further details one is referenced to the literature [257, 258].

C.3.1   Coherent states for Bosons and Gaussian integrals

The n_i-times repeated action of the bosonic annihilation operator $\hat{a}_i$ (C.33) on $|\Phi\rangle^+$ as defined in Eq. (C.29) yields

$$\hat{a}_i^{n_i} |\Phi\rangle^+ = \sum_{n_1,\dots,n_i,\dots} c_{n_1,\dots,n_i,\dots} \sqrt{n_i!} |n_1,\dots,0_i,\dots\rangle^+ = a_i^{n_i} |\Phi\rangle^+ . \tag{C.57}$$

Note that the summation encoded in $|\Phi\rangle^+$ according to Eq. (C.29) includes the complete Fock space. Therefore each ket $|n_1,\dots,0_i,\dots\rangle^+$ appearing in the middle of Eq. (C.57) has an equivalent in $|\Phi\rangle^+$ (C.29) assigned with the expansion coefficient $c_{n_1,\dots,0_i,\dots}$. Consequently, by matching the prefactor of each summand in the middle of Eq. (C.57) with the expansion coefficient $c_{n_1,\dots,0_i,\dots}$ associated with the corresponding ket in $|\Phi\rangle^+$ on the r.h.s. of Eq. (C.57) yields to

$$c_{n_1,\dots,n_i,\dots} = \frac{a_i^{n_i}}{\sqrt{n_i!}} c_{n_1,\dots,0_i,\dots}. \tag{C.58}$$

Due to the commutation of any pair of bosonic annihilation operators (C.42) one obtains

$$c_{n_1,\dots,n_i,\dots} = \prod_j \frac{a_j^{n_j}}{\sqrt{n_j!}} c_{0_1,\dots,0_i,\dots}, \tag{C.59}$$

where $c_{0_1,\dots,0_i,\dots} = 1$ for convenience [257], by repetition of Eq. (C.57) for $\hat{a}_1, \hat{a}_2, \dots$. Insertion of this relation (C.59) into the definition of $|\Phi\rangle^+$ (C.55) results in a *coherent state*, defined by

$$|\Phi\rangle^+ = C \sum_{n_1,\dots,n_i,\dots} \prod_j \frac{(a_j \hat{a}_j^\dagger)^{n_j}}{n_j!} |0\rangle^+ = C \prod_j e^{a_j \hat{a}_j^\dagger} |0\rangle^+ , \tag{C.60}$$

where $C \in \mathbb{C}$ denotes the normalization constant. Note that within similar considerations one finds that there exists no eigenbasis for the creation operator.

Since $[\hat{a}_i, [\hat{a}_j, \hat{a}_k^\dagger]] = [\hat{a}_i^\dagger, [\hat{a}_j^\dagger, \hat{a}_k]] = 0 \ \forall i, j, k$, one can apply the simplified version of the Baker-Campbell-Hausdorff formula [243–245],

$$e^{a_i' \hat{a}_i} e^{a_j \hat{a}_j^\dagger} = e^{a_j \hat{a}_j^\dagger} e^{a_i' \hat{a}_i} e^{a_i' a_j [\hat{a}_i, \hat{a}_j^\dagger]}, \tag{C.61}$$

to obtain the scalar product of two coherent states from Eq. (C.60)

$$^+\langle\Phi'|\Phi\rangle^+ = \prod_{i,j} {}^+\langle 0| e^{a_i' \hat{a}_i} e^{a_j \hat{a}_j^\dagger} |0\rangle^+ = \prod_i e^{a_i' a_i}. \tag{C.62}$$

From Eq. (C.62) follows for $^+\langle a'| \neq {}^+\langle\Phi|$ which is known as *over-completeness* of the coherent states, meaning that the basis provided by a set of coherent states is linear-dependent. As a consequence of that, any coherent state can be represented as the linear combination of other coherent states. In view of the definition of the bosonic coherent state (C.60) the

explicit execution [140, 257] of the integral

$$\int d\boldsymbol{\alpha}^\dagger d\boldsymbol{\alpha}\, e^{-\boldsymbol{\alpha}^\dagger \boldsymbol{\alpha}}\, |\Phi\rangle^{+\,+}\langle\Phi| = 1, \quad d\boldsymbol{\alpha}^\dagger d\boldsymbol{\alpha} = \prod_i \frac{da_i^* da_i}{\pi} \tag{C.63}$$

proofs its equivalence to the completeness relation of Fock states (C.25) and thus in turn proving that coherent states provide a (over-)complete basis for the Fock space as well. Thereby, $\boldsymbol{\alpha} = (a_1, a_2, \dots)^T$ and $\boldsymbol{\alpha}^\dagger = (a_1^*, a_2^*, \dots)$ are vector-representations of the complex eigenvalues of the corresponding bosonic annihilation operators. Complex conjugation of the eigenvalue equation (C.56) yields to ${}^+\langle\Phi|\hat{a}_i^\dagger = {}^+\langle\Phi|a_i^*$, so that the expectation value of the occupation number operator $\hat{n}_i = \hat{a}_i^\dagger \hat{a}_i$ reads

$${}^+\langle\Phi|\hat{n}_i|\Phi\rangle^+ = |a_i|^2. \tag{C.64}$$

Therefore, the absolute value of the eigenvalue a_i of a creation operator $\hat{a}_i$ is associated with the occupation of the corresponding single-particle state i.

Though there exists no eigenbasis of the creation operator $\hat{a}_i^\dagger$ one may evaluate its action on a coherent state, i.e.

$$\begin{aligned}
\hat{a}_i^\dagger |\Phi\rangle^+ &= \prod_{j\neq i} e^{a_j \hat{a}_j^\dagger} \sum_{k=0}^\infty \frac{a_i^k (\hat{a}_i^\dagger)^{k+1}}{k!} |0\rangle^+ \\
&= \prod_{j\neq i} e^{a_j \hat{a}_j^\dagger} \sum_{k=1}^\infty \frac{(\partial_{a_i} a_i^k)(\hat{a}_i^\dagger)^k}{k!} |0\rangle^+ \\
&= \partial_{a_i} |\Phi\rangle^+ .
\end{aligned} \tag{C.65}$$

Thus, the creation operator $\hat{a}_i^\dagger$ is in coherent-state representation (C.60) equivalent to the derivative with respect to the complex eigenvalue a_i of the corresponding annihilation operator $\hat{a}_i$. In fact, this is not surprising, since $\hat{a}_i^\dagger, \hat{a}_i$ fulfill the canonical commutation relation (C.41) similar to momentum and position operator $\hat{p}_i, \hat{x}_i$ in single-particle quantum mechanics. Thereby the position-space representation of the momentum operator is also given by the derivative with respect to the eigenvalue x_i of the position operator $\hat{x}_i$. The validity of the canonical commutation relations (C.41, C.42) remains in coherent-state representation as easily confirmed, i.e.

$$[\hat{a}_i, \hat{a}_j^\dagger]|\Phi\rangle^+ = (a_i \partial_{a_j} - \partial_{a_j} a_i) \quad |\Phi\rangle^+ = \delta_{i,j}|\Phi\rangle^+, \tag{C.66}$$

$$[\hat{a}_i, \hat{a}_j]|\Phi\rangle^+ = (a_i a_j - a_j a_i) \qquad |\Phi\rangle^+ = 0, \tag{C.67}$$

$$[\hat{a}_i^\dagger, \hat{a}_j^\dagger]|\Phi\rangle^+ = (\partial_{a_i} \partial_{a_j} - \partial_{a_j} \partial_{a_i})|\Phi\rangle^+ = 0. \tag{C.68}$$

One of the most important integrals in quantum field theory is the Gaussian integral of the following form

$$I^+ = \int d\boldsymbol{\alpha}^\dagger d\boldsymbol{\alpha}\, e^{-\frac{1}{2}\boldsymbol{\alpha}^\dagger \mathbb{A} \boldsymbol{\alpha}} = \det(\mathbb{A})^{-1}, \tag{C.69}$$

Coherent state	$\lvert\Phi\rangle^+ = \prod_i e^{a_i \hat{a}_i^\dagger} \lvert 0\rangle^+$
Representation of $\hat{a}_i$	$\hat{a}_i \lvert\Phi\rangle^+ = a_i \lvert\Phi\rangle^+$
Representation of $\hat{a}_i^\dagger$	$\hat{a}_i^\dagger \lvert\Phi\rangle^+ = \partial_{a_i} \lvert\Phi\rangle^+$
Number operator	${}^+\langle\Phi\lvert\hat{n}_i\lvert\Phi\rangle^+ = \lvert a_i\rvert^2$
Scalar product	${}^+\langle\Phi'\lvert\Phi\rangle^+ = \prod_i e^{a_i'^* a_i}$
Resolution of identity	$\int \mathrm{d}\boldsymbol{\alpha}^\dagger \mathrm{d}\boldsymbol{\alpha}\, e^{-\boldsymbol{\alpha}^\dagger\boldsymbol{\alpha}}\, {}^+\lvert\Phi\rangle\langle\Phi\rvert^+ = 1$
Gaussian integral	$\int \mathrm{d}\boldsymbol{\alpha}^\dagger \mathrm{d}\boldsymbol{\alpha}\, e^{-\boldsymbol{\alpha}^\dagger \mathbb{A}\boldsymbol{\alpha}} = \det(\mathbb{A})^{-1}$

TABLE C.1: Summary [257] of the basic properties of bosonic coherent states $\lvert\Phi\rangle^+$ as eigenstates of the bosonic annihilation operator $\hat{a}_i$ to the eigenvalue $a_i \in \mathbb{C}$. $\boldsymbol{\alpha} = (a_1, a_2, \dots)^T$ and $\boldsymbol{\alpha}^\dagger = (a_1^*, a_2^*, \dots)$ denote the vector-representation of the eigenvalues, whereas the coefficient matrix $\mathbb{A}$ is assumed to be diagonalizable. The integration measure $\mathrm{d}\boldsymbol{\alpha}^\dagger \mathrm{d}\boldsymbol{\alpha}$ is defined in Eq. (C.69).

where the integration measure is defined in Eq. (C.63). Consequently, $\mathbb{A}$ denotes a coefficient matrix. Since the evaluation of this integral and proving its equality to the inverse of the determinant of $\mathbb{A}$ is a standard procedure discussed in various textbooks on the topic [257] it is not outlined here. Table C.1 provides a final summary of the main properties of bosonic coherent states and related quantities. However, the evaluation of the fermionic equivalent to (C.69) is subsequently discussed since it shows some peculiarities due to the anti-commutativity of those particles.

C.3.2 Coherent states for Fermions and Gaussian integrals

Similar to the considerations for the bosonic case the fermionic creation operator cannot posses an eigenstates. The scheme for the derivation of the coherent state for fermions [257, 258],

$$|\Phi\rangle^- = e^{-\sum_i c_i \hat{c}_i^\dagger} |0\rangle^- \tag{C.70}$$

follows similar steps as outlined for the bosonic case. The main differences arise from the anti-commutativity inherent to fermions in contrast to the commutativity of bosons which yields not only to a negative sign in the exponential of the fermionic coherent state (C.70). Even more, the consequences of the anti-commutativity become most obvious by investigating on the anti-commutation relation concerning two fermionic creation operators $\hat{c}_i, \hat{c}_j$ (C.44) in coherent-state representation,

$$\{\hat{c}_i, \hat{c}_j\} |\Phi\rangle^- = (c_i c_j + c_j c_i) |\Phi\rangle^- = 0, \tag{C.71}$$

which fairly alters from its bosonic equivalent (C.67). It is quite obvious, that this condition for c_i, c_j cannot be fulfilled by complex numbers and rather needs the introduction of a new mathematical framework. This accomplished by introducing the associative *Grassmann algebra* [259, 260] $\mathbb{G}$ over the field of complex numbers. A few important properties of the Grassmann number concerning the arithmetic calculus, differentiation and integration are outlined in Sec.

Gaussian integral with Grassmann numbers [257]
Similar to the bosonic case, Gaussian integrals on Grassmann numbers

$$I^- = \int d\boldsymbol{\rho}^\dagger d\boldsymbol{\rho}\, e^{-\boldsymbol{\rho}^\dagger \mathbb{M} \boldsymbol{\rho}}, \quad d\boldsymbol{\rho}^\dagger d\boldsymbol{\rho} = \prod_i dc_i^* dc_i, \tag{C.72}$$

are commonly found within the field of quantum field theory. Regarding the special properties of Grassmann numbers the Gaussian integral appears in an essentially simpler way as the bosonic equivalent. Since all powers of a Grassmann number higher than 1 are zero the Gaussian integral I (C.72) transforms into a simple Berezin integral:

$$I^- = \int d\boldsymbol{\rho}^\dagger d\boldsymbol{\rho} \left(1 - \boldsymbol{\rho}^\dagger \mathbb{M} \boldsymbol{\rho}\right) = -\int d\boldsymbol{\rho}^\dagger d\boldsymbol{\rho}\, \boldsymbol{\rho}^\dagger \mathbb{M} \boldsymbol{\rho}. \tag{C.73}$$

Suppose the complex matrix $\mathbb{M}$ to be diagonalizable, i.e. there exists a unitary transformation $\mathbb{S}$, so that $\mathbb{S}^\dagger \mathbb{M} \mathbb{S} = \tilde{\mathbb{M}}$, where $\tilde{\mathbb{M}} = \text{diag}(\lambda_1, \ldots, \lambda_N)$, with the eigenvalues $\lambda_i \in \mathbb{C}$ $\forall i = 1, 2, \ldots, N$. If $\mathbb{M}$ is hermitian the eigenvalues $\lambda_i \in \mathbb{\shortparallel} \forall i = 1, 2, \ldots, N$. Anyway, the

function f (E.22) can be expressed in a diagonalized form, reading

$$\tilde{f}(\tilde{\boldsymbol{\rho}}^\dagger, \tilde{\boldsymbol{\rho}}) = \tilde{\boldsymbol{\rho}}^\dagger \tilde{\mathbb{M}} \tilde{\boldsymbol{\rho}} = \sum_i \tilde{c}_i^* \lambda_i \tilde{c}_i = f(\boldsymbol{\rho}^\dagger, \boldsymbol{\rho}), \tag{C.74}$$

where $\tilde{\boldsymbol{\rho}} = \mathbb{S}^\dagger \boldsymbol{\rho}$ and $\tilde{\boldsymbol{\rho}}^\dagger = \boldsymbol{\rho} \mathbb{S}$ denote the vectors of Grassmann numbers in the diagonal basis of $\mathbb{M}$. Therefore, each entry $\tilde{c}_i^{(*)}$ of $\tilde{\boldsymbol{\rho}}^{(\dagger)}$ is a linear combination of the Grassmann numbers $c_1^{(*)}, c_2^{(*)}, \ldots, c_N^{(*)}$.
As easily proven, the Jacobian of this transformation equals 1, so that the transformed integral measure reads $\mathrm{d}\tilde{\boldsymbol{\rho}}^\dagger \mathrm{d}\tilde{\boldsymbol{\rho}} = \mathrm{d}\boldsymbol{\rho}^\dagger \mathrm{d}\boldsymbol{\rho}$.
Along with this, the Gaussian integral (C.73) reads

$$I^- = - \int \mathrm{d}\tilde{\boldsymbol{\rho}}^\dagger \mathrm{d}\tilde{\boldsymbol{\rho}} \, \tilde{\boldsymbol{\rho}}^\dagger \tilde{\mathbb{M}} \tilde{\boldsymbol{\rho}} = - \int \prod_i \mathrm{d}\tilde{c}_i^\dagger \mathrm{d}\tilde{c}_i \sum_j \tilde{c}_j^\dagger \lambda_j \tilde{c}_j. \tag{C.75}$$

Due to the linearity of the berenzin integral the product and the sum are interchangeable. Anti-commuting the integration variables c_j, c_j^* and first evaluating the integral over c_j yields to

$$\begin{aligned}
I^- &= \sum_j \int \prod_i \mathrm{d}\tilde{c}_i^\dagger \mathrm{d}\tilde{c}_i \, \tilde{c}_j \lambda_j \tilde{c}_j^\dagger = \sum_j \int \prod_i \mathrm{d}\tilde{c}_i^\dagger \delta_{i,j} \lambda_j \tilde{c}_j^\dagger = \prod_i \lambda_i \\
&= \det(\mathbb{M}),
\end{aligned} \tag{C.76}$$

where it is used that $\det(\tilde{\mathbb{M}}) = \det(\mathbb{M})$ in accordance with linear algebra. To conclude the considerations on fermionic coherent states $|\Phi\rangle^-$ table (C.2) summarizes their most important properties.

Coherent state	$\vert\Phi\rangle^- = e^{-\sum_i c_i \hat{c}_i^\dagger} \vert 0\rangle^-$
Representation of $\hat{c}_i$	$\hat{c}_i \vert\Phi\rangle^- = c_i \vert\Phi\rangle^-$
Representation of $\hat{c}_i^\dagger$	$\hat{c}_i^\dagger \vert\Phi\rangle^- = \partial_{c_i} \vert\Phi\rangle^-$
Number operator	$^-\langle\Phi\vert\hat{n}_i\vert\Phi\rangle^- = \vert c_i\vert^2$
Scalar product	$^-\langle\Phi'\vert\Phi\rangle^- = e^{\sum_i c_i'^* c_i}$
Resolution of identity	$\int \mathrm{d}\boldsymbol{\rho}^\dagger \mathrm{d}\boldsymbol{\rho}\, e^{-\boldsymbol{\rho}^\dagger\boldsymbol{\rho}}\, {}^-\vert\Phi\rangle\langle\Phi\vert^- = 1$
Gaussian integral	$\int \mathrm{d}\boldsymbol{\rho}^\dagger \mathrm{d}\boldsymbol{\rho}\, e^{-\boldsymbol{\rho}^\dagger\mathbb{M}\boldsymbol{\rho}} = \det(\mathbb{M})$

TABLE C.2: Summary of the basic properties of fermionic coherent states $\vert\Phi\rangle^-$ based on Ref. [257]. Similar to the coherent sates $\vert\Phi\rangle^+$ being eigenstates of the bosonic annihilation operators $\hat{a}_i$, $\vert\Phi\rangle^-$ are eigenstates to the fermionic annihilation operators $\hat{c}_i$. The respective eigenvalues as are anticommuting Grassmann numbers c_i. $\boldsymbol{\rho} = (c_1, c_2, \dots)^T$ and $\boldsymbol{\rho}^\dagger = (c_1^*, c_2^*, \dots)$ denote the vector-representation of the eigenvalues, whereas the coefficient matrix $\mathbb{M}$ is assumed to be diagonalizable. The integration measure $\mathrm{d}\boldsymbol{\alpha}^\dagger\mathrm{d}\boldsymbol{\alpha}$ is defined in Eq. (C.72). All relations given in the table are easily derived in view of the properties of Grassmann numbers, see Sec. E.2.

Appendix D

Path integral representation of partition sums

The key quantity of statistical physics in thermal equilibrium is the partition function, since it contains the entire information about the statistical properties of a system according to the considered statistical ensemble. The partition sum is defined as

$$Z(\beta, X) = \text{Tr} \left[e^{-\beta \hat{H}} \right] = \sum_q \langle q | e^{-\beta \hat{H}} | q \rangle, \tag{D.1}$$

where $\beta = 1/(k_B T)$ and $\hat{H}$ denote thermal energy and Hamiltonian, respectively. According to basic linear algebra the trace over a matrix is independent on the choice of basis, so that $\{|q\rangle\}$ marks a, yet unspecified, basis. For convenience, $\{|q\rangle\}$ is chosen to be discrete. In case of a continuous basis the sum over states q is replaced by an integral. The argument X of the partition sum (D.1) represents all further state functions and parameters that characterize the considered system. In case of Eq. (D.1) the chosen ensemble exemplarily is the canonical ensemble. Thereby the system is allowed to exchange energy with its environment whereas the number of particles remains constant.

Quantum statistical mechanics
By knowing the complete set of eigenstates $\{|n\rangle\}$ of the Hamiltonian $\hat{H}$,

$$\hat{H} | n \rangle = \epsilon_n | n \rangle, \tag{D.2}$$

the partition function simplifies according to

$$Z(\beta, X) = \sum_n \langle n | e^{-\beta \hat{H}} | n \rangle = \sum_n e^{-\beta \epsilon_n}. \tag{D.3}$$

With this representation the striking significance of the partition function becomes more obvious. Thus, the partition function or the negative of its logarithm, which is defined as the free energy in the case of the canonical ensemble,

$$F(\beta, X) = -\frac{1}{\beta} \ln \left[Z(\beta, X) \right], \tag{D.4}$$

contains not only information about the thermal properties but it is also determined by the properties of the micro states n, such as the masses or spins of the considered particles.

It also allows for quantifying the probability P_n of the system occupying a specific micro state n, which is given by

$$P_n(\beta, X) = \frac{e^{-\beta \epsilon_n}}{Z(\beta, X)}, \quad \sum_n P_n(\beta, X) = 1. \tag{D.5}$$

However in most cases, the computation of the micro states is difficult or even analytically impossible. The representation of the partition function by means of a path integral provides a powerful and elegant method to gain further insights in such situations. Therefore, the derivation of a path integral representation of Z in the case of bosonic and fermionic particles is outlined in the following. As briefly discussed in Sec. D.2, the analytic continuation from the real Minkowski to a complex or Euclidean time axis provides an analogy between statistical and quantum mechanics. Therefore it is convenient to demonstrate the main aspects of the derivation of a path integral representation on the, probably more familiar, example of the quantum propagator according to Feynman [261] in Minkowski space. The subsequent adaption of the scheme of derivation is then easily performed within the transformation from Minkowski to Euclidean space-time.

D.1 Prelude: Feynman's path integral representation of the quantum propagator

The first path integral approach was invented by Feynman [261] considering the propagation of a quantum particle from the initial position $|q_\mathrm{i}\rangle$ at time t_i to a final state localized at $|q_\mathrm{f}\rangle$ at time $t_\mathrm{f} > t_\mathrm{i}$. The time evolution of an initial state $|q_\mathrm{i}\rangle$ at time t_i to a final state $|q_\mathrm{f}\rangle$ at time t_f is facilitated by the time-evolution operator (B.4) according to Eq. (B.5). The probability of the transition $|q_\mathrm{i}\rangle \rightarrow |q_\mathrm{f}\rangle$ is given by the respective matrix element known as the *propagator*,

$$K(q_\mathrm{f}, t_\mathrm{f}; q_\mathrm{i}, t_\mathrm{i}) = \langle q_\mathrm{f}| \hat{U}(t_\mathrm{f}, t_\mathrm{i}) |q_\mathrm{i}\rangle = \langle q_\mathrm{f}| e^{-\frac{i}{\hbar}\hat{H}(\hat{q},\hat{p})(t_\mathrm{f}-t_\mathrm{i})} |q_\mathrm{i}\rangle. \tag{D.6}$$

The Hamiltonian is assumed to be not explicitly time dependent. The generalization of the subsequently discussed scheme of derivation is easily performed.

According to the properties of the time-evolution operator [119] one can decompose $\hat{U}(t_\mathrm{f}, t_\mathrm{i})$ into N products of $N+1$ equally time-sliced operators [261, 262]

$$\hat{U}(t_\mathrm{f}, t_\mathrm{i}) = \hat{U}(t_\mathrm{f}, t_N) \cdot \left[\prod_{i=N}^{2} \hat{U}(t_i, t_{i-1}) \right] \cdot \hat{U}(t_1, t_\mathrm{i})$$

$$= e^{-\frac{i}{\hbar}\hat{H}(\hat{q},\hat{p})\epsilon} \cdot \left[\prod_{i=N}^{2} e^{-\frac{i}{\hbar}\hat{H}(\hat{q},\hat{p})\epsilon} \right] \cdot e^{-\frac{i}{\hbar}\hat{H}(\hat{q},\hat{p})\epsilon}, \tag{D.7}$$

with $\epsilon = t_i - t_{i-1} = (t_\mathrm{f} - t_\mathrm{i})/(N+1) > 0$ denotes the time interval. By inserting resolutions of identity in terms of

$$1 = \int \mathrm{d}q_i\, |q_i\rangle \langle q_i|, \quad i = 1, 2, \dots, N, \tag{D.8}$$

where each $\{|q_i\rangle\}$ denotes a complete set of position eigenstates, between each pair of time-evolution operators one can rewrite the expression for the propagator (D.6) in the following way

$$
\begin{aligned}
K(q_\mathrm{f}, t_\mathrm{f}; q_\mathrm{i}, t_\mathrm{i}) &= \prod_{i=1}^{N}\left[\int \mathrm{d}q_i\right]\prod_{i=1}^{N+1} K(q_i, t_i; q_{i-1}, t_{i-1}) \\
&= \prod_{i=1}^{N}\left[\int \mathrm{d}q_i\right]\prod_{i=1}^{N+1}\langle q_i|\, e^{-\frac{i}{\hbar}\hat{H}(\hat{q},\hat{p})\epsilon}\,|q_{i-1}\rangle ,
\end{aligned}
\tag{D.9}
$$

where $q_\mathrm{f} = q_{N+1}$ at $t_\mathrm{f} = t_{N+1}$ and $q_\mathrm{i} = q_0$ at $t_\mathrm{i} = t_0$, respectively. Assuming the Hamiltonian to consist of kinetic and potential part, $\hat{H}(\hat{q}, \hat{p}) = \hat{T}(\hat{p}) + \hat{V}(\hat{q})$, each contribution in Eq. (D.9) can be factorized in the following manner according to *Baker-Campbell-Hausdorff formula* [119, 243–245, 249]

$$
\begin{aligned}
K(q_i, t_i; q_{i-1}, t_{i-1}) &= \langle q_i|\, e^{-\frac{i}{\hbar}\hat{T}(\hat{p})\epsilon} e^{-\frac{i}{\hbar}\hat{V}(\hat{q})\epsilon} e^{-\frac{i}{\hbar}\mathcal{O}(\epsilon^2)}\,|q_{i-1}\rangle \\
&\approx \langle q_i|\, e^{-\frac{i}{\hbar}\hat{T}(\hat{p})\epsilon} e^{-\frac{i}{\hbar}\hat{V}(\hat{q})\epsilon}\,|q_{i-1}\rangle .
\end{aligned}
\tag{D.10}
$$

If $[\hat{T}, \hat{V}] = 0$, the left and right hand side of Eq. (D.10) will exactly be equal. Otherwise, the error within the factorization (D.10) tends to zero in the limit $N \to \infty$ and thus in turn $\epsilon \to 0$, again retrieving equality between the left and right hand side of expression (D.10). Mapping this back onto Eq. (D.7) yields the *Trotter product formula* [263]

$$
e^{-\frac{i}{\hbar}\hat{H}(\hat{q},\hat{p})(t_\mathrm{f}-t_\mathrm{i})} = \lim_{N\to\infty}\left(e^{-\frac{i}{\hbar}\hat{T}(\hat{p})\epsilon} e^{-\frac{i}{\hbar}\hat{V}(\hat{q})\epsilon}\right)^{N+1}.
\tag{D.11}
$$

For convenience N is maintained final during the following steps so that the limit $N \to \infty$ is taken only at the end.

Now, by first inserting the resolution of identity according to Eq. (D.8) between the product of the exponentials of kinetic and potential operator

$$
K(q_i, t_i; q_{i-1}, t_{i-1}) \approx \int \mathrm{d}q\, \langle q_i|\, e^{-\frac{i}{\hbar}\hat{T}(\hat{p})\epsilon}\,|q\rangle\, \langle q|\, e^{-\frac{i}{\hbar}\hat{V}(\hat{q})\epsilon}\,|q_{i-1}\rangle ,
\tag{D.12}
$$

one can insert identity resolved in terms of the momentum space eigenstates $\{|p_i\rangle\}$,

$$
1 = \int \frac{\mathrm{d}p_i}{2\pi\hbar}\, |p_i\rangle\, \langle p_i| ,
\tag{D.13}
$$

between the exponential of the kinetic operator and the ket $|q\rangle$. Equation (D.12) then reads

$$
K(q_i, t_i; q_{i-1}, t_{i-1}) \approx \int \frac{\mathrm{d}p_i}{2\pi\hbar} \int \mathrm{d}q\, e^{-\frac{i}{\hbar}T(p_i)\epsilon} e^{-\frac{i}{\hbar}V(x)\epsilon}\, \langle q_i|p_i\rangle\, \langle p_i|x\rangle\, \langle x|q_{i-1}\rangle ,
\tag{D.14}
$$

where it was used that the momentum / position representation is the eigenbasis of the momentum / position operator, respectively. Thus, also the kinetic and potential operator are represented in their respective eigenbasis. Therefore the operators entering

Eq. (D.14) are replaced by their complex eigenvalues. Under usage of

$$\langle q_i | p_j \rangle = e^{\frac{i}{\hbar} q_i p_j} = (\langle p_j | q_i \rangle)^\dagger ,$$
$$\langle q_i | q_j \rangle = \delta(q_i - q_j), \tag{D.15}$$

and after executing the integration over position space the propagator (D.14) transforms into

$$K(q_i, t_i; q_{i-1}, t_{i-1}) \approx \int \frac{\mathrm{d}p_i}{2\pi\hbar} e^{\frac{i}{\hbar}\epsilon \left[p_i \frac{q_i - q_{i-1}}{\epsilon} - H(q_i, p_i) \right]} , \tag{D.16}$$

where the Hamiltonian enters in its eigenbasis representation. Inserting the intermediate result (D.16) into the full propagator (D.6) yields

$$K(q_\mathrm{f}, t_\mathrm{f}; q_\mathrm{i}, t_\mathrm{i}) = \prod_{i=1}^{N} \left[\int \mathrm{d}q_i \right] \prod_{i=1}^{N+1} \left[\int \frac{\mathrm{d}p_i}{2\pi\hbar} \right] e^{\frac{i}{\hbar}\epsilon \sum_{i=1}^{N+1} \left[p_i \frac{q_i - q_{i-1}}{\epsilon} - H(q_i, p_i) \right]} , \tag{D.17}$$

In the limit of $N \to \infty$ the time slice $\epsilon \to 0$, so that the discrete set of time steps $t_i = i\epsilon$, for $i = 1, 2, \dots, N$, is dense on the interval $[t_\mathrm{i}, t_\mathrm{f}]$.
Accordingly, the set of phase space points $\{(q_i, p_i); i = 1, 2, \dots, N\}$ can be regarded as continuous functions of time $(x(t), p(t))$ on the interval l $[t_\mathrm{i}, t_\mathrm{f}]$ and

$$\lim_{N \to \infty} \frac{q_i - q_{i-1}}{\epsilon} = \partial_t q(t),$$
$$\lim_{N \to \infty} \epsilon \sum_{i=1}^{N+1} = \int_{t_\mathrm{i}}^{t_\mathrm{f}} \mathrm{d}t. \tag{D.18}$$

The convergence of the discretized Hamiltonian (D.17) into a continuous function of time $H(q(t), p(t))$ is strictly valid only for smooth potentials $V(q(t), t)$ without singularities. Summarizing, in the limit $N \to \infty$ the propagator (D.17) can be written in the following *path integral* representation

$$K(q_\mathrm{f}, t_\mathrm{f}; q_\mathrm{i}, t_\mathrm{i}) = \int_{q(t_\mathrm{i})=q_\mathrm{i}}^{q(t_\mathrm{f})=q_\mathrm{f}} \mathcal{D}'x \, e^{\frac{i}{\hbar} \int_{t_\mathrm{i}}^{t_\mathrm{f}} \mathrm{d}t [p(t)\partial_t q(t) - H(q(t), p(t))]} , \tag{D.19}$$

where

$$\int_{q(t_\mathrm{i})=q_\mathrm{i}}^{q(t_\mathrm{f})=q_\mathrm{f}} \mathcal{D}'x = \lim_{N \to \infty} \prod_{i=1}^{N} \left[\int \mathrm{d}q_i \right] \prod_{i=1}^{N+1} \left[\int \frac{\mathrm{d}p_i}{2\pi\hbar} \right] \tag{D.20}$$

defines the integration measure. The integral in the exponential of the path integral representation (D.19) is known as the *classical canonical action*

$$\mathcal{S}[q, p] = \int_{t_\mathrm{i}}^{t_\mathrm{f}} \mathrm{d}t \mathcal{L}\left[q(t), \dot{q}(t) \right], \tag{D.21}$$
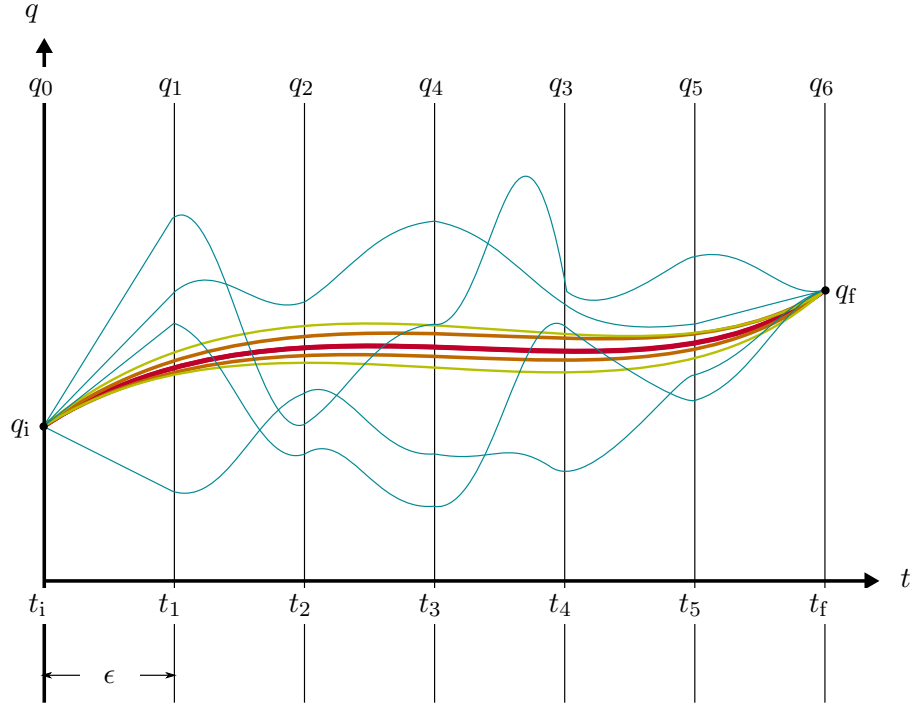
FIGURE D.1:   Illustration of classical and quantum trajectories connecting the initial coordinate q_i at time t_i with the final coordinate q_f at time t_f. The thick red curve illustrates a classical path according to Hamilton's principle. Whereas trajectories in the vicinity of this classical path lead still contribute in first order, the thin blue lines depict classically forbidden paths. When the time-steps ϵ become infinitesimal small, these paths interfere destructively so that their contribution to the quantum propagator vanishes.

of all trajectories $t \mapsto q(t)$ that connect initial and final coordinate, $q_i = q(t_i)$ and $q_f = q(t_f)$, respectively, according to the *classical Lagrangian*

$$\mathcal{L}\left[q(t), \dot{q}(t)\right] = p(t)\dot{q}(t) - H(q(t), p(t)), \tag{D.22}$$

the *Legendre transform* of the *classical Hamiltonian* H. Thereby $\partial_t q(t) = \dot{q}(t)$ defines the time derivative of the generalized coordinate $q(t)$, the generalized velocity. Furthermore, *Hamilton's principle*

$$\frac{\delta S[q, p]}{\delta q(t)} = 0 \tag{D.23}$$

states, that only paths, that satisfy the classical equations of motions in accordance with the *Euler-Lagrange-equations*

$$\frac{\partial \mathcal{L}\left[q(t), \dot{q}(t)\right]}{\partial q(t)} - \frac{\mathrm{d}}{\mathrm{d}t}\frac{\partial \mathcal{L}\left[q(t), \dot{q}(t)\right]}{\partial \dot{q}(t)} = 0 \tag{D.24}$$

are stationary points of the action $\mathcal{S}$ and therefore providing the dominant contribution to the propagator (D.19). This situation is depicted by Fig. D.1 for the example of six

time-steps.

Assuming the particle to return to its initial point after a time t, i.e. claiming periodic boundary conditions $q = q_i = q(0) = q_f = q(t)$ for the paths, yields a special case of the propagator

$$K(q,t) = \langle q| \, e^{-\frac{i}{\hbar}\hat{H}t} \, |q\rangle = \oint \mathcal{D}'[x] e^{\frac{i}{\hbar}S[q,p]}, \tag{D.25}$$

where

$$\oint \mathcal{D}'[x] = \int_{q(0)=q}^{q(t)=q} \mathcal{D}'[x]. \tag{D.26}$$

This is starting point for the discussion of the path integral representation of the partition sum.

D.2   Partition sum of the canonical ensemble and Wick rotation

The formal connection between quantum and statistical mechanics is provided by the concept of *imaginary time* $\tau = it$. This becomes obvious by comparison of the quantum propagator for periodic paths with the definition of the partition sum according. Each summand contributing to the partition function (D.1) matches a quantum propagator for periodic boundary conditions (D.25) evaluated at the imaginary time $t \mapsto -i\hbar\beta$, i.e.

$$Z(\beta, X) = \sum_q K(q,t)|_{t \mapsto -i\hbar\beta} \,. \tag{D.27}$$

Starting from the ordinary Minkowski space with its defined metric

$$\mathrm{d}s^2 = -\mathrm{d}t^2 + \mathrm{d}\boldsymbol{q}^2, \tag{D.28}$$

where $\mathrm{d}t \in \mathbb{R}$ and $\mathrm{d}\boldsymbol{q} \in \mathbb{R}^3$. Within the concept of imaginary time, the real time axis t in Minkowski space is extended to the complex plane, as illustrated in Fig. D.2 a). The analytic continuation of a integration contour γ from the real time axis t to a complex time $t \mapsto e^{-i\varphi}t$ is called *Wick rotation* [249]. The space coordinates remain unchanged by the rotation of the time-frame. In the depicted example, Fig. D.2 a), and in accordance with the sign convention for position space introduced in Ref. [249]) the rotation is performed clockwise, i.e. $\varphi > 0$. By claiming $\varphi = \pi/2$ a path is analytically continued from t to a purely imaginary time $-it$, i.e.$\gamma(t) \mapsto \gamma(-it)$ Thereby the direction of integration alters from positive on the real axis to negative on the imaginary time axis as the sign in the argument of the analytically continued path γ indicates. Accordingly, a Wick rotation in momentum space, where the time coordinate corresponds to the energy ϵ, is performed counterclockwise [249], so that the direction of integration remains unchanged[1]. Within this sign convention [249] the product of time and energy is invariant under Wick rotation as easily proven. After the rotation of an integration path in position space, one may put $it = \tau$, where τ is postulated to be the real time coordinate in a four-dimensional Euclidean space and therefore also sometimes referred to as *Euclidean time*. Thereby the

---

[1]Some authors use a different sign convention, which is possible as long as consistently applied.
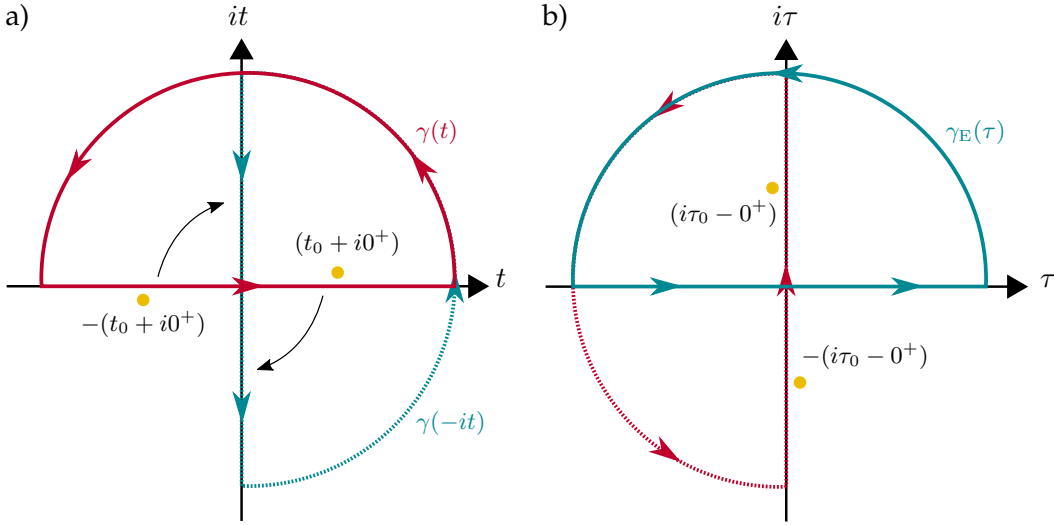
FIGURE D.2: a) Illustration of the Wick rotation of a integration path γ in Minkowski space from real time coordinate t (solid red line) to imaginary time $-it$ (dotted blue line) [249]. The black arrows denote the direction of rotation, $t \mapsto e^{-i\varphi}t$, where $\varphi = \pi/2$. Thereby the direction of integration in position space is changed from positive, on the real time axis t, to negative, on the imaginary time axis it. The integration along $-it$ corresponds to a integration in positive direction along the real axis τ in Euclidean space as depicted by the solid blue line in panel b). The dotted red line corresponds to the inverted Wick rotation leading from Euclidean to the original curve (red solid line in panel a)) in Minkowski space. The orange dots represent potential singularities of a quantum propagator similar to Eq. (D.19). In the depicted example, the positions of the singularities correspond to the anti-time-ordered Greens function according to the Feynman path integral. Any different, but consistent choice depending on the demand of the theory is valid as well. The direction of circulation of the path around the enclosed pole $t_0 + i0^+$ remains unchanged by the Wick rotation.

Wick rotation corresponds to a mapping from the Minkowski space-time to Euclidean space-time [249], with its assigned Euclidean metric

$$\mathrm{d}s_{\mathrm{E}}^2 = \mathrm{d}\tau^2 + \mathrm{d}\boldsymbol{q}^2, \tag{D.29}$$

where $\mathrm{d}\tau \in \mathbb{R}$ and $\mathrm{d}\boldsymbol{q} \in \mathbb{R}^3$. With this, one can introduce the short-hand notation $t \mapsto -i\tau$ for the Wick rotation from the real time axis t in Minkowski space to the real time axis τ in Euclidean space. According to the introduced sign convention [249], the direction of integration of the transformed path in Euclidean space, $\gamma_E(\tau) = \gamma(-it)$, is again positive, as Fig. D.2 b) illustrates. Similar to the definition of the integration path γ_E in Euclidean space, one can define

$$q(t) \mapsto q(-it) = q(\tau) = q_{\mathrm{E}}(\tau) \tag{D.30}$$

for the transformation of generalized coordinates. Having regard to

$$\partial_t \mapsto i\partial_\tau, \quad \mathrm{d}t \mapsto -i\mathrm{d}\tau \tag{D.31}$$

the transformation of time-dependent quantities under Wick rotation is straightforward. For example one finds for the generalized velocities in Euclidean space This coincidence holds not for the generalized velocities:

$$\dot{q}(t) = \partial_t q(t) \mapsto \dot{q}(-it) = i\partial_\tau q_{\mathrm{E}}(\tau) = i\dot{q}_{\mathrm{E}}(\tau). \tag{D.32}$$

Similarly the Euclidean Lagrangian is obtained from the Minkowski Lagrangian (D.22) by

$$\mathcal{L}\left[q(t), \dot{q}(t)\right] \mapsto \mathcal{L}\left[q(t), \dot{q}(-it)\right] = \mathcal{L}_{\mathrm{E}}\left[q(\tau), \dot{q}_{\mathrm{E}}(\tau)\right]. \tag{D.33}$$

This directly leads to the Euclidean action

$$\mathcal{S}\left[q, p\right] \mapsto i\hbar \int_0^\beta \mathrm{d}\tau \, \mathcal{L}_{\mathrm{E}}\left[q(\tau), \dot{q}_{\mathrm{E}}(\tau)\right] = i\hbar \mathcal{S}_{\mathrm{E}}\left[q, p\right], \tag{D.34}$$

so that one concludes for the quantum propagator with periodic boundary conditions (D.25) in Euclidean space

$$K(q, t) = \oint \mathcal{D}'[x] \, e^{\frac{i}{\hbar}\mathcal{S}[q,p]} \mapsto K_{\mathrm{E}}(q, \beta) = \oint \mathcal{D}'[x] \, e^{-\mathcal{S}_{\mathrm{E}}[q,p]}. \tag{D.35}$$

Concluding in view of Eq. (D.25), the result for propagator for a periodic path q in Euclidean space-time corresponds to a summand of the partition sum in path-integral representation, so that the final result of this section reads

$$Z(\beta, X) = \int_{-\infty}^{\infty} \mathrm{d}q \, K_{\mathrm{E}}(q, \beta) = \oint \mathcal{D}[x] \, e^{-\mathcal{S}_{\mathrm{E}}[q,p]}. \tag{D.36}$$

The integration measure is explicitly given by

$$\oint \mathcal{D}[x] = \int_{-\infty}^{\infty} \mathrm{d}q \oint \mathcal{D}'[x], \tag{D.37}$$

whereas $\oint \mathcal{D}'[x]$ is defined in Eqs. (D.20, D.26).

D.3 Grand-canonical partition sum for many-body systems

Within the framework of bosonic or fermionic coherent states (cf. Sec. C.3) the derivation of a path-integral approach for the many-body partition function

$$\mathcal{Z} = \mathrm{Tr}\left[e^{-\beta(\hat{\mathcal{H}} - \mu\hat{\mathcal{N}})}\right] = \sum_n {}^{\pm}\langle n|e^{-\beta(\hat{\mathcal{H}} - \mu\hat{\mathcal{N}})}|n\rangle^{\pm} \tag{D.38}$$

can be achieved in the same way as the derivation in the single-particle case considered in Sec. D.2. The subsequently discussed scheme of derivation mainly follows Ref. [257]. Without loss of generality the partition sum as written in Eq. (D.38) refers to the *grand canonical ensemble*, where the system is allowed to exchange energy and particles with its environment. Thereby, the chemical potential μ is a measure of the energy required to add a particle to the system. The many-body Hamiltonian $\hat{\mathcal{H}}$ in Eq. (D.38) is assumed to

be of the general form

$$\hat{\mathcal{H}} = \sum_{i,j} \hat{b}_i^\dagger \, h_{i,j} \, \hat{b}_j, \tag{D.39}$$

where $\hat{b}_i^\dagger, \hat{b}_j$ denote either bosonic or fermionic creation annihilation operators for the single-particle states i, j. The matrix element $h_{i,j} = \langle \psi_i | \, \hat{H} \, | \psi_j \rangle \in \mathbb{C}$ is obtained from associated single-particle state vectors $|\psi_i\rangle$ and $|\psi_j\rangle$ and the corresponding single-particle Hamiltonian $\hat{H}$, as discussed in Subsec. C.2.5. Furthermore, the number operator $\hat{\mathcal{N}}$ reads

$$\hat{\mathcal{N}} = \sum_i \hat{n}_i = \sum_{i,j} \hat{b}_i^\dagger \, \delta_{i,j} \, \hat{b}_j, \tag{D.40}$$

with $\hat{n}_i$ as defined in Eq. (C.39). The basis states $\{|n\rangle^\pm\}$ shall denote the a complete set of Fock states for either the symmetrized ($+$) or anti-symmetrized ($-$) Fock space (C.30). By insertion of the identity resolution in terms of coherent states, Eq. (C.63) and Tab. C.2, between the Fock-state bra and the operator exponential, Eq. (D.38) takes the following form

$$\mathcal{Z} = \int \mathrm{d}\boldsymbol{\beta}^\dagger \mathrm{d}\boldsymbol{\beta} \, e^{-\boldsymbol{\beta}^\dagger \boldsymbol{\beta}} \sum_n {}^\pm\langle n | \Phi \rangle^\pm \, {}^\pm\langle \Phi | e^{-\beta(\hat{\mathcal{H}} - \mu \hat{\mathcal{N}})} | n \rangle^\pm. \tag{D.41}$$

The integration measure explicitly reads

$$\int \mathrm{d}\boldsymbol{\beta}^\dagger \mathrm{d}\boldsymbol{\beta} = \int \prod_i \frac{\mathrm{d}b_i^* \mathrm{d}b_i}{\sqrt{\pi}^{1\pm 1}}, \tag{D.42}$$

where b^*, b denote either bosons or fermions. Similarly, $\boldsymbol{\beta}^{(\dagger)}$ denotes the vector representation of complex or Grassmann numbers. In Eq. (D.41) the normalizing exponential contains no operators so that it is pulled from the right side of the Fock-state bra to its left side. By permuting ${}^\pm\langle n | \Phi \rangle^\pm$ with ${}^\pm\langle \Phi | e^{-\beta(\hat{\mathcal{H}} - \mu \hat{\mathcal{N}})} | n \rangle^\pm$ one is able to represent the trace only by means of the coherent states according to the completeness of Fock states (C.25). In the fermionic case, the sign in the exponential assigned with the creation operators in ${}^-\langle \Phi |$ (C.70) changes [257] according to the anti-commutation of fermionic operators (C.43) and Grassmann numbers (C.71). This can be seen from the following:
The operator exponential in Eq. (D.41) yields no change in the sign since the considered Hamiltonian (C.7) as well as the number operator (D.40) consist of an even number of fermionic operators. Note that also the fermionic part of the Hamiltonian (5.44 – 5.47), regarded in the main part of this thesis, contains an even number of fermionic operators. Therefore, one can regard the permutation of ${}^\pm\langle n | \Phi \rangle^\pm$ with ${}^\pm\langle \Phi | n \rangle^\pm$ only when concerned with the origin of the sign change. From the generation of Fock states from the vacuum by action of the creation operators $\hat{b}_i^\dagger$ according to Eq. (C.36) and the definition of the coherent states as eigenstates of the annihilation operator one finds

$${}^-\langle n | \Phi \rangle^- \, {}^-\langle \Phi | n \rangle^- = {}^-\langle 0 | \sum_i \frac{(c_i)^{n_i}}{\sqrt{n_i!}} | \Phi \rangle^- \, {}^-\langle \Phi | \sum_i \frac{(c_i^*)^{n_i}}{\sqrt{n_i!}} | 0 \rangle^-, \tag{D.43}$$

where c_i^*, c_i denote Grassmann numbers. With regard to the definition of anti-commuting multiplication of Grassmann numbers (C.71) it is obvious that

$$
{}^-\langle n|\Phi\rangle^-\, {}^-\langle\Phi|n\rangle^- = {}^-\langle\Phi|\sum_i \frac{(-c_i^*)^{n_i}}{\sqrt{n_i!}}\,|0\rangle^-\, {}^-\langle 0|\sum_i \frac{(c_i)^{n_i}}{\sqrt{n_i!}}\,|\Phi\rangle^- = {}^-\langle -\Phi|n\rangle^-\, {}^-\langle n|\Phi\rangle^-,
$$

$$(D.44)$$

where

$$
{}^-\langle -\Phi| = {}^-\langle 0|e^{+\sum_i \hat{c}_i c_i^*}.
$$

$$(D.45)$$

Along with this, it follows from Eq. (D.41) for the partition sum

$$
\mathcal{Z} = \int \mathrm{d}\boldsymbol{\beta}^\dagger \mathrm{d}\boldsymbol{\beta}\, e^{-\boldsymbol{\beta}^\dagger\boldsymbol{\beta}}\, {}^\pm\langle\pm\Phi|e^{-\beta(\hat{\mathcal{H}}-\mu\hat{\mathcal{N}})}\,|\Phi\rangle^\pm,
$$

$$(D.46)$$

where the trace is given in terms of the coherent states. According to the anti-commutativity of Grassmann numbers, the corresponding representation of the fermionic trance is referred to as anti-diagonal. This condition results in anti-periodic boundary conditions for the respective fermionic fields as it becomes clear during the following.

As a next step, the exponential of the Hamiltonian is expanded into $N+1$ equally spaced pieces ($\delta = \beta/N$) whereas a resolution of identity expressed in terms of coherent states, Eq. (C.63) and Tab. C.2, is inserted between each pair of exponentials:

$$
\mathcal{Z} = \prod_{n=1}^{N+1}\left[\int \mathrm{d}\boldsymbol{\beta}_n^\dagger \mathrm{d}\boldsymbol{\beta}_n\right] \prod_{n=1}^{N+1} e^{-\boldsymbol{\beta}_n^\dagger\boldsymbol{\beta}_n}\, {}^\pm\langle\Phi_n|e^{-\beta(\hat{\mathcal{H}}-\mu\hat{\mathcal{N}})}\,|\Phi_{n-1}\rangle^\pm.
$$

$$(D.47)$$

The product over matrix elements is thereby to read in descending order, i.e.

$$
{}^\pm\langle\Phi_{N+1}|\,|\Phi_{N-1}\rangle^\pm\, {}^\pm\langle\Phi_{N-1}|\,|\Phi_{N-1}\rangle^\pm\ldots{}^\pm\langle\Phi_1|\,|\Phi_0\rangle^\pm.
$$

$$(D.48)$$

According to the definition of the trace in terms of coherent states (D.46) the conditions

$$
{}^\pm\langle\Phi_{N+1}| = {}^\pm\langle\pm\Phi|, \quad |\Phi_0\rangle^\pm = |\Phi\rangle^\pm
$$

$$(D.49)$$

have to be satisfied. Note that the expansion of the Hamiltonian into time-sliced products (D.47) is exact. Furthermore, each coherent state $|\Phi_n\rangle^\pm$ is a function of a complete set of eigenvalues $\boldsymbol{\beta}_n = (b_{1_n}, b_{2_n}, \ldots)^T$ of the corresponding annihilation operators. Thereby each of the indices $i = 1, 2, \ldots$ denotes a single-particle state, so that i_n refers to the single-particle state i at Euclidean time $n\delta$. Accordingly, the integration measure in (D.47) is explicitly given by

$$
\prod_{n=1}^{N+1}\left[\int \mathrm{d}\boldsymbol{\beta}_n^\dagger \mathrm{d}\boldsymbol{\beta}_n\right] = \prod_{n=1}^{N+1}\left[\int \prod_{i_n} \frac{\mathrm{d}b_{i_n}^* \mathrm{d}b_{i_n}}{\sqrt{\pi}^{1\pm1}}\right].
$$

$$(D.50)$$

Each exponential entering each matrix element in Eq. (D.47) is then expanded into a Tailor series of normal-ordered contributions [257]:

$$
{}^\pm\langle\Phi_n|e^{-\delta(\hat{\mathcal{H}}-\mu\hat{\mathcal{N}})}\,|\Phi_{n-1}\rangle^\pm = {}^\pm\langle\Phi_n|1 + \delta\sum_{i,j}\hat{b}_i^\dagger c_{i,j}\,\hat{b}_j + \mathcal{O}(\delta^2)\,|\Phi_{n-1}\rangle^\pm,
$$

$$(D.51)$$

where the expansion coefficients $c_{i,j} \in \mathbb{C}$ and $\hat{b}_i^\dagger$, $\hat{b}_j$ correspond to the creation and annihilation operator of the respective single-particle states. In general, this is valid for any Hamiltonian containing an even number of particle operators. In case of the particular example for Hamiltonian given by Eq. (D.39), the complex coefficients satisfy $c_{i,j} = h_{i,j} - \mu\delta_{i,j}$. Remembering the coherent states being eigenstates of the annihilation operator further simplifies the Tailor expansion in first order approximation:

$$
\begin{aligned}
{}^{\pm}\langle\Phi_n|e^{-\delta(\hat{\mathcal{H}}-\mu\hat{\mathcal{N}})}|\Phi_{n-1}\rangle^{\pm} &\approx {}^{\pm}\langle\Phi_n|\Phi_{n-1}\rangle^{\pm}(1+\delta\sum_{i,j}b_i^* c_{i,j} b_j) \\
&\approx {}^{\pm}\langle\Phi_n|\Phi_{n-1}\rangle^{\pm}e^{-\delta\left[\mathcal{H}(\boldsymbol{\beta}_n^\dagger,\boldsymbol{\beta}_{n-1})-\mu\mathcal{N}(\boldsymbol{\beta}_n^\dagger,\boldsymbol{\beta}_{n-1})\right]},
\end{aligned}
\tag{D.52}
$$

where b_i^* and b_j are either complex or Grassmann numbers and $\boldsymbol{\beta}^\dagger$, $\boldsymbol{\beta}$ denote the corresponding vector representation. Accordingly, $\mathcal{H}$ and $\mathcal{N}$ in Eq. (D.52) refer to the coherent-state representation of each corresponding operator $\hat{\mathcal{H}}$, $\hat{\mathcal{N}}$, i.e.

$$
\mathcal{H}(\boldsymbol{\beta}_n^\dagger,\boldsymbol{\beta}_{n-1}) = \frac{{}^{\pm}\langle\Phi_n|\hat{\mathcal{H}}|\Phi_{n-1}\rangle^{\pm}}{{}^{\pm}\langle\Phi_n|\Phi_{n-1}\rangle^{\pm}} = \sum_{i,j}b_{i_n}^* h_{i,j}, b_{j_{n-1}},
\tag{D.53}
$$

The same holds for the number operator.
The scalar product entering expression (D.52),

$$
{}^{\pm}\langle\Phi_n|\Phi_{n-1}\rangle^{\pm} = e^{\boldsymbol{\beta}_n^\dagger\boldsymbol{\beta}_{n-1}},
\tag{D.54}
$$

satisfies in accordance with Eq. (D.49) the following boundary conditions for $n = N+1$

$$
{}^{\pm}\langle\Phi_{N+1}|\Phi_N\rangle^{\pm} = e^{\pm\boldsymbol{\beta}_{N+1}^\dagger\boldsymbol{\beta}_N}.
\tag{D.55}
$$

Thus, each contribution to the partition sum (D.47) is given by

$$
e^{-\boldsymbol{\beta}_n^\dagger\boldsymbol{\beta}_n}{}^{\pm}\langle\Phi_n|e^{-\delta(\hat{\mathcal{H}}-\mu\hat{\mathcal{N}})}|\Phi_{n-1}\rangle^{\pm} \approx e^{-\delta\left[\boldsymbol{\beta}_n^\dagger\frac{\boldsymbol{\beta}_n-\boldsymbol{\beta}_{n-1}}{\delta}+\mathcal{H}(\boldsymbol{\beta}_n^\dagger,\boldsymbol{\beta}_{n-1})-\mu\mathcal{N}(\boldsymbol{\beta}_n^\dagger,\boldsymbol{\beta}_{n-1})\right]},
\tag{D.56}
$$

so that $\mathcal{Z}$ can be written as

$$
\mathcal{Z} \approx \prod_{n=1}^{N+1}\left[\int d\boldsymbol{\beta}_n^\dagger d\boldsymbol{\beta}_n\right]e^{-\delta\sum_{n=1}^{N+1}\left[\boldsymbol{\beta}_n^\dagger\frac{\boldsymbol{\beta}_n-\boldsymbol{\beta}_{n-1}}{\delta}+\mathcal{H}(\boldsymbol{\beta}_n^\dagger,\boldsymbol{\beta}_{n-1})-\mu\mathcal{N}(\boldsymbol{\beta}_n^\dagger,\boldsymbol{\beta}_{n-1})\right]}.
\tag{D.57}
$$

According to expression (D.55), the boundary conditions in the bosonic case, $\boldsymbol{\beta}^{(\dagger)} = \boldsymbol{\alpha}^{(\dagger)}$, are periodic:

$$
\boldsymbol{\alpha}_0 = \boldsymbol{\alpha}_{N+1}.
\tag{D.58}
$$

By contrast, the anti-diagonal condition (D.55) for fermions, $\boldsymbol{\beta}^{(\dagger)} = \boldsymbol{\rho}^{(\dagger)}$, results in anti-periodic boundary conditions:

$$
\boldsymbol{\rho}_0 = -\boldsymbol{\rho}_{N+1}.
\tag{D.59}
$$

Similar to the single-particle case, discussed in Sec. D.1, the partition sum (D.57) becomes exact in the continuum limit, $N \to \infty$, according to the Trotter product formula (D.11). Within similar considerations, the set of discrete eigenvalue vectors $\{\boldsymbol{\beta}_n, \boldsymbol{\beta}_n^\dagger\}$ becomes

continuous on the Euclidean time interval $[\tau_i = 0, \tau_f = \beta]$, so that

$$\lim_{N\to\infty} \{\boldsymbol{\beta}_n, \boldsymbol{\beta}_n^\dagger\} = \{\boldsymbol{\beta}(\tau), \boldsymbol{\beta}^\dagger(\tau)\} \tag{D.60}$$

are referred to as fields of complex or Grassmann variables, depending on the considered species of particles. Correspondingly, the final result for the many-body partition sum refers to a quantum field integral rather than a quantum path integral as in the single-particle case, Eq (D.36).

In the continuum limit the mismatch of eigenvalue vectors evaluated at different time slices $\delta \cdot n$ and $\delta \cdot (n - 1)$ entering the Hamiltonian and the number operator becomes arbitrary small, resulting in

$$\lim_{N\to\infty} \left[\mathcal{H}(\boldsymbol{\beta}_n^\dagger, \boldsymbol{\beta}_{n-1}) - \mu\mathcal{N}(\boldsymbol{\beta}_n^\dagger, \boldsymbol{\beta}_{n-1}) \right] = \mathcal{H}[\boldsymbol{\beta}^\dagger(\tau), \boldsymbol{\beta}(\tau)] - \mu\mathcal{N}[\boldsymbol{\beta}^\dagger(\tau), \boldsymbol{\beta}(\tau)]. \tag{D.61}$$

By obtaining for the difference of the sets $\boldsymbol{\beta}_n$ and $\boldsymbol{\beta}_{n-1}$ in Eq. (D.57) the corresponding derivative with respect to the Euclidean time τ and replacing the sum by an integral,

$$\lim_{N\to\infty} \frac{\boldsymbol{\beta}_n - \boldsymbol{\beta}_{n-1}}{\delta} = \partial_\tau \boldsymbol{\beta}(\tau),$$

$$\lim_{N\to\infty} \delta \sum_{n=1}^{N+1} = \int_0^\beta \mathrm{d}\tau, \tag{D.62}$$

the many-body path-integral formulation of the partition sum is given by

$$\mathcal{Z} = \oint \mathcal{D}[\boldsymbol{\beta}]\, e^{-\mathcal{S}_\mathrm{E}[\boldsymbol{\beta}^\dagger, \boldsymbol{\beta}]}, \tag{D.63}$$

with the Euclidean action of the quantum fields

$$\mathcal{S}_\mathrm{E}[\boldsymbol{\beta}^\dagger, \boldsymbol{\beta}] = \int_0^\beta \mathrm{d}\tau \left[\boldsymbol{\beta}^\dagger(\tau)\partial_\tau\boldsymbol{\beta}(\tau) + \mathcal{H}[\boldsymbol{\beta}^\dagger(\tau), \boldsymbol{\beta}(\tau)] - \mu\mathcal{N}[\boldsymbol{\beta}^\dagger(\tau), \boldsymbol{\beta}(\tau)] \right]. \tag{D.64}$$

The integration measure of the quantum field integral (D.63) explicitly reads

$$\oint \mathcal{D}[\boldsymbol{\beta}] = \int_{\boldsymbol{\beta}^{(\dagger)}(0)}^{\boldsymbol{\beta}^{(\dagger)}(\beta) = \pm\boldsymbol{\beta}^{(\dagger)}(0)} \mathcal{D}[\boldsymbol{\beta}] = \int_{\boldsymbol{\beta}^{(\dagger)}(0)}^{\boldsymbol{\beta}^{(\dagger)}(\beta) = \pm\boldsymbol{\beta}^{(\dagger)}(0)} \prod_{n=1}^{\infty} \frac{\mathrm{d}\boldsymbol{\beta}_n^\dagger \mathrm{d}\boldsymbol{\beta}_n}{\sqrt{\pi}^{1\pm1}}, \tag{D.65}$$

where the boundary conditions of the closed field integral are either periodic (+) in the bosonic case or anti-periodic (−) in the fermionic case. A discussion of the concept of Euclidean time and the connection between quantum and statistical mechanics is found in Sec. D.2. According to the thermal energy β entering the quantum field integral as the Euclidean time parameter, the class of integrals (D.63) is also referred to as thermal quantum field integrals in literature [264].

For the evaluation of $\mathcal{Z}$ it is convenient to introduce the Fourier transform of the quantum fields $\{\boldsymbol{\beta}^\dagger(\tau), \boldsymbol{\beta}(\tau)\}$ with respect to the Euclidean time τ [240, 257, 264]:

$$
\boldsymbol{\beta}^\dagger(\tau) = \frac{1}{\sqrt{\beta}} \sum_{\omega_n^\pm} \tilde{\boldsymbol{\beta}}_n^\dagger e^{i\omega_n^\pm \tau}, \qquad \tilde{\boldsymbol{\beta}}_n^\dagger = \frac{1}{\sqrt{\beta}} \int_0^\beta \mathrm{d}\tau \, \boldsymbol{\beta}^\dagger(\tau) e^{-i\omega_n^\pm \tau},
$$

$$
\boldsymbol{\beta}(\tau) = \frac{1}{\sqrt{\beta}} \sum_{\omega_n^\pm} \tilde{\boldsymbol{\beta}}_n e^{-i\omega_n^\pm \tau}, \quad \tilde{\boldsymbol{\beta}}_n = \frac{1}{\sqrt{\beta}} \int_0^\beta \mathrm{d}\tau \, \boldsymbol{\beta}(\tau) e^{i\omega_n \tau},
$$

(D.66)

where $\tilde{\boldsymbol{\beta}}_n$ denotes the short-hand notation for the vector representation of the complex or Grassmann numbers in frequency space, i.e. $\tilde{\boldsymbol{\beta}}_n = \tilde{\boldsymbol{\beta}}(\omega_n^\pm) = (\tilde{b}_1(\omega_n^\pm), \tilde{b}_2(\omega_n^\pm), \dots)^T$. The particular periodic or anti-periodic boundary conditions (D.65) are precisely satisfied [240, 257, 264] by choice of the following so-called Matsubara frequencies [265]

$$
\omega_n^\pm = \begin{cases} \frac{2\pi n}{\beta}, & (+) \text{ for bosons}, \\ \frac{(2n+1)\pi}{\beta}, & (-) \text{ for fermions}, \end{cases} \qquad n \in \mathbb{Z}.
$$

(D.67)

Under usage of the identity $\int_0^\beta \mathrm{d}\tau \, e^{-i\omega_n^\pm \tau} = \delta_{n,0}$ the Euclidean action (D.64) is easily transformed into

$$
\mathcal{S}_{\mathrm{E}}[\tilde{\boldsymbol{\beta}}^\dagger, \tilde{\boldsymbol{\beta}}] = \sum_n \left[\tilde{\boldsymbol{\beta}}_n^\dagger(-i\omega_n^\pm)\tilde{\boldsymbol{\beta}}_n + \mathcal{H}\left[\tilde{\boldsymbol{\beta}}_n^\dagger, \tilde{\boldsymbol{\beta}}_n \right] - \mu\mathcal{N}\left[\tilde{\boldsymbol{\beta}}_n^\dagger, \tilde{\boldsymbol{\beta}}_n \right] \right].
$$

(D.68)

In particular, for $\hat{\mathcal{H}}$ and $\hat{\mathcal{N}}$ being of the general form (D.39, D.39), the Euclidean action can be written as

$$
\mathcal{S}_{\mathrm{E}}[\tilde{\boldsymbol{\beta}}^\dagger, \tilde{\boldsymbol{\beta}}] = \sum_n \sum_{i,j} \left[\tilde{b}_i^*(\omega_n^\pm) \left[(-i\omega_n^\pm - \mu)\delta_{i,j} + h_{i,j} \right] \tilde{b}_j(\omega_n^\pm) \right] = \sum_n \tilde{\boldsymbol{\beta}}_n^\dagger \, \mathbb{S}(i\omega_n^\pm)\tilde{\boldsymbol{\beta}}_n.
$$

(D.69)

By adapting the integration measure $\mathcal{D}[\boldsymbol{\beta}]$ to the Fourier representation,

$$
\mathcal{D}[\tilde{\boldsymbol{\beta}}] = \prod_{\omega_n^\pm} \frac{\mathrm{d}\tilde{\boldsymbol{\beta}}_n^\dagger \mathrm{d}\tilde{\boldsymbol{\beta}}_n}{\sqrt{\pi}^{1\pm 1}},
$$

(D.70)

one obtains the equivalent of the partition sum in frequency representation:

$$
\mathcal{Z} = \oint \mathcal{D}[\tilde{\boldsymbol{\beta}}] \, e^{-\mathcal{S}_{\mathrm{E}}[\tilde{\boldsymbol{\beta}}^\dagger, \tilde{\boldsymbol{\beta}}]}.
$$

(D.71)

Regarding the particular example of $\mathcal{S}_{\mathrm{E}}$ given by Eq. (D.69) the thermal field integral is easily evaluated by means of Gaussian integration as discussed in Sec. C.3 for bosons and fermions, respectively. Therefore, the partition sum in this case is given by

$$
\mathcal{Z} = \prod_{\omega_n^\pm} \det \left[\mathbb{S}(i\omega_n^\pm) \right]^{\mp 1},
$$

(D.72)

where the matrix $\mathbb{S}$ is defined in Eq. (D.69). The product over Matsubara frequencies can be transformed into a sum by considering the logarithm of the partition sum, referred to

as the grand-canonical potential:

$$\Omega = -\frac{1}{\beta}\log\mathcal{Z} = \pm\frac{1}{\beta}\sum_{\omega_n^\pm}\log\left[\det\left[\mathbb{S}(i\omega_n^\pm)\right]\right]. \tag{D.73}$$

The evaluation of this infinite sum over Matsubara frequencies can be accomplished by means of the Residue theorem, as demonstrated in Sec. E.3.

If the matrix $\mathbb{S}(i\omega_n^\pm)$ assumes diagonal form,

$$\mathbb{S}_{j,j}^{\mathrm{diag}}(i\omega_n^\pm) = -i\omega_n^\pm - \mu + \epsilon_j \quad \Leftrightarrow \quad \det\left[\mathbb{S}^{\mathrm{diag}}(i\omega_n^\pm)\right] = \prod_j \mathbb{S}_{j,j}^{\mathrm{diag}}(i\omega_n^\pm), \tag{D.74}$$

where $\epsilon_j = h_{j,j}$ denotes the single-particle eigenenergy of state j and $h_{i,j} = 0 \; \forall i \neq j$, the evaluation of the partition sum $\mathcal{Z}$ will be seemingly easy and yields

$$\mathcal{Z} = \prod_{\omega_n^\pm}\left[\prod_j\left(-i\omega_n^\pm - \mu + \epsilon_j\right)\right]^{\mp 1}. \tag{D.75}$$

By evaluation of the Matsubara sum (cf. Sec. E.3) one finds the grand-canonical potential of the many-body system in the familiar form

$$\Omega = \pm\frac{1}{\beta}\sum_{\omega_n^\pm}\sum_j\log\left(-i\omega_n^\pm - \mu + \epsilon_j\right) \stackrel{(E.41)}{=} \pm\frac{1}{\beta}\sum_j\log\left[1 \mp e^{-\beta(\epsilon_j - \mu)}\right], \tag{D.76}$$

where the upper sign refers to bosons and the lower one to fermions. Note that the information entering Ω and thus in turn the many-body partition sum is only based on single-particle information and the chemical potential determining the number of occupied levels at a given temperature $1/\beta$. Hence, for $\beta \to \infty$ one obtains the many-body ground state of the grand-canonical ensemble.

Appendix E

Mathematical concepts

E.1 Fourier transformation

The Fourier transform of a scalar field or a component of a vector field $f : \mathbb{R}^3 \to \mathbb{R}$, $\boldsymbol{q} \mapsto f(\boldsymbol{q})$ from real space to reciprocal space is defined by

$$\tilde{f}(\boldsymbol{k}) = \int_{\mathbb{R}^3} \mathrm{d}^3 q \, f(\boldsymbol{q}) e^{-i\boldsymbol{k}\cdot\boldsymbol{q}}, \tag{E.1}$$

where $\tilde{f} : \mathbb{R}^3 \to \mathbb{R}$, $\boldsymbol{k} \mapsto \tilde{f}(\boldsymbol{k})$ is a map in reciprocal or momentum space. Likewise, the inverse transformation is defined by

$$f(\boldsymbol{q}) = \int_{\mathbb{R}^3} \frac{\mathrm{d}^3 k}{(2\pi)^3} \tilde{f}(\boldsymbol{k}) e^{i\boldsymbol{k}\cdot\boldsymbol{q}}. \tag{E.2}$$

From these definitions follows a variety of relations, such as the Plancherel identity [266]

$$\int_{\mathbb{R}^3} \mathrm{d}^3 q \, f(\boldsymbol{q}) g(\boldsymbol{q}) = \int_{\mathbb{R}^3} \frac{\mathrm{d}^3 k}{(2\pi)^3} \tilde{f}(\boldsymbol{k}) \tilde{g}(-\boldsymbol{k}) \tag{E.3}$$

concerned with the Fourier transform of the product of two fields $f(\boldsymbol{q})$ and $g(\boldsymbol{q})$. The identity can be derived from the definitions (E.1, E.2) and the δ distribution in reciprocal space,

$$\delta(\boldsymbol{q} - \boldsymbol{q}') = \int_{\mathbb{R}^3} \frac{\mathrm{d}^3 k}{(2\pi)^3} e^{i\boldsymbol{k}\cdot(\boldsymbol{q}-\boldsymbol{q}')} \quad \Leftrightarrow \quad e^{-i\boldsymbol{k}\cdot\boldsymbol{q}'} = \int_{\mathbb{R}^3} \mathrm{d}^3 q \, \delta(\boldsymbol{q} - \boldsymbol{q}') \, e^{-i\boldsymbol{k}\cdot\boldsymbol{q}} \tag{E.4}$$

$$(2\pi)^3 \delta(\boldsymbol{k} - \boldsymbol{k}') = \int_{\mathbb{R}^3} \mathrm{d}^3 q \, e^{-i(\boldsymbol{k}-\boldsymbol{k}')\cdot\boldsymbol{q}} \quad \Leftrightarrow \quad e^{i\boldsymbol{k}'\cdot\boldsymbol{q}} = \int_{\mathbb{R}^3} \mathrm{d}^3 k \, \delta(\boldsymbol{k} - \boldsymbol{k}') e^{i\boldsymbol{k}\cdot\boldsymbol{q}} \tag{E.5}$$

as follows

$$\begin{aligned}
\int_{\mathbb{R}^3} \mathrm{d}^3 q \, f(\boldsymbol{q}) g(\boldsymbol{q}) &= \int_{\mathbb{R}^3} \mathrm{d}^3 q \int_{\mathbb{R}^3} \frac{\mathrm{d}^3 k}{(2\pi)^3} \int_{\mathbb{R}^3} \frac{\mathrm{d}^3 k'}{(2\pi)^3} \tilde{f}(\boldsymbol{k}) \tilde{g}(\boldsymbol{k}') \, e^{-i(\boldsymbol{k}+\boldsymbol{k}')\boldsymbol{q}} \\
&= \int_{\mathbb{R}^3} \frac{\mathrm{d}^3 k}{(2\pi)^3} \int_{\mathbb{R}^3} \mathrm{d}^3 k' \, \tilde{f}(\boldsymbol{k}) \tilde{g}(\boldsymbol{k}') \delta(\boldsymbol{k} + \boldsymbol{k}') \\
&= \int_{\mathbb{R}^3} \frac{\mathrm{d}^3 k}{(2\pi)^3} \tilde{f}(\boldsymbol{k}) \tilde{g}(-\boldsymbol{k})
\end{aligned} \tag{E.6}$$

E.2 Grassmann numbers: eigenvalues of the fermionic annihilation operator

The Grassmann algebra is generated from an identity element 1 and anti-commuting *Grassmann numbers* c_i, whereas the multiplication is precisely defined by Eq. (C.71). A profound derivation of the properties of the Grassmann algebra can be found, for example, in Ref. [258]. Therefore the following outlines a few important aspects of the properties of Grassmann numbers needed to investigate on a fermionic path integral.

From the definition of the multiplication of two Grassmann numbers (C.71) one can deduce the following properties among others:

1. The addition of Grassmann numbers is commutative:

$$c_i + c_j = c_j + c_i, \quad (c_i + c_j) + c_k = c_i + (c_j + c_k) \tag{E.7}$$

2. The addition and multiplication of a Grassmann number and a complex number a is commutative:

$$c_i + a = a + c_i, \quad c_i a = a c_i. \tag{E.8}$$

3. As anticipated in Eq. (C.70) it is possible to define the complex conjugate c_i^* of a Grassmann number $c_i = c_i^{\mathrm{R}} + i c_i^{\mathrm{I}}$, where c_i^{q}, c_i^{I} are Grassmann numbers and i is the imaginary unit. Therefore

$$(c_i^*)^* = (c_i^{\mathrm{R}} - i c_i^{\mathrm{I}})^* = c_i^{\mathrm{R}} + i c_i^{\mathrm{I}} \tag{E.9}$$

and the square of the absolute value is imaginary

$$|c_i|^2 = c_i^* c_i = (c_i^{\mathrm{R}} - i c_i^{\mathrm{I}})(c_i^{\mathrm{R}} + i c_i^{\mathrm{I}}) = 2 i c_i^{\mathrm{R}} c_i^{\mathrm{I}}. \tag{E.10}$$

4. The multiplication is associative by definition

$$(c_i c_j) c_k = c_i (c_j c_k). \tag{E.11}$$

5. The multiplication of two Grassmann numbers c_j, c_k yields a complex number. This follows from

$$c_i (c_j c_k) = -c_j c_i c_k = (c_j c_k) c_i \tag{E.12}$$

in view of Eqs. (C.71, E.11) and the commutativity of the multiplication of c_i with a complex number (E.8).

6. Any power of a Grassmann number higher than 1 is zero:

$$c_i^0 = 1, \quad c_i^1 = c_i, \tag{E.13}$$

$$c_i^2 = c_i^3 = \ldots = 0. \tag{E.14}$$

Consequently there exists no inverse to a Grassmann number with respect to the multiplication (C.71).

7. From 6 directly follows, that any function of a set of Grassmann numbers can maximally be of first order in each Grassmann number. For example any function of N Grassmann numbers is of the following form

$$f(c_1, c_2, \ldots, c_N) = m_0 + \sum_{i=1}^{N} m_1(i)c_i + m + \sum_{i=1}^{N} \sum_{j=i+1}^{N} m_2(i,j)c_i c_j + \ldots$$
$$+ m_N(1, 2, \ldots, N)c_1 c_2 \ldots c_N, \tag{E.15}$$

where $m_i(\ldots) \in \mathbb{C} \ \forall i = 0, 1, 2, \ldots, N$.

According to the properties of the complex differentiation one can define the derivative of the elements of the Grassmann algebra by

$$\partial_{c_j} 1 = 0, \tag{E.16}$$
$$\partial_{c_j} c_i = \delta_{i,j}. \tag{E.17}$$

Thus, for $N = 2$, the derivative of the exemplary function f (E.15) with respect to a Grassmann number c_k in reads

$$\partial_{c_k} f(c_1, c_2) = [m_1(1) + m_2(1,2)c_2] \, \delta_{1,k} + [m_1(2) - m_2(1,2)c_1] \, \delta_{2,k}. \tag{E.18}$$

The integration over a Grassmann number c_i is defined as the linear *Berezin integral* [267] with the follwing properties

$$\int \mathrm{d}c_j \, 1 = 0, \tag{E.19}$$
$$\int \mathrm{d}c_j \, c_i = - \int c_i \, \mathrm{d}c_j = \delta_{i,j}. \tag{E.20}$$

The differential $\mathrm{d}c_j$ is anti-commutative under multiplication (C.71) similar to an ordinary Grassmann number. Summarizing, mathematical analysis of functions of Grassmann numbers is seemingly easy by virtue of their properties resulting from the anti-commutative multiplication (C.71) and the equality (up to a sign) of derivative (E.16, E.17) and integration (E.19, E.20), i.e.

$$\partial_{c_k} f(c_1, c_2, \ldots, c_N) = \int \mathrm{d}c_k \, f(c_1, c_2, \ldots, c_N) = - \int f(c_1, c_2, \ldots, c_N) \, \mathrm{d}c_k. \tag{E.21}$$

Within the framework of this thesis a slightly generalized version of functions (E.15), which are quadratic in Grassmann numbers, i.e. $m_i(\ldots) = 0 \ \forall i = 0, 1, 3, \ldots$, are of special interest: By introducing the vector-representation of the N pairs of conjugated Grassmann numbers, $\boldsymbol{\rho} = (c_1, c_2, \ldots, c_N)^T$ and $\boldsymbol{\rho}^\dagger = (c_1^*, c_2^*, \ldots, c_N^*)$, functions of this type are from the following form

$$f(\boldsymbol{\rho}^\dagger, \boldsymbol{\rho}) = \boldsymbol{\rho}^\dagger \mathbb{M} \boldsymbol{\rho} = \sum_{i,j} c_i^* m_{i,j} c_j, \tag{E.22}$$

where $\mathbb{M}$ denotes a $N \times N$-matrix-representation of complex coefficients $m_{i,j} = m_2(i,j)$, $i, j = 1, 2, \ldots, N$.

E.3 Evaluation of Matsubara sums

The aim of the following subsection is to outline a general scheme [268, 269] for the evaluation of a Matsubara frequency sum [265] of the following form

$$\sigma^{\pm} = \frac{1}{\beta} \sum_{\omega_n^{\pm}} f(i\omega_n^{\pm}), \tag{E.23}$$

where $f(z)$, $z \in \mathbb{C}$, is an arbitrary function of complex numbers regarded to be regular at each Matsubara frequency $i\omega_n^{\pm}$, where $\omega_n^{\pm}$ is defined in Eq. (D.67). Thereby the summation in Eq. (E.23) extends over all Matsubara frequencies indexed by n, i.e. $n \in \mathbb{Z}$.

As a first step one expresses the prefactor by the complex residue of the auxiliary functions

$$\eta^{\pm}(z) = \pm \frac{1}{\exp(z\beta) \mp 1}, \tag{E.24}$$

matching the Bose-Einstein ($+$) and Fermi-Dirac ($-$) statistics up to the negative sign for the latter. It is straightforward to see, that $z = i\omega_n^{\pm}$ is a pole of $\eta^{\pm}(z)$ and the residue of this pole precisely coincides with the prefactor in Eq. (E.23), i.e.

$$\mathrm{Res}_{i\omega_n^{\pm}} \left[\eta^{\pm}(z) \right] = \frac{1}{\beta}. \tag{E.25}$$

Since $f(z)$ is regarded to be regular at each Matsubara frequency one can express σ (E.23) in the following way

$$\sigma^{\pm} = \sum_{\omega_n^{\pm}} \mathrm{Res}_{i\omega_n^{\pm}} \left[\eta^{\pm}(z) f(z) \right]. \tag{E.26}$$

From the residue theorem [270] follows that the residue of a function $g(z)$ at its pole a can be determined by the integration along a closed contour $\partial U(a)$ around the pole,

$$\mathrm{Res}_a \left[g(z) \right] = \frac{\mathrm{ind}(a)}{2\pi i} \oint_{\partial U(a)} \mathrm{d}z\, g(z), \tag{E.27}$$

where the winding number $\mathrm{ind}(a)$ counts the number and the direction of circulation around a pole a performed by a certain path of integration. In the case discussed here the paths are chosen to circumvent each pole once, whereas

$$\mathrm{ind}(a) = \begin{cases} -1 & \text{for clockwise,} \\ +1 & \text{for counter-clockwise} \end{cases} \tag{E.28}$$
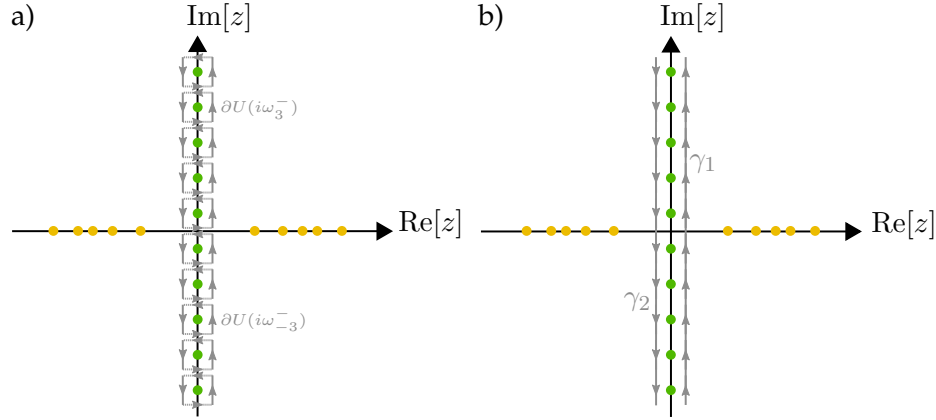
circulation around a.

FIGURE E.1: Poles of the auxiliary function $\eta^-(z)$ according to fermionic Matsubara frequencies (D.67) are marked by green dots. The orange dots illustrate potential poles of the function $f(z)$ (E.23). Without loss of generality these poles are chosen to be real in the depicted example. Panel a) illustrates the counter-clockwisely enclosed integration contours $\partial U(i\omega_n^-)$ (gray rectangles) in the vicinity of each imaginary Matsubara frequency. For pedagogical reasons those contours are depicted as rectangular paths, so that the cancellation of the horizontal contribution (dotted segments) of two subsequent paths becomes obvious. Therefore, the integration can be reduced to the vertical contributions (solid segments) of each integration contour $\partial U(i\omega_n^-)$ resulting in the paths γ_1, γ_2 as shown in gray by panel b).

For convenience a counter-clockwise direction of integration is chosen, so that

$$\sigma^\pm = \frac{1}{2\pi i} \sum_{\omega_n^\pm} \oint_{\partial U(i\omega_n^\pm)} \mathrm{d}z \, \eta^\pm(z) f(z). \tag{E.29}$$

As depicted by Fig. E.1 a) for fermionic Matsubara frequencies the horizontal contributions of two subsequent integration contours, $\partial U(i\omega_n^\pm)$ and $\partial U(i\omega_{n+1}^\pm)$, cancel with each other since the direction of integration is opposite. Therefore, the integration contour reduces to the vertical contributions resulting in the path γ_1 on the right half plane and γ_2 on the left half plane as clarified by Fig. E.1 b). Consequently $\sigma^\pm$ simplifies to the sum of both contributions according to the integration along the effective paths γ_1 and γ_2,

$$\sigma^\pm = \sigma_1^\pm + \sigma_2^\pm, \quad \sigma_i^\pm = \frac{1}{2\pi i} \int_{\gamma_i} \mathrm{d}z \, \eta^\pm(z) f(z). \tag{E.30}$$

The evaluation of these integrals can be achieved by means of the residue theorem [270]. Therefore the integration along both effective paths, γ_1 and γ_2, has to be transformed into an integration along closed contours. Note that the choice of the closed integration contour depends upon the properties of the integrand $\eta^\pm f$. The particular example subsequently outlined refers to f being well-behaved and injective. However, also the evaluation of the Matsubara sum (E.23) for $f(z) = \log(z - \epsilon)$, which has a branch cut for $z \leq \epsilon$ along the real axis, is relevant for this thesis (cf. Sec. D.3). In this case the subsequently outlined scheme applies as well for a proper choice of the closed integration contour, such as depicted in Fig. E.2 b). For further details on the evaluation of the Matsubara
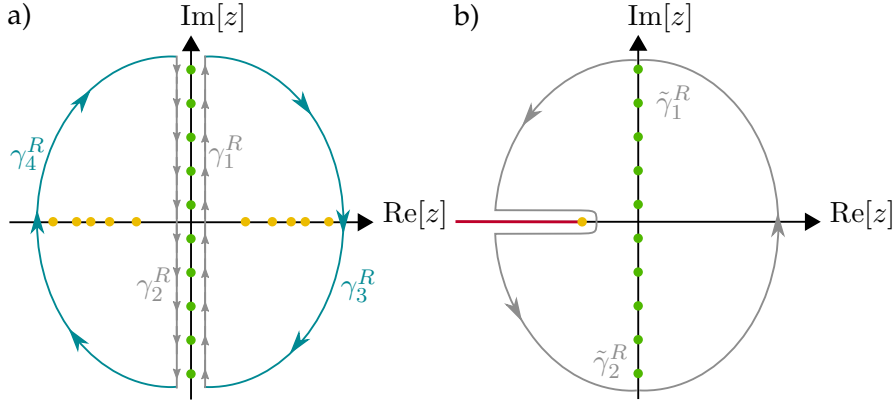
FIGURE E.2: Panel a): Following Fig. E.1. Closure of the effective integration contours γ_1^R and γ_2^R by the blue solid semicircular contours, γ_3^R and γ_4^R, respectively. Note that this holds only for injective complex integrands. Panel b): Following Ref. [257]. Suitable integration contour for $f(z) = \log(z - \epsilon)$, where ϵ is marked by the orange dot. The red labeled region on the real axis for $z \leq \epsilon$ illustrates the branch cut of the complex logarithm. The integration contour is composited from $\tilde{\gamma}_1^R$ and $\tilde{\gamma}_2^R$ which result from the distorted contours γ_1 and γ_2 as depicted in Fig. E.1.

sum in case of $f(z) = \log(z - \epsilon)$ one is also referred to Ref. [257].

With this, the discussion of the evaluation of the Matsubara sum for f being injective and regular is proceeded. Thus, by extending the integration path γ_1 with a semicircular path γ_3^R with radius R, as depicted by Fig. E.2 a), a closed integration contour $\gamma_r^R = \gamma_1^R + \gamma_3^R$ results on the right half plane. Similar, one can close the integration on the left half plane by adding to $\sigma_2^{\pm}$ the integration along γ_4^R, i.e. $\gamma_1^R = \gamma_2^R + \gamma_4^R$. According to the residue theorem, the value of the integration of $\eta^{\pm}(z)f(z)$ along either closed contours, $\gamma_{r/l}^R$, equals the sum over the residues of $f(z)$ at its enclosed poles, $z_i^{r/l}$. Thus, one finds, for instance, in the right half plane

$$\frac{1}{2\pi i} \lim_{R\to\infty} \oint_{\gamma_1^R + \gamma_3^R = \gamma_r^R} \mathrm{d}z\, \eta^{\pm}(z)f(f) = -\sum_{z_i^r} \mathrm{Res}_{z_i^r}\left[\eta^{\pm}(z)f(z)\right] \qquad (E.31)$$

Note that the poles of the auxiliary function $\eta^{\pm}(z)$ lie on the outside of the enclosed region by definition. With $z_i^{r/l}$ denoting the i-th pole of $f(z)$ in the right / left half plane one finds for each contribution $\sigma_i^{\pm}$, $i = 1, 2$, to $\sigma^{\pm}$, Eq. (E.30):

$$\sigma_{1/2}^{\pm} = -\sum_{z_i^{r/l}} \mathrm{Res}_{z_i^{r/l}}\left[\eta^{\pm}(z)f(z)\right] - \frac{1}{2\pi i} \lim_{R\to\infty} \int_{\gamma_{3/4}^R} \mathrm{d}z\, \eta^{\pm}(z)f(z). \qquad (E.32)$$

The negative sign in front of the sum over residues results from the integration around the poles in clockwise direction as Fig. E.2 a) depicts. Up to the integration along the semicircles, γ_3^R and γ_4^R, the resulting expression for $\sigma_{1/2}^{\pm}$ and thus in turn $\sigma^{\pm}$ have essentially simplified. In many cases and also applicable to the one of interest during this thesis, the remaining integration on the r.h.s. of Eq. (E.32) can be evaluated taking account

for Jordan's lemma [270]:

$$\int_{\gamma_3^R} \mathrm{d}z\, g(z) e^{-\alpha z} \xrightarrow{R \to \infty} 0, \tag{E.33}$$

$$\int_{\gamma_4^R} \mathrm{d}z\, g(z) e^{\alpha z} \xrightarrow{R \to \infty} 0, \tag{E.34}$$

if a complex function $g(z)$ that fulfills

$$g(z) \xrightarrow{|z| \to \infty} 0, \quad \text{if } \alpha > 0, \tag{E.35}$$

$$zg(z) \xrightarrow{|z| \to \infty} 0, \quad \text{if } \alpha \geq 0. \tag{E.36}$$

This is at least the case, if $g(z) = P(z)/Q(z)$, where $P(z)$ and $Q(z)$ are polynomials with

$$\mathrm{degree}(Q) \geq \begin{cases} 1 + \mathrm{degree}(P), & \text{if } \alpha > 0 \\ 2 + \mathrm{degree}(P), & \text{if } \alpha \geq 0. \end{cases} \tag{E.37}$$

Applying these conditions to the present discussion, one substitutes $g(z) = \eta^{\pm}(z)f(z)$. In the case of interest during this thesis the function $f(z)$ is a polynomial fulfilling Eq. (E.37). Due to the factor $\eta^{\pm}(z)$ convergence of $\eta^{\pm}(z)f(z) \to 0$ or $z\eta^{\pm}(z)f(z) \to 0$, when $|z| \to 0$, is self-sufficiently guaranteed as long as $\eta^{\pm}(z)$ tends faster to zero than $f(z)$. With this the final result of this Sec. can be summarized as follows:

$$\sigma^{\pm} = \frac{1}{\beta} \sum_{\omega_n^{\pm}} f(i\omega_n^{\pm}) = - \sum_{z_i} \mathrm{Res}_{z_i}[\eta^{\pm}(z)f(z)], \tag{E.38}$$

where the summation over the poles z_i of the function $f(z)$ include the poles on the right and left half plane as well.

Remarks on the Matsubara sum over the complex logarithm
Figure E.2 b) depicts a proper choice of the integration contour in the case of $f(z) = \log(z - \epsilon)$ [257]. By application of Jordan's lemma, one can show that the contributions from both semicircles in the upper and lower half plane vanish in the limit $R \to \infty$. Thus from accounting for the suitable choice of integration, one finds for Eq. (E.29) [257]

$$\sigma^{\pm} = \frac{1}{2\pi i} \int_{-\infty}^{\infty} \mathrm{d}z\, \eta^{\pm}(z) \left[\log(z + i0^+ - \epsilon) - \log(z - i0^+ - \epsilon) \right], \tag{E.39}$$

where the displacement of z in each argument of the logarithm is necessary to avoid the integration along the branch cut on the real axis. The integration (E.39) accounts for both directions along the branch cut. As the contributions to (E.39) compensate for $z > \epsilon$ the integration interval was extended from $]-\infty, \epsilon]$ to $]-\infty, \infty[$ in accordance with Ref. [257].

Finally, integrating by parts in view of the definition of $\eta^{\pm}$, Eq. (E.39), yields [203, 257]

$$
\begin{aligned}
\sigma^{\pm} &= -\frac{1}{\beta}\frac{1}{2\pi i}\int_{-\infty}^{\infty}\mathrm{d}z\,\log\left(1\mp e^{-\beta z}\right)\left(\frac{1}{z+i0^{+}-\epsilon}-\frac{1}{z-i0^{+}-\epsilon}\right)\\
&= -\frac{1}{\beta}\log\left(1\mp e^{-\beta\epsilon}\right),
\end{aligned}
\tag{E.40}
$$

where $\eta^{\pm}(z) = \partial_z \log(1 \mp e^{-\beta z})$ [257] was used. Thus, summarizing, one finds for the Matsubara sum over the complex logarithm

$$
\sigma^{\pm} = \frac{1}{\beta}\sum_{\omega_n^{\pm}}\log(i\omega_n^{\pm}-\epsilon) = \frac{1}{\beta}\log\left(1\mp e^{-\beta\epsilon}\right),
\tag{E.41}
$$

where the upper sign refers to bosons and the lower one to fermions.

E.4   Useful commutation relations

Assuming two quantum operators $\hat{A}$ and $\hat{B}$, which do not commute in the most general case. The following considerations are basically captured by the Baker-Campbell-Hausdorff formula [243–245] as given by Eq. (B.26). Likewise, the subsequently derived expressions can be regarded precisely as the basis for the derivation of that particular formula. Nevertheless, one might gain further insight in the commutation relation between the operator $\hat{A}$ and the kth power of $\hat{B}$ by detailed investigation according to

$$
\begin{aligned}
[\hat{A},\hat{B}^k] &= \hat{B}^{k-1}[\hat{A},\hat{B}] + [\hat{A},\hat{B}^{k-1}]\hat{B}\\
&= \hat{B}^{k-1}[\hat{A},\hat{B}] + \hat{B}^{k-2}[\hat{A},\hat{B}] + [\hat{A},\hat{B}^{k-2}]\hat{B}\\
&\;\;\vdots\\
&= \sum_{l=1}^{k}\hat{B}^{k-l}[\hat{A},\hat{B}]\hat{B}^{l-1}
\end{aligned}
\tag{E.42}
$$

With this, it follows

$$
\hat{A}\hat{B}^k = \hat{B}^k\hat{A} + \sum_{l=1}^{k}\hat{B}^{k-l}[\hat{A},\hat{B}]\hat{B}^{l-1}
\tag{E.43}
$$

By defining

$$
\hat{X}_i = [\hat{X}_{i-1},\hat{B}], \quad \text{where } \hat{X}_0 = \hat{A}
\tag{E.44}
$$

one finds for the general situation, where $[\hat{A}, \hat{B}] \neq 0$:

$$
\begin{aligned}
[\hat{A}, \hat{B}^k] &= \sum_{l=1}^{k} \hat{B}^{k-l} \hat{X}_1 \hat{B}^{l-1} \\
&\overset{(E.43)}{=} \sum_{l=1}^{k} \hat{B}^{k-1} \hat{X}_1 + \sum_{l=1}^{k} \sum_{m=1}^{l-1} \hat{B}^{k-m-1} \hat{X}_2 \hat{B}^{m-1} \\
&\overset{(E.43)}{=} \sum_{l=1}^{k} \hat{B}^{k-1} \hat{X}_1 + \sum_{l=1}^{k} \sum_{m=1}^{l-1} \hat{B}^{k-2} \hat{X}_2 + \sum_{l=1}^{k} \sum_{m=1}^{l-1} \sum_{n=1}^{m-1} \hat{B}^{k-n-2} \hat{X}_3 \hat{B}^{n-1} \qquad \text{(E.45)} \\
&\;\;\vdots \\
&= \sum_{l=1}^{k} \frac{\prod_{i=0}^{l-1}(k-i)}{l!} \hat{B}^{k-l} \hat{X}_l.
\end{aligned}
$$

It follows for the commutator of $\hat{A}$ with the exponential of $\hat{B}$,

$$
[\hat{A}, e^{\hat{B}}] = \sum_{k=0}^{\infty} \frac{[\hat{A}, \hat{B}^k]}{k!} = \sum_{k=0}^{\infty} \sum_{l=1}^{k} \frac{1}{k!} \left[\frac{\prod_{i=0}^{l-1}(k-i)}{l!} \hat{B}^{k-l} \hat{X}_l \right]. \qquad \text{(E.46)}
$$

With this, one is able to discover the most general condition for $[\hat{A}, e^{\beta \hat{B}}] = 0$, where $\beta \in \mathbb{C}$. Let the commutator $\hat{X}_l$ (E.44) be given by

$$
\hat{X}_l = \alpha^l f(\hat{A}, \hat{B}), \qquad \text{(E.47)}
$$

where $\alpha \in \mathbb{C}$ and $f(\hat{A}, \hat{B})$ denotes some function of both operator contributions which is independent on l. Then it follows for the commutator of $\hat{A}$ and $e^{\beta \hat{B}}$

$$
[\hat{A}, e^{\beta \hat{B}}] = e^{\beta \hat{B}} (e^{\alpha \beta} - 1) f(\hat{A}, \hat{B}). \qquad \text{(E.48)}
$$

This expression will precisely yield zero, if

1. $f(\hat{A}, \hat{B}) = 0$, which is identical to $[\hat{A}, \hat{B}] = 0$, or if

2. $\alpha \beta = 2\pi i n$, for $n \in \mathbb{Z}$.

For proving the parity operator to commute with the Dicke Hamiltonian, as discussed in Subsec. 3.3.5, it is helpful to consider the case of $\hat{A}$ and $\hat{B}$ each being composed two different operator contributions. Therefore, assuming $\hat{A} = \hat{A}_1 \hat{A}_2$ and $\hat{B} = \hat{B}_1 + \hat{B}_2$, where the equally labeled contributions, $\hat{A}_1, \hat{B}_1$ and $\hat{A}_2, \hat{B}_2$, operate in different Hilbert subspaces, i.e.

$$
[\hat{A}_1, \hat{A}_2] = [\hat{A}_1, \hat{B}_2] = [\hat{B}_1, \hat{A}_2] = [\hat{B}_1, \hat{B}_2] = 0. \qquad \text{(E.49)}
$$

For the most general consideration, it is assumed

$$
[\hat{A}_1, \hat{B}_1] \neq 0, \quad [\hat{A}_2, \hat{B}_2] \neq 0. \qquad \text{(E.50)}
$$

The equivalent to Eq. (E.46) is then of the form

$$
\begin{aligned}
[\hat{A}_1\hat{A}_2, e^{\beta_2\hat{B}_1}e^{\beta_2\hat{B}_2}] &= \hat{A}_2[\hat{A}_1, e^{\beta_1\hat{B}_1}]e^{\beta_2\hat{B}_2} + e^{\beta_1\hat{B}_1}[\hat{A}_2, e^{\beta_2\hat{B}_2}]\hat{A}_1 \\
&\overset{(E.46)}{=} \hat{A}_2 e^{\beta_1\hat{B}_1}(e^{\alpha_1\beta_1} - 1)f_1(\hat{A}_1, \hat{B}_1)e^{\beta_2\hat{B}_2} \\
&\quad + e^{\beta_1\hat{B}_1}e^{\beta_2\hat{B}_2}(e^{\alpha_2\beta_2} - 1)f_2(\hat{A}_2, \hat{B}_2)\hat{A}_1,
\end{aligned}
\tag{E.51}
$$

where $\alpha_1, \alpha_2 \in \mathbb{C}$ and $\beta_1, \beta_2 \in \mathbb{C}$. In order to investigate on the properties of β, α_1 and α_2 which need to be satisfied in order provide the operator products (E.51) to commute, it is necessary to order change the order of $\hat{A}_2$ and $e^{\beta_2\hat{B}_2}$ in the first expression in the last line of Eq. (E.51). This is achieved by means of relation (E.46), yielding for Eq. (E.51) the following expression

$$
\begin{aligned}
[\hat{A}_1\hat{A}_2, e^{\beta_1\hat{B}_1}e^{\beta_2\hat{B}_2}] &= e^{\beta_1\hat{B}_1}e^{\beta_2\hat{B}_2}\Big[(e^{\alpha_1\beta_1} - 1)f_1(\hat{A}_1, \hat{B}_1)\hat{A}_2 \\
&\quad + (e^{\alpha_1\beta_1} - 1)(e^{\alpha_2\beta_2} - 1)f_1(\hat{A}_1, \hat{B}_1)f_2(\hat{A}_2, \hat{B}_2) + (e^{\alpha_2\beta_2} - 1))\hat{A}_1 f_2(\hat{A}_2, \hat{B}_2)\Big].
\end{aligned}
\tag{E.52}
$$

If the functions f_1 and f_2 are not specified further, this is the final result. In this case, similar conditions as for the single-particle operator apply to ensure commutation.

By contrast, if it is assumed that $f_1 = \hat{A}_1$ and $f_2 = \hat{A}_2$ expression (E.52) will simplify to

$$
[\hat{A}_1\hat{A}_2, e^{\beta_1\hat{B}_1}e^{\beta_2\hat{B}_2}] = e^{\beta_1\hat{B}_1}e^{\beta_2\hat{B}_2}(e^{\alpha_1\beta_1+\alpha_2\beta_2} - 1)\hat{A}_1\hat{A}_2.
\tag{E.53}
$$

Thus, in this case

$$
[\hat{A}_1\hat{A}_2, e^{\beta_1\hat{B}_1}e^{\beta_2\hat{B}_2}] = 0 \quad \Leftrightarrow \quad \alpha_1\beta_1 + \alpha_2\beta_2 = 2\pi i n, \text{ for } n \in \mathbb{Z}.
\tag{E.54}
$$

Appendix F

Fourth-order contributions to the effective Dicke-like Hamiltonian

F.1 Contributions from the Landau-level doublet M and $M + 1$

For the derivation of the relevant contributions arising from the fourth-order correction to the effective Hamiltonian, Eq. (8.43), discussed in Chap. 8, it is convenient to decompose $\hat{\mathcal{H}}^{(4)}$, Eq. (8.48), into three components:

$$\hat{\mathcal{H}}^{(4)} = \hat{\mathcal{H}}_1^{(4)} + \hat{\mathcal{H}}_2^{(4)} + \hat{\mathcal{H}}_3^{(4)}, \tag{F.1}$$

where the single parts,

$$\hat{\mathcal{H}}_1^{(4)} = -\frac{1}{2}[\hat{\mathcal{V}}_o, \mathcal{L}([\hat{\mathcal{V}}_d, \mathcal{L}([\hat{\mathcal{V}}_d, \hat{\mathcal{S}}_1])])], \tag{F.2}$$

$$\hat{\mathcal{H}}_2^{(4)} = -\frac{1}{6}[\hat{\mathcal{V}}_o, \mathcal{L}([\hat{\mathcal{S}}_1, [\hat{\mathcal{S}}_1, \hat{\mathcal{V}}_o]])], \tag{F.3}$$

$$\hat{\mathcal{H}}_3^{(4)} = -\frac{1}{24}[\hat{\mathcal{S}}_1, [\hat{\mathcal{S}}_1, [\hat{\mathcal{S}}_1, \hat{\mathcal{V}}_o]]], \tag{F.4}$$

are sequentially discussed. It is beneficial, to recap the general structure of the three operators entering the expressions:

$$\hat{\mathcal{V}}_d = \hat{v} \otimes \hat{V}_d, \tag{F.5}$$

$$\hat{\mathcal{V}}_o = \hat{v} \otimes (\hat{V}_o + \hat{V}_o^\dagger), \tag{F.6}$$

$$\hat{\mathcal{S}}_1 = \hat{s} \otimes \hat{S} - \hat{s}^\dagger \otimes \hat{S}^\dagger, \tag{F.7}$$

where the capital letters refer to the fermionic part and the small letters denote the bosonic contribution. This notation helps to evaluate the nested commutators in a more transparent way. For convenience, the explicit notation of the tensor product, $\otimes$, will be omitted during the following. The microscopic details of each contribution can be found in Subsec. 8.1.2 and Subsec. 8.2.3.

Derivation of $\hat{\mathcal{H}}_1^{(4)}$

The innermost commutator is easily evaluated in view of Eqs. (F.5, F.7). Thereby one decomposes the bosonic and fermionic parts similar as in Eq. (8.54) where the second-order contribution is considered:

$$\mathcal{L}([\hat{\mathcal{V}}_d, \hat{\mathcal{S}}_1]) = \mathcal{L}(\hat{v}\hat{s}[\hat{V}_d, \hat{S}]) - \mathcal{L}(\hat{v}\hat{s}^\dagger[\hat{V}_d, \hat{S}^\dagger]) + \mathcal{L}([\hat{v}, \hat{s}]\hat{S}\hat{V}_d) - \mathcal{L}([\hat{v}, \hat{s}^\dagger]\hat{S}^\dagger\hat{V}_d). \tag{F.8}$$

According to the arguments discussed in Subsec. 8.2.7, only the following parts of the first nested commutator yield expressions similar to Eq. (8.54)

$$\mathcal{L}([\hat{\bar{\mathcal{V}}}_d, \mathcal{L}([\hat{\mathcal{V}}_d, \hat{\mathcal{S}}_1]]))_R = \mathcal{L}([\hat{v}, \mathcal{L}(\hat{v}\hat{s}[\hat{V}_d, \hat{S}])]\hat{\bar{V}}_d) - \mathcal{L}([\hat{v}, \mathcal{L}(\hat{v}\hat{s}^\dagger[\hat{V}_d, \hat{S}^\dagger])]\hat{\bar{V}}_d)$$
$$+ \mathcal{L}(\hat{v}, [\hat{\bar{V}}_d, \mathcal{L}([\hat{v}, \hat{s}]\hat{S}\hat{V}_d)]) - \mathcal{L}(\hat{v}, [\hat{\bar{V}}_d, \mathcal{L}([\hat{v}, \hat{s}^\dagger]\hat{S}^\dagger\hat{V}_d)]), \tag{F.9}$$

where R indicates, that only the terms expected to dominantly contribute are considered. Furthermore, the operators marked with the bar are identical to the plane ones. However, as expression (F.9) is regarded as a short-hand notation where the summation over each set of quantum numbers has to be taken into account, this notation helps to keep track. Note Eq. (F.9) can be further reduced as the first two nested commutators yield no contribution in the ground-state average. This can be seen from the innermost commutators, $[\hat{V}_d, \hat{S}]$ and $[\hat{V}_d, \hat{S}^\dagger]$, which already "consuming" the first commutator of relation (8.97). However, each of them yields a block-off diagonal contribution which clearly is not diagonal and hence the ground-state expectation value assumes zero. Thus, proceeding with the remaining last two terms in Eq. (F.9) and taking the last commutator with $\hat{\mathcal{V}}_o$ yields

$$[\hat{\mathcal{V}}_o, \mathcal{L}([\hat{\mathcal{V}}_d, \mathcal{L}([\hat{\mathcal{V}}_d, \hat{\mathcal{S}}_1])]))]_R = \hat{v}[\hat{V}_o + \hat{V}_o^\dagger, \mathcal{L}(\hat{v}[\hat{\bar{V}}_d, \mathcal{L}([\hat{v}, \hat{s}]\hat{S}\hat{V}_d)])]$$
$$- \hat{v}[\hat{V}_o + \hat{V}_o^\dagger, \mathcal{L}(\hat{v}[\hat{\bar{V}}_d, \mathcal{L}([\hat{v}, \hat{s}^\dagger]\hat{S}^\dagger\hat{V}_d)])]. \tag{F.10}$$

However, this expression still contains terms which vanish when taking the ground-state average $\langle \ldots \rangle_0$. These terms can only be identified when taking into account the microscopic definitions of the single contributions along with the action of the superoperator $\mathcal{L}$. To this end, consider the innermost commutators of Eq. (F.10):

$$[\hat{v}, \hat{s}]\hat{S}\hat{V}_d = -\frac{[\hat{a}, \hat{a}^\dagger]}{\mathcal{N}} \sum_{\substack{M \in \mathbb{H}_M \\ N \in \mathbb{H}_{m \; n_M^-}}} \sum_{\substack{S, S' \in \mathbb{H}_M \\ S, S' \in \mathbb{H}_N}} \mathcal{M}_{M,N} \mathcal{M}_{S,S'} \mathcal{C}_{M,N} \, \hat{c}_M^\dagger \hat{c}_N \, \hat{c}_S^\dagger \hat{c}_{S'}, \tag{F.11}$$

$$[\hat{v}, \hat{s}^\dagger]\hat{S}^\dagger\hat{V}_d = \frac{[\hat{a}, \hat{a}^\dagger]}{\mathcal{N}} \sum_{\substack{M \in \mathbb{H}_M \\ N \in \mathbb{H}_{m \; n_M^-}}} \sum_{\substack{S, S' \in \mathbb{H}_M \\ S, S' \in \mathbb{H}_N}} \mathcal{M}_{M,N} \mathcal{M}_{S,S'} \mathcal{C}_{M,N} \, \hat{c}_N^\dagger \hat{c}_M \, \hat{c}_S^\dagger \hat{c}_{S'}, \tag{F.12}$$

where $\mathcal{C}_{M,N}$ is defined in Eq. (8.60). In order to ensure a Hermitian result it is necessary to symmetrize these expressions with respect to the ordering of the fermionic perturbation and the SW generator contribution, i.e. $[\hat{v}, \hat{s}]\hat{S}\hat{V}_d = 1/2\,[\hat{v}, \hat{s}](\hat{S}\hat{V}_d + \hat{V}_d\hat{S})$ and similar fo the second contribution. This is furthermore well justified, as the anti-commutator of this relation yields a one-body contribution which is not relevant. Thus, the action of the

superoperator onto the symmetrized equivalent of expression (F.11) is given by

$$
\mathcal{L}(\frac{1}{2}[\hat{v},\hat{s}](\hat{S}\hat{V}_d + \hat{S}\hat{V}_d))_R = -\frac{[\hat{a},\hat{a}^\dagger]}{2\mathcal{N}}\left[\sum_{\substack{M\in\mathbb{H}_M \\ N,\bar{N},N'\in\mathbb{H}_N}} \mathcal{M}_{M,N}\mathcal{M}_{\bar{N},N'}\mathcal{C}_{M,N} E^{M,N}_{\bar{N},N'}\,\hat{c}^\dagger_M\hat{c}_N\,\hat{c}^\dagger_{\bar{N}}\hat{c}_{N'}\right.
$$

$$
\left.+\sum_{\substack{M,\bar{M},M'\in\mathbb{H}_M \\ N\in\mathbb{H}_N}} \mathcal{M}_{M,N}\mathcal{M}_{\bar{M},M'}\mathcal{C}_{M,N} E^{M,N}_{M',\bar{M}}\,\hat{c}^\dagger_{M'}\hat{c}_{\bar{M}}\,\hat{c}^\dagger_M\hat{c}_N\right], \quad \text{(F.13)}
$$

where

$$
E^{M,N}_{K,L} = \frac{1}{\Delta_{M,N}+\Delta_{K,L}} \tag{F.14}
$$

for $\Delta_{M,N}$ as defined in Eq. (8.52). The corresponding expression for the remaining inner-most commutator in Eq. (F.10), $1/2\,[\hat{v},\hat{s}^\dagger](\hat{S}^\dagger\hat{V}_d + \hat{V}_d\hat{S}^\dagger)$, is obtained likewise.

As a next step, the commutator with $\hat{\mathcal{V}}_d$ is evaluated. However, not all contributions appearing from the fermionic commutators are relevant with respect to the ground-state average. Consider, for instance, the commutator

$$
[\hat{c}^\dagger_O\hat{c}_{O'},\hat{c}^\dagger_M\hat{c}_N\,\hat{c}^\dagger_{\bar{N}}\hat{c}_{N'}] = \hat{c}^\dagger_M\hat{c}_N[\hat{c}^\dagger_O\hat{c}_{O'},\hat{c}^\dagger_{\bar{N}}\hat{c}_{N'}] + [\hat{c}^\dagger_O\hat{c}_{O'},\hat{c}^\dagger_M\hat{c}_N]\hat{c}^\dagger_{\bar{N}}\hat{c}_{N'}, \tag{F.15}
$$

where O and O' label states within either the Hilbert subspace $\mathbb{H}_M$ or $\mathbb{H}_N$. The last contribution on the r.h.s. yields a block-off diagonal term which gives zero when taking the ground-state expectation value. Thus, only the commutator between both block-diagonal operators will contribute in the end. However, there are still terms appearing in the commutators of block-diagonal contributions in the Hilbert subspace $\mathbb{H}_N$ which do not contribute to the ground-state average. These terms appear from the dipole selection rules as it is seen from the following: From the relevant commutator in Eq. (F.15) one obtains

$$
\sum_{\substack{O,O'\in\mathbb{H}_N \\ \bar{N},N'}} \mathcal{M}_{O,O'}\mathcal{M}_{\bar{N},N'}f_{\bar{N},N'}[\hat{c}^\dagger_O\hat{c}_{O'},\hat{c}^\dagger_{\bar{N}}\hat{c}_{N'}]
$$

$$
= \sum_{N,\bar{N},N'}\mathcal{M}_{N,\bar{N}}\mathcal{M}_{\bar{N},N'}(f_{\bar{N},N'}\,\hat{c}^\dagger_N\hat{c}_{N'} - f_{N',\bar{N}}\,\hat{c}^\dagger_{N'}\hat{c}_N), \quad \text{(F.16)}
$$

where $f_{\bar{N},N'}$ denotes some function which, for instance, could be given by Eq. (F.14). The product of the matrix elements is explicitly given by

$$
\mathcal{M}_{N,\bar{N}}\mathcal{M}_{\bar{N},N'} \overset{(5.48)}{=} \lambda_n\lambda_{\bar{n}}\,w_{+,n}w_{+,n+1}\,\delta_{n+1,\bar{n}}\delta_{n+2,n'}
$$
$$
+\lambda_n\lambda_{n'}\,w_{+,n}w_{+,n'}\,\delta_{n+1,\bar{n}}\delta_{n,n'}
$$
$$
+\lambda_{\bar{n}}\lambda_{\bar{n}}\,w^2_{+,\bar{n}}\,\delta_{n,\bar{n}+1}\delta_{n,n'}
$$
$$
+\lambda_{\bar{n}}\lambda_{n'}\,w_{+,\bar{n}}w_{+,n'}\,\delta_{n,\bar{n}+1}\delta_{n,n'+2}, \tag{F.17}
$$

where it its obvious that the first and last term promote non-diagonal operator contributions in Eq. (F.16). As these non-diagonal contributions vanish in the ground-state average, they are omitted straight away such that the relevant contribution from (F.16) is given by

$$\sum_{N,\bar{N}} \mathcal{M}^2_{N,\bar{N}}(f_{\bar{N},N} - f_{N,\bar{N}})\, \hat{c}^\dagger_N \hat{c}_N, \tag{F.18}$$

where the squared matrix elements are then explicitly reading

$$\mathcal{M}^2_{N,\bar{N}} = w^2_{+,n}\,\delta_{n+1,\bar{n}} + w^2_{+,n-1}\,\delta_{n-1,\bar{n}}. \tag{F.19}$$

With this, one finds for the relevant terms of the commutator of $\hat{\mathcal{V}}_d$ with Eq. (F.13)

$$\hat{v}[\hat{\bar{V}}_d, \mathcal{L}(\frac{1}{2}[\hat{v},\hat{s}](\hat{S}\hat{V}_d + \hat{S}\hat{V}_d))]_R$$

$$= -\frac{(\hat{a}^\dagger + \hat{a})}{2\sqrt{\mathcal{N}}^3}\left[\sum_{\substack{M\in\mathbb{H}_M \\ N,\bar{N},N'\in\mathbb{H}_N}} \mathcal{M}_{M,N}\mathcal{M}^2_{\bar{N},N'}\mathcal{C}_{M,N}\mathcal{E}^{M,N}_{\bar{N},N'}\,\hat{c}^\dagger_M\hat{c}_N\,\hat{c}^\dagger_{\bar{N}}\hat{c}_{\bar{N}} \right.$$

$$\left. + \sum_{\substack{M,\bar{M},M'\in\mathbb{H}_M \\ N\in\mathbb{H}_N}} \mathcal{M}_{M,N}\mathcal{M}^2_{\bar{M},M'}\mathcal{C}_{M,N}\mathcal{E}^{M,N}_{M',\bar{M}}\,\hat{c}^\dagger_{\bar{M}}\hat{c}_{\bar{M}}\,\hat{c}^\dagger_M\hat{c}_N \right], \quad \text{(F.20)}$$

where

$$\mathcal{E}^{M,N}_{K,L} = E^{M,N}_{K,L} - E^{M,N}_{L,K} = -\frac{2\Delta_{K,L}}{\Delta^2_{M,N} - \Delta^2_{K,L}}. \tag{F.21}$$

This function requires that $\Delta_{M,N} \neq \Delta_{K,L}$ in order to avoid divergence. This yields one particular contribution arising from the evaluation of the commutators to be necessarily regularized or excluded from the discussion. Postponing further considerations on this issue to the subsequent discussion, the evaluation of the nested commutator is proceeded.

Thus, the equivalent to Eq. (F.20) is found for the remaining commutator in Eq. (F.10) by identical derivation:

$$\hat{v}[\hat{\bar{V}}_d, \mathcal{L}(\frac{1}{2}[\hat{v},\hat{s}](\hat{S}^\dagger\hat{V}_d + \hat{S}^\dagger\hat{V}_d))]_R$$

$$= \frac{(\hat{a}^\dagger + \hat{a})}{2\sqrt{\mathcal{N}}^3}\left[\sum_{\substack{M\in\mathbb{H}_M, N\in\mathbb{H}_{m\ n_M^-} \\ \bar{N},N'\in\mathbb{H}_N}} \mathcal{M}_{M,N}\mathcal{M}^2_{\bar{N},N'}\mathcal{C}_{M,N}\mathcal{E}^{N,M}_{\bar{N},N'}\,\hat{c}^\dagger_{\bar{N}}\hat{c}_{\bar{N}}\,\hat{c}^\dagger_N\hat{c}_M \right.$$

$$\left. + \sum_{\substack{M,\bar{M},M'\in\mathbb{H}_M \\ N\in\mathbb{H}_{m\ n_M^-}}} \mathcal{M}_{M,N}\mathcal{M}^2_{\bar{M},M'}\mathcal{C}_{M,N}\mathcal{E}^{N,M}_{M',\bar{M}}\,\hat{c}^\dagger_N\hat{c}_M\,\hat{c}^\dagger_{\bar{M}}\hat{c}_{\bar{M}} \right]. \quad \text{(F.22)}$$

By interchanging the position of the block-diagonal and block-off diagonal fermionic operator pairs, which is justified when considering only dominant contributions, the combination of Eq. (F.20) and (F.22) simplifies to

$$\hat{v}[\hat{\bar{V}}_d, \mathcal{L}(\frac{1}{2}[\hat{v}, \hat{s}](\hat{S}\hat{V}_d + \hat{S}\hat{V}_d))]_R - \hat{v}[\hat{\bar{V}}_d, \mathcal{L}(\frac{1}{2}[\hat{v}, \hat{s}](\hat{S}^\dagger \hat{V}_d + \hat{S}^\dagger \hat{V}_d))]_R$$

$$= \frac{(\hat{a}^\dagger + \hat{a})}{2\sqrt{\mathcal{N}}^3} \left[\sum_{\substack{M \in \mathbb{H}_M, N \in \mathbb{H}_{m\ n_M^-} \\ O, O' \in \mathbb{H}_M \dot\cup \mathbb{H}_N}} \mathcal{M}_{M,N} \mathcal{M}_{O,O'}^2 \mathcal{C}_{M,N} \mathcal{E}_{O,O'}^{M,N} \, \hat{c}_O^\dagger \hat{c}_O \, (\hat{c}_M^\dagger \hat{c}_N + \hat{c}_N^\dagger \hat{c}_M) \right], \quad \text{(F.23)}$$

where the quantum numbers O and O' are defined within the disjoint union of the Hilbert subspaces $\mathbb{H}_M$ and $\mathbb{H}_N$. The action of the superoperator $\mathcal{L}$ onto Eq. (F.23) is then obtained as

$$\mathcal{L}(\hat{v}[\hat{\bar{V}}_d, \mathcal{L}(\frac{1}{2}[\hat{v}, \hat{s}](\hat{S}\hat{V}_d + \hat{S}\hat{V}_d))] - \hat{v}[\hat{\bar{V}}_d, \mathcal{L}(\frac{1}{2}[\hat{v}, \hat{s}](\hat{S}^\dagger \hat{V}_d + \hat{S}^\dagger \hat{V}_d))])_R$$

$$= \frac{(\hat{a}^\dagger + \hat{a})}{2\sqrt{\mathcal{N}}^3} \left[\sum_{\substack{M \in \mathbb{H}_M, N \in \mathbb{H}_{m\ n_M^-} \\ O, O' \in \mathbb{H}_M \dot\cup \mathbb{H}_N}} \mathcal{M}_{M,N} \mathcal{M}_{O,O'}^2 \mathcal{C}_{M,N} \mathcal{E}_{O,O'}^{M,N} \, \hat{c}_O^\dagger \hat{c}_O \, (\hat{s}_{M,N} \hat{c}_M^\dagger \hat{c}_N - \hat{s}_{M,N}^\dagger \hat{c}_N^\dagger \hat{c}_M) \right]$$

$$\text{(F.24)}$$

where $\hat{s}_{M,N}$ is defined in Eq. (8.51). Finally, one finds for the last commutator with the block-off diagonal contribution $\hat{\mathcal{V}}_o$ the expression

$$[\hat{\mathcal{V}}_o, \mathcal{L}([\hat{\mathcal{V}}_d, \mathcal{L}([\hat{\mathcal{V}}_d, \hat{\mathcal{S}}_1])])]_R$$

$$= -\frac{(\hat{a}^\dagger + \hat{a})^2}{2\mathcal{N}^2} \left[\sum_{\substack{M \in \mathbb{H}_M, N \in \mathbb{H}_{m\ n_M^-} \\ O, O' \in \mathbb{H}_M \dot\cup \mathbb{H}_N}} \mathcal{M}_{M,N}^2 \mathcal{M}_{O,O'}^2 \mathcal{C}_{M,N} \mathcal{D}_{M,N} \mathcal{E}_{O,O'}^{M,N} \, \hat{c}_O^\dagger \hat{c}_O \, (\hat{c}_M^\dagger \hat{c}_M - \hat{c}_N^\dagger \hat{c}_N) \right]$$

$$\text{(F.25)}$$

where, again, only the terms are kept which survive the ground-state average. This contribution is also diamagnetic as expected. The ground-state expectation value of the contribution $\hat{\mathcal{H}}_1^{(4)}$ is given by

$$\langle \hat{\mathcal{H}}_1^{(4)} \rangle_0 = -\frac{(\hat{a}^\dagger + \hat{a})^2}{4\mathcal{N}^2} \left[\sum_{\substack{M \in \mathbb{H}_M, N \in \mathbb{H}_{m\ n_M^-} \\ O, O' \in \mathbb{H}_M \dot\cup \mathbb{H}_N}} \mathcal{M}_{M,N}^2 \mathcal{M}_{O,O'}^2 \mathcal{C}_{M,N} \mathcal{D}_{M,N} \mathcal{E}_{O,O'}^{M,N} \, n_O^- \, (n_M^- - n_N^-) \right],$$

$$\text{(F.26)}$$

where n_K^- is given by the Fermi-Dirac distribution, Eq. (8.140). Note that the negative

sign in the definition of $\hat{\mathcal{H}}_1^{(4)}$, Eq. (F.2), is compensated by the negative sign of the relevant term in the ground-state average, Eq. (8.99).

Now, the detailed evaluation of each sum over quantum numbers is demonstrated, starting with the summation over M and N. Therefore, it is beneficial to define

$$\mathcal{F}_{O,O'}^{M,N} = \mathcal{C}_{M,N}\mathcal{D}_{M,N}\mathcal{E}_{O,O'}^{M,N} = \frac{8\,\hbar\omega_0\,\Delta_{M,N}\Delta_{O,O'}}{[\Delta_{M,N}^2 - (\hbar\omega_0)]^2(\Delta_{M,N}^2 - \Delta_{O,O'}^2)} \tag{F.27}$$

such that one finds for the summation over M and N in Eq. (F.26)

$$\sum_{\substack{M\in\mathbb{H}_M \\ N\in\mathbb{H}_{m\ n_M^-}}} \mathcal{M}_{M,N}^2 \mathcal{F}_{O,O'}^{M,N}\,(n_M^- - n_N^-) \tag{F.28}$$

$$\begin{aligned}
=\mathcal{N}\Big[\ & w_{+,M-1}^2\big[\mathcal{F}_{O,O'}^{M,-(M-1)}(n_M^- - n_{-(M-1)}^-) && + \mathcal{F}_{O,O'}^{M,(M-1)}(n_M^- - n_{(M-1)}^-)\big] \\
+ & w_{+,M}^2\ \big[\mathcal{F}_{O,O'}^{M,-(M+1)}(n_M^- - n_{-(M+1)}^-) && + \mathcal{F}_{O,O'}^{M+1,-M}(n_{M+1}^- - n_{-M}^-)\big] \\
+ & w_{+,M+1}^2\big[\mathcal{F}_{O,O'}^{M+1,-(M+2)}(n_{M+1}^- - n_{-(M+2)}^-) + \mathcal{F}_{O,O'}^{M+1,M+2}(n_{M+1}^- - n_{M+2}^-)\big]\Big].
\end{aligned}$$

The sum over k, encoded in the short-hand notation, yields the factor of $\mathcal{N}$. In the zero-temperature limit, all states beneath the Fermi level are occupied and hence $n_K^- = 1$ for $K \leq M$. All other levels are completely empty. Thus, the terms remaining in Eq. (F.28) are

$$\sum_{\substack{M\in\mathbb{H}_M \\ N\in\mathbb{H}_{m\ n_M^-}}} \mathcal{M}_{M,N}^2 \mathcal{F}_{O,O'}^{M,N}\,(n_M^- - n_N^-) = -\mathcal{N}(w_{+,M}^2 \mathcal{F}_{O,O'}^{M+1,-M} + w_{+,M+1}^2 \mathcal{F}_{O,O'}^{M+1,-(M+2)}) \tag{F.29}$$

$$= -\mathcal{N}\,\mathcal{T}_{O,O'},$$

where $\mathcal{T}_{O,O'}$ is now a function of O and O' and M and N have been fixed. Before evaluating the sum over these remaining quantum numbers, the intermediate result for $\langle\hat{\mathcal{H}}_1^{(4)}\rangle_0$, Eq. (F.26), is summarized:

$$\langle\hat{\mathcal{H}}_1^{(4)}\rangle_0 = \frac{(\hat{a}^\dagger + \hat{a})^2}{4\mathcal{N}}\left[\sum_{O,O'\in\mathbb{H}_N} \mathcal{M}_{O,O'}^2 \mathcal{T}_{O,O'}\, n_O^-\right], \tag{F.30}$$

After carrying out the sum over the remaining k encoded in the short-hand notation and then summing over O' one obtains:

$$\begin{aligned}
\sum_{O,O'} \mathcal{M}_{O,O'}^2 \mathcal{T}_{O,O'} n_O^- = \mathcal{N}\sum_O \Big[& w_{+,O}^2\left(\mathcal{T}_{O,O+1} + \mathcal{T}_{O,-(O+1)}\right) \\
+ & w_{+,O-1}^2\left(\mathcal{T}_{O,O-1} + \mathcal{T}_{O,-(O-1)}\right)\Big]\,n_O^-.
\end{aligned} \tag{F.31}$$

Thereby it was explicitly accounted for both energy bands as it is also required for the final summation over O. Thus, carrying out the sum over the band indices encoded in

the short-hand notation $O = (\lambda, o) = (\lambda, |O|)$ one finds

$$\sum_{O,O'} \mathcal{M}^2_{O,O'} \mathcal{T}_{O,O'} n_O^- = \mathcal{N} \sum_{|O|} \left[w^2_{+,O} \left(\mathcal{T}_{O,O+1} + \mathcal{T}_{O,-(O+1)} \right) \right.$$
$$\left. + w^2_{+,O-1} \left(\mathcal{T}_{O,O-1} + \mathcal{T}_{O,-(O-1)} \right) \right] \left(n_O^- - n_{-O}^- \right), \tag{F.32}$$

where the symmetry properties of $\mathcal{T}_{O,O'}$ as a function of O and O' were used. At $T = 0$ this expression is given by

$$\frac{1}{\mathcal{N}} \sum_{O,O'} \mathcal{M}^2_{O,O'} \mathcal{T}_{O,O'} n_O^- = - \left[2 \sum_{|O|=M+3}^{\nu-2} w^2_{+,O} \mathcal{T}_{O+1,-O} + w^2_{+,M} \mathcal{T}_{M+1,M} \right.$$
$$\left. + w^2_{+,M+2} \left(\mathcal{T}_{M+3,M+2} + \mathcal{T}_{M+3,-(M+2)} \right) + w^2_{+,\nu-1} \left(-\mathcal{T}_{\nu,\nu-1} + \mathcal{T}_{\nu,-(\nu-1)} \right) \right]. \tag{F.33}$$

By defining

$$\mathcal{CD}_{M,N} = \mathcal{C}_{M,N} \mathcal{D}_{M,N} = -\frac{4\Delta_{M,N}\hbar\omega_0}{[\Delta^2_{M,N} - (\hbar\omega_0)^2]^2} \xrightarrow{\omega_0 \to 0} 0, \tag{F.34}$$

$$\mathcal{J}^{\nu-2}_{M+3}(\Delta_{M,N}) = 2 \sum_{|O|=M+3}^{\nu-2} \mathcal{E}^{M,N}_{O+1,-O}, \tag{F.35}$$

one can express the sum over $\mathcal{T}_{O,O'}$ in terms of

$$2 \sum_{|O|=M+3}^{\nu-2} w^2_{+,O} \mathcal{T}_{O+1,-O} = w^2_{+,M} \mathcal{CD}_{M+1,-M} \mathcal{J}^{\nu-2}_{M+3}(\Delta_{M+1,-M})$$
$$w^2_{+,M+1} \mathcal{CD}_{M+1,-(M+2)} \mathcal{J}^{\nu-2}_{M+3}(\Delta_{M+1,-(M+2)}). \tag{F.36}$$

Thereby, each sum $\mathcal{J}^{\nu-2}_{M+3}$ is bounded by

$$J^{\nu-2}_{M+4}(\Delta_{M,N}) \leq \mathcal{J}^{\nu-2}_{M+3}(\Delta_{M,N}) \leq J^{\nu-2}_{M+3}(\Delta_{M,N}), \tag{F.37}$$

where

$$J^{\nu-2}_{M+3}(\Delta_{M,N}) = -2 \int_{M+3}^{\nu-2} do \frac{2 \times 2\,\hbar\omega_c\sqrt{o}}{\Delta^2_{M,N} - (2\,\hbar\omega_c\sqrt{o})^2}$$
$$= \left[\frac{4\sqrt{o}}{\hbar\omega_c} + \frac{\Delta_{M,N}}{(\hbar\omega_c)^2} \log\left(\frac{2\,\hbar\omega_c\sqrt{o} - \Delta_{M,N}}{2\,\hbar\omega_c\sqrt{o} + \Delta_{M,N}} \right) \right]^{o=\nu-2}_{o=M+3} \tag{F.38}$$
$$= J^{\nu-2}(\Delta_{M,N}) - J_{M+3}(\Delta_{M,N}),$$

denotes the integral approximation of $\mathcal{J}^{\nu-2}_{M+3}$. The short-hand notation introduced in the last line of Eq. (F.38) reads as follows: The superscript denotes the evaluation of the expression in the second line at the upper boundary of the integral. Likewise, the expression in the second line is evaluated at the lower boundary of the integral when the J

carries a subscript. Without regularization, $J^{\nu-2}_{M+4}$ and thus $\mathcal{J}^{\nu-2}_{M+3}$ diverges as $\sqrt{\nu}$ in the limit $\nu \to \infty$.

Any photon frequency in the order of a cyclotron transition, $\omega_0 \leq \omega_c$, yields Eq. (F.33) to be positive. Thus, the ground-state average of the first forth-order contribution,

$$\langle \hat{\mathcal{H}}^{(4)}_1 \rangle_0 = \frac{(\hat{a}^\dagger + \hat{a})^2}{4} \left[\sum_{O,O' \in \mathbb{H}_N} \mathcal{M}^2_{O,O'} \mathcal{T}_{O,O'} \, n^-_O \right], \tag{F.39}$$

is also positive for any $\omega_0 \leq \omega_c$.

Derivation of $\hat{\mathcal{H}}^{(4)}_2$ and $\hat{\mathcal{H}}^{(4)}_3$

With this, the second contribution, $\hat{\mathcal{H}}^{(4)}_2 = -\frac{1}{6}[\hat{\mathcal{V}}_o, \mathcal{L}([\hat{\mathcal{S}}_1, [\hat{\mathcal{S}}_1, \hat{\mathcal{V}}_o]])]$, to $\hat{\mathcal{H}}^{(4)}$ is discussed. Therefore, one first evaluates the contribution of the nested commutator in the argument of the superoperator and keeps only the relevant terms precisely consisting of one commutator of fermionic operators. By means of basic commutator algebra one finds for the relevant terms

$$\begin{aligned}
[\hat{\bar{\mathcal{S}}}, [\hat{\mathcal{S}}, \hat{\mathcal{V}}_o]]_R =& \hat{\bar{s}}[\hat{s}, \hat{v}][\hat{\bar{S}}, \hat{V}^\dagger_o]\hat{S} + \hat{\bar{s}}^\dagger[\hat{s}, \hat{v}]\hat{V}_o[\hat{S}, \hat{\bar{S}}^\dagger] + \hat{\bar{s}}^\dagger[\hat{s}, \hat{v}][\hat{V}_o, \hat{\bar{S}}^\dagger]\hat{S} \\
& - \hat{\bar{s}}[\hat{s}^\dagger, \hat{v}]\hat{V}^\dagger_o[\hat{\bar{S}}, \hat{S}^\dagger] - \hat{\bar{s}}[\hat{s}^\dagger, \hat{v}][\hat{\bar{S}}, \hat{V}^\dagger_o]\hat{S}^\dagger - \hat{\bar{s}}^\dagger[\hat{s}^\dagger, \hat{v}][\hat{V}_o, \hat{\bar{S}}^\dagger]\hat{S}^\dagger \\
& + ([\hat{\bar{s}}, \hat{s}]\hat{v} + \hat{s}[\hat{\bar{s}}, \hat{v}])[\hat{S}, \hat{V}^\dagger_o]\hat{\bar{S}} - (\hat{s}[\hat{\bar{s}}^\dagger, \hat{v}] + [\hat{\bar{s}}^\dagger, \hat{s}]\hat{v})[\hat{S}, \hat{V}^\dagger_o]\hat{\bar{S}}^\dagger \\
& + (\hat{s}^\dagger[\hat{\bar{s}}, \hat{v}] + [\hat{\bar{s}}, \hat{s}^\dagger]\hat{v})[\hat{V}_o, \hat{S}^\dagger]\hat{\bar{S}} - (\hat{s}^\dagger[\hat{\bar{s}}^\dagger, \hat{v}] + [\hat{\bar{s}}^\dagger, \hat{s}^\dagger]\hat{v})[\hat{V}_o\hat{S}^\dagger]\hat{\bar{S}}^\dagger.
\end{aligned} \tag{F.40}$$

As the final result obtained from this relation will also be evaluated within the ground-state average, one keeps only diagonal operator contributions. Thus, all non-diagonal contributions arising from the commutators are dropped right away. After careful examination, one thereby finds the nested commutator to simplify to

$$\begin{aligned}
[\hat{\bar{\mathcal{S}}}, [\hat{\mathcal{S}}, \hat{\mathcal{V}}_o]]_R =& -\frac{\hat{a}^\dagger + \hat{a}}{\sqrt{\mathcal{N}}^3} \Big[3\mathcal{C}_{\hat{\bar{\mathcal{S}}}} \mathcal{D}_{\hat{\mathcal{S}}} (\hat{\bar{S}} + \hat{\bar{S}}^\dagger)[\hat{S}, \hat{V}^\dagger_o] \\
& + \mathcal{C}\mathcal{D}_{\hat{\mathcal{S}}} (\hat{V}_o + \hat{V}^\dagger_o)[\hat{S}, \hat{\bar{S}}^\dagger] \Big],
\end{aligned} \tag{F.41}$$

where, for instance, $\mathcal{C}_{\hat{\mathcal{S}}}$ is a short-hand notation implicating that the function $\mathcal{C}_{M,N}$ has to be evaluated with respect to the quantum numbers assigned with the operator $\hat{\mathcal{S}}$, which are here M and N. The function $\mathcal{CD}$ is defined in Eq. (F.34). The superoperator $\mathcal{L}$ transforms this expression into

$$\begin{aligned}
\mathcal{L}([\hat{\bar{\mathcal{S}}}, [\hat{\mathcal{S}}, \hat{\mathcal{V}}_o]])_R =& -\frac{1}{\sqrt{\mathcal{N}}^3} \Big[3\mathcal{C}_{\hat{\bar{\mathcal{S}}}} \mathcal{D}_{\hat{\mathcal{S}}} (\hat{\bar{s}}\hat{\bar{S}} - \hat{\bar{s}}^\dagger \hat{\bar{S}}^\dagger)[\hat{S}, \hat{V}^\dagger_o] \\
& + \mathcal{C}\mathcal{D}_{\hat{\mathcal{S}}} (\hat{s}_{\hat{\mathcal{V}}_o} \hat{V}_o - \hat{s}^\dagger_{\hat{\mathcal{V}}_o} \hat{V}^\dagger_o)[\hat{S}, \hat{\bar{S}}^\dagger] \Big],
\end{aligned} \tag{F.42}$$

where $\hat{s}_{\hat{\mathcal{V}}_o}$ is defined just like $\hat{s}$ or $\hat{\bar{s}}$, Eq. (8.51) where the indices have been adapted to the summation defined within $\hat{\mathcal{V}}_o$. Thus, the remaining commutator with $\hat{\mathcal{V}}_o$ can be evaluated

keeping again, only terms which contribute to the ground-state average:

$$
[\hat{\mathcal{V}}_o, \mathcal{L}([\hat{\mathcal{S}}_1, [\hat{\mathcal{S}}_1, \hat{\mathcal{V}}_o]])]_R = \frac{(\hat{a}^\dagger + \hat{a})^2}{\mathcal{N}^2} \left(3 \mathcal{CD}_{\hat{\mathcal{S}}} \mathcal{D}_{\hat{\mathcal{S}}} [\hat{\bar{V}}_o, \hat{\bar{S}}^\dagger][\hat{S}, \hat{V}_o^\dagger] + \mathcal{CD}_{\hat{\mathcal{S}}} \mathcal{D}_{\hat{\mathcal{V}}_o} [\hat{\bar{V}}_o, \hat{V}_o^\dagger][\hat{S}, \hat{\bar{S}}^\dagger] \right)
$$

$$
= 4 \frac{(\hat{a}^\dagger + \hat{a})^2}{\mathcal{N}^2} \mathcal{CD}_{\hat{\mathcal{S}}} \mathcal{D}_{\hat{\mathcal{S}}} [\hat{\bar{V}}_o, \hat{\bar{S}}^\dagger][\hat{S}, \hat{V}_o^\dagger], \tag{F.43}
$$

where the reordering in the second line is permitted in view of the definitions of each fermionic operator contribution. From Eq. (F.41) it is easy to check that the nested commutator of the last contribution to the effect, $\hat{\mathcal{H}}_3^{(4)}$, is identical to the negative of expression (F.43). Thus, the ground-state expectation values of $\hat{\mathcal{H}}_2^{(4)}$ and $\hat{\mathcal{H}}_3^{(4)}$ can be evaluated together, yielding

$$
\langle \hat{\mathcal{H}}_2^{(4)} \rangle_0 + \langle \hat{\mathcal{H}}_3^{(4)} \rangle_0 = \frac{(\hat{a}^\dagger + \hat{a})^2}{2\mathcal{N}^2} \left[\sum_{M,N} \mathcal{M}_{M,N}^2 \mathcal{CD}_{M,N} (n_M^- - n_N^-) \right] \tag{F.44}
$$

$$
\times \left[\sum_{M,N} \mathcal{M}_{M,N}^2 \mathcal{D}_{M,N} (n_M^- - n_N^-) \right]
$$

$$
= \frac{(\hat{a}^\dagger + \hat{a})^2}{2} \left(w_{+,M}^2 \mathcal{CD}_{M+1,-M} + w_{+,M+1}^2 \mathcal{CD}_{M+1,-(M+2)} \right) \tag{F.45}
$$

$$
\times \left(w_{+,M}^2 \mathcal{D}_{M+1,-M} + w_{+,M+1}^2 \mathcal{D}_{M+1,-(M+2)} \right),
$$

where the factor of $1/2$ results from the prefactors assigned to $\hat{\mathcal{H}}_2^{(4)}$ and $\hat{\mathcal{H}}_3^{(4)}$ according to Eqs. (F.3, F.4) along with the factor of 4 in Eq. (F.43). Relation (F.45) follows from expression (F.44) in analogy to Eq. (F.28). Thereby it was used that each sum in both brackets of Eq. (F.44) contributes a factor of $\mathcal{N}$ which stems from the summation over the quantum number k encoded in the short-hand notation.

By expanding the brackets in the second line, one finds for this contribution explicitly

$$
\langle \hat{\mathcal{H}}_2^{(4)} \rangle_0 + \langle \hat{\mathcal{H}}_3^{(4)} \rangle_0 = -\frac{(\hat{a}^\dagger + \hat{a})^2}{2} \left(\frac{8 \, w_{+,M}^4 \, \hbar \omega_0 \, \Delta_{M+1,-M}^2}{\left[\Delta_{M+1,-M}^2 - (\hbar \omega_0)^2 \right]^3} + \frac{8 \, w_{+,M+1}^4 \, \hbar \omega_0 \, \Delta_{M+1,-(M+2)}^2}{\left[\Delta_{M+1,-(M+2)}^2 - (\hbar \omega_0)^2 \right]^3} \right.
$$

$$
+ \frac{8 \, w_{+,M}^2 \hbar \omega_0 \, \Delta_{M+1,-M} \Delta_{M+1,-(M+2)}}{\left[\Delta_{M+1,-M}^2 - (\hbar \omega_0)^2 \right]^2 \left[\Delta_{M+1,-(M+2)}^2 - (\hbar \omega_0^2) \right]}
$$

$$
\left. + \frac{8 \, w_{+,M+1}^2 \hbar \omega_0 \, \Delta_{M+1,-M} \Delta_{M+1,-(M+2)}}{\left[\Delta_{M+1,-(M+2)}^2 - (\hbar \omega_0)^2 \right]^2 \left[\Delta_{M+1,-M}^2 - (\hbar \omega_0^2) \right]} \right). \tag{F.46}
$$

For any photonic energy comparable with a cyclotron transition, $\hbar \omega_0 \leq \hbar \omega_c$, the contribution from $\langle \hat{\mathcal{H}}_2^{(4)} \rangle_0 + \langle \hat{\mathcal{H}}_3^{(4)} \rangle_0$ is negative. Furthermore, one can estimate the upper and lower bounds of this contribution by approximating $\Delta_{M+1,-M} \approx 2 \hbar \omega_c \sqrt{M}$ and

$\Delta_{M+1,-(M+2)} \approx 2\,\hbar\omega_c\,\sqrt{M+1}$:

$$H_M^{(4)} < \langle\hat{\mathcal{H}}_2^{(4)}\rangle_0 + \langle\hat{\mathcal{H}}_3^{(4)}\rangle_0 < H_{M+1}^{(4)}, \tag{F.47}$$

where

$$H_M^{(4)} = -\frac{(\hat{a}^\dagger + \hat{a})^2}{2}\,\frac{128\,\hbar\omega_0\,(\hbar\omega_c)^2\,M}{[4(\hbar\omega_c)^2 M - (\hbar\omega_0)^2]^3}. \tag{F.48}$$

Summary of the forth-order contribution to the block-diagonal Hamiltonian

With this, the results for the fourth-order contribution, $\hat{\mathcal{H}}^{(4)}$, of the decoupled Hamiltonian $\hat{\mathcal{H}}^{\mathrm{eff}}$ can be summarized. Thus, from Eqs. (F.39, F.44) one finds for the ensemble average of $\hat{\mathcal{H}}^{(4)}$ at $T = 0$:

$$\langle\hat{\mathcal{H}}^{(4)}\rangle_0^{M,\nu} = (\hat{a}^\dagger + \hat{a})^2\,\chi_{M,\nu}^{(4)}(\hbar\omega_0), \tag{F.49}$$

where the function

$$\chi_{M,\nu}^{(4)}(\hbar\omega_0) = \frac{1}{4}\left[\sum_{O,O'\in\mathbb{H}_N} \mathcal{M}_{O,O'}^2\,\mathcal{T}_{O,O'}\,n_O^-\right] + \frac{1}{2}\left[\sum_{M,N} \mathcal{M}_{M,N}^2\,\mathcal{CD}_{M,N}(n_M^- - n_N^-)\right]$$
$$\times\left[\sum_{M,N} \mathcal{M}_{M,N}^2\,\mathcal{D}_{M,N}(n_M^- - n_N^-)\right]. \tag{F.50}$$

vanishes in the static limit. In order to discuss the two different techniques of regularization it is beneficial to decompose $\chi_{M,\nu}^{(4)}$ into its ν-independent and ν-dependent parts, denoted by $\chi_M^{(4)}$ and $\chi_\nu^{(4)}$, respectively:

$$\chi_{M,\nu}^{(4)}(\hbar\omega_0) = \chi_M^{(4)}(\hbar\omega_0) + \chi_\nu^{(4)}(\hbar\omega_0). \tag{F.51}$$

From Eqs. (F.33, F.45) one finds for both contributions and $M \geq 1$

$$\chi_M^{(4)}(\hbar\omega_0) = \frac{1}{4}\left[\mathcal{W}_{M+1,-M}(M) + \mathcal{W}_{M+1,-(M+2)}(M) + \mathcal{Y}(M)\right], \tag{F.52}$$

$$\chi_\nu^{(4)}(\hbar\omega_0) = -\frac{1}{4}\left[\mathcal{W}'_{M+1,-M}(\nu) + \mathcal{W}'_{M+1,-(M+2)}(\nu)\right], \tag{F.53}$$

where the following definitions were introduced

$$\mathcal{W}_{K,L}(M) = \mathcal{CD}_{K,L}\left[J_{M+3}(\Delta_{K,L}) + 2\mathcal{D}_{K,L} - \mathcal{E}_{M+1,M}^{K,L} - \mathcal{E}_{M+3,M+2}^{K,L} - \mathcal{E}_{M+3,-(M+2)}^{K,L}\right], \tag{F.54}$$

$$\mathcal{Y}(M) = \mathcal{CD}_{M+1,-M}\mathcal{D}_{M+1,-(M+2)} + \mathcal{CD}_{M+1,-(M+2)}\mathcal{D}_{M+1,-M}, \tag{F.55}$$

$$\mathcal{W}'_{K,L}(\nu) = \mathcal{CD}_{K,L}\left[J^{\nu-2}(\Delta_{K,L}) - \mathcal{E}_{\nu,\nu-1}^{K,L} + \mathcal{E}_{\nu,-(\nu-1)}^{K,L}\right]. \tag{F.56}$$

Further discussion on these contributions are found in Subsec. 8.2.7.

F.2 Contributions from the approximate diagonalization

The derivation of the fourth-order contributions stemming from the approximate diagonalization of the term $\hat{\mathcal{H}}_{i,N}$ according to Eq. (8.125) is performed in analogy to the investigations on $\hat{\mathcal{H}}_2^{(4)}$ and $\hat{\mathcal{H}}_3^{(4)}$ discussed in Sec. F.1. Again, it is helpful to review the definition of $\hat{\mathcal{H}}^{(4)}$ which is given by

$$\hat{\mathcal{H}}_N^{(4)} = -\frac{1}{6}[\hat{\mathcal{V}}_o', \mathcal{L}([\hat{\mathcal{R}}_1, [\hat{\mathcal{R}}_1, \hat{\mathcal{V}}_o']])] - \frac{1}{24}[\hat{\mathcal{R}}_1, [\hat{\mathcal{R}}_1, [\hat{\mathcal{R}}_1, \hat{\mathcal{V}}_o']]], \tag{F.57}$$

where the block-off diagonal contribution $\hat{\mathcal{V}}_o' = \hat{v} \otimes (\hat{V}_o' + \hat{V}_o'^\dagger)$ is defined in Eq. (8.114). The lowest-order SW generator, $\hat{\mathcal{R}}_1$, is given in Eq. (8.126), where the convenient shorthand notation $\hat{\mathcal{R}}_1 = \hat{r} \otimes \hat{R} - \hat{r}^\dagger \otimes \hat{R}^\dagger$ will be applied during the following. For the sake of brevity, the tensor product will not be marked explicitly anymore from now on. Furthermore, one defines

$$\hat{\mathcal{H}}_{2,N}^{(4)} = -\frac{1}{6}[\hat{\mathcal{V}}_o', \mathcal{L}([\hat{\mathcal{R}}_1, [\hat{\mathcal{R}}_1, \hat{\mathcal{V}}_o']])], \tag{F.58}$$

$$\hat{\mathcal{H}}_{3,N}^{(4)} = -\frac{1}{24}[\hat{\mathcal{R}}_1, [\hat{\mathcal{R}}_1, [\hat{\mathcal{R}}_1, \hat{\mathcal{V}}_o']]] \tag{F.59}$$

in analogy to the discussion in Sec. F.1. According to the formal similarity between the definitions of $\hat{\mathcal{S}}_1$, $\hat{\mathcal{V}}_o$ and $\hat{\mathcal{R}}_1$, $\hat{\mathcal{V}}_o'$, one can adapt the results obtained for the former one onto the latter one, finding the relevant commutator contributions of $\hat{\mathcal{H}}_{2,N}^{(4)}$:

$$
\begin{aligned}
[\hat{\mathcal{V}}_o', \mathcal{L}([\hat{\mathcal{R}}_1, [\hat{\mathcal{R}}_1, \hat{\mathcal{V}}_o']])]_R &= \frac{(\hat{a}^\dagger + \hat{a})^2}{\mathcal{N}^2} \left(3\mathcal{CD}_{\hat{\mathcal{R}}} \mathcal{D}_{\hat{\mathcal{R}}}[\hat{\bar{V}}_o', \hat{\bar{R}}^\dagger][\hat{R}, \hat{V}_o'^\dagger] + \mathcal{CD}_{\hat{\mathcal{R}}} \mathcal{D}_{\hat{\mathcal{V}}_o'}[\hat{\bar{V}}_o', \hat{V}_o'^\dagger][\hat{R}, \hat{\bar{R}}^\dagger] \right) \\
&= 4\frac{(\hat{a}^\dagger + \hat{a})^2}{\mathcal{N}^2} \mathcal{CD}_{\hat{\mathcal{R}}} \mathcal{D}_{\hat{\mathcal{R}}}[\hat{\bar{V}}_o', \hat{\bar{R}}^\dagger][\hat{R}, \hat{V}_o'^\dagger], \tag{F.60} \\
&= -[\hat{\mathcal{R}}_1, [\hat{\mathcal{R}}_1, [\hat{\mathcal{R}}_1, \hat{\mathcal{V}}_o']]]_R
\end{aligned}
$$

where $\mathcal{CD}$ is defined in Eq. (F.34) and $\mathcal{D}$ is given by Eq. (8.62). Thus, one finds for the relevant contributions to the ground-state expectation value of $\hat{\mathcal{H}}_{2,N}^{(4)}$ and $\hat{\mathcal{H}}_{3,N}^{(4)}$:

$$
\begin{aligned}
\langle \hat{\mathcal{H}}_{2,N}^{(4)} \rangle_0 + \langle \hat{\mathcal{H}}_{3,N}^{(4)} \rangle_0 = \frac{(\hat{a}^\dagger + \hat{a})^2}{2\mathcal{N}^2} &\left[\sum_{N,N'} m_{N,N'}^2 \mathcal{CD}_{N,N'}(n_N^- - n_{N'}^-) \right] \\
&\times \left[\sum_{N,N'} m_{N,N'}^2 \mathcal{D}_{N,N'}(n_N^- - n_{N'}^-) \right],
\end{aligned} \tag{F.61}
$$

where n_N^- denotes the Fermi-Dirac distribution according to Eq. (8.140). The definition of the matrix elements $m_{N,N'}$ is found in Eq. (5.48). The summation over each set of quantum numbers in either of the two brackets is then performed as follows: Setting $\mathcal{X}_{N,N'}$ as a space holder for either $\mathcal{CD}_{N,N'}$ or $\mathcal{D}_{N,N'}$, one finds for the evaluation of the

sum over N':

$$
\sum_{N,N'} m_{N,N'}^2 \mathcal{X}_{N,N'}(n_N^- - n_{N'}^-) = \mathcal{N} \sum_N w_{+,N}^2 \left[\mathcal{X}_{N,N+1}(n_N^- - n_{N+1}^-) \right.
$$
$$
\left. + \mathcal{X}_{N,-(N+1)}(n_N^- - n_{-(N+1)}^-) \right]
$$
$$
= \mathcal{N} \sum_N \left[\left[w_{+,N}^2 \left(\mathcal{X}_{N,N+1} + \mathcal{X}_{N,-(N+1)} \right) \right. \right.
$$
$$
\left. \left. - w_{+,N-1}^2 \mathcal{X}_{N-1,N} \right] n_N^- - w_{+,N-1}^2 \mathcal{X}_{N-1,-N} \, n_{-N}^- \right] ,
$$
(F.62)

where the factor of $\mathcal{N}$ is due to the sum over k encoded in the short-hand notation. Now, the sum over $N = (\lambda, n) = (\lambda, |N|)$ is carried out yielding

$$
\sum_{N,N'} m_{N,N'}^2 \mathcal{X}_{N,N'}(n_N^- - n_{N'}^-) = \mathcal{N} \sum_{|N|} \left[w_{+,N}^2 \left(-\mathcal{X}_{N+1,N} + \mathcal{X}_{N+1,-N} \right) \right.
$$
$$
\left. + w_{+,N-1}^2 \left(\mathcal{X}_{N,N-1} + \mathcal{X}_{N,-(N-1)} \right) \right] \left[n_N^- - n_{-N}^- \right] ,
$$
(F.63)

where the symmetry properties of $\hat{\mathcal{X}}_{N,N'}$ where used. The sum over $|N|$ explicitly includes the quantum numbers $[0, \dots, M-2, M+3, \dots, \nu-1]$. At $T = 0$, the Fermi-Dirac distribution is given by a Heaviside step function and the contributions of the sum over $[0, \dots, M-2]$ precisely vanish, such that

$$
\sum_{N,N'} m_{N,N'}^2 \mathcal{X}_{N,N'}(n_N^- - n_{N'}^-) = -\mathcal{N} \sum_{|N|=M+3}^{\nu-1} \left[w_{+,N}^2 \left(-\mathcal{X}_{N+1,N} + \mathcal{X}_{N+1,-N} \right) \right.
$$
$$
\left. + w_{+,N-1}^2 \left(\mathcal{X}_{N,N-1} + \mathcal{X}_{N,-(N-1)} \right) \right] .
$$
(F.64)

By shifting the indices of the last bracket, $N \to N+1$, one eventually finds

$$
\sum_{N,N'} m_{N,N'}^2 \mathcal{X}_{N,N'}(n_N^- - n_{N'}^-) = -\mathcal{N} \left[2 \sum_{|N|=M+3}^{\nu-2} w_{+,N}^2 \mathcal{X}_{N+1,-N} \right.
$$
$$
+ w_{+,\nu-1}^2 \left(-\mathcal{X}_{\nu,\nu-1} + \mathcal{X}_{\nu,-(\nu-1)} \right)
$$
$$
\left. + w_{+,M+2}^2 \left(\mathcal{X}_{M+3,M+2} + \mathcal{X}_{M+3,-(M+2)} \right) \right] .
$$
(F.65)

Thus, by defining

$$
\chi_{N,M,\nu}^{(4)}(\hbar\omega_0) = \frac{1}{2} \left[\mathcal{K}_{M+3}^{\nu-2}(\hbar\omega_0) + w_{+,\nu-1}^2 \left(-\mathcal{CD}_{\nu,\nu-1} + \mathcal{CD}_{\nu,-(\nu-1)} \right) \right.
$$
$$
+ w_{+,M+2}^2 \left(\mathcal{CD}_{M+3,M+2} + \mathcal{CD}_{M+3,-(M+2)} \right) \right] \left[\mathcal{J}_{M+3}^{\nu-2} + w_{+,\nu-1}^2 \left(-\mathcal{D}_{\nu,\nu-1} + \mathcal{D}_{\nu,-(\nu-1)} \right) \right.
$$
$$
\left. + w_{+,M+2}^2 \left(\mathcal{D}_{M+3,M+2} + \mathcal{D}_{M+3,-(M+2)} \right) \right] , \quad \text{(F.66)}
$$

where the definition of $\mathcal{J}_{M+3}^{\nu-2}(\hbar\omega_0)$ is found in Eq. (F.35) and

$$\mathcal{K}_{M+3}^{\nu-2}(\hbar\omega_0) = 2 \sum_{|N|=M+3}^{\nu-2} w_{+,N}^2 \mathcal{CD}_{N+1,-N}, \qquad (F.67)$$

the fourth-order contribution to the approximate diagonalized Hamiltonian $\hat{\mathcal{H}}_D$ reads

$$\langle \hat{\mathcal{H}}_N^{(4)} \rangle_0 = (\hat{a}^\dagger + \hat{a})^2 \chi_{N,M,\nu}^{(4)}(\hbar\omega_0). \qquad (F.68)$$

Similar to $\mathcal{J}_{M+3}^{\nu-2}$ being bound by the integrals $J_{M+4}^{\nu-2}$ and $J_{M+3}^{\nu-2}$, Eq. (F.38), one finds the bounds of $\mathcal{K}_{M+3}^{\nu-2}$,

$$K_{M+4}^{\nu-2}(\hbar\omega_0) \leq \mathcal{K}_{M+3}^{\nu-2}(\hbar\omega_0) \leq K_{M+3}^{\nu-2}(\hbar\omega_0), \qquad (F.69)$$

where

$$K_{M+3}^{\nu-2}(\hbar\omega_0) = \left[\frac{2 \times 2\,\hbar\omega_c\sqrt{o}\,\hbar\omega_0}{\hbar\omega_c\left[(2\,\hbar\omega_c\sqrt{o})^2 - (\hbar\omega_0)^2\right]} - \frac{1}{(\hbar\omega_c)^2} \log\left(\frac{2\,\omega_c\sqrt{o} - \omega_0}{2\,\omega_c\sqrt{o} + \omega_0}\right) \right]_{o=M+3}^{o=\nu-2}. \qquad (F.70)$$

As $K_{M+3}^{\nu-2}(0) = 0$, the function $\chi_{N,M,\nu}^{(4)}(0) = 0$ such that there is no unphysical static contribution arising from $\langle \hat{\mathcal{H}}_N^{(4)} \rangle_0$. Similar to the decomposition of $\chi_{m\,n_M}^{(4)}$ into a ν-dependent and -independent part, one finds for $\chi_{N,M,\nu}^{(4)} = \chi_{N,M}^{(4)} + \chi_{N,\nu}^{(4)}$, where

$$\begin{aligned}
\chi_{N,M}^{(4)}(\hbar\omega_0) &= \frac{1}{2}\left[-K_{M+3}(\hbar\omega_0) + w_{+,M+2}^2\left(\mathcal{CD}_{M+3,M+2} + \mathcal{CD}_{M+3,-(M+2)}\right)\right] \\
&\quad \times \left[-J_{M+3}(\hbar\omega_0) + w_{+,M+2}^2\left(\mathcal{D}_{M+3,M+2} + \mathcal{D}_{M+3,-(M+2)}\right)\right] \\
&= \frac{1}{2}\left[-K_{M+3}(\hbar\omega_0) - \frac{8\,\omega_0\omega_c\left[\left[\omega_c^2 - \omega_0^2\right]^2 + 4\omega_c^4(M+2)\right]\sqrt{M+3}}{\hbar^2\left[\omega_0^4 + \omega_c^4 - 2(\omega_0\omega_c)^2\left[1 + 2(M+2)\right]\right]^2}\right] \\
&\quad \times \left[-J_{M+3}(\hbar\omega_0) + \frac{4\omega_c\left[\omega_c^2 - \omega_0^2\right]\sqrt{M+3}}{\hbar\left[\omega_0^4 + \omega_c^4 + 2(\omega_0\omega_c)^2\left[1 + 2(M+2)\right]\right]}\right].
\end{aligned} \qquad (F.71)$$

This contribution is positive for $\Omega_M \leq \omega_0 \leq \omega_c$. The ν-dependent term is given by

$$
\begin{aligned}
\chi^{(4)}_{\mathrm{N},\nu}(\hbar\omega_0) ={} & \frac{1}{2} \left[K^{\nu-2}(\hbar\omega_0) + w^2_{+,\nu-1}\left(-\mathcal{CD}_{\nu,\nu-1} + \mathcal{CD}_{\nu,-(\nu-1)}\right)\right] \\
& \times \left[J_{\nu-2}(\hbar\omega_0) + w^2_{+,\nu-1}\left(-\mathcal{D}_{\nu,\nu-1} + \mathcal{D}_{\nu,-(\nu-1)}\right)\right] \\
& + \frac{1}{2}\left[K^{\nu-2}(\hbar\omega_0) + w^2_{+,\nu-1}\left(-\mathcal{CD}_{\nu,\nu-1} + \mathcal{CD}_{\nu,-(\nu-1)}\right)\right] \\
& \times \left[-J_{M+3}(\hbar\omega_0) + w^2_{+,M+2}\left(\mathcal{D}_{M+3,M+2} + \mathcal{D}_{M+3,-(M+2)}\right)\right] \\
& + \frac{1}{2}\left[-K_{M+3}(\hbar\omega_0) + w^2_{+,M+2}\left(\mathcal{CD}_{M+3,M+2} + \mathcal{CD}_{M+3,-(M+2)}\right)\right] \\
& \times \left[J_{\nu-2}(\hbar\omega_0) + w^2_{+,\nu-1}\left(-\mathcal{D}_{\nu,\nu-1} + \mathcal{D}_{\nu,-(\nu-1)}\right)\right] \\
={} & \frac{1}{2}\left[K^{\nu-2}(\hbar\omega_0) - \frac{8\omega_0\omega_c\left[\omega_0^4 + 2(\omega_0\omega_c)^2 - \omega_c^4\left[4 + 3(\nu-1)\right]\right]\sqrt{\nu-1}}{\hbar^2\left[\omega_0^4 + \omega_c^4 - 2(\omega_0\omega_c)^2\left[1 + 2(\nu-1)\right]\right]^2}\right] \\
& \times \left[J^{\nu-2}(\hbar\omega_0) - \frac{4\omega_c\left(\omega_c^2 + \omega_0^2\right)\sqrt{\nu}}{\hbar\left[\omega_0^4 + \omega_c^4 - 2(\omega_0\omega_c)^2\left[1 + 2(\nu-1)\right]\right]}\right] \qquad \text{(F.72)} \\
& + \frac{1}{2}\left[K^{\nu-2}(\hbar\omega_0) - \frac{8\omega_0\omega_c\left[\omega_0^4 + 2(\omega_0\omega_c)^2 - \omega_c^4\left[4 + 3(\nu-1)\right]\right]\sqrt{\nu-1}}{\hbar^2\left[\omega_0^4 + \omega_c^4 - 2(\omega_0\omega_c)^2\left[1 + 2(\nu-1)\right]\right]^2}\right] \\
& \times \left[-J_{M+3}(\hbar\omega_0) + \frac{4\omega_c\left[\omega_c^2 - \omega_0^2\right]\sqrt{M+3}}{\hbar\left[\omega_0^4 + \omega_c^4 + 2(\omega_0\omega_c)^2\left[1 + 2(M+2)\right]\right]}\right] \\
& + \frac{1}{2}\left[-K_{M+3}(\hbar\omega_0) - \frac{8\,\omega_0\omega_c\left[\left[\omega_c^2 - \omega_0^2\right]^2 + 4\omega_c^4(M+2)\right]\sqrt{M+3}}{\hbar^2\left[\omega_0^4 + \omega_c^4 - 2(\omega_0\omega_c)^2\left[1 + 2(M+2)\right]\right]^2}\right] \\
& \times \left[J^{\nu-2}(\hbar\omega_0) - \frac{4\omega_c\left(\omega_c^2 + \omega_0^2\right)\sqrt{\nu}}{\hbar\left[\omega_0^4 + \omega_c^4 - 2(\omega_0\omega_c)^2\left[1 + 2(\nu-1)\right]\right]}\right] ,
\end{aligned}
$$

and yields a negative contribution for ν according to Eq. (8.31) and $\Omega_M \leq \omega_0 \leq \omega_c$.

Bibliography

[1] A. Demming, *King of the elements?* Nanotechnology **21**, 300201 (2010).

[2] S. Mouras, A. Hamm, D. Djurado, and J.-D. Cousseins, *Synthesis of first stage graphite intercalation compounds with fluorides,* Revue de Chimie Minerale **24**, 572 (1987), eng.

[3] M. Sharon and M. Sharon, *Graphene: An Introduction to the Fundamentals and Industrial Applications* (John Wiley & Sons, Inc., 2015).

[4] P. R. Wallace, *The Band Theory of Graphite,* Phys. Rev. **71**, 622 (1947).

[5] J. W. McClure, *Diamagnetism of Graphite,* Phys. Rev. **104**, 666 (1956).

[6] D. P. DiVincenzo and E. J. Mele, *Self-consistent effective-mass theory for intralayer screening in graphite intercalation compounds,* Phys. Rev. B **29**, 1685 (1984).

[7] G. W. Semenoff, *Condensed-Matter Simulation of a Three-Dimensional Anomaly,* Phys. Rev. Lett. **53**, 2449 (1984).

[8] Kroto H. W., Heath J. R., O'Brien S. C., Curl R. F., and Smalley R. E., *C60: Buckminsterfullerene,* Nature **318**, 162 (1985).

[9] Iijima, S., *Helical microtubules of graphitic carbon,* Nature **354**, 56 (1991), 10.1038/354056a0.

[10] G. Ruess and F. Vogt, *Höchstlamellarer Kohlenstoff aus Graphitoxyhydroxyd.* Monatsh. Chem. **78**, 222 (1948).

[11] H. P. Boehm, A. Clauss, G. O. Fischer, and U. Hofmann, *Das Adsorptionsverhalten sehr dünner Kohlenstoff-Folien,* Z. Anorg. Allg. Chem. **316**, 119 (1962).

[12] R. Peierls, *Quelques propriétés typiques des corps solides,* Annales de l'institut Henri Poincaré **5**, 177 (1935).

[13] L. D. Landau, *Zur Theorie der phasenumwandlungen II,* Phys. Z. Sowjetunion **11**, 26 (1937).

[14] L. D. Landau and E. M. Lifshitz, *Statistical Physics (Part 1)*, 3rd ed. (Pergamon Press, Oxford, 1980).

[15] N. D. Mermin and H. Wagner, *Absence of Ferromagnetism or Antiferromagnetism in One- or Two-Dimensional Isotropic Heisenberg Models,* Phys. Rev. Lett. **17**, 1133 (1966).

[16] N. D. Mermin, *Crystalline Order in Two Dimensions,* Phys. Rev. **176**, 250 (1968).

[17] P. C. Hohenberg, *Existence of Long-Range Order in One and Two Dimensions,* Phys. Rev. **158**, 383 (1967).

[18] A. O'Hare, F. V. Kusmartsev, and K. I. Kugel, *A Stable "Flat? Form of Two-Dimensional Crystals: Could Graphene, Silicene, Germanene Be Minigap Semiconductors?* Nano Letters **12**, 1045 (2012).

[19] K. S. Novoselov, A. K. Geim, S. V. Morozov, D. Jiang, Y. Zhang, S. V. Dubonos, I. V. Grigorieva, and A. A. Firsov, *Electric Field Effect in Atomically Thin Carbon Films,* Science **306**, 666 (2004).

[20] K. S. Novoselov, D. Jiang, F. Schedin, T. J. Booth, V. V. Khotkevich, S. V. Morozov, and A. K. Geim, *Two-dimensional atomic crystals,* Proceedings of the National Academy of Sciences of the United States of America **102**, 10451 (2005).

[21] Novoselov K. S., Geim A. K., Morozov S. V., Jiang D., Katsnelson M. I., Grigorieva I. V., Dubonos S. V., and Firsov A. A., *Two-dimensional gas of massless Dirac fermions in graphene,* Nature **438**, 197 (2005).

[22] Zhang Yuanbo, Tan Yan-Wen, Stormer Horst L., and Kim Philip, *Experimental observation of the quantum Hall effect and Berry's phase in graphene,* Nature **438**, 201 (2005).

[23] A. H. Castro Neto, F. Guinea, N. M. R. Peres, K. S. Novoselov, and A. K. Geim, *The electronic properties of graphene,* Rev. Mod. Phys. **81**, 109 (2009).

[24] M. O. Goerbig, *Electronic properties of graphene in a strong magnetic field,* Rev. Mod. Phys. **83**, 1193 (2011).

[25] D. R. Cooper, B. D'Anjou, N. Ghattamaneni, B. Harack, M. Hilke, A. Horth, N. Majlis, M. Massicotte, L. Vandsburger, E. Whiteway, and V. Yu, *Experimental Review of Graphene,* ISRN Condens. Matter Phys. , 501686 (2012).

[26] Schwierz, F., *Graphene transistors,* Nat. Nano. **5**, 487 (2010).

[27] Wu Yanqing, Lin Yu-ming, Bol Ageeth A., Jenkins Keith A., Xia Fengnian, Farmer Damon B., Zhu Yu, and Avouris Phaedon, *High-frequency, scaled graphene transistors on diamond-like carbon,* Nature **472**, 74 (2011).

[28] M. L. Sadowski, G. Martinez, M. Potemski, C. Berger, and W. A. de Heer, *Landau Level Spectroscopy of Ultrathin Graphite Layers,* Phys. Rev. Lett. **97**, 266405 (2006).

[29] P. Plochocka, C. Faugeras, M. Orlita, M. L. Sadowski, G. Martinez, M. Potemski, M. O. Goerbig, J.-N. Fuchs, C. Berger, and W. A. de Heer, *High-Energy Limit of Massless Dirac Fermions in Multilayer Graphene using Magneto-Optical Transmission Spectroscopy,* Phys. Rev. Lett. **100**, 087401 (2008).

[30] M. Orlita, C. Faugeras, P. Plochocka, P. Neugebauer, G. Martinez, D. K. Maude, A.-L. Barra, M. Sprinkle, C. Berger, W. A. de Heer, and M. Potemski, *Approaching the Dirac Point in High-Mobility Multilayer Epitaxial Graphene,* Phys. Rev. Lett. **101**, 267601 (2008).

[31] Crassee Iris, Levallois Julien, Walter Andrew L., Ostler Markus, Bostwick Aaron, Rotenberg Eli, Seyller Thomas, v. d. M. Dirk, and Kuzmenko Alexey B., *Giant Faraday rotation in single- and multilayer graphene,* Nat. Phys. **7**, 48 (2011).

[32] C. Drexler, S. Tarasenko, P. Olbrich, J. Karch, M. Hirmer, F. Muller, M. Gmitra, J. Fabian, R. Yakimova, S. Lara-Avila, S. Kubatkin, M. Wang, R. Vajtai, A. P. M., J. Kono, and G. S. D., *Magnetic quantum ratchet effect in graphene,* Nat Nano **8**, 104 (2013).

[33] Ponomarenko L. A., Gorbachev R. V., Yu G. L., Elias D. C., Jalil R., Patel A. A., Mishchenko A., Mayorov A. S., Woods C. R., Wallbank J. R., Mucha-Kruczynski M., Piot B. A., Potemski M., Grigorieva I. V., Novoselov K. S., Guinea F., Fal/'ko V. I., and Geim A. K., *Cloning of Dirac fermions in graphene superlattices,* Nature **497**, 594 (2013).

[34] Z. Jiang, E. A. Henriksen, L. C. Tung, Y.-J. Wang, M. E. Schwartz, M. Y. Han, P. Kim, and H. L. Stormer, *Infrared Spectroscopy of Landau Levels of Graphene,* Phys. Rev. Lett. **98**, 197403 (2007).

[35] R. S. Deacon, K.-C. Chuang, R. J. Nicholas, K. S. Novoselov, and A. K. Geim, *Cyclotron resonance study of the electron and hole velocity in graphene monolayers,* Phys. Rev. B **76**, 081406 (2007).

[36] E. A. Henriksen, P. Cadden-Zimansky, Z. Jiang, Z. Q. Li, L.-C. Tung, M. E. Schwartz, M. Takita, Y.-J. Wang, P. Kim, and H. L. Stormer, *Interaction-Induced Shift of the Cyclotron Resonance of Graphene Using Infrared Spectroscopy,* Phys. Rev. Lett. **104**, 067404 (2010).

[37] Y. Kawano, *Wide-band frequency-tunable terahertz and infrared detection with graphene,* Nanotechnol. **24**, 214004 (2013).

[38] R. Jago, T. Winzer, A. Knorr, and E. Malic, *Graphene as gain medium for broadband lasers,* Phys. Rev. B **92**, 085407 (2015).

[39] S. Brem, F. Wendler, and E. Malic, *Proposal for a tunable graphene-based terahertz Landau-level laser,* arXiv (2016).

[40] V. Ryzhii, M. Ryzhii, and T. Otsuji, *Negative dynamic conductivity of graphene with optical pumping,* J. Appl. Phys. **101**, 083114 (2007).

[41] T. Winzer, E. Malić, and A. Knorr, *Microscopic mechanism for transient population inversion and optical gain in graphene,* Phys. Rev. B **87**, 165413 (2013).

[42] T. Li, L. Luo, M. Hupalo, J. Zhang, M. C. Tringides, J. Schmalian, and J. Wang, *Femtosecond Population Inversion and Stimulated Emission of Dense Dirac Fermions in Graphene,* Phys. Rev. Lett. **108**, 167401 (2012).

[43] S. Boubanga-Tombet, S. Chan, T. Watanabe, A. Satou, V. Ryzhii, and T. Otsuji, *Ultrafast carrier dynamics and terahertz emission in optically pumped graphene at room temperature,* Phys. Rev. B **85**, 035443 (2012).

[44] Gierz Isabella, Petersen Jesse C., Mitrano Matteo, Cacho Cephise, Turcu I. C. Edmond, Springate Emma, Stöhr Alexander, Köhler Axel, Starke Ulrich, and Cavalleri Andrea, *Snapshots of non-equilibrium Dirac carrier distributions in graphene,* Nat. Mater **12**, 1119 (2013).

[45] T. Watanabe, T. Fukushima, Y. Yabe, S. A. B. Tombet, A. Satou, A. A. Dubinov, V. Y. Aleshkin, V. Mitin, V. Ryzhii, and T. Otsuji, *The gain enhancement effect of surface plasmon polaritons on terahertz stimulated emission in optically pumped monolayer graphene,* New J. Phys. **15**, 075003 (2013).

[46] Wendler F. and Malic E., *Towards a tunable graphene-based Landau level laser in the terahertz regime,* Sci. Rep. **5**, 12646 (2015).

[47] Gunter G., Anappara A. A., Hees J., Sell A., Biasiol G., Sorba L., De Liberato S., Ciuti C., Tredicucci A., Leitenstorfer A., and Huber R., *Sub-cycle switch-on of ultrastrong light-matter interaction,* Nature **458**, 178 (2009).

[48] P. Forn-Díaz, J. Lisenfeld, D. Marcos, J. J. García-Ripoll, E. Solano, C. J. P. M. Harmans, and J. E. Mooij, *Observation of the Bloch-Siegert Shift in a Qubit-Oscillator System in the Ultrastrong Coupling Regime,* Phys. Rev. Lett. **105**, 237001 (2010).

[49] Niemczyk T., Deppe F., Huebl H., Menzel E. P., Hocke F., Schwarz M. J., Garcia-Ripoll J. J., Zueco D., Hummer T., Solano E., Marx A., and Gross R., *Circuit quantum electrodynamics in the ultrastrong-coupling regime,* Nat. Phys. **6**, 772 (2010).

[50] T. Schwartz, J. A. Hutchison, C. Genet, and T. W. Ebbesen, *Reversible Switching of Ultrastrong Light-Molecule Coupling,* Phys. Rev. Lett. **106**, 196405 (2011).

[51] M. Geiser, F. Castellano, G. Scalari, M. Beck, L. Nevou, and J. Faist, *Ultrastrong Coupling Regime and Plasmon Polaritons in Parabolic Semiconductor Quantum Wells,* Phys. Rev. Lett. **108**, 106402 (2012).

[52] G. Scalari, C. Maissen, D. Turčinková, D. Hagenmüller, S. De Liberato, C. Ciuti, C. Reichl, D. Schuh, W. Wegscheider, M. Beck, and J. Faist, *Ultrastrong Coupling of the Cyclotron Transition of a 2D Electron Gas to a THz Metamaterial,* Science **335**, 1323 (2012).

[53] S. Gambino, M. Mazzeo, A. Genco, O. Di Stefano, S. Savasta, S. Patanè, D. Ballarini, F. Mangione, G. Lerario, D. Sanvitto, and G. Gigli, *Exploring Light–Matter Interaction Phenomena under Ultrastrong Coupling Regime,* ACS Photonics **1**, 1042 (2014).

[54] M. Goryachev, W. G. Farr, D. L. Creedon, Y. Fan, M. Kostylev, and M. E. Tobar, *High-Cooperativity Cavity QED with Magnons at Microwave Frequencies,* Phys. Rev. Applied **2**, 054002 (2014).

[55] C. Maissen, G. Scalari, F. Valmorra, M. Beck, J. Faist, S. Cibella, R. Leoni, C. Reichl, C. Charpentier, and W. Wegscheider, *Ultrastrong coupling in the near field of complementary split-ring resonators,* Phys. Rev. B **90**, 205309 (2014).

[56] L. Garziano, R. Stassi, V. Macrì, A. F. Kockum, S. Savasta, and F. Nori, *Multiphoton quantum Rabi oscillations in ultrastrong cavity QED,* Phys. Rev. A **92**, 063830 (2015).

[57] H. K. Avetissian, A. K. Avetissian, G. F. Mkrtchian, and K. V. Sedrakian, *Creation of particle-hole superposition states in graphene at multiphoton resonant excitation by laser radiation,* Phys. Rev. B **85**, 115443 (2012).

[58] B. Dóra, K. Ziegler, P. Thalmeier, and M. Nakamura, *Rabi Oscillations in Landau-Quantized Graphene,* Phys. Rev. Lett. **102**, 036803 (2009).

[59] Enamullah, Kumar Vipin, and Setlur Girish S., *Crossover of coherent Rabi oscillations in graphene,* Physica B **407**, 4600 (2012).

[60] Enamullah, V. Kumar, U. Kumar, and G. S. Setlur, *Quantum Rabi oscillations in graphene,* J. Opt. Soc. Am. B **31**, 484 (2014).

[61] K. Hepp and E. H. Lieb, *Equilibrium Statistical Mechanics of Matter Interacting with the Quantized Radiation Field,* Phys. Rev. A **8**, 2517 (1973).

[62] C. Emary and T. Brandes, *Chaos and the quantum phase transition in the Dicke model,* Phys. Rev. E **67**, 066203 (2003).

[63] R. H. Dicke, *Coherence in Spontaneous Radiation Processes,* Phys. Rev. **93**, 99 (1954).

[64] N. Skribanowitz, I. P. Herman, J. C. MacGillivray, and M. S. Feld, *Observation of Dicke Superradiance in Optically Pumped HF Gas,* Phys. Rev. Lett. **30**, 309 (1973).

[65] M. Gross, P. Goy, C. Fabre, S. Haroche, and J. M. Raimond, *Maser Oscillation and Microwave Superradiance in Small Systems of Rydberg Atoms,* Phys. Rev. Lett. **43**, 343 (1979).

[66] M. Gross, C. Fabre, P. Pillet, and S. Haroche, *Observation of Near-Infrared Dicke Superradiance on Cascading Transitions in Atomic Sodium,* Phys. Rev. Lett. **36**, 1035 (1976).

[67] M. Gross, J. M. Raimond, and S. Haroche, *Doppler Beats in Superradiance,* Phys. Rev. Lett. **40**, 1711 (1978).

[68] Y. Kaluzny, P. Goy, M. Gross, J. M. Raimond, and S. Haroche, *Observation of Self-Induced Rabi Oscillations in Two-Level Atoms Excited Inside a Resonant Cavity: The Ringing Regime of Superradiance,* Phys. Rev. Lett. **51**, 1175 (1983).

[69] R. Röhlsberger, K. Schlage, B. Sahoo, S. Couet, and R. Rüffer, *Collective Lamb Shift in Single-Photon Superradiance,* Science **328**, 1248 (2010).

[70] A. Goban, C.-L. Hung, J. D. Hood, S.-P. Yu, J. A. Muniz, O. Painter, and H. J. Kimble, *Superradiance for Atoms Trapped along a Photonic Crystal Waveguide,* Phys. Rev. Lett. **115**, 063601 (2015).

[71] Mlynek J. A., Abdumalikov A. A., Eichler C., and Wallraff A., *Observation of Dicke superradiance for two artificial atoms in a cavity with high decay rate,* Nat. Commun. **5**, 5186 (2014).

[72] T. Laurent, Y. Todorov, A. Vasanelli, A. Delteil, C. Sirtori, I. Sagnes, and G. Beaudoin, *Superradiant Emission from a Collective Excitation in a Semiconductor,* Phys. Rev. Lett. **115**, 187402 (2015).

[73] Q. Zhang, T. Arikawa, E. Kato, J. L. Reno, W. Pan, J. D. Watson, M. J. Manfra, M. A. Zudov, M. Tokman, M. Erukhimova, A. Belyanin, and J. Kono, *Superradiant Decay of Cyclotron Resonance of Two-Dimensional Electron Gases,* Phys. Rev. Lett. **113**, 047601 (2014).

[74] F. Dimer, B. Estienne, A. S. Parkins, and H. J. Carmichael, *Proposed realization of the Dicke-model quantum phase transition in an optical cavity QED system,* Phys. Rev. A **75**, 013804 (2007).

[75] D. Nagy, G. Kónya, G. Szirmai, and P. Domokos, *Dicke-Model Phase Transition in the Quantum Motion of a Bose-Einstein Condensate in an Optical Cavity,* Phys. Rev. Lett. **104**, 130401 (2010).

[76] J. Keeling, M. J. Bhaseen, and B. D. Simons, *Fermionic Superradiance in a Transversely Pumped Optical Cavity,* Phys. Rev. Lett. **112**, 143002 (2014).

[77] F. Piazza and P. Strack, *Umklapp Superradiance with a Collisionless Quantum Degenerate Fermi Gas,* Phys. Rev. Lett. **112**, 143003 (2014).

[78] Y. Chen, Z. Yu, and H. Zhai, *Superradiance of Degenerate Fermi Gases in a Cavity,* Phys. Rev. Lett. **112**, 143004 (2014).

[79] P. Kirton and J. Keeling, *Suppressing and Restoring the Dicke Superradiance Transition by Dephasing and Decay,* Phys. Rev. Lett. **118**, 123602 (2017).

[80] Baumann K., Guerlin C., Brennecke F., and Esslinger T., *Dicke quantum phase transition with a superfluid gas in an optical cavity,* Nature **464**, 1301 (2010), 10.1038/nature09009.

[81] K. Baumann, R. Mottl, F. Brennecke, and T. Esslinger, *Exploring Symmetry Breaking at the Dicke Quantum Phase Transition,* Phys. Rev. Lett. **107**, 140402 (2011).

[82] J. Klinder, H. Keßler, M. R. Bakhtiari, M. Thorwart, and A. Hemmerich, *Observation of a Superradiant Mott Insulator in the Dicke-Hubbard Model,* Phys. Rev. Lett. **115**, 230403 (2015).

[83] Kollár Alicia J., Papageorge Alexander T., Vaidya Varun D., Guo Yudan, Keeling Jonathan, and Lev Benjamin L., *Supermode-density-wave-polariton condensation with a Bose–Einstein condensate in a multimode cavity,* Nat. Commun. **8**, 14386 (2017).

[84] M. P. Baden, K. J. Arnold, A. L. Grimsmo, S. Parkins, and M. D. Barrett, *Realization of the Dicke Model Using Cavity-Assisted Raman Transitions,* Phys. Rev. Lett. **113**, 020408 (2014).

[85] K. Rzażewski, K. Wódkiewicz, and W. Żakowicz, *Phase Transitions, Two-Level Atoms, and the A^2 Term,* Phys. Rev. Lett. **35**, 432 (1975).

[86] K. Rzażewski, K. Wódkiewicz, and W. Żakowicz, *Remark on the superradiant phase transition,* Phys. Lett. A **58**, 211 (1976).

[87] K. Rzażewski and K. Wódkiewicz, *Thermodynamics of two-level atoms interacting with the continuum of electromagnetic field modes,* Phys. Rev. A **13**, 1967 (1976).

[88] J. M. Knight, Y. Aharonov, and G. T. C. Hsieh, *Are super-radiant phase transitions possible?* Phys. Rev. A **17**, 1454 (1978).

[89] A. Vukics, T. Grießer, and P. Domokos, *Fundamental limitation of ultrastrong coupling between light and atoms,* Phys. Rev. A **92**, 043835 (2015).

[90] I. Bialynicki-Birula and K. Rzążewski, *No-go theorem concerning the superradiant phase transition in atomic systems,* Phys. Rev. A **19**, 301 (1979).

[91] V. A. Slyusarev and R. P. Yankelevich, *On the impossibility of a phase transition to the superradiant state in a thermodynamically equilibrium gauge-invariant system,* Theoretical and Mathematical Physics **40**, 641 (1979).

[92] B. M. Garraway, *The Dicke model in quantum optics: Dicke model revisited,* Phil. Trans. R. Soc. A **369**, 1137 (2011).

[93] D. Hagenmüller and C. Ciuti, *Cavity QED of the Graphene Cyclotron Transition,* Phys. Rev. Lett. **109**, 267403 (2012).

[94] L. Chirolli, M. Polini, V. Giovannetti, and A. H. MacDonald, *Drude Weight, Cyclotron Resonance, and the Dicke Model of Graphene Cavity QED,* Phys. Rev. Lett. **109**, 267404 (2012).

[95] F. M. D. Pellegrino, L. Chirolli, R. Fazio, V. Giovannetti, and M. Polini, *Theory of integer quantum Hall polaritons in graphene,* Phys. Rev. B **89**, 165406 (2014).

[96] M. Polini, A. H. MacDonald, and G. Vignale, *Drude weight, plasmon dispersion, and pseudospin response in doped graphene sheets,* arXiv , 0901.4528 (2009).

[97] A. Principi, M. Polini, and G. Vignale, *Linear response of doped graphene sheets to vector potentials,* Phys. Rev. B **80**, 075418 (2009).

[98] V. P. Gusynin, S. G. Sharapov, and J. P. Carbotte, *Sum rules for the optical and Hall conductivity in graphene,* Phys. Rev. B **75**, 165407 (2007).

[99] J. Sabio, J. Nilsson, and A. H. Castro Neto, *f-sum rule and unconventional spectral weight transfer in graphene,* Phys. Rev. B **78**, 075410 (2008).

[100] R. Roldán, J.-N. Fuchs, and M. O. Goerbig, *Collective modes of doped graphene and a standard two-dimensional electron gas in a strong magnetic field: Linear magnetoplasmons versus magnetoexcitons,* Phys. Rev. B **80**, 085408 (2009).

[101] J. Sári, C. Tőke, and M. O. Goerbig, *Magnetoplasmons of the tilted anisotropic Dirac cone material $\alpha - (\mathrm{BEDT - TTF})_2\mathrm{I}_3$,* Phys. Rev. B **90**, 155446 (2014).

[102] J. Sári, M. O. Goerbig, and C. Tőke, *Magneto-optics of quasirelativistic electrons in graphene with an inplane electric field and in tilted Dirac cones in $\alpha - (BEDT\ TTF)_2\mathrm{I}_3$,* Phys. Rev. B **92**, 035306 (2015).

[103] C. Cohen-Tannoudji, J. Dupont-Roc, and G. Grynberg, *Photons and Atoms: Introduction to Quantum Electrodynamics* (Wiley, New York, 1997).

[104] W. E. Lamb and R. C. Retherford, *Fine Structure of the Hydrogen Atom by a Microwave Method*, Phys. Rev. **72**, 241 (1947).

[105] H. A. Bethe, *The Electromagnetic Shift of Energy Levels,* Phys. Rev. **72**, 339 (1947).

[106] H. B. G. Casimir, *On the attraction between two perfectly conducting plates,* Proceedings of the KNAW **51**, 793 (1948).

[107] M. Sparnaay, *Measurements of attractive forces between flat plates,* Physica **24**, 751 (1958).

[108] S. K. Lamoreaux, *Demonstration of the Casimir Force in the 0.6 to 6μm Range,* Phys. Rev. Lett. **78**, 5 (1997).

[109] C. H. Henry, *Theory of the linewidth of semiconductor lasers,* IEEE J. Quant. Electron. **18**, 259 (1982).

[110] C. H. Henry, *Theory of spontaneous emission noise in open resonators and its application to lasers and optical amplifiers,* J. Lightwave Technol. **4**, 288 (1986).

[111] P. A. M. Dirac, *The Quantum Theory of the Emission and Absorption of Radiation,* Proc. R. Soc. A **114**, 243 (1927).

[112] H. Goldstein, *Classical mechanics* (Addison-Wesley, Massachusetts, 1980).

[113] P. A. M. Dirac, *The Principles of Quantum Mechanics* (Oxford University Press, Oxford, 1958).

[114] N. Bohr, *Über die Serienspektra der Elemente,* Z. Phys. **2**, 423 (1920).

[115] W. Greiner, *Quantum Mechanics – An Introduction* (Springer, Berlin, Heidelberg, 2000).

[116] D. Kleppner, *Inhibited Spontaneous Emission,* Phys. Rev. Lett. **47**, 233 (1981).

[117] K. Kakazu and Y. S. Kim, *Quantization of electromagnetic fields in cavities and spontaneous emission,* Phys. Rev. A **50**, 1830 (1994).

[118] M. Hayn, *On superradiant phase transitions in generalised Dicke models* (Dissertation, Technische Universität Berlin, 2017).

[119] C. Cohen-Tannoudji, B. Diu, and F. Laloë, *Quantenmechanik* (de Gruyter, Berlin, 2007).

[120] M. O. Scully and M. S. Zubairy, *Quantum Optics* (Cambridge University Press, 1997).

[121] E. T. Jaynes and F. W. Cummings, *Comparison of quantum and semiclassical radiation theories with application to the beam maser,* Proc. IEEE **51**, 89 (1963).

[122] I. I. Rabi, *Space Quantization in a Gyrating Magnetic Field,* Phys. Rev. **51**, 652 (1937).

[123] H. G. Reik, P. Lais, M. E. Stutzle, and M. Doucha, *Exact solution of the $E \otimes \epsilon$ Jahn-Teller and Rabi Hamiltonian by generalised spheroidal wavefunctions?* J. Phys. A **20**, 6327 (1987).

[124] Y. Wang and J. Y. Haw, *Bridging the gap between the Jaynes–Cummings and Rabi models using an intermediate rotating wave approximation,* Physics Letters A **379**, 779 (2015).

[125] G. S. Agarwal, *Rotating-Wave Approximation and Spontaneous Emission,* Phys. Rev. A **4**, 1778 (1971).

[126] D. Walls, *Higher order effects in the single atom field mode interaction,* Phys. Lett. A **42**, 217 (1972).

[127] P. L. Knight and L. Allen, *Rotating-Wave Approximation in Coherent Interactions,* Phys. Rev. A **7**, 368 (1973).

[128] M. Tavis and F. W. Cummings, *Exact Solution for an N-Molecule—Radiation-Field Hamiltonian,* Phys. Rev. **170**, 379 (1968).

[129] M. Tavis and F. W. Cummings, *Approximate Solutions for an N-Molecule-Radiation-Field Hamiltonian,* Phys. Rev. **188**, 692 (1969).

[130] W. R. Mallory, *Solution of a Multiatom Radiation Model Using the Bargmann Realization of the Radiation Field,* Phys. Rev. **188**, 1976 (1969).

[131] J. J. Hopfield, *Theory of the Contribution of Excitons to the Complex Dielectric Constant of Crystals,* Phys. Rev. **112**, 1555 (1958).

[132] Nataf, P. and Ciuti, C., *No-go theorem for superradiant quantum phase transitions in cavity QED and counter-example in circuit QED,* Nat. Commun. **1**, 72 (2010).

[133] A. Shnirman, G. Schön, and Z. Hermon, *Quantum Manipulations of Small Josephson Junctions,* Phys. Rev. Lett. **79**, 2371 (1997).

[134] D. Averin, *Adiabatic quantum computation with Cooper pairs,* Solid State Commun. **105**, 659 (1998).

[135] Makhlin Yuriy, Scohn Gerd, and Shnirman Alexander, *Josephson-junction qubits with controlled couplings,* Nature **398**, 305 (1999), 10.1038/18613.

[136] Nakamura Y., Pashkin Yu. A., and Tsai J. S., *Coherent control of macroscopic quantum states in a single-Cooper-pair box,* Nature **398**, 786 (1999).

[137] A. Blais, R.-S. Huang, A. Wallraff, S. M. Girvin, and R. J. Schoelkopf, *Cavity quantum electrodynamics for superconducting electrical circuits: An architecture for quantum computation,* Phys. Rev. A **69**, 062320 (2004).

[138] A. B. Klimov and S. M. Chumakov, *A Group-Theoretical Approach to Quantum Optics* (Wiley, Weinheim, 2009).

[139] C. Hamner, C. Qu, Y. Zhang, J. Chang, M. Gong, C. Zhang, and P. Engels, *Dicke-type phase transition in a spin-orbit-coupled Bose–Einstein condensate,* Nat. Commun. **5**, 4023 (2014).

[140] R. J. Glauber, *Coherent and Incoherent States of the Radiation Field*, Phys. Rev. **131**, 2766 (1963).

[141] A. Moroz, *A hidden analytic structure of the Rabi model*, Ann. Phys. **340**, 252 (2014).

[142] J. M. Raimond, M. Brune, and S. Haroche, *Manipulating quantum entanglement with atoms and photons in a cavity*, Rev. Mod. Phys. **73**, 565 (2001).

[143] Reithmaier J. P., Sek G., Loffler A., Hofmann C., Kuhn S., Reitzenstein S., Keldysh L. V., Kulakovskii V. D., Reinecke T. L., and Forchel A., *Strong coupling in a single quantum dot-semiconductor microcavity system*, Nature **432**, 197 (2004).

[144] Khitrova G., Gibbs H. M., Kira M., Koch S. W., and Scherer A., *Vacuum Rabi splitting in semiconductors*, Nat Phys **2**, 81 (2006).

[145] F. Beaudoin, J. M. Gambetta, and A. Blais, *Dissipation and ultrastrong coupling in circuit QED*, Phys. Rev. A **84**, 043832 (2011).

[146] C. Ciuti and I. Carusotto, *Input-output theory of cavities in the ultrastrong coupling regime: The case of time-independent cavity parameters*, Phys. Rev. A **74**, 033811 (2006).

[147] S. De Liberato and C. Ciuti, *Quantum model of microcavity intersubband electroluminescent devices*, Phys. Rev. B **77**, 155321 (2008).

[148] S. De Liberato, *Light-Matter Decoupling in the Deep Strong Coupling Regime: The Breakdown of the Purcell Effect*, Phys. Rev. Lett. **112**, 016401 (2014).

[149] E. M. Purcell, Spontaneous Emission Probabilities at Radio Frequencies, in *Confined Electrons and Photons: New Physics and Applications*, edited by E. Burstein and C. Weisbuch (Springer US, Boston, MA, 1995) pp. 839–839.

[150] F. T. Arecchi, E. Courtens, R. Gilmore, and H. Thomas, *Atomic Coherent States in Quantum Optics*, Phys. Rev. A **6**, 2211 (1972).

[151] X. Wang and K. Mølmer, *Pairwise entanglement in symmetric multi-qubit systems*, EPJ D **18**, 385 (2002).

[152] J. J. Sakurai, *Modern quantum mechanics* (Addison-Wesley, 1994).

[153] H. Carmichael, C. Gardiner, and D. Walls, *Higher order corrections to the Dicke superradiant phase transition*, Phys. Lett. A **46**, 47 (1973).

[154] K. Hepp and E. H. Lieb, *On the superradiant phase transition for molecules in a quantized radiation field: the dicke maser model*, Ann. Phys. **76**, 360 (1973).

[155] Y. K. Wang and F. T. Hioe, *Phase Transition in the Dicke Model of Superradiance*, Phys. Rev. A **7**, 831 (1973).

[156] S. Sachdev, *Quantum Phase Transitions* (Cambridge University Press, 1999).

[157] R. K. Bullough, *Photon, quantum and collective, effects from rydberg atoms in cavities*, Hyperfine Interactions **37**, 71 (1987).

[158] R. K. Bullough, G. S. Agarwal, B. M. Garraway, S. S. Hassan, G. P. Hildred, S. V. Lawande, N. Nayak, R. R. Puri, B. V. Thompson, J. Timonen, and M. R. B. Wahiddin, Giant Quantum Oscillators from Rydberg Atoms: Atomic Coherent States and Their Squeezing from Rydberg Atoms, in *Squeezed and Nonclassical Light*, edited by P. Tombesi and E. R. Pike (Springer US, Boston, MA, 1989) pp. 81–106.

[159] T. Holstein and H. Primakoff, *Field Dependence of the Intrinsic Domain Magnetization of a Ferromagnet,* Phys. Rev. **58**, 1098 (1940).

[160] E. Ressayre and A. Tallet, *Holstein-Primakoff transformation for the study of cooperative emission of radiation,* Phys. Rev. A **11**, 981 (1975).

[161] F. Persico and G. Vetri, *Coherence properties of the N-atom-radiation interaction and the Holstein-Primakoff transformation,* Phys. Rev. A **12**, 2083 (1975).

[162] Johansson J.R., Nation P.D., and Nori Franco, *QuTiP: An open-source Python framework for the dynamics of open quantum systems,* Comput. Phys. Commun. **183**, 1760 (2012).

[163] Johansson J.R., Nation P.D., and Nori Franco, *QuTiP 2: A Python framework for the dynamics of open quantum systems,* Comput. Phys. Commun. **184**, 1234 (2013).

[164] M. Hayn, C. Emary, and T. Brandes, *Superradiant phase transition in a model of three-level-Λ systems interacting with two bosonic modes,* Phys. Rev. A **86**, 063822 (2012).

[165] C. Emary and T. Brandes, *Quantum Chaos Triggered by Precursors of a Quantum Phase Transition: The Dicke Model,* Phys. Rev. Lett. **90**, 044101 (2003).

[166] S. He, L. Duan, and Q.-H. Chen, *Exact solvability, non-integrability, and genuine multipartite entanglement dynamics of the Dicke model,* New J. Phys. **17**, 043033 (2015).

[167] M. A. Bastarrachea-Magnani and J. G. Hirsch, *Peres lattices and chaos in the Dicke model,* J. Phys. Conf. Ser. **512**, 012004 (2014).

[168] M. A. Bastarrachea-Magnani, B. López-del Carpio, S. Lerma-Hernández, and J. G. Hirsch, *Chaos in the Dicke model: quantum and semiclassical analysis,* Phys. Scripta **90**, 068015 (2015).

[169] A. Relaño, M. A. Bastarrachea-Magnani, and S. Lerma-Hernández, *Approximated integrability of the Dicke model,* EPL **116**, 50005 (2016).

[170] M. A. Bastarrachea-Magnani, A. Relaño, S. Lerma-Hernández, B. López-del Carpio, J. Chávez-Carlos, and J. G. Hirsch, *Adiabatic invariants for the regular region of the Dicke model,* J. Phys. A **50**, 144002 (2017).

[171] L. Bakemeier, A. Alvermann, and H. Fehske, *Dynamics of the Dicke model close to the classical limit,* Phys. Rev. A **88**, 043835 (2013).

[172] V. Bužek, M. Orszag, and M. Roško, *Instability and Entanglement of the Ground State of the Dicke Model,* Phys. Rev. Lett. **94**, 163601 (2005).

[173] R. A. Robles Robles, S. A. Chilingaryan, B. M. Rodríguez-Lara, and R.-K. Lee, *Ground state in the finite Dicke model for interacting qubits*, Phys. Rev. A **91**, 033819 (2015).

[174] L. Bakemeier, A. Alvermann, and H. Fehske, *Quantum phase transition in the Dicke model with critical and noncritical entanglement*, Phys. Rev. A **85**, 043821 (2012).

[175] C. Dunning, K. E. Hibberd, and J. Links, *On quantum phase crossovers in finite systems*, J. Stat. Mech. Theor. Exp. **2006**, P11005 (2006).

[176] D. C. Brody, D. W. Hook, and L. P. Hughston, *Quantum phase transitions without thermodynamic limits*, Proc. R. Soc. A **463**, 2021 (2007).

[177] Q.-H. Chen, Y.-Y. Zhang, T. Liu, and K.-L. Wang, *Numerically exact solution to the finite-size Dicke model*, Phys. Rev. A **78**, 051801 (2008).

[178] J. Vidal and S. Dusuel, *Finite-size scaling exponents in the Dicke model*, Europhys. Lett. **74**, 817 (2006).

[179] R. Botet, R. Jullien, and P. Pfeuty, *Size Scaling for Infinitely Coordinated Systems*, Phys. Rev. Lett. **49**, 478 (1982).

[180] N. Lambert, C. Emary, and T. Brandes, *Entanglement and the Phase Transition in Single-Mode Superradiance*, Phys. Rev. Lett. **92**, 073602 (2004).

[181] O. Tsyplyatyev and D. Loss, *Dicke model: Entanglement as a finite size effect*, J. Phys. Conf. Ser. **193**, 012134 (2009).

[182] G. C. Duncan, *Effect of antiresonant atom-field interactions on phase transitions in the Dicke model*, Phys. Rev. A **9**, 418 (1974).

[183] T. Makhviladze, A. Rez, and M. Saritchev, *On the thermodynamics of radiating molecules strongly coupled to resonant field*, Phys. Lett. A **49**, 293 (1974).

[184] A. Messina and F. Persico, *Tunneling ground state in the nonresonant superradiant phase transition*, Phys. Rev. A **13**, 367 (1976).

[185] M. Orszag, *Phase transition of a system of two-level atoms*, J. Phys. A **10**, 1995 (1977).

[186] D. Stepanenko, M. Trif, O. Tsyplyatyev, and D. Loss, *Field-dependent superradiant quantum phase transition of molecular magnets in microwave cavities*, Semicond. Sci. Technol. **31**, 094003 (2016).

[187] M.-J. Hwang and M.-S. Choi, *Variational study of a two-level system coupled to a harmonic oscillator in an ultrastrong-coupling regime*, Phys. Rev. A **82**, 025802 (2010).

[188] S. Ashhab and F. Nori, *Qubit-oscillator systems in the ultrastrong-coupling regime and their potential for preparing nonclassical states*, Phys. Rev. A **81**, 042311 (2010).

[189] S. Ashhab, *Superradiance transition in a system with a single qubit and a single oscillator*, Phys. Rev. A **87**, 013826 (2013).

[190] Zhu Hanjie, Zhang Guofeng, and Fan Heng, *Quantum Criticality in the Biased Dicke Model,* Sci. Rep. **6**, 19751 (2016).

[191] M.-J. Hwang, R. Puebla, and M. B. Plenio, *Quantum Phase Transition and Universal Dynamics in the Rabi Model,* Phys. Rev. Lett. **115**, 180404 (2015).

[192] J. Lolli, A. Baksic, D. Nagy, V. E. Manucharyan, and C. Ciuti, *Ancillary Qubit Spectroscopy of Vacua in Cavity and Circuit Quantum Electrodynamics,* Phys. Rev. Lett. **114**, 183601 (2015).

[193] N. N. Bogoljubov, *On a new method in the theory of superconductivity,* Il Nuovo Cimento (1955-1965) **7**, 794 (1958).

[194] J. G. Valatin, *Comments on the theory of superconductivity,* Il Nuovo Cimento (1955-1965) **7**, 843 (1958).

[195] R. F. Bishop and A. Vourdas, *Displaced and squeezed parity operator: Its role in classical mappings of quantum theories,* Phys. Rev. A **50**, 4488 (1994).

[196] C. M. Bowden and C. C. Sung, *Effect of spin-spin interaction on the super-radiant phase transition for the Dicke Hamiltonian,* J. Phys. A **11**, 151 (1978).

[197] R. Gilmore, *Persistence of the phase transition in the Dicke model with external fields and counter-rotating terms,* Phys. Lett. A **55**, 459 (1976).

[198] A. Vukics, T. Grießer, and P. Domokos, *Elimination of the A-Square Problem from Cavity QED,* Phys. Rev. Lett. **112**, 073601 (2014).

[199] W. Thomas, *Über die Zahl der Dispersionselektronen, die einem stationären Zustande zugeordnet sind. (Vorläufige Mitteilung),* Naturwissenschaften **13**, 627 (1925).

[200] W. Kuhn, *Über die Gesamtstärke der von einem Zustande ausgehenden Absorptionslinien,* Zeitschrift für Physik **33**, 408 (1925).

[201] F. Reiche and W. Thomas, *Über die Zahl der Dispersionselektronen, die einem stationären Zustand zugeordnet sind,* Zeitschrift für Physik **34**, 510 (1925).

[202] S. Wang, *Generalization of the Thomas-Reiche-Kuhn and the Bethe sum rules,* Phys. Rev. A **60**, 262 (1999).

[203] I. S. Gradshtein, I. M. Ryzhik, A. Jeffrey, and D. Zwillinger, *Table of integrals, series and products,* Academic Press (Academic Press, New York, 2007).

[204] G. Giuliani and G. Vignale, *Quantum Theory of the Electron Liquid* (Cambridge University Press, Cambridge, 2005).

[205] K. W. Post, B. C. Chapler, M. K. Liu, J. S. Wu, H. T. Stinson, M. D. Goldflam, A. R. Richardella, J. S. Lee, A. A. Reijnders, K. S. Burch, M. M. Fogler, N. Samarth, and D. N. Basov, *Sum-Rule Constraints on the Surface State Conductance of Topological Insulators,* Phys. Rev. Lett. **115**, 116804 (2015).

[206] R. G. Woolley, *Gauge invariant wave mechanics and the Power-Zienau-Woolley transformation,* J. Phys. A **13**, 2795 (1980).

[207] M. Bamba and T. Ogawa, *Stability of polarizable materials against superradiant phase transition,* Phys. Rev. A **90**, 063825 (2014).

[208] O. Viehmann, J. von Delft, and F. Marquardt, *Superradiant Phase Transitions and the Standard Description of Circuit QED,* Phys. Rev. Lett. **107**, 113602 (2011).

[209] C. Ciuti and P. Nataf, *Comment on "Superradiant Phase Transitions and the Standard Description of Circuit QED",* Phys. Rev. Lett. **109**, 179301 (2012).

[210] O. Viehmann, J. von Delft, and F. Marquardt, *Reply to Comment on "Superradiant Phase Transitions and the Standard Description of Circuit QED",* arXiv , 1202.2916 (2012).

[211] T. Jaako, Z.-L. Xiang, J. J. Garcia-Ripoll, and P. Rabl, *Ultrastrong-coupling phenomena beyond the Dicke model,* Phys. Rev. A **94**, 033850 (2016).

[212] J. R. Schrieffer and P. A. Wolff, *Relation between the Anderson and Kondo Hamiltonians,* Phys. Rev. **149**, 491 (1966).

[213] D. R. Hamann and A. W. Overhauser, *Electron-Gas Spin Susceptibility,* Phys. Rev. **143**, 183 (1966).

[214] S. Bravyi, D. P. DiVincenzo, and D. Loss, *Schrieffer–Wolff transformation for quantum many-body systems,* Ann. Phys. **326**, 2793 (2011).

[215] L. Pauling, *The nature of the chemical bond. Application of results obtained from the quantum mechanics and from a theory of paramagnetic susceptibility to the structure of molecules.* J. Am. Chem. Soc. **53**, 1367 (1931).

[216] M. Wimmer, *Quantum transport in nanostructures: From computational concepts to spintronics in graphene and magnetic tunnel junctions* (Dissertation, Universität Regensburg, 2009).

[217] D. Rössler, *Solid State Theory* (Springer Berlin Heidelberg, 2009).

[218] Geim A. K. and Novoselov K. S., *The rise of graphene,* Nat. Mater. **6**, 183 (2007).

[219] D. Porezag, T. Frauenheim, T. Köhler, G. Seifert, and R. Kaschner, *Construction of tight-binding-like potentials on the basis of density-functional theory: Application to carbon,* Phys. Rev. B **51**, 12947 (1995).

[220] K. Sasaki, S. Murakami, and R. Saito, *Stabilization mechanism of edge states in graphene,* Appl. Phys. Lett. **88**, 113110 (2006).

[221] F. D. M. Haldane, *Model for a Quantum Hall Effect without Landau Levels: Condensed-Matter Realization of the "Parity Anomaly",* Phys. Rev. Lett. **61**, 2015 (1988).

[222] Bostwick, A., Ohta, T., Seyller, T., Horn, K., and Rotenberg, E., *Quasiparticle dynamics in graphene,* Nat. Phys. **3**, 36 (2007).

[223] R. Roldán, M. O. Goerbig, and J.-N. Fuchs, *The magnetic field particle–hole excitation spectrum in doped graphene and in a standard two-dimensional electron gas,* Semicond. Sci. Technol. **25**, 034005 (2010).

[224] A. R. Akhmerov and C. W. J. Beenakker, *Detection of Valley Polarization in Graphene by a Superconducting Contact*, Phys. Rev. Lett. **98**, 157003 (2007).

[225] T. Ando, *Theory of Electronic States and Transport in Carbon Nanotubes*, J. Phys. Soc. Jpn. **74**, 777 (2005).

[226] J. K. Jain, *Composite Fermions* (Cambridge University Press, Cambridge, 2007).

[227] L. Onsager, *Interpretation of the de Haas-van Alphen effect*, Philos. Mag. **43**, 1006 (1952).

[228] C. Kittel, *Introduction to Solid State Physics* (Addison-Wesley, Boca Raton, 1995).

[229] A. Messiah, *Quantum Mechanics* (North-Holland, Amsterdam, 1961).

[230] M. Frasca, *Theory of dressed states in quantum optics*, Phys. Rev. A **60**, 573 (1999).

[231] R. Peierls, *Zur Theorie des Diamagnetismus von Leitungselektronen*, Z. Phys. **80**, 763 (1933).

[232] M. Graf and P. Vogl, *Electromagnetic fields and dielectric response in empirical tight-binding theory*, Phys. Rev. B **51**, 4940 (1995).

[233] A. Alexandrov and H. Capellmann, *Energy of electrons on a two-dimensional lattice in a magnetic field: perturbation theory versus "Peierls substitution"*, Z. Phys. B **83**, 237 (1991).

[234] J. Ibañez-Azpiroz, A. Eiguren, A. Bergara, G. Pettini, and M. Modugno, *Breakdown of the Peierls substitution for the Haldane model with ultracold atoms*, Phys. Rev. A **90**, 033609 (2014).

[235] W. Kohn, *Theory of Bloch Electrons in a Magnetic Field: The Effective Hamiltonian*, Phys. Rev. **115**, 1460 (1959).

[236] T. B. Boykin, R. C. Bowen, and G. Klimeck, *Electromagnetic coupling and gauge invariance in the empirical tight-binding method*, Phys. Rev. B **63**, 245314 (2001).

[237] L. Heße and K. Richter, *Orbital magnetism of graphene nanostructures: Bulk and confinement effects*, Phys. Rev. B **90**, 205424 (2014).

[238] C. W. Groth, M. Wimmer, A. R. Akhmerov, and X. Waintal, *Kwant: a software package for quantum transport*, New J. Phys. **16**, 063065 (2014).

[239] V. N. Popov and S. A. Fedotov, *Behavior of the partition function of Dicke type models in the limit of a large number of atoms*, Theor. Math. Phys. **51**, 363 (1982).

[240] M. Le Bellac, *Thermal Field Theory*, Cambridge Monographs on Mathematical Physics (Cambridge University Press, 1996).

[241] M. A. Alcalde, J. Stephany, and N. F. Svaiter, *A path integral approach to the full Dicke model with dipole–dipole interaction*, J. Phys. A **44**, 505301 (2011).

[242] M. A. Alcalde and B. Pimentel, *Path integral approach to the full Dicke model*, Physica A **390**, 3385 (2011).

[243] H. F. Baker, *Alternants and Continuous Groups,* Proc. London Math. Soc. **3**, 24 (1905).

[244] J. E. Campbell, *On a Law of Combination of Operators (Second Paper)*,* Proc. London Math. Soc. **29**, 14 (1897).

[245] F. Hausdroff, *Die symbolische Exponentialformel in der Gruppentheorie,* Ber. Verh. Sächs. Akad. Wiss. Leipzig, Math.-Naturwiss. Kl. **58**, 19 (1906).

[246] G. L. Celardo and L. Kaplan, *Superradiance transition in one-dimensional nanostructures: An effective non-Hermitian Hamiltonian formalism,* Phys. Rev. B **79**, 155108 (2009).

[247] J. D. Jackson, *Classical Electrodynamics Third Edition*, 3rd ed. (Wiley, 1998).

[248] D. Strauch, *Classical Mechanics* (Springer Berlin Heidelberg, 2009).

[249] W. Greiner, *Field Quantization* (Springer, Berlin, Heidelberg, 1996).

[250] B. Sagan, *The Symmetric Group – Representations, Combinatorial Algorithms, and Symmetric Functions* (Springer-Verlag, New York, 2001).

[251] J. C. Slater, *The Theory of Complex Spectra,* Phys. Rev. **34**, 1293 (1929).

[252] A. Stern, *Anyons and the quantum Hall effect—A pedagogical review,* Ann. Phys. **323**, 204 (2008).

[253] C. Nayak, S. H. Simon, A. Stern, M. Freedman, and S. Das Sarma, *Non-Abelian anyons and topological quantum computation,* Rev. Mod. Phys. **80**, 1083 (2008).

[254] R. F. Streater and A. S. Wightman, *PCT, Spin and Statistics, and All That* (Princeton University Press, 1989).

[255] W. Pauli, *The Connection Between Spin and Statistics,* Phys. Rev. **58**, 716 (1940).

[256] W. Nolting, *Fundamentals of Many-body Physics* (Springer Berlin Heidelberg, 2009).

[257] A. Altland and B. Simons, *Condensed Matter Field Theory* (Cambridge University Press, New York, 2010).

[258] B. J. Dalton, J. Jeffers, and B. S. M., *Phase Space Methods for Degenerate Quantum Gases* (Oxford University Press, Oxford, 2015).

[259] H. Graßmann, *Die lineare Ausdehnungslehre – ein neuer Zweig der Mathematik* (O. Wigand, Leipzig, 1844).

[260] W. Clifford, *Applications of Grassmann's Extensive Algebra,* Am. J. Math. **1**, 350 (1878).

[261] R. P. Feynman, *Space-Time Approach to Non-Relativistic Quantum Mechanics,* Rev. Mod. Phys. **20**, 367 (1948).

[262] P. A. M. Dirac, *The Lagrangian in quantum mechanics,* Physikalische Zeitschrift der Sowjetunion **3**, 64 (1933).

[263] H. F. Trotter, *On the product of semi-groups of operators,* Proc. Amer. Math. Soc. **10**, 545 (1959).

[264] M. Laine and A. Vuorinen, *Basics of Thermal Field Theory* (Springer International Publishing, 2016).

[265] T. Matsubara, *A New Approach to Quantum-Statistical Mechanics,* Prog. Theor. Phys. **14**, 351 (1955).

[266] D. C. Champeney, *Fourier Transforms and their Physical Applications* (Academic Press, New York, 1973).

[267] F. Berezin, *The method of second quantization*, Pure and applied physics. A series of monographs and textbooks (Academic Press, London, 1966).

[268] A. Nieto, *Evaluating sums over the Matsubara frequencies,* Comput. Phys. Commun. **92**, 54 (1995).

[269] A. Abrikosov, L. Gor'kov, and I. Dzyaloshinskii, *Methods of Quantum Field Theory in Statistical Physics* (Dover Publ., New York, 1975).

[270] J. W. Brown and R. V. Churchill, *Complex Variables and Applications* (McGraw Hill, New York, 2009).